Lecture Notes in Electrical Engineering 699

Om Hari Gupta
Vijay Kumar Sood *Editors*

Recent Advances in Power Systems

Select Proceedings of EPREC 2020

Springer

Lecture Notes in Electrical Engineering

Volume 699

The book series *Lecture Notes in Electrical Engineering* (LNEE) publishes the latest developments in Electrical Engineering - quickly, informally and in high quality. While original research reported in proceedings and monographs has traditionally formed the core of LNEE, we also encourage authors to submit books devoted to supporting student education and professional training in the various fields and applications areas of electrical engineering. The series cover classical and emerging topics concerning:

- Communication Engineering, Information Theory and Networks
- Electronics Engineering and Microelectronics
- Signal, Image and Speech Processing
- Wireless and Mobile Communication
- Circuits and Systems
- Energy Systems, Power Electronics and Electrical Machines
- Electro-optical Engineering
- Instrumentation Engineering
- Avionics Engineering
- Control Systems
- Internet-of-Things and Cybersecurity
- Biomedical Devices, MEMS and NEMS

For general information about this book series, comments or suggestions, please contact leontina.dicecco@springer.com.

To submit a proposal or request further information, please contact the Publishing Editor in your country:

China

Jasmine Dou, Associate Editor (jasmine.dou@springer.com)

India, Japan, Rest of Asia

Swati Meherishi, Executive Editor (Swati.Meherishi@springer.com)

Southeast Asia, Australia, New Zealand

Ramesh Nath Premnath, Editor (ramesh.premnath@springernature.com)

USA, Canada:

Michael Luby, Senior Editor (michael.luby@springer.com)

All other Countries:

Leontina Di Cecco, Senior Editor (leontina.dicecco@springer.com)

**** Indexing: The books of this series are submitted to ISI Proceedings, EI-Compendex, SCOPUS, MetaPress, Web of Science and Springerlink ****

More information about this series at http://www.springer.com/series/7818

Om Hari Gupta · Vijay Kumar Sood
Editors

Recent Advances in Power Systems

Select Proceedings of EPREC 2020

Springer

Editors
Om Hari Gupta
Department of Electrical Engineering
National Institute of Technology
Jamshedpur
Jamshedpur, India

Vijay Kumar Sood
Faculty of Engineering and Applied Science
Ontario Tech University
Oshawa, ON, Canada

ISSN 1876-1100 ISSN 1876-1119 (electronic)
Lecture Notes in Electrical Engineering
ISBN 978-981-15-7993-6 ISBN 978-981-15-7994-3 (eBook)
https://doi.org/10.1007/978-981-15-7994-3

This Springer imprint is published by the registered company Springer Nature Singapore Pte Ltd.
The registered company address is: 152 Beach Road, #21-01/04 Gateway East, Singapore 189721, Singapore

Preface

The Electric Power and Renewable Energy Conference (EPREC-2020), organized by the Department of Electrical Engineering, National Institute of Technology Jamshedpur, India, during May 29 to 30, 2020, has been a unique conference during the difficult times of a global pandemic necessitating the usage of online presentations. We thank all the contributors for maintaining the high standard and making EPREC-2020 a huge success. Out of total 351 valid submissions, only 142 were selected for publication in three different volumes, i.e., an acceptance rate of nearly 40%. The conference attracted an international audience from the following countries: Bangladesh, Brazil, Canada, China, India, Norway, Qatar, Slovakia, Thailand, Ukraine, and USA. This volume, i.e., Recent Advances in Power System, is one of three volumes published by Springer in the book series "Lecture Notes in Electrical Engineering (LNEE)." It contains 49 high-quality papers which provide an overview of recent developments in modern power systems.

We thank all the organizing committee members, technical program committee members, reviewers, and student volunteers for their valuable support and volunteer work. We also appreciate the role of session chairs/co-chairs. We also thank the series editors of LNEE and Ms. Priya Vyas and Dr. Akash Chakraborty, Associate Editors—Applied Sciences and Engineering, Springer, for their help and quick responses during the preparation of the volume.

The editors hope that this volume will provide the readers relevant information on the latest trends in renewable energy, microgrid/smart grid operation, control, protection, HVDC systems, power system protection, etc.

Jamshedpur, India — Om Hari Gupta
Oshawa, Canada — Vijay Kumar Sood

Contents

About the Editors

Om Hari Gupta is currently an Assistant Professor at the Department of Electrical Engineering, National Institute of Technology Jamshedpur, India. He received the B.Tech degree (Electrical & Electronics Engineering) from UP Technical University, Lucknow, India, M.Tech degree (Power Electronics & ASIC Design) from the MN National Institute of Technology Allahabad, Prayagraj, India, and Ph.D. degree (Electrical Engineering) from the Indian Institute of Technology Roorkee, Roorkee, India. He is a recipient of the Canadian Queen Elizabeth II Diamond Jubilee Scholarship for research visiting the University of Ontario Institute of Technology, Oshawa, ON, Canada in 2017. His major areas of research interests include power system compensation and protection, microgrid control and protection, and control of drives. Dr. Gupta is a reviewer for various international journals including IEEE Transactions on Power Delivery, Electric Power Components and Systems, International Journal of Electrical Power and Energy Systems, etc.

Vijay Kumar Sood was a Senior Researcher with the Research Institute of Hydro-Québec, Montreal, QC, Canada, for many years. Currently, he is an Associate Professor in the Electrical Engineering Department, Ontario Tech University (formerly University of Ontario Institute of Technology), Oshawa, ON, Canada where he joined in 2007. He is also a Professional Engineer in Ontario. Dr. Sood received the Ph.D. degree from the University of Bradford, Yorkshire, England, UK in 1977. He has authored over 150 articles and written 2 books on HVDC and FACTS transmission systems and has been the Editor of the IEEE Transactions on Power Delivery, Associate Editor of IEEE Canadian Journal of Electrical and Computer Engineering, and Associate Editor of IEEE Canadian Review quarterly magazine. His current research interests include the monitoring, control, and protection of power systems. Dr. Sood is a life fellow of the Institute of Electrical and Electronics Engineers, a fellow of the Engineering Institute of Canada and Emeritus, and a fellow of the Canadian Academy of Engineers.

Ground Fault Detection Using Pole Differential Current Measurement for 2-Terminal Bipolar HVDC Lines

Ravi Shankar Tiwari, Om Hari Gupta, and Vijay K. Sood

1 Introduction

Long-distance bulk power transmission is one of the essentials in today's electricity grids. Extra high-voltage alternating current (HVAC) transmission lines are traditionally being used for long-distance and bulk power transmission. However, high-voltage direct current (HVDC) transmission system is also gaining in popularity over existing HVAC transmission system. Some typical recent examples are the 2375 km, Rio Madeira link in Brazil, 1750 km, ±800 kV, Bishwanath–Agra corridor, in India and many more. The reasons for HVDC transmission popularity are its ability for bulk power transmission over long distances, fast and precise control of power due to asynchronous interconnection, increased line-loading (close to the thermal limit), nearly zero reactive power loss, high efficiency, cost-effectiveness, etc [1]. To ensure the smooth and reliable power flow, fast and effective transmission protection schemes are required.

Protecting HVDC lines needs a different approach as compared to HVAC lines. The HVDC line protection requires detection and interruption of DC short-circuit currents. Interrupting a DC short-circuit current is much more complex in HVDC lines as compared to HVAC lines because of the absence of natural current zero crossings and quick increase of short-circuit current to an unacceptable value. However, the

R. S. Tiwari (✉)
GLA University, Mathura, Uttar Pradesh 281406, India
e-mail: ravishankar.tiwari@gla.ac.in

O. H. Gupta
National Institute of Technology Jamshedpur, Jamshedpur, Jharkhand 831014, India
e-mail: omhari.ee@nitjsr.ac.in

V. K. Sood
Ontario Tech University, Oshawa, ON, Canada
e-mail: vijay.sood@ontariotechu.ca

O. H. Gupta and V. K. Sood (eds.), *Recent Advances in Power Systems*, Lecture Notes in Electrical Engineering 699, https://doi.org/10.1007/978-981-15-7994-3_1

HVDC converter control technologies provide options for clearing the fault beyond the notable approach of employing circuit breakers in the AC system [2].

Therefore, the function of HVDC line protection is to detect the DC line faults and force DC line current to zero by means of rapid control actions so as to clear the fault and restore the normal system operation as quickly as possible. Most of the faults in DC lines are temporary in nature [3] and get cleared within a short time duration. If the DC fault is permanent in nature, then converter controls are unable to extinguish the fault arc and AC breakers are used to interrupt the DC system.

Some characteristics of DC line faults are noteworthy. The magnitudes of DC fault current in HVDC systems are much lower (typically, 2–3 P.U.) when compared to AC systems. Also, a sharp voltage dip during DC line faults results in a sudden drop in DC power transmission causing huge disturbances in the attached AC systems [4, 5]. This speaks to the need and significance of rapid fault detection, clearing and system recovery.

The major challenges are to achieve the desired speed, sensitivity and reliability to clear the fault within few AC cycles. This depends on accurate real-time voltage and current measurements and high-speed communication to transfer the crucial decision-making information from one station to other. Giant magneto resistance (GMR) and Hall effect sensors based on magnetic field can be used for accurate current measurements. The GMR and Hall current sensors have a high sensitivity and dynamic range of the value of 10 mT (10 mA–35 kA) and 0.001 mT (1 mA–10 kA), respectively [6]. The principle used to implement the protection algorithm can be based on local measurement or measurement via communication at distinct locations on the DC lines [7].

In the literature, the commonly available algorithms utilize traveling wave [8], current derivative [3], differential [3] and voltage level and voltage derivative protections [9]. These protection algorithms are discussed next.

1.1 Voltage Derivative Protection [8]

The decrease in voltage and increase in current of DC line use the concept of traveling waves and calculate the derivates of measured voltage $\frac{\partial V}{\partial t}$ and current $\frac{\partial I}{\partial t}$ waves to construct the criteria for detecting faults. The polarity of the current derivative indicated whether the fault is internal or external. The weighted sum of these derivatives ($k = k_1 \frac{\partial I}{\partial t} + k_2 \frac{\partial V}{\partial t}$) is compared with a set threshold, and if found to be greater than the said threshold, a DC line fault is detected. Both the poles are required to be equipped with this function and can detect the fault within 2–3 ms. However, the technique is unable to detect remote-end faults as well as faults with high resistance because of its impedance dependency [8].

1.2 Traveling Wave (TW) Protection [8]

Traveling waves are the high-frequency transient current/voltage waves generated in the event of DC line faults and tend to move from fault point to the ends of line [8]. The protection algorithm detects the wave front of generated traveling wave from instantaneous current and voltage samples. A number of consecutive sample differences are measured and compared with a threshold value to check whether the wave has enough magnitude for a certain time period. If all the measured difference crosses the threshold, it indicates the presence of a line fault. However, the detection of wave front gets affected in long lines and large impedance faults and it is difficult to detect double-pole faults [10].

1.3 Current Differential Protection [3, 11]

In this algorithm, differential current calculated by measurement at the two ends of the DC line is compared with a threshold. If the differential current exceeds the threshold, this information is relayed to converter stations and protection is initiated. The sensitivity of this gets affected by charging and discharging currents produced due to voltage variations, especially in cables. Moreover, line current information needs to be transferred to other stations, which adds a delay, and may affect the response of the scheme. The reliability indirectly depends on reliability of telecommunication method used [3, 11].

1.4 Distance Protection [10, 12]

The distance protection scheme is widely used for AC lines. The authors of [12] suggested time-domain distance protection scheme based on distributed line model. In [10], a distance protection criterion is proposed which is based on linear distribution of low-frequency voltage signal along the line. If the polarity of low-frequency filtered voltage is opposite to the compensating voltage, it indicates the presence of an internal fault.

1.5 DC Voltage-Level Protection [3]

This method detects high impedance faults near the inverter end by measuring a dip in voltage over a large time. The time and level delays are kept so as not to cause mal-operation during normal switching or voltage transients. This method is also used as backup for traveling wave and voltage derivative schemes [3].

1.6 Protection Based on Signal Processing Techniques [13–15]

The use of signal processing techniques such as wavelets, artificial neural networks (ANNs) and support vector machines (SVMs) has also increased as a powerful tool for AC as well as DC line protection. The authors of [13] propose a complete fault detection, localization and classification algorithm based on SVM for HVDC lines. In [14], ANN architecture is used to accurately locate the fault using AC rms voltage, DC voltage and line currents at rectifier end. A wavelet multi-resolution signal decomposition algorithm [15] is used to calculate traveling wave transient voltage energy distribution to identify the short circuit and lightning fault in HVDC line [15].

Now, to address the aforementioned issues—mainly the problem of delay in protection due to involvement of data exchange and communication—this paper proposes a local fault detection criteria (independent of information from remote station) to reduce the fault detection time and improve the converter controls.

The rest of the manuscript is organized as follows. Section 2 deals with the control strategy for steady-state and dynamic operation of HVDC system. Section 3 explains proposed pole differential current algorithm for pole-to-ground fault detection, threshold criteria and its coordination with VDCO control. Section 4 presents the PSCAD/EMTDC simulation of the test system. Finally, Sect. 5 concluded the work performed.

2 HVDC Line Control Strategies

The line-commutated 6-pulse converter bridges are the basic components of the bipolar HVDC transmission system, as shown in Fig. 1. The objectives of HVDC control [1] are (a) to limit the maximum DC line current, (b) to maintain the maximum

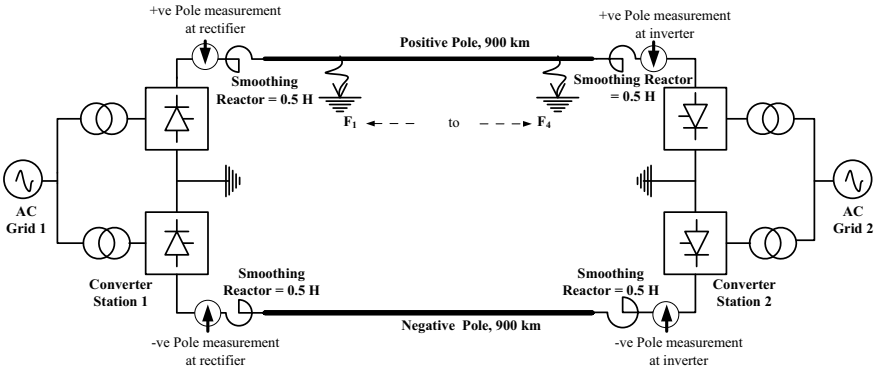

Fig. 1 2-terminal bipolar HVDC test system

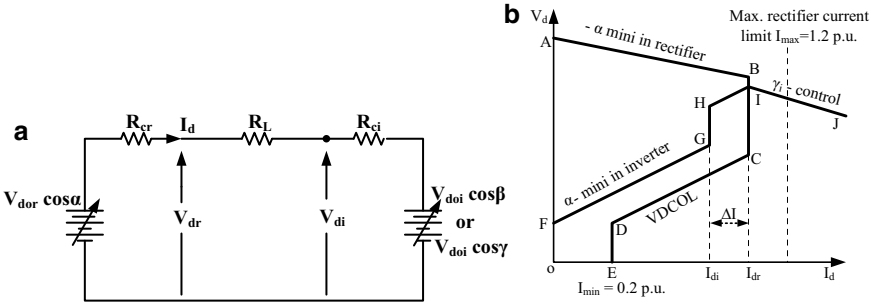

Fig. 2 **a** Steady-state equivalent circuit. **b** Controller characteristics

DC voltage for transmission and (c) to minimize reactive power consumption for steady-state and dynamic conditions of the HVDC system. The steady-state requirements are to limit the non-characteristic harmonic generation, maintaining control variable DC line current (I_d) and firing angle α to accommodate any AC network topology variations. The dynamic requirements are to minimize sudden changes in the power, current, power reversal and associated AC system frequency variations.

The control strategies implemented to fulfill the steady-state and dynamic requirements are constant current (CC), minimum firing angle at rectifier end and constant voltage control, minimum extinction angle at the inverter end. The controller functions are illustrated via DC system equivalent and controller characteristics, as shown in Fig. 2(a) and 2(b), respectively.

The converter valve voltages and line current for steady-state equivalent circuit of a 2-terminal HVDC (Fig. 2(a)) are defined as

At rectifier end

$$V_{dr} = V_{dor} \cos \alpha - R_{cr} I_d \tag{1}$$

$V_{dor} = \frac{3}{\pi}\sqrt{2} V_{LLr}$, $R_{cr} = \frac{3}{\pi}\omega L_{cr}$,

$$I_d = \frac{V_{dor} \cos \alpha - V_{doi} \cos \gamma}{R_{cr} + R_L - R_{ci}} \tag{2}$$

At inverter end

$$-V_{di} = V_{doi} \cos \beta + R_{ci} I_d \tag{3}$$

Or

$$-V_{di} = V_{doi} \cos \gamma - R_{ci} I_d \tag{4}$$

$$V_{doi} = \frac{3}{\pi}\sqrt{2} V_{LLi} \tag{5}$$

where V_{LLr}, V_{LLi} are the AC-side line-to-line voltages at rectifier and inverter stations. R_L is the DC line resistance, and R_{cr}, R_{ci} are the equivalent commutation resistances of rectifier and inverter bridges. Figure 2(b) shows the modified control characteristics ABCDE and FGHIJ of rectifier and inverter stations, respectively. The details for both are described in Tables 1 and 2 to fulfill the steady-state and dynamic requirements.

Table 1 Rectifier station requirements and control implementation

Line section	Control implemented	Features obtained	Reason
AB	α-minimum	Higher loading and minimized reactive power consumption	To enhance power flow, power factor
BC	Constant current (CC) $I_{dr(limit)} = 1$ P.U.	Limit maximum DC line current I_d (during inverter-side voltage dip rectifier operates in CC)	For valve protection
CD	Voltage-dependent current order limit (VDCOL)	Operates the HVDC link with reduced power flowing under sudden huge voltage dip	To maintain lower current margin for reduced power flow
DE	Minimum current $I_{min} = 0.2$ P.U.	To avoid zero current through converter valves due to harmonics generates HV stresses	Valve protection

Table 2 Inverter station requirements and control implementation

Point on curve	Control implemented	Features obtained	Reason
IJ	γ-minimum (CEA)	Provide voltage controller at inverter, and maintain constant voltage for steady-state operation	Improved power factor during operation
HI	Constant β	Stable operation during heavy voltage dip at rectifier during week AC system interconnection	Avoided multiple operation of controller
GH	Constant current (CC)	To get an intersection point between rectifier and inverter characteristics, CC must be provided at inverter	Maintain power flow in HVDC link
FG	α-minimum	Operates the HVDC link with reduced power flowing under sudden large voltage dip	To avoid commutation failure during AC faults

The intersection point of the two characteristics shows the operating point of HVDC link.

3 Proposed Pole Differential Current Algorithm

3.1 Protection Principle

The probability of faults in the DC line is higher as compared to any other part of the HVDC system. Most of the faults in DC lines are temporary which are initiated due to pollution or lightning strikes. Pole-to-ground fault is one of the most frequently caused faults due to insulation failure between line conductor and ground [16].

The traditional current differential protection algorithm has good reliability but depends on the communication channel. To minimize the dependency on the communication channel and enhance the reliability and sensitivity, single-end measurement-based protection scheme is introduced. The proposed scheme uses a measurement at rectifier side using high-sensitivity GMR or Hall sensors. The measurement performed on both poles is shown in Fig. 1. The measured samples of instantaneous currents are used to obtain the pole differential current (PDC) as shown in (6) which is compared with the threshold, and if found greater than the said threshold, an internal fault is declared.

For normal load and external fault conditions, the PDC will be negligible. The sudden rise in differential current guaranties the presence of an internal fault, but to enhance the security; it should be compared with a set threshold. The amplitude of differential current gets affected by fault resistance and fault location. Still the scheme is sensitive enough for fault resistances up to 500 Ω.

The current measurements are performed at each station, i.e., $I_{\mathrm{PR}}(t)$, $I_{\mathrm{NR}}(t)$, $I_{\mathrm{PI}}(t)$ and $I_{\mathrm{NI}}(t)$. The PDC calculated at inverter and rectifier stations is given by

Pole differential current (PDC) at rectifier end $\Delta I_{\mathrm{Pole1}}(t)$ is given below in (6):

$$\Delta I_{\mathrm{Pole1}}(t) = (I_{\mathrm{PR}}(t) - I_{\mathrm{NR}}(t)) \tag{6}$$

Pole differential current (PDC) at inverter end $\Delta I_{\mathrm{Pole2}}(t)$ is given below in (7):

$$\Delta I_{\mathrm{Pole2}}(t) = (I_{\mathrm{PI}}(t) - I_{\mathrm{NI}}(t)) \tag{7}$$

where $\Delta I_{\mathrm{Pole1}}(t)$ and $\Delta I_{\mathrm{Pole2}}(t)$ are PDC obtained by subtracting positive and negative instantaneous current samples at both stations. The pole-to-ground fault is detected when it satisfies the criteria of (8):

$$\Delta I_{\mathrm{Pole}}(t) > I_{\mathrm{th}} \tag{8}$$

where I_{th} is the threshold for PDC. Whenever this criterion is satisfied—giving an indication of fault—the local or master controller was instructed for necessary actions.

3.2 Selection of Threshold

Since the bipolar HVDC transmission system, under normal or external fault operation, gives negligible PDC, so the selection of minimum threshold current increases the sensitivity with low fault detection time. Based on the rigorous simulation study presented in the next section, the threshold used for identifying the fault detection time is set at 0.25 P.U.

3.3 Coordination of PDC and VDCOL Control Characteristics

The normal control-based protection against DC line faults is the use of the static VDCOL characteristic. This is effective to reduce the DC fault current to a level of 0.2 P.U. as indicated in Fig. 2 and works well in most cases of a temporary DC line fault. However, in the case of a permanent DC line fault, the VDCOL characteristic is unable to extinguish the DC fault arc and reduce the DC fault current to zero. In such a case, the PDC will activate the opening of the AC-side breaker at the rectifier end to extinguish the DC fault arc after a preselected period of time.

4 Simulation Results and Discussion

A 2-terminal bipolar HVDC transmission system (Fig. 1) is simulated in PSCAD/EMTDC, and pole-to-ground faults are created at various locations, i.e., at F_1, F_2, F_3 and F_4. System data and controller details are provided in the Appendix. The measured and sampled data is exported to MATLAB software for the implementation of the protection algorithm.

For a pole-to-ground fault at location F_1 (0 km from the rectifier end) and fault resistance R_1, the DC pole currents and PDC are plotted in Fig. 3. Similarly, Fig. 4 presents the DC pole currents and PDCs for fault at F_4 (900 km) with fault resistance R_4. In both the cases, the current of the faulty pole varies largely and the current of healthy pole hardly changes. The PDCs at the rectifier and inverter ends also detect and cross the thresholds—indicating the internal pole-to-ground fault. A few cases for various fault locations F_1 to F_4 where $F_1 = 0$ km, $F_2 = 300$ km, $F_3 = 600$ km and $F_4 = 900$ km are considered with the variations in fault resistance and fault

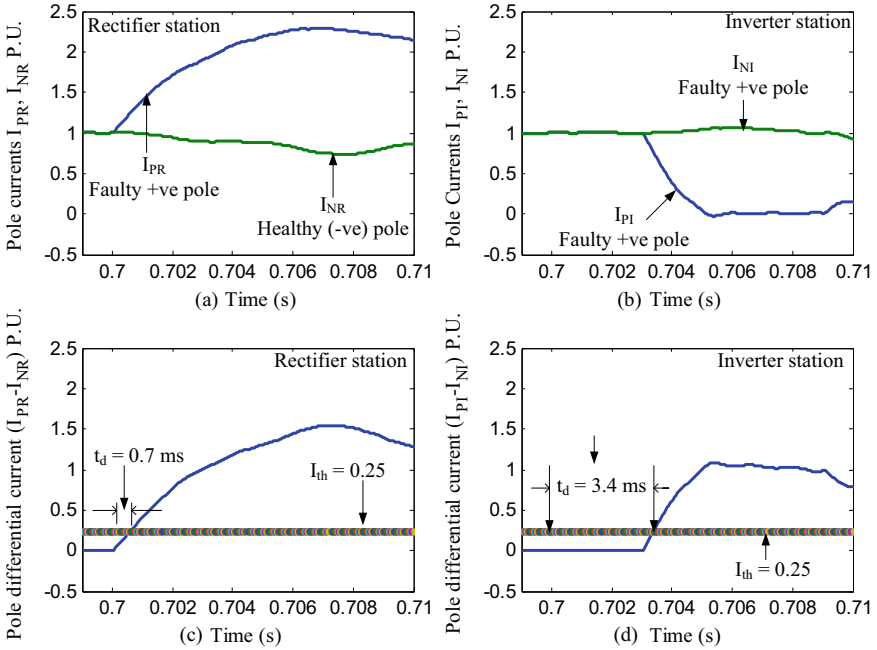

Fig. 3 DC line currents, PDCs and fault detection time (t_d) for F_1, R_1

detection time is recorded (Table 3). From the obtained results, it is found that the highest fault detection time is at 500 Ω fault resistance at location F_4 which is 5.1ms. Similar measurement and calculation are performed at inverter station also to obtain various fault detection times based on different fault locations and resistances. The results show smaller fault detection time as compared to other schemes, and thus the scheme can be preferred for primary protection against ground faults in DC lines.

Here, t_{dr} and t_{di} are the fault detection times at rectifier and inverter stations, respectively, as listed in Table 3.

The proposed PDC algorithm gives stable response during any variations in reference power through the HVDC link. Figure 5 presents the reference current, positive and negative pole currents, and PDC in response to changes in the reference loading condition from 1 to 0.5 P.U. for time duration of 1 s. Since the master control is same for both the poles, any variation in reference power is simultaneously applied to both positive and negative poles. Thus, similar variation in each DC line current to accommodate the command from master controller leads to nearly zero PDC which is desired for stable operation.

Similarly, the PDC algorithm gives stable response at inverter end also for any step variation in reference power in the HVDC link. Thus, the scheme is accurate for protection against ground fault having least detection time, good sensitivity and high reliability due to elimination of data transfer and communication delay.

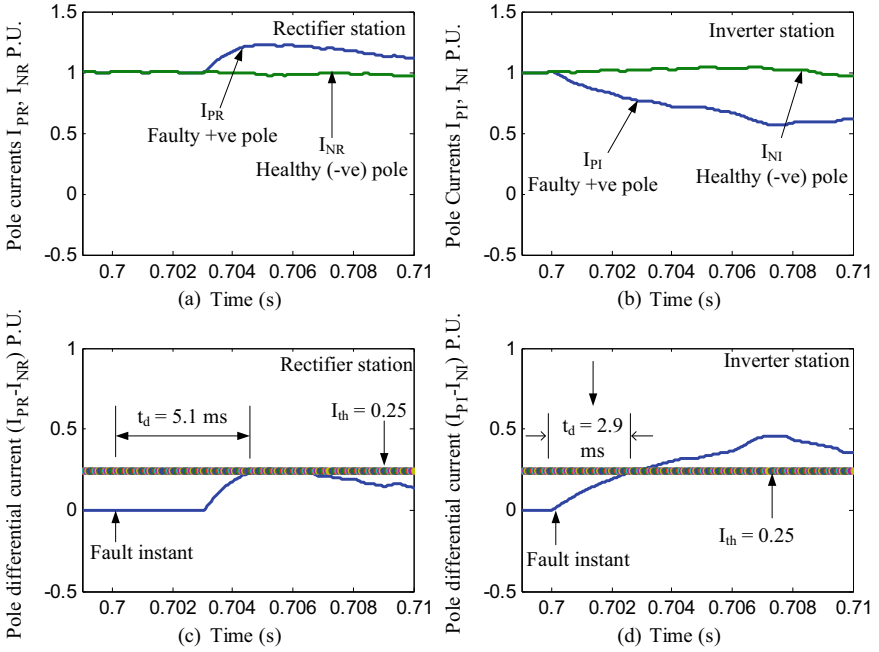

Fig. 4 DC line currents, PDCs and fault detection time (t_d) for F_4, R_4

Table 3 Fault detection time with fault location and transition resistance

Fault location	Fault detection times t_{dr}/t_{di} (ms) for threshold $I_{th} = 0.25$ P.U.				Fault detection status			
	$R_1 = 10\ \Omega$	$R_2 = 100\ \Omega$	$R_3 = 300\ \Omega$	$R_4 = 500\ \Omega$	R_1	R_2	R_3	R_4
F_1	0.7/3.4	0.9/3.6	1.6/4.0	3.1/4.8	✓	✓	✓	✓
F_2	1.4/2.4	1.7/2.7	2.5/3.5	4.7/4.3	✓	✓	✓	✓
F_3	2.4/1.3	2.7/1.7	3.6/2.5	4.4/4.0	✓	✓	✓	✓
F_4	3.5/0.7	3.6/1.0	4.1/1.8	5.1/2.9	✓	✓	✓	✓

5 Conclusion

The paper presents a thorough analysis of a 2-terminal bipolar HVDC system control and the protection algorithm against DC line faults. Importance of fast fault detection and response from these faults by control strategies are explained. Most of the available detection algorithms have delay in protection due to communication between inverter and rectifier ends for measured data transmission. The proposed algorithm is based on the calculation of pole differential currents at both ends to avoid the delay due to information exchange and therefore speeds up the protection. The HVDC

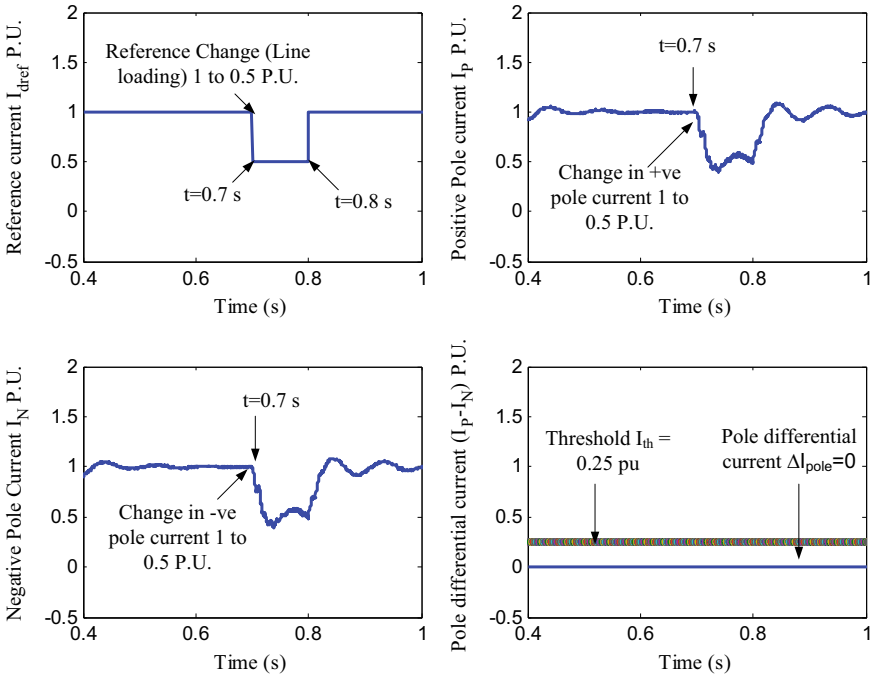

Fig. 5 PDC algorithm response during change in reference power loading at rectifier end

line faults, i.e., pole-to-ground faults, were implemented with the combination of various fault resistances and fault locations to observe the effect on fault detection. The simulated results show that the proposed PDC algorithms have the advantage of improved fault detection time and protection reliability and are useful as primary protection schemes for HVDC lines against line-to-ground short-circuit faults.

Appendix 1

Bipolar HVDC Test System

The data for the system configuration (Fig. 1) is obtained from the MATLAB model (based on a Hydro-Quebec-)mono-polar HVDC model which is modified into a bipolar HVDC system. The Hydro-Quebec system was developed for steady-state and transient analysis of a 12-pulse, 1000 MW (500 kV–2kA) 50/60 Hz HVDC transmission system. The system consists of two overhead transmission line conductors acting as forward paths for positive and negative poles and solidly grounding acting as return path. The HVDC link interconnects the two asynchronous AC grids. The sending end of the HVDC link is connected with 500 kV, 60 Hz, and receiving end

Table 4 Various parameters of converters and HVDC bipolar system

Components of HVDC system	Rating and specifications
Type of HVDC link	Bipolar solid grounded
Power rating	2000 MW (1000 MW each pole)
DC voltage level	±500 kV each pole
Current rating	2 kA of each pole
Converter	1200 MVA of each pole
AC grid 1 voltage	500 kV, 60 Hz, 500 MVA
AC grid 2 voltage	345 kV, 50 Hz, 10,000 MVA
Smoothing reactor	0.5 H at both ends
AC filter 1	1200 Mvar at 60 Hz
AC filter 2	1200 Mvar at 50 Hz

AC grid is of 345 kV, 50 Hz system. The line-commutated converter bipolar HVDC test system consists of two 6-pulse series-connected converters forming 12-pulse converter configuration which is connected to a 900 km distributed parameter line and smoothing reactors of 0.5 H at both ends. The various parameters of converter and HVDC bipolar system are shown in Table 4. The two 600 MVAr AC filters are connected in the system.

Appendix 2

Current Controller and Constant Extinction Angle Control (CEA)/γ-Control

The prime objective of HVDC system control is to obtain fast and flexible power control between rectifier and inverter stations under steady-state and transient operation. Usually, this system operates in constant power control mode where power order is decided by user. Power controller derives the current order supplied to VDCOL and current controller amplifier (CCA). The α-order generated from CCA is communicated to converter firing angle control to determine valve firing instants. The converter controls at rectifier and inverter stations are set to operate in constant current and constant voltage control modes, respectively; during any DC line faults, the controllers of both ends shift their operational modes from steady state so as to minimize the effect of fault on both AC–DC sides. The various converter control modes are current control (CC), voltage control, VDCOL, minimum alpha (CIA), gamma control (CEA), β-control modes. Figures 6, 7 and 8 present the pole control, current control and overview of control blocks of HVDC system.

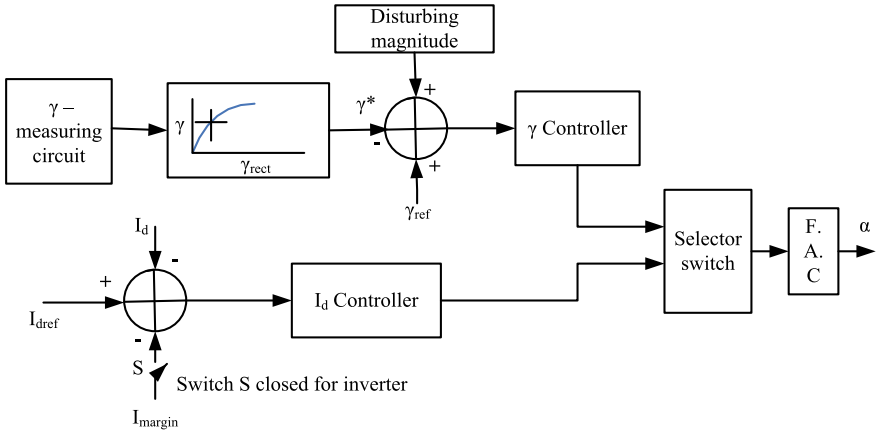

Fig. 6 Pole and converter control

Fig. 7 Current controller

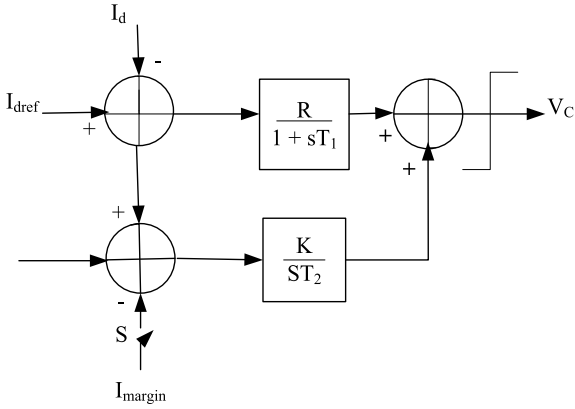

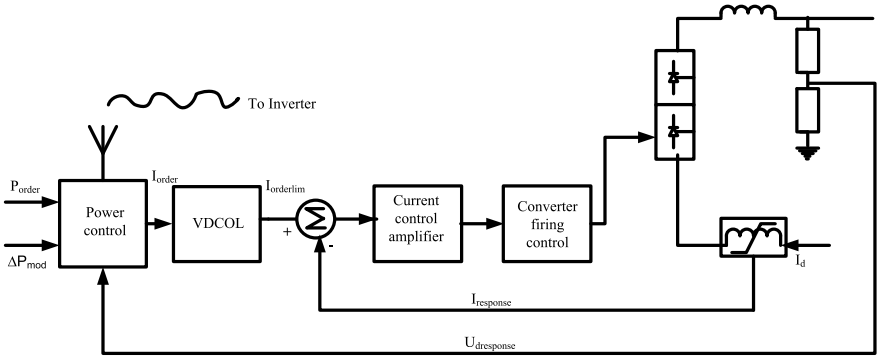

Fig. 8 HVDC control overview

References

1. Sood, V.K.: HVDC transmission. In: Power Electronics Handbook, pp. 823–849. Elsevier, Amsterdam (2011)
2. Leterme, W., Jahn, I., Ruffing, P., Sharifabadi, K., Van Hertem, D.: Designing for high-voltage dc grid protection: fault clearing strategies and protection algorithms. IEEE Power Energy Mag. **17**(3), 73–81 (2019). https://doi.org/10.1109/MPE.2019.2897188
3. Naidoo, D., Ijumba, N.M.: HVDC line protection for the proposed future HVDC systems. In: 2004 International Conference on Power System Technology, POWERCON 2004, 2004, vol. 2, pp. 1327–1332. https://doi.org/10.1109/icpst.2004.1460207
4. Ademi, S., Tzelepis, D., Dyśko, A., Subramanian, S., Ha, H.: Fault current characterisation in VSC-based HVDC systems. In: IET Conference Publications, 2016, vol. 2016, no. CP671. https://doi.org/10.1049/cp.2016.0043
5. Kontos, E., Pinto, R.T., Rodrigues, S., Bauer, P.: Impact of HVDC transmission system topology on multiterminal DC network faults. IEEE Trans. Power Deliv. **30**(2), 844–852 (2015). https://doi.org/10.1109/TPWRD.2014.2357056
6. Ouyang, Y., He, J., Hu, J., Wang, S.X.: A current sensor based on the giant magnetoresistance effect: design and potential smart grid applications. Sensors (Switzerland) **12**(11), 15520–15541 (2012). https://doi.org/10.3390/s121115520
7. Leterme, W., Pirooz Azad, S., Van Hertem, D.: A local backup protection algorithm for HVDC grids. IEEE Trans. Power Deliv. **31**(4), 1767–1775 (2016). https://doi.org/10.1109/tpwrd.2016.2543306
8. (PDF) Traveling wave fault location in power transmission systems: an overview. https://www.researchgate.net/publication/249313007_Traveling_wave_fault_location_in_power_transmission_systems_An_overview. Accessed 21 May 2020
9. Gao, B., Zhang, R., Zhang, X.: A novel procedure for protection setting in an HVDC system based on fault quantities. J. Electr. Eng. Technol. **12**(2), 513–521 (2017). https://doi.org/10.5370/JEET.2017.12.2.513
10. Qin, Y., Wen, M., Zheng, J., Bai, Y.: A novel distance protection scheme for HVDC lines based on R-L model. Int. J. Electr. Power Energy Syst. **100**, 167–177 (2018). https://doi.org/10.1016/j.ijepes.2018.02.037
11. Abu-Elanien, A.E.B., Elserougi, A.A., Abdel-Khalik, A.S., Massoud, A.M., Ahmed, S.: A differential protection technique for multi-terminal HVDC. Electr. Power Syst. Res. **130**, 78–88 (2016). https://doi.org/10.1016/j.epsr.2015.08.021
12. Suonan, J., Zhang, J., Jiao, Z., Yang, L., Song, G.: Distance protection for HVDC transmission lines considering frequency-dependent parameters. IEEE Trans. Power Deliv. **28**(2), 723–732 (2013). https://doi.org/10.1109/TPWRD.2012.2232312
13. Johnson, J.M., Yadav, A.: Complete protection scheme for fault detection, classification and location estimation in HVDC transmission lines using support vector machines. IET Sci. Meas. Technol. **11**(3), 279–287 (2017). https://doi.org/10.1049/iet-smt.2016.0244
14. Johnson, J.M., Yadav, A.: Fault location estimation in HVDC transmission line using ANN. Smart Innov. Syst. Technol. **50**, 205–211 (2016). https://doi.org/10.1007/978-3-319-30933-0_22
15. Li, Z.Q., Lv, Y.P.: A novel scheme of HVDC transmission line voltage traveling wave protection based on wavelet transform. In: 2008 International Conference on High Voltage Engineering and Application, ICHVE 2008, Nov. 2008, pp. 163–167. https://doi.org/10.1109/ichve.2008.4773899
16. Khaimar, A.K., Shah, P.J.: Study of various types of faults in HVDC transmission system. In: Proceedings of the International Conference on Global Trends in Signal Processing, Information Computing and Communication ICGTSPICC 2016, no. Lcc, pp. 480–484, 2017. https://doi.org/10.1109/icgtspicc.2016.7955349

A Review on Islanding Detection Schemes for DC Microgrids

Bhabani Kumari Choudhury and Premalata Jena

1 Introduction

Recently, renewable energy sources (RESs)-based power plants have attained significant attention because of the fast depletion of fossil fuels and global warming [1]. Distributed generations (DGs), loads, and a bidirectional converter is interfaced with the utility grid in order to exchange powers [2]. DGs enhance the profit of power generation, reduce the effect of global warming, and improve power quality. Therefore, the application of DGs provides the reliability and security to the system [3, 4]. MGs are of two types, namely AC MGs and DC MGs. Operation modes of MGs can be either isolated or grid-connected modes [5]. AC MGs research is well developed because of its mature technologies, protection, and standards. Most of the DGs generate power in the form of DC, and it is converted into AC power through DC-to-AC converter (inverter) in order to connect them with the AC MGs [6]. It is important to note that DC loads need DC power supply, and hence, AC power is converted back to DC power. Here, the number of conversions, number of required converters, and losses are more, so it reduces the efficiency of the system [7]. Apart from these, stability, synchronization, and reactive power requirement are the built-in disadvantages of AC MGs. Therefore, DC MGs are a better alternative and solution to the above problems [8, 9]. Moreover, DC MGs are easily scalable because of the absence of limiting equipment, such as transformers and relays.

During islanding, utility grid connection is absent. So, DGs are the main sources at this time. But, the power can reach to the consumers without any interruption during islanding due to DGs [10]. Here, employees can be affected by islanding as

B. K. Choudhury (✉) · P. Jena
Department of Electrical Engineering Indian Institute of Technology Roorkee, Roorkee 247667, India
e-mail: bkumarichoudhury@ee.iitr.ac.in

P. Jena
e-mail: pjenafee@iitr.ac.in

O. H. Gupta and V. K. Sood (eds.), *Recent Advances in Power Systems*, Lecture Notes in Electrical Engineering 699, https://doi.org/10.1007/978-981-15-7994-3_2

they may not notice that some part of the circuit is working, which may stop reconnection of devices automatically [11]. In order to maintain stability, it is essential to maintain a balance between load and generation in the islanded circuit. The above-stated reasons can be avoided by rapidly detecting the islanding, so that it can be disconnected from the primary circuit as quickly as possible. This process is known as anti-islanding [12]. The requirements for IDSs in DGs are outlined in [13], which clearly indicates that DGs should disconnect from the grid within 2 s. Otherwise, it will draw a significantly high amount of current to keep the balance. Due to this, DGs are damaged.

In [14–17], some AC MGs islanding is reported. However, DC MG IDSs are in the initial stage and not rigorously studied in the literature. This paper presents an overview of islanding detection schemes, which is used for DC MGs. The requirements of DC MGs IDSs along with their advantages over the AC MGs IDSs are reported. Recent research and developments in this field are presented with possible challenges, and classification of the same is highlighted.

The rest of the paper is organized as follows. DC MGs IDSs and their advantages and disadvantages are presented in Sect. 2. Different types of passive IDSs for DC MGs are explained in Sect. 3, and active IDSs concepts and its types are reported in Sect. 4. At last, final conclusions are drawn in Sect. 5 with some future insights.

2 DC MGs Islanding Detection Schemes

Islanding detection methods which detect the islanding situation with fewer false positives is the leading research area. When the electrical system parameters crosses a certain threshold value, a trip signal is generated. Here, tripping time is the time which is required to successfully separate the two systems during islanding as reported in [18]. No fuse circuit breakers and solid-state circuit breakers are commonly used circuit breakers in DC MGs [19]. The author in [20] mentioned that in DC MGs, the detection time is with in 0.2 s. The advantages and disadvantages of DC and AC MGs IDSs are given in Table 1.

2.1 Intentional/Planned IDSs

Intentional/Planned IDSs are a detection method where generation and loads are scheduled prior to islanding. It means that which parts of the load to be isolated is decided before islanding [21, 22]. This type of detection technique is applicable to AC MGs as well as DC MGs. The leading cause of this type of islanding detection is a preplanned switching event. During such cases, the number of transients is less in MGs.

Table 1 Comparison between AC MG and DC MG IDSs

Parameters	AC MGs IDSs	DC MGs IDSs
Standards	Available (IEEE 1547)	Not available (Required Reconsideration)
System Parameters	Voltage, current, impedance, Active power, reactive power, frequency, harmonics, and phase	Voltage, current, active power, and impedance
IDSs available	Passive, active, and hybrid	Passive and active
Complexity	Easier than DC MG IDSs	Complex
Accuracy	Less accurate	Accurate
Tripping time	Less than 0.5 s	Less than 0.2 s

2.2 Unintentional/Unplanned IDSs

Unintentional/Unplanned IDSs are a detection method that is uncertain in nature. The leading cause of these type of IDSs is unplanned switching events [23, 24]. Islanding detection should be quick in order to maintain the reliability and stability of MGs, with a proper control strategy. In this case, the severity of the transients is more. During islanding conditions, electrical characteristics like current, voltage, impedance, frequency, active, reactive power output, etc., of DGs are changed significantly. In order to detect islanding, it is essential to observe the electrical parameters of the system continuously. IDSs are of two types, namely remote IDSs and local IDSs. The detailed classification is shown in Fig. 1.

Remote IDSs The communication medium between the grids and the DGs of MGs is required in this type of IDSs. Due to this, the cost of the islanding circuit increases, which is the major challenge of this type of IDSs. The examples of these IDSs, which are applicable for DC MGs are transfer trip, impedance insertion, and power line carrier communication (PLCC) IDSs. In transfer trip IDSs, supervisory control and data acquisition (SCADA) are used to monitor the status of circuit breakers and reclosures, which are present near to the point of common coupling (PCC) [25]. In the impedance insertion method, a low-value impedance is inserted nearer to the PCC in order to obtain proper power balance between generations and load [26]. In the PLCC method, a low energy signal transmits from the transmitter (utility side) to the receiver (DGs side). The disappearance of the signal represents the islanding condition [17]. Remote IDSs are more accurate and reliable than local detection schemes, but these are uneconomical because of their communication equipment.

Local IDSs Local IDSs utilize measurement and monitoring of electrical parameters like impedance, voltage, active power, etc., on the DGs side. The detailed classification of local IDSs is represented in Fig. 1.

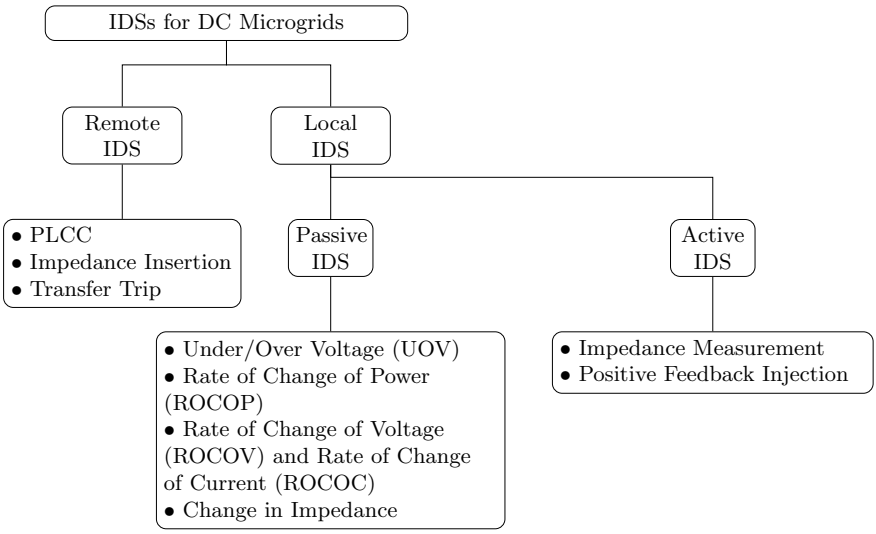

Fig. 1 Classification of DC MGs IDSs

3 Passive IDSs for DC MGs

Passive IDSs monitor the electrical system parameters like voltage, impedance, active and reactive power, frequency of DGs, etc., to identify the islanding. In DC MGs, the system parameters are voltage, impedance, and active power output of DGs. The islanding situation can be identified when the system parameters deviate from a predefined threshold value. In [27], passive IDSs for DC MGs have been explained. Note that, the implementation of passive detection schemes is simple and easy. Non-detection zone (NDZ) is the major challenge of this IDSs [28]. However, suitable threshold selection is also a complicated and challenging task.

3.1 Under/Over-Voltage-Based IDSs

In this type of IDS, it is required to sample the voltage v periodically and monitor to detect sudden changes in voltage in order to detect a fault condition. UOV IDS is important for grid-interfaced converters as the primary function of this type of converters is to maintain proper balance. A sudden change in voltage occurs commonly in the grid due to frequent removal and attachment of loads, so a threshold needs to be set to avoid faults [29]. The IDSs calculate the change in terminal voltage of DC/DC converter with t window length. Then, the obtained signal is compared continuously.

When it crosses a predefined trip setting, tripping occurs. The trip condition for UOV IDSs is stated as follows.

$$|\sum_{n=0}^{t}(\Delta v_n)| > \text{Trip Setting} \tag{1}$$

where the number of sampling instants is denoted as n. Here, Δv_n is the change in the voltage. The trip setting, Trip Setting, can be accurately chosen, so that the relay trips suddenly whenever any disturbance occurs for loss of mains. If the absolute value does not cross the trip setting, then the change in voltage is set to zero. This IDS is economical and simple in nature. Moreover, it can be used for several other reasons besides islanding as voltage deviations are common in the power system. However, it causes relatively large NDZ, and the reaction times for these IDSs may be unpredictable, which are the major challenges for this IDSs.

3.2 ROCOP-Based IDSs

The integration of digital technology with a protection scheme needs a number of input data to make an accurate decision. ROCOP-based IDSs is one of them. Since the loss of mains results sudden change in load, continuously monitoring the output power deviation of the DGs provides a direct method of detecting islanding [25]. This IDSs monitor output power deviation and integrate the change in output power signal over a pre-defined sample period. The instantaneous power output from the DGs is mathematically represented as follows.

$$P = vi \tag{2}$$

where v is the sampling voltage, i is the sampling current measured at the terminals of DGs, and P is the instantaneous power. Here, tripping occurs when the integrated signal crosses the trip setting K_{s1}. A trip criterion for this IDSs is as follows.

$$\sum_{n=0}^{t}(P_n - P_{n-1}) > K_{s1} \tag{3}$$

where n is the number of sampling instants and t is the window length, which is used for sampling. Here, P_n is the present value of instantaneous power, which is compared with the previous value P_{n-1} to detect the islanding. In extreme load unbalancing cases, integrating action provides immunity to mal-operation. Note that, this IDSs is simple during the loss of the grid. But high NDZ and selection of proper threshold is also a challenge in this case.

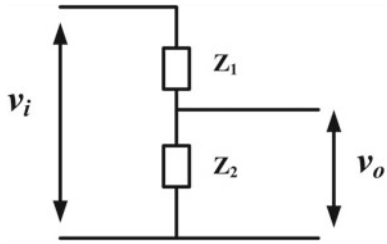

Fig. 2 Circuit representation of CII-based IDSs

3.3 Change in Impedance-Based IDSs

The impedance of the utility grid is much smaller as compared to the impedance of islanding power. This is because the impedance of an isolated section is suddenly increased during islanding [30]. Due to the change of impedance level, a change in the system fault level occurs. When the system impedance rises significantly, and it is higher than the routine situations, loss of mains happens, and the system trips. These IDSs cause unnecessary trips during network faults or grid frequency transients [31]. Here, the complete accuracy is not required in this impedance measurement equipment. A voltage divider represents the circuit diagram of this IDSs. When a signal v_i is applied to a voltage divider circuit, it produces an output, which is v_0, which is given in Fig. 2.

When the value of Z_2 (system impedance) varies, the output voltage (V_o) also varies. It helps to make a decision about whether the system is operating in an islanding case or not. The output voltage is represented as follows.

$$v_0 = v_i \frac{Z_2}{Z_2 + Z_1} \tag{4}$$

where v_0 is the output voltage, v_i is the input voltage, Z_2 is the system impedance, and Z_1 is the driver circuit impedance. The input to voltage divider circuit is coupled to the utility mains through a capacitor. The impedance across the capacitor can be denoted as Z_1. The value of Z_1 can is chosen, such that the ripple on the mains is negligible when synchronized to the utility. The value of Z_2 increases in case of loss of mains. The islanding detection circuit monitors the magnitude of the output signal (v_0) continuously, and when it crosses a specific predetermined value, the system trips. Here, it is challenging to distinguish between islanding and non-islanding events.

3.4 ROCOV- and ROCOC-Based IDSs

When generation is not equal to load, real power mismatch occurs. This causes transients and variations in voltage and current. ROCOV- and ROCOC-based IDSs

are used to detect islanding in such situations [27]. DC voltage and current can be measured continuously at the terminal of each DG separately, which is used to calculate the rate of change of voltage and current as follows.

$$\text{ROCOV} = \frac{v(t_1) - v(t_1 - \Delta t_1)}{\Delta t} \tag{5}$$

$$\text{ROCOC} = \frac{i(t_1) - i(t_1 - \Delta t_1)}{\Delta t} \tag{6}$$

where t_1 is the window length, Δt_1 is the small variation in a particular time instant, and Δt is the variation in the total time. The variations in the voltage and the current during islanding is a function of power mismatch, which are stated as follows.

$$\text{ROCOV} = \frac{v}{2P_L}\frac{\Delta P}{\Delta t} \tag{7}$$

$$\text{ROCOC} = \frac{i}{2P_L}\frac{\Delta P}{\Delta t} \tag{8}$$

where ΔP is the power mismatch and P_L is the active load power. However, demerits of this IDSs is that voltage and current deviate gradually during small power mismatch situations. Therefore, it is challenging to identify islanding from different non-islanding events.

4 Active IDSs for DC MGs

In active IDS, a small disturbance in the form of signal is applied to the system, and then, the response of the system is monitored to determine the islanding situation. The main motive is that the small disturbance results a necessary modification in the system parameters in islanding conditions with respect to that of the grid-connected condition. The impedance measurement-based active IDSs and the positive feedback signal injection-based active IDSs are commonly used methods that are explained in [20, 31–35]. Due to the injection of external disturbances, it may effect the power quality of the system and also produce harmonics in to the system. So, performance of the system degrades.

4.1 Impedance Measurement IDSs

In this IDSs, a lock-in amplifier (LIA) [36] is used as a tool to measure the impedance with a sensor. The benefit of this method is that it can identify and act quickly when the

loss of mains occurs. In this IDSs, a low amplitude signal is injected, and its detection speed is high because of which this method is highly sensitive. Here, the interfaced converters can able to find the islanding condition even when the load nearly matches the converter output power. DGs connected to the DC grid through a bidirectional converter, which can collect the energy from DGs and deliver that to the load side. One link, which is bidirectional in nature, is used to maintain voltage regulation with the utility. In the case of islanding, the converter disconnects, and the grid voltage regulation is disturbed, which can cause damage to the consumer's appliances. In this IDSs, incremental impedance can be calculated using output voltage and output current of the converter, which is used as a critical element to finding the islanding situation to deactivate the converter. In this IDSs, a small signal as a disturbance is injected to find incremental impedance using a digital IDSs, which is represented as follows.

$$Z_{gc} = \frac{dv_o}{di_o} = \frac{\Delta v_o}{\Delta i_o} \tag{9}$$

where Z_{gc} is the impedance in case of grid-connected mode or non-islanding mode, dv_0 is the change in the output voltage of the DG, di_0 is the change in the terminal current of the DG, Δv_0, and Δi_0 are the discrete domain representation.

Figure 3 represents a non-islanded mode. Here, voltage regulation (v_{dc}) is provided by the grid-connected converter, while DGs can be described as a current source i_s. Depending on maximum power point tracking (MPPT) techniques, DGs can inject the required amount of current. The equivalent load resistance (R_{eq}) is a sum of all load resistances. R_{1eq} and R_{2eq} are the resistance of line 1 and line 2, respectively. The equivalent resistance is given by the effect of the disturbance on Z in case of grid-connected mode, which is stated as follows.

$$Z_{gc} = \frac{\Delta v_o}{\Delta i_o} = (Z_{1eq} + \frac{Z_{2eq} Z_{eq}}{Z_{2eq} + Z_{eq}}) \tag{10}$$

where $Z_{1eq} = R_{1eq} + j\omega L_{1eq}$ and $Z_{2eq} = R_{2eq} + j\omega L_{2eq}$ represent the equivalent line impedances, L_{1eq} and L_{2eq} are the inductances of line 1 and line 2, respectively, and w is the angular frequency. Z_{gc} value is very small and doesn't dependent on the source converters. When a small disturbance is applied to the source current of the converter, it effects the other variables also. In the case of islanding, the equivalent circuit changes as shown in Fig. 4.

$$Z_{\text{island}} = \frac{\Delta v_o}{\Delta i_o} = (Z_{1eq} + R_{eq}) \tag{11}$$

where Z_{island} is the impedance in the case of islanding mode. In this case, v_{dc} is disconnected, and Z_{2eq} term is not present in the equation.

The impedance measurement-based IDSs use a digital LIA to find the real (R) and imaginary (X) parts of impedance. Depending on R and X, this IDS can calculate the impedance and detect the islanding. In this scheme, a disturbance of a given

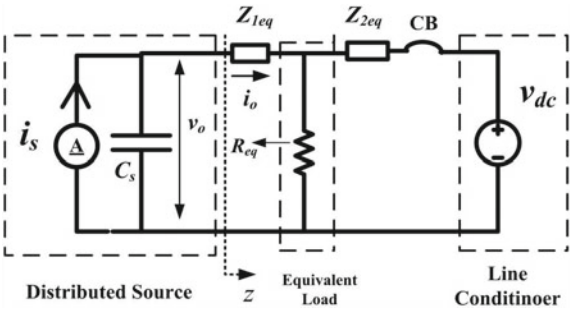

Fig. 3 IDSs circuit in the grid-connected situation

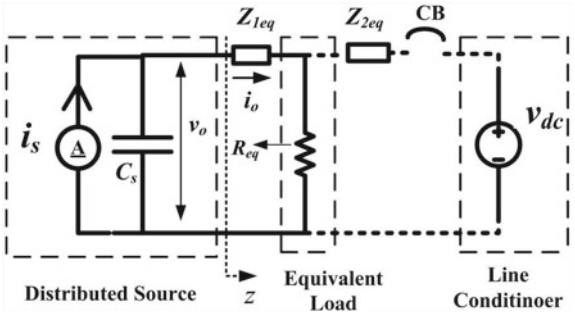

Fig. 4 IDSs circuit in the islanded situation

frequency is injected in the source and measured the output voltage and current. Then, the signal is to be passed through a filter, which consists of a low pass filter and an analog-to-digital converter. Next, both the signals are applied to different LIA in order to calculate impedance.

4.2 Positive Feedback IDSs

Positive feedback technique-based IDSs can be applied only to the voltage signals. It is of two types, namely power injection-based IDSs and current injection-based IDSs. These are explained as follows.

Power Injection Scheme (PIS) In this IDSs, disturbance in the form of power is injected in the DC/DC controller of DGs. Here, the voltage variation (ΔV) at the PCC is directly proportional to the disturbance, and it is processed with a feedback gain constant (K). Then, the obtained signal is compared with the nominal power. The error (ΔP) is applied to an outer control loop of a DG controller. During islanding, DGs become unstable because of the disturbance (ΔP). The block diagram representation of the outer control loop is given in Fig. 5. In order to cause sufficient instability, the proper selection of the gain K is required [20].

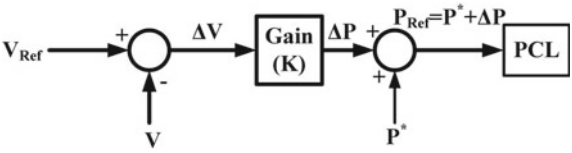

Fig. 5 PCL for power injection-based IDSs

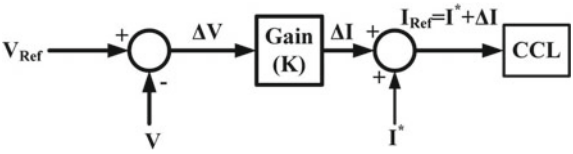

Fig. 6 CCL for current injection-based IDSs

The change of the power command is applied to the power control loop (PCL) of the DG. This is equal to the power disturbance signal which can be represented as follows.

$$P_{\text{Ref}} = KV \tag{12}$$

Current Injection Scheme In this IDSs, disturbance in the form of current is injected in the inner loops of DC/DC converter of DGs. Here, the disturbance is a current signal. It is a function of the PCC voltage variation, which is injected into the inner current control loop (CCL) of the converter. The relation between variation in reference to current, voltage, and power is given as follows.

$$I_{\text{Ref}} = -P\left(K1 + \frac{K2}{S}\right) + KV \tag{13}$$

where $K1$ and $K2$ are the proportional and integral gain of the CCL. Figure 6 shows the inner CCL representation of this IDSs.

5 Conclusion

In this paper, an overview of various DC MGs IDSs is reported in details. At first, the advantages and disadvantages of DC MGs over AC MGs along with the requirement of IDSs in MGs are presented and stated the efficacy of considering DC MGs IDSs. Next, the classification of DC MGs IDSs is explained, and the comparison of each IDSs is presented rigorously. Here, the advantage and disadvantages of each IDSs are stated clearly. Finally, a few challenges in these DC MG IDSs which are going to help the research community to carry out further research in this field are reported.

The need for developing IDSs for DC MGs is a challenging task as it is difficult to implement remote IDSs for all DGs. Moreover, the use of passive IDSs cannot differentiate islanding and non-islanding events. Therefore, in the future, it is suggested to develop such IDSs, which are more efficient like active IDSs and traveling wave-

based IDSs. These IDSs can identify islanding quickly and can distinguish between islanding events and non-islanding situation, which can increase the effectiveness of the IDSs.

References

1. Salomonsson, D., Soder, L., Sannino, A.: Protection of low-voltage dc microgrids. IEEE Trans. Power Delivery **24**(3), 1045–1053 (2009)
2. Jun-fang, Z., Si-min, D., Yin-li, H., Guang, H.: Research on distributed generation source placement. In: 2009 International Conference on Sustainable Power Generation and Supply, pp. 1–4. IEEE, New York (2009)
3. Abu-Rub, H., Malinowski, M., Al-Haddad, K.: Power Electronics for Renewable Energy Systems, Transportation and Industrial Applications. Wiley (2014)
4. Buccella, C., Cecati, C., Abu-Rub, H.: An overview on distributed generation and smart grid concepts and technologies. In: Power Electronics for Renewable Energy Systems, Transportation and Industrial Applications, pp. 50–68 (2014)
5. Hatziargyriou, N., Asano, H., Iravani, R., Microgrids Marnay, C.: IEEE power and energy magazine (July/august 2007)
6. Peças Lopes, J.A., Moreira, C.L., Madureira, A.G.: Defining control strategies for microgrids islanded operation. IEEE Trans. Power Syst. **21**(2), 916–924 (2006)
7. Rocabert, J., Luna, A., Blaabjerg, F., Rodriguez, P.: Control of power converters in ac microgrids. IEEE Trans. Power Electron. **27**(11), 4734–4749 (2012)
8. Baran, M.E., Mahajan, N.R.: Dc distribution for industrial systems: opportunities and challenges. IEEE Trans. Ind. Appl. **39**(6), 1596–1601 (2003)
9. Elsayed, A.T., Mohamed, A.A., Mohammed, O.A.: Dc microgrids and distribution systems: An overview. Electr. Power Syst. Res. **119**, 407–417 (2015)
10. Pouryekta, A., Ramachandaramurthy, V.K., Mithulananthan, N., Arulampalam, A.: Islanding detection and enhancement of microgrid performance. IEEE Syst. J. **12**(4):3131–3141 (2017)
11. Bekhradian, R., Davarpanah, M., Sanaye-Pasand, M.: Novel approach for secure islanding detection in synchronous generator based microgrids. IEEE Trans. Power Delivery **34**(2), 457–466 (2018)
12. Katiraei, F., Iravani, M.R., Lehn, P.W.: Micro-grid autonomous operation during and subsequent to islanding process. IEEE Trans. Power Delivery **20**(1), 248–257 (2005)
13. Committee, I., et al.: IEEE standard for interconnecting distributed resources with electric power systems. IEEE Standard **1547**, 1–28 (2003)
14. Serban, E., Pondiche, C., Ordonez, M.: Islanding detection search sequence for distributed power generators under ac grid faults. IEEE Trans. Power Electron. **30**(6), 3106–3121 (2014)
15. De Mango, F., Liserre, M., Dell'Aquila, A., Pigazo, A.: Overview of anti-islanding algorithms for PV systems. Part I: Passive methods. In: 2006 12th International Power Electronics and Motion Control Conference, pp. 1878–1883. IEEE, New York (2006)
16. De Mango, F., Liserre, M., Dell'Aquila, A.: Overview of anti-islanding algorithms for PV systems. Part II: Activemethods. In: 2006 12th International Power Electronics and Motion Control Conference, pp. 1884–1889. IEEE, New York (2006)
17. Xu, W., Zhang, G., Li, C., Wang, W., Wang, G., Kliber, J.: A power line signaling based technique for anti-islanding protection of distributed generators—part I: Scheme and analysis. IEEE Trans. Power Delivery **22**(3), 1758–1766 (2007)
18. Tobin, P.: Pspice for analog communications engineering. Synthesis Lect. Digital Circuits Syst. **2**(1), 1–139 (2007)
19. Augustine, S., Quiroz, J.E., Reno, M.J., Brahma, S.: Dc microgrid protection: Review and challenges. Technical report, Sandia National Lab.(SNL-NM), Albuquerque, NM (United States) (2018)

20. Mohamad, A.M.I., Abdel-Rady, Y., Mohamed, I.: Assessment and performance comparison of positive feedback islanding detection methods in dc distribution systems. IEEE Trans. Power Electron. **32**(8), 6577–6594 (2016)
21. Esmaeilian, A., Kezunovic, M.: Prevention of power grid blackouts using intentional islanding scheme. IEEE Trans. Ind. Appl. **53**(1), 622–629 (2016)
22. Balaguer, I.J., Lei, Q., Yang, S., Supatti, U., Peng, F.Z.: Control for grid-connected and intentional islanding operations of distributed power generation. IEEE Trans. Ind. Electron. **58**(1), 147–157 (2010)
23. Issa, W.R., Abusara, M.A., Sharkh, S.M.: Control of transient power during unintentional islanding of microgrids. IEEE Trans. Power Electron. **30**(8), 4573–4584 (2014)
24. Li, Y., Zhang, P., Li, W., Debs, J.N., Ferrante, D.A, Kane, D.J., Woolard, S.N., Kalbfleisch, R., Bowes, K.B., Kasznay, A.J.: Nondetection zone analytics for unintentional islanding in a distribution grid integrated with distributed energy resources. IEEE Trans. Sustain. Energy **10**(1), 214–225 (2018)
25. Redfern, M.A., Usta, O., Fielding, G.: Protection against loss of utility grid supply for a dispersed storage and generation unit. IEEE Trans. Power Delivery **8**(3), 948–954 (1993)
26. Ropp, M., Ginn, J., Stevens, J., Bower, W., Gonzalez, S.: Simulation and experimental study of the impedance detection anti-islanding method in the single-inverter case. In: 2006 IEEE 4th World Conference on Photovoltaic Energy Conference, vol. 2, pp. 2379–2382. IEEE, New York (2006)
27. Makkieh, A., Florida-James, A., Tzelepis, D., Emhemed, A., Burt, G., Strachan, S., Junyent-Ferre, A.: Assessment of passive islanding detection methods for dc microgrids (2019)
28. Cui, Q., El-Arroudi, K., Joós, G.: Islanding detection of hybrid distributed generation under reduced non-detection zone. IEEE Trans. Smart Grid **9**(5), 5027–5037 (2017)
29. Redfern, M.A., Barrett, J., Usta, O.: A new microprocessor based islanding protection algorithm for dispersed storage and generation units. IEEE Trans. Power Delivery **10**(3), 1249–1254 (1995)
30. O'kane, P., Fox, B.: Loss of mains detection for embedded generation by system impedance monitoring (1997)
31. Papadimitriou, C.N., Kleftakis, V.A., Hatziargyriou, N.D.: A novel method for islanding detection in dc networks. IEEE Trans. Sustain. Energy **8**(1), 441–448 (2016)
32. Mohamad, A.M.I., Abdel-Rady, Y., Mohamed, I.: Impedance-based analysis and stabilization of active dc distribution systems with positive feedback islanding detection schemes. IEEE Trans. Power Electron. **33**(11), 9902–9922 (2018)
33. Mohamad, A.M.I., Abdel-Rady, Y., Mohamed, I.: Analysis and mitigation of interaction dynamics in active dc distribution systems with positive feedback islanding detection schemes. IEEE Trans. Power Electron. **33**(3), 2751–2773 (2017)
34. Seo, G.-S., Lee, K.-C., Cho, B.-H.: A new dc anti-islanding technique of electrolytic capacitorless photovoltaic interface in dc distribution systems. IEEE Trans. Power Electron. **28**(4), 1632–1641 (2012)
35. Paz, F., Ordonez, M.: An impedance-based islanding detection method for dc grids. In: 2018 9th IEEE International Symposium on Power Electronics for Distributed Generation Systems (PEDG), pp. 1–7. IEEE, New York (2018)
36. Lin, J., Boon, C.C., Yi, X., Feng, G.: A 50–59 GHZ CMOS injection locking power amplifier. IEEE Microwave Wireless Components Lett. **25**(1), 52–54 (2014)

Novel Fault Detection Scheme Using Stockwell Transform for Transmission Lines with Wind Power Penetration

Nishant Saxena, Rachit Saxena, and Krishna Murari

1 Introduction

In electric power systems, transmission system plays an important and significant role where compatible increases in electrical power demand with increase in demand all globally, to supply bulk power from generation terminals or from gird to load centers. Faults will affect the rigidness of electrical power system resulting in disturbance in power flow in utility network. Accurate and fast detection of faults facilitate the power engineer to repair and restoration of power supply within stipulated minimum time.

Hassan et al. [1] have proposed a filter-based artificial neural network for faults detection where the trained hybrid framework was evaluated on the process of fault detection for a short duration of one cycle providing better results. Shaik et al. have developed a novel wavelet-based fault identification and segregation on short transmission line, wherein the fault indices were used to compare the results from the threshold values to identify the category of fault [2]. Advanced mathematical technique and signal processing methodology have been proposed to assured power system protection; furthermore, it is also used for identification and segregation of healthy system from faulty network. Efficient relay operations are ensured by such methodology used in power system protection. Moslem et al. [3] have proposed the fuzzy system and singular wavelet for the classification and detection of faults

N. Saxena (✉) · R. Saxena
Suresh Gyan Vihar University, Jaipur, Rajasthan 302017, India
e-mail: nishant.saxena@mygyanvihar.com

R. Saxena
e-mail: rachit.saxena@mygyanvihar.com

K. Murari
The University of North Carolina at Charlotte, Charlotte, NC, USA
e-mail: kmurari@uncc.edu

O. H. Gupta and V. K. Sood (eds.), *Recent Advances in Power Systems*, Lecture Notes in Electrical Engineering 699, https://doi.org/10.1007/978-981-15-7994-3_3

and in an primary distribution network in association to DG sources. Furthermore, Hussain et al. [4] have proposed a novel algorithm residing on the non-synchronized measurement for the location of faults in the multi-transmission line. Also, Aleena et al. have proposed an algorithm for the detection of fault location depicting multiple types of faults specifically shunt faults [5]. A novel approach of classification of types of faults and prediction has been proposed in [6] using the two approaches, i.e., WT and support vector machine (SVM) by measuring terminal bus voltages and current's transient signals. In the presence of UPFC for a double circuit, differential relaying is used for mutually coupled extra high-power transmission line [7]. A novel approach of high-speed protection of an extra high-voltage transmission line, where relaying point technique is used to identify the faults [8]. Singular value decomposition (SVD) and discrete wavelet transform (DWT)-based algorithms are used for the detection of faults [9]. Later, Zhara et al. [10] have proposed the DWT method to identify the faults. Coasta et al. have proposed the novel and effective approach for real-time fault identification where the algorithm has been developed based on overlap discrete wavelet transform coefficient analysis [11]. Furthermore, in [12] penetration of wind energy into the power system using Weibull's probability density function has been discussed, and the impact over the economic load dispatch problem is implemented. Krishna Murari et al. have carried out an analysis in which impact of protection cost has been investigated on the consumers affiliated with wind integrated distribution system [13].

In the STATCOM transmission line, DWT and Naïve Bayes technique are used to identify and localize the faults on the system resulting the proposed method more accurate with less misclassification rate, RMSE, % RRSE, and % RAE [14]. Furthermore, electromagnetic time reversal techniques are used to detect fault in HVDC system, and localization of the fault is done where DC faults are differentiated from external faults. Also, pole to pole and pole to ground faults are used for discrimination [15].

In the proposed approach, Stockwell transform (ST) technique has been used to identify and classify the distinguished type of faults. This method gives the very impressive classification along with the identification of the distinguished types of faults on the network. The test mentioned in subsequent section has been contemplated for our analysis and investigation purpose, and above test system has been implemented on MATLAB–Simulink platform. It is divulge from the simulation results that the proposed approach provides more efficient and accurate results.

Later, in the subsequent section, i.e., Sect. 2, the proposed approach has been thoroughly explained. In Sect. 3, the data related to the test system has been provided. In the last two Sects. 4 and 5, simulation results and conclusion, respectively, have been presented and thoroughly discussed.

2 Methodology Descriptions

In the given approach, fault index and ST are implemented to detect the type of fault in power system network. These fault indices are mentioned in given subsections.

2.1 Fault Index

The unhealthy phases are discriminated from the healthy phases on EHV transmission lines of a power system network by using fault index. Fault indices are determined using the following steps:

(i) Phase currents are recorded from bus 800 of proposed test network.
(ii) Current waveforms are featured to obtain the ST at Fs 20 kHz.
(iii) From the S-matrix later, median is determined.
(iv) Later, fault index is determined from the absolute value obtained which will be used to distinguish the faults and identify the position of it.

2.2 S-Transform

Short-time Fourier transform (STFT) of the signal c(t) can be presented by the following relation.

$$\mathrm{STFT}(\tau, f) = \int_{-\infty}^{+\infty} c(t)h(\tau - t)\mathrm{e}^{-j2\pi ft}\mathrm{d}t \tag{1}$$

where f and τ, respectively, indicate the Fourier frequency and spectrum localization time. The $h(t)$ defines a window function. This function $h(t)$ is swapped with Gauss function in Eq. 1 to obtain the ST as shown in Fig. 2.

$$h(t) = \frac{|f|}{\sqrt{2\pi}} e^{-\frac{f^2t^2}{2}} \tag{2}$$

Hence,

$$S(\tau, f) = \int_{-\infty}^{+\infty} c(t)\frac{|f|}{\sqrt{2\pi}}\mathrm{e}^{\frac{f^2(\tau-t)^2}{2}}\mathrm{e}^{-j2\pi ft}\mathrm{d}t \tag{3}$$

This S-transform reflects a case of short-time Fourier transform (STFT); by implementing in time domain with wider window, it can provide improved frequency resolution for lower frequency which results perfect time resolution for higher frequency by using the narrower window. S-matrix defines the output of S-transform in the

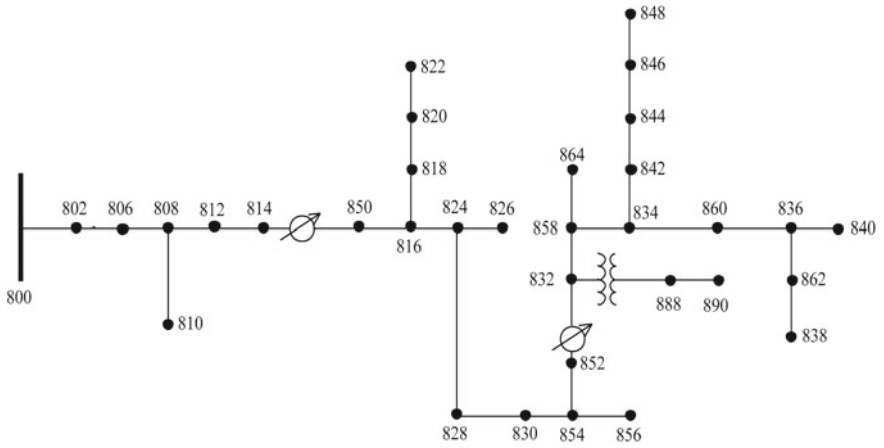

Fig. 1 Test system (Standard IEEE 34)

Table 1 Transformer used in test system

Transformer	kVA	kV high	kV low	*R*(%)	*X* (%)
Substation transformer	2500	69-D	24.9 -Gr. W	1	8
Transformer used in the system	500	24.9- Gr.W	4.16-Gr. W	1.9	4.08

matrix form. The data related to the amplitude and frequency concluded from the S-matrix [11, 12].

3 Proposed Test System

IEEE 34-bus test system is utilized for the proposed method described in Fig. 1. Wherein three-phase test feeders are used each of equal to length of original feeder length. The loads are considered as three-phase loads which are simulated by loads spots, capacitor banks, distributed loads, and line sections as shown in Table 1, 2 and 3, 4 and 5, respectively.

4 Results and Discussion

Results obtained after simulation are presented and discussed in the section, where test system has been implemented and tested on various types of faults. Current measurement of all phases was monitored at bus 800, and plots were obtained corresponding to 12 cycles. Faults are triggered at sixth cycle.

Table 2 Test system load description

Node	Load model	Ph-1 (kW)	Ph-I (kVAr)	Ph-2 (kW)	Ph-2 (kVAr)	Ph-3 (kW)	Ph-4 (kVAr)
860	Y-PQ	20	16	20	16	20	16
840	Y-l	9	7	9	7	9	7
844	Y-Z	135	105	135	105	135	105
848	D-PQ	20	16	20	16	20	16
890	D-l	150	75	150	75	150	75
830	D-Z	10	5	10	5	25	10
Total		344	224	344	224	359	229

Table 3 Description of test system capacitor data

Node	Ph-A (kVAr)	Ph-B (kVAr)	Ph-C (kVAr)
844	100	100	100
848	150	150	150
Total	250	250	250

4.1 Line to Ground Fault (SLG)

Unsymmetrical grounding of A phase, a line to ground (SLG) fault was triggered and current waveform is obtained as shown in Fig. 2, and it can be clearly seen that 600% increase in magnitude in current from 50 to 300 A.

Figure 3 depicts the numerical values of fault index of collated phases at the event of LG fault. It has been seen that fault index is higher than its threshold comparing to fault indices during healthy lines. Fault index value is 13 in the case, and hence, LG fault is detected efficiently.

4.2 Double Line Fault

Unsymmetrical connection between line A and line B, an line to line (LL) fault is triggered and current waveform is obtained as shown in Fig. 4, and it can be clearly seen that 700% increase in magnitude in current from 50 to 350 A.

Figure 5 depicts the numerical values of fault index of collated phases at the occurrence LL fault. It has been observed that fault index is much higher than its threshold comparing to fault indices during healthy phases. Fault index value is 16 in the case, and hence, LL fault is detected efficiently, and fault index is less than threshold and equal to zero.

Figure 5 depicts the numerical values from proposed fault index of collated phases at the event of LL fault. It has been seen that Fault index is higher than the threshold comparing to fault indices during healthy lines. Fault index value is 16 in this case,

Table 4 Description of test system line data

Bus A	Bus B	Length (feet)	Configuration
800	802	2580	300
802	806	1730	300
806	808	32230	300
808	810	5804	303
808	812	37500	300
812	814	29730	300
814	850	10	301
816	818	1710	302
816	824	10210	301
818	820	48150	302
820	822	13740	302
824	826	3030	303
824	828	840	301
828	830	20440	301
830	854	520	301
832	858	4900	301
832	888	0	XFM-1
834	860	2020	301
834	842	280	301
836	840	860	301
836	862	280	301
842	844	1350	301
844	846	3640	301
846	848	530	301
850	816	310	301
852	832	10	301
854	856	23330	303
854	852	36830	301
858	864	1620	302
858	834	5830	301
860	836	2680	301
862	838	4860	304
888	890	10560	300

Table 5 Node to node per phase kW and kVAr values on load model

Node A	Node B	Load model	Ph-1 (kW)	Ph-1 (kVAr)	Ph-2 (kW)	Ph-2 (kVAr)	Ph-3 (kW)	Ph-3 (kVAr)
802	806	Y-PQ	0	Q	30	15	25	14
808	810	Y-I	0	0	16	8	0	0
818	820	Y-Z	34	17	0	0	0	0
820	822	Y-PQ	135	70	0	0	0	0
816	824	D-I	0	0	5	2	0	0
824	826	Y-I	0	0	40	20	0	0
824	828	Y-PQ	0	0	0	0	4	2
828	830	Y-PQ	7	3	0	0	0	0
854	856	Y-PQ	0	0	4	2	0	0
832	858	D-Z	7	3	2	1	6	3
858	864	Y-PQ	2	1	0	0	0	0
858	834	D-PQ	4	2	15	8	13	7
834	860	D-Z	16	8	20	10	110	55
860	836	D-PQ	30	15	10	6	42	22
836	840	D-I	18	9	22	1 1	0	0
862	838	Y-PQ	0	0	28	14	0	0
842	844	Y-PQ	9	5	0	0	0	0
844	846	Y-PQ	0	0	25	12	20	11
846	848	Y-PQ	0	0	23	11	0	0
Total			262	133	240	120	220	114

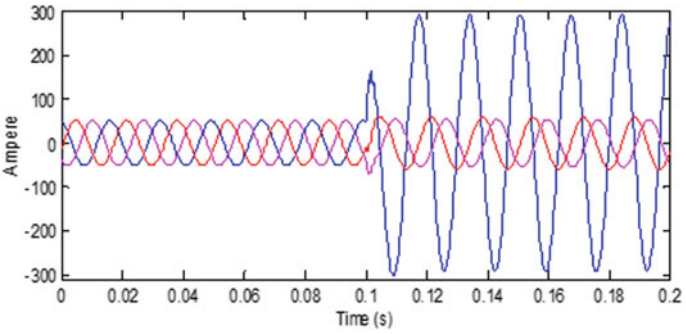

Fig. 2 LG fault current (If) waveform on bus no. 838

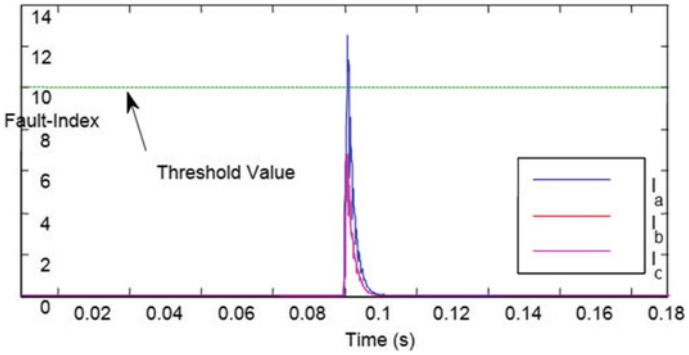

Fig. 3 Fault index level during LG fault at bus 838

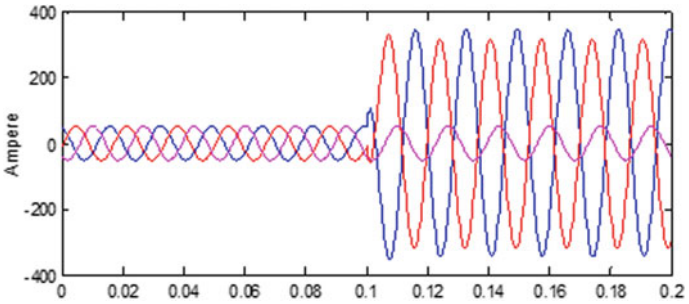

Fig. 4 Current waveforms when line to line fault is triggered at bus 838

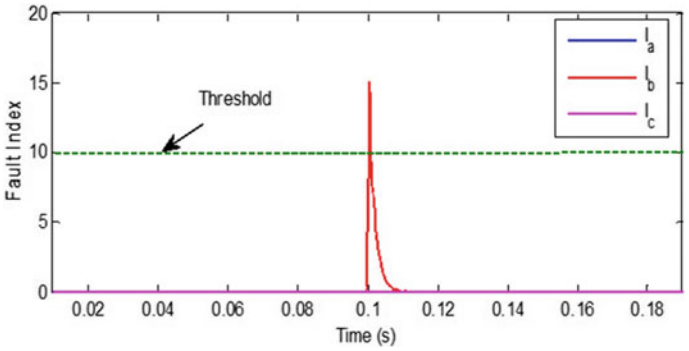

Fig. 5 Fault level as per fault index when line to line fault is triggered at bus 838

and hence, LL fault is detected efficiently, and fault index is less than threshold and equal to zero.

4.3 Double Line Grounded Fault

An line A to line B and to ground (LLG) fault is triggered and current waveform is obtained as shown in Fig. 6, and it can be clearly seen that 750% increase in magnitude in current from 50 to 375 A. The fault index of the line C will remain same due to healthy line comparing to fault line A and B.

Figure 7 depicts the numerical values of proposed fault index of collated phases on the occurrence of double LG fault. It has been observed that fault index is higher than the threshold comparing to fault indices during healthy phases. Fault index value is 16 in the case, and hence, LLG fault is detected efficiently, and fault index is less than threshold and equal to four.

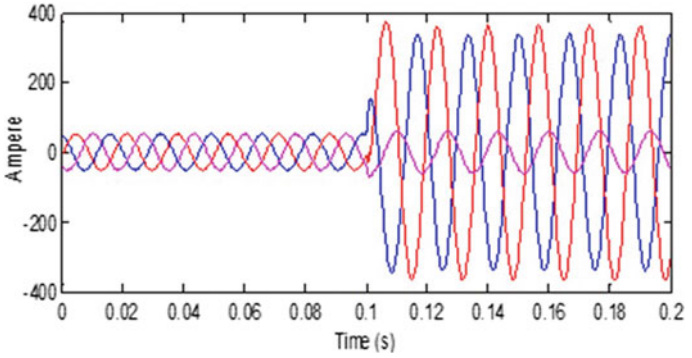

Fig. 6 LLG fault current waveform at bus 838

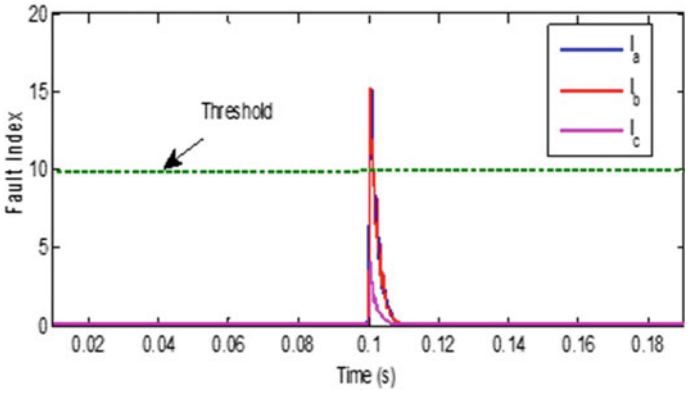

Fig. 7 Fault index during LLG fault bus 838

4.4 *Phase line Fault with Ground*

The fault has been initiated and simulated between all the three lines and to the ground of the transmission line and called as line to line to line fault (LLLG). The current waveform has been generated using scope in simulink and depicted in Fig. 8 wherein is has been cleared seen that current increases from 50 to 400 A resulting an 800% increment.

Figure 9 depicts the numerical values of proposed fault index of collated phases at the event of LLLG fault. It has been seen that index is higher than the threshold comparing to fault indices during healthy phases. Fault index value is above 25 in the case, and hence, LLG fault is detected efficiently.

The peak fault indices has been described in Table 6 for all types of phases initiated as mentioned previously above and can be seen distinctly.

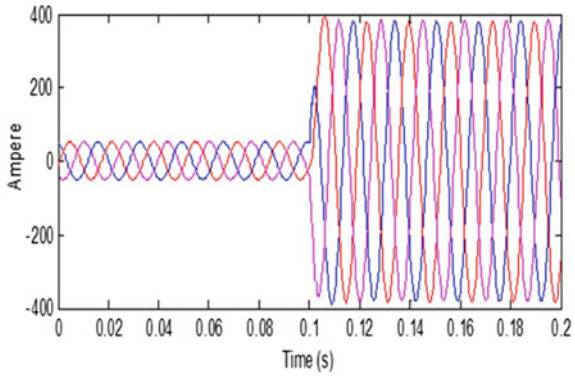

Fig. 8 Fault at bus 838 and bus 800 current waveform during three phase fault

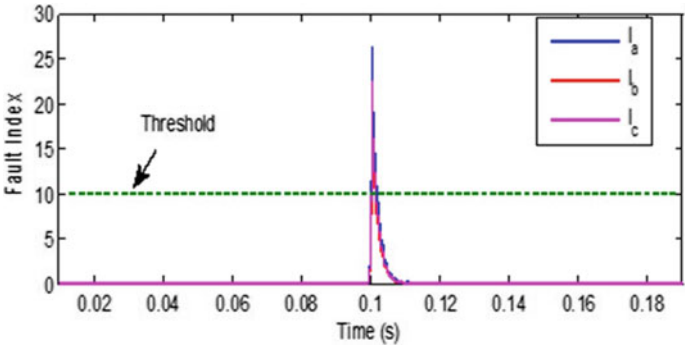

Fig. 9 Fault index level during fault bus 838

Table 6 Fault index peak values

S. no.	Type of fault	Phase A	Phase B	Phase C
1	LG	13	7	7
2	LL	16	16	0
3	LLG	16	16	4
4	LLLG	27	24	24

5 Conclusion

A proposed algorithm has been implemented and simulated in MATLAB/SIMULINK with described test system (IEEE-34 bus). The fault indices were calculated and compared with the threshold values to determine the various types of faults triggered in the system, and type of the fault has been identified and discriminated. Fault indices facilitate us to infer that different faults have different index values, and effectively type of faults can be predicted just by the observation. As mentioned in Table 6, during LG fault, only Phase A has the value above the threshold value, and rest two phases are below it. Similarly, in LL fault except Phase C both the phases have crossed the threshold value (10 as in the case study). Furthermore, in LLG and LLLG phase faults, all the phases have crossed the threshold values and reached to maximum values at 27, 24, and 24, respectively, for Phase A, B, and C, respectively. Hence, the proposed test system is evaluated as per the proposed methodology.

References

1. Fathabadi, Hassan: Novel filter based ANN approach for short-circuit faults detection, classification and location in power transmission lines. Int. J. Electr. Power Energy Syst. **74**, 374–383 (2016)
2. Shaik, A.G., Pulipaka, R.R.V.: A new wavelet based fault detection, classification and location in transmission lines. Int. J. Electr. Power Energy Syst. **64**, 35–40 (2015)
3. Dehghani, M., Khooban, M.H., Niknam, T.: Fast fault detection and classification based on a combination of wavelet singular entropy theory and fuzzy logic in distribution lines in the presence of distributed generations. Int. J. Electr. Power Energy Syst. **78**, 455–462 (2016)
4. Hussain, S., Osman, A.H.: Fault location scheme for multi-terminal transmission lines using unsynchronized measurements. Int. J. Electr. Power Energy Syst. **78**, 277–284 (2016)
5. Swetapadma, Aleena, Yadav, Anamika: All shunt fault location including cross-country and evolving faults in transmission lines without fault type classification. Electr. Power Syst. Res. **123**, 1–12 (2015)
6. Ekici, Sami: Support vector machines for classification and locating faults on transmission lines. Appl. Soft Comput. **12**, 1650–1658 (2012)
7. Tripathy, L.N., Samantaray, S.R., Dash, P.K.: A fast time–frequency transform based differential relaying scheme for UPFC based double-circuit transmission line. Int. J. Electr. Power Energy Syst. **77**, 404–417 (2016)
8. Bo, Z.Q., Redfern, M.A., Weller, G.C.: Positional protection of transmission line using fault generated high frequency transient signals. IEEE Trans. Power Delivery **15**(3), 888–894 (2000)

9. Guillen, D., Paternina, M.R.A., Zamora, A., Ramirez, J.M., Idarraga, G.: Detection and classification of faults in transmission lines using the maximum wavelet singular value and Euclidean norm. IET Generation Transmiss. Distrib. **9**(15), 2294–2302 (2015)
10. Moravej, Z., Pazoki, M., Khederzadeh, M.: New pattern-recognition method for fault analysis in transmission line with UPFC. IEEE Trans. Power Delivery **30**(3), 1231–1242 (2015)
11. Costa, F.B.: Fault-induced transient detection based on real-time analysis of the wavelet coefficient energy. IEEE Trans. Power Delivery **29**(1), 140–153 (2014)
12. Saxena, N., Ganguli, S.: Solar and wind power estimation and economic load dispatch using firefly algorithm. Procedia Comput. Sci. **70**, 688–700 (2015)
13. Murari, K., Padhy, N.P., Pradhan, A.K., Li, F.: Investigating the impact of protection system reinforcement cost on the consumers associated with renewable integrated distribution network. IET Gener. Transmiss. Distrib. **13**(9), 1572–1588 (2019)
14. Aker, E., Othman, M.L., Veerasamy, V., Aris, I., Wahab, N.I.A., Hizam, H.: Fault detection and classification of shunt compensated transmission line using discrete wavelet transform and naive bayes classifier. Energies **13**, 243 (2020)
15. Tailor, K., Ukil, A.: Fault detection and locating using electromagnetic time reversal (EMTR) technique for HVDC Transmission Network. In: 2019 IEEE PES Asia-Pacific Power and Energy Engineering Conference (APPEEC), Macao, Macao, pp. 1–5 (2019)

Optimization of Load Distribution Between Distributed Generation Units of a Similar Technology Using Dynamic Programming

Illia Diahovchenko and Anastasiia Horbul

1 Introduction

Extension of the generation capacity of the power system and mitigation of climate worsening is possible through integration of alternative energy sources and distributed generation (DG). In recent years, their share in the global electric energy generation has been rising rapidly, and the related technologies are maturing. However, unreasonable access location and capacity of DERs may bring about power losses increasing, voltage profile, and power quality violation [1, 2]. Thus, it is of concern to select optimal type(s) and size of grid-connected DERs and allocate them properly.

Various methods have been created for optimal allocation of DG in distribution power systems. The manuscript [3] proposes an analytical technique to define the optimum size and location of DERs. In [4], the authors tested an improved analytical (IA) method and came up with the conclusion that the operating power factor (PF) of DG units for losses lowering should be closer to the PF of combined load of the considered systems. In paper [5], an efficient analytical (EA) technique was applied to allocate different DG units with the aim to reduce power losses in distribution power networks. An improved artificial bee colony (IABC) algorithm that selects initial solution by using path priority and real power restrictions was proposed in [6], aiming to find an optimal placement of DGs of photovoltaic (PV) nature. In article [7], advancements of an ant lion optimization algorithm (ALOA) for optimal location and sizing of DGs were introduced, and a comparison with several other methods was done. A backward–forward sweep (BFS) method was employed in [8] to determine the optimal capacity of DG sources to minimize network power losses and to improve bus voltage profile.

I. Diahovchenko (✉) · A. Horbul
Sumy State University, Rymskogo-Korsakova st. 2, 40007 Sumy, Ukraine
e-mail: i.diahovchenko@etech.sumdu.edu.ua

O. H. Gupta and V. K. Sood (eds.), *Recent Advances in Power Systems*, Lecture Notes in Electrical Engineering 699, https://doi.org/10.1007/978-981-15-7994-3_4

Once the size and locations of DG units are determined, an electrical engineer should consider ways to optimize load distribution between the available energy resources. An approach to optimize power generation of a hydropower station by minimizing water consumption is presented in the work [9]; the equal micro-increment rate technique and the dynamic programming method were used for this purpose. In the work [10], the authors discussed an analytical-based short-term optimization of load distribution between electric power stations within the power system. The solution was obtained by the criterion of minimum cost of fuel and electricity, based on the characteristics of electric power stations. A strategy to satisfy load demands of a hydropower station by means of classical and sophisticated dynamic programming is presented in [11]. However, not much attention has been given to optimization of load distribution between DG units in the scientific literature.

This paper aims to propose an alternative method for load distribution between several DGs. The approach consists of two phases. On the first stage, an optimal size and allocation of DG is to be determined, and on the second stage, an optimal load distribution between several DG units is to be defined by means of dynamic programming. Simulation is performed on a typical radial distribution system.

2 Optimal Allocation of Distributed Generation Units

2.1 Method Selection and Operational Constraints

The DG units can be deployed in a power system after the load flow and voltage profile of the distribution network are identified. For this purpose, the BSF-based MATLAB code from the work [12] can be applied. Further, the local search optimization is to be used to allocate power source at a certain bus in a distribution system. The description of the BFS operational algorithm is given in [8].

The objective is to minimize power losses in the distribution power network [6]

$$P_{\text{loss}} = \min f(B_{\text{DG}}, C_{\text{DG}}) = \sum_{i=1}^{K} \frac{P_n^2 + Q_n^2}{U_{n+1}^2} \cdot R_n, \tag{1}$$

where $B_{\text{DG}} = [b_{\text{DG1}}, b_{\text{DG2}}\ldots]$ are the locations of grid-tied DGs; $C_{\text{DG}} = [c_{\text{DG1}}, c_{DG2}\ldots]$ are the capacities of grid-tied DGs; P_i and Q_i are the active and reactive power flow at the end of the line n after the DG is installed at bus $n + 1$, respectively. In each branch, the reference direction of power flow is from the bus with a smaller number to the bus with a higher number. U_{n+1} is the bus voltage of bus $n + 1$ after a DG is injected at the bus $n + 1$. R_n is the line resistance of a branch between the buses n and $n + 1$ (nth line); K is the total number of lines in the network.

The constraints include the limitations related to voltage magnitude, maximum penetration, and discrete capacity of the available DGs:

$$U_{n\min} \leq U_n \leq U_{n\max}, \tag{2}$$

$$\sum P_{\mathrm{DG}} \leq \sum P_{\mathrm{DG\,max}}, \tag{3}$$

$$P_{\mathrm{DG}n\min} \leq P_{\mathrm{DG}n} \leq P_{\mathrm{DG}n\max}, \tag{4}$$

where U_n, $U_{n\min,}$ and $U_{n\max}$ are the actual bus voltage, minimum voltage, and maximum voltage at bus n, respectively; $P_{\mathrm{DG}n\max}$ and $P_{\mathrm{DG}n\min}$ are the maximum and minimum active power restrictions of DG that will be installed at bus n in the distribution network, respectively.

$U_{n\min}$ and $U_{n\max}$ correspond to the minimal and maximal voltage magnitude deviations established in the EN 50160-2010. In the standard, it is indicated that the acceptable range of variation of the root mean square (rms) voltage magnitude should not exceed ±10% for 95% of a week.

2.2 Optimal Allocation of a Single Grid-Connected DG Unit

The IEEE 33-bus radial distribution system (see Fig. 1) was chosen for this study [13]. The voltage amplitude at the head bus of the system was adjusted in accordance with the Ukrainian rated value for rural distribution networks, which is 10.5 kV. The total real and reactive loads are 3715 kW and 2300 kVAr.

The selected method suggests allocating the DG units at bus 6. A notable reduction in total electric energy losses (64.47%) is achieved. The calculation results are provided in Table 1, alongside with the comparison of the BSF method with other techniques mentioned in Sect. 1. The intelligent optimization approaches differ by criteria of program running time, amount of computation, convergence rate, and

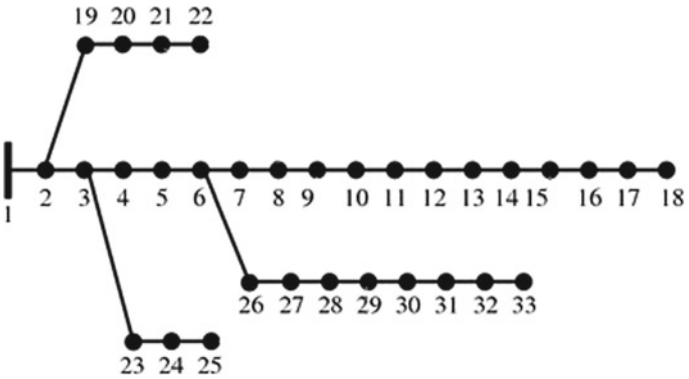

Fig. 1 Single-line diagram of the IEEE 33-bus radial distribution system

Table 1 Estimation of the optimal DG placement in the 33-bus system by various approaches

Method	Analytical method [3]	IA [4]	EA [5]	IABC [6]	ALOA [7]	BFS [8, 12]	
Rated voltage of the system (kV)	12.62	12.62	12.62	12.62	12.62	12.62	10.5
Optimal location (bus)	6	6	6	7	6	6	6
Optimal DG unit size (kW)	2490	2601	2530	2440.97	2450	2481.1	2508.5
Real power losses without DG (kW)	211.2	211.2	211.05	202.69	210.98	211.29	228.26
Real power losses after DG deployment (kW)	111.24	111.1	68.17	104.99	103.05	74.91	81.09
Real power losses reduction (%)	47.33	47.39	67.7	48.2	51.15	64.55	64.47

parameters needed to be set, which leads to some variations between the solutions. But in general, the accepted technique gives results similar to those obtained by other methods.

In Fig. 2, the voltage profiles of each bus obtained by the BFS method before (red curve with stars) and after DG unit deployment (blue curve with asterisks) are shown. The lowest voltage is supervised at the bus 18, which is the most remoted from the swing bus 1. Without a DG installed in the system, the lowest voltage in the system is 0.8547 p.u., which violates the requirements of the EN 50160, and, in turns, is lower than $U_{n\min}$. After a DG is injected, the voltage of each bus increased, but no bus voltage is higher than $U_{n\max}$. At the bus 18, the voltage increased by

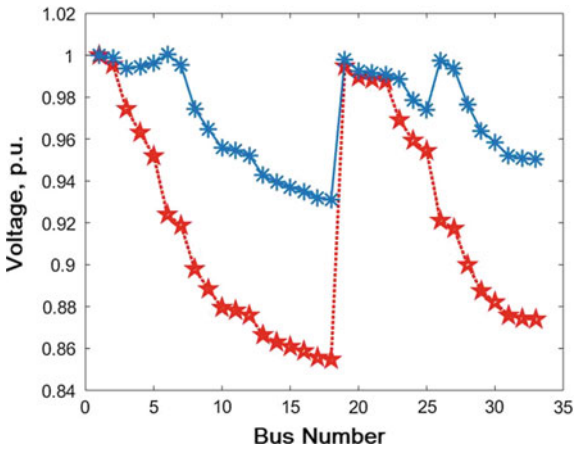

Fig. 2 Voltage profiles of the 33-bus system before and after the injection of a DG unit

8.93%, reaching a value of 0.931 p.u., which is appropriate, in accordance with the EN 50160.

3 Optimization of Load Distribution Between DG Units by Means of Dynamic Programming

3.1 Selection of a Distributed Generation Source

On the previous stage, the optimal location and capacity of the DG have been determined. Next, it is assumed that PV-based and biofuel-based DGs are installed at the bus 6 in the proportion of 25% and 75%, respectively, to cover the power deficiency of 2508.5 kW. Microturbines (MTs) are chosen as biofuel power sources. DERs of a PV type are not absolutely reliable due to the impermanence, unpredictability, and solar activity dependence variability. Thus, PV technology is to be used to feed non-critical loads, which are 75% of consumers. On the contrary, MTs strengthen energy security and can be employed for standby or backup power hospitals or data centers, where power availability is critical, as well as in less sensitive commercial settings, if the reliability of a grid supply is not sufficient [14]. Their advantages are modular size, low emission, low operation, and maintenance cost [15]. Given this MTs are selected to supply the rest 25% of consumers, which are the critical loads (CLs), where continuous and uninterrupted power delivery are crucial to maintain a high power system reliability and resiliency [13].

MTs range in power output from 25 to 330 kW and have the following major parts [15]: compressor, turbine, combustor, recuperator, and alternator (see Fig. 3). This

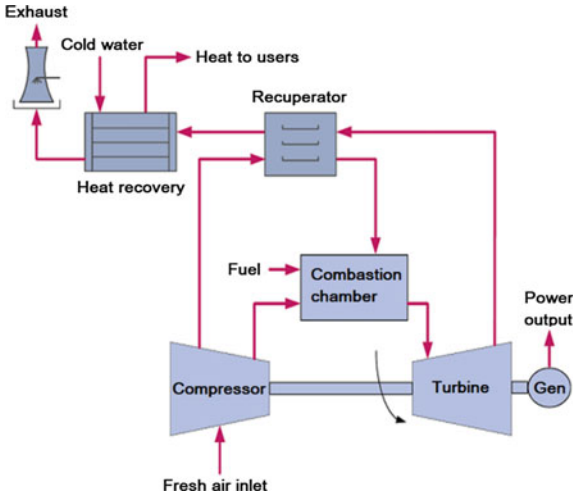

Fig. 3 Scheme of a MT with recuperator and waste heat recovery

power generation technology is characterized by fuel flexibility, good cogeneration efficiency, low greenhouse gases emissions [16].

3.2 Problem Statement and Initial Data

The optimality criterion is an objective indicator that allows to compare the considered options for solving problems with each other [17]. To find the extreme value of the optimality criterion, it is represented as a targeting function of the optimization parameters. Mode or system parameters are accepted as optimizers.

In engineering practice resource distribution is very common. Here resources can be understood as money, people, generating capacity, fuel at cogeneration plants or water at hydroelectric power stations, etc. This article deals with the problem of optimization of load distribution between several microturbines.

To serve 25% of DG's output, determined in Sect. II, B, three Capston C250 microturbines with 250 kW unit capacity and 240 kW net capacity are to be deployed at the sixth bus of the 33-bus system. Let us assume that the installed capacity of the MTs corresponds to the maximal loading. Since the load schedule is uneven through the day, the electric energy output of the microturbines should vary. Suppose that the total load varies from 50% during minimum demand hours to 100% during peak hours. The optimization problem is to distribute the total hourly load of the CLs between the three MT units so as to obtain a minimum of fuel consumption.

Let us assume that a biogas, which is essentially composed of CH_4, H_2S, H_2, and CO_2, is the feed for the MT. Biogas has lower emissions compared to natural gas and traditional fuels. The dependence of electricity generation versus fuel consumption at different rated power loads was derived from article [18], where a similar MT, but of smaller rated power, was tested. The obtained curve is shown in Fig. 4 and referred

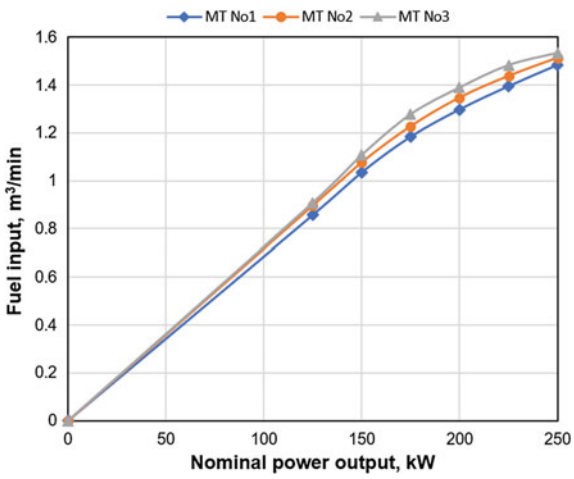

Fig. 4 Power output versus fuel consumption at different rated power loads

Table 2 Consumption data of MT units at different rated loads

No. of MT	Fuel consumption Q_j (m^3/min) depending on loading P_i (kW)						
	P_1	P_2	P_3	P_4	P_5	P_6	P_7
	0	125	150	175	200	225	250
1	0	0.857	1.035	1.184	1.298	1.395	1.483
2	0	0.896	1.076	1.227	1.347	1.437	1.513
3	0	0.908	1.107	1.277	1.388	1.482	1.533

as MT No. 1. The related curves MT No. 2 and MT No. 3 were obtained from MT No. 1, taking into account that the fuel consumption of microturbines of even the same type may slightly differ and depend on the state of the unit, fuel quality, service life, periodicity of routine maintenance, etc. Consumption data of MT units are given in Table 2.

3.3 Optimization Approach with Dynamic Programming

In dynamic programming, the indicated problem is considered as multi-step processes by the number of microturbines and is solved through calculations on the forward and reverse run of the basic algorithm, describing the general scheme of solving problems of this class. On the forward run, the following sequence of functions is to be calculated

$$Q_j^e\left(P_j^e\right) = \min\left[Q_j\left(P_j\right) - Q_{j-1}^e\left(P_j^e - P_j\right)\right] \tag{5}$$

where P_j^e is the total capacity of j combined units; Q_j^e is their minimum fuel consumption, at what $Q_1^e(P_1^e) = Q_1(P_1)$.

Power output of DG units is considered as a "resource," which is also a parameter of the state. In the j-th step of the forward course, the total minimum biogas consumption rate Q_j^e of the two units, P_j and $P_{j=1}^e$, is sought by a complete search, according to (5). Initially, the first step (the first object) is planned so that it by itself ensures minimal fuel consumption. A second object P_2 is then added to the first one so that the result of these two steps is optimal. For this hop, an equivalent cost characteristic is constructed as a table of correspondence of the specified load total $P_2^e = P_1 + P_2$ versus the minimum fuel consumption Q_2^e and the optimal power output of the second unit P_2. The third step deals with the joint work of the following two units: The third P_3 and the two previous units represented by the equivalent generator P_2^e, and the consumption characteristic of which $Q_2^e(P_2^e)$ was obtained in the previous step. Next, optimum power distribution corresponding to the minimum total fuel consumption Q_3^e and the optimal power output of the third unit P_3 are to be selected.

In the last step of the forward run, when all variables P_j are considered, we will have a function Q_j^e, the minimum of which will be the optimal solution.

The reverse run converges quickly, since there is no consumption optimization here, but only the conditionally optimal equation $P_j\ (P_1^e) = n$, where $n = 1, 2, \ldots$, obtained in the forward run is used. The optimal value of the last variable P_n is determined from the dependency

$$P_n = P_n\left(P_n^e\right) \tag{6}$$

Knowing P_n, it is possible to calculate the optimal value $P_{n-1}^e = P_n^e - P_n$. Then, referring to (6), the penultimate variable P_{n-1} can be determined. Continuing to unfold this process from end to beginning, we similarly determine the optimal values of $P_{n-2}, P_{n-3}, \ldots, P_1$.

The objective function is

$$Q_{\text{MT}} = \sum_{j=1}^{n} Q_j\left(P_j\right) \Rightarrow \min \tag{7}$$

The calculation starts with optimizing the mode of the two DG units. Total capacity range is from 125 to 500 kW. The optimization starts with the power of 500 kW, which is to be reduced with a constant step $h = 25$ kW. Results are combined in Table 3, and the optimal load chart of the two DG units is demonstrated in Fig. 5.

Table 3 Optimal load distribution for two microturbines

P_2^e (kW)	P_1 (kW)	P_2 (kW)	Q_2^e (m^3/min)	Optimum MT composition	
500	250	250	2.996	1	1
475	225	250	2.908	1	1
450	200	250	2.811	1	1
425	175	250	2.697	1	1
400	150	250	2.548	1	1
375	125	250	2.37	1	1
350	225	125	2.291	1	1
325	200	125	2.194	1	1
300	175	125	2.08	1	1
275	150	125	1.931	1	1
250	250	0	1.483	1	0
225	225	0	1.395	1	0
200	200	0	1.298	1	0
175	175	0	1.184	1	0
150	150	0	1.035	1	0
125	125	0	0.857	1	0

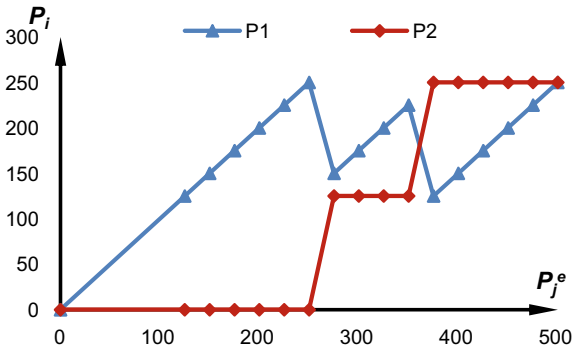

Fig. 5 Optimal load chart for two MTs

Table 4 Optimal load distribution for three microturbines

P_3^e (kW)	P_1 (kW)	P_2 (kW)	P_3 (kW)	Q_3^e (m^3/min)	Optimum MT composition		
750	250	250	250	4.530	1	1	1
625	125	250	250	3.903	1	1	1
500	250	0	250	3.017	1	0	1
375	125	0	250	2.390	1	0	1
250	250	0	0	1.483	1	0	0
125	125	0	0	0.857	1	0	0

Next let us consider the work of three DG units. Total fuel consumption can be determined by the equation

$$Q_3^e\left(P_3^e\right) = \min\left\{Q_3(P_3) + Q_2^e\left(P_3^e - P_3\right)\right\} \tag{8}$$

The step is $h = 125$ kW. With a load of 750 kW all MTs operate at maximum capacity, with a total fuel consumption of 4.530 m^3/min. The load of 625 kW can be covered in six ways. The modes are calculated similarly. The results are given in Table 4, and the corresponded optimal load chart of the three DG units is shown in Fig. 6.

4 Conclusions

In this paper, an approach for optimization of load distribution between several DERs has been presented. On the first stage optimal sizing and placement of distributed energy resources for reducing total power losses were determined. PV power technology and microturbines are chosen as DGs to feed non-critical and critical loads of the considered power network. It is supposed that the total power demand of CLs

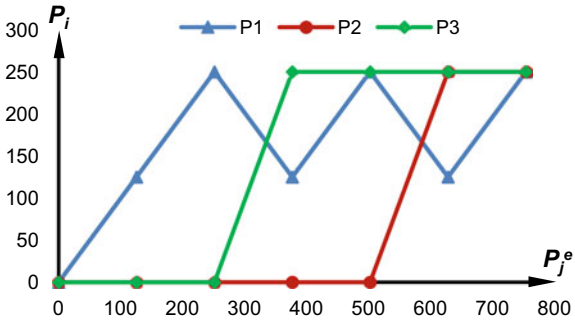

Fig. 6 Optimal load chart for three MTs

varies from 50% during minimum demand hours to 100% during peak hours, and the optimization problem is to distribute the total hourly load of the CLs between the three MT units to achieve a minimal fuel consumption. This problem has been addressed using dynamic programming. The task of optimization was considered as multi-step processes by the number of microturbines and is solved through calculations on the forward and reverse run of the basic algorithm.

Optimal load distribution and MTs composition for operation at different electric energy demands were determined. Depending on the power demand, two or three microturbines can serve to feed critical loads. For the mode with two operating MTs (i.e. power capacity in the range 125–500 kW) the optimization starts from 500 kW, which is reduced with a 25 kW step. For three operating MTs the optimization starts with a maximum load of 750 kW, which is then being descended with a 125 kW step.

The presented approach can be employed to solve numerous engineering problems, e.g. to find optimal distribution of other resources, such as money, people, generating capacity, fuel at cogeneration plants or water at hydroelectric power stations.

References

1. Diahovchenko, I., Kolcun, M., Čonka, Z., Savkiv, V., Mykhailyshyn, R.: Progress and challenges in smart grids: distributed generation, smart metering, energy storage and smart loads. Iran. J. Sci. Technol. Trans. Electr., Eng (2020)
2. Volokhin, V. V., Diahovchenko, I. M., Derevyanko, B.V.: Electric energy accounting and power quality in electric networks with photovoltaic power stations. In: 2017 IEEE International Young Scientists Forum on Applied Physics and Eng., YSF 2017, Lviv , pp. 36–39 (2017)
3. Acharya, N., Mahat, P., Mithulananthan, N.: An analytical approach for DG allocation in primary distribution network. Int. J. Electr. Power Energy Syst. **28**(10), 669–678 (2006)
4. Hung, D.Q., Mithulananthan, N.: Multiple distributed generator placement in primary distribution networks for loss reduction. IEEE Trans. Ind. Electron. **60**(4), 1700–1708 (2013)
5. Mahmoud, K., Yorino, N., Ahmed, A.: Optimal distributed generation allocation in distribution systems for loss minimization. IEEE Trans. Power Syst. **31**(2), 960–969 (2016)

6. Hui, W., Zai-Lin, P., Xiao-Fang, M., Dan, G., Jun, W.: An optimization approach based on improved artificial bee colony algorithm for location and capacity of grid-connected photovoltaic systems. Tech. Electrodyn. **5**, 68–76 (2019)
7. Ali, E.S., Abd Elazim, S.M., Abdelaziz A. Y.: Ant Lion Optimization Algorithm for optimal location and sizing of renewable distributed generations. Renew. En. **101**, 1311–1324 (2017)
8. Rupa, J.M., Ganesh, S.: Power flow analysis for radial distribution system using backward/forward sweep method. Int. J. Electr. Comput. Energ. Electron. Commun. Eng. **8**(10), 1628–1632 (2014)
9. Li, J., Saw, M.M.M., Chen, S., Yu, H.: Short-term optimal operation of baluchaung II hydropower plant in Myanmar. Water (2020)
10. Kuvakin, P.Z., et al.: Short term optimisation of load distribution between electric power stations within the power system. Lett. High. Educ. Inst. Electromechanics **5**, 80–82 (2003)
11. Liao, S., Liu, J., Liu, B., Cheng, C., Zhou, L., Wu, H.: Multicore parallel dynamic programming algorithm for short-term hydro-unit load dispatching of huge hydropower stations serving multiple power grids. Water Resour. Manag. **34**(1), 1–18 (2020)
12. Malladi, R.: Radial distribution system with multiple distribution generator (DG) (2020). https://www.mathworks.com/matlabcentral/fileexchange/60286-radial-distribution-system-with-multiple-distribution-generator-dg. Last accessed 28 Feb 2020
13. Diahovchenko, I., Kandaperumal, G., Srivastava A.K.: Distribution power system resiliency improvement using distributed generation and automated switching. 2019 IEEE 6th International Conference on Energy Smart Systems, Kyiv, pp. 126–131 (2019)
14. Breeze, P.: Microturbines. Gas-Turbine Power Generation. Academic, New York (2016)
15. Adefarati, T., Bansal, R.C.: Energizing Renewable Energy Systems and Distribution Generation, Pathways to a Smarter Power System, pp. 29–65 (2019)
16. Darrow, K., Tidball, R., Wang, J., Hampson, A.: Technology characterization—Microturbines. Catalog of CHP Technologies, U.S. Environmental Protection Agency Combined Heat and Power Partnership (2015)
17. Soshinov, A.G., Bakhtiarov, K.N.: Matematicheskiye zadachi elektroenergetiki [*Mathematical Problems of Electric Power Industry*]. Volgograd: ESLP Volgograd STU (2012)
18. Chang, C.C., et al.: A case study on the electricity generation using a micro gas turbine fueled by biogas. Energies **12**(12) (2019)

Improvement of Voltage Regulation in an IEEE 9-Bus Radial Microgrid Feeder Using Regression Model

Yuvraj Praveen Soni and Eugene Fernandez

1 Introduction

For simplicity in layout, microgrid structure adopted for rural area is basically radially structured distribution system. For the system operator, the voltage at each bus and the overall system loss are the prime planning and design objectives which depends upon several factors such as configuration, connected load value and its type, length and parameter of the line. While system losses are not very critical, the VR is one mandatory requirement to be addressed for satisfying the utility customer's load operational requirements.

Numerous parameters have to be controlled to ensure voltage limit compliance in the individual buses of the feeder. For the estimation of voltage at a feeder bus under a specific loading, the acceptable method is the load flow technique which can be used to determine the bus voltage, with some known quantity like active (P) and reactive power (Q), section line resistance (R), and inductance (X). Certain characteristics are possessed by the distribution system such as the higher value of R/X ratio, radial-type and loop-type configuration, load consists of linear, nonlinear, balanced, and unbalanced type, and distributed generation makes it inadequate for conventional load flow methods such as Newton–Raphson (NR) and Gauss–Seidel (GS) for the system analysis. These transmission line load flow techniques such as NR and GS are hence not suitable for the distribution system, and hence, separate load flow methods are explicitly developed to be implemented in the distribution sector.

Y. P. Soni (✉) · E. Fernandez
Indian Institute of Technology, Roorkee, Roorkee, Uttarakhand 247667, India
e-mail: yuvraj.soni21092@gmail.com

E. Fernandez
e-mail: eugenefdz@gmail.com

O. H. Gupta and V. K. Sood (eds.), *Recent Advances in Power Systems*, Lecture Notes in Electrical Engineering 699, https://doi.org/10.1007/978-981-15-7994-3_5

The backward and forward sweep (BFS) load flow is the most common method to be implemented in the distribution system. BFS method assumes the system that consists of impedance and voltage control current source. Analysis for the load flow considers the two main steps, backward and forward. As the name indicates, first current at each branch is calculated from end bus to start bus that is in the backward direction. In the second step, voltages at each bus are calculated considering the voltage drops at line impedances. Various reports are available in the literature [1–5] that explores applications of this method. Other methods are also available for load flow analysis of distribution networks [6–13].

Traditionally, load flow analysis in distribution networks involves iterative solutions, which may be time-consuming for large bus systems. Also, when frequent updating of the load scenario is involved, a non-iterative solution may prove to yield quicker solutions. Regression analysis (RA) is one such methodology that may be tried. This is a robust technique which can be efficiently utilized for the computation of specified variable with the specific input(s). Several research papers [14–21] highlight studies based on RA implemented in diverse operations in general systems or power systems. Here, we attempt to apply the regression as a method for estimation of voltages at radial feeder buses under loading.

In this paper, an IEEE 9-bus radial feeder has been analyzed to improve VR at the weakest bus (the last bus). Also, voltage estimation at each bus has been computed using a multiple linear regression model which consists of five inputs variables, namely R, X, P, Q, and prior bus voltage. Proposed method efficacy is analyzed with fitness variable (R^2), adjusted R^2, standard error, and residuals calculated in the system. The sections included in this paper are as follows: Sect. 2 discusses the multiple linear regression model applied to the system, and the implementation in the model are discussed and explained in Sect. 3. Section 4 examines the results with discussions obtained, and finally, the paper presents conclusions and future extensions of the work.

2 Regression Model

It is a technique which formulates the relation between output, i.e., "dependent variable" and input or "independent variable" so that if inputs are known, the output can be calculated [22]. Expressions comprising of only one independent variable are solved using a simple linear regression method, and if independent variables are more than one, then this method is known as multiple regression method. The expression for the multiple regression model is as follows:

$$y_i = \beta_0 + \beta_1 x_{i1} + \cdots + \beta_p x_{ip} + \varepsilon_i = x_i^T \beta + \epsilon_i \quad i = 1, 2, \ldots n \tag{1}$$

In Eq. (1) y_i denotes the dependent variable and ith independent variables. ε_i denotes the error term involved and β_i denote the associated coefficients with x_i. The above equation can be grouped and collectively expressed in the vector form as:

$$y = x\beta + \epsilon \tag{2}$$

where

$$y = \begin{pmatrix} y_1 \\ y_2 \\ : \\ : \\ y_n \end{pmatrix} \tag{3}$$

$$x = \begin{pmatrix} x_1^T \\ x_2^T \\ : \\ : \\ x_n^T \end{pmatrix} \begin{pmatrix} 1 & x_{11} & \cdots & x_{1p} \\ 1 & x_{21} & \cdots & x_{2p} \\ \vdots & \vdots & \ddots & \vdots \\ 1 & x_{n1} & \cdots & x_{np} \end{pmatrix} \tag{4}$$

$$\beta = \begin{pmatrix} \beta_0 \\ \beta_1 \\ : \\ : \\ \beta_P \end{pmatrix}, \quad \epsilon = \begin{pmatrix} \epsilon_1 \\ \epsilon_2 \\ : \\ : \\ \epsilon_n \end{pmatrix} \tag{5}$$

Ordinary least squares (OLS) is used to calculate unknown parameter β in the regression model. OLS finds the nearest value of β by a given set of independent variables by the least square method. It is a process of reducing the sum of square differences between the actual and calculated value.

$$\hat{\beta} = (x^T X)^{-1} X^T y = \left(\sum x_i x_i^T\right)^{-1} \left(\sum x_i y_i\right) \tag{6}$$

Error is found to have finite variance, and it is also uncorrelated with the regression. This indicates that the estimator is unbiased and consistent, i.e.,

$$E[x_i \epsilon_i] = 0 \tag{7}$$

Fitness of linear model can be computed by determining R^2 which lies between 0 to 1, with 0 being the poorer and 1 being the indication of a good fit of the linear system.

3 The Model for the Study

Numerous literatures are addressed to the voltage estimation and control techniques problems. For a better understanding of the effect of reactive power injection on bus

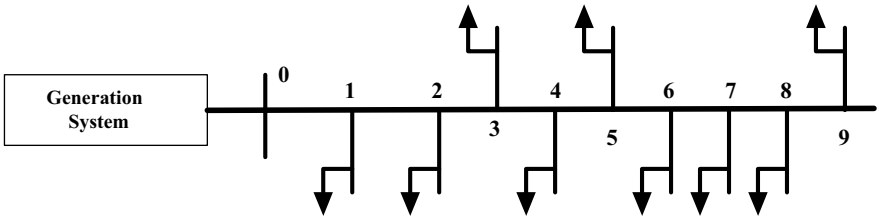

Fig. 1 Schematic representation of the IEEE 9-bus radial distribution system

voltage in the radial distribution system, in this paper, an IEEE 9-bus radial distribution system [23] represented in Fig. 1 has been modeled. Proposed configuration consists of a power generator or substation and unequal loads connected at each bus with the distribution feeder line sections (R, X) interconnecting the buses. Bus 0 represents the substation bus with 23 kV (considered as 1 per unit), and other buses have connected loads of constant P, Q type with individual loading. Data for the study is referred from the literature [24].

The multiple linear regression has been formulated using Eq. (8) as:

$$V_i = K + A * V_{i-1} + B * \sum_{i-1}^{N} R + C * \sum_{i-1}^{N} X + D * \sum_{i}^{N} P + E * \sum_{i}^{N} (Q) - \Delta q \tag{8}$$

where $i = 2, 3, \ldots, N$; $N =$ No. of bus; $K, A, B \ldots E$ are constants.

To compute the bus voltage using regression, five parameters have been considered, which make this method more robust and accurate. A, B, C, D and E are the respective coefficients of the input parameters V_{i-1}, R, X, P and Q. K is the intercept constant. Δq represents the change in reactive power loading in the weakest bus. R, X, P, and Q are summed to address the effect on current due to change in line and loading parameter. Current I in the feeder section is a function of the section impedances, the voltage at the particular bus, and the loadings in the feeder buses following the bus which is being considered. Thus, the current can be expressed as:

$$I = f(R, X, P, Q) \tag{9}$$

It is to be noted that Δq represents reactive power loading change in the weakest bus and is subtracted from the net reactive power involved. The effectiveness of the RA is represented by fitness parameter R^2, F statistics, and standard error.

The initial load flow bus voltage solution for the IEEE 9-bus radial feeder is required for constructing the regression model. This can be obtained either using the *BFS* method or using actual available field data. Since the latter is not available in this case, the only option is to use available results of the *BFS* method. In actual use of the regression model for distribution load flow studies, it is best to use available field data for developing the model.

Table 1 Initial load flow solution for bus voltages in an IEEE 9-bus radial feeder

S. no.	Bus no.	Bus voltage (kV)
1	0	23.00
2	1	22.84
3	2	22.72
4	3	22.18
5	4	21.83
6	5	21.14
7	6	20.91
8	7	20.50
9	8	19.84
10	9	19.38

Table 1 shows the initial load flow bus voltages obtained for constructing the regression model.

The initial voltage falls expressed as *VR* at the last bus is 15.73%. Using the initial load flow bus voltages obtained in Table 1, regression modeling is carried out [23, 24] and the following results (Table 2) have obtained using *MS EXCEL* software.

Figure 2 shows the percentage of errors obtained between the actual and calculated values using the regression model developed. It may be seen that the percentage errors are minimal at each bus of the feeder (generally <1%), and so this shows that the regression model developed can be used as an effective load flow tool for analyzing the IEEE 9-bus radial feeder system bus voltages.

Table 2 Results of the regression model for the IEEE 9-bus feeder system

S. no.	Feature	Value
1	Multiple *R*	0.993534
2	R^2	0.98711
3	Adjusted R^2	0.965628
4	Standard error	227.4856
5	No. of observations	9
6	*F*-Statistics	45.94918
Constants		
7	K	26277.36
8	A	−0.41107
9	B	81.22648
10	C	143.2287
11	D	0.000205
12	E	0.000125

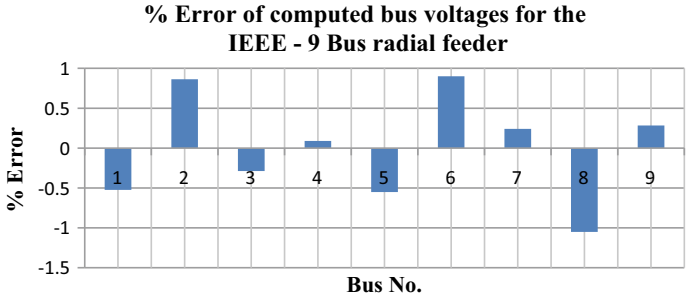

Fig. 2 Percentage errors obtained for the model

4 Results

The object of the study is to inject leading VAR in the last bus (the weakest bus) to improve the VR. Injecting leading VAR in the bus is the same as reducing the reactive power drawn by the load connected to the last bus. For the study, the injected VARs used are 10, 30, 50, 80, and 90% of the Q drawn by the last bus (i.e., Q_9). This will amount to $\Delta q = j(0.1 * Q_9)$, $j(0.3 * Q_9)$, $j(0.5 * Q_9)$, $j(0.8 * Q_9)$, and $j(0.9 * Q_9)$, respectively. Complete elimination of reactive loading is not practical and hence an upper limit of 90% of the rated load is imposed in reactive loading reduction. Reducing this reactive load will enhance the voltage resulting in VR improvement, and results of this reduction are shown in Fig. 3.

Figure 3 shows that there is a marginal improvement in the VR at the last bus on the injection of reactive VAR. However, the fall is minimal (15.73–15.10%). Also, after 30% VAR injection, the regulation remains virtually stable at 15.15% up to 90% VAR injection. This will mean that there is not much advantage in trying to improve VR at the last bus by VAR injection beyond 30%.

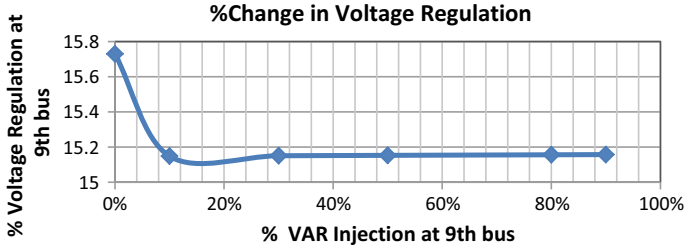

Fig. 3 Effect of injection of reactive *VAR* on *VR* of the last bus

5 Conclusions

In this paper, *RA* has been applied to analyze the IEEE 9-bus radial microgrid feeder bus voltages. The formulation of the model and its findings indicates that the regression model is acceptable for estimating the bus voltage of the distribution system. The model was subsequently applied to observe the effect of reactive power injection at the weak bus. A slight change in voltage can be observed by injecting leading VAR; however, improvement is not significant even after reducing 90% of the reactive loading of the last bus.

The main conclusions are, therefore, as follows:

1. *RA* can be used as an alternative methodology for load flow analysis in distribution feeders. It may reduce computational time for online control of voltage profile under fluctuating load demand.
2. If VAR injection is used as a means of improving the voltage regulation of the last bus, then in the present case, the improvement is found to be marginal and possibly not justifying the cost of implementation of the corrective scheme.
3. However, the method (RA) may be tried on other radial bus feeder systems before generalizations can be made.
4. The present work may be extended by trying VAR injection at other buses in the feeder and observing the extent of improvements that may result in the VR.

References

1. Salama, M.M.A., Chikhani, A.Y.: A simplified network approach to the VAR control problem for radial distribution systems. IEEE Trans. Power Delivery **8**(3), 1529–1535 (1993)
2. Berg Jr., R., Hawkins, E.S., Pleines, W. W.: Mechanized calculation of unbalanced load flow on radial distribution circuits. IEEE Trans. Power Apparatus Syst. **86**(4), 415–421 (1967)
3. Chang, G.W., Chu, S.Y., Wang, H.L.: An improved backward–forward sweep load flow algorithm for radial distribution systems. IEEE Trans. Power Syst. **22**(2), 882–884 (2007)
4. Singh, N., Ghosh, S., Murari, K.: Optimal sizing and placement of DG in a radial distribution network using sensitivity based methods. Int. Electr. Eng. J. (IEEJ) **6**(1), 1727–1734 (2015)
5. Wang, Z., Chen, F., Li, J.: Implementing transformer nodal admittance matrices into backward/forward sweep based power flow analysis for unbalanced radial distribution system. IEEE Trans. Power Syst. **19**(4), 1831–1836 (2004)
6. Zhang, F., Cheng, C.S.: A modified Newton method for radial distribution system power flow analysis. IEEE Trans. Power Syst. **12**(1), 389–397 (1997)
7. Exposito, A.G., Ramos, E.R.: Reliable load flow technique for radial distribution networks. IEEE Trans. Power Syst. **14**(3), 1063–1069 (1999)
8. Chen, T.H., Chen, M.S., Hwang, K.J., Kotas, P., Chebli, E.A.: Distribution system power flow analysis—a rigid approach. IEEE Trans. Delivery **6**(3), 1146–1153 (1991)
9. Thukaram, D., Banda, H.M.W., Jerome, J.: A robust three-phase power flow algorithm for radial distribution systems. Electr. Power Syst. Res. **50**(3), 227–236 (1999)
10. Das, D., Nagi, H.S., Kothari, D.P.: Novel method for solving radial distribution networks. IEE-Part C **141**(4), 291–298 (1994)
11. Das, D, Kothari, D.P., Kalam, A.: Simple and efficient method for radial distribution networks. Electr. Power Energy Syst.**17**(5), 335–346 (1995)

12. Ghosh, S., Das, D.: Method for load flow solution of radial distribution networks. IEE Proc. Gen. Trans. Distribution **146**(6), 641–648 (1999)
13. Teng, J.H.: A Direct approach for distribution system load flow solutions. IEEE Trans. Power Delivery **18**(3), 882–887 (2003)
14. Anwar, S., Mikami, Y.: Comparing accuracy performance of ANN, MLR, and GARCH model in predicting time deposit return of Islamic Bank. Int. J. Trade Econ. Finance **2**(1), 1–8 (2011)
15. Desai, V.S., Bharati, R.: A comparison of linear regression and neural network methods for predicting excess returns on large stocks. Ann. Oper. Res. **78**(1), 127–163 (1998)
16. Tosun, E., Aydin, K., Bilgili, M.: Comparison of linear regression and artificial neural network model of a diesel engine fueled with biodiesel-alcohol mixtures. Alexandria Eng. J. **55**(1), 3081–3089 (2016)
17. Tsekouras, G.J., Dialynas, E.N., Hatziargyriou, N.D., Kavatza, S.: A non-linear multivariable regression model for midterm energy forecasting of power systems. Electr. Power Syst. Res. **77**(12), 1560–1568 (2007)
18. Marčiukaitis, M., Žutautaitė, I., Martišauskas, L., Jokšas, B., Gecevičius, G.S, Sfetsos, A.: Nonlinear regression model for wind turbine power curve. Renewable Energy **113**(1), 732–741 (2017)
19. Hahne, J.M.: Linear and nonlinear regression techniques for simultaneous and proportional myoelectric control. IEEE Trans. Neural Syst. Rehabil. Eng. **22**(2), 269–279 (2014)
20. de Matos, E.O., Mota Soares, T., Bezerra, U.H., Tostes, M.E.D. L., Manito, A.R.A., Costa, B.C.: Using linear and non-parametric regression models to describe the contribution of non-linear loads on the voltage harmonic distortions in the electrical grid. IET Generation Transmission Distrib. **10**(8), 1825–1832 (2016)
21. Shakouri, H., Nadimi, G.R., Ghaderi, F.: Fuzzy linear regression models with absolute errors and optimum uncertainty. In: International Conference on Industrial Engineering and Engineering Management, pp. 917–921. IEEE, Singapore (2007)
22. Gujarati, D.N.: Basic Econometrics. 4th edn. Mc Graw-Hill Companies, New York (2004)
23. Soni, Y.P., Fernandez, E., Singh, R.: Evaluation of loading of individual buses on voltage regulation in a radial microgrid feeder. In: International Conference on Electrical, Electronics and Computer Engineering (UPCON), pp. 1–4. IEEE, ALIGARH, India (2019)
24. Babu, G.K., Samala, R.K.: Load flow analysis of a 9-bus system using BFSLF algorithm. Int. J. Electron. Commun. Eng. (IJECE) **4**(6), 17–22 (2015)

Optimal Power Dispatch of Renewable Energy-Based Microgrid with AC/DC Constraints

Sunil Kumar and G. L. Pahuja

Notations

Symbols

PV_s	Symbol for solar power generating units
W	Symbol for wind generating units
g	Symbol for DG sets
i, j	Symbol for system buses
Ω_1	Group of all system branches
Ω_B	Group of all system buses
Ω_{th}	Group of all DG units
Ω_i^l	Group of all system buses connected to bus i
Ω_i^{th}	Group of all DG units connected to bus i

Parameters

W_i^{cap}	Capacity of wind generation at bus i (kW)
RUp_g/RDp_g	Active power up/down ramp rate constrains of generators (kW)
RUq_g/RDq_g	Reactive power up/down ramp rate constrains of generators (kVar)
$w_{i,t}$	Wind generation available at bus i at time t (in the ratio of W_i^{cap})

S. Kumar (✉) · G. L. Pahuja
National Institute of Technology, Kurukshetra, Kurukshetra, Haryana 136119, India
e-mail: Sunil_31804302@nitkkr.ac.in

G. L. Pahuja
e-mail: glpahuja@nitkkr.ac.in

O. H. Gupta and V. K. Sood (eds.), *Recent Advances in Power Systems*, Lecture Notes in Electrical Engineering 699, https://doi.org/10.1007/978-981-15-7994-3_6

$P_{\mathrm{i},t}^{\mathrm{ch,min}}/\mathrm{P}_{\mathrm{i},t}^{\mathrm{ch,max}}$	Charging limits of battery at bus i at time t (kW)
$P_{\mathrm{i},t}^{\mathrm{dis,min}}/P_{\mathrm{i},t}^{\mathrm{dis,max}}$	Discharging limits of battery at bus i at time t (kW)
S_i^{cap}	Capacity of solar power generation at bus i (kW)
$S_{i,t}$	Solar radiation available to photovoltaic module at bus i at time t (in the ratio of S_i^{cap})
C_i^{nb}	Nominal battery capacity connected to bus i (kW h)
$\eta_{\mathrm{ch}}/\eta_{\mathrm{dis}}$	Battery charge and discharge efficiency
$P_{\mathrm{i},t}^{L}$	Required active power at ith bus at time t (kW)
$Q_{\mathrm{i},t}^{L}$	Required reactive power at ith bus at time t (kW)
$a_{\mathrm{g}}, b_{\mathrm{g}}, c_{\mathrm{g}}$	Coefficients of fuel cost function of diesel generator g
$\mathrm{DOD}_i^{\mathrm{max}}$	Maximum value of depth of discharge of the battery connected to bus i
$P_{\mathrm{g}}^{\mathrm{min}}/P_{\mathrm{g}}^{\mathrm{max}}$	Active power generation limits of diesel generator g (kW)
$Q_{\mathrm{g}}^{\mathrm{min}}/Q_{\mathrm{g}}^{\mathrm{max}}$	Reactive power generation limits of diesel generator g (kVar)
$\mathrm{SOC}_i^{\mathrm{min}}/\mathrm{SOC}_i^{\mathrm{max}}$	Limiting values of state of charge of the battery connected to bus i (kW h)
P_{ij}^{max}	Maximum value of active power flow in line from bus i to j (kW)
Q_{ij}^{max}	Maximum value of reactive power flow in line from bus i to j (kVar)
VWC	Estimate of wind curtailment (Rs/kWhr)
$X_{i,j}$	Reactance of line between bus i an j (per unit)
VOLL	Loss of load value (Rs/kWhr)
$r_{i,j}$	Resistance of line between bus i and j (per unit)

Variables

$P_{ij,t}$	Active power flow for line between bus i and j at time t (kW)
$Q_{ij,t}$	Reactive power flow for line between bus i and j at time t (kVar)
$\mathrm{DOD}_{i,t}$	Battery depth of discharge at bus location i at time t
$P_{i,t}^{\mathrm{ch}}/P_{i,t}^{\mathrm{dis}}$	Battery charge/discharge power at bus location i at time t (kW)
$P_{g,t}$	Generation of active power from diesel generator g at time t (kW)
$Q_{g,t}$	Generation of reactive power from diesel generator g at time t (kVar)
$V_{i,t}$	Magnitude of voltage at bus location i at time t (pu)
$\mathrm{SOC}_{i,t}$	Battery state of charge at bus location i at time t (kWhr)
$P_{i,t}^{w}$	Active wind power generation at ith bus at time t (kW)
$P_{i,t}^{s}$	Active solar power generation at bus i at time t (kW)
$\mathrm{Lsh}_{i.t}$	Shedding of load at ith bus location at time t (kW)
$\delta_{i,t}$	Angle of voltage at bus location i at time t (rad).
$P_{i,t}^{wc}$	Wind power curtailment at ith bus at time t (kW)
$\lambda_{i,t}^{p}$	Active power marginal price at ith bus location at time t (Rs/kWh)

$\lambda_{i,t}^{q}$ Reactive power marginal price at *i*th bus location at time *t* (Rs/kWh)

1 Introduction

1.1 Literature Review

Current trends in the electricity industry, redistribution and deregulation of the electricity industry, and changing electricity sector all contribute to localized electricity generation and storage called distributed power generation [6]. Solar photovoltaic units, wind power, thermal diesel generators, and energy storage systems like batteries and capacitors are widely used in power generation and distribution at the local level [12]. Some of these majorly used technologies are considered in this paper. Solar and wind energy systems have become an integral part of the modern power systems. But due to intermittent characteristics of these energy resources, power distribution in such systems is difficult [10]. As wind energy and solar energy are irregular and affected by weather conditions, the output power of these energy sources is not constant and cause problems when connecting to the grid and thus require optimal power flow solutions [5]. Higher injection of renewable energy into the grid causes frequent issues of power balance. Batteries and storage devices are used to overcome the problem of intermittency of renewable energy sources [3]. Thus, it is important to examine the issue of power distribution with renewable energy sources and battery storage systems (Fig. 1).

Economic dispatch gives optimal power flow solutions to supply the demands as per the requirements of MG. Economic dispatch of solar power generation and wind energy with uncertainty is proposed in Nemati et al. [8]. To account for wind energy output uncertainty and generate a dispatch schedule, a scenario-based probabilistic method is used in Peng et al. [9]. However, in general, wind power is evaluated and the probability distribution function is used to solve the problems of wind dynamics [1]. Nazari-Heris et al. [7] describe an economic dispatch representation that takes account of the randomness of solar and wind power generation using Weibull distribution for solar radiation and wind speed. Practices that enhance microgrid development and usage are energy diversification, reduced gas emissions, regulated power usage, global electricity demand, improved power planning, power generation at a local level, and competitive energy market [6]. Economic advantages like lower expenditure requirements and easier placement of small generator sets are also considered.

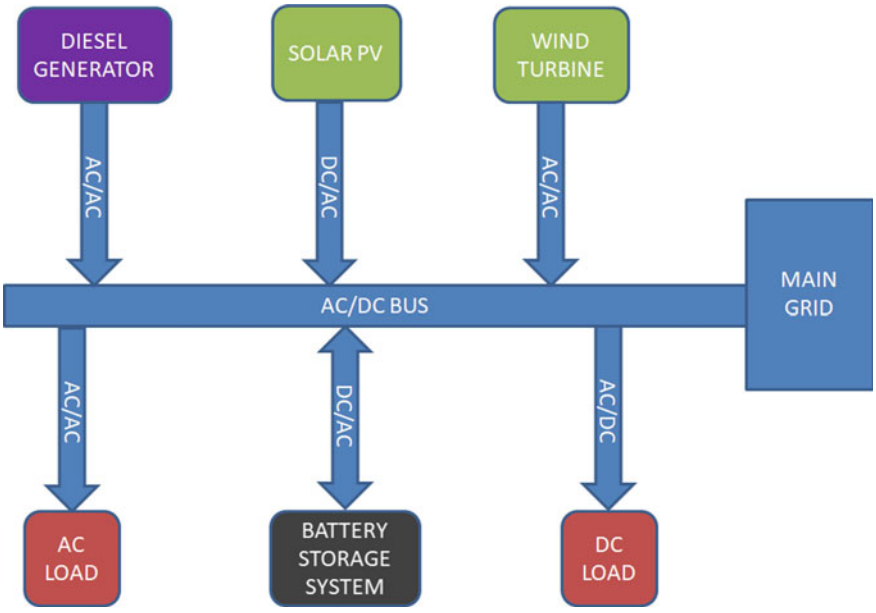

Fig. 1 Block diagram of test system

1.2 Contributions

This paper proposes an economical dispatch optimization architecture for microgrids (Fig. 2), consisting of dynamic sources of energy (solar power plants and wind power), thermal generators, and battery storage systems. An IEEE standard 33-bus modified system for the microgrid is described which is investigated under an islanded mode of operation. Network constraints such as AC/DC power flow technical restrictions are also considered, and the effects of renewable power penetration and storage of energy are investigated for a 24-hour timeframe to get the best solution for MG's economic dispatch.

The main objectives are summarized as:

i. Economic dispatch solution that involves renewable energy sources in microgrid is described considering solar and wind power dynamics.
ii. An optimal power flow technique is used to get decision variables for the optimization problem.
iii. The importance of energy storage systems in enhancing the efficiency of the microgrid and reduction in the cost of thermal generation is discussed.
iv. Consider and discuss various cases to highlight the accuracy and authenticity of the given model.

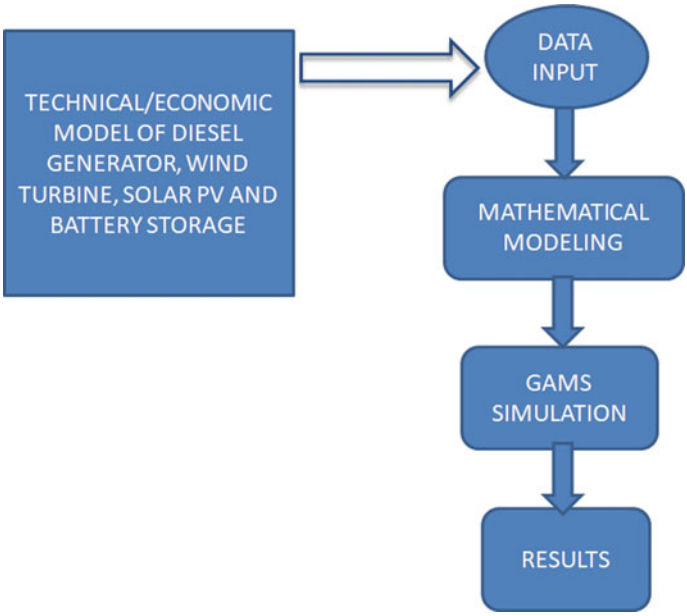

Fig. 2 Simulation architecture

1.3 Paper Structure

The following section is organized as follows: The issue of economic dispatch is explained in part 2 with system modeling. Part 3 provides detailed information about the dataset and related studies. Simulation outputs are described in part 4. Lastly, this article is concluded in part 5.

2 Problem Formulation

Taking three main elements of cost function namely the cost of diesel generating units, wind curtailment cost, and load shedding cost, the economic allocation problem of renewable energy-based microgrid is represented by minimizing costs. An optimized model using wind turbines, solar cells, and battery storage systems is described in this section. The given model is analyzed using AC and DC optimal power flow solution methods, and the comparison of results is done for both. The optimization method is discussed below. The results are obtained with the standard IEEE 33-bus modified system.

2.1 Objective Function

$$\min_{P_i^{\text{th}}, P_{i,t}^{\text{wc}}, \text{Lsh}_{i,t}} \text{OF} = F^{\text{th}} + F^{\text{wc}} + F^{\text{Lsh}} \tag{1}$$

where F^{th} is fuel cost for diesel generators, cost of curtailment of wind is F^{wc}, and load shedding cost is F^{Lsh}.

$$F^{\text{th}} = \sum_{g,t} a_g . P_{g,t}^2 + b_g . P_{g,t} + c_g \tag{2}$$

F^{th} is function of active output power $P_{\text{g},t}$ of the thermal generator which is quadratic in nature [8]. The values of cost coefficients of the generator can be taken from heat test.

$$F^{\text{wc}} = \sum_{i,t} \text{VWC} \times P_{\text{i},t}^{\text{wc}} \tag{3}$$

The operators have to pay for wind curtailment if they do not use the full capacity of wind power plant. This is called the wind curtailment cost F^{wc} which varies linearly with curtailment of wind power $P_{\text{i},t}^{\text{wc}}$. This situation arises when generators run at minimum limits under lightly loaded condition while at the same time wind generation is also serviceable [11]. One of the methods to reduce wind curtailment cost is to apply load shedding method at lightly loaded places.

$$F^{\text{Lsh}} = \sum_{i,t} \text{VOLL} \times \text{Lsh}_{i,t} \tag{4}$$

Penalty for load shedding is given by the system operators for not providing the required amount of power to some customers. Cost function for load shedding F^{Lsh} varies linearly with load shedding $\text{Lsh}_{i,t}$ [11].

2.2 Thermal Power Generators

The constraints of thermal power plant is

$$P_g^{\min} \leq P_{g,t} \leq P_g^{\max} \tag{5}$$

Generator constraints for reactive power are also taken into account case of AC network given by

$$Q_g^{\min} \leq Q_{g,t} \leq Q_g^{\max} \tag{6}$$

Generator active and reactive power ramp rate constrains is given by

$$P_{g,t-1} - P_{g,t} \leq \mathrm{RDp}_g \tag{7}$$

$$P_{g,t} - P_{g,t-1} \leq \mathrm{RUp}_g \tag{8}$$

$$Q_{g,t-1} - Q_{g,t} \leq \mathrm{RDq}_g \tag{9}$$

$$Q_{g,t} - Q_{g,t-1} \leq \mathrm{RUq}_g \tag{10}$$

2.3 Wind Turbine Model

The cubic curve representation of wind generation is considered [2] in this paper given by Fig. 3.

$$P^w = \begin{cases} P^r \times \left(\frac{v - v_{\text{in}}}{v_r - v_{\text{in}}}\right)^3; & v_c \leq v \leq v_r \\ P^r; & v_r \leq v \leq v_f \\ 0; & v \leq v_c \text{ or } v \geq v_f \end{cases} \tag{11}$$

where the output power of the turbine is P^w. Wind velocity is v at a given time, P^r is rated power, v_f is cut out and v_c is cut in velocity of the turbine and rated power is generated at minimum velocity v_r of the wind. The ratio of wind availability $w_{i,t}$ is calculated with available 24 h duration data of wind speed.

$$w_{i,t} = P_{i,t}^{w,\text{avl}} / W_i^{\text{cap}} \tag{12}$$

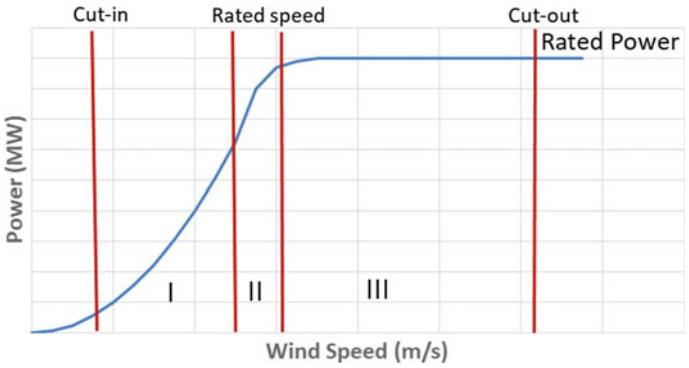

Fig. 3 Wind generation power output curve

where P_i^r and W_i^{cap} are similar to power rating for wind turbine available at *i*th bus. The curtailed for power wind turbine is given by

$$P_{i,t}^{\text{wc}} = w_{i,t} \times W_i^{\text{cap}} - P_{i,t}^{w} \tag{13}$$

Using full capacity of generated wind power is always recommended to minimize overall cost of operation and avoid any environmental damage, therefore $P_{i,t}^{\text{wc}}$ is kept minimum. Wind turbine capacity constraints are given as

$$0 \leq P_{i,t}^{w} \leq w_{i,t} \times W_i^{\text{cap}} \tag{14}$$

2.4 Solar Photovoltaic Model

Irradiance of solar energy on inclined surface [4] is used to calculate the amount of power generated by PV module given by

$$I_t = I_d \times \cos\theta_\beta + I_{\text{dif}} \times \frac{(1+\cos\beta)}{2} + \rho \times I_g \times \frac{(1-\cos\beta)}{2} \tag{15}$$

Here, I_g, is global horizontal irradiance, I_{dif} is diffuse horizontal irradiance, and I_d is direct normal irradiance.θ_β and β are incidence angles for solar radiation on a tilted surface and tilt angle, respectively. Reflection in the surrounding is given by ρ [10]. $P_{i,t}^{\text{PV}}$ is generated power from PV module given by:

$$P_{i,t}^{\text{PV}} = P_{\text{stc}}^{\text{PV}} \times n_s^{\text{PV}} \times n_p^{\text{PV}} \times (I_t/1000) \times \left[1 - \in \left(T_t^c - 25\right)\right] \tag{16}$$

Under standard test condition, the power output of solar cell module at the maximum power point is given by $P_{\text{stc}}^{\text{PV}}$. n_p^{PV} and n_s^{PV} are number of panels for PV module placed in parallel and in series, T_t^c and $\in$ is cell temperature and temperature coefficient [10]. Temperature of the solar cell is related to the ambient temperature given by

$$T_t^c = T_t^a + (I_t/800) \times (\text{NOTC} - 20) \tag{17}$$

In the above equation, NOCT and T_t^a are nominal cell temperature and ambient temperature, respectively. Solar power availability $s_{i,t}$ is given by

$$s_{i,t} = P_{i,t}^{s}/S_i^{\text{cap}} \tag{18}$$

Here, S_i^{cap} is similar to power rating of PV module available at bus *i*. Capacity constraints for output power of PV system is written as

$$0 \leq \mathrm{P}_{i,t}^{s} \leq s_{i,t} \times S_i^{\mathrm{cap}} \tag{19}$$

2.5 Modeling for Battery Storage System

To facilitate uninterrupted power supply to emergency and critical loads in MG, it becomes essential to have backup energy storage devices connected to the system. Nominal capacity determines the maximum SOC of the battery while depth of discharge determines its minimum value [7].

$$\mathrm{SOC}_i^{\min} = \mathrm{C}_i^{\mathrm{nb}}\left(1 - \mathrm{DOD}_i^{\max}\right) \tag{20}$$

$$\mathrm{SOC}_i^{\max} = \mathrm{C}_i^{\mathrm{nb}} \tag{21}$$

$$\mathrm{SOC}_{i,t} = \mathrm{SOC}_{i,t-\Delta t} \cdot \left(1 - \mathrm{DOD}_{i,t}\right) + \left(\mathrm{P}_{i,t}^{\mathrm{ch}} \cdot \eta_{\mathrm{ch}} - P_{i,t}^{\mathrm{dis}} \cdot \frac{1}{\eta_{\mathrm{dis}}}\right) \cdot \Delta t \tag{22}$$

Battery charging, discharging, and SOC constraints are as follows

$$\mathrm{SOC}_i^{\min} \leq \mathrm{SOC}_{i,t} \leq \mathrm{SOC}_i^{\max} \tag{23}$$

$$P_{i,t}^{\mathrm{ch,\,min}} \leq \mathrm{P}_{i,t}^{\mathrm{ch}} \leq \mathrm{P}_{i,t}^{\mathrm{ch,max}} \tag{24}$$

$$P_{i,t}^{\mathrm{dis,min}} \leq \mathrm{P}_{i,t}^{\mathrm{dis}} \leq \mathrm{P}_{i,t}^{\mathrm{dis,\,max}} \tag{25}$$

2.6 Model for Load Shedding

Load shedding of non-essential loads is done when power generation is not sufficient to meet the load demand. Upper and lower limits for load shedding [11] are given by

$$0 \leq \mathrm{Lsh}_{i,t} \leq L_{i,t} \tag{26}$$

2.7 DC Power Flow Constraints Modeling

Power (active) balance equation for each node bus and for every time interval is given by the equation

$$\sum_{\Omega_i^{\text{th}}} P_{g,t} + \text{Lsh}_{i,t} + P_{i,t}^{w} + P_{i,t}^{s} + P_{i,t}^{\text{dis}} - P_{i,t}^{\text{ch}} - P_{i,t}^{L} = \sum_{\Omega_i^{\text{l}}} P_{ij,t} : \lambda_{i,t}^{p} \tag{27}$$

The above equation is used to calculate locational marginal price (LMP) values. Taking 1 p.u. voltage at each bus, power flowing between any two buses is given by

$$P_{ij,t} = \left(\delta_{i,t} - \delta_{j,t}\right)/_{x_{ij}} \tag{28}$$

Power flow constraints in the lines is given as

$$-P_{ij}^{\max} \leq P_{ij,t} \leq P_{ij}^{\max} \tag{29}$$

Angle of voltage at each bus is constrained as

$$-\pi/2 \leq \delta_{i,t} \leq \pi/2 \tag{30}$$

2.8 Constraints Modeling for AC Power Flow

Considering AC power flow, reactive power balance equation for each node bus and for every time interval is given by the equation

$$\sum_{\Omega_i^{\text{th}}} Q_{g,t} - Q_{i,t}^{L} = \sum_{\Omega_i^{l}} Q_{ij,t} : \lambda_{i,t}^{q} \tag{31}$$

Line active and reactive flows are given as

$$P_{ij,t} = \frac{V_{i,t}^2}{z_{ij}} \cos\theta_{ij} - \frac{V_{i,t}V_{j,t}}{z_{ij}} \cos\left(\delta_{i,t} - \delta_{j,t} + \theta_{ij}\right) \tag{32}$$

$$Q_{ij,t} = \frac{V_{i,t}^2}{z_{ij}} \sin\theta_{ij} - \frac{V_{i,t}V_{j,t}}{z_{ij}} \sin\left(\delta_{i,t} - \delta_{j,t} + \theta_{ij}\right) - b\frac{V_{i,t}^2}{2} \tag{33}$$

where $z_{ij} = \sqrt{r_{ij}^2 + x_{ij}^2}$ is impedance for the line joining bus i to j.

Constraints for reactive power flow in the lines are given as

$$-Q_{ij}^{\max} \leq Q_{ij,t} \leq Q_{ij}^{\max} \tag{34}$$

Bus voltage is varied in the range given by

$$0.95\,\text{p.u.} \leq V_{i,t} \leq 1.05\,\text{p.u.} \tag{35}$$

3 Data Used for the Modeling

Optimal power flow solutions are obtained considering bus 19 as slack bus in both AC and DC networks. IEEE modified 33-bus network is taken for analysis purpose with scalar values are VWC = 150, $\eta_{\text{dis}} = 0.951$, $\eta_{\text{ch}} = 0.96$ and VOLL = 1000.

Figure 4 shows that wind generation is present all day while solar power is generated only during day time from t4 to t18 h, and the maximum generation of wind and solar power occurs at t16 and t13, respectively. Power curve is assumed to be identical for wind turbines, and all PV modules are also identical. But capacities PV modules and wind turbines connected at different buses are assumed to be different.

Constraints for load at each bus for AC/DC power flow are given by

$$P_{i,t}^{L} = l_{i,t} \times P_{d,i}^{\max} \tag{36}$$

$$Q_{i,t}^{L} = l_{i,t} \times Q_{d,i}^{\max} \tag{37}$$

Ratings of solar panels, wind turbine, and maximum SOCs of batteries installed at different buses are given in Table 1.

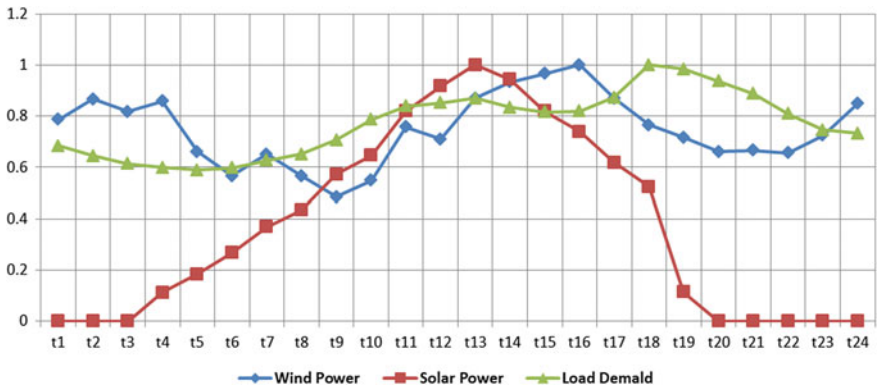

Fig. 4 Fractional availability load, solar and wind power w.r.t. time

Table 1 Ratings of the wind turbines, solar panels, and maximum state of charge of batteries connected to different buses

Bus no.	Wind capacity (kW)	Solar capacity (kW)	SOC^{max} (kW h)
3	129	120	–
8	101	–	255
9	115	151	
10	130	132	–
15	–	90	260
18	–	–	260
19	80	–	190
21	50	109	180
28	–	153	–
29	130	–	231
32	112	–	–

4 Simulation Results and Discussions

Ultrabook core i5-based processor with DDR3 RAM of 8GBs is utilized for the simulation purpose. GAMS build 24.4.3 is used to run the optimization programming codes in Windows 10 operating system to get the solutions. Nonlinear program modeling of the system is done. Three cases are studied each for DC and AC network.

i. Case 1: Only conventional thermal generators (DG) are operating.
ii. Case 2: DG along with renewable energy sources (wind and solar) is operating.
iii. Case 3: Energy storage system (ESS) is operating along with renewable energy sources and diesel generators.

It is to be noted that power generation curves for both DC and AD analysis are similar but their corresponding values are very much different which is reflected in Tables 2 and 3.

Table 2 Cost comparison of different cases for DC analysis

DC-OPF	Case 1	Case 2	Case 3
Total cost of operation (Rs)	15,394,250	4,358,685	3,312568
Congestion cost (Rs)	2,188,526	805,813	1,147,093
Change in operating cost w.r.t case 1 (%)	–	71.68	78.48
Change in congestion cost w.r.t case 1 (%)	–	63.18	47.58

Table 3 Cost comparison of different cases for AC analysis

DC-OPF	Case 1	Case 2	Case 3
Total cost of operation (Rs)	15,650,900	4,481,341	3,432,015
Congestion cost (Rs)	2,432,992	1,495,912	1,396,638
Change in operating cost w.r.t case 1 (%)	–	71.36	78.07
Change in congestion cost w.r.t case 1 (%)	–	38.51	42.59

4.1 Case 1

DC Power Flow: Fig. 5 shows time duration power curves which includes load requirement, power generation, and load shedding. It is noticed that load shedding occurs at t1 and then from t8 to t24, as load is more than generation capacity of MG. Because of high power demand at t18, peak value load shedding is obtained at this time interval with value of 1700 kW.

AC Power Flow: AC optimal power flow gives better results than DC. It is seen that load shedding occurs at the same time duration, but AC optimal power flow analysis gives better results than DC. Because of high power demand at t18, peak value load shedding is increased to 1715 kW.

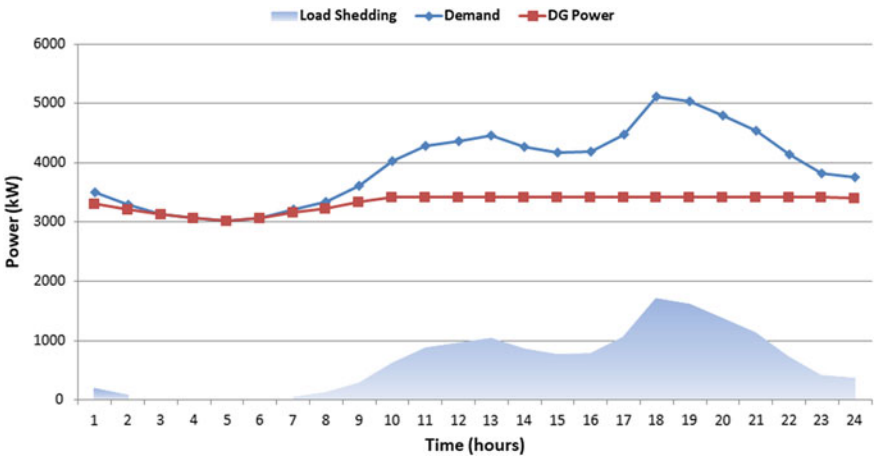

Fig. 5 Power generation curves for DC/AC analysis of case 1

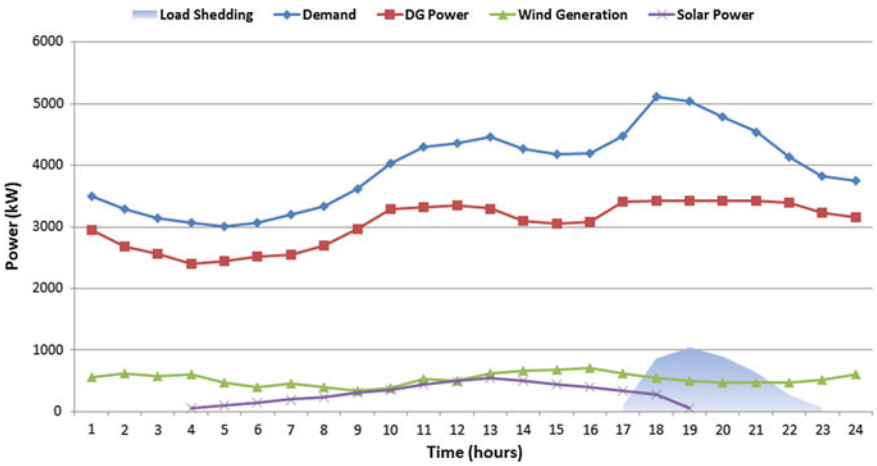

Fig. 6 Power generation for DC/AC analysis of case 2

4.2 Case 2

DC Power Flow: Fig. 6 shows the power curves. It is noticed that load shedding occurs at t12 and from t17 to t23 and its value has decreased drastically. This has happened on account of huge amount of renewable energy penetration into the network. At t19, peak value load shedding is obtained at this time interval with value of 1046 kW.

AC Power Flow: It is seen that load shedding occurs at t10, t12 and from t17 to t23, but their values are very low compared to case 1 AC analysis. As compared to case 1 AC analysis due to large amount of renewable energy availability at t18, maximum value of load shedding is shifted from t18 to t19 with value of 1064 kW.

4.3 Case 3

DC Power Flow: Fig. 7 shows the power curves, and Fig. 8 shows battery parameters. Due to extra energy provided by battery, maximum value of load shedding is reduced to 788 kW. Maximum SOC occurs at t8 and t16 in all the corresponding buses. Initial SOC is assumed to be 20% of maximum SOC. Figure 8 shows that charging of batteries takes place during lightly loaded conditions and they supply power during high loads.

AC Power Flow: It is seen that load shedding occurs at only from t17 to t23, but their values are very low compared to case 2 AC analysis. As compared to case 2 AC analysis due to large amount of renewable energy and now battery storage

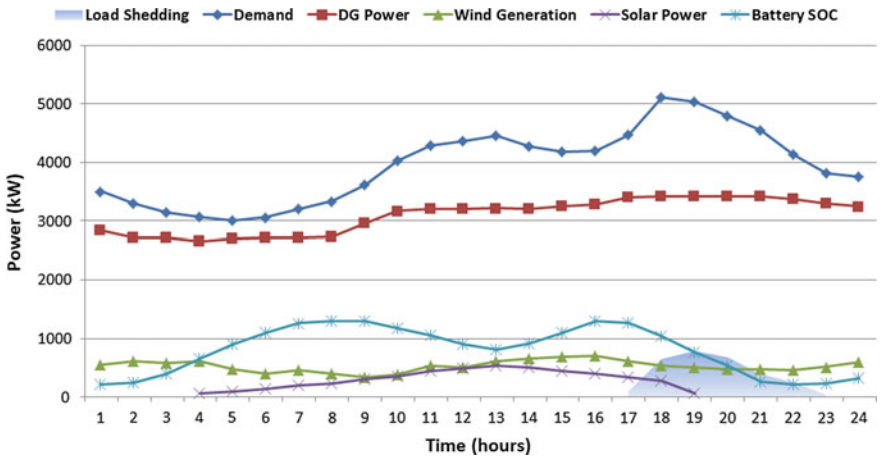

Fig. 7 Power generation for DC/AC analysis of case 3

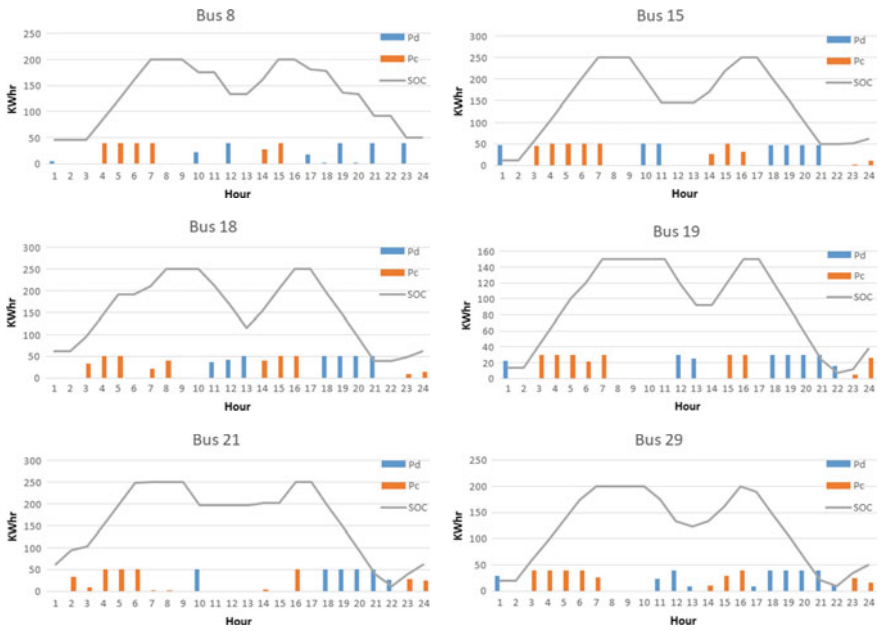

Fig. 8 Charging, discharging, and state of charge for the individual batteries for DC-OPF case 3

availability, maximum value of load shedding is further reduced to 806 kW at t19. Maximum SOC occurs at t7, t8, t9, and t16 in all the corresponding buses where batteries are connected. Initial SOC is again assumed to be 20% of maximum SOC. Figure 9 shows that charging of batteries takes place during lightly loaded conditions and they supply power during high loads.

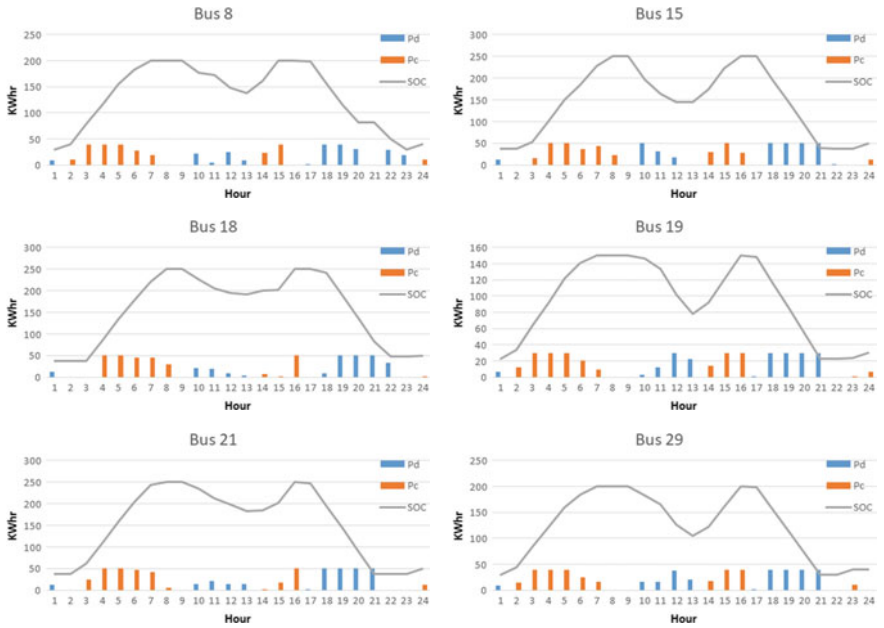

Fig. 9 Charging, discharging, and state of charge for the individual batteries for AC-OPF case 3

DC analysis shows that there is a sharp reduction in the overall cost of operation when power from renewable sources is injected into the system as mentioned in Fig. 10. As compared to case 1 there is more than 70% reduction in total cost in case 2 given in Table 2. The cost of line congestion is reduced by more than 60% in case 2 when renewable sources are connected to the network but the reduction is only 47% when battery storage system is also connected along with renewable sources in case 3. This happens because batteries are also charging and storing certain amount of energy when system is lightly loaded leading to an increase in the congestion of the line.

AC analysis also shows that there is a sharp reduction in the overall cost of operation when power from renewable sources is injected into the system as mentioned

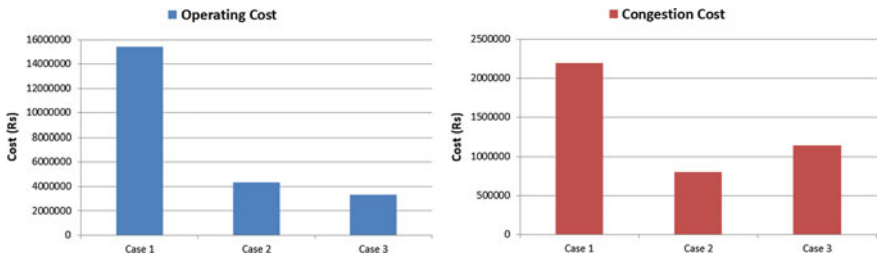

Fig. 10 Variation of total operating cost and congestion cost of MG for DC-OPF

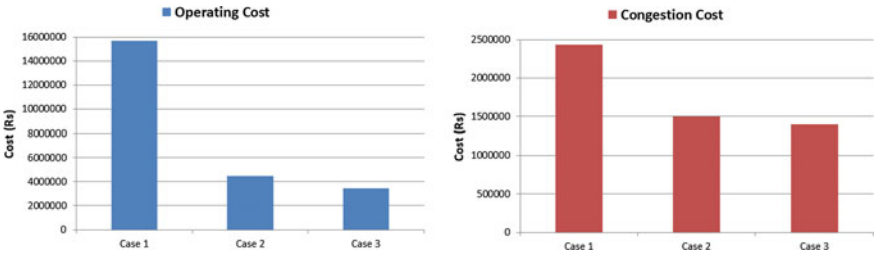

Fig. 11 Variation of total operating cost and congestion cost of MG for AC-OPF

in Fig. 11. As compared to case 1, there is more than 70% reduction in total cost in case 2 given in Table 3. Congestion cost is continuously decreasing as we move from case 1 to case 3. This happens because AC analysis takes into account variables for reactive power and voltage magnitude at various buses and is more complex but accurate.

5 Conclusion

The paper gives an economic dispatch optimization scheme for microgrid connected to renewable and non-renewable sources of energy such as thermal generators, energy storage devices, wind and solar power systems. Considering the dynamics and randomness of solar and wind power generation, modeling of the system is done in IEEE modified 33-bus system. Advantage of using energy storage technologies like battery storage in enhancing the system efficiency and cost reduction is discussed. The role of renewable energy integration in economic dispatch considering power flow constraints is explained. Three cases for each DC/AC optimal power flow network are analyzed.

References

1. Bahmani-Firouzi, B., Farjah, E., Azizipanah-Abarghooee, R.: An efficient scenario-based and fuzzy self-adaptive learning particle swarm optimization approach for dynamic economic emission dispatch considering load and wind power uncertainties. Energy **50**(1), 232–244 (2013). https://doi.org/10.1016/j.energy.2012.11.017
2. Chedid, R., Akiki, H., Rahman, S.: A decision support technique for the design of hybrid solar-wind power systems. IEEE Trans. Energy Convers. **13**(1), 76–83 (1998). https://doi.org/10.1109/60.658207
3. Eldesouky, A.A.: Security constrained generation scheduling for grids incorporating wind, photovoltaic and thermal power. Electr. Power Syst. Res. **116**, 284–292 (2014). https://doi.org/10.1016/j.epsr.2014.06.017
4. Giglmayr, S., Brent, A.C., Gauché, P., Fechner, H.: Utility-scale PV power and energy supply outlook for South Africa in 2015. Renew. Energy **83**, 779–785 (2015). https://doi.org/10.1016/j.renene.2015.04.058

5. Jiang, S., Zhang, C., Wu, W., Chen, S.: Combined economic and emission dispatch problem of wind-thermal power system using gravitational particle swarm optimization algorithm. Math. Problems Eng. (2019). https://doi.org/10.1155/2019/5679361
6. Mohammed, A., Refaat, S.S., Bayhan, S., Abu-Rub, H.: AC microgrid control and management strategies: evaluation and review. IEEE Power Electron. Mag. **6**(2), 18–31 (2019). https://doi.org/10.1109/MPEL.2019.2910292
7. Nazari-Heris, F., Mohammadi-ivatloo, B., Nazarpour, D.: Network constrained economic dispatch of renewable energy and CHP based microgrids. Int. J. Electr. Power Energy Syst. **110**(January), 144–160 (2019). https://doi.org/10.1016/j.ijepes.2019.02.037
8. Nemati, M., Braun, M., Tenbohlen, S.: Optimization of unit commitment and economic dispatch in microgrids based on genetic algorithm and mixed integer linear programming. Appl. Energy **210**, 944–963 (2018). https://doi.org/10.1016/j.apenergy.2017.07.007
9. Peng, C., Sun, H., Guo, J., Liu, G.: Dynamic economic dispatch for wind-thermal power system using a novel bi-population chaotic differential evolution algorithm. Int. J. Electr. Power Energy Syst. **42**(1), 119–126 (2012). https://doi.org/10.1016/j.ijepes.2012.03.012
10. Riffonneau, Y., Bacha, S., Barruel, F., Ploix, S.: Optimal power flow management for grid connected PV systems with batteries. IEEE Trans. Sustain. Energy **2**(3), 309–320 (2011). https://doi.org/10.1109/TSTE.2011.2114901
11. Soroudi, A. (2019). Alireza Soroudi power system optimization modeling in GAMS. https://link-springer-com.dianus.libr.tue.nl/content/pdf/10.1007%2F978-3-319-62350-4.pdf
12. Zhang, H., Yue, D., Xie, X.: Robust optimization for dynamic economic dispatch under wind power uncertainty with different levels of uncertainty budget. IEEE Access **4**, 7633–7644 (2016). https://doi.org/10.1109/ACCESS.2016.2621338

An Overview of Implementation Issues of Smart Grid

Mayank Srivastava

1 Introduction

The modernization of the existing grid is presently in progress to manage the rising complexities of today's energy systems. The smart grid is one of the possible solutions that can pave way for developing solution which can handle the drawbacks of the existing grid technologies for energy transmission. It permits society to transit from a centralized energy system to a distributed energy system, i.e., the power is transferred at a short distance as compared to long distance in a centralized energy system [1].

Smart grids are skilled to better manage the energy generation of intermittent sources of electricity. It can manage the load side demand accurately and predictably. Due to technology-enabled sensors, its energy efficiency is improved due to the reduction of transmission losses. Smart grids integrate the action of all users in a two-way computer-based network. A smart grid consists of different computer-based equipment that works in synchronization with the grid and responds quickly according to the required electricity demand [2].

2 Review of the Literature

The area of smart grid is one of the ongoing research domains in which a good number of researchers are working. Some of the major contributions of this area are as follows.

Chebbo [3] highlights the importance of smart vision, smart technologies, smart processes, smart roadmap, and finally smart stakeholders for energy innovation.

M. Srivastava (✉)
Department of CEA, GLA University, Mathura, UP 281406, India
e-mail: mayank.srivastava@gla.ac.in

O. H. Gupta and V. K. Sood (eds.), *Recent Advances in Power Systems*, Lecture Notes in Electrical Engineering 699, https://doi.org/10.1007/978-981-15-7994-3_7

Amin et al. [4] identify some of the current challenges of power system which includes the lack of transmission capability, planning of power system, and operation of the grid in a competitive domain. The paper finally gives insight on centralized and decentralized control for power generation. Farhangi [5] focusses on the concepts, technologies, and systems of the smart grid. It also mentions that many research centers are developing solutions to perform an easy transition to these next-generation technologies. Fang et al. [6] explore various management objectives and methods to achieve factors such as improvement of energy efficiency, utility maximization, cost reduction, and controlling the emission. The author also identifies various ways to improve security, reliability, and privacy issues of the smart grid. Wei [7] summarizes the important features of smart grid like integration, optimization, self-healing, and compatibility. The paper finally co-relates the smart grid with economic and technological development.

Atwa et al. [8] focus on identifying the constraints for distributed generation (DG), which includes the important attributes of maximum penetration limit, the capacity of the feeder, discrete size of DG units, etc. Baumeister [9] proposed work which is divided into five different categories of process control, smart meter, power system state estimation, communication protocol, and simulation for security analysis of smart grid. Berthier et al. [10] gives the emphasis on using the secure protocols and the enforcement of strong security properties to prevent the network from being exploited. The paper also explores the need for monitoring and intrusion detection by analyzing different types of threats. Bose [11] suggests the requirements to handle ubiquitous phasor measurements to handle a large amount of data. The paper also gives the path for a smooth transition from present-day systems and applications. Wang et al. [12] firstly discuss the challenging problems of network reliability and security associated with smart grid. The paper finally ends by highlighting that planning of the network must be done carefully to meet the changing performance requirements of energy management.

Bigerna et al. [13] perform the literature review pertaining to the social costs affecting the development of the smart grid. The paper finally presents the opportunities and challenges in the business, applications, policy, and security issues of the smart grid. Tuballa et al. [14] present an overview of the related technologies of the smart grid. The paper also highlights the contribution of these latest technologies in shaping the existing grid to align themselves with rising energy demand and supply. Kakran et al. [15] provide a detailed description related to the key progress and advantage of demand side management, demand response programs, and distributed generation in smart grids. Mrabet et al. [16] provide a cyber-security strategy to deal with several severe cyberattacks. Wang et al. [17] present a comprehensive review of various cyber-security issues for the smart grid. It presents a thorough understanding of vulnerabilities and solutions in context to the infrastructure of the smart grid.

3 State Estimation of Smart Grid

This section presents a comparison between the existing and the smart grid infrastructure. Figures 1 and 2 below highlights the basic infrastructure required in both existing and smart grid, respectively. It is evident from Fig. 1 that the existing grid architecture includes the phases of generation, transmission, and distribution. The electricity in the existing grid is firstly generated, transmitted to substations over long distances, and finally distributed to the consumers. The electricity generation phase includes energy from non-renewable sources like coal and renewable sources like solar.

Figure 2 below shows a smart grid architecture. A smart grid is a combination of an existing grid along with a computer network for sensing, analyzing, and distributing data related to energy consumption. Typically, any smart grid consists of power generation and consumption entities, where all the entities are strongly connected through a computer network. In the smart grid, the energy producers provide energy to the grid intelligently, and the consumers also consume the energy from the grid intelligently.

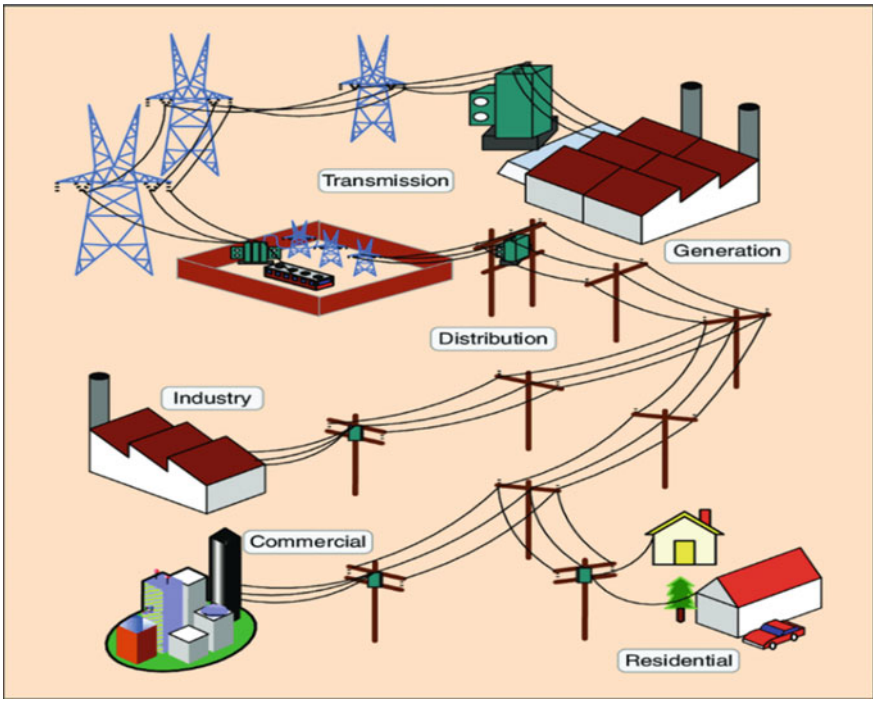

Fig. 1 Existing grid architecture [18]

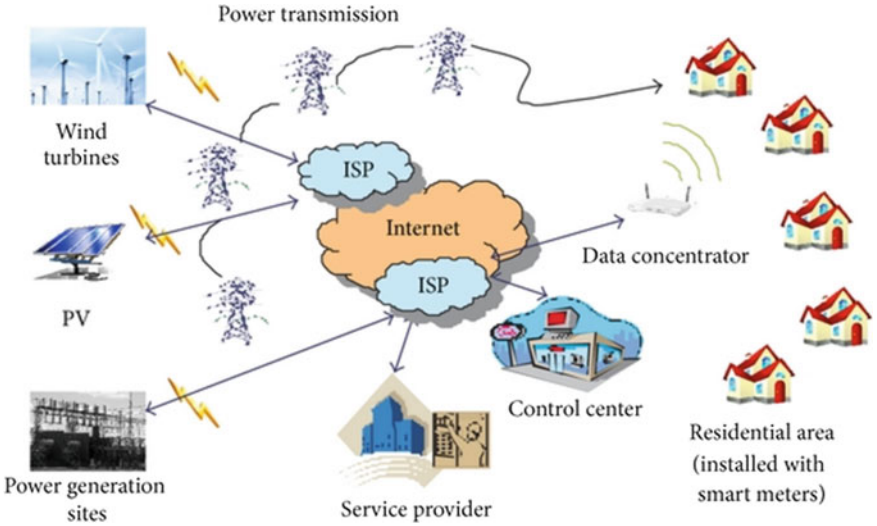

Fig. 2 Smart grid architecture [19]

The existing grid infrastructure is compared with the smart grid on the basis of different performance and functional parameters. Some of the important parameters which were used for comparison are given below by using Table 1.

Technology:

EG: It is based on electromechanical devices.
SG: It is based on digital circuits that allow communication and self-regulation.

Distribution:

EG: The distribution of power is one-way from the generation unit to consumers.
SG: It gives two-way communication between the generation unit and the consumer.

Table 1 Comparison between existing grid and smart grid

Parameters	Existing grid (EG)	Smart grid (SG)
Technology	Electromechanical	Digital circuit
Distribution	Unidirectional	Bidirectional
Generation	Centralized	Distributive
Sensor	Few	Large
Monitoring	Manual	Digitally
Restoration	Manual	Automated
Equipment	Error prone	Accurate
Control	Less	More
User choices	Few	More

Generation:

EG: The power is generated centrally.
SG: The power can be disseminated from various power generation units.

Sensors:

EG: It is normally not equipped to handle sensors.
SG: In this multiple sensors are used to increased system performance.

Monitoring:

EG: Monitoring is done manually.
SG: Monitoring is done digitally to balance power loads and troubleshooting.

Restoration:

EG: Faults need to be repaired manually.
SG: It can do simple troubleshooting and repairing automatically.

Equipment:

EG: Its infrastructure is prone to failures.
SG: The devices are accurate which helps in developing a reliable system.

Control:

EG: It is having less control over power after generation.
SG: It is having more control over power after generation.

Users Choice:

EG: Users will have no choice in receiving the electricity.
SG: Users will have a choice to access one of the different forms of energy.

4 Significant Findings of the Study

Smart grid is a modernized form of the existing grid which provides smart and secure electrical service. In the previous section, we compared the two domains of EG and SG, which show that smart grid infrastructure is superior to existing infrastructure in many aspects, and it is the future of the energy sector. However, the current state of smart grid technology still needs to address a number of issues before it can be put for commercial use. Some of the major issues concerning the smart grid are as follows:

- **Infrastructure**: One needs to build entirely new infrastructure for the smart grid which includes smart devices at the grid, network, and consumer level. The possible solution to this is to develop infrastructure optimally, so that the development of such an infrastructure needs less number of devices.

- **Cost**: The development of the entire smart infrastructure with various kinds of smart devices requires huge investment costs. The possible solution to this is to develop and use cheap smart devices so that the overall cost of developing such an infrastructure reduces.
- **Network Security**: Smart grid technology is based on network communication. We know that the communication network is vulnerable to various types of attacks and to handle this, the communication network must use the protocol and devices which are free from any vulnerabilities.
- **Data Storage**: The large number of network devices used in the smart grid continuously generates a large amount of data for accurate system operation. One possible solution to store this voluminous data is to use RAID or cloud-based storage architecture.
- **Communication concerns**: Communication issues pertaining to a smart grid is mainly related to broadband issues of both the wireless and wired domain. A large number of access points along with high-speed routers on optical fiber networks need to be used to address the connectivity issues.
- **Confidentiality**: Consumers will connect to the smart grid network by means of smart devices from their homes. Such a scenario definitely required us to look for the privacy issues of the customer. Encryption algorithms can be used as a solution to achieve the privacy issues of the customer.
- **Accuracy**: The entire smart grid infrastructure is based on a number of smart devices including sensors, which may operate in different physical conditions and gives feedback for correct system performance. It is therefore very important to use the devices which give precise results for correct system operation.
- **Reliability**: A smart grid network is reliable if all the connected devices of the network give accurate results continuously over a longer duration of time. To make the system reliable, one has to use the precise devices which can sustain for a longer duration of time.

5 Conclusion

Smart grid technology is an ongoing research area which focusses on addressing the issues of existing grid infrastructure. The smart grid can be used to monitor the grid-oriented system activities, load side preferences, and to perform real-time actions. The paper highlights the key differences between the existing grid and the smart grid on the basis of several attributes. Despite many advantages of the smart grid, there are multiple challenges in its implementation which involves large-scale coordination and adoption of the new technology, huge investments in infrastructure, etc. The paper, therefore, focusses on the identification of issues related to the current state of a smart grid that needs to be addressed for making the implementation of the smart grid successful.

References

1. Zhou, J., He, L., Li, C., Cao, Y., Liu, X., Geng, Y.: What's the Difference between traditional Power Grid and Smart Grid? Dispatching Perspective. In: IEEE PES Asia-Pacific Power and Energy Engineering Conference (APPEEC), Kowloon, pp. 1–6(2013)
2. Kappagantu, R., Daniel, S.A.: Challenges and issues of smart grid implementation: a case of Indian scenario. J. Electr. Syst. Inform. Technol. **5**(3), 453–467 (2018)
3. Chebbo, M.: EU Smart grids fFramework "Electricity Networks of the future 2020 and beyond". In: IEEE Power Engineering Society General Meeting, Tampa, pp. 1–8 (2007)
4. Amin, S.M., Wollenberg, B.F.: Toward a smart grid: power delivery for the 21st century. IEEE Power Energ. Mag. **3**(5), 34–41 (2005)
5. Farhangi, H.: The path of the smart grid. IEEE Power Energ. Mag. **8**(1), 18–28 (2009)
6. Fang, X., Misra, S., Xue, G., Yang, D.: Smart grid—the new and improved power grid: a survey. IEEE Commun. Surv. Tutorials **14**(4), 944–980 (2011)
7. Wei, C.: A conceptual framework for smart grid. In: Asia-Pacific Power and Energy Engineering Conference, Chengdu, pp. 1–4 (2010)
8. Atwa, M., El-Saadany, E.F., Salama, M.M.A., Seethapathy, R.: Optimal renewable resources mix for distribution system energy loss minimization. IEEE Trans. Power Syst. **25**(1), 360–370 (2009)
9. Baumeister, T.: Literature review on smart grid cyber security. Collaborative Software Development Laboratory at the University of Hawaii, Manoa (2010)
10. Berthier, R., Sanders, W. H., Khurana, H.: Intrusion detection for advanced metering infrastructures: Requirements and architectural directions. In: First IEEE International Conference on Smart Grid Communications, Gaithersburg, pp. 350–355 (2010)
11. Bose, A.: Smart transmission grid applications and their supporting infrastructure. IEEE Trans. Smart Grid **1**(1), 11–19 (2010)
12. Wang, W., Xu, Y., Khanna, M.: A survey on the communication architectures in smart grid. Comput. Netw. **55**, 3604–3629 (2011)
13. Bigerna, S., Bollino, C.A., Micheli, S.: Socio-economic acceptability for smart grid development—a comprehensive review. J. Clean. Prod. **131**, 399–409 (2016)
14. Tuballa, M.L., Abundo, M.L.: A review of the development of smart grid technologies. Renew. Sustain. Energy Rev. **59**, 710–725 (2016)
15. Kakran, S., Chanana, S.: Smart operations of smart grids integrated with distributed generation: a review. Renew. Sustain. Energy Rev. **81**, 524–535 (2018)
16. Mrabet, Z.E., Kaabouch, N., Ghazi, N.E., Ghazi, H.E.: Cyber-security in smart grid: Survey and challenges. Comput. Electr. Eng. **67**, 469–482 (2018)
17. Wang, W., Lu, Z.: Cyber security in the smart grid: survey and challenges. Comput. Netw. **57**(5), 1344–1371 (2013)
18. Yu, X., Cecati, C., Dillon, T., Simões, M.G.: The new frontier of smart grids. IEEE Ind. Electron. Mag. **5**(3), 49–63 (2011)
19. Bari, A., Jiang, J., Saad, W., Arunita, J.: Challenges in the smart grid applications: an overview. Int. J. Distrib. Sens. Networks **10**(2) (2014)

A Performance Evaluation of SO_2 Gas and SO_2/CO_2 Gas Mixture as Potential SF_6 Gas Alternatives in Power Transmission and Distribution System

Akhilesh Kumar Pandey, Pushpendra Singh, Jitendra Kumar Singh, and Shahnawaz Khan

1 Introduction

Modern transmission and distribution system is looking for better reliability, greener technology with lessor footprints and reduction in emission of greenhouse gases (GHG). From reliability and lessor land utilization view point, SF_6 gas-insulated switching elements like Circuit-breakers, Isolators, and Instrument transformers as well as substations are most adopted solution in this system. The application range is from medium voltage (MV) 33 kV to ultra high voltage (UHV) of 1200 kV for switch elements and SF_6/N_2 mixture in gas-insulated transmission lines (GITL). Despite these benefits, SF6 gas-based solutions have few drawbacks also like potential GHG gas [1], high cost, and sensitive toward non-uniform electric fields [8]. These drawbacks led to find suitable alternatives since 1970s. SO_2 gas and its mixture with gases like CO_2 or N_2 are also one of the potential alternatives suggested in various studies [1, 2]. As reported in very few experimental works in, SO_2 gas have comparable dielectric strength with respect to SF_6 gas [11–13] as well as the higher corona starting gradient among other non-halogenated gas and second to SF_6 gas [14]. In addition to dielectric strength for this gas and its mixtures, various gaseous discharge processes which encompasses streamer discharge, corona discharge, using swarm parameters under stressed electric and magnetic field and microscopic collision mechanism, need to be understood to be used an suitable SF_6 alternative. These investigational aspects are still missing for SO_2 gas and its mixture. Based on swarm parameters like drift velocity and effective ionization coefficients, we are analyzing the insulating performance SO_2 gas and SO_2/CO_2 gas mixture and comparing with SF_6 and SF_6/N_2. We are also calculating these parameters for existing gas mixture like SF_6/N_2 and

A. K. Pandey (✉) · P. Singh · J. K. Singh · S. Khan
JK Lakshmipat University, P.O. Mahapura, Near Mahindra SEZ, Ajmer Road, Jaipur, Rajasthan 302026, India
e-mail: Pandey.akh@gmail.com

O. H. Gupta and V. K. Sood (eds.), *Recent Advances in Power Systems*, Lecture Notes in Electrical Engineering 699, https://doi.org/10.1007/978-981-15-7994-3_8

calculated data is also compared with experimentally reported data. The valuated values are generally in agreement with reported values.

These parameters are calculated based on several macroscopic collision mechanism of gas like attachment, excitation vibration, and ionization which occurred during operating conditions in switchgears [8]. As reported in several literatures, BOLSIG+ [7] is a useful tool to calculate these data as reported in several works [9, 10] owing to faster calculations and lessor memory requirement. The methods used in this paper are described in Sect. 2. The results are reported and discussed in Sect. 3 followed by conclusions Sect. 4.

2 Research Methodology

To calculate the swarm parameters like drift velocity, diffusion coefficients mean energy, mobility, collision frequencies (total collision frequency, momentum frequency, ionization coefficients, attachment coefficients, effective ionization coefficients, various numerical techniques like Monte Carlo simulation (MCS) and Boltzmann transport (BE) led to fluid modeling with an enhanced understanding of various microscopic physical process [8] in last 2 to 3 decades. In this paper, we prefer to use the BOLSIG+ tool [7] for the estimation of these parameters as MCS required more computation time and large memory. BOLSIG+ is a very user-friendly tool and openly accessible for the estimation of swarm parameters. The BOLSIG+ is based on the numerical solution of the Boltzmann equation (1) for electrons in weakly ionized gases in uniform electric fields, conditions which occur in swarm transports in various types of gas discharges and collisional low-temperature plasmas.

$$\frac{\partial f}{\partial t} + \vec{v}.\nabla f - \frac{e}{m}\vec{E}.\nabla_v f = C[f] \tag{1}$$

where f is the electron energy distribution in six-dimensional phase space, e the elementary charge, m the electron mass, E an electric field, v the velocity, ∇_v the velocity gradient operator, and C the rate of change of f due to the elastic and inelastic collisions. The expression for drift velocity, ionization coefficients, attachment coefficient, and effective ionization coefficients are reported in various kinds of the literature as shown below and quite useful in analyzing these parameters.

$$w = \frac{1}{3}E\int_0^\infty \frac{\epsilon}{N\,\theta}\frac{\mathrm{d}}{\mathrm{d}\epsilon}\frac{f(\epsilon)}{\epsilon^{1/2}}\mathrm{d}\epsilon \tag{2}$$

$$\alpha/N = \frac{1}{w}\int_{\epsilon_i}^\infty Q_i\epsilon^{1/2}f(\epsilon)\,\mathrm{d}\epsilon \tag{3}$$

$$\eta/N = \frac{1}{w}\int_{\epsilon_i}^{\infty} Q_a \epsilon^{1/2} f(\epsilon)\, \mathrm{d}\epsilon \tag{4}$$

$$((\bar{\alpha}/N = \alpha/N - \eta/N)) \tag{5}$$

w: drift velocity (m/s); E: electric field; θ: momentum transfer cross section (m^2); ϵ: mean energy(eV); N: gas number density (m^{-3}); $F(\epsilon)$: electron energy distribution; Q_i: ionization cross section (m^2); Q_a: attachment cross section (m^2); α/N: ionization coefficients (m^2); η/N: attachment coefficients; $\bar{\alpha}/N$ :: effective ionization coefficients.

3 Result and Discussion

Gaseous electronics is specialized field of electrical engineering and started with discovery of cathode rays in 1876. The numerous industrial applications of this field are illumination, gas lasers, eye surgery, metal cutting, and power and distribution system. In this field, electrons interactions with neutrals, excited, and charged gas molecules are studied theoretically, numerically, and experimentally. In power transmission and distribution system, gases are being used as dielectric insulating medium since 1960s. The main reason for this application is that the gases are naturally insulating owing to no or low free electrons but changes its behavior to current carrying conductors under influence of photoelectric, thermal, electromagnetics, and electrostatics stress which are experienced during normal and switching operations in this system. This behavioral change in gas due to free electron and gas molecule interaction are function of various microscopic collisions cross sections and swarm parameters. The various collision cross sections are attachment, ionization, momentum, vibrational and rotational, and function of electron energy. The swarm parameters are drift velocity (w), ionization coefficient (α/N), attachment coefficients (η/N), collision frequencies, rate constant, and rate coefficient and studied as function of reduced electrical field (E/N). The swarm parameter is selected as they play very important role in analyses of gases dielectric behavior as shown in Eqs. (2)–(5). In this study, we are focusing on SO_2 gas and SO_2/CO_2 gas mixture as potential SF_6 gas alternatives using these swarm parameters

3.1 Electron Drift Velocity for SF_6 and SO_2 Gas

As shown in Eqs. (2) and (3), the ionization coefficient and attachment coefficients are function of drift velocity of electron and ions in gas discharge process. In below graph (see Fig. 1), the drift velocity is calculated for SF_6 and SO_2 gas based on

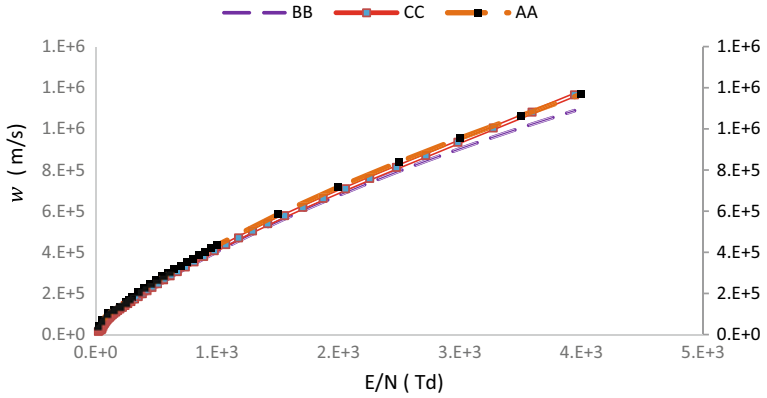

Fig. 1 Drift velocity (m/s) vs reduced electric field *E/N* (Td) for SO_2 and SF_6 gas. AA: SF_6 [15], BB: SF_6 (calculated), CC: SO_2 (calculated)

respective scattering momentum cross section and compared the same with reported values of SF_6 gas [3, 4]. Between *E/N* of 23 Td to 100 Td, the calculated drift velocity of SO_2 gas is 30–35% higher by SF_6 gas, and in *E/N* of 100 Td to 2000 Td, drift velocity of SO_2 gas is within range to 90–95% of SF_6 gas. Experimentally reported drift velocity of SF_6 gas is higher by 50% than calculated values of SF_6 gas. The difference may be due to variation in momentum cross section is shown (see Fig. 2) as well as different conditions of calculations and experimental conditions. The effective ionization coefficient which is difference of ionization and attachment coefficient and critical in deciding to the dielectric strength of gas are inversely proportion of drift velocity as relation shown in Eq. (5). Since high attachment coefficients with lowest drift velocity for high range of reducing electric filed is preferable conditions for any gas to better insulating gas, SO_2 shows considerable proximity with values of SF_6 gas.

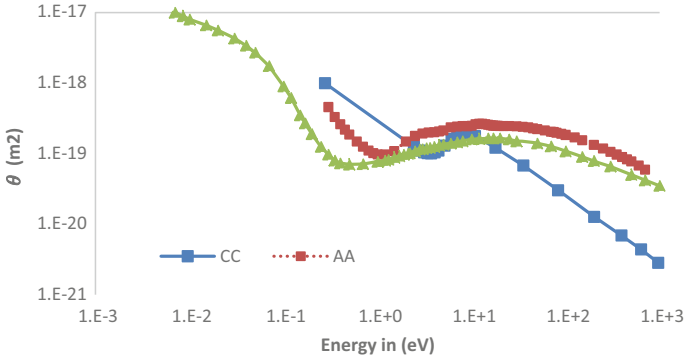

Fig. 2 SF_6 and SO_2 gas momentum cross section (m^2) vs eV. AA: SF_6 [3], BB: SF_6 [4], CC: SO_2 [5]

3.2 *Electron Drift Velocity for CO_2 and SO_2 Gas*

In below graph (see Fig. 3), the electron drift velocity of CO_2 and SO_2 gas is calculated with respect to reduced electric field. The calculated values of CO_2 are approximately 3–3.5 times higher than SO_2 gas over *E*/*N* range of 20 Td to 4000 Td. This behavior of drift velocity might be due to 20–35% of higher value of elastic momentum cross section CO_2 gas over SO_2 as shown in below graph (see Fig. 4). At around 5000 Td, drift velocity of SO_2 gas cross-over the same for CO_2 gas (see Fig. 3) which may be due to change in electron energy distribution function. The higher values of drift velocity in the lower range of reduced electric field reduce the attachment coefficients of CO_2 gas and not suitable to be used as in insulating gas.

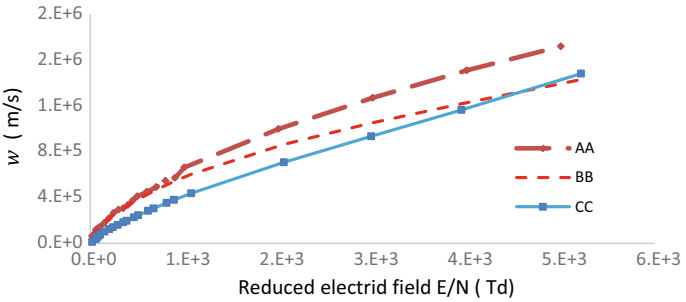

Fig. 3 Drift velocity (m/s) vs reduced electric field *E*/*N* (Td) for SO_2 and CO_2 gas. AA: CO_2 [14]; BB: CO_2 (calculated); CC: SO_2 (calculated)

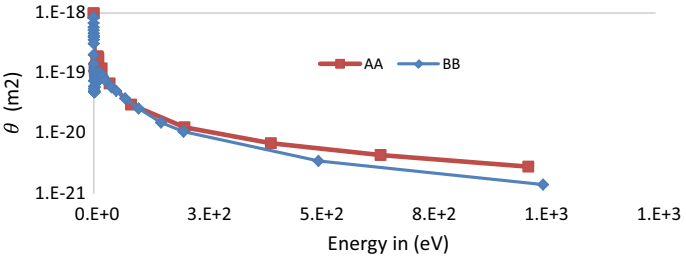

Fig. 4 CO_2 and SO_2 gas momentum cross section (m^2) vs Energy (eV). AA: CO_2 [5], BB: SO_2 [5]

3.3 *Effective Ionization Coefficients and Drift Velocity of the Gas Mixture*

We have made a comparative study of effective ionization coefficients and drift velocity of SF_6/N_2 gas mixture, and the SO_2/CO_2 gas mixture is done over the range of 200 Td to 500 Td. The calculated data are at lower pressure, at ambient temperature, and at relative concentration. Since saturation vapor pressure of SO_2 gas is very high, the SO_2/CO_2 gas mixture is chosen on account of as saturation vapor pressure of CO_2 gas as shown in graph (see Fig. 10). The SF_6/N_2 gas mixture is already an industrially acceptable SF_6 alternative in gas-insulated lines for power transmission and distribution.

SF_6/N_2 Mixture: Effective Ionization Coefficients

Using BOLSIG+ [7], the effective ionization coefficients divided by gas number density ($\bar{\alpha}/N$) is calculated and compared with other reported data [6]. The calculated results are in closure agreement with reported data in as shown in below graph (see in Figs. 5 and 6). In calculated results, it appears that there is no linear increase in effective ionization with an increase in the percentage of SF_6 in N_2 as expected. It also appears there is a general agreement between calculated data in this paper with

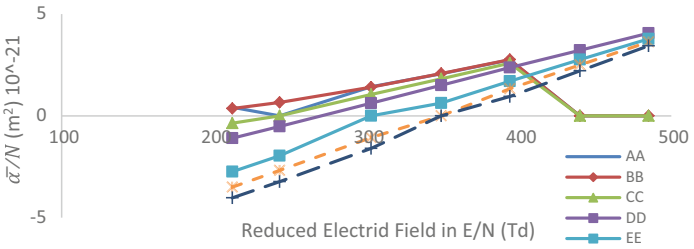

Fig. 5 Effective ionization coefficients vs reduced electric Field for SF_6/N_2 Mixture [6]. AA: 0% SF_6; AA; BB: 1% SF_6; CC: 10% SF_6; DD: 20% SF_6; EE: 50% SF_6; FF: 75% SF_6; GG: 100% SF_6

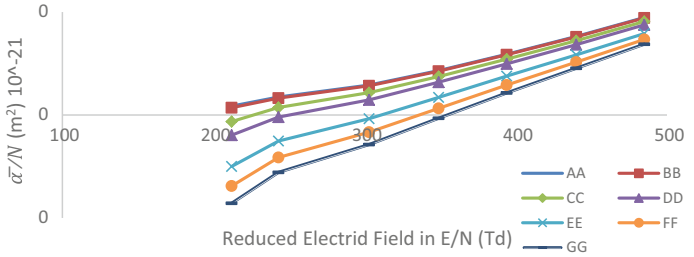

Fig. 6 Effective ionization coefficients for SF_6/N_2 Mixture as calculated. AA: 0% SF_6; AA; BB: 1% SF_6; CC: 10% SF_6; DD: 20% SF_6; EE: 50% SF_6; FF: 75% SF_6; GG: 100% SF_6

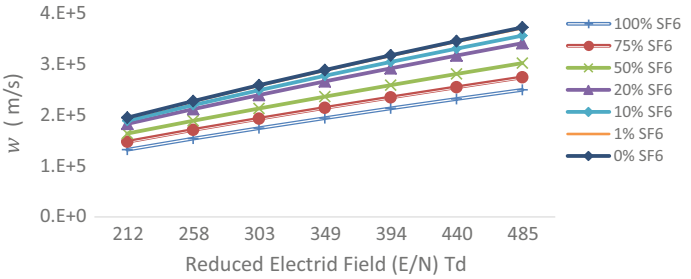

Fig. 7 Electron drift velocity w (m/s) vs reduced electric field (E/N) Td for SF_6/N_2 in range of 200 Td to 500 Td as calculated

reported data. The abnormal behavior in reported data is due to non-available data from 0% SF_6 to 10% of SF_6 for 440 Td and 485 Td.

SF_6/N_2 Mixture: Drift Velocity

A new data set of electron drift velocity for SF_6 and N_2 gas mixture is calculated using the BOLSIG+ tool [7] in the nearby range of E_{Cric} of SF_6, i.e., 358 Td, i.e., 200 Td to 500 Td. As shown in below graph (see in Fig. 7), the mixture composition of SF_6/N_2 gas has very slight impact on drift velocity. The calculated values in this paper are in reasonable agreement with other calculation made for this composition by several authors [6].

SO_2/CO_2 Mixture: Effective Ionization Coefficients

The effective ionization of the SO_2/CO_2 gas mixture is calculated using the BOLSIG+ tool [7] for the first time over a range of 200 Td to 500 Td. With an increase in concentration of SO_2 gas this mixture, there is a no linear increase in effective ionization coefficients up to 50% of SO_2 gas and between 75% and 95% concentration of SO_2 gas in CO_2 gas and there is linear change with a negative slope. The critical electric field (E_{cric}) at which the effective ionization is zero is also changes with change in concentration of SO_2 gas in CO_2 gas (Fig. 8).

SO_2/CO_2 Mixture: Drift Velocity

The drift velocity of the SO_2/CO_2 gas mixture is calculated for the first time for concentration range of SO_2 gas from 0 to 100%. The accuracy of data could not be ascertained owing to the non-availability of any data related to drift velocity for this mixture as far as per the author's knowledge. There is a linear decrease in drift for this mixture with an increase in the concentration of CO_2 gas from 0 to 100% in SO_2 gas. The adopted method fails to explain an abrupt change in drift velocity of this mixture for 20% of SO_2 concentration of in CO_2 gas (Figs. 9 and 10).

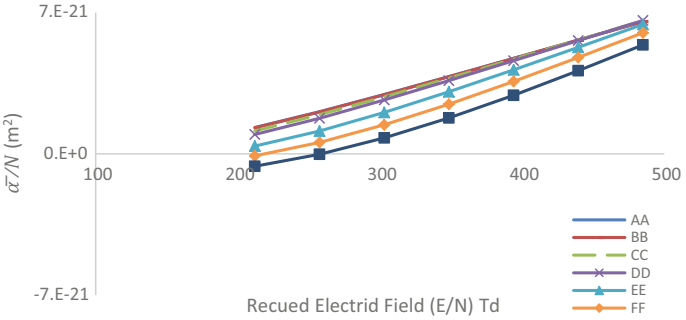

Fig. 8 Effective ionization coefficients vs reduced electric field (*E*/*N*) Td for SO_2/CO_2 mixture as calculated [7]. AA: 0% SO_2; BB: 1% SO_2; CC: 10% SO_2; DD: 20% SO_2; EE: 50% SO_2; FF: 75% SO_2; GG: 100% SO_2

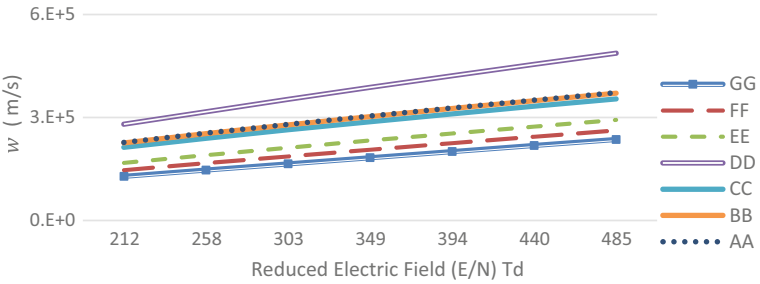

Fig. 9 Drift velocity w (m/s) vs reduced electric (*E*/*N* Td) field for SO_2/CO_2 mixture as calculated [7]. AA: 0% SO_2; BB: 1% SO_2; CC: 10% SO_2; DD: 20% SO_2; EE: 50% SO_2; FF: 75% SO_2; GG: 100% SO_2

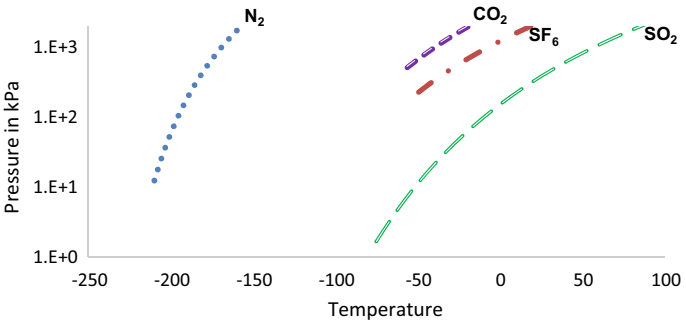

Fig. 10 Saturation pressure vs temperature overlay [16]

4 Conclusion

SF_6 gas free power transmission and distribution is need of hour. In this connection, we have evaluated the insulating performance of SO_2 and SO_2/CO_2 gas mixture based on parameter like drift velocity and effective ionization coefficients. These parameters are calculated using BOLSIG+ tool for SO_2, SF_6, N_2, and CO_2 gases as well as binary mixtures like SF_6, N_2, and SF_6/N_2 and compared with experimentally reported data for these gases. The following conclusion is made in this study.

1. SO_2 and SO_2/CO_2 gas mixtures have comparable insulating performance with respect to SF_6 and SF_6/N_2 gas mixture. The effective ionization coefficient of SO_2/CO_2 gas mixtures is lower by 30–35% of SF_6/N_2 gas mixture. Since these values are density and pressure dependent, better values can be obtained with increased density and pressure.
2. The drift velocity of SO_2/CO_2 gas mixtures is higher by 15–20% of SF_6/N_2 gas mixture, since drift velocity is depended to elastic and inelastic momentum transfer collision cross section. With availability of sufficient cross section database, better values of drift velocity may be obtained.
3. BOLSIG+ is useful tool to calculate swarm parameters which are required for study of various gas physical process like streamer discharge, corona discharge. The values calculated are in close agreement with experimentally reported values. Other aspects of any SF_6 gas alternative require further work toward understanding of gas discharge process like behavior in non-uniform electric field, streamer discharge, and corona discharge as well as chemical stability during discharge at high pressure and temperate for SO_2 and SO_2/CO_2 gas mixtures.

References

1. Loucas, L.G., Christophorou, K.J., Olthoff, S.D.: Gases for Electrical Insulation and Arc Interruption: Possible Present and Future Alternatives to Pure SF_6. National Institute of Standards and Technology (NIST), U.S. Department of Commerce's, Washington, USA, no. November 1997
2. Electric Power Research Institute, "Gases Superior to SF6 for Insulation and Interruption," Report EPRI EL 2620 September 1982
3. For SF_6, Christopher database, www.lxcat.net, retrieved on June 24, 2019. https://fr.lxcat.net/data/set_type.php
4. For SF_6, Phelps database, www.lxcat.net, retrieved on July 11, 2019. https://fr.lxcat.net/data/set_type.php
5. CO_2 and SO_2 Hayashi database. www.lxcat.net, retrieved on June 24, 2019. https://fr.lxcat.net/data/set_type.php
6. Loucas, L.G., Christophorou, Van Brunt, R.J.: SF_6/N_2 mixtures: basic and HV insulation properties. IEEE Trans. Dielec Electr. Insul. **DEIS-2**(5) (1995)
7. Hagelaar, G.J.M., Pitchford, L.C.: Solving the Boltzmann equation to obtain electron transport coefficients and rate coefficients for fluid models, Plasma Sources Sci. Technol. **14**, 722–733 (2005). Brief documentation of BOLSIG+ version 03/ 2016, Web, pp. 1–20, 2015.

http://www.bolsig.laplace.univ-tlse.fr/. https://fr.lxcat.net/data/set_type.php“BriefdocumentationofBOLSIG+version03/2016,” Web, pp. 1–20, 2015.
8. Christophorou, L.G.: Insulating gases. Nucl. Inst. Methods Phys. Res. A **268**(2–3), 424–433 (1988)
9. Rabie, M.: A systematic approach to identify and quantify gases for electrical insulation. Ph.D. Thesis, University of Innsbruck (2017)
10. Chen, L., Widger, P., Kamarudin, M.S., Griffiths, H., Haddad, A.: CF3I gas mixtures: breakdown characteristics and potential for electrical insulation. IEEE Trans. Power Delivery **32**(2), 1089–1097 (2017). https://doi.org/10.1109/tpwrd.2016.2602259
11. Vijh, A.K.: Electric strength and molecular properties of gaseous dielectrics. IEEE Trans. Electr. Insul. **EI-12**(4), 313–315 (1977). https://doi.org/10.1109/tei.1977.297984
12. Brand, K.P.: Dielectric strength, boiling point and toxicity of gases—Different aspects of the same basic molecular properties. IEEE Trans. Electr. Insulation **EI-17**(5), 451–456 (1982). https://doi.org/10.1109/tei.1982.298489
13. Berger, L.: Dielectric strength of insulating materials. CRC Handb. Chem. Phys. pp. 15.44–15.47 (2006)
14. Meek, J.M., Craggs, J.D.: Electric Breakdown of Gases. Clarendon Press, Oxford (1953)
15. Raju, G.: Gaseous Electronics. CRC Press, Boca Raton (2012). https://doi.org/10.1201/9781315217437
16. Linstrom, P.J., Mallard, W.G. (eds.): NIST Chemistry WebBook, NIST Standard Reference Database Number 69, National Institute of Standards and Technology, Gaithersburg MD, 20899. https://doi.org/10.18434/T4D303, (retrieved August 30, 2020)

An Islanding Detection Methodology for SOFC-Based Static DG Using DWT

Salauddin Ansari, Om Hari Gupta, and Manoj Tripathy

1 Introduction

The use of distributed generation (DG) is increasing due to declining availability of fossil fuel. Islanding is the condition when utility grid is electrically separated and power system is being energized by the DGs. Now, according to IEEE standard 1547-2003 [1], it is the responsibility of the DGs to detect the condition of islanding and remove themselves within 2 s.

There are few passive methods of islanding detection [2], these methods work satisfactorily only if there is some considerable active and/or reactive power mismatch between DG and load, and for matched or small mismatched active and reactive powers, there is always a non-detectable zone (NDZ) [3, 4], in which these detection methods fail to work [5]. Wavelet-based approaches have also been used for the islanding detection of islanded microgrid formed by the DGs and loads [6–12]. In the non-converter-based DGs, islanding injects some switching transients into the islanded network, which may help wavelet to find the condition of islanding. In [7], the detection time is quite large (over 100 ms). Most of the DGs use converters to connect DGs with the utility grid. Converters inject high-frequency harmonics into the power system; wavelet uses these high-frequency components to detect islanding condition. Under usual operation, the high-frequency components at point of common coupling (PCC) differ than that of the islanding condition [13]. But, the

S. Ansari (✉) · O. H. Gupta
Department of Electrical Engineering, NIT Jamshedpur, Jamshedpur 831014, India
e-mail: 2019rsee006@nitjsr.ac.in

O. H. Gupta
e-mail: omhari.ee@nitjsr.ac.in

M. Tripathy
Department of Electrical Engineering, IIT Roorkee, Roorkee 247667, India
e-mail: manojfee@iitr.ac.in

O. H. Gupta and V. K. Sood (eds.), *Recent Advances in Power Systems*, Lecture Notes in Electrical Engineering 699, https://doi.org/10.1007/978-981-15-7994-3_9

change in load will also cause difference in high-frequency components in voltage at PCC, which will also affect the wavelet-based islanding schemes. Surprisingly, many of the literatures have not shown the effect of sudden load change during normal condition [6, 7, 9, 10, 12, 13]. In [10], the attention has been given to the wavelet of levels 3 and 4 as these two levels contain 5th and 7th voltage harmonic information, and it is also said that nuisance tripping may occur due to any transient disturbance if simple threshold settings are used. The proposed scheme in [10] is robust against transient and noise disturbances but if during normal operation of microgrid, sudden load change occurs, this scheme fails.

Solid oxide fuel cells (SOFCs) can reach great efficiency with good performance [14, 15]. So here in this work, firstly, the effect of sudden load change during normal operation of SOFC-based DG has been observed, and secondly, wavelet scheme, which is able to differentiate between load change and islanding condition, has been proposed.

1.1 Feature Extraction Using Discrete Wavelet Transform

Figure 1 shows the process of decomposing a signal by filtering and down-sampling. The original signal is filtered using half-band low-pass filter (HBLPF) and half-band high-pass filter (HBHPF), that provide the approximations and details, which is further down-sampled by 2 to get approximation coefficient (Ac) and detailed coefficient (Dc). Again Ac is further filtered using its HBLPF and other HBHPF and further down-sampled by 2. This procedure is repeated unless the required level is achieved.

1.2 Test System Considered

Figure 2 shows the one-line circuit diagram of the test system considered, which consists of a SOFC connected to the inverter, load and a grid, with which the SOFC-based DG is connected. L_{FC} and R_{FC} consist of line and transformer parameters, while L_g and R_g are the grid-side parameters.

2 Proposed Scheme

Figure 3 demonstrates the flow diagram of the proposed scheme. First, the PCC voltage has to be measured. Then, it is checked whether the manual trip signal (MTS) is enabled or not. If MTS is not enabled, then features of the PCC voltage have to be extracted using db-5, at the level of 5. Now, this extracted signal is processed and new featured signal x_r is obtained such that it is a moving discrete true root mean square

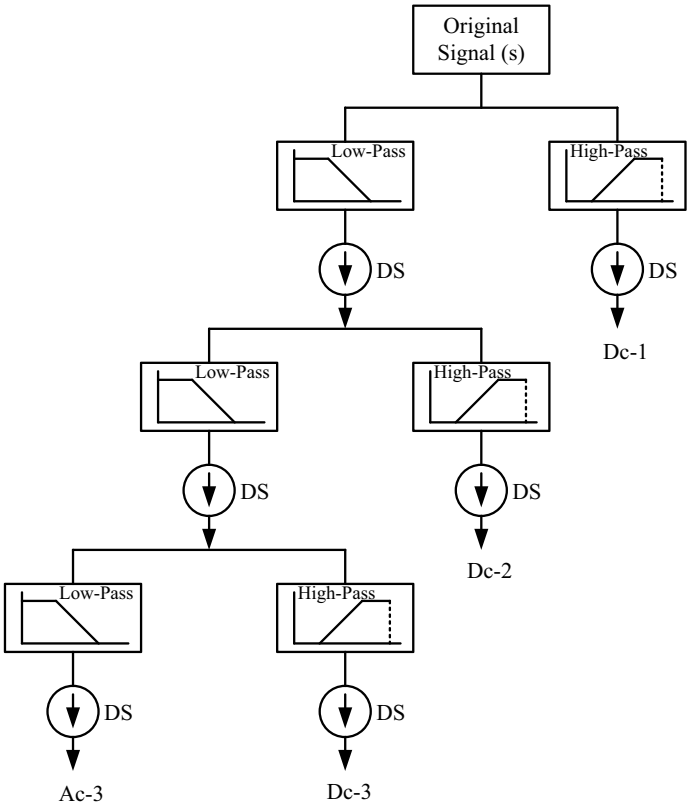

Fig. 1 Wavelet decomposition

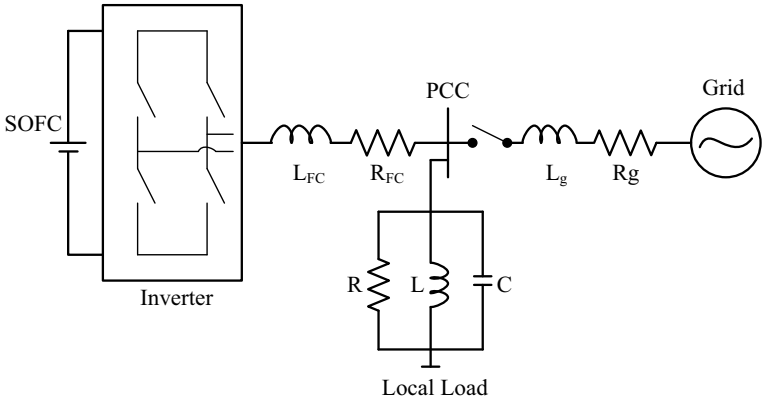

Fig. 2 One line diagram of the microgrid considered for study

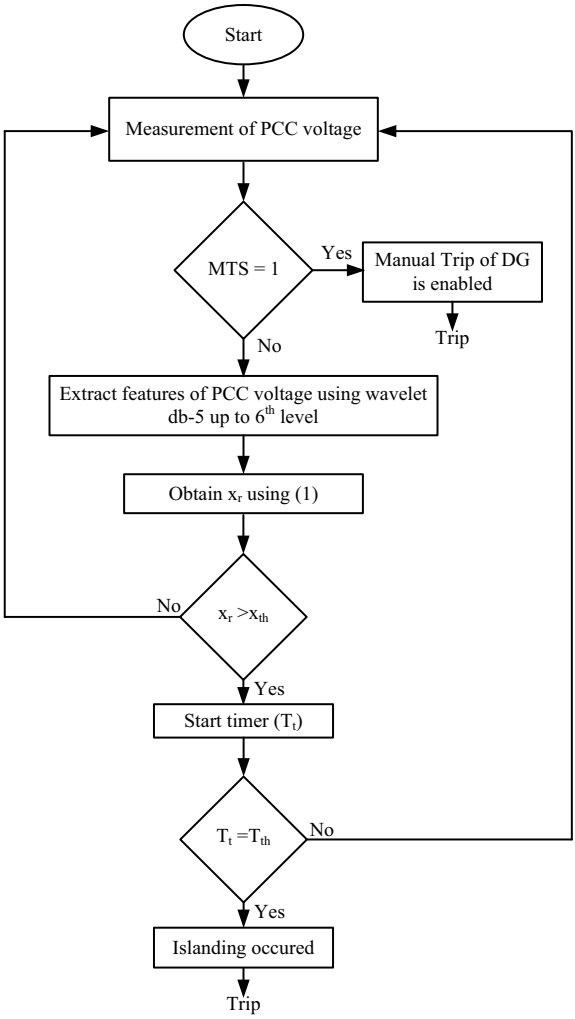

Fig. 3 Flow diagram of the proposed scheme

(MDTrms) of the extracted signal. This MDTrms is obtained at power frequency so as to minimize the effect of ripples. The x_r can be expressed as

$$x_r = \sqrt{\frac{1}{n}\left(x_1^2 + x_2^2 + \cdots + x_n^2\right)} \tag{1}$$

where n is corresponding to the power frequency; i.e., for 50 Hz power frequency and 1000 Hz sampling frequency, n will be 20. And x_1, $x_{2,}$ … are the one-cycle samples of extracted featured signal. In the next block—which is signal comparison block—signal x_r is compared with the threshold signal x_{th} and if found greater than x_{th}, this block enables and provides a high output, i.e., 1; otherwise, it provides a low

output, 0. High output of this signal comparison block enables the timer, and low output disables the timer. When the timer reaches the set threshold value t_{th}, it will be an islanding condition and an alert signal will be sent to the DG.

3 Results

To check the performance of the proposed DWT-based islanding detection scheme, a typical microgrid model as shown in Fig. 2 is simulated in MATLAB. The DG supply and load connected are of unity power factor. The complete system and load data are given in Tables 1 and 2. Different switching events were also performed along with the islanding event. Figure 4 represents the PCC voltage, detailed coefficient of db-5 at level-6 and active and reactive power absorbed by the grid. Firstly, the local load and DG powers are kept equal, and then at $t = 0.3$ s, load gets doubled; therefore, grid is supplying 1 PU of active power which is clear from Fig. 4c. At $t = 0.6$ s, the load is returned back to 1 PU and grid is now not supplying any active power since DG is capable to supply the same. It can be observed from Fig. 4b that there are no variations in the detailed coefficient of DWT during load change. Now, at $t = 0.7$, the islanding event has occurred and the detailed coefficient has significant changes. The MDTrms is obtained as per (1), and after 36.1 ms (i.e., at $t = 0.7361$ s), the islanding has been detected. So, it is found that proposed system is robust enough to ignore large load change and can successfully detect the islanding even when grid is not supplying any power. Similarly, the scheme has been tested for other switching events such as capacitor switching (Fig. 5), nonlinear load switching (Fig. 6), induction motor switching (Fig. 7) and three-phase fault at PCC (Fig. 8). From the results, it was found that the scheme is unaffected by all these non-islanding events and MDTrms does not cross the threshold. For the last case, the MDTrms (x_r) is plotted in Fig. 9. It is clear that it crosses the threshold after the islanding event only.

4 Conclusion

The discrete wavelet transform is one of the feature extraction techniques that was utilized to form a criterion for the detection of an islanding event in this study. A converter-based distributed generation and a local load are attached to the grid for the investigation of performance of DWT-based islanding detection technique. Different switching events were considered for the evaluation of the proposed methodology such as capacitor switching, nonlinear and linear load switching, induction motor switching and occurrence of fault. The simulated results proved the accuracy, reliability and selectivity of the proposed methodology since it is found to be unaffected by all non-islanding events and can detect the islanding event.

Table 1 Specifications of simulated model

Parameter	Value
SOFC	
Absolute temperature	1273 K
Current at initial	100 A
Constant of Faraday's	96.487×10^6 c/kmol
Constant for universal gas	8314 j/kmol K
Standard voltage for ideal case	1.18 V
Number of series-connected cells	450
Maximum, minimum and optimal fuel utilization	0.9, 0.8 and 0.85
Response time for hydrogen, water and oxygen flow	26.6, 78.3 and 2.91 s
Per cell ohmic loss	0.32813 milli-ohm
Response time for electrical	0.8 s
Response time for fuel processor	5 s
Hydrogen-to-oxygen ratio	1.145
Rated output power	50 kW
Transformer	
Rated kVA and frequency	1000 kVA and 50 Hz
Rated voltage	200/440 V (star–star)
$R_1 = R_2$, $L_1 = L_2$ and $R_m = L_m$	0.04 PU, 0.0001 PU and 500 PU
Main grid	
Rated voltage and frequency	440 V rms (L-L) and 50 Hz
Local load	
Rated power	50 kW
R, L and C	3.872 Ohm, 41.0832 milli H and 246.6244 micro F
Load resonance frequency	50 Hz

Table 2 Non-islanding and islanding events simulated

Parameter	Value
Real load switching	
Configuration	Star-connected parallel RLC load
Rated real power	50 kW
Rated voltage	440 V rms (L-L)
R, L and C	3.872 Ohm, 41.0832 milli H and 246.6244 micro F
Capacitor switching	
Configuration	Star-connected capacitor bank
Capacitive reactive power	50 kVAR
Rated voltage	440 V rms (L-L)
Nonlinear load	
Configuration	Three-phase bridge uncontrolled rectifier
Real power consumed	50 kW
Resistance	38.805 Ohm
Rated voltage	440 V rms (L-L)
Induction motor	
Nominal power	50 kVA
Rated voltage	440 V rms
Number of poles and frequency	2 and 50 Hz
Three-phase fault	
Resistance of faulty path	0.001 Ohm
Resistance of grounded path	0.01 Ohm

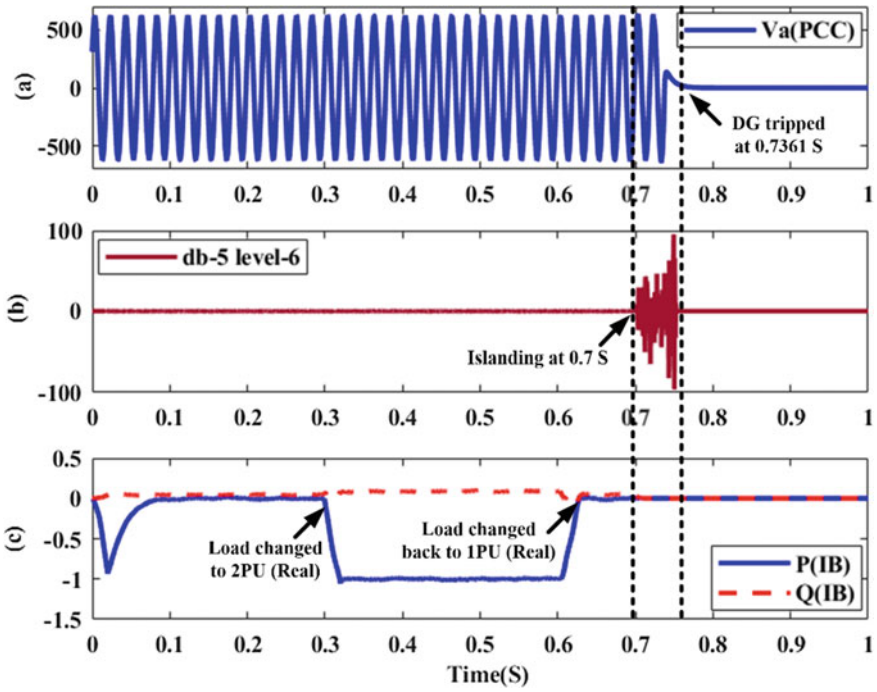

Fig. 4 **a** Voltage at PCC in volts, **b** detailed coefficient of db-5 at level-6 and **c** active and reactive power absorbed in PU by infinite bus (IB)

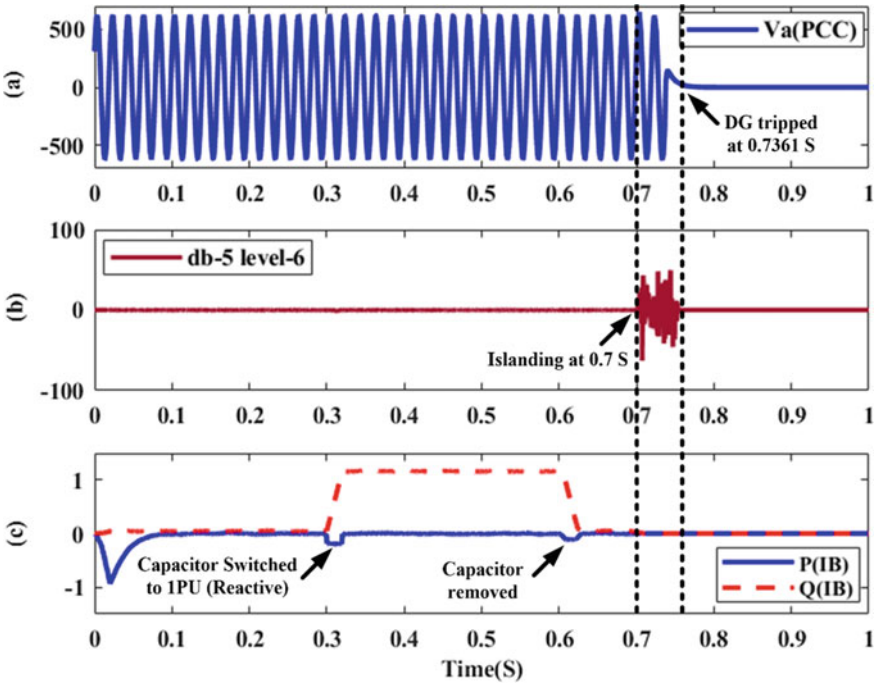

Fig. 5 **a** Voltage at PCC in volts, **b** detailed coefficient of db-5 at level-6 and **c** active and reactive power absorbed in PU by infinite bus (IB)

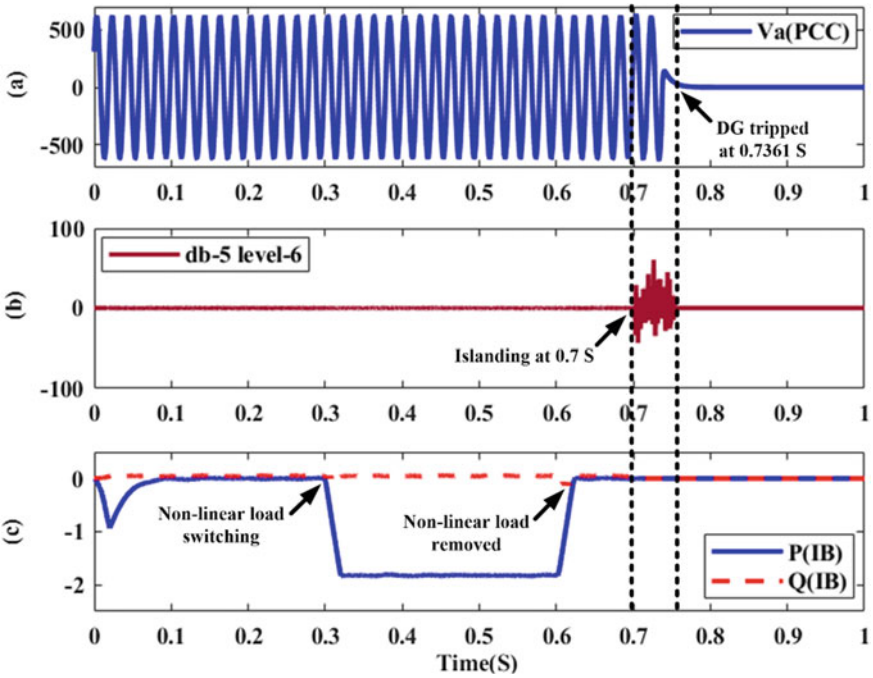

Fig. 6 **a** Voltage at PCC in volts, **b** detailed coefficient of db-5 at level-6 and **c** active and reactive power absorbed in PU by infinite bus (IB)

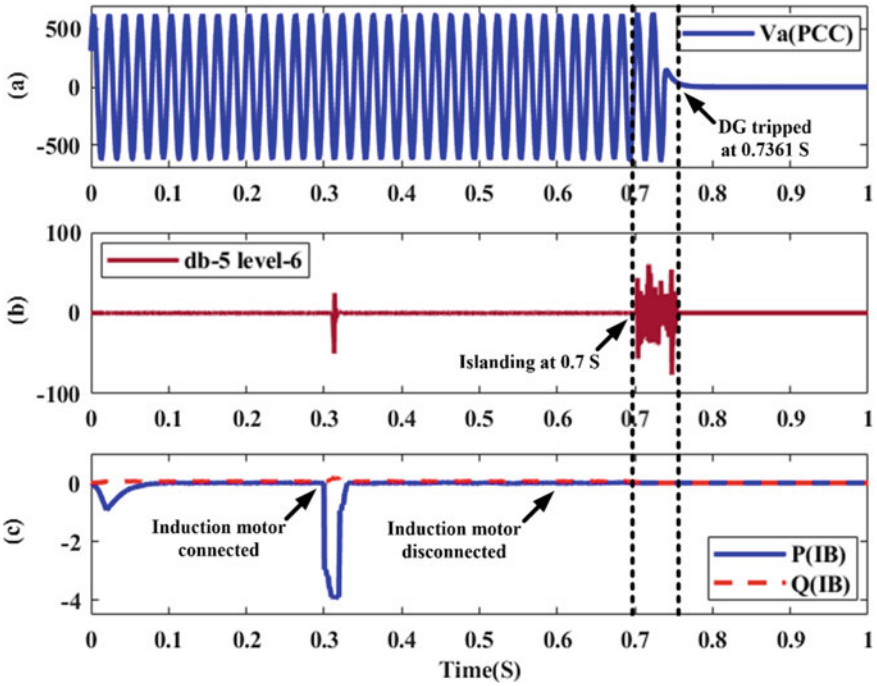

Fig. 7 **a** Voltage at PCC in volts, **b** detailed coefficient of db-5 at level-6 and **c** active and reactive power absorbed in PU by infinite bus (IB)

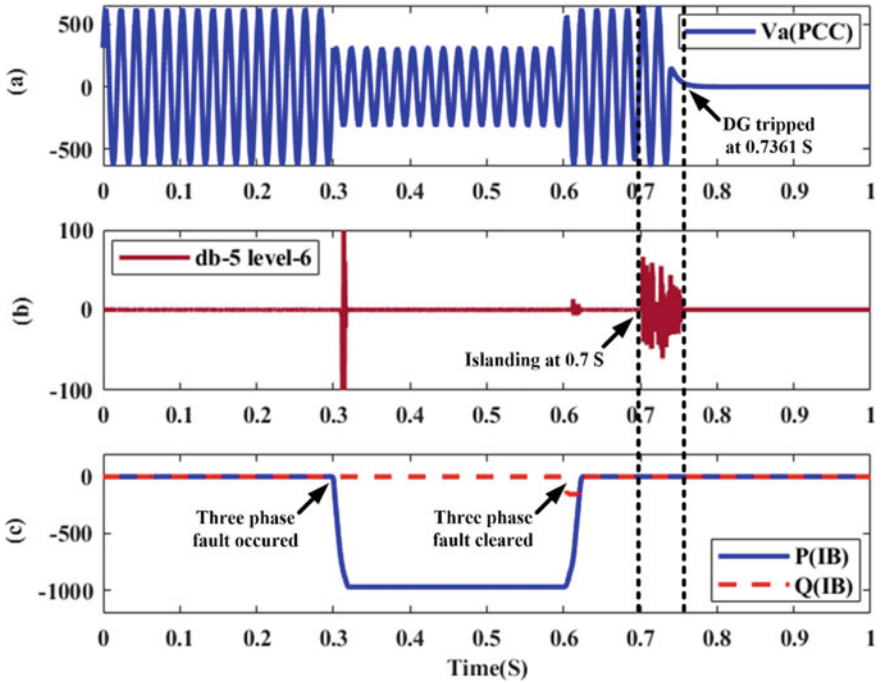

Fig. 8 **a** Voltage at PCC in volts, **b** detailed coefficient of db-5 at level-6 and **c** active and reactive power absorbed in PU by infinite bus (IB)

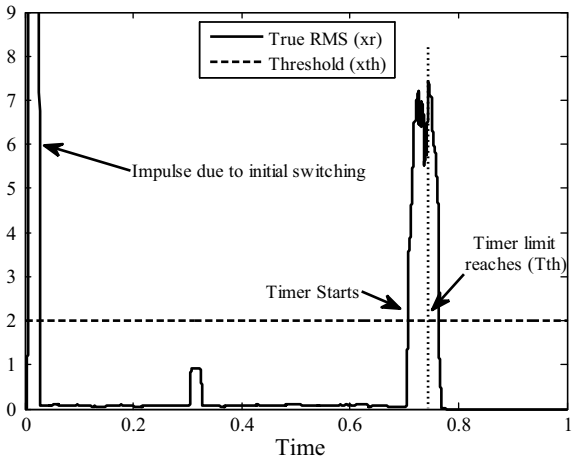

Fig. 9 Processed signal (x_r) and threshold signal (x_{th})

References

1. IEEE Standard for Interconnecting Distributed Resources with Electric Power Systems, July 2003
2. Chowdhury, S.P., Chowdhury, S., Crossley, P.A.: Islanding protection of distribution systems with distributed generators—a comprehensive survey report. In: 2008 IEEE Power Energy Society General Meeting—Conversion and Delivery of Electrical Energy 21st Century, pp 1–8, July 2008
3. Gupta, O.H., Tripathy, M., Sood, V.K.: Islanding detection scheme for converter-based DGs with nearly zero non-detectable zone. IET Gener. Transm. Distrib. **13**(23), 5365–5374 (2019)
4. Gupta, O.H., Tripathy, M., Sood, V.K.: Hybrid event classification scheme for converter-based DG with improved power quality. In: Lecture Notes in Electrical Engineering, vol. 625, pp. 207–238. Springer, Berlin (2020)
5. Yuyama, S., et al.: A high speed frequency shift method as a protection. **35**, 477–486 (1993)
6. Heidari, M., Seifossadat, G., Razaz, M.: Application of decision tree and discrete wavelet transform for an optimized intelligent-based islanding detection method in distributed systems with distributed generations. Renew. Sustain. Energy Rev. **27**, 525–532 (2013)
7. Karegar, H.K., Sobhani, B.: Wavelet transform method for islanding detection of wind turbines. Renew. Energy **38**(1), 94–106 (2012)
8. Samui, A., Member, S., Samantaray, S.R., Member, S.: Wavelet singular entropy-based islanding detection in distributed generation. IEEE Trans. Power Deliv. **28**(1), 411–418 (2013)
9. Hsieh, C.-T.T., Lin, J.-M.M., Huang, S.-J.J.: Enhancement of islanding-detection of distributed generation systems via wavelet transform-based approaches. Int. J. Electr. Power Energy Syst. **30**(10), 575–580 (2008)
10. Hanif, M., Basu, M., Gaughan, K.: Development of EN50438 compliant wavelet-based islanding detection technique for three-phase static distributed generation systems. IET Renew. Power Gener. **6**(4), 289 (2012)
11. Shayeghi, H., Sobhani, B.: Zero NDZ assessment for anti-islanding protection using wavelet analysis and neuro-fuzzy system in inverter based distributed generation. Energy Convers. Manag. **79**, 616–625 (2014)
12. Pigazo, A., Liserre, M., Mastromauro, R.A., Moreno, V.M., Dell'Aquila, A.: Wavelet-based islanding detection in grid-connected PV systems. IEEE Trans. Ind. Electron. **56**(11), 4445–4455 (2009)
13. Mohammadzadeh Niaki, A.H., Afsharnia, S.: A new passive islanding detection method and its performance evaluation for multi-DG systems. Electr. Power Syst. Res. **110**, 180–187 (2014)
14. Zhu, Y., Tomsovic, K.: Development of models for analyzing the load-following performance of microturbines and fuel cells. Electr. Power Syst. Res. **62**(1), 1–11 (2002)
15. Liu, J., Su, C., Wang, C., Zhu, L., He, J.: Influence of solid oxide fuel cell on power system transient stability. J. Eng. **2019**(16), 1081–1086 (2019). https://doi.org/10.1049/joe.2018.8511

A Novel Firing Angle-Based Power-Flow Model of TCSC

Palak, Pawan Yadav, Vedant Tiwari, and Suman Bhowmick

1 Introduction

The electric power-flow problem, a part of power engineering, requires accurate and real-time calculation of loading at demand (receiving end) and generation (transmission end) levels. The calculation of load flow, which is subjected to balancing proficiency of generator, provides voltages and power flows for a specific power system. One of the prerequisites of power system is to address the continuously fluctuating demand of power due to occurrence of unavoidable conditions such as line fault, generator fault, and line tripping. To control the performance of a power network under these conditions, FACTS devices like TCSC are incorporated [1, 2]. A TCSC can be used to adjust the magnitudes of voltage, angles, reactances between lines, and the power flow [3]. It has the inherent capability to vary transmission line reactance continuously up to a certain level. The components of TCSC include a parallel combination of TCR [4–9] and a fixed capacitor. Figure 1 shows the composition of TCSC.

Several methods exist to solve the power flow in transmission systems. Gauss–Siedel as well as Newton–Raphson methods are most commonly used. Unlike Gauss–Siedel, due to its faster convergence, the Newton–Raphson method has been adopted as the de facto power-flow method in the industry [11].

In this paper, a novel firing angle-based Newton–Raphson power-flow model of the TCSC has been presented, which had been recently implemented on IEEE 30- and 118-bus systems [8]. It is implemented in the IEEE 14- and IEEE 300-bus test systems in this paper to further evaluate its performance.

Palak (✉) · P. Yadav · V. Tiwari · S. Bhowmick
Department of Electrical Engineering, Delhi Technological University, Bawana Road, Delhi, India 110042
e-mail: palak987@gmail.com

O. H. Gupta and V. K. Sood (eds.), *Recent Advances in Power Systems*, Lecture Notes in Electrical Engineering 699, https://doi.org/10.1007/978-981-15-7994-3_10

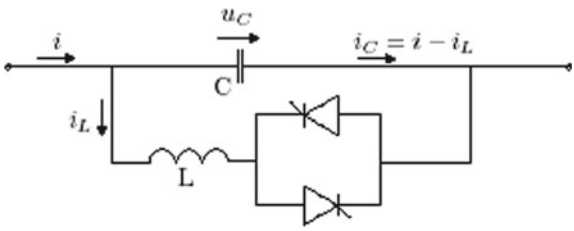

Fig. 1 Thyristor controlled series capacitor model [10]

2 TCSC—A Series FACTS Device

To provide better and faster active power-flow regulation, TCSC can be used to change the transmission line electrical length. In turn, it helps in controlling the line power flow, damping power oscillations which in turn helps in the increasing the overall stability of the system [12]. A recently proposed model exploits the nonlinearity between reactance of TCSC and characteristic of firing angle [13]. In this model, state variable of Newton–Raphson algorithm is chosen as TCSC firing angle. The correlation between TCSC equivalent reactance, X_{TCSC} and its firing angle, α, shown in Fig. 2, at steady-state, can be expressed mathematically using the following equations:

$$X_{\mathrm{tcsc}} = \frac{X_c\left[\pi\left(k^2-1\right)^2 - k^2\left(k^2-1\right)(2\beta + \sin 2\beta) + 4k^2\cos^2\beta(k\tan k\beta - \tan\beta)\right]}{\pi\left(k^2-1\right)^2} \tag{1}$$

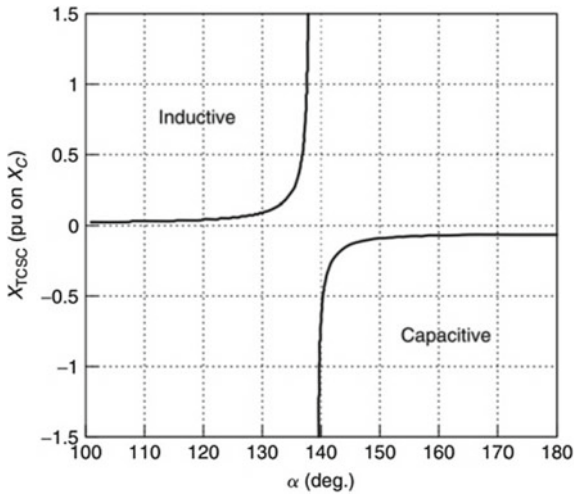

Fig. 2 TCSC fire angle characteristics [10]

where $k = \sqrt{\frac{X_c}{X_L}}$, $\beta = \pi - \alpha$, $X_L = \omega L$ is linear inductance and $X_C = \frac{1}{\omega C}$ is linear capacitance.

Operating range of firing angles for TCSC is from 90° to 180°. The operating region of the TCSC, capacitive or inductive, is decided by the firing angle.

3 Power-Flow Solution with TCSC Using Newton–Raphson

The power flow in TCSC from the transmission side to receiving side (bus 'a' to bus 'b'), can be formulated as:

$$S_{ab} = V_a I_{ab}^* = V_a Y_{ab}^* (V *_a - V_b^*) \tag{2}$$

$$Y_{ab}^* = \frac{1}{R_{ab} + j(X_{ab} - X_{\text{tcsc}})} = G_{ab} - j B_{ab} \tag{3}$$

The equations for power flow at the sending bus are formulated as:

$$P_a = V_a V_b B_{ab} \sin(\theta_a - \theta_b) \tag{4}$$

$$Q_a = -V_a^2 B_{aa} - V_a V_b B_{ab} \cos(\theta_a - \theta_b) \tag{5}$$

Similarly, the equations at the receiving side are given as:

$$P_b = V_b V_a B_{ab} \sin(\theta_b - \theta_a) \tag{6}$$

$$Q_b = -V_b^2 B_{bb} - V_b V_a B_{ba} \cos(\theta_b - \theta_a) \tag{7}$$

where

$V_a \angle\theta_a$ = Voltage at bus 'a'

$V_b \angle\theta_b$ = Voltage at bus 'b'

$B_{ab}\theta$ = maginary part of (a, b)th element of Y bus

Newton–Raphson method uses linear approximation in each subsequent iteration to determine the next value of the unknown variable. If TCSC is incorporated in the line between two PQ buses 'a' and 'b,' then following expression gives the Newton–Raphson power-flow equation with TCSC:

$$\begin{bmatrix} \frac{\partial P_a}{\partial V_a} & \frac{\partial P_a}{\partial \theta_a} & \frac{\partial P_a}{\partial V_b} & \frac{\partial P_a}{\partial \theta_a} & \frac{\partial P_a}{\partial \alpha} \\ \frac{\partial Q_a}{\partial V_a} & \frac{\partial P_a}{\partial \theta_a} & \frac{\partial Q_a}{\partial V_b} & \frac{\partial Q_a}{\partial \theta_a} & \frac{\partial P_a}{\partial \alpha} \\ \frac{\partial P_b}{\partial V_a} & \frac{\partial P_a}{\partial \theta_a} & \frac{\partial P_b}{\partial V_b} & \frac{\partial P_b}{\partial \theta_b} & \frac{\partial P_b}{\partial \alpha} \\ \frac{\partial Q_b}{\partial V_a} & \frac{\partial P_b}{\partial \theta_a} & \frac{\partial Q_b}{\partial V_b} & \frac{\partial Q_b}{\partial \theta_b} & \frac{\partial Q_b}{\partial \alpha} \\ \frac{\partial P_{ab}}{\partial V_a} & \frac{\partial P_{ab}}{\partial \theta_a} & \frac{\partial P_{ab}}{\partial V_b} & \frac{\partial P_{ab}}{\partial \theta_b} & \frac{\partial P_{ab}}{\partial \alpha} \end{bmatrix} \begin{bmatrix} \Delta V_a \\ \Delta \theta_a \\ \Delta V_b \\ \Delta \theta_b \\ \Delta \alpha \end{bmatrix} = \begin{bmatrix} \Delta P_a \\ \Delta Q_a \\ \Delta P_b \\ \Delta Q_b \\ \Delta P_{ab} \end{bmatrix} \tag{8}$$

When the mismatch between the calculated and scheduled values is within the specified range of tolerance, the algorithm stops.

4 Results

The suggested TCSC model has been implemented and examined using IEEE 14- and IEEE 300-bus test systems. The performance of these systems has been studied and monitored. In all the case studies, the value of k has been taken to be equal to 2.88 (SLATT TCSC, USA.).

4.1 IEEE 14-Bus Test System

Figure 3 shows the connections between buses in the IEEE 14-bus system. First, the basecase power flow for all the lines of the bus system is calculated without TCSC. Depending on the values of the basecase powers and the rate of convergence, a line is chosen from the system where TCSC is incorporated.

TCSC is incorporated between the buses 3 and 4. The system requires 5 iterations to converge to the final value with an error equal to 1e−16. The TCSC parameters used in calculations and the results obtained for line 3–4 are summarized in Table 1.

The voltage profile of the IEEE 14-bus with and without TCSC placed in between the buses 3 and 4 are given in Fig. 4a, b, respectively.

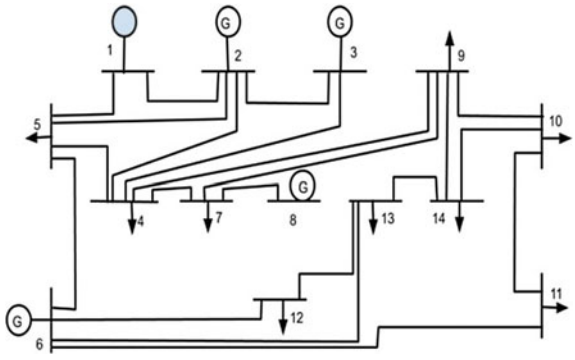

Fig. 3 IEEE 14-bus system

Table 1 TCSC parameters and results for IEEE 14-bus system

Initial value of X_{TCSC} (Ω)	Basecase real power (p.u.)	Capacitance reactance X_C (p.u.)	Active power with TCSC (p.u.)	Firing angle value obtained	Increase in voltage at bus 4 (%)
−0.629	0.447	0.5	0.7	157°	4.5

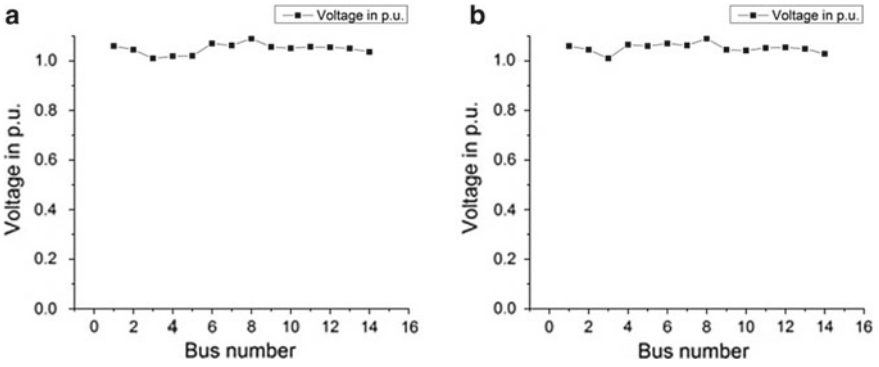

Fig. 4 **a** Variation in voltage with bus number (without TCSC). **b** Variation in voltage with bus number (TCSC in line 3–4)

4.2 IEEE 300-Bus Test System

The same procedure is followed in calculating the real powers, for all the lines before and after incorporating TCSC, for IEEE 300-bus as was done for IEEE 14-bus system. TCSC is incorporated between the buses 16 and 36. The system requires 15 iterations to converge to the final value with an error equal to 1e−7. The TCSC parameters and the results for line 16–36 are summarized in Table 2.

The voltage profile of the IEEE 14-bus with and without TCSC placed in between the buses 16 and 36 are given in Fig. 5a, b, respectively.

Table 2 TCSC parameters and results for IEEE 300-bus system

Initial value of X_{TCSC} (Ω)	Basecase real power (p.u.)	Capacitance reactance X_C (p.u.)	Active power with TCSC (p.u.)	Firing Angle value obtained	Increase in voltage at bus 36 (%)
−1.410	0.3	0.15	0.42	156°	0.71

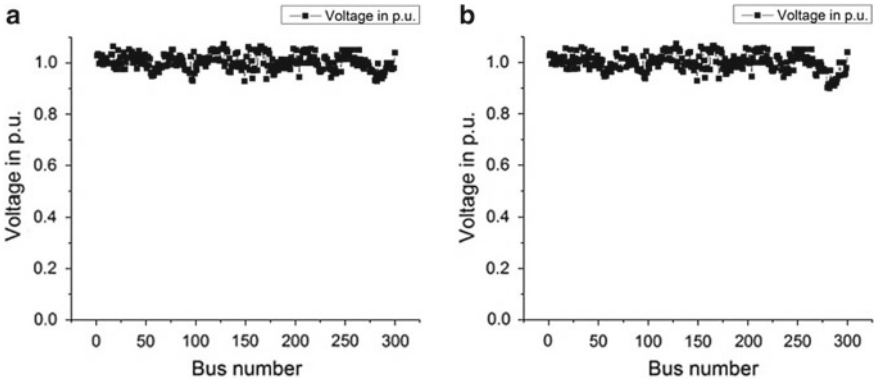

Fig. 5 **a** Variation in voltage with bus number (without TCSC). **b** Variation in voltage with bus number (TCSC in line 16–36)

5 Conclusion

We have presented an efficient firing angle-based Newton–Raphson model of the TCSC. The presented work enlightens on a clear choice in placing the TCSC optimally in the given bus systems. Also, it offers the range of increase in power flowing through the chosen line while operating the TCSC in the vernier capacitive mode. However, the limit constraint violations of the TCSC have not been considered. Hence, further investigations are obligatory in order to take it to the experimental phase. The proposed model has been implemented in the IEEE 14- and 300-bus test systems. It can similarly be used for other bus systems. The quadratic convergence of the Newton–Raphson algorithm is validated by the results.

References

1. Advanced Solutions in Power Systems: HVDC, FACTS, and Artificial Intelligence. Wiley (2016)
2. Sen: Improvement of System Performances Using FACTS and HVDC. Electricity Pricing (2014)
3. Wang, X., Song, Y.H., Lu, Q., Sun, Y.Z.: Optimal allocation of transmission rights in systems with FACTS devices. IEE Proc. G.T.D. **149**(3), 359–366 (2002)
4. Zhang, X.-P., Rehtanz, C., Pal, B.: Flexible AC Transmission Systems: Modelling and Control. Springer Science and Business Media LLC (2012)
5. Tiwari, R., Niazi, K.R., Gupta, V.: Variable series impedance model of a unified power flow controller for load flow analysis. Electr. Power Comp. Syst. (2011)
6. Johnson, B.K.: Design of TCSC for classroom and research applications on an analog model power system. In: 2006 IEEE Power Engineering Society General Meeting (2006)
7. Luor, T.-S., et al.: Application of Thyristor-Controlled series compensators to enhance oscillatory stability of a longitudinal power system. IEEE Trans. Power Syst. **14**

8. Sreejith, S., Simon, S.P., Selvan, M.P.: Power flow analysis incorporating firing angle model based TCSC. In: 2010 5th International Conference on Industrial and Information Systems (2010)
9. Nair, N.-K.C.: Incorporating TCSC into the voltage stability constrained OPF formulation. In: IEEE Power Engineering Society Summer Meeting PESS-02 (2002)
10. Mohan Mathur, R., Verma, R.K.: Thyristor-Based FACTS Controllers for Electrical Transmission Systems. Wiley (2002)
11. Vijayvargia, A., Jain, S., Meena, S., Gupta, V., Lalwani, M.: Comparison between different load flow methodologies by analyzing various bus systems. Int. J. Electr. Eng. **9**(2) (2016)
12. Singh, S.N.: Optimal location of FACTS devices for congestion management. Electr. Power Syst. Res. 0621 (2001)
13. Fuerte-Esquivel, C.R., Acha, E., Ambriz-Pervez, H.: A thyristor controlled series compensator model for the power flow solution of practical networks. IEEE Trans. Power Syst. **15** (2000)

Impact of Responsive Demand Scheduling on Optimal Operation of Smart Reconfigurable Distribution System

Tanuj Rawat, K. R. Niazi, Nikhil Gupta, and Sachin Sharma

Nomenclature

Indices	
n, m	Node index
br	Branch index
t	Time index
Parameters	
N	Total nodes
N_{br}	Total branches
T	Total number of time intervals
ρ_t	Retail tariff
$\gamma_{n,t}^{\max}$	Maximum demand flexibility
$V^{\min}/V^{\max}$	Minimum/maximum voltage
R_{br}	Resistance of branch br
P^{gridmax}	Substation active power limit
Q^{gridmax}	Substation reactive power limit
Y_{mn}	Admittance
$P_{n,t}^{\text{BDR}}$	Active demand before DR
Variables	
$P_{n,t}^{\text{DR}}$	Active demand after DR
$\gamma_{n,t}$	Demand flexibility
δ	Average load demand
$I_{br,t}$	Current through branch
$V_{n,t}$	Voltage magnitude
$\mu_{n,t}$	Phase angle of voltage
$\theta_{mn,t}$	Admittance phase angle
$P_{n,t}^{\text{inj}}/Q_{n,t}^{\text{inj}}$	Active/reactive power injected
P_{loss}	Power loss

T. Rawat (✉) · K. R. Niazi · N. Gupta · S. Sharma
Malaviya National Institute of Technology, Jaipur, India
e-mail: tanujsometime@gmail.com

O. H. Gupta and V. K. Sood (eds.), *Recent Advances in Power Systems*, Lecture Notes in Electrical Engineering 699, https://doi.org/10.1007/978-981-15-7994-3_11

1 Introduction

Due to scarcity of fossil fuels, environmental problems and rising load demand, the traditional distribution network is unfolding into a modern smart distribution network. The smart distribution system will have bulk of innovative products and technologies. In this regard, two key components of smart distribution system are demand response (DR) and automated distribution feeder reconfiguration (DFR). The DR aims to reduce the stress on grid by modifying the energy consumption pattern of an electric utility customer. Moreover, integration of DR will also provide an opportunity for customers to reduce their electricity consumption bill [14]. Furthermore, using remote-controlled switches DFR can be implemented which results in flexible automated networks [16]. Therefore, the participation of DR with DFR will enhance the operational quality of distribution system.

In recent years, large number of work is reported in the literature investigating the impact of DR on operation of grid. Effect of customer's participation rate in emergency DR programs on peak demand reduction and operation cost is studied in [6]. Impact of various price-based and incentive-based DR programs on techno-economic performance of smart distribution company is detailed in [13]. DR programs are modeled using customer benefit function and price elasticity in [6, 13]. A dual-objective-based approach coordinated by DR aggregator for scheduling of responsive demand in distribution system is presented in [9]. A two-layer interactive framework based on mixed-integer second-order cone approach for demand-side management in distribution system is reported in [12]. The authors have addressed both economic concern of customers and technical performance of network while carrying out scheduling of responsive demand in [9, 12]. However, role of DFR is not investigated in [6, 9, 12, 13].

Combined impact of multi-period DR based on hourly pricing and critical peak pricing, and DFR on operation of distribution network is studied in [5]. A model for simultaneous scheduling of incentive-based DR based on responsive load economic model and DFR to minimize operation cost of grid is presented in [4]. A framework for scheduling of hourly DFR and responsive loads for a distribution network in the presence of different price-based DR actions is reported in [3]. Multi-objective optimization approach for DFR in existence of time of use (TOU)-based DR is investigated in [7]. Impact of DR services based on responsive load model in reducing operation cost and energy losses of a distribution system with effect of DFR is explored in [1]. However, the capability of DFR in enhancing the operation of distribution network in the presence of responsive demand scheduling from viewpoint of customers and network operator has not been reported.

Therefore, the main contribution of this work is to investigate the impact of responsive demand scheduling carried out from perspective of only customers, only network operator and both customers and network operator simultaneously on reconfigurable distribution system. Toward this goal, a two-layer optimization framework is proposed in this paper. In the first layer, scheduling of responsive demand is performed for both individual and simultaneous optimizations of customer and network opera-

tor's objective. The objective function considered from customers and network operator's perspective is minimization of energy consumption cost and load variance of network's load profile, respectively. In the second layer, DFR is implemented with the modified load profile obtained from first layer to optimize energy losses. For simultaneously minimizing the objectives of customers and network operator, the problem is modeled as a multi-objective optimization. The developed multi-objective model is solved using augmented ϵ-constraint method, and the trade-off solution is evaluated using fuzzy satisfying technique.

2 Problem Formulation

2.1 First Layer

In the first layer of the proposed two-layer optimization mechanism, the base demand profile is modified by shifting responsive demands of distribution system using load shifting DR strategy. The responsive demand is shifted to minimize either energy payments or load variance of distribution system or both the objectives simultaneously.

Minimize electricity payments Due to integration of DR in distribution system, the customers will be billed based on time-varying tariff structure, such as TOU. The customers would prefer to make economic benefits by shift responsive demands when the prices are high- to low-price periods. Therefore, in this case, the shifting of responsive demand is carried out to minimize customer's electricity payments. It is mathematically expressed as:

$$\text{Min} \sum_{t=1}^{T} \sum_{n=1}^{N} P_{n,t}^{\text{DR}} \times \rho_t \tag{1}$$

Minimize load variance The interest of system operator is to shift the responsive demand such that performance of the distribution network is enhanced and an infrastructure investment is delayed/avoided. The cost of capital expenditure and energy losses can be reduced by minimizing the peak load in a distribution network. Similarly, network asset utilization can be improved by filling valley in the load curve. Therefore, from the viewpoint of system operator, the objective is to schedule responsive demands such that load variance is minimized, which is evaluated as [10]:

$$\text{Min} \frac{1}{T} \sum_{t=1}^{T} \left(\sum_{n=1}^{N} P_{n,t}^{\text{DR}} - \delta \right)^2 \tag{2}$$

where

$$\delta = \frac{1}{T} \sum_{t=1}^{T} \sum_{n=1}^{N} P_{n,t}^{\mathrm{DR}} \tag{3}$$

The objective function in Eqs. (1) and (2) is subjected to the following constraints [12]:

$$P_{n,t}^{\mathrm{DR}} = P_{n,t}^{\mathrm{BDR}} \times \gamma_{n,t} \quad \forall n, \forall t \tag{4}$$

$$\sum_{t=1}^{T} P_{n,t}^{\mathrm{DR}} = \sum_{t=1}^{T} P_{n,t}^{\mathrm{BDR}} \quad \forall n \tag{5}$$

$$(1 - \gamma_{n,t}^{\max}) \leq \gamma_{n,t} \leq (1 + \gamma_{n,t}^{\max}) \quad \forall n, \forall t \tag{6}$$

After DR, active demand is calculated using Eq. (4). Equation (5) ensures that one day energy consumption remains constant. Demand flexibility will be restricted by its minimum and maximum limits as shown by constraint (6).

2.2 Second Layer

In the second layer, DFR is performed to improve the performance of distribution system. It is important to note that while carrying out DFR the modified load profile of distribution system as obtained from first layer is utilized. The objective of DFR is to determine radial topology of distribution which results in minimum energy losses. The objective for DFR is expressed as [16]:

$$\text{Min } P_{\mathrm{loss}} = \sum_{t=1}^{T} \sum_{\mathrm{br}=1}^{N_{\mathrm{br}}} I_{br,t}^{2} \times R_{\mathrm{br}} \tag{7}$$

The objective in Eq. (7) is subjected to radiality constraint which is adopted from [16]. In addition, power balance constraints (8 and 9), voltage and angle constraint of slack node (10), substation active and reactive power limits (11 and 12) and node voltage limits (13) should also be ensured.

$$P_{n,t}^{\mathrm{inj}} = \sum_{m=1}^{N} \mid V_{n,t} \mid\mid V_{m,t} \mid\mid Y_{mn} \mid \cos\left(\theta_{mn,t} + \mu_{m,t} - \mu_{n,t}\right) \quad \forall n, \forall t \tag{8}$$

$$Q_{n,t}^{\mathrm{inj}} = \sum_{m=1}^{N} \mid V_{n,t} \mid\mid V_{m,t} \mid\mid Y_{mn} \mid \sin\left(\theta_{mn,t} + \mu_{m,t} - \mu_{n,t}\right) \quad \forall n, \forall t \tag{9}$$

$$V_{n,t} = 1, \ \mu_{n,t} = 0 \ \text{ if } n = \text{slack bus} \tag{10}$$

$$P_{n,t}^{\text{grid}} \leq P^{\text{gridmax}} \quad \forall n, \forall t \tag{11}$$

$$Q_{n,t}^{\text{grid}} \leq Q^{\text{gridmax}} \quad \forall n, \forall t \tag{12}$$

$$V^{\min} \leq V_{n,t} \leq V^{\max} \quad \forall n, \forall t \tag{13}$$

3 Numerical Simulation

The proposed two-layer framework is investigated on 33-bus radial distribution system. Details of this test system are available in [2]. The TOU price structure is adopted from [9]. The participation rate of responsive demand is taken as 30% [9]. The input parameter such as maximum and minimum voltage limits, and branch current limits is adopted from [12]. The joint optimization of customer energy payment and load variance of network in the first layer is formulated as a multi-objective model and solved using an augmented ϵ-constraint method [8], and the trade-off solution is obtained using fuzzy min–max satisfying criteria [11]. The optimizations of first stage are solved using CPLEX 12.8.0, while DFR in the second stage is handled using genetic algorithm [15].

In this study, the following three scenarios are considered.

- Scenario 1 (S1): In this scenario, responsive demand of customers is shifted such that customer's energy cost is minimized.
- Scenario 2 (S2): In this scenario, demand of customers which participate in DR is shifted so as to minimize load variance of network.
- Scenario 3 (S3): In this scenario, the responsive demand of customers is scheduled to simultaneously minimize the customer electricity cost and load variance of distribution system.

For comparative purpose, a base case, without any responsive demand, is also considered.

In the base case, the customer payment and load variance are Rs 266489.30 and 1.037×10^7 kWsq, respectively. The results of single-objective optimization for S1 and S2 are presented in Table 1. It is observed that as compared to base case the customer payment is reduced by 6.73% along with 3.18% reduction in load variance in S1. Similarly, the load variance is improved by 5.08% and customer's cost is reduced by 4.03% in S2 in comparison with base case. It can be noted from the table that enhancement in one objective function degrades the value of other objective function. Therefore, the two objectives are contradictory and a single solution which optimizes both customer's energy cost and load variance does not exist. In this regard, multiple trade-off solutions are obtained under S3 using augmented ϵ-constraint approach. The Pareto-solutions when both customer's energy cost and load variance are minimized simultaneously are depicted in Fig. 1. The most compromising solution is

Table 1 Comparison of objective functions for S1 and S2

	Customer's cost (Rs)	Load variance (kWsq)
Customer's cost (Rs)	248554.50	1.004×10^7
Load variance (kWsq)	255783.30	9.768×10^6

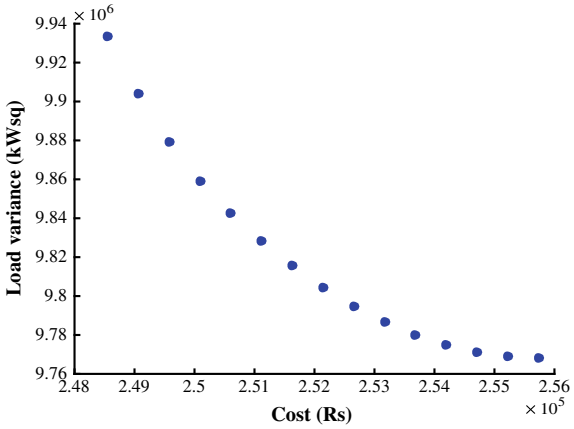

Fig. 1 Pareto-solutions

Table 2 Compromising solution

Customer's cost (Rs)	Load variance (kWsq)
251633.30	9.8156×10^6

shown in Table 2. The customer payment and load variance are reduced by 5.57% and 5.34% in comparison with base case. Thus, in comparison with S1 and S2, the best compromising solution obtained in S3 represents good performance with respect to both the objectives.

The variation of load profiles of distribution network for each Pareto solution is shown in Fig. 2. The peak demand is reduced by 10.81%, 30% and 30% in S1, S2 and S3, respectively, in comparison with base case. In S1, demand is shifted in the time intervals in which the prices are less to minimize the electricity bill of customers. In S2, the responsive demand is shifted from peak demand periods to time intervals when demand is less. Consequently, load profile in this scenario results in both peak shaving and valley filling. It is worth noting that the load profile obtained in S3 falls in between load profiles of S1 and S2. Subsequently, both the objectives get benefit and remain close to their optimal values.

The energy losses of distribution network under the three scenarios without DFR and with DFR are shown in Table 3. In comparison with base case, without DFR the losses are reduced by 9.56%, 13.09% and 12.10% in S1, S2 and S3, respectively. The

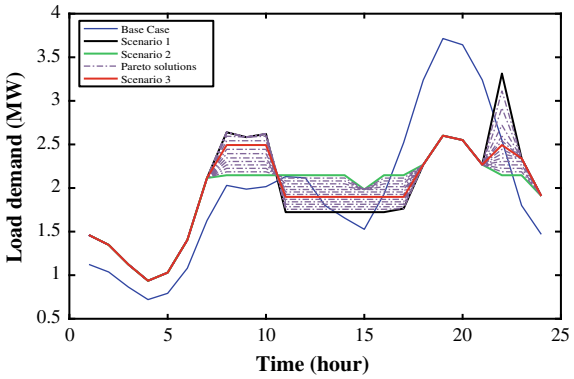

Fig. 2 Load profiles for different Pareto-solutions

Table 3 Comparison of energy losses (in kWh)

	Base case	S1	S2	S3
Without DFR	1512.40	1367.80	1314.40	1329.30
With DFR	–	961.40	925.90	935.90

losses are minimum in S2 when responsive demand is shifted to obtain a leveled load profile. The reduction in energy losses in S3 is improved considerably as compared with S1. Further, it is observed that application of DFR results in substantial reduction in losses. The application of DFR leads to 406.40 kW, 388.50 kW and 393.40 kW reduction in losses for S1, S2 and S3, respectively.

The minimum voltage obtained at each node for all three scenarios without and with DFR is shown in Fig. 3. For all three scenarios, the minimum voltage profile is significantly enriched as compared to base case. It is noted that the multi-objective optimization results in minimum voltage profile for S3 which overlaps with that of voltage profile of S2. The voltage profile is better in S2 as compared with S1 due load leveling objective function. Furthermore, the minimum voltage profile is improved for all scenarios after the application of DFR. The minimum voltage for S1, S2 and S2 is 0.9232 p.u, 0.9407 p.u and 0.9407 p.u. before DFR and 0.9449 p.u., 0.9572 p.u. and 0.9572 p.u. after the application of DFR. Therefore, DFR assists in reducing energy losses and enhancing voltage quality of the system.

4 Conclusions

This work presents a comparative study investigating the impact of responsive demand scheduling from viewpoint of customers and network operator on distribution system in the presence of DFR. The objective of customer and network operator

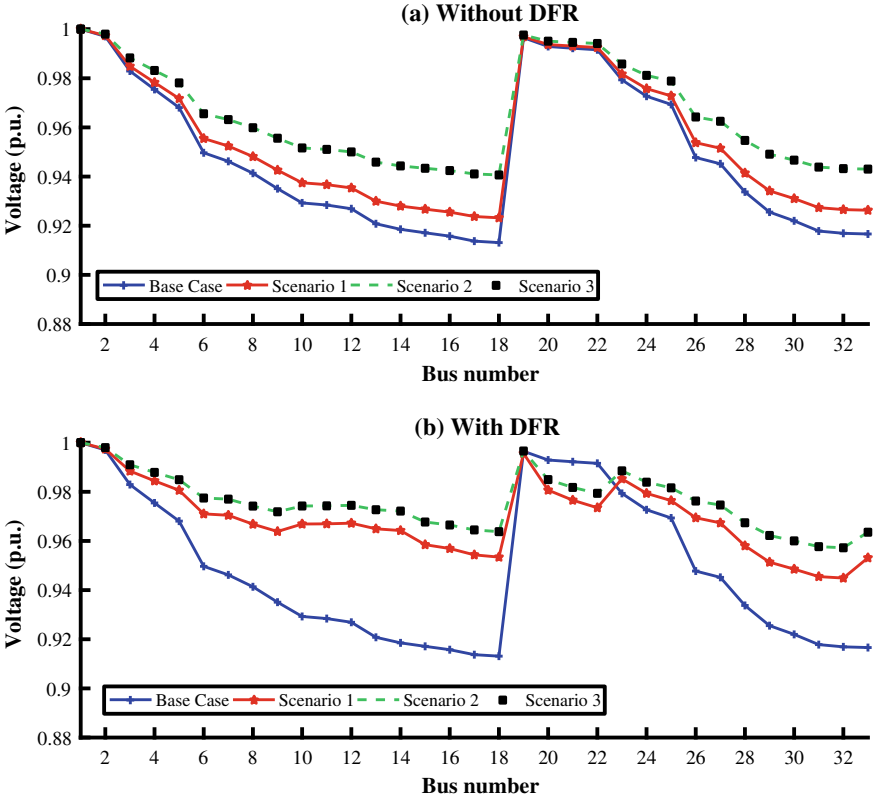

Fig. 3 Minimum voltage profile

is minimized individually and simultaneously, and the results are compared using a two-layer optimization framework. Simulation results show that the augmented ϵ-constraint method achieves the desired trade-off between energy consumption cost of customers and load variance of network. It is found that DR plays a vital role in enhancing the operation of grid. Further, it is also observed that DFR results in substantial improvement in minimum voltage level and energy losses of distribution system.

References

1. Ajoulabadi, A., Ravadanegh, S.N., Mohammadi-Ivatloo, B.: Flexible scheduling of reconfigurable microgrid-based distribution networks considering demand response program. Energy **196**, 117024 (2020)
2. Baran, M.E., Wu, F.F.: Network reconfiguration in distribution systems for loss reduction and load balancing. IEEE Power Eng. Rev. **9**(4), 101–102 (1989)

3. Esmaeili, S., Anvari-Moghaddam, A., Jadid, S., Guerrero, J.M.: Optimal simultaneous day-ahead scheduling and hourly reconfiguration of distribution systems considering responsive loads. Int. J. Electr. Power Energy Syst. **104**, 537–548 (2019)
4. Gazijahani, F.S., Salehi, J.: Integrated DR and reconfiguration scheduling for optimal operation of microgrids using Hong's point estimate method. Int. J. Electr. Power Energy Syst. **99**, 481–492 (2018)
5. Gutiérrez-Alcaraz, G., Tovar-Hernández, J., Lu, C.N.: Effects of demand response programs on distribution system operation. Int. J. Electr. Power Energy Syst. **74**, 230–237 (2016)
6. Imani, M.H., Niknejad, P., Barzegaran, M.: The impact of customers' participation level and various incentive values on implementing emergency demand response program in microgrid operation. Int. J. Electr. Power Energy Syst. **96**, 114–125 (2018)
7. Jahani, M.T.G., Nazarian, P., Safari, A., Haghifam, M.: Multi-objective optimization model for optimal reconfiguration of distribution networks with demand response services. Sustain. Cities Soc. **47**, 101514 (2019)
8. Mavrotas, G.: Effective implementation of the ε-constraint method in multi-objective mathematical programming problems. Appl. Math. Comput. **213**(2), 455–465 (2009)
9. Panwar, L.K., Konda, S.R., Verma, A., Panigrahi, B.K., Kumar, R.: Demand response aggregator coordinated two-stage responsive load scheduling in distribution system considering customer behaviour. IET Gener. Transm. Distrib. **11**(4), 1023–1032 (2017)
10. Rawat, T., Niazi, K.R., Gupta, N., Sharma, S.: Impact assessment of electric vehicle charging/discharging strategies on the operation management of grid accessible and remote microgrids. Int. J. Energy Res. **43**(15), 9034–9048 (2019)
11. Rawat, T., Niazi, K.R.: Comparison of EV smart charging strategies from multiple stakeholders' perception. J. Eng. **2017**(13), 1356–1361 (2017)
12. Rawat, T., Niazi, K., Gupta, N., Sharma, S.: A two stage interactive framework for demand side management in smart grid. In: 2019 IEEE 16th India Council International Conference (INDICON), pp. 1–4. IEEE, New York (2019)
13. Sadati, S.M.B., Moshtagh, J., Shafie-khah, M., Catalão, J.P.: Smart distribution system operational scheduling considering electric vehicle parking lot and demand response programs. Electr. Power Syst. Res. **160**, 404–418 (2018)
14. Safdarian, A., Degefa, M.Z., Lehtonen, M., Fotuhi-Firuzabad, M.: Distribution network reliability improvements in presence of demand response. IET Gener. Transm. Distrib. **8**(12), 2027–2035 (2014)
15. Singh, J., Tiwari, R.: Cost benefit analysis for v2g implementation of electric vehicles in distribution system. IEEE Trans. Industry Appl. pp. 1–1 (2020)
16. Singh, J., Tiwari, R.: Real power loss minimisation of smart grid with electric vehicles using distribution feeder reconfiguration. IET Gener. Transm. Distrib. **13**(18), 4249–4261 (2019)

Optimal Sharing of Real Power Using Robust Controller in Multi-terminal DC Systems

Himanshu Singh, Suyash Singh, Sheetla Prasad, and Lokesh Garg

1 Introduction

A high voltage DC system is used to transmit power to large distances. Due to continuous increase in power demand, the grid system stability and power quality are a challenging task. So, multi-terminal DC grids are used to provide a meshed-type interconnection between powers generating stations and far control areas where electricity is required. It is also helpful in maintaining the reliability between AC and DC system networks [1, 2]. Hence, multi-terminal DC grids can be used to make system economical and increase its efficiency through transmitting power using terminal converter controls. The execution of a transmission line in effective way depends on both converter and its controllability. Due to two degrees of freedom, VSC-MTDC can operate individually in the active control mode or reactive power control mode and both simultaneously. Thus, VSC-MTDC transmission network is enhanced to control easily its capability, stability, and its feasibility of wind farm integration with networks.

A current sharing on each terminal in MTDC system plays an important role to stabilize DC power flow, and it is achieved through a current sharing technique [3]. The current sharing control scheme has the ability to share voltages and power on all terminals with minimum oscillations in LCC MTDC. To increase a MTDC system operation flexibility region, the frequency droop control strategy developed and analyzed its interaction with AC grid through two cases isolated and interconnected to grid [4, 5]. The performance of VSC-MTDC is reduced due to unknown and uncertainties in distributed power generation systems and becomes a challenging task. Hence, several coordinated control schemes were developed to enhance DC voltage

H. Singh · S. Singh · S. Prasad (✉) · L. Garg
School of Electrical, Electronics and Communication Engineering, Galgotias University, Delhi-NCR, India
e-mail: sheetla.prasad@galgotiasuniversity.edu.in

O. H. Gupta and V. K. Sood (eds.), *Recent Advances in Power Systems*, Lecture Notes in Electrical Engineering 699, https://doi.org/10.1007/978-981-15-7994-3_12

and power characteristics operation regions [6–9]. A back-step control approach is used to regulate DC voltage and real power operating region through Lyapunov approach in [10]. A model predictive control approach is applied on VSC-MTDC system to adjust the gains of droop controllers against variation in DC power flow as described in [11]. In converter droop control mode, a control strategy is proposed to modulate power reference and enhanced power sharing capability in VSC-MTDC system even in the presence of variations [12]. Thus, real power and DC voltage distribution on different terminals in MTDC system with minimum oscillations in power and voltage profile are a formidable task to researchers.

To control and dynamic analysis of VSC-MTDC, it is linearized through small-signal approach in the presence of small perturbation [13, 14] due to the slow convergence rate and its large time constant. The advancement in control strategy and its necessity in the MTDC system is discussed in [15, 16] based on international power markets. A linear-quadratic model Gaussian control strategy is designed to reduced system dynamics oscillations against variations and called power oscillation damping controller in embedded VSC-MTDC system [17]. Critical values of VSC-MTDC system are also tuned using model linear quadratic Gaussian controller approach even in the presence of small disturbances [18]. Hence, linear quadratic Gaussian applied and used to improve system dynamics in several engineering fields for its simplicity and applicability.

In this study, a linear matrix inequality (LMI)-based linear-quadratic regulator control strategy is made for five terminal VSC-MTDC distribution networks [19]. The proposed controller aims to distribute and minimize the oscillations in real terminal power and terminal voltages in the presence of power demand variation. The proposed controller weight matrices are tuned and calculated using LMI tool framework. The stability convergence of the proposed controller proves using Lyapunov theorem. The performance of the proposed strategy enhances in terms of time response characteristics and its applicability.

Remaining segments of the present study are arranged as: Five terminal VSC-MTDC is represented in state-space dynamics in Sect. 2, trailed by proposed control strategy structure for mentioned five terminal VSC-MTDC systems under Sect. 3 followed by detailed closed-loop stability is analyzed in Sect. 3. The simulated result analysis of the proposed controller is done in Sect. 4. Conclusion is lastly drained from the illustrated work done which is given in Sect. 5.

2 System Description

In presence of small perturbation, the VSC-MTDC system is linearized due to its large time constant and represented in state-space dynamics approach [19–21]. Hence, the linearized state-space representation is sufficient to analyze for five terminal VSC-MTDC system and given in Fig. 1a. The two terminals of VSC-MTDC are operated in constant power zone (terminal-3 and terminal-5), and rest terminals are operated in DC voltage drop control zone with fix drop constant, respectively. The

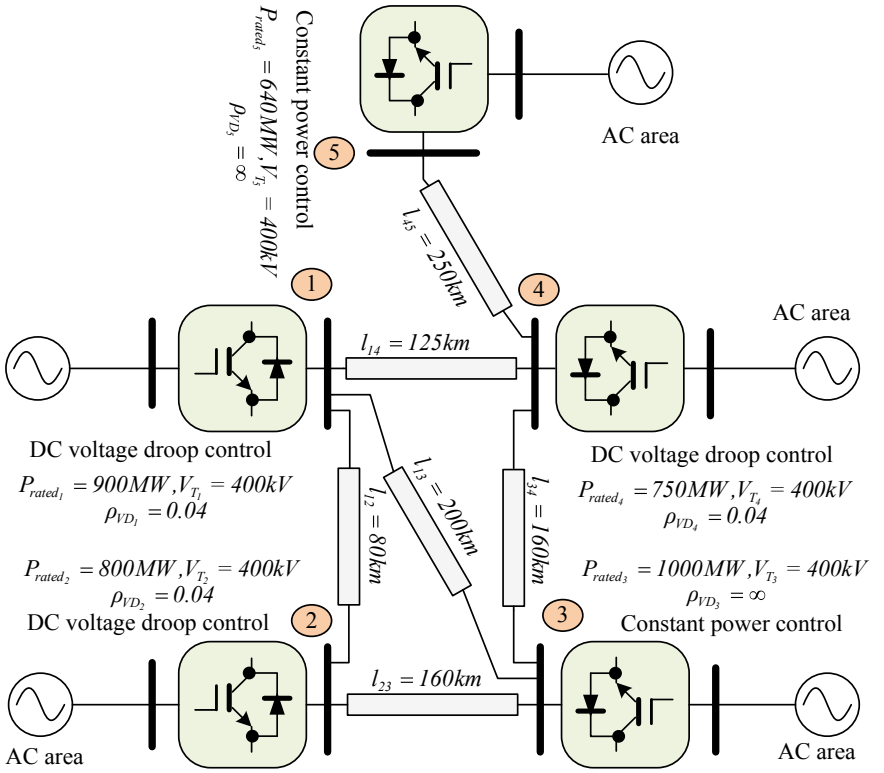

a) Schematic representation of five terminal MTDC System

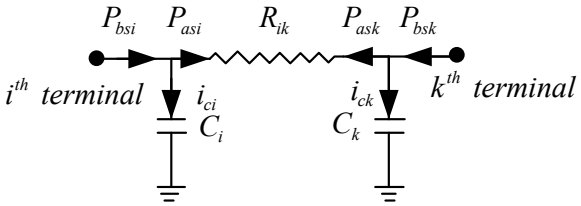

b) DC resistive equivalent network between i^{th} terminal and j^{th} terminal

Fig. 1 MTDC system representation and its equivalent circuit

bipolar DC transmission lines are represented in π-network with its resistance and capacitance, and negligible inductance. The value of DC transmission line resistance and all capacitance is 0.01 Ω/km and 5.0 μF/km, respectively. The *i*th terminal shunt capacitance $C_i = C_{fi} + C_{li}$ is represented as summation of DC filter capacitance C_{fi} and transmission line capacitance C_{li} and also represented in Fig. 1b. The *i*th terminal power flow equation is written as:

$$P_{bsi} - P_{asi} = V_i * i_{ci} = V_i C_i \frac{\mathrm{d}V_i}{\mathrm{d}t} \tag{1}$$

Apply small variation in signal and it becomes:

$$P_{bsi} - P_{bsi}^0 + P_{asi}^0 - P_{asi} = V_i^0 C_i \frac{\mathrm{d}(V_i^0 + V_i)}{\mathrm{d}t} = V_i^0 C \frac{\mathrm{d}V_i}{\mathrm{d}t} \tag{2}$$

At steady state, Eq. (2) simplifies as:

$$\Delta \dot{V}_i = \frac{\Delta P_{bsi} - \Delta P_{asi}}{V_i^0 C_i} = F_i(\Delta P_{bsi} - \Delta P_{asi}) \tag{3}$$

where $F_i = \left(V_i^0 C_i\right)^{-1}$

From Fig. 1b, the power flow is written as:

$$\Delta P_{asi} = P_{asi} - P_{asi}^0 \tag{4}$$

In DC resistive network, the change in power with respect to voltage can be represented with DC Jacobian matrix as:

$$J_{\mathrm{DC}i} = \frac{\partial P_{asi}}{\partial V_i} \tag{5}$$

From Eqs. (3), (4), and (5), it gives:

$$\Delta \dot{V}_i = F_i \Delta P_{bsi} - F_i J_{\mathrm{DC}i} \Delta V_i \tag{6}$$

The complete control dynamic characteristics of VSC-MTDC system [19] can be written as:

$$\Delta \dot{P}_{bsi} = a\Delta P_{bsi} + (b + cJ_{\mathrm{DC}i})\Delta V_i + d\Delta P_{bsi}^{\mathrm{ref}} + e\Delta V_i^{\mathrm{ref}} \tag{7}$$

The DC terminal voltage $V = \begin{bmatrix} V_1 & V_2 & V_3 & V_4 & V_5 \end{bmatrix}^{\mathrm{T}}$ and the DC node power behind and after shunt capacitances are written as $\Delta P_{bs} = \begin{bmatrix} \Delta P_{bs1} & \Delta P_{bs2} & \Delta P_{bs3} & \Delta P_{bs4} & \Delta P_{bs5} \end{bmatrix}^{\mathrm{T}}$ and $\Delta P_{as} = \begin{bmatrix} \Delta P_{as1} & \Delta P_{as2} & \Delta P_{as3} & \Delta P_{as4} & \Delta P_{as5} \end{bmatrix}^{\mathrm{T}}$, respectively. The state-space representation for all five VSC-MTDC is simplified using Eqs. (6) and (7) as:

$$\begin{bmatrix} \Delta \dot{P}_{bs} \\ \Delta \dot{V} \end{bmatrix} = \begin{bmatrix} A_{11} & A_{12} \\ A_{21} & A_{22} \end{bmatrix} \begin{bmatrix} \Delta P_{bs} \\ \Delta V \end{bmatrix} + \begin{bmatrix} B_{12} \\ B_{22} \end{bmatrix} \Delta P_{bs}^{\mathrm{ref}} + \begin{bmatrix} B_{11} \\ B_{21} \end{bmatrix} \Delta V^{\mathrm{ref}} \tag{8}$$

where the system matrices are $A_{11} = \text{diag}(a)$, $A_{12} = \text{diag}(b) + \text{diag}(c)J_{\text{DC}}$, $A_{21} = \text{diag}(F)$, $A_{22} = -\text{diag}(F)J_{\text{DC}}$, $B_{11} = \text{diag}(d)$, $B_{12} = \text{diag}(e)$, $B_{21} = \text{diag}(0)$ and $B_{22} = \text{diag}(0)$, respectively.

The equivalent state-space representation of Eq. (8) can be written as:

$$\dot{x} = Ax + Bu + D\Delta P_{bs}^{\text{ref}} \tag{9}$$

where $x = \left[\Delta P_{bs}\ \Delta V\right]^{\text{T}}, u = \Delta V^{\text{ref}}$ are state variable, control DC reference voltage, and disturbance reference power, respectively.

3 Proposed Control Strategy and Its Convergence

The proposed controller design steps and convergence analysis are illustrated in this section. Due to its simple design steps and its wide applications, the linear quadratic regulator (LQR)-based controller has a significant role in state feedback approach. It can be represented easily through mathematical dynamics inequalities in terms of LMIs [22]. The performance of LQR control approach is evaluated and optimized linearly through a quadratic criterion function. The quadratic function is composed with state energy dynamics and required control signals. The quadratic function criteria are used to avoid mismatch between system state trajectory response speed and the strength of the maintained signals. For obtaining every system state, trajectory response time and strength of control signal u simultaneously define the quadratic function criteria as:

$$J_{\min} = \int_0^{\infty} \left(x^{\text{T}} Q\, x + u^{\text{T}} R\, u\right) \text{d}t \tag{10}$$

where $Q = Q^{\text{T}} > 0$ and $R = R^{\text{T}} > 0$ are basic tuned design parameters and both are positive definite matrices.

The weights value of matrix Q is used to punish system state trajectories convergence speed from any initial point, and similarly, weights value of matrix R is used to punish in terms of required control signals intensity. Thus, the choice of weight matrices Q and R can be only diagonal valued matrix or complete valued matrix is challenging task in MTDC systems. The schematic representation of the proposed controller structure is shown in Fig. 2.

The control law is described as:

$$u = -Kx \tag{11}$$

where K is state feedback gain matrix.

Proof Let a quadratic Lyapunov function

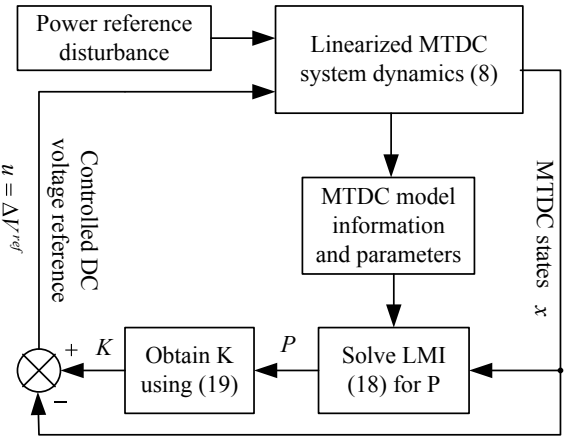

Fig. 2 Controller schematics representation

$$v = x^{\mathrm{T}} P x \tag{12}$$

Equations (10) and (12) are differentiated with respect to time. To obtain an optimal solution equate both dynamics using Eq. (11) as:

$$x^{\mathrm{T}}\big(Q + K^{\mathrm{T}} R K\big)x = -\frac{\mathrm{d}(x^{\mathrm{T}} P\, x)}{\mathrm{d}t} \tag{13}$$

Using Eq. (9) and after simplification, it gives

$$x^{\mathrm{T}}\big(Q + K^{\mathrm{T}} R K\big)x = -x^{\mathrm{T}}\big[(A - BK)^{\mathrm{T}} P + P(A - BK)\big]x - x^{\mathrm{T}} 2PD\Delta P_{bs}^{\mathrm{ref}} \tag{14}$$

$$x^{\mathrm{T}}\big[A^{\mathrm{T}} P + PA + Q - K^{\mathrm{T}} R K - K^{\mathrm{T}} B^{\mathrm{T}} P - PBK\big]x - x^{\mathrm{T}} 2PD\Delta P_{bs}^{\mathrm{ref}} < 0 \tag{15}$$

The term $-(K^{\mathrm{T}} R K + K^{\mathrm{T}} B^{\mathrm{T}} P + PBK) \cong -B^{\mathrm{T}} P R^{-1} PB$ is represented using [23], and Eq. (15) gives:

$$x^{\mathrm{T}}\big[A^{\mathrm{T}} P + PA + Q - B^{\mathrm{T}} R^{-1} PB\big]x - x^{\mathrm{T}} 2PD\Delta P_{bs}^{\mathrm{ref}} < 0 \tag{16}$$

Thus, to get $\dot{v} < 0$, Eq. (16) may be written in LMI [23] as:

$$\big[A^{\mathrm{T}} P + PA + Q - B^{\mathrm{T}} R^{-1} PB\big] < 0 \tag{17}$$

Hence, this proves the linear stability of the entire system.

However, the LMI Eq. (17) can be converted into LMI optimization framework as given:

Select P in such way that following LMIs holds simultaneously with minimum of $J_{\min}$.

$$P > 0$$
$$Q > 0$$
$$R > 0$$
$$(A^{\mathrm{T}}P + PA + Q - B^{\mathrm{T}}R^{-1}PB) < 0 \tag{18}$$

Then control law is defined as:

$$u = -R^{-1}PB\,x \tag{19}$$

Thus, this completes proof and optimization.

4 Results and Discussions

The designed control strategy is applied on five terminal MTDC system and demonstrated its performance through MATLAB© simulation. The proposed control strategy aims to distribute power against unpredictable nature of power demand disturbance and applied on five terminal MTDC systems [19, 20]. The five terminal MTDC system matrices and its parameters are given in [19, 20]. Three simulation scenarios are considered to define the effectiveness of the designed controlled scheme and described as:

1. *Step change in power demand at constant power terminal*
2. *Step change in power demand at fix voltage droop control terminal*
3. *Random difference in power demand at constant power terminal.*

The rating of five terminal MTDC systems is shown in Fig. 1.

4.1 Step Change in Power Demand at Constant Power Terminal

A step change in power reference of $\Delta P_{bs5}^{\mathrm{ref}} = -250$ MW at constant power terminal is given here. The total changes in nodal power and corresponding voltages of all five terminals are shown in Fig. 3. It is seen that the overshoot and undershoot at every terminal even in the presence of sudden change in power load demand with the proposed control scheme are completely removed. From the said figure, it is seen that the settling time is negligible and distributes power load demand accurately and the closed-loop system stability is improved. The proposed controller scheme is self-capable to eliminate oscillations and enhanced power reserve capacity of each terminal. The difference of power at terminal-3 is zero because of constant power operation mode.

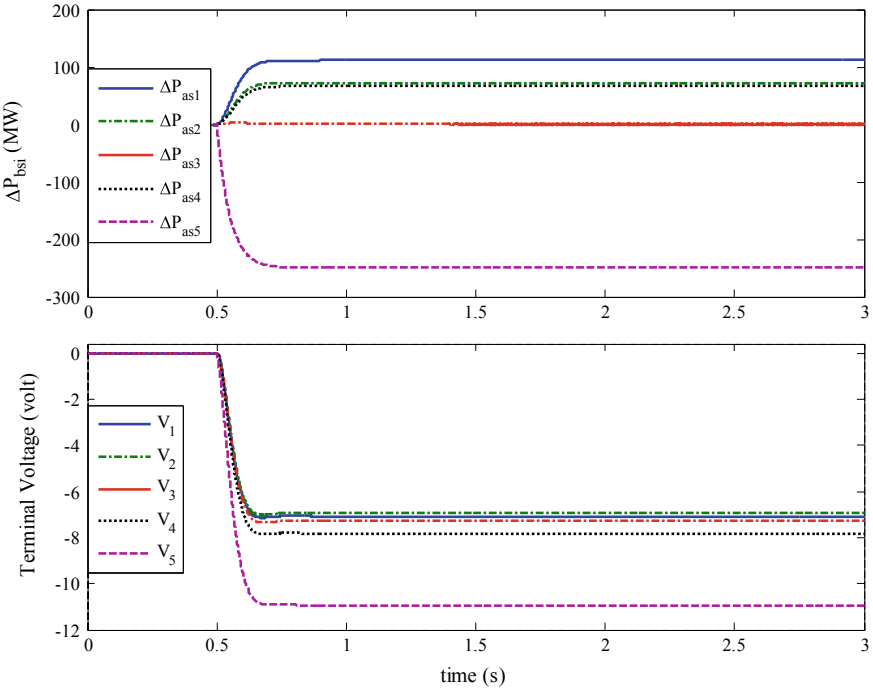

Fig. 3 MTDC system responses with the proposed controller against step change in power load demand at constant power terminal-5

4.2 Step Change in Power Demand on Fix Voltage Droop Control Terminal

In this subsection, a step change in power reference at terminal-2 $\Delta P_{bs2}^{\text{ref}} = 300$ MW is employed and terminal-2 is operated in DC voltage droop zone. The total changes in nodal power and corresponding voltages of all five terminals are shown in Fig. 4. The power distribution at terminal-3 and terminal-5 is operated in constant power mode. Hence, total power load demand is shared by other terminals smoothly. The change in voltages at each terminal is also changed smoothly. It is observed that the time responses of each terminal are improved even in the presence of load demand. The proposed controller scheme is self-capable to eliminate oscillations and enhanced power reserve capacity of each terminal.

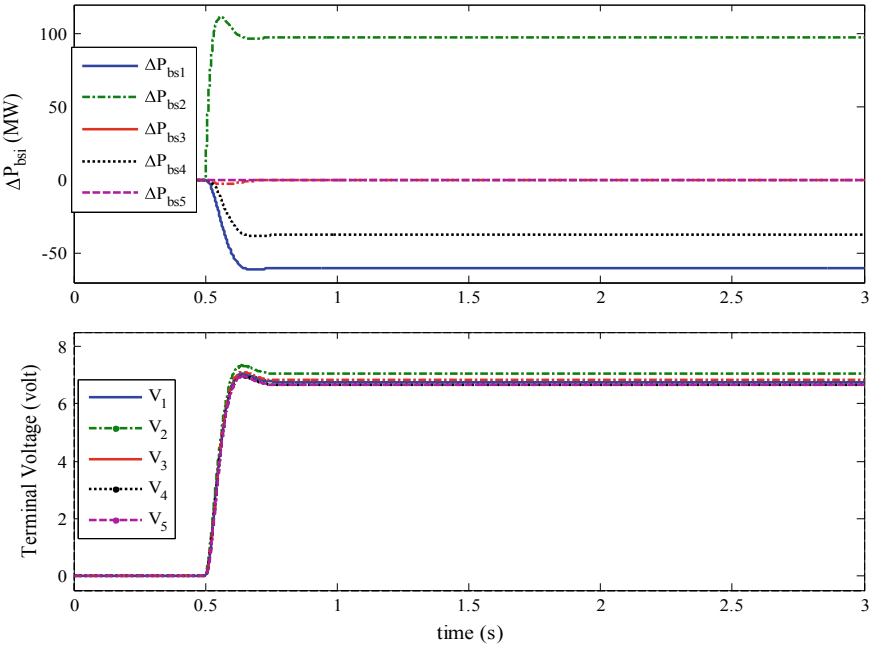

Fig. 4 MTDC system responses with the proposed controller against step change in power load demand at DC voltage droop terminal-2

4.3 Random Difference in Power Demand at Fix Power Terminal

In this subsection, an arbitrary power load demand is considered at each terminal in MW and given in Fig. 5. The deviation in power and voltage at each terminal are shown in Fig. 6 against random change in power load demand.

It can be seen that there is no change at constant power terminal-3 and terminal-5 when power load demand changed at other terminals. It is evident that the designed controller is able to minimize the oscillations with power load demand varying conditions. From said Fig. 6, it is seen that the settling time is negligible and distributes power load demand accurately and the closed-loop system stability is improved. Thus, terminal reserve power capacity is less affected.

5 Conclusion

In this study, a linear matrix inequality (LMI)-based linear quadratic regulator control strategy was designed for five terminal VSC-MTDC systems. The proposed controller was able to distribute and minimize the oscillations in real terminal power

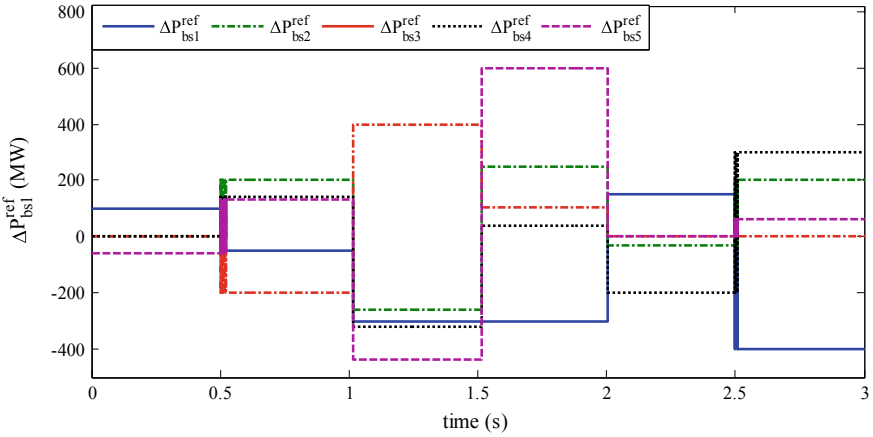

Fig. 5 Random power load demand at five terminals

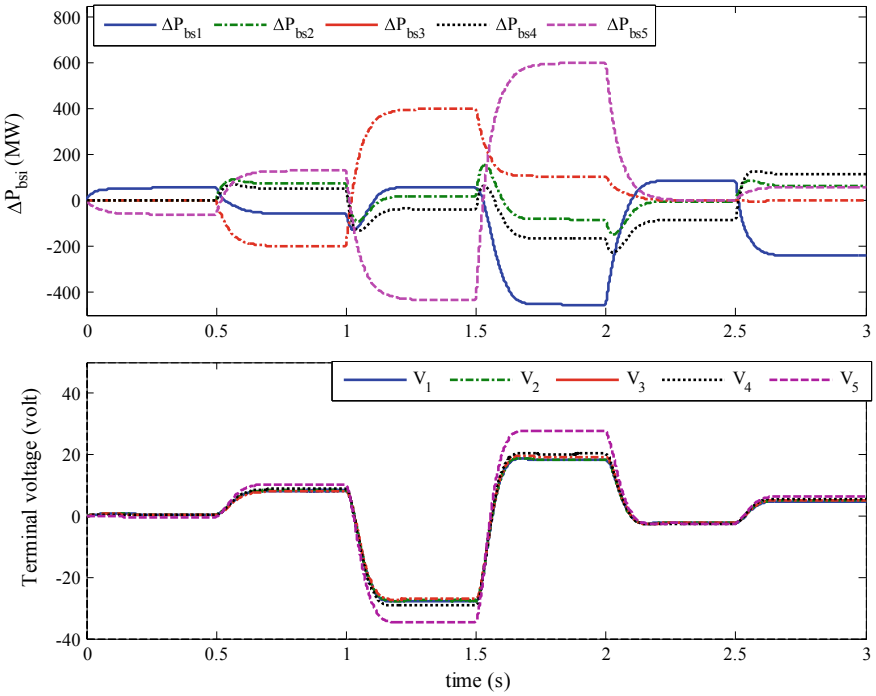

Fig. 6 MTDC system responses with the proposed controller against random reference power load demand

and terminal voltages in the presence of power load demand variations. The proposed controller weight matrices were tuned and calculated using LMI tool framework. The stability convergence of the proposed controller proved using Lyapunov theorem. The simulations are demonstrated on five terminal VSC-MTDC systems to illustrate effectiveness against step and random power load demand variations. The proposed controller was reduced to inject undesired oscillations in the grid and enhanced power system stability. The performance of the proposed strategy enhances in terms of time response characteristics and its applicability.

References

1. Mohan, M., Singh, B., Panigrahi, B.K.: Design, control, and modeling of a new voltage source converter for HVDC system. Int. J. Emerg. Electr. Power Syst. **14**(2), 123–138 (2013)
2. Zhang, L., Zou, Y., Yu, J., Qin, J., Vittal, V., Karady, G.G., Shi, D., Wang, Z.: Modeling, control, and protection of modular multilevel converter-based multi-terminal HVDC systems: a review. CSEE J. Power Energy Syst. **3**(1), 340–352 (2017)
3. Marene Larruskain, D., Zamora, I., Abarrategui, O., Iturregi, A.: A solid-state fault current limiting device for VSC-HVDC systems. Int. J. Emerg. Electric Power Syst. **14**(5), 375–384 (2013)
4. Martínez, S., Torres, F., Roa, C., López, E.: Interaction between AC grids and MTDC systems based on droop controllers. In: 2018 IEEE International Conference on Automation/XXIII Congress of the Chilean Association of Automatic Control (ICA-ACCA), pp. 1–6 (2018)
5. Wang, R., Chen, L., Zheng, T., Mei, S.: VSG-based adaptive droop control for frequency and active power regulation in the MTDC system. CSEE J. Power Energy Syst. **3**(3), 260–268 (2017)
6. Gao, Y., Ai, Q.: Multi point voltage control for DFIG wind farms in VSC-MTDC network. Int. J. Emerg. Electr. Power Syst. **18**(2), 20160174 (2017)
7. Ren, J., Li, K., Zhao, J., Dong, X., Zhang, X.: A multi-point DC voltage control strategy of VSCMTDC transmission system for integrating large scale offshore wind power. IEEE PES Innov. Smart Grid Technol. pp. 1–6 (2012)
8. Pratap, A., Howlader, A.M., Senjyu, T., Yona, A., Urasaki, N., Funabashi, T.: Different strategies for controlling output power smoothing of a PMSG-based wind energy conversion systems. Int. J. Emerg. Electr. Power Syst. **13**(4), 1–31 (2012)
9. Jing Lyu, Xu, Cai, X., Molinas, M.: Optimal design of controller parameters for improving the stability of MMC-HVDC for wind farm integration. IEEE J. Emerg. Sel. Top. Power Electron. **6**(1), 40–53 (2018)
10. Ayari, M., Belhaouane, M.M., Guillaud, X., Braiek, N.B.: Nonlinear control design of VSC-MTDC systems based on backstepping approach. In: 12th International Conference on Informatics in Control, Automation and Robotics (ICINCO), pp. 1–6 (2015)
11. Li, G., Du, Z., Shen, C., Yuan, Z., Wu, G.: Coordinated design of droop control in MTDC grid based on model predictive control. IEEE Trans. Power Syst. **33**(3), 2816–2828 (2018)
12. Zhou, G., Ma, W.: Model predictive control-based coordinated control strategy for VSC-MTDC systems. In: 22nd International Conference on Electrical Machines and Systems (ICEMS), pp. 1–6 (2019)
13. Rault, P., Colas, F., Guillaud, X., Nguefeu, S.: Method for Small Signal Stability Analysis of VSC-MTDC Grids. In: IEEE Power and Energy Society General Meeting, pp. 1–6 (2012)
14. Amin, M., Suul, J.A., D'Arco, S., Tedeschi, E., Molinas, M.: Impact of state-space modelling fidelity on the small-signal dynamics of VSC-HVDC systems. In: IET International Conference on AC and DC Power Transmission, pp. 1–11 (2015)

15. Li, G.-J., Ruan, S.-Y., Lie, T.: Real power regulation design for multi-terminal VSC-HVDC systems. Int. J. Emerg. Electr. Power Syst. **3**(2), 243–252 (2013)
16. Rodriguez, P., Rouzbehi, K.: Multi-terminal DC grids: challenges and prospects. J. Mod. Power Syst. Clean Energy **5**(4), 515–523 (2017)
17. Kotb, O., Ghandhari, M., Renedo, J., Rouco, L., Eriksson, R.: On the design and placement of a supplementary damping controller in an embedded VSC-MTDC network. In: IEEE PES Innovative Smart Grid Technologies Conference Europe (ISGT-Europe), pp. 1–6 (2017)
18. Preece, R., Milanović, J.V.: Tuning of a damping controller for multiterminal VSC-HVDC grids using the probabilistic collocation method. IEEE Transa. Power Del. **29**(1), 318–326 (2017)
19. Yadav, Omkar, Kishor, Nand, Negi, Richa: Power imbalance sharing among the power converters in MTDC system. Int. J. Electr. Power Energy Syst. **109**, 584–596 (2019)
20. Haileselassie, T.M.: Control, Dynamics and Operation of Multi-terminal VSC-HVDC Transmission System, Ph. D. thesis, NTNU-Trondheim (2012)
21. Assis, T.M.L., Kuenzel, S., Chandra Pal, B.: Impact of multi-terminal HVDC grids on enhancing dynamic power transfer capability. IEEE Trans. Power Syst. **32**(4), 2652–2663 (2015)
22. Zhao, X., Jiang, Z., Han, J., Liu, G.: Adaptive robust LQR control with the application to the yaw control of small-scale helicopter. In: Proceedings of the 2006 IEEE International Conference on Mechatronics and Automation, pp. 1–6 (2006)
23. Boyd, S., Ghaoui, E.L., Feron, E., et al. LMI in Systems and Control Theory. SIAM Philadelphia, version 5.2 (1994)

Voltage Ripple-Based Islanding Technique on Modified IEEE-13 Bus Test Feeder for Photovoltaic Inverter

Salauddin Ansari and Om Hari Gupta

1 Introduction

Electric power systems worldwide are being rigorously burdened by rising power demand [1]. Strict natural guidelines and the exorbitant prices of modern power production factories make distributed energy resources (DER) systems a smart option to supplement the prevailing power framework foundation. Moreover, huge concentrated electricity plants are most likely to destructive shutdowns, because they constitute one location of collapse impacting a huge operating region. Because of these demerits, scientists and governing bodies have promoted a comprehensive way to incorporate DER systems with the prevailing power framework foundation [2]. On the other hand, the main problem that may be caused by using the DER source is the unexpected islanding event [3]. Islanding identification is not just essential to the function of DER systems, in addition to it is also compulsory to maintain by standardized guidelines [4]. Islanding detection methods are categorized as local or remote [5–8]. Local methods are again categorized among passive methods [9–15], active methods [16, 17], and neural computing-based methods [18]. In passive methods, system variables like frequency and voltage, over PCC among the power grid and the DER source are continuously monitoring. Whenever PCC voltage and frequency go beyond the preset threshold limits, islanding is reported [19–21]. However, the passive technique is easy to apply, yet shows wide NDZ and might not identify islanding events if the power mismatch is small [11]. In active methods, a perturbation signal is locally injected into the power system, during grid-connected mode of

S. Ansari (✉) · O. H. Gupta
Department of Electrical Engineering, National Institute of Technology Jamshedpur, Jamshedpur, JH 831014, India
e-mail: 2019rsee006@nitjsr.ac.in

O. H. Gupta
e-mail: omhari.ee@nitjsr.ac.in

O. H. Gupta and V. K. Sood (eds.), *Recent Advances in Power Systems*, Lecture Notes in Electrical Engineering 699, https://doi.org/10.1007/978-981-15-7994-3_13

operation. At the instant when islanding occurs, clear and remarkable changes in the system parameter are reported. Since this method depends upon the perturbation in the signal which reduced the power quality of the power system, they are reliable but expensive in terms of requirement of signal equipment. Neural-based method suited for islanding detection in case of rule-based method fails to detect islanding. It is able to recognize voltage and frequency behavior simultaneously during islanding condition because neural-based method considers simultaneously both the variable. Neural-based method is able to read example and recognize structures of input signal. So, with the using of neural-based approach, it is possible to detect structure that hardly detected by conventional method. In the present article, an effective passive islanding identification method for PV systems attached to the IEEE-13 bus feeder is described. In this method, the voltage ripple [23] of the inverter at the PCC is inspected to variations under a time domain study that can be readily applied in the inverter. Now, once the voltage ripple of the inverter at the PCC is more than the preset threshold limit for a particular duration of time, then islanding is reported. This method does not have NDZ restrictions and can recognize islanding although in the case of perfectly matched power situations, where passive method neglects to identify islanding. Furthermore, this method can identify islanding within 210 ms. The remaining of the paper is arranged out as follows. Model of inverter-connected DER is described in Sect. 2. Scheme of islanding detection is investigated in Sect. 3. Section 4 is described in Results and Discussion. At last, Sect. 5 introduced the Conclusions.

2 Model of Inverter Connected DER

Figure 1 demonstrates an electrical single-line diagram of the scheme that comprises panels of PV, DC-DC converter, DC-AC converter, filter, local load, and finally step-up transformer coupled to the IEEE-13 bus feeder at 671 nodes. In the present scheme, the PV cell configured to produce 50 kW of nominal power at the standard working environment (1000 W/m^2 irradiance at 25 °C temperature). Therefore, to extract maximum output power obtained by the PV cell, the DC-DC converter is inserted whose duty ratio is governed by the maximum power point tracking approach (MPPTA). The MPPTA employed in this model works with the principle of "Incremental Conductance" which settled output voltage in the best possible way. A reference signal for the active part of current (I_d) is generated, and in order to inject only real power to the grid, reactive part of current (I_q) is fixed to be zero. To eliminate any high-order harmonic due to switching of the inverter, a filter is used. To the PCC, both transformer and load are connected that are further coupled at 671 nodes of the IEEE-13 bus feeder. The simulated specification is provided in Table 1.

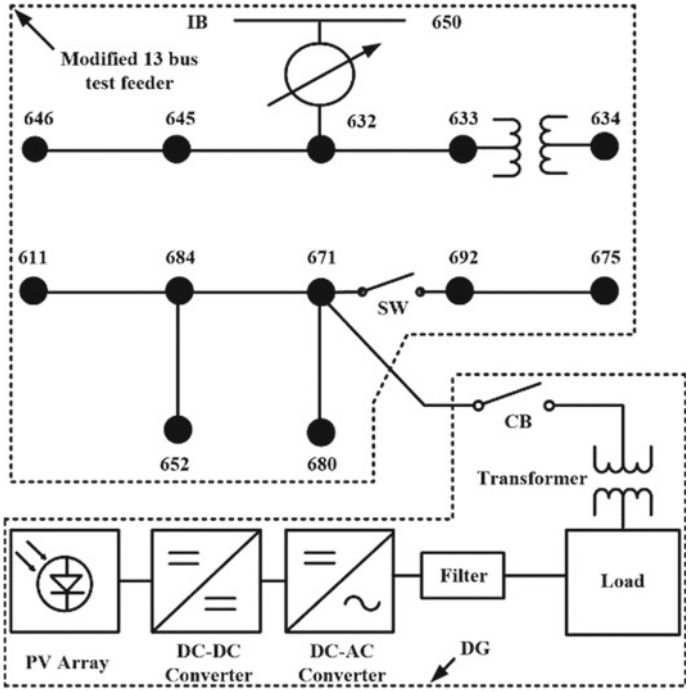

Fig. 1 Electrical single-line diagram of general PV system connected to 671 nodes of IEEE-13 bus feeder system

Table 1 Specification of simulated model

Parameter	Value
Rated PV power	100 kW
Load real power	100 kW
Load resonance frequency	60 Hz
Switching frequency	1980 Hz
Transformer rated power	100 kVA
Filter resistance	1.9 mΩ

3 Scheme of Islanding Detection

Based on ripple content in instantaneous inverter voltage magnitude at PCC in the time domain, the islanding detection scheme has been established. Single-phase voltage V_r to the PCC followed by islanding may be written as [22]:

$$V_{\text{rms}} = V_{\text{grd}} \sqrt{\frac{P_{\text{iv}}}{3P}} \tag{1}$$

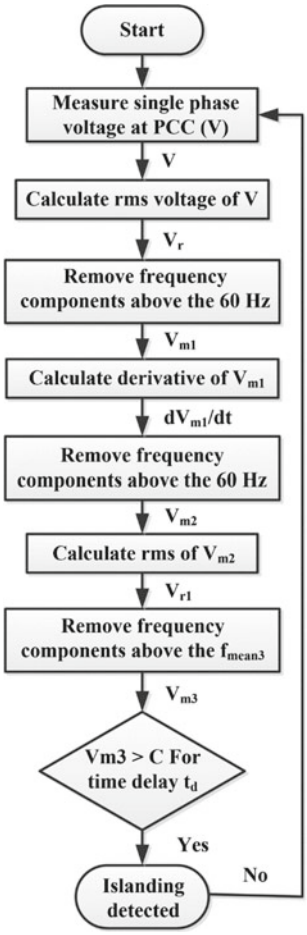

Fig. 2 Algorithm of the islanding detection scheme

where V_{rms} is the single-phase rms voltage to the PCC, V_{grd} is the rms value of single-phase voltage at the grid side, P_{iv} is the power of three-phase inverter, and P is the single-phase active power absorbed to the load. Every power change in P_{iv} is immediately reported back into V_{rms} because V_{grd} and P are assumed to be constant. From Fig. 3a, it is clear that after islanding, the prolonged oscillations in single-phase voltage at PCC have been reported which are especially distinct out of other disturbances, like three-phase fault conditions as shown in Fig. 3b. In the case of a three-phase fault which is shown in Fig. 3b, within three cycles, the fault was seen to be clear, whereas in the case of islanding, sustained voltage oscillations are noticed as shown in Fig. 3a. Based on such a concept, this technique is successfully applied to detect islanding by keeping close eye on voltage ripple content in the V_r waveform. Figure 4 represents the islanding detection waveform output in terms of two cases as shown in Fig. 4. From Fig. 4, it is noticed that there is consistent dissimilarity

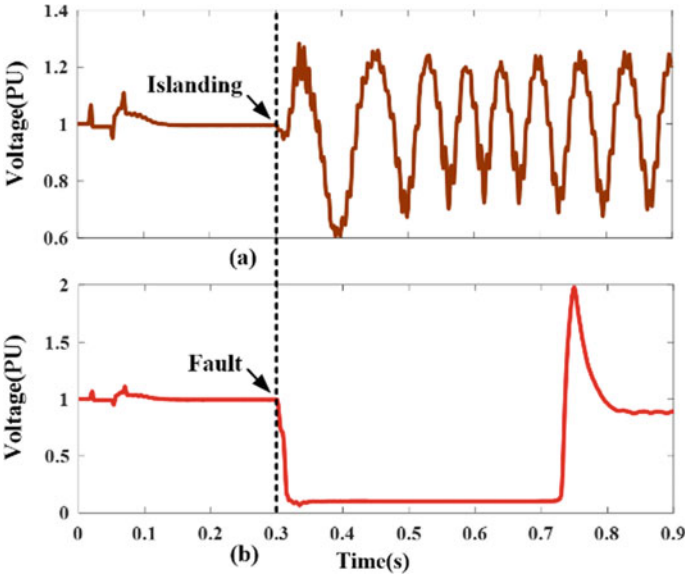

Fig. 3 Instantaneous voltage waveform at PCC, **a** islanding condition and **b** a three-phase fault condition

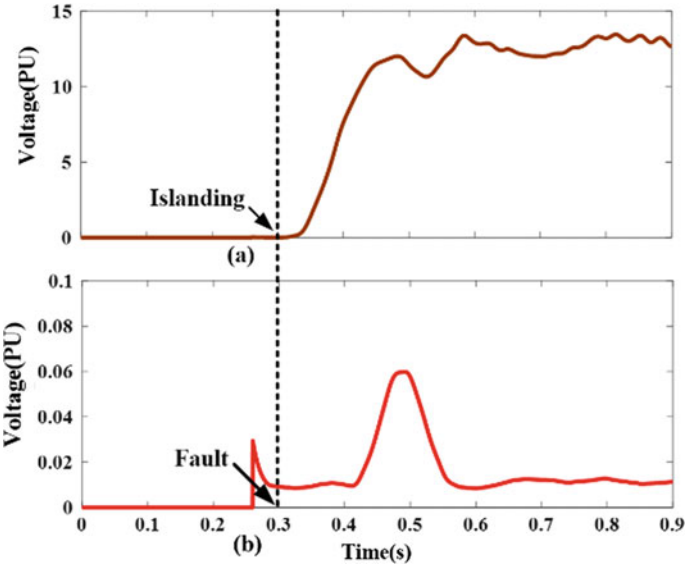

Fig. 4 Islanding detection output waveform, **a** islanding conditions and **b** three-phase fault condition

before and after the islanding in waveform. In the case of a three-phase fault, initially some spike is present in the waveform and after that, it comes to rest comparatively faster. Thus, a threshold is used to discriminate among non-islanding and islanding waveforms. In addition to that, a delay of time was provided in the last to prevent wrong tripping because of transient due to non-islanding events like faults, capacitor switching, load switching, and starting of the motor. Figure 5 depicts the seven steps of islanding detection waveform output under this technique. Step 1 represents the instantaneous single-phase input voltage (V) to the PCC. Step 2 represents rms value (V_r) of waveform V.

The V_r computed under the one time period, for a rated frequency of 60 Hz in the following way:

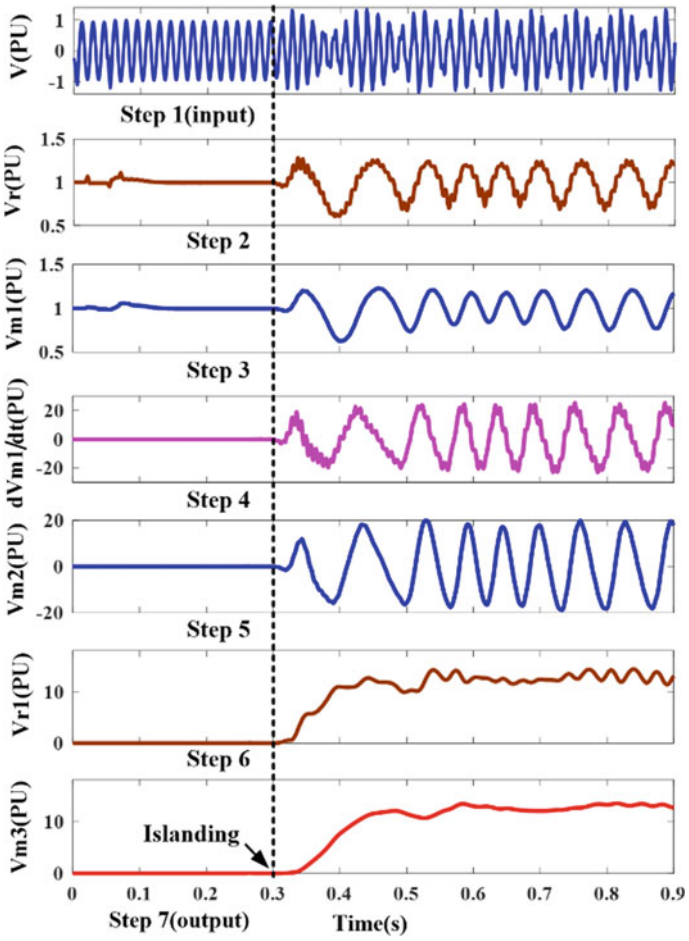

Fig. 5 Entire steps of the islanding detection method

$$V_r = \sqrt{\frac{1}{T}\int_0^T V^2 \mathrm{dt}} \tag{2}$$

whereby $T = 1/60$ s and entire frequency component more than 60 Hz in the V_r waveform assumed to be noise and they are removed by mean-1 block in the following way:

$$V_{m1} = \frac{1}{\mathrm{T}}\int_0^T V_r \mathrm{d}t \tag{3}$$

where V_{m1} be the mean of V_r under one time period for a rated frequency of 60 Hz. The role of the mean block is the same as that of a low-pass filter that removes all frequency, more than 60 Hz into Fig. 5 (step 3). Since the magnitude of V_{m1} is small so to increase scaling and technique to work, it is necessary to magnify V_{m1}. This is fulfilled by taking derivative of V_{m1} which is demonstrated in Fig. 5 (step 4). Moreover, to enhance the effectiveness of the technique, the frequency which is more than 60 Hz in the $\mathrm{d}V_{m1}/\mathrm{d}t$ is removed by another one filter to get the V_{m2} depicted in Fig. 5 (step 5).

The V_{m2} is computed under one time period for a rated frequency of 60 Hz in the following way:

$$V_{m2} = \frac{1}{T}\int_0^T \left(\frac{V_{m1}}{\mathrm{d}t}\right)\mathrm{d}t \tag{4}$$

In order to extend the ripple present and to remove DC component from the V_{m2}, rms value of V_{m2} was calculated under time period of T_{rms1} to get the V_{r1} in the following way:

$$V_{r1} = \sqrt{\frac{1}{T_{\mathrm{rms1}}}\int_0^{T_{\mathrm{rms1}}} V_{m2}\mathrm{d}t} \tag{5}$$

The waveform of V_{r1} demonstrated in Fig. 5 (step 6). Lastly, to remove any frequency component which is more than f_{mean1} in the waveform of $V_{r1,}$ the mean value of V_{r1} is computed in the time period of T_{man3} in the following way:

$$V_{m2} = \frac{1}{T_{\mathrm{mean3}}}\int_0^{T_{\mathrm{mean3}}} V_{r1}\mathrm{d}t \tag{6}$$

The waveform of V_{m3} is demonstrated in Fig. 5 (step 7), where $T_{\text{rms1}} = 1/f_{\text{rms1}}$ s and $T_{\text{mean3}} = 1/f_{\text{mean3}}$ s. The choice of f_{rms1} and f_{mean3} performs a vital duty in the technical design and later on investigated in Sect. 4.1. The islanding detection output waveform (V_{m3}) is now cross-checked with the preset threshold (C). When V_{m3} more than the C for a preset time (t_s) then islanding is detected. Let Δt_s be the time interval for which V_{m3} more than C. The alert signal A_d can be generated as follows:

$$A_d = \begin{cases} 1 \text{ if } V_{m3} > C, \ \Delta t_s > t_s \\ 0 \text{ otherwise} \end{cases} \tag{7}$$

where $A_d = 1$ implies islanding is detected whereas $A_d = 0$ implies there is no islanding. The comprehensive procedure of the islanding identification approach is portrayed in Fig. 2.

4 Results and Discussion

A lot of different cases of feasible islanding and non-islanding events are studied to validate the effectiveness of the technique in the MATLAB/Simulink. The summarized information of the results is as per the following:

4.1 Effect of Working Frequency on Blocks mean-3 and rms-1

The choice of the working frequency for mean-3 shown in Fig. 6 and rms-1 block shown in Fig. 7 performs a vital duty in the process of designing. There is a minor

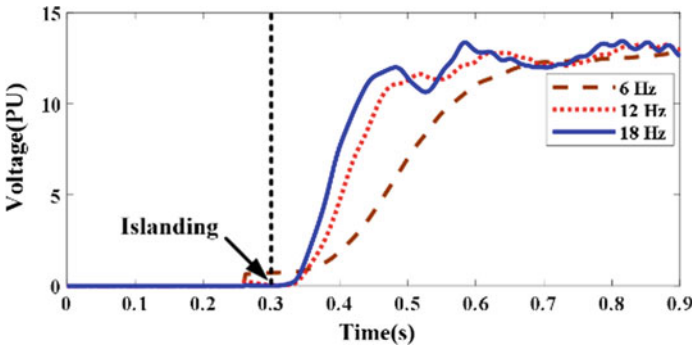

Fig. 6 Impact on islanding detection waveform on mean-3 block at the different working frequency

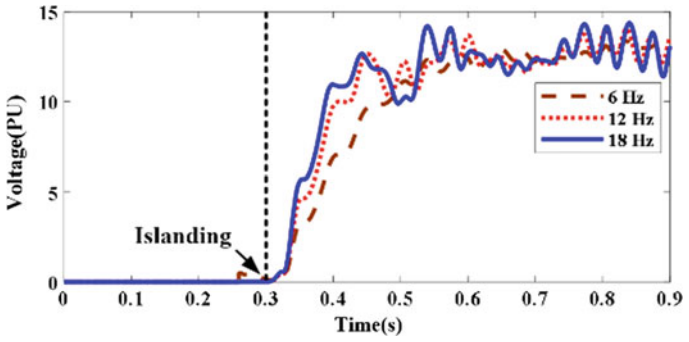

Fig. 7 Impact on islanding detection waveform on rms-1 block at the different working frequency

effect on the shape of a detected waveform in case of non-islanding, whereas in the case of islanding, there is a significant effect reported. However, lower frequency supports in obtaining a significant difference between the level of islanding and non-islanding event. Thus, there is the best possible frequency for both two blocks that must be selected in order to get sufficient difference among the islanding and non-islanding level.

4.2 Islanding During Various Real Power of Mismatch

Whenever islanding takes place at 0.3 s during various real power mismatch (say 0, +10, −10, 20, and −20%), islanding detection waveform and its corresponding alert signal are generated because it crossed the threshold (i.e., 2 PU), and therefore, the islanding case is detected. Figures 8 and 9 represent islanding detection waveform and its corresponding alert signal, respectively, with various active power mismatch (say 0, +10, −10, 20 and −20%).

4.3 Islanding During Various Reactive Power Mismatch

Figures 10 and 11 demonstrate the islanding detection wave and its corresponding alert signal, respectively, during various reactive power mismatch (say 0, 1, −1, 4, and −4%).

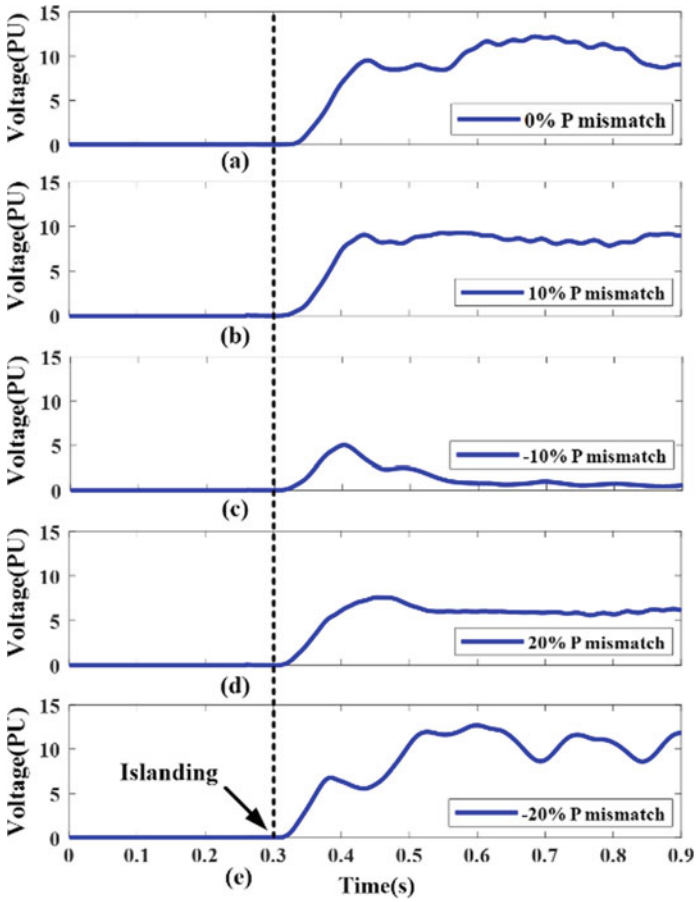

Fig. 8 Islanding detection waveform during various active power mismatch

4.4 Three-Phase Faults

The three-phase fault has occurred at 0.3 s, and its islanding detection waveform and alert signal are demonstrated in Fig. 12. Initially, for a moment, some spike is present in the islanding detection waveform which returns to zero within the intentional delay time. Now, according to technique, this event will not be mistakenly detected as islanding but can be regarded as another switching event.

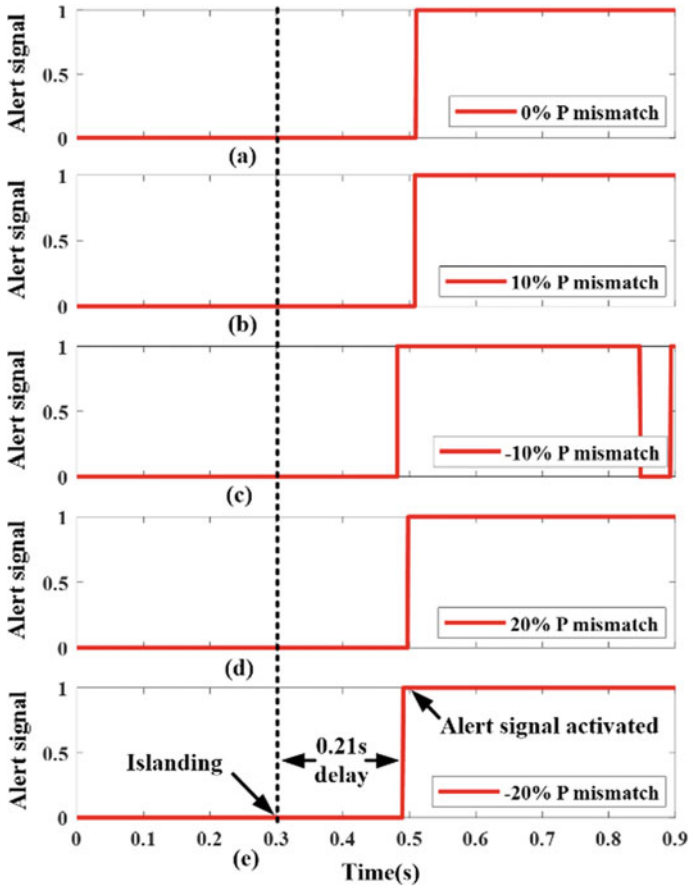

Fig. 9 Alert signal waveform during various active power mismatch

4.5 Load Switching

The load on the distribution power system changes irregularly. Thus, to find out the impact of abrupt load change, 100% of the nominal load abruptly rises at 0.3 s. An alert signal generated because of the change in the islanding detection waveform. Initially for a moment, it crossed the threshold but again comeback to zero which is depicted in Fig. 14. Therefore, the islanding case is not reported.

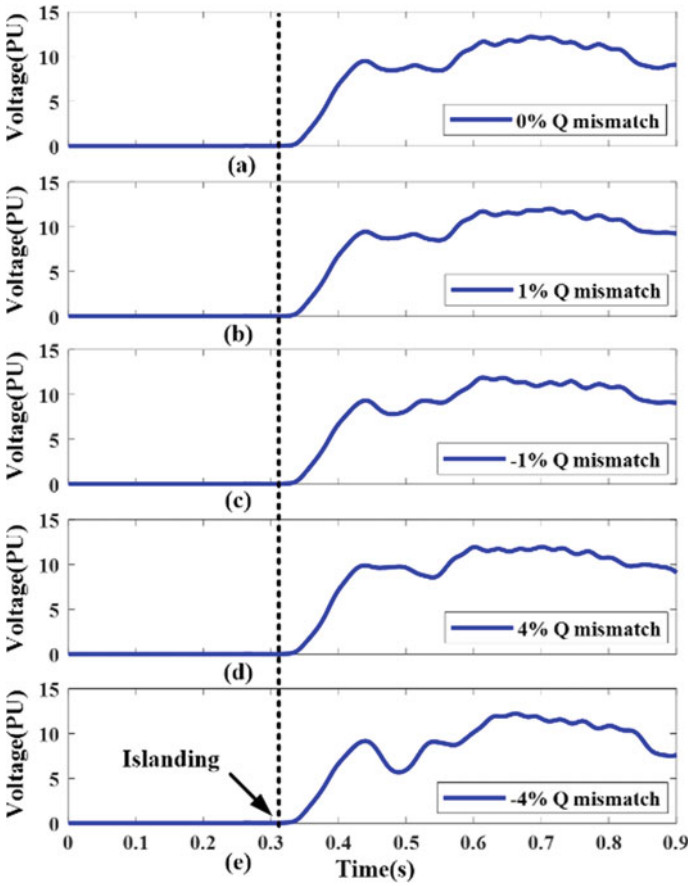

Fig. 10 Islanding detection waveform during various reactive power mismatch

4.6 Capacitor Switching

At 0.3 s, a bank capacitor of 10 kVAR (0.1 PU) is attached to the PCC. The islanding detection waveform gets changed as a result; an alert signal is generated which is shown in Fig. 13. After some oscillation, the islanding detection waveform dropped down the threshold. It will be regarded as capacitor switching.

4.7 Nonlinear Load Connected

To study the effectiveness of the technique subjected to nonlinear load, a three-phase full-wave rectifier was connected at 0.3 s to the PCC. The power absorbed

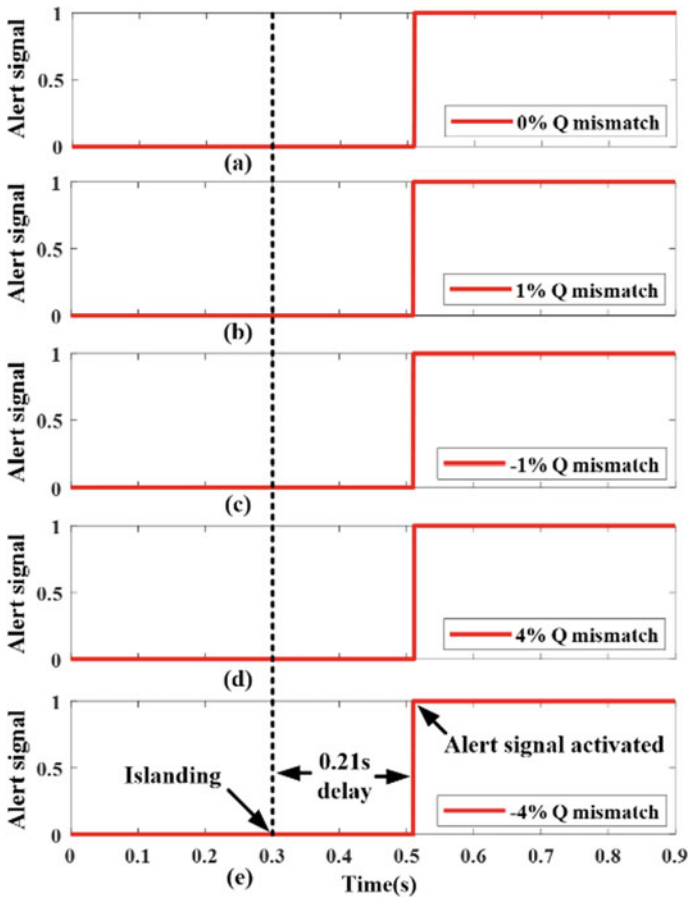

Fig. 11 Alert signal waveform during various reactive power mismatch

by the rectifier is 0.676 PU. After the rectifier is switched on, a spike is present in the islanding detection waveform which settles down fastly and its corresponding alert signal is generated which is shown in Fig. 15. Thus, the event is considered as switching of the nonlinear load.

5 Conclusion

In the present article, a passive islanding detection method for PV-incorporated inverter on modified IEEE-13 bus feeder is simulated in MATLAB/Simulink. In this method, the ripple present in the output of inverter voltage at the PCC is inspected to variations under time domain study. Now, once the ripple present in it is more than

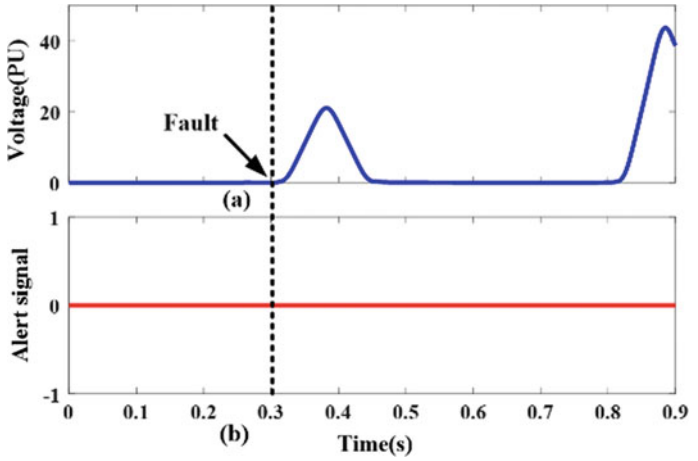

Fig. 12 Three-phase fault at PCC, **a** islanding detection waveform and **b** alert signal

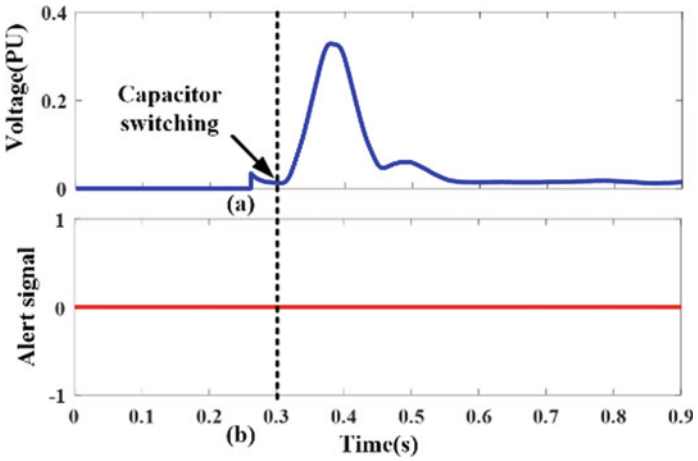

Fig. 13 Effect of switching capacitor bank, **a** islanding detection waveform and **b** alert signal

the preset threshold limit for a particular duration of time, then islanding is reported. The technique has been fully tested under various possible islanding conditions, including mismatch of active and reactive power and non-islanding situations, such as three-phase fault, load switching, capacitor switching, and presence on nonlinear load. Even in the more serious situation where the power mismatch is zero, the technique effectively detects islanding. Moreover, it can precisely differentiate islanding from the verified non-islanding cases. This technique can detect islanding less than 210 ms, which is far under the 2 s specified by the IEEE 1547 standard. Furthermore,

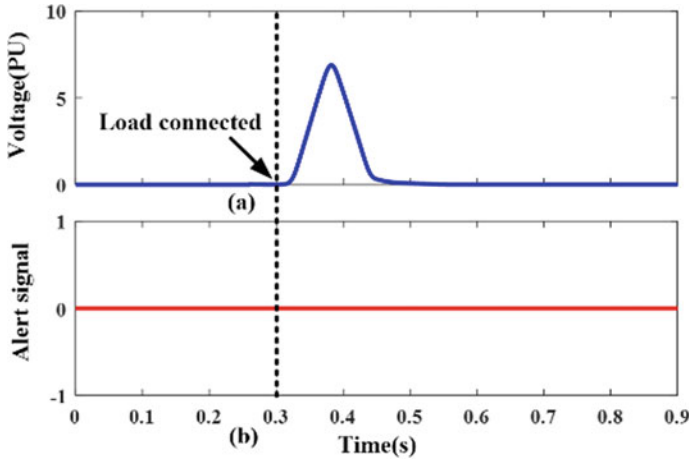

Fig. 14 Effect of load switching, **a** islanding detection waveform and **b** alert signal

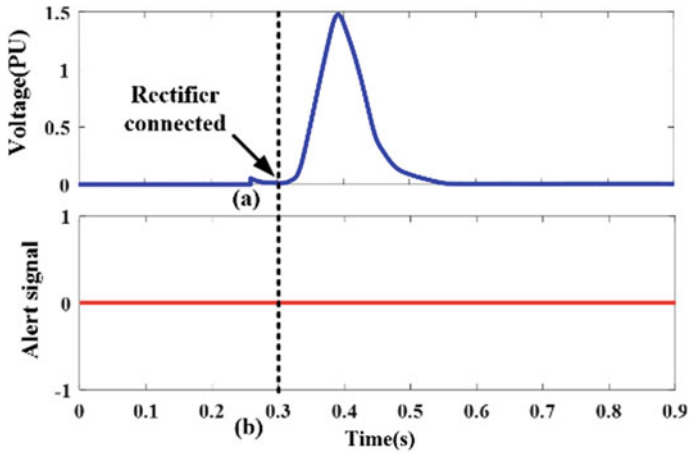

Fig. 15 Effect on nonlinear load, **a** islanding detection waveform and **b** alert signal

this technique is easy to implement and can be applied at a lower cost to the PV inverter.

References

1. Momoh, J., Meliopoulos, S., Saint, R.: Centralized and distributed generated power systems-a comparison approach. Future and grid initiative white paper, and undefined (2012)

2. Murdock, H., Gibb, D., André, T., Appavou, F., Brown, A.: Renewables 2019 Global Status Report (2019)
3. Razavi, S.E., et al.: Impact of distributed generation on protection and voltage regulation of distribution systems: a review. Renew. Sustain. Energy Rev. **105**, 157–167 (2019). https://doi.org/10.1016/j.rser.2019.01.050
4. Photovoltaics, D., Storage, E.: IEEE application guide for IEEE Std 1547™, IEEE Standard for Interconnecting Distributed Resources with Electric Power Systems (2009)
5. Pvps, I.: Task 5: evaluation of islanding detection methods for photovoltaic utility—interactive power systems. Task V Report IEA-PVPS T5-09 : 2002 March 2002, no. March 2002 (2018)
6. Xu, W., Zhang, G., Li, C., Wang, W., Wang, G., Kliber, J.: A power line signaling based technique for anti-islanding protection of distributed generators-Part I: scheme and analysis. IEEE Trans. Power Del. **22**, 3 (2007). https://doi.org/10.1109/TPWRD.2007.899618
7. Kim, M.-S., Haider, R., Cho, G.-J., Kim, C.-H., Won, C.-Y., Chai, J.-S.: Comprehensive review of islanding detection methods for distributed generation systems. Energies **12**(5), 837 (2019). https://doi.org/10.3390/en12050837
8. Tang, Y., Sun, R., Thomas, K., Burgos, R.: Synchrophasor based transmission system anti-islanding scheme. IEEE Power Energy Soc. Gen. Meet. **1**, 1–5 (2018). https://doi.org/10.1109/PESGM.2017.8274354
9. Ye, Z., Kolwalkar, A., Zhang, Y., Du, P., Walling, R.: Evaluation of anti-islanding schemes based on nondetection zone concept. IEEE Trans. Power Electron. **19**(5), 1171–1176 (2004). https://doi.org/10.1109/TPEL.2004.833436
10. Velasco, D., Trujillo, C.L., Garcerá, G., Figueres, E.: Review of anti-islanding techniques in distributed generators. Renew. Sustain. Energy Rev. **14**(6), 1608–1614 (2010). https://doi.org/10.1016/j.rser.2010.02.011
11. Bower, W., Ropp, M.: SANDIA REPORT evaluation of islanding detection methods for utility-interactive inverters in photovoltaic systems
12. Pigazo, A., Liserre, M., Mastromauro, R.A., Moreno, V.M., Dell'Aquila, A.: Wavelet-based Islanding detection in grid-connected PV systems. IEEE Trans. Ind. Electron. **56**(11), 4445–4455 (2009). https://doi.org/10.1109/TIE.2008.928097
13. ElNozahy, M.S., El-Saadany, E.F., Salama, M.M.A.: A robust wavelet-ANN based technique for islanding detection. In: IEEE Power and Energy Society General Meeting (2011). https://doi.org/10.1109/pes.2011.6039158
14. Ray, P.K., Kishor, N., Mohanty, S.R.: Islanding and power quality disturbance detection in grid-connected hybrid power system using wavelet and S-transform. IEEE Trans. Smart Grid **3**(3), 1082–1094 (2012). https://doi.org/10.1109/TSG.2012.2197642
15. Gupta, O.H., Tripathy, M., Sood, V.K.: Islanding detection scheme for converter-based DGs with nearly zero non-detectable zone. IET Gener. Transm. Distrib. **13**(23), 5365–5374 (2019). https://doi.org/10.1049/iet-gtd.2018.5168
16. Hernández-González, G., Iravani, R.: Current injection for active islanding detection of electronically- interfaced distributed resources. IEEE Trans. Power Deliv. **21**(3), 1698–1705 (2006). https://doi.org/10.1109/TPWRD.2006.876980
17. Chiang, W.J., Jou, H.L., Wu, J.C., Der Wu, K., Feng, Y.T.: Active islanding detection method for the grid-connected photovoltaic generation system. Electr. Power Syst. Res. **80**(4), 372–379 (2010). https://doi.org/10.1016/j.epsr.2009.09.018
18. Balamurugan, M., Sahoo, S.K., Sukchai, S.: Application of soft computing methods for grid connected PV system: a technological and status review. Renew. Sustain. Energy Rev. **75**, 1493–1508 (2017)
19. Yingram, M., Premrudeepreechacharn, S.: Investigation over/under-voltage protection of passive islanding detection method of distributed generations in electrical distribution systems. In: 2012 International Conference on Renewable Energy Research and Applications, ICRERA 2012 (2012). https://doi.org/10.1109/icrera.2012.6477399
20. Institute of Electrical and Electronics Engineers., *Electrical Power Distribution Networks (EPDC)*. In: *2012 Proceedings of 17th Conference on* [IEEE] (2012)

21. Khamis, A., Shareef, H., Bizkevelci, E., Khatib, T.: A review of islanding detection techniques for renewable distributed generation systems. Renew. Sustain. Energy Rev. **28**, 483–493 (2013). https://doi.org/10.1016/j.rser.2013.08.025
22. Jeraputra, C., Enjeti, P.N.: Development of a robust anti-islanding algorithm for utility interconnection of distributed fuel cell powered generation. IEEE Trans. Power Electron. **19**(5), 1163–1170 (2004). https://doi.org/10.1109/TPEL.2004.833439
23. Guha, B., Haddad, R.J., Kalaani, Y.: Voltage ripple-based passive islanding detection technique for grid-connected photovoltaic inverters. IEEE Power Energy Technol. Syst. J. **3**(4), 143–154 (2016). https://doi.org/10.1109/jpets.2016.2586847

Overview of Electric Vehicle: Opportunities and Challenges with Smart Grid

Atma Ram Gupta, Rishabh Gupta, Saurav, Aditya Tiwari, and Ranjana Purohit

1 Introduction

EV uses electricity as a fuel and converts it into kinetic energy, which is required for running the vehicle. The electricity can be extracted either from a battery or renewable sources of energy. EV has many advantages such as high performance, high response, no noise, low maintenance and driving cost, highly safe, and there is no need of fuel tanks, carburetor, and smog controllers in them. EVs are not new, although they were around us since the 1800 s. At that time out of 4200 vehicles, 38% were EVs but due to low cost gasoline fuel, evolution, and development of electric starter for gasoline engine, the interest in EV declined. Gasoline vehicles are easy to operate due to electric starter which curb the need for hand crank for starting the engine and due to which most of the electric car manufacturer stopped their production [1]. EV has come into limelight due to the problem of environmental hazards related to the conventional vehicle. The first ever made EV was developed by 'Anyos Jedlik' in 1828. In early 1980s, EV activity again rose but with the development of plug-in hybrid EV (PHEV) and hybrid electric vehicles (HEV), the interest in pure EV again decline. In 2003, T (an automobile company) launched its first pure EV "Tesla roadster." Tesla overcome all the challenges of EV such as they use lithium-ion battery to power the vehicles, and the problem of short range is also overcome to some extent. Some issues related to EV development are: profit determination becomes uncertain considering the high capital cost and uncertainties in policies related to EV production. The government has made various comments about their thoughts for EV but nothing has been put down to policies. This discourages the investment industries. Cost of the EV is also an issue of concern [2]. There is a need for lowering the operating cost of the EVs by optimal usage of the renewable energy resource with the help of a microgrid. A

A. R. Gupta (✉) · R. Gupta · Saurav · A. Tiwari · R. Purohit
Department of Electrical Engineering, NIT Kurukshetra, Kurukshetra, Haryana, India
e-mail: arguptanitd@gmail.com

O. H. Gupta and V. K. Sood (eds.), *Recent Advances in Power Systems*, Lecture Notes in Electrical Engineering 699, https://doi.org/10.1007/978-981-15-7994-3_14

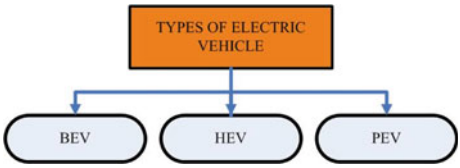

Fig. 1 Block diagram for types of EV

microgrid can extract information and be interfaced to technologies to manage loads [3]. The battery material made is quite expensive which hinders with the development rate of the EVs. The EV manufacturing unit must shift from mechanical to electronic component [4]. Since EV is a necessity these days and to overcome the problems mentioned above in manufacturing an EV, makes it the most researchable topic.

Lithium ion is the major ingredient for making the EV's battery. The main problem with EVs from the time of its development is that it has short range and choice of suitable propulsion motor [5]. Motor is a major component of EV which is going to replace the gasoline engines. Motor must possess high torque-to-inertia ratio, ruggedness, must be compact in size, convenience of control, low maintenance, and minimal cost. Several types of motor were used in EVs such as permanent magnet (PM), induction motor, switched reluctance motor, synchronous reluctance motor, etc. Some of the major factors for the choice of induction motor are its performance and efficiency. Induction motor can also be used as a generator for regenerative action which will help in recovering some of the lost energy and therefore increasing the range of EV per charge.

As far as EV is concerned, it is mainly of three types as shown in Fig. 1: (1) Battery electric vehicles (BEV) in which the batteries need to be charged again by removing from the vehicle. (2) Hybrid electric vehicles (HEV) in which the batteries are charged with the help of either regenerative braking or internal combustion engine. (3) Plug-in EV (PEV) in which the batteries are charged by direct plugging [6, 7]. Basically, both direct current and alternating current can be used to recharge the batteries. When the direct current is used, there is no need of an external charger as no conversion is required whereas when the batteries are charged by alternating current, then an external charger is required for conversion of the alternating current into direct current. Thus, EV can be used to reduce the per mile cost incurred [5].

2 Components of EV

The different components of EV are shown in Fig. 2. The detail findings of the main components are as follows:

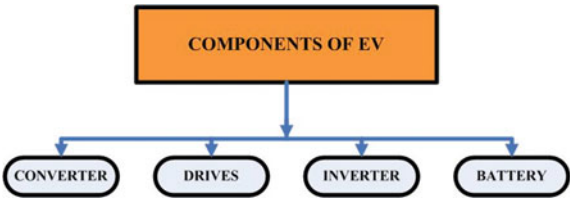

Fig. 2 Block diagram for components of EV

2.1 Converter

The designing of converters is one of the major issues in manufacturing of EV to ensure safety of the passengers. Its major use is to regulate circulation of power between battery and drives. EV can have both DC–AC and DC–DC converters. DC–AC converters are majorly used to power electric drives and other basic components such as air conditioners whereas DC–DC converters are used to supply low voltages in the electric vehicle. DC–DC converters can be soft switched or hard switched whereas they can also be classified on the basis of direction of power circulation, which implies they can be either bidirectional or unidirectional in nature. The switches used in these converters are either IGBT's or MOSFET's. The battery supplies power to the DC–DC converter which converts unregulated DC to regulated DC which then supplies power to the inverter that transforms DC into AC and that AC supply powers to the electric drives or motors of the electric vehicle [8].

2.2 Electrical Machines and Drives

Electrical machines and drives is one of the most important units of electric vehicles. The basic characteristics of these machines required in electric vehicles are high torque, higher power density, higher efficiency, high maximum speed capability, less noise, and low torque ripple. The typical machines required for traction purpose are induction machines (IM), brushless dc machines, and switched reluctance machines (SRMs) [9–17].

2.3 Inverter

Inverter is a device which converts DC to AC. An inverter can be a current source inverter or a voltage source inverter. A 3-phase VSI at 180° conduction mode is preferred. A 3-phase VSI inverter has 3 bridge networks each bridge containing apair of power MOSFET each. Now, why did we used MOSFET and why not BJT since MOSFET performs fast switching as compared to the BJT switching and losses are also less when both are compared. MOSFET can work on wide frequency range. The

DC supply is provided with the help of 12 V lithium batteries and the firing angle of the H-bridged inverter is controlled using peripheral interface controller which provides a proper ON–OFF duration to individual switches so that 180 degree conduction can be achieved. A capacitor is also connected across the branches so as to reduce the harmonics and a diode generally called a freewheeling diode is also connected across the branch. There are various methods for the control of output voltage of a VSI which are pulse width modulation control (PWM), space vector modulation control (SVM), phase displacement control, etc. Nowadays, the DC motors which control the wheels of the EV are directly connected through the converters, though this increases the complexity of the converters but gives a good performance [18].

2.4 Battery

Battery acts as a fuel for EVs. One of the major problems regarding the implementation of EV is its cost and the size of the battery required. The various types of batteries used are Lithium–nickel–cobalt, Lithium–iron–phosphate, Lithium air, Lithium titanate, Lithium-ion battery, Lithium–sulfur [19]. Nowadays, Lithium-ion (Li-ion) battery is the best choice among all rechargeable batteries, as it possesses high energy density, high range, lower self-discharge rate, longer life span, and efficient charging properties [20, 21]. Battery is a key component of an EV but their designing is more challenging as it is based on their chemical composition. Battery can also be destructive in nature due to thermal runaway and may catch fire both externally and internally. Therefore, it is important to wisely choose or design a battery for the safety of consumers [22–28].

3 Interaction of EV with Smart Grid

EV is an attracting concept to lower down the CO_2 emissions but it has also increased the load on grid by extracting power to get charged. So, there is a great need of renewable energy sources to mitigate power deficit issue and to increase the ratio of clean energy. There are great chances of randomness and intermittency of renewable energy sources [29].

There are various feasible networks of integrated technology such as DC, AC, and hybrid microgrid. The DC is most advantageous in respect to cost and efficiency as it requires least number of power electronics converters between renewable energy sources (RES) and DC bus. Also, no interference of harmonics would exist. A special DC microgrid based on PV has been designed which provides multiple ports for charging PHEV and HEV [30].

The AC microgrid is almost same as DC one except the fact that it requires more power electronic converters to provide final DC supply to the EV. The greatest advantage of an AC microgrid is V2G and this power reversal could be controlled through a switch at the point of common coupling (PCC).

The hybrid system utilizes the advantages of both AC and DC. The DC part provides fast charging whereas AC part provides with V2G. A smart charging method for EV is proposed which gets connected to both DC and AC [31]. However, this proposed scheme may have many disadvantages too, to mitigate it; the idea of vehicle-to-grid (V2G) was developed. V2G technology controls and manages EV loads via aggregators and by communication between vehicle and grid. The classifications of V2G are:

Unidirectional V2G: It controls the charging rate of EV which helps in preventing overloading of grids, fixing the overvoltage issue, and keeping the system stable. It exploits the communication between EV and the grid operators to perform this task. Spinning reserves is one of the main services provided by unidirectional V2G. Spinning reserve is additional power that is available due to increased power output of generators connected to the power system itself.

Bidirectional V2G: It allows power flow in both directions, i.e., it provides EV charging as well as grid support. Its major benefit is that it provides much more pliability for power transfer to regulate the energy of the battery so that it improves the reliability and power system sustainability. The major benefits that bidirectional V2G provides are: active and reactive power assistance, load leveling, power factor correction, it filters harmonics, controls frequency, provides the integration of RES with the power grid, etc. The bidirectional charger works as an active power filter [32]. It works either way, i.e., charger the battery via grid and transfers the power to grid when needed. The majority of modes of operation of battery chargers these days in smart grids and homes are discussed in [33]. Bidirectional V2G uses AC–DC and DC–DC converter to function. AC–DC converter converts AC power from the grid to usable DC power for charging of battery. Similarly, DC–AC conversion is required during energy transfer from vehicle to grid. Buck or boosts DC–DC converters are used during charging and discharging, respectively.

Challenges in V2G:

A. Degradation of battery

Due to frequent charging and discarding, battery quality gets degraded the most, although there are other factors like depth of discharge (DOD), temperature, and voltages.

B. Investment cost

Since two ways approach is required in bidirectional power flow, it requires more equipment to accomplish the task of power transfer. As the complexity of the structure increases, so does its cost. Social barriers: The presence of large number of EV owner is a must in V2G technology. Since the EV technology is not mature yet, there is less number of owners which proves to be a social barrier.

C. Optimization objectives

- Operation cost. The main aim is operating cost minimization.
- CO_2 emission. This too has to be minimized.
- Profit for V2G technique. There is a need to maximize the ease of the users and power system aggregators using optimization techniques.V2G serves this purpose.
- Sustenance of renewable energy generation. EV acts as battery banks for renewable energy sources. They can provide energy to them in times of insufficient renewable energy. During the time of high energy generation, EVs can store energy from them. This way, EV gives an opportunity to have green energy around [34].

4 Opportunities and Challenges

On the basis of energy sources available, i.e., diesel, battery, gasoline, etc., and the devices of propulsion, i.e., motor and engine, all kinds of vehicles whether EV or any other internal combustion energy vehicle (ICEV), are basically classified as Battery EV, hybrid EV or fuel cell electric vehicle. Hybrid EV is further classified into plug-in HEV, range-extended EV. The plug-in HEV, battery EV, and range-extended EV are capable of getting charged directly from power grid, therefore, all these are called as grid EV or GEV.

4.1 Vehicle to Home (V2H)

V2H configuration uses lead acid or Li-ion battery. This system is supported by reactive power with bidirectional charger capacitor. A single GEV can only be appointed for a single house. It is the simplest and least flexible of the three concepts and very easily installed with simple infrastructure requirements and negligible transmission losses. V2H EV acts as a home backup generator and cooperates with domestic electrical devices for load shift. Most of the time, EV's are parked at parking lots, with the help of bidirectional charger and controller EVs can used to deliver the stored energy to the building to reduce the high demand and EVs can be charged by taking supply from the building during low demand according to the necessary [35, 36]. Considering the power electronics for V2H, single-phase AC–DC converter is used for GEV on board charger. They provide reactive power support with capacitors [37–39]. This will help to reduce the electricity bills because during the peak load, when load demand is high, the distribution companies charges high price as compared to price during low load demand because sometimes, the distribution company had to brought electricity at high price to fulfill the load demands [40].

4.2 Vehicle to Vehicle (V2V)

This configuration is supported by bidirectional charger capacitor. It is a convenient but less pliable configuration due to small transmission losses. It acts as an energy source to other local GEVs. It reduces tariff by trading with local grid. Single-phase current or voltage source converter is used in V2V scheme. This configuration is flexible in power transferring between the chargers within the GEVs.

5 Charging Station

There are two kinds of charging station one is the slow charging station which is generally used for residential purposes and the other one is the fast charging stations which are used during emergencies [41]. Moreover, charging station must be at a place where it is easily accessible and a power grid close to its proximities will be very appreciable. Taking into account the users interest such as outside a mall or a restaurant or at any parking area will make it convenient for the user to charge their vehicle while they are busy with their own interest.

Now let us analyze the effect of fast charging station on the distribution system, talking about the load density, it is seen that there is a nominal increase in the load density which is quite less than the other installed loads in the system. To dismiss the possibility of overloading in the transmission line, a possible strategy must be implemented which leads the EV owner to charge their vehicle at low load density areas, and the results shows that there is no overloading if we follow this trend. The apparent power flow in a distribution system is toward the place where the power consumption is more as compared to the other places. The study shows that the places not having fast charging station do not report a significant change in the apparent power whereas the places having a fast charging station draw the apparent power from the neighboring feeders. Now taking into account the voltage drop and it is noticed that only few percentage increases is observed up to 0.2%. The main factor that must be taken into account is the effect on the harmonic distortion which mainly tells us the quality of power that is being supplied. Total harmonic distortion (THD) factor for the voltage is likely to increase by 1–2% and the distortion of current from its fundamental value is under acceptable range as proposed by the IEEE standard 519-2014 [42].

5.1 Smart Charging

First of all, why do we need SCMA (smart charging management algorithms)? It is because our fossil fuels are depleting, we have a storage problem and due to environment degradation and to all this, we have only one solution EV. So, there is

a need for a SCMA for improving its efficiency. Power grid is affected because of uncontrolled charging time. Moreover, control of 1000 s EVs at one time will be a challenge and that too when we are unaware of the charging habits of the consumer. The SCMA model proposed has various benefits; it not only provides the driver the most effective path to reach the nearest parking lot or a charging station (CS) but also reduces time and money of the driver and the problem of congestion on the roads and CS.

The proposed model also helps in reducing the peak power and voltage drop. First of all, we need to have a clear view of all the components of the model such as workplace, charging station, EV, and distribution system of the place under observation. Workplaces like campus where there are a lot of parking lots are very best places to start the observations such as the driving habits of the people. Distribution system of that area taking into account the number of transformers connected to supply the whole workplace. An EV present in the area is also important to note as the type of EV and the driver's behavior will decide the amount of load that it would exert on our system. Recharging is the main problem; this strategy helps in suggesting the best possible route to reach the CS. There are some objectives which the consumer must follow and some prerequisites which the system must get before proposing a model. According to the transformer loading rate, the strategy and the optimum path proposed can change to decrease the voltage drop of the system. Connecting vehicle to grid is also a very good option as their will be no unbalancing at any point of time [43].

Due to short range and large recharging time of EV, there is need for the fast charging stations. We know that it is impossible to charge the batteries alike that of filling the tanks of oil-based vehicles with the present technology but with DC fast charging, it possible to boost the battery level from 0 to 80% of a 39 kWh battery pack in 57 min. This paper demonstrates the consequences of DC fast charging station for an EV [44]. Basically, DC fast charging stations connect the EV to the grid via a charger to charge the batteries. Power electronic devices such as IGBT, Thyristor, and MOSFET are used in inverter units for AC to variable DC conversion for the EV charging. The major problem faced by the EV consumer is the lack of infrastructure of EV stations. The same problem was faced in case of oil-based vehicles at the starting. Although, number of EVs are on roads have increased but there are only few recharging stations.

Apart from charging stations, charging is also a major concern. The new launched Hyundai 'Kona' takes about 1 h to charge up to 80% with DC fast charging station. Therefore, we need station where up to 8–10 vehicles can be charged simultaneously without affecting the main grid.

5.2 Solar-Powered Electric Vehicle

EV has not become an acceptable solution due to its short range and large recharging time. For improving driving range of EV, we require a high energy density battery with

less weight. Till date, we have Lithium-ion battery which are fulfilling requirement but their charging time is large. These problems of EV can be overcome to some extent by using solar power. Basically, an EV completely or partially powered by direct solar energy by using solar panel is known as the solar vehicle, by using photovoltaic cells in solar array which converts the sun light directly into electrical energy [45]. Many cities in India has good solar electrical potential, so we can use solar energy to recharge Lithium-ion batteries of EV which eliminate the time required for charging at workplace or EV charging stations. The existing solar panel which can be mounted on the top of vehicle has a capacity to produce 125 W per hour. At least 3 solar panels can be used with the existing dimension of EV [46]. As we know solar power produced by solar panels are DC which can be directly stored in batteries which will result in a large range per charge. Solar energy can also be used to charge EV with Solar Edge inverter integrated EV charger which allows fast charging as compared to level 1 charger (Household charger). Basically it is an EV charger that is integrated with an inverter. This charger combines the DC power provided by the solar panel and the AC power by the grid which results in fast charging and further reducing the electricity bills. EV level 1 charger adds 5 miles in 1 h but by using Solar Edge inverter integrated EV charger, we can charge 25–30 miles in 1 h which is more effective. Therefore, EV owner can charge 6 times faster than the standard level 1 charger [47].

It uses single-phase inverter for converting DC power from the solar panel to AC power and combines it with the AC power from the grid. It is the most economical, simpler, and reliable method [48]. Can really the EV have a positive impact on the Economics of Electric Energy Usage?

"TIME OF USE" policy [49] is used by several companies. This policy changes the price of the electricity as per usage of it during the day. The price of electricity rises when its demand is at peak whereas it reduces when the demand is low.

5.3 Future Trends

Charging time is also a vital factor while considering for implementation of EV. The e-rickshaw launched by Mjindal Group [50] also known as "SHAGUN" takes about 6 h to charge and gives a mileage of 90 km. The major cost of the vehicle is covered by the battery. About 50–60% of the quoted price includes just the battery. So, one solution to the problem is that battery size should be reduced. But if the battery size is reduced, the mileage of the EV would further reduce thus making the condition worse of long distance travels. But if the vehicle is charged while it is moving, then the battery size can be reduced without compromising with the mileage. The concept of wireless charging comes from smart phones which use electromagnetic induction to charge. Similarly, here, the load is the vehicle which is in motion. A metal plate named power track [51] is laid on the road which has coils beneath it. The power track is connected to an inverter which turns ON only when a vehicle passes over it. As the vehicle passes over the power track, the battery is charged due to electromagnetic

induction. These tracks can be laid at equal distances thus the battery gets charged while the vehicle is not idle. Thus there is no need of using battery with high rating. This can lead to more economical and convenient way of implementing an EV. The vehicles need not to be charged for long hours continuously thus reducing the impact on supply grid. As compared to conventional vehicle, the EV charged by wireless charger would be more cost effective and cheaper. This could lead to a reduction in the price of the EV.

6 Conclusions

EV is the major means of transportation for tomorrow. The future demands a large-scale development of EV and as per the present scenario, it is going to be an inevitable trend. In this paper, there are various types of EVs discussed. The characteristics, design requirements, and control schemes of battery, inverter, and converter and various machines and drives have been reviewed. Also, the upcoming technology of power exchange between grid and vehicle is highlighted. EV and its integration with grid are long-term goal which is quite beneficial for the environment as well as to the grid itself but it requires government support, power utilities to make it happen. Also, mathematical analysis regarding performance of EV is required to observe its challenges to integrate with the grid.

References

1. https://en.wikipedia.org/wiki/history_of_the_electric_vehicle
2. https://www.sciencedirect.com/science/article/pii/S1364032113006370#bibliog0005
3. Liu, L., Kong, F., Liu, X., Peng, Y., Wang, Q.: A review on electric vehicles interacting with renewable energy in smart grid. Renew. Sustain. Energy Rev. **51**, 648–661 (2015). https://doi.org/10.1016/j.rser.2015.06.036
4. https://www.industr.com/en/ev-manufacturing-in-india-opportunities-challenges-2343489
5. https://en.wikipedia.org/wiki/Electricity_sector_in_India
6. https://inc42.com/buzz/bajaj-md-rajiv-bajaj-slams-confusing-government-ev-policy-for-electric-vehicles/
7. Rastogi, S.K., Sankar, A., Manglik, K., Mishra, S.K., Mohanty, S.P.: Toward the vision of all-electric vehicles in a decade [energy and security]. IEEE Consum. Electron. Mag. **8**(2), 103–107 (2019). https://doi.org/10.1109/mce.2018.2880848
8. Bellur, D.M., Kazimierczuk, M.K.: DC–DC converters for electric vehicle applications. In: 2007 Electrical Insulation Conference and Electrical Manufacturing Expo, Nashville, TN, pp. 286–293 (2007). https://doi.org/10.1109/eeic.2007.4562633
9. Bahrin, S.Z.A.S.K., Razali, N.M.M., Jalal, T.S., Anisa, U., Amirulddin, U.: Evaluating the potential of solenoid motion system for electric vehicle—challenging the conventional usage of electric motor. In: 2008 IEEE 2nd International Power and Energy Conference, Johor Bahru, pp. 726–730 (2008). https://doi.org/10.1109/pecon.2008.4762570
10. Ehsani, M., Rahman, K.M., Toliyat, H.: Propulsion system design of electric and hybrid vehicles. IEEE Trans. Ind. Electron. **44**(1), 19–27 (1997)

11. Novotny, D.W., Lipo, T.A.: Vector control and dynamics of AC drives. Clarendon, UK, Oxford (1996)
12. Khater, F.M.H., Novotny, D.W.: Efficiency optimization for constant horsepower operation of induction machines. In: Proceedings of International Conference on Evolution and Modern Aspects of Induction Machines, pp. 9–16, July 1986
13. Kirscehn, D.S., Novotny, D.W., Lipo, T.A.: Optimal efficiency control of an induction motor drive. IEEE Trans. Energy Convers. **2**(1), 70–76 (1987)
14. Fahimi, B., Emadi, A., Sepe, R.B.: A switched reluctance machine-based starter/alternator for more-electric cars. IEEE Trans. Energy Convers. **19**(1), 116–124 (2004)
15. Rahman, K.M., Schulz, S.E.: Design of high-efficiency and high-torque-density switched reluctance motor for vehicle propulsion. IEEE Trans. Ind. Appl. **38**(6), 1500–1507 (2002)
16. Ramamurthy, S.S., Balda, J.C.: Sizing a switched reluctance motor for electric vehicles. IEEE Trans. Ind. Appl. **37**(5), 1256–1263 (2001)
17. Rahman, K.M., Fahimi, B., Suresh, G., Rajarathnam, A.V., Ehsani, M.: Advantages of switched reluctance motor applications to EV and HEV: design and control issues. IEEE Trans. Ind. Appl. **36**(1), 111–121 (2000)
18. Umamaheswari, S., Thakura, P.R., Keshri, R.K.: Hardware development of voltage source inverter for hybrid electric vehicle. In: 2011 1st International Conference on Electrical Energy Systems, Newport Beach, CA, pp. 67–71 (2011). https://doi.org/10.1109/icees.2011.5725304
19. Frieske, B., Kloetzke, M., Mauser, F.: Trends in vehicle concept and key technology development for hybrid and battery electric vehicles. 2013 World Electric Vehicle Symposium and Exhibition (EVS27), Barcelona, pp. 1–12 (2013). https://doi.org/10.1109/evs.2013.6914783
20. Khaligh, A., Li, Z.: Battery ultra capacitor fuel cell and hybrid energy storage systems for electric hybrid electric fuel cell and plug-in hybrid electric vehicles: state of the art. IEEE Trans. Veh. Tech. **59**(6), 2806–2814 (2010)
21. Zou, Y., Li, S.E., Shao, B., Wang, B.: State-space model with non-integer order derivatives for lithium-ion battery. Appl. Energy **161**, 330–336 (2018)
22. Weiss, H., Winkler, T., Ziegerhofer, H.: Large lithium-ion battery-powered electric vehicles—from idea to reality. 2018 ELEKTRO, Mikulov, pp. 1–5 (2018). https://doi.org/10.1109/elektro.2018.8398241
23. Kuhn, B.T., Pitel, G.E., Krein, P.T.: Electrical properties and equalization of lithium-ion cells in automotive applications. In: 2005 IEEE Vehicle Power and Propulsion Conference, Chicago, IL, pp. 5 (2005). https://doi.org/10.1109/vppc.2005.1554532
24. Frieske, B., Kloetzke, M., Mauser, F.: Trends in vehicle concept and key technology development for hybrid and battery electric vehicles. In: 2013 World Electric Vehicle Symposium and Exhibition (EVS27), Barcelona, pp. 1–12 (2013). https://doi.org/10.1109/evs.2013.6914783
25. Zhang, L., Hu, X., Wang, Z., Sun, F., Dorrell, D.G.: Experimental impedance investigation of an ultracapacitor at different conditions for electric vehicle applications. J. Power Sour. **287**, 129–138 (2015)
26. Deshpande, V.S., Talele, M.N.: Nanotechnology enabled hybrid power system suitable for batteries in hybrid electric vehicle. In: 2017 Third International Conference on Advances in Electrical, Electronics, Information, Communication and Bio-Informatics (AEEICB), Chennai, pp. 33–35 (2017). https://doi.org/10.1109/aeeicb.2017.7972378
27. Wilcke, W.W., Kim, H.: The 800-km battery lithium-ion batteries are played out. Next up: lithium-air. IEEE Spectr. **53**(3), 42–62 (2016). https://doi.org/10.1109/MSPEC.2016.7420398
28. Rajashekara, K.: Present status and future trends in electric vehicle propulsion technologies. IEEE J. Emerg. Sel. Top. Power Electron. **1**(1), 3–10 (2013). https://doi.org/10.1109/JESTPE.2013.2259614
29. Ota, Y., Taniguchi, H., Nakajima, T. et al.: Effect of autonomous distributed vehicle-to-grid (V2G) on power system frequency control. In: International Conference on Industrial and Information Systems (ICIIS) (2010)
30. Chen, Z., Liu, Q., Xiao, X., Liu, N., Yan, X.: Integrated mode and key issues of renewable energy sources and electric vehicles' charging and discharging facilities in microgrid. In: 2nd IET Renewable Power Generation Conference (RPG 2013), Beijing, pp. 1–4 (2013). https://doi.org/10.1049/cp.2013.1759

31. Ota, Y., Taniguchi, H., Nakajima, T. et al.: Effect of autonomous distributed vehicle-to-grid (V2G) on power system frequency control. International Conference on Industrial and Information Systems (ICIIS) (2010)
32. Zgheib, R., Al-Haddad, K., Kamwa, I.: V2G G2V and active filter operation of a bidirectional battery charger for electric vehicles. In: Proceedings of IEEE International Conference Industrial Technologies Taipei Taiwan, pp. 1260–1265 (2016)
33. Monteiro, V., Pinto, J.G., Afonso, J.L.: Operation modes for the electric vehicle in smart grids and smart homes: present and proposed modes. IEEE Trans. Veh. Technol. **65**(3), 1007–1020 (2016)
34. Mwasilu, F., Justo, J.J., Kim, E.-K., Do, T.D., Jung, J.-W.: Electric vehicles and smart grid interaction: a review on vehicle to grid and renewable energy sources integration. Renew. Sustain. Energy Rev. **34**, 501–516 (2014). https://doi.org/10.1016/j.rser.2014.03.031
35. Li, C., Luo, F., Chen, Y., Xu, Z., An, Y., Li, X.: Smart home energy management with vehicle-to-home technology. In: 2017 13th IEEE International Conference on Control & Automation (ICCA), Ohrid, pp. 136–142 (2017). https://doi.org/10.1109/icca.2017.8003048
36. Wi, Y., Lee, J., Joo, S.: Smart electric vehicle charging for smart home/building with a photovoltaic system. In: 2013 IEEE International Conference on Consumer Electronics (ICCE), Las Vegas, NV, pp. 548–549 (2013). https://doi.org/10.1109/icce.2013.6487014
37. Ehsani, M., Falahi, M., Lotfifard, S.: Vehicle to grid services: potential and applications. Energies **5**(10), 4076–4090 (2012)
38. Kisacikoglu, M.C., Ozpineci, B., Tolbert, L.M.: Examination of a PHEV bidirectional charger system for V2G reactive power compensation. In: Proceedings of IEEE Applications Power Electronics Conference Exposition pp. 458–465, Feb 2010
39. Turisyn, K., Sulc, P., Backhaus, S., Chertkov, M.: Local control of reactive power by distributed photovoltaic generators. In: Proceedings of IEEE International Conference on Smart Grid Communications, pp. 79–84, Oct 2010
40. Pang, C., Kezunovic, M., Ehsani, M.: Demand side management by using electric vehicles as distributed energy resources. In: 2012 IEEE International Electric Vehicle Conference, Greenville, SC, pp. 1–7 (2012). https://doi.org/10.1109/ievc.2012.6183273
41. González, L.G., Siavichay, E., Espinoza, J.L.: Impact of EV fast charging stations on the power distribution network of a Latin American intermediate city. Renew. Sustain. Energy Rev. **107**, 309–318 (2019). https://doi.org/10.1016/j.rser.2019.03.017
42. NT: 519-2014 IEEE Recommended Practice and Requirements for Harmonic Control in Electric Power Systems. n.d
43. Yagcitekin, B., Uzunoglu, M.: A double-layer smart charging strategy of electric vehicles taking routing and charge scheduling into account. Appl. Energy **167**, 407–419 (2016). https://doi.org/10.1016/j.apenergy.2015.09.040
44. Etezadi-Amoli, M., Choma, K., Stefani, J.: Rapid-charge electric-vehicle stations. IEEE Trans. Power Del. **25**(3), 1883–1887 (2010). https://doi.org/10.1109/tpwrd.2010.2047874
45. https://en.wikipedia.org/wiki/Solar_vehicle
46. Hussin, M.A., Abdalla, A.N., Ishak, R., Abdullah, R., Ali, Z.M.: Study on improving electric vehicle drive range using solar energy. In: International Conference on Electrical, Control and Computer Engineering 2011 (InECCE), Pahang, pp. 373–376 (2011).https://doi.org/10.1109/inecce.2011.5953909
47. https://www.civicsolar.com/article/charging-electric-cars-solar-power
48. Cheng, Y., Duan, F., Cui, S.: The design principle of electric motors and drive systems for electric vehicles. In: 2005 International Conference on Electrical Machines and Systems, Nanjing, vol. 1, pp. 802–805. https://doi.org/10.1109/icems.2005.20264727
49. Dufo-López, R., Artal-Sevil, J.S., Bernal-Agustín, J.L., Domínguez-Navarro, J.A.: Can electric vehicles reduce electricity bill? In: 2014 IEEE International Electric Vehicle Conference (IEVC), Florence, pp. 1–4 (2014). https://doi.org/10.1109/ievc.2014.7056109

50. http://www.mjindalgroup.in/
51. Jeong, S., Jang, Y.J., Kum, D., Lee, M.S.: Charging automation for electric vehicles: is a smaller battery good for the wireless charging electric vehicles? IEEE Trans. Autom. Sci. Eng. **16**(1), 486–497 (2019). https://doi.org/10.1109/TASE.2018.2827954

HVDC Transmission Topology and Control Analysis

Ravi Shankar Tiwari

1 Introduction

The energy is dispersed to the surrounding into various forms out of electrical energy which is one of the highest forms easily transported and converted into other forms of energy. Industrial growth and rising per-capita energy consumption shoot its demand on every part of the world. This creates an efficient and economical power transmission requirement between remotely located generation and consumers. Power is being traditionally transported using high voltage alternating current (HVAC) transmission of 132, 220, 400, 765 kV and more for long distance to get the advantage of reduction in losses, cost of power. However, transmission cost, system stability, and power flow control are the important issues for power transmission beyond 500 km. The innovation in power electronics, deregulation, and restructuring in power sector encourages the transmission utility to trade power among the remotely located generator to consumers [1]. Thus, bulk power transmission over long-distance and interconnected local, regional, national, and international generations is a win-win situation for both consumers and generation utilities.

The high voltage direct current transmission (HVDC) is one of economical, secure, and fast controllable alternative of power transmission for distance beyond 500 km. The main constituents are three-phase controllable power electronics converter valves, which serve the function conversion from AC to DC and vice versa and provide interfacing between AC-DC systems [2]. The present installed capacity of HVDC transmission is greater than 75,000 MW in 90 projects worldwide. The highest transmission voltage is 1100 kV over 3300 km with power capacity of 12 GW started between Northwest China's Xinjiang and southern Anhui province leading to 2385 km, ± 600 kV Rio Madeira Brazil. The encouraging features of HVDC

R. S. Tiwari (✉)
GLA University, Mathura, UP 281406, India
e-mail: ravishankar.tiwari@gla.ac.in

O. H. Gupta and V. K. Sood (eds.), *Recent Advances in Power Systems*, Lecture Notes in Electrical Engineering 699, https://doi.org/10.1007/978-981-15-7994-3_15

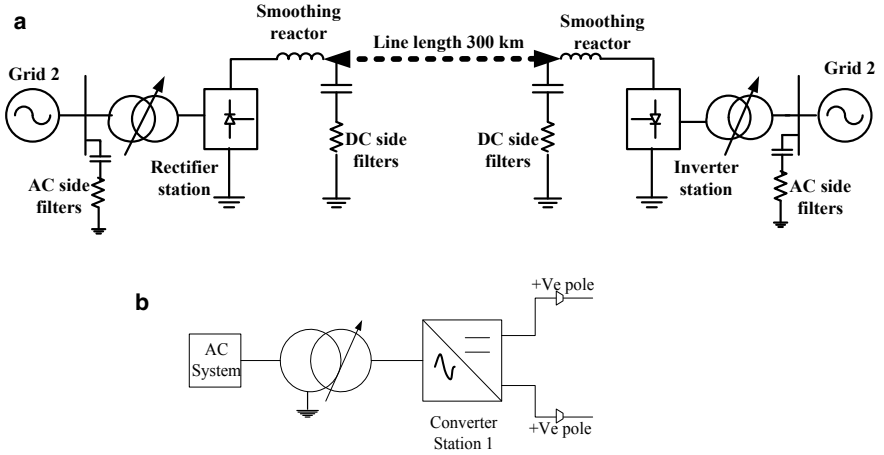

Fig. 1 **a** 2-terminal mono-polar HVDC configuration, **b** symmetrical mono-polar configuration

transmission over HVAC are its ability of controlled power transmission, improved stability, limited fault currents, and independent of reactive compensation for lines and loading ability closer to thermal limit. However, in HVAC transferable power is a function of distance, steady state, transient and thermal limits and the requirement of reactive compensation based on line loading [3]. The aforementioned advantages do not anticipate that HVDC transmission totally eliminates the AC but advancement in technology and development in multi-terminal direct current (MTDC) transmission are expected to increase its scope and future. Thus, it is fruitful to understand and enhance the research in the field of HVDC transmission. The rest of the paper is organized as: Sect. 2 covers the various configurations of HVDC system and their application. Section 3 explains about HVDC control and characteristics. Similarly, Sect. 4 analyzes the steady state and transients system operation due to AC or DC disturbances using test system Fig. 1a. Of mono-polar HVDC transmission system using PSCAD/EMTDC, lastly Sect. 5 concludes the results.

2 HVDC System and Converter Topology

The HVDC systems are configured into four basic structures to attain the desired requirement and performance, namely mono-polar, bipolar, back to back and multi-terminal HVDC which can further be divided into symmetric and unsymmetrical topologies.

2.1 Symmetric and Asymmetric Mono-Polar Topology

The mono-polar DC lines uses single wire of negative polarity with grounding or metallic return path in line commutated converters (LCC) or midpoint grounding of DC link capacitor in voltage source converter (VSC)-based DC lines. This configuration is having advantage that any pole to ground faults do not feed by AC side current and transformer is independent of any DC voltage stress. Asymmetric mono-polar consisting of single converter with neutral grounded [4].

2.2 Bipolar Configuration

This topology uses two mono-polar at both terminal with ground or metallic return to achieve double the power rating compared to mono-polar configuration. The two poles are usually of opposite polarities to reduce corona losses and eliminate the current through ground or metallic return. Two different transformer groups are employed to connect each converter from AC grid one uses Yg-Δ while other uses Yg-Y configurations to minimize the AC side harmonic distortion [5].

2.3 Back-to-Back Configuration

This configuration is used to interconnect two asynchronous AC systems where both the inverter and rectifier are located at the same station. The total system cost decreases due to the absence of cable or line length but the electrical length present due to the presence of reactor in series.

2.4 Multi-terminal Configuration (MTDC)

MTDC consisting of more than two sets of converter station operating independently either as an inverter or a rectifier station interconnect into the DC network. This configuration is helpful in accessing power from various distributed generations such as offshore wind and solar generations [6]. Figures 1a, b and 2a, b represent the various HVDC system topologies.

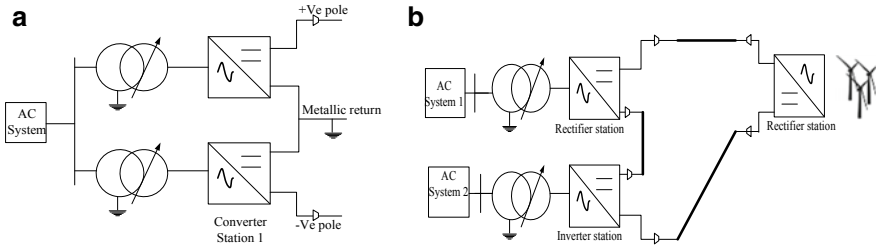

Fig. 2 **a** Bipolar metallic return system, **b** 3-terminal MTDC system

2.5 Converter Topologies

The HVDC system converts the AC power at sending station into DC for long-distance transmission and again into AC at the receiving station by rectifier and inverters, respectively. These converters are based on line commutated current (LCC) and voltage source converter (VSC) technologies. LCC also known as current source converters (CSC) consisting of thyristor-based unidirectional switch triggered by gate pulse and stays on until zero crossing of current occurs and having reverse voltage blocking capacity of 10 kV and current ratings of 6 kA [7]. The power reversal in DC link is obtained by reversing the polarities of voltages at both sending end and receiving end converter stations while the direction of current flow remains the same. The LCC is the most popular for HVDC transmission system due to its lower converter losses, good reliability, and overload capability. Moreover, LCC technology faces the shortcoming of the generation of higher harmonics on both DC and AC side, huge filter requirement, needs strong associate AC network and unable to black start.

The VSC is another insulated gate bipolar transistor (IGBT) or gate turn off (GTO)-based self-commutated HVDC converter technology offering wide and flexible power flow control [8]. High-frequency pulse width modulation (PWM) provides the capability of instantaneous phase and amplitude control to any value; thus, active and reactive power can be controlled independently unlike to conventional LCC HVDC [9]. VSC consumes and generates a wide range of reactive power even at zero active power situations via fast control action. Power inversion is achieved by inverting the current instead of reversing the voltage polarities as for conventional CSC. In contrast with LCC HVDC, VSC possessed multi-terminal configuration and easier expansibility and makes possible the connection of number of converters to a common bipolar DC bus. The post-fault transient stability for interconnected wind firms is improved by controlling active power of VSC converters [10, 11]. Besides these merits, VSC presents certain drawbacks compared to the LCC technology such as higher converter cost and losses, not capable of emergency power supply during tripping of one pole, more expository DC line to ground faults, etc., restricts its application for 2-terminal HVDC transmission [12].

3 System Control Analysis

The idea of HVDC control is to regulate the power flow between the terminals, stabilize the AC system under small disturbance. It is anticipated that control system tolerate the changes in voltage magnitude, phase, and transient in AC system without creating problem of sub-synchronous resonance, non-characteristic harmonics, electromechanical oscillation, voltage instability, and operating point instability. Furthermore, the HVDC control is also expected to refine its performance and reliability [13]. The conventional control of HVDC system is termed as marginal current control method (MCCM) where hierarchical control supplies reference power to the power used to calculate the current order (I_{order}) which is compared with measured DC line current. The generated error passed through current control (CC) amplifier and to converter α angle control to calculate the firing instant of valves [14]. Figure 3 presents an overview of HVDC system control.

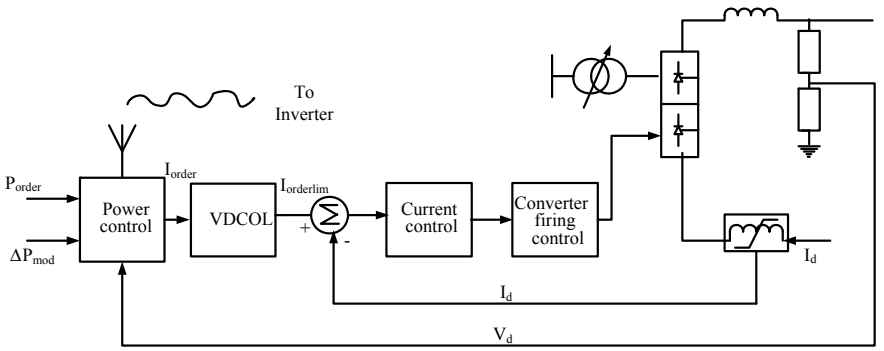

Fig. 3 Overview of HVDC system control

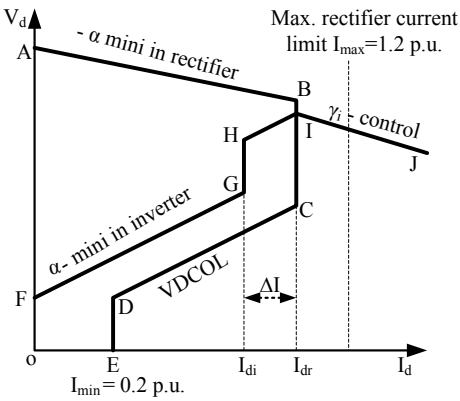

Fig. 4 V-I characteristics of HVDC rectifier and inverter station

The calculation of the exact instant of firing provides the benefits of reduced overvoltage across and short-circuit current through the valves. It minimizes the consumption of reactive power and avoids multiple commutation failures. The firing control unit determines the rated voltage by utilizing the output of current control, voltage control, minimum α-control (CIA) or maximum α control (γ-control) or constant extinction angle control (CEA) to determine the exact firing instant. Normally, inverter operates in constant voltage control mode also provided with DC current error control (CER), CC, and CEA control modes [15].

Figure 4 shows the $V_d - I_d$ characteristics of HVDC to understand its operation. Conventionally, inverter controls the voltage by constant commutation control or CEA control and rectifier in constant current under steady-state operation. In order to maintain the stability, the deviation in current ($I_{\text{order}} - I_d$) and ($\gamma_{\text{ref}} - \gamma_{\text{meas}}$) should be minimum and the intersection point of the two current and voltage control characteristics gives its operating point.

The equation determining the minimum firing angle characteristics at rectifier end is expressed by Eqs. 1 and 2.

$$V_{\text{dc}} = V_{di0} \cos\alpha - (T_{xN} + T_{rN}) \frac{V_{di0N}}{I_{dcN}} I_{\text{dc}} \tag{1}$$

$$V_{\text{dc}} = V_{di0} \cos\gamma - (T_{xN} + T_{rN}) \frac{V_{di0N}}{I_{dcN}} I_{\text{dc}} \tag{2}$$

Voltage across converter for a minimum firing angle α and transformer reactance $(T_{xN} + T_{rN}) \frac{V_{di0N}}{I_{dcN}} I_{\text{dc}}$ can be determined. Pre-firing voltage and reactance of transformer are assumed to be constant so DC voltage reduces with increase in line current. The CC characteristics can also obtain by Eq. 1 by considering variable α and constant DC current I_{dc}. Equation 2 determines the constant extinction angle characteristics of inverter operated at maximum α-angle. Normally, Υ maintained at 17° and not allow to rise or fall below this to avoid variation in reactive power demand and commutation failure. The minimum α at inverter is used to maintain at 110° so that during fault both converter can operate as inverter to limit the fault current as early as possible. So inverters are provided with minimum α limit. Both the inverter and rectifier are provided with current controller with a difference in current margin of 10%. Inverter current margin kept lower the rectifier and usually inactive. Maximum current margin at rectifier 1.2 P.U. and not allowed to be zero any time.

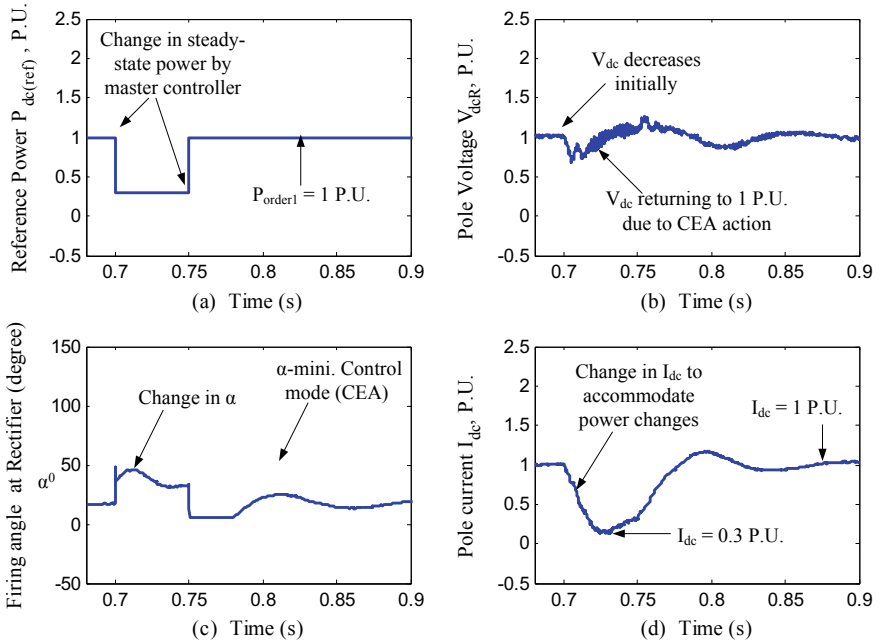

Fig. 5 HVDC control response during steady-state change

4 Results and Discussion

4.1 Steady-State Operation and Control Analysis

Out of the above-discussed control strategies, CC, VDCO, and γ minimum are analyzing the test system (Fig. 1) under steady-state and transient action condition. The system data is reported in Appendix 1. Figure 3a–d shows the variation of reference power, DC line voltage, α-angle, and DC line current, respectively. The change in P_{order} from 1 P.U. to 0.3 P.U. leads reduction in $I_{\text{dref,}}$ and the current controller determines α shifted to 45°−50° to reduce DC line current such that HVDC system can operate in constant power mode. The CEA or γ-control maintains DC the voltage fluctuation negligible and restores the DC bus voltage to 1 P.U (Fig. 5).

4.2 Transient Operation and Control Analysis

The transient conditions on HVDC interconnected system may be over-voltage due to lightning, under voltages, and short-circuit condition due to faults in AC–DC, etc. Figure 4a–d shows the rectifier end waveform during short-circuit faults at inverter

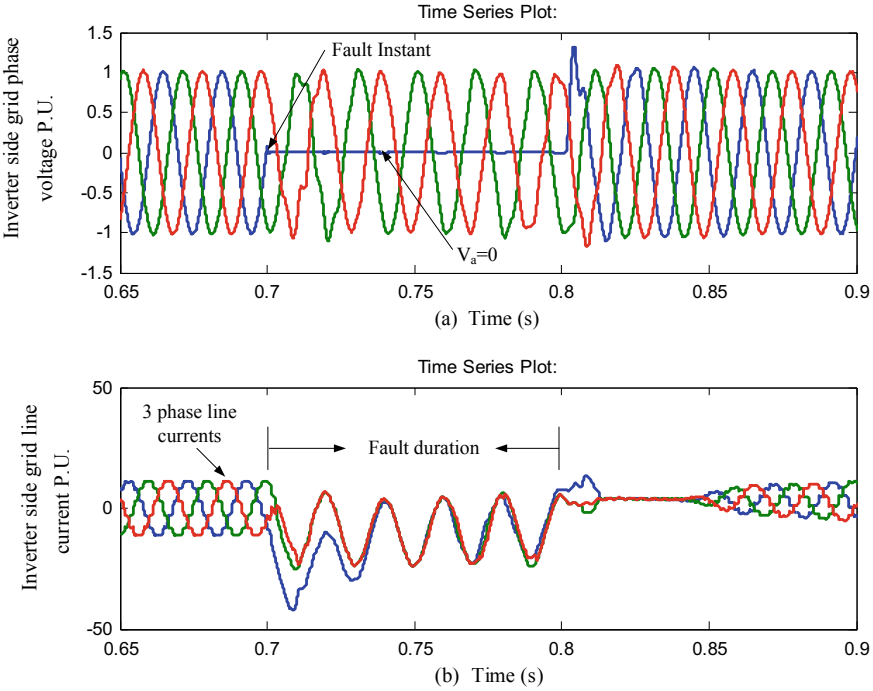

Fig. 6 Inverter side grid waveform during single phase to ground short circuit

side AC system. Single-phase short circuit fault results quick rise in DC line current may cause damage to the converter valves. The VDCOL controller shift its current margin supplied to the current control amplifier. The controller at rectifier shifted from CC to α-maximum ($\alpha > 90°$) system so as to pull rectifier into inverter mode and to limit the DC line current (Figs. 6 and 7).

5 Conclusion

The innovation and development in power electronics popularize the long distance, bulk DC power transmission via HVDC lines. The various HVDC line configurations and two dominant converter technologies are discussed based on application, cost, and efficiency. The paper also covers the converter control strategy for 2-terminal HVDC configurations to understand its operation during steady-state and dynamic conditions. A mono-polar 2-terminal HVDC transmission system is simulated using PSCAD/EMTDC to analyze the control behavior. The results show that the current controller (CC) and constant extinction angle controller (CEA) together with VDCOL control at rectifier and inverter ends tries to stabilize the disturbance generated during steady-state and transient condition on both AC–DC sides.

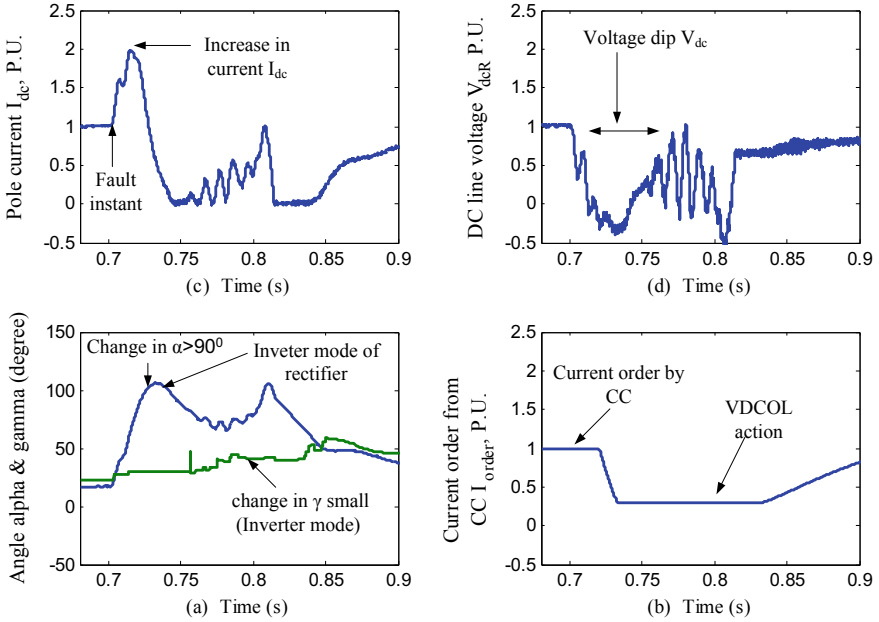

Fig. 7 HVDC system response for inverter side AC system disturbance

Appendix 1

The test system Fig. 1a data of MATLAB Hydro-Quebec mono-polar HVDC model of DC line length 300 km is provided in Table 1.

Table 1 Test system parameters

Components	Rating
Power	1000 MW
DC voltage level	± 500 kV
DC line current	2 kA
Converter	1200 MVA
Rectifier side grid 1 voltage, frequency, and power	500 kV, 60 Hz, 5000 MVA
Inverter side grid 2 voltage, frequency, and power frequency and power	345 kV, 50 Hz, 10,000 MVA
Smoothing reactor	0.5 H
AC filter 1	600 Mvar at 60 Hz
AC filter 2	600 Mvar at 50 Hz

References

1. Ahmad, F., Alam, M.S.: Assessment of power exchange based electricity market in India. Energy Strateg. Rev. **23**, 163–177 (2019). https://doi.org/10.1016/j.esr.2018.12.012
2. Kim, C.K., Sood, V.K., Jang, G.S., Lim, S.J., Lee, S.J.: Development of HVDC Technology. HVDC Transm., pp. 1–35 (2010). https://doi.org/10.1002/9780470822975.ch1
3. Kincic, S., Papic, M.: Impact of series compensation on the voltage profile of transmission lines. In: 2013 IEEE Power & Energy Society General Meeting, pp. 1–5 2013. https://doi.org/10.1109/PESMG.2013.6672105
4. Sellick, R.L., Åkerberg, M.: Comparison of HVDC light (VSC) and HVDC classic (LCC) site aspects, for a 500 MW 400 kV HVDC transmission scheme. In: 10th IET International Conference on AC and DC Power Transmission (ACDC 2012), vol. 2012, no. 610 pp. 23–23 (2012). https://doi.org/10.1049/cp.2012.1945
5. Okba, M.H., Saied, M.H., Mostafa, M.Z., Abdel-Moneim, T.M.: High voltage direct current transmission—a review, Part II—converter technologies. In: 2012 IEEE Energytech, May 2012, pp. 1–7 (2012). https://doi.org/10.1109/energytech.2012.6304651
6. Kontos, E., Pinto, R.T., Rodrigues, S., Bauer, P.: Impact of HVDC transmission system topology on multiterminal DC network faults. IEEE Trans. Power Del. **30**(2), 844–852 (2015). https://doi.org/10.1109/TPWRD.2014.2357056
7. Oni, O.E., Mbangula, K.I., Davidson, I.E.: A review of LCC-HVDC and VSC-HVDC technologies and applications. Trans. Environ. Electr. Eng. **1**(3), 68 (2016). https://doi.org/10.22149/teee.v1i3.29
8. Bandaru, T., Dhawa, U., Chatterjee, D., Bhattacharya, T.: Improving the Transient Stability by Modifying the Power Exchange by the HVDC Transmission
9. Abbas, A.M., Lehn, P.W.: PWM based VSC-HVDC systems; a review. In: 2009 IEEE Power & Energy Society General Meeting, Jul 2009, pp. 1–9. https://doi.org/10.1109/pes.2009.5275751
10. Mitra, A., Chatterjee, D.: Active power control of DFIG-based wind farm for improvement of transient stability of power systems. IEEE Trans. Power Syst. **31**(1), 82–93 (2016). https://doi.org/10.1109/TPWRS.2015.2397974
11. Patari, N., Chatterjee, D., Bhattacharya,, T.: Transient stability improvement by pre-fault and post-fault modifications in wind power plant control
12. Alassi, A., Bañales, S., Ellabban, O., Adam, G., MacIver, C.: HVDC transmission: technology review, market trends and future outlook. Renew. Sustain. Energy Rev. **112**, 530–554 (2019). https://doi.org/10.1016/j.rser.2019.04.062
13. Povh, D., Thepparat, P., Westermann, D.: Further development of HVDC control. In: 2011 IEEE Trondheim PowerTech, Jun. 2011, pp. 1–8. https://doi.org/10.1109/ptc.2011.6019447
14. Xu, J., et al.: A coordinated marginal current control method for LCC-HVDC. IEEE Trans. Power Syst. **34**(6), 4569–4582 (2019). https://doi.org/10.1109/TPWRS.2019.2912865
15. Shah, S., Hassan, R., Sun, J.: HVDC transmission system architectures and control—a review. In: 2013 IEEE 14th Workshop on Control and Modeling for Power Electronics (COMPEL), Jun. 2013, pp. 1–8. https://doi.org/10.1109/compel.2013.6626396

Modeling and Simulation of Photovoltaic Solar Cell Microgrid

Munna Kumar, Kanak Bhengra, and Jitendra Kumar

1 Introduction

As traditional energy sources are limited so we need new energy sources such as solar energy, wind energy. Instantly, we have to use new resources and natural energy such as solar, bio, wind, tides are very suitable [1, 2]. Renewable energy is limitless on this planet. In our country, the authority revises their report that solar installed capacity has expanded from 2.60 GW to more than 12.20 GW in the last three years, a 370.0% increase. At Paris climate, GW to over e-summit held in 2017 the prime minister of India promises to increases total renewable energy capacity to 175.0 GW by 2022 [3]. At the same time, microgrids are programmed to effectively preserve different DGs and territorial capacities of load. The standard solar emission around country is 300–5000 W/m^2/day (equivalent to 3–5 h at 1000 W/m^2/day) [4]. By connecting the microgrid to the system, the transitional spiral distribution grid arrangement turns into a multi-sources system that challenges a universal protection scheme [5].

Further, traditional safety strategy cannot assure microgrid in island network. Accordingly, contemporary protection of networks with grid-connected microgrids and non-grid connected mode microgrids needs to be considered [6]. Figure 1 presents the essential modules of a microgrid. Table 1 is the input given to the solar panel, and at each irradiance, there is a separate voltage and current.

M. Kumar (✉) · K. Bhengra · J. Kumar
Electrical Department, National Institute of Technology Jamshedpur, Jamshedpur, JH, India
e-mail: meakmunna@gmail.com

K. Bhengra
e-mail: saumyakanak@gmail.com

J. Kumar
e-mail: jitendra.ee@nitjsr.ac.in

O. H. Gupta and V. K. Sood (eds.), *Recent Advances in Power Systems*, Lecture Notes in Electrical Engineering 699, https://doi.org/10.1007/978-981-15-7994-3_16

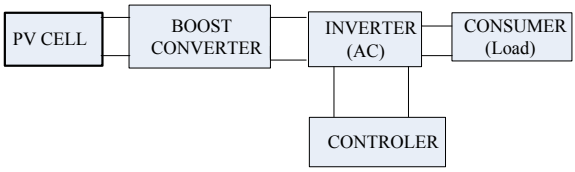

Fig. 1 Basic microgrid scheme

Table 1 Irradiant voltage and current value

Irradiant	Voltage	Current
1000	$Volt_1$	$Current_1$
900	$Volt_2$	$Current_2$
800	$Volt_3$	$Current_3$
700	$Volt_4$	$Current_4$
600	$Volt_5$	$Current_5$
500	$Volt_6$	$Current_6$

2 Micro-Grid Scheme

2.1 PV Array

The universe is developing through a photovoltaic solar system, but it depends entirely on temperature [1]. The photovoltaic units are automatically associated in parallel or/and series circuits to outcome high currents, power, and voltages levels. PV modules consist of photovoltaic unit circuits fixed in natural friendly laminates and are the basic component of photovoltaic systems [7]. A photovoltaic panel has separate or more PV modules massed as a wired system that can be installed on-site. PV is a complete power unit subsisting of several PV panels and modules [1, 7]. The characteristics of the photovoltaic array V–I are given different illuminations for different voltages and currents [Table 1]. By these value, V–I characteristics are found in simulation. As in all season or in morning, evening and noon time sun irradiance is not same so we need to track maximum irradiance. The 100 kW photovoltaic array is combined to a 2500 kW network system through a DC-to-DC converter and a 3-level VSC system. MPPT is carry out in boost converters using Simulink models. The output of module depends upon the irradiance and temperature (Figs. 2 and 3).

2.2 A Step Up Converter (DC–DC)

A step up converter or boost converter is especially the simplest shift-mode converters that boost the voltage in a power supply to a load. Step up converter is a switch-mode power supply and it consists of at least two semiconductors (transistors and diodes)

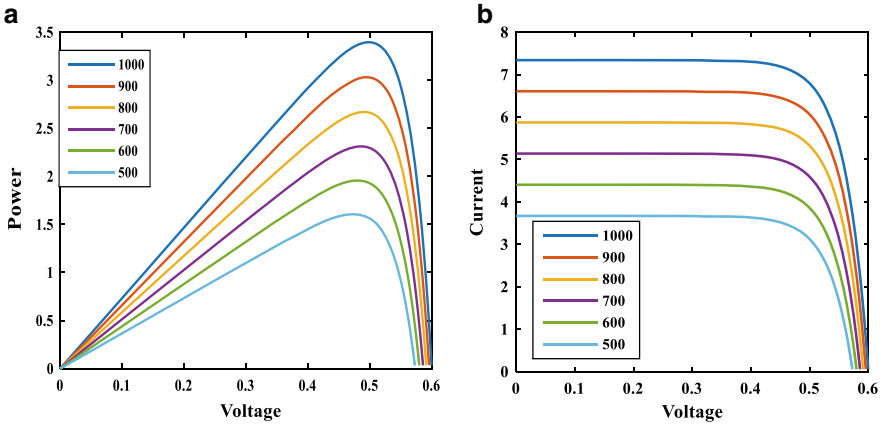

Fig. 2 Simulation result of the photovoltaic array at different irradiants, **a** voltage versus power, **b** current versus voltage

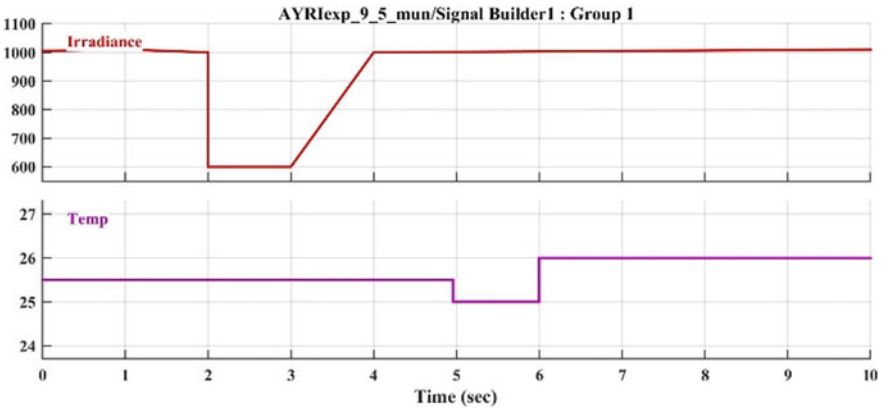

Fig. 3 Signal builder at fixed irradiance (1000) and temperature (25.5 °C)

and one energy storage integral. To decreases surge voltage, filters made along capacitors are mostly supplemental as load-side filters at the output of such converters, and inputs as supply-side filters. [8, 9]. To boost the voltage of the Photovoltaic array 213.15–422.20, a MOSFET was used. The increased voltage can be managed by using MPPT, which provides maximum output power.

2.3 MPPT Method

There is a complex communication between the absolute climate of the solar units and the resistance, resulting in a complex nonlinear output capability that can be analyzed according to the curve of I–V [10]. The function of the MPPT model is to collect the result of a photovoltaic cell under any given environmental condition and apply a suitable load to obtain high power [11]. MPPT devices are usually unified into power converter structure. To provide voltage or current conversion, filtering, and regulation to drive a variety of loads, including the supply grid, motors, or batteries [12].

2.3.1 Control Scheme of MPPT

In the MPPT algorithm (Fig. 8), duty cycle D is the initial point. Power is calculated by $P = V * I$, where P can be considered as $P_{\text{new.}}$ For perturbing the operating, let, initial operating point $D = 0.5$ and perturbation value is ΔD and ΔD is very small (0.001). The decision block decide is $P_{\text{old}} < P_{\text{new}}$ or not. If it is satisfied, it update the value of $D = D+\Delta D$ and goes to a $+\Delta D$. If the condition is not satisfied $P_{\text{old}} < P_{\text{new}}$, then it goes to $-\Delta D$ and again decision block decide is $P_{\text{old}} < P_{\text{new}}$. If it is satisfied, it goes to $D = D - \Delta D$; otherwise, it goes to decision block and this cycle is continued to track maximum power. This algorithm always works with the difference in the previous power and instantaneous power after the perturbation (Fig. 4).

2.4 Design of VSC in dq-Framework

To step down the 480.00 V DC bus voltage to 213.15 AC and maintain the power element of the VSC converter. Two control loops are required for the operation of the inverter. The loop command result maintains the three-level voltage source controller at +240 V to −240 V. To provide a single power factor detail, this control loop is used [13]. To adjust the current, there should be an arrangement of active and reactive components. Invalid components are set to 0 when the power factor will be 1 (Fig. 5).

3 Result and Discussion

Through this simulation, it was tested with PV array by using the MPPT algorithm method at different irradiant (1000–500) on 25–26 °C temperature. Then, to boost up the voltage from 213 to 422 V, a boost converter is used. For control, the solar output and network voltage, a voltage source control is layout in MATLAB software and attached with a boost converter using PV array simulation. The simulation results

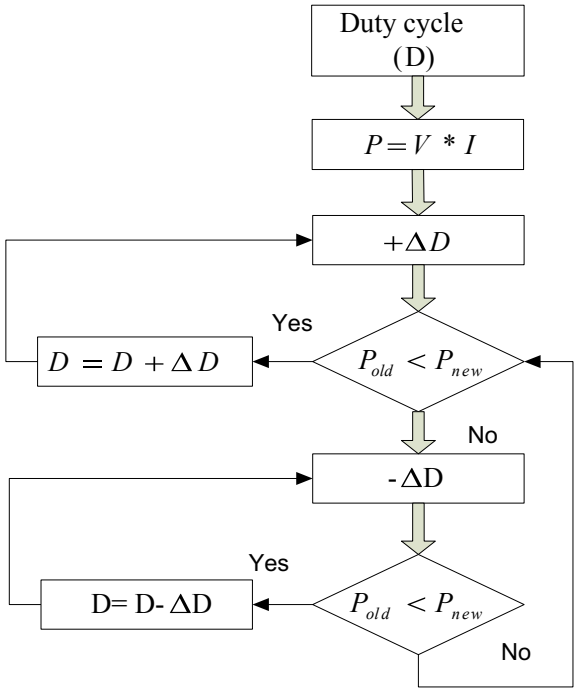

Fig. 4 MPPT algorithm [8, 15]

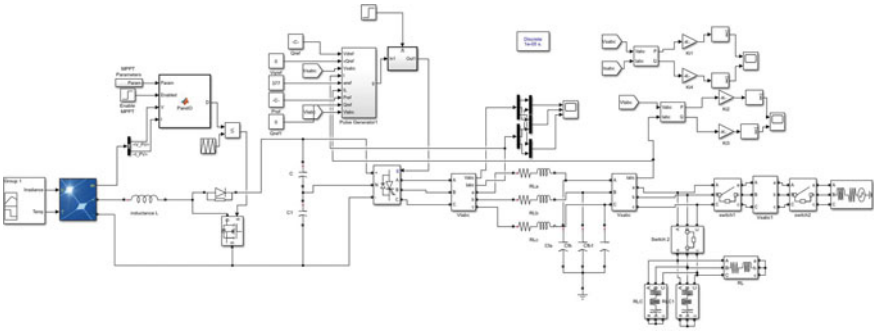

Fig. 5 Micro-grid simulation with the controller

are shown below. Active segment gates the output DC voltage of the controller as output [12, 14].

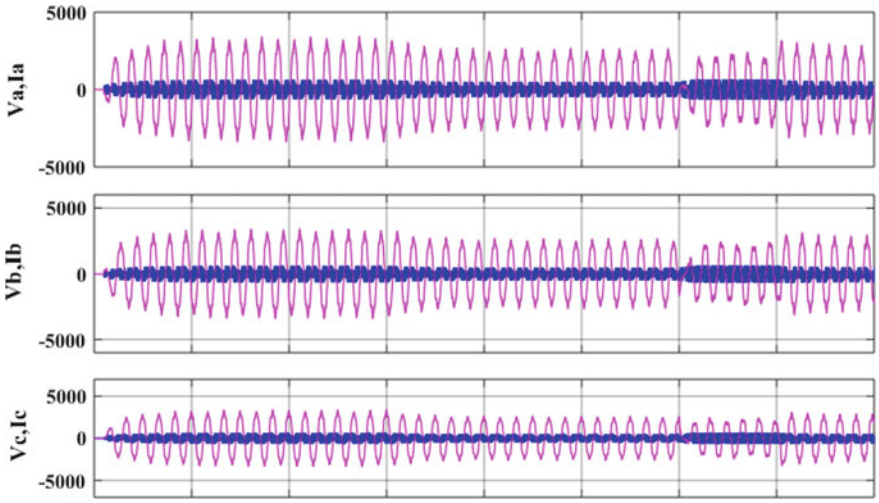

Fig. 6 Output of three-phase voltage and current variation with time

3.1 Autonomous Network Utility

The network has an ideal 2500 kW circulation channel and a 1.2 mV correspondent communication line system. A 260/24 kV generator with a rated power of 100 kVA is used to connect the microgrid to the power structure [12].

Figure 6 displays the huge harmonics at the end side because of high load and sudden fall is also observed in voltage and current. At the time of 0.6, the islanding occurs and the system acts as an islanding condition. At 0.6–0.7 s, the trip switch accessible and the microgrid continues the supply. After 0.7 s, again trip switch closed and system acts as a non-islanding condition (Figs. 7, 8 and 9).

Figure 10 shows the formation of the island is detected; the operation mode is switched to the controlled frequency mode. In Fig. 10a, voltage value is pi * 2 = 6.283 and in Fig. 10b, angular frequency φ is set to $\varphi = 314$ rad/s. As input frequency is 50 Hz, so $\varphi = 50 * 2 * \Pi$.

4 Conclusion

Through this paper, the MATLAB Simulink is done in MATLAB 2015a to develop a microgrid for a grid-connected approach as well as an islanding approach. A photovoltaic cell is allied with a step up converter to step up the input voltage. The DC–DC step up converter and MPPT method make the scheme an enticing result to develop the photovoltaic system capability. Then VSC is arranging and connects with the PV model, load, and grid. The result clearly shows that the harmonics problem

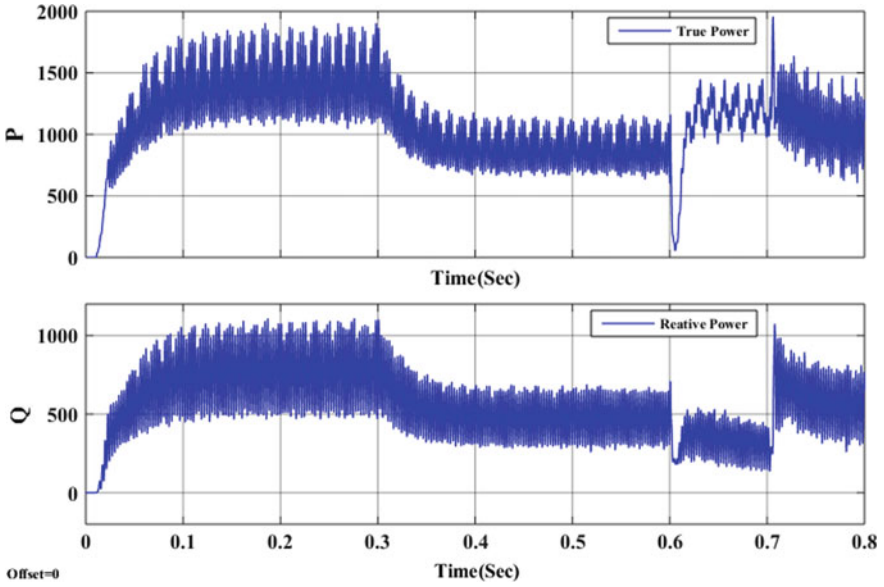

Fig. 7 Output of true and reactive power oscillation time 0.6–0.7 at the load side of the grid

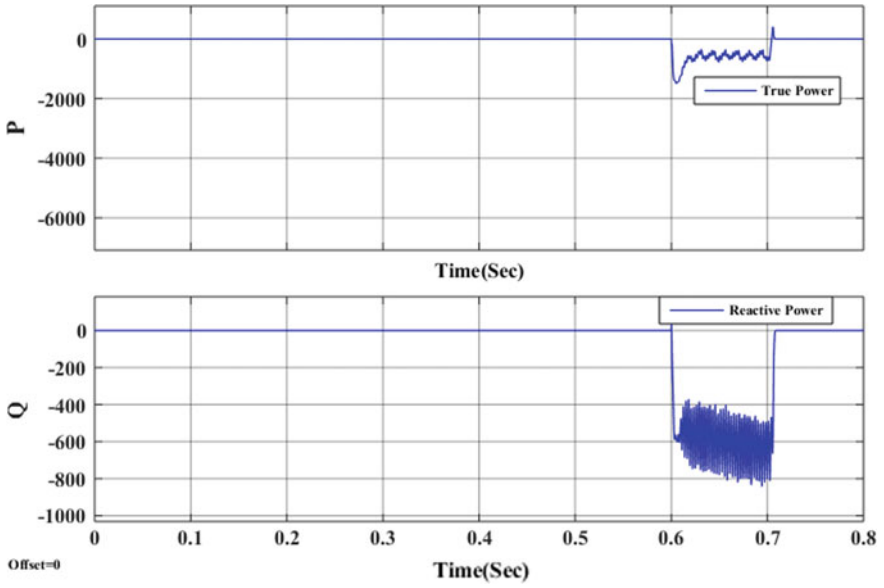

Fig. 8 The output of real and reactive power at the network side

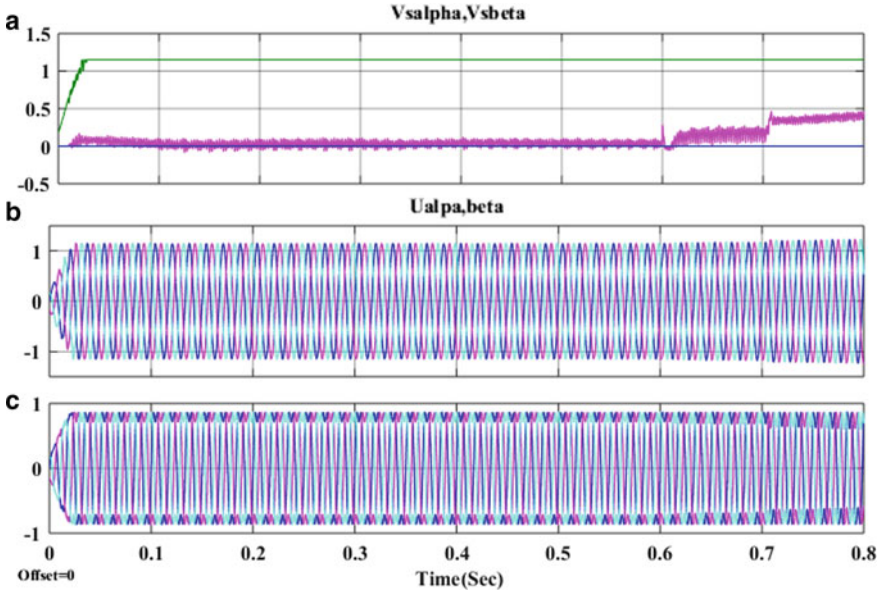

Fig. 9 **a**, **b**, **c** Startup transient and step up response of the controlled frequency VSC system under moderately loaded status, **b** is without 3rd harmonic and **c** with 3rd harmonic

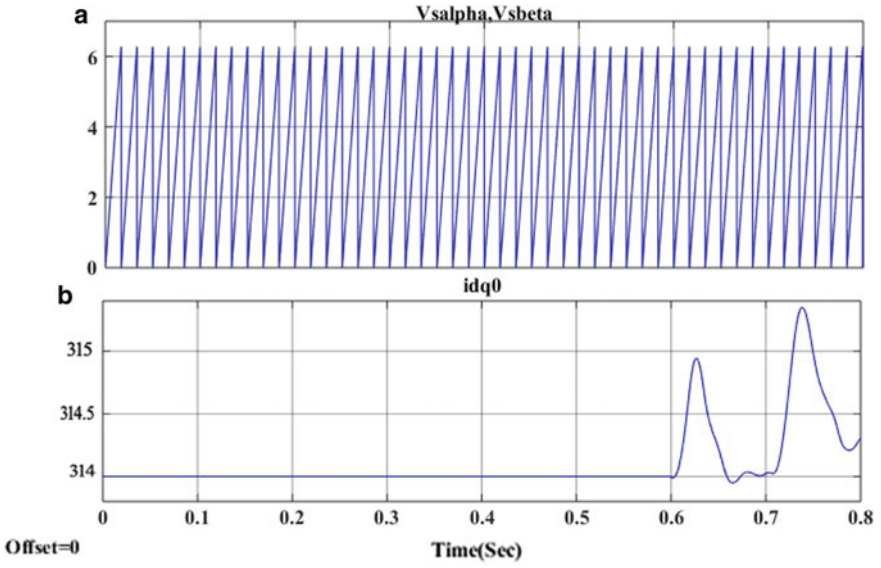

Fig. 10 **a**, **b** Response of the VSC system for a random condition with an island detection delay of 0.6 ms

arises at the same time as the transition from grid connected to islanding approach. VSC's recommended method can be used in other grid connections to adjust current, power, and voltage exchange with the grid. The system act as islanding as well as non-islanding.

References

1. Galád, M., Špánik, P.: Design of photovoltaic solar cell model for stand-alone renewable system. 2014 ELEKTRO, Rajecke Teplice, pp. 285–288 (2014)
2. Nthontho, M.P., Chowdhury, S.P., Winberg, S., Chowdhury, S.: Protection of domestic solar photovoltaic based microgrid. In: 11th IET International Conference on Developments in Power Systems Protection (DPSP 2012), Birmingham, UK, pp. 1–6 (2012)
3. AbdelHady, R.: Modeling and simulation of a micro grid-connected solar PV system. National Research Center, Ministry of Water Resources and Irrigation, April 2017
4. Chattopadhyay, T.M., Banerjee, S., Maity, D., Chanda, C.K.: Microgrid: planning of active and reactive power loss reduction in distribution network. In: 3rd International Conference on Electrical, Electronics, Engineering Trends, Communication, Optimization and Sciences (EEECOS 2016), Tadepalligudem, pp. 1–5 (2016)
5. Tavakoli, A., Negnevitsky, M., Lyden, S., Haruni, O.: A decentralized control strategy for multiple distributed generation in islanded mode. In: 2014 IEEE PES General Meeting|Conference & Exposition, National Harbor, MD, pp. 1–5 (2014)
6. Nordin, A.H.M., Omar, A.M.: Modeling and simulation of photovoltaic (PV) array and maximum power point tracker (MPPT) for grid-connected PV system. In: 2011 3rd International Symposium & Exhibition in Sustainable Energy & Environment (ISESEE), Melaka, pp. 114–119 (2011)
7. Atallah, A.M., Almoataz, Y.: Abdelaziz, Jumaah, R.S.: Implementation of perturb and observe mppt of PV system with direct control method using buck and buckboost converters. Emerg. Trends Electr. Electron. Instrum. Eng. Int. J. (EEIEJ), **1**(1), February 2014
8. www.ministryofnewandrenewablesource. India
9. Sahu, P., Verma, D., Nema, S.: Physical design and modelling of boost converter for maximum power point tracking in solar PV systems. In: 2016 International Conference on Electrical Power and Energy Systems (ICEPES) Maulana Azad National Institute of Technology, Bhopal, India. Dec 14–16, 2016
10. Muhtadi, A., Saleque, A.M.: Modeling and simulation of a microgrid consisting solar PV & DFIG based wind energy conversion system for St. Martin's island. In: 2017 IEEE 3rd International Conference on Engineering Technologies and Social Sciences (ICETSS), Bangkok, pp. 1–6 (2017)
11. Surawdhaniwar, Sonali, Diwan, Ritesh: Study of maximum power point tracking using perturb and observe method. Int. J. Adv. Res. Comput. Eng. Technol. **1**(5), 106–110 (2012)
12. Sharma, V., Fatima, M., Prakash, A.: Performance analysis of grid connected and islanded mode photovoltaic system. In: 2017 4th IEEE Uttar Pradesh Section International Conference on Electrical, Computer and Electronics (UPCON), Mathura, pp. 145–149 (2017)
13. Yazdani, A., Iravani, R: Voltage-Sourced Converters in Power Systems—Modeling, Control, and Applications. IEEE Press. Wiley Sons Inc. Publication, pp. 204–269
14. Jie, L., Ziran, C.: Research on the MPPT algorithms of photovoltaic system based on PV neural network. In: 2011 Chinese Control and Decision Conference (CCDC), Mianyang, pp. 1851–1854 (2011)
15. Kumar, M., Morla, S.K., Mahanty, R.N.: Modeling and simulation of a Microgrid connected with PV solar cell and its protection strategy. In: 2019 4th International Conference on Recent Trends on Electronics, Information, Communication & Technology (RTEICT), Bangalore, India, pp. 146–150 (2019)

Effect of Electrical Vehicles Charging on Distribution System with Distributed Generation

Nilesh Bhut and Bhargav Vyas

1 Introduction

Electric vehicles are simple creations in which wheels are turned by electric motors rather than gasoline/diesel powered drive train. They are energy efficient and convert about 59–62% of the electrical energy from the grid. Whereas energy stored in gasoline converted just 17–21%. It is also as old as the Internal Combustion (IC) vehicle as the first practical EV developed in 1834 by Thomas Davenport. Due to improvement in EV technology, EV shows revival of their era. Moreover, an increased focus on renewable energy [1] made it more relevant in recent time. India leaping to achieve 175 GW in terms of renewable energy by 2022 according to commitment under global climate change accord. Out of these, the target of solar energy will be of 100 GW.

There are different kind of Battery electric vehicles (BEVs); Hybrid electric vehicles (HEVs); Plug-in hybrid electric vehicles (PHEVs). A higher portion is expected to be PHEV as convenient in practical cases. The electrical distribution grid will experience an impact due to connected PHEVs. This is mainly because they consumes a large quantum of electrical energy from the distribution grid it is connected. Sudden switching for charging can result in unwanted power peaks in the electricity consumption [2, 3]. Moreover, it also leads to change and degrade the quality of the power. This is primarily in terms of change in THD, large variation in current and degradation of the voltage levels.

Distribution grid refers to 'The last stage of the electricity network in which electricity is distributed to households, industry and other end products. The main

N. Bhut (✉) · B. Vyas
Gujarat, India
e-mail: bhutnilesh.0303@gmail.com

B. Vyas
e-mail: bhargavonline@gmail.com

O. H. Gupta and V. K. Sood (eds.), *Recent Advances in Power Systems*, Lecture Notes in Electrical Engineering 699, https://doi.org/10.1007/978-981-15-7994-3_17

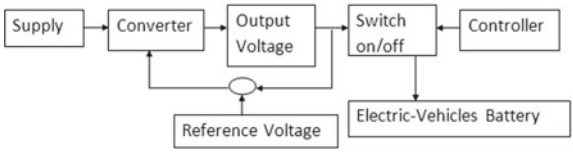

Fig. 1 Electric vehicles charging circuit

function of electric power distribution system is to supply energy to the premises of individual consumers. Electrical energy is distributed to various consumers with low voltage levels. Distribution of electric power is done by distribution network' [4].

Distributed Generation (DG) is basically generation of electricity from small energy sources less than 10 MW. Nowadays renewable sources mostly use as DG due to reduce reliance of fossil fuels, i.e., Photo-Voltaic (PV) or Solar [5].

Specification The Bharat DC-001 (Moderate level) charger has selected for Electric vehicles charging parameter according to standard. Its power rating 15 kW voltage rating 72 V or higher and current rating maximum 200 A. Converter Efficiency is greater than 92% at nominal output power [6, 7]. New lunched electric vehicle (Tata tiago and Mahindra e20 plus) have based on this parameter. For EV Lithium-ion battery used it's parameter [8]: Nominal voltage 72 V, Rated capacity 11,000 Ah [3] (Fig. 1).

Charger is power converter that performs the necessary function for charging battery [1, 9]. The charging of battery is considered in this work; however, discharging of battery in case of grid requirement is omitted. The charging conditions for any EV considered through circuit breaker depend on two conditions:

(1) Output of converter must be greater than 72.5 Voltage
(2) Battery state of charge is less than 90%.

2 Related Work and Background Information

The article [2] selects simulation of the daily load profile of China for which the EV penetration considered are 5, 10, 20%. The results of the article establish the best time of electric vehicle charging during off-peak hours. The findings are more efficient in terms of grid stress; however, its implementation is difficult as load profile varies much. The article [10] demonstrates distribution system model on Dig SILENT software. The grid connection of the PEV's has been evaluated in term of the load profile. These connections include both types of charging: controlled a dun-controlled. According to the available load profile, the article provides the concept of controlled charging. Moreover, it also finds voltage unbalance at transformer according to definition of the National Electrical Manufacture Association (NEMA) and IEEE. The unbalance of the voltage has been defined in this article as the ratio of voltage deviation (maximum) from the average voltage to the average of line voltage.

A comparison of daily load profile for winter and summer daily load for household consumers in the UK were presented in [11]. Connected EV penetration considered were 10, 20 and 30%. EV has a constant 10 A charging current for six hours to standard outlet of residential supply. EV charging with different strategies, i.e., uncontrolled, off-peak, smart charging were simulated and results were produced for obtained voltage and demand profile of each case. This article also defines and compare few terms like:

- Uncontrolled charging: may increase about 18% of maximum demand
- Off-Peak charging: This includes a simple controller that controls switching of the charger during off-peak period.
- Smart charging: In this type of charging, 'smart' charging control circuitry made demand uniform by separating (phasing) the charging cycle. This is done by dividing total charging requirement into four distinct charging schedules according to their priority.

Result of this article shows the charging operation by restricting the voltage profile within 20% of its regular level with the on-load tap changer. The article [12] shows impact of EV charging on IEEE 34 node test feeder. The simulation was provided with electrical distribution design (EDD) software with summer season load curve for the California Independent System Operator (CAISO). The load flow analysis was conducted for each of the cases and monitors transformer loading limit; current rating; voltage limit; line loading limit. The findings were provided with randomly increased 10% load for every load bus to find out the system limit. Then finally, increment of load by 5–20% of load in each step to find out maximum loading that system can withstand. They concluded that larger size transformers are needed to solve EV connection or may connect Distribution Generator (DG).

The article [13] analyzes impact of EV charging in terms of power quality with a distribution grid of fifteen houses. Fundamentally, the non-linear current consumed by load will positively affect the quality of the power. Results show that the THD in current taken by load has been reduced to 1.8% for smart charges than 51.6% for a traditional EV charger. The reduction in the voltage level is of 7.3% has been reported for the most distinct home from the distribution transformed. This will result in malfunctioning of the equipment in that house. Another article mostly focuses on current limit, harmonic, effect on transformer and a maximum loading capacity [14].

From the system operator point of view, in the distribution system, the losses occur due to charging are a major concern on the economic front. Moreover, it also can result in overloads that eventually results in change of Voltage profile; Unbalance of current; THD; Transformer loading limit; reduced efficiency; Difficulty operation control; Stress on customer equipment; new requirement for distribution network planning.

3 System Simulation

3.1 Analysis of IEEE-15 BUS System

To check the effect of plug-in EV charger on the distribution grid, an IEEE-15 bus system has been simulated with inclusion of EV charger [15–18]. IEEE-15 bus system is a well-defined distribution network; its parameters are provided in Table 2. The model of distribution grid is simulated on MATLAB software with rated voltage 11 kV. It's consists sources is rated 1.26 MW and total load is connected on bus 1.23 MW [19, 20].

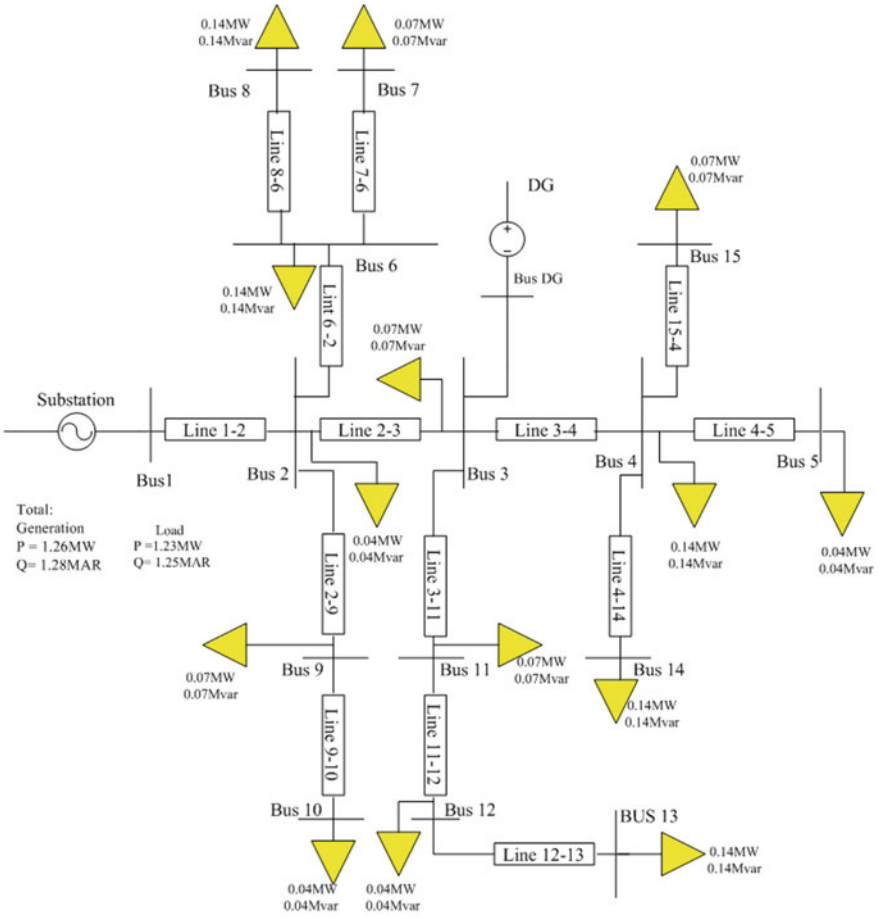

Fig. 2 IEEE 15 distribution system

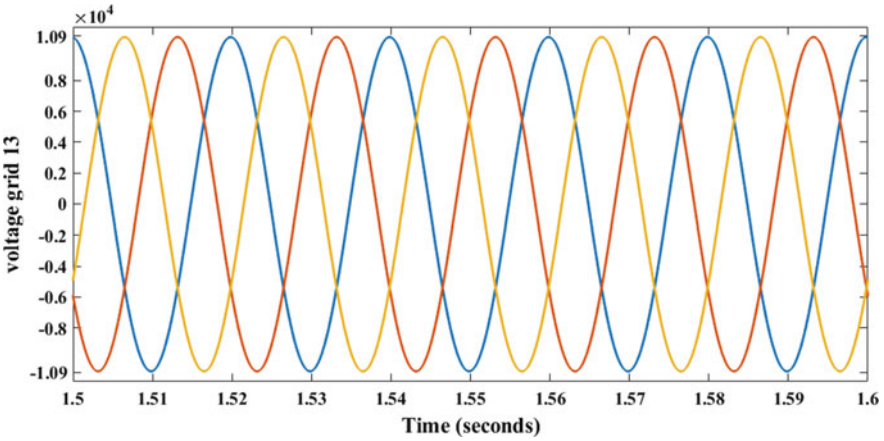

Fig. 3 Bus voltage waveform without PV charging or DG

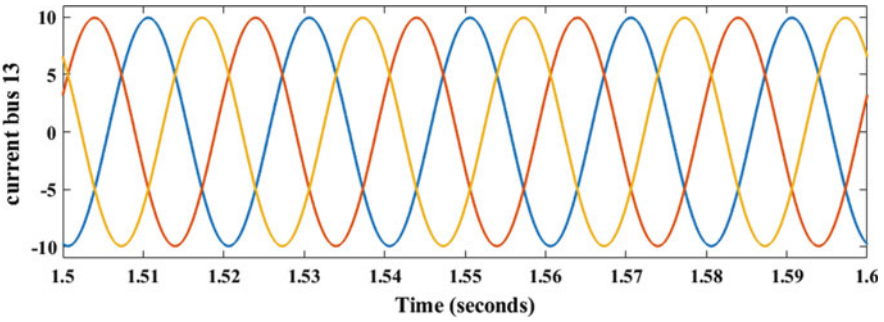

Fig. 4 Bus current waveform without PV charging or DG

The simulation of IEEE-15 bus system has been shown in Fig. 2. This is simulated without inclusion of any PV or EV charger. The waveform of the bus voltage and bus current at bus number 13 (the weakest bus) is shown in Figs. 3 and 4 (Table 1).

3.2 IEEE-15 Bus System with EVC

Now, to evaluate the effect of the electric vehicle based charger with converter, it has been integrated with IEEE-15 bus systems as shown Fig. 5. The EV charging module is group of electronic circuitry. It converts available AC distribution power into DC of appropriate level to charge vehicle batteries. Usually these chargers can work with multiple voltage and power levels to increase its operation universally. With progress in technology, charges can perform multiple operations for better grid integration, mainly taking into account the power quality [19, 21] (Fig. 6).

Table 1 Line and load data

S. No.	Line	*R*	*L*	*P* (kW)	*Q* (kW)
1	1–2	1.3	0.0035	44.1	44.99
2	2–3	1.17	0.0030	70	71.41
3	2–6	2.557	0.004	140	142.82
4	2–9	2.013	0.003	70	71.41
5	3–4	0.84	0.0021	140	142
6	3–11	1.79	0.0032	70	71.41
7	4–5	1.53	0.00275	44.1	44.99
8	4–14	2.2308	0.00399	140	142.82
9	4–15	1.197	0.00214	70	71.41
10	6–7	1.088	0.0019	70	71.41
11	6–8	1.25	0.002	140	142.82
12	9–10	1.68	0.0031	44.1	44.99
13	11–12	2.448	0.004	44.1	44.99
14	12–13	2.01	0.003	150	150.82

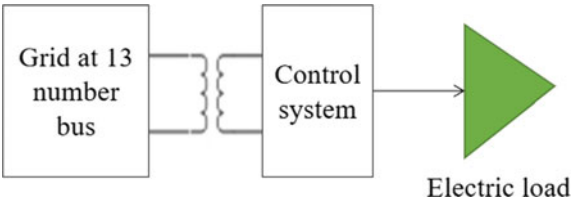

Fig. 5 Block diagram the EVC of grid connected to EVC

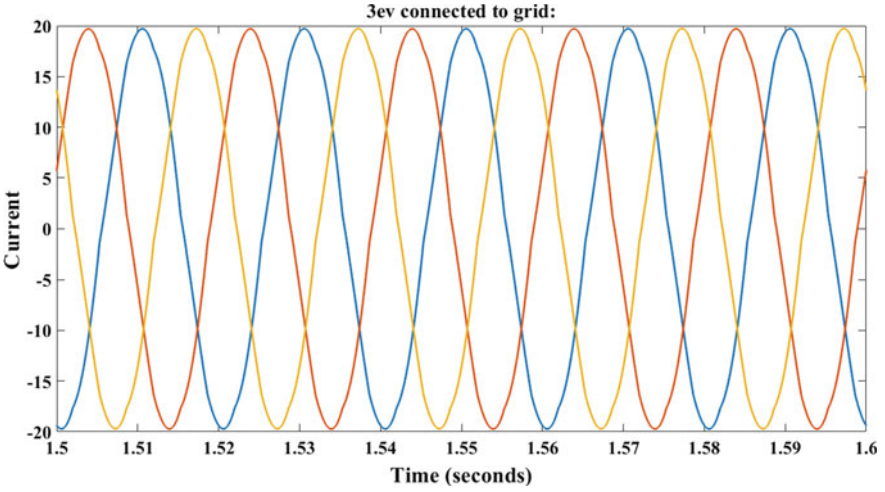

Fig. 6 Bus current waveform grid with EV

Figure 7 shown that the maximum voltage deviation during three electric vehicles charging from the grid. The analysis shows voltage (10,145 V) compare to (10,828 V) without EV charging, current (20 A) compare to (9.95 A) without EV charging, battery voltage (74.34 V) and battery current (167 A) on bus number 13. It can be observed that, the voltage has decreased considerably and current increases (Fig. 6). The voltage on the last bus (load that is more distant from the generator bus) is affected by 7.7% voltage drop, which can cause problems. Grid connected EV Charger output current waveform and voltage waveform is provided in Figs. 8 and 9 respectively.

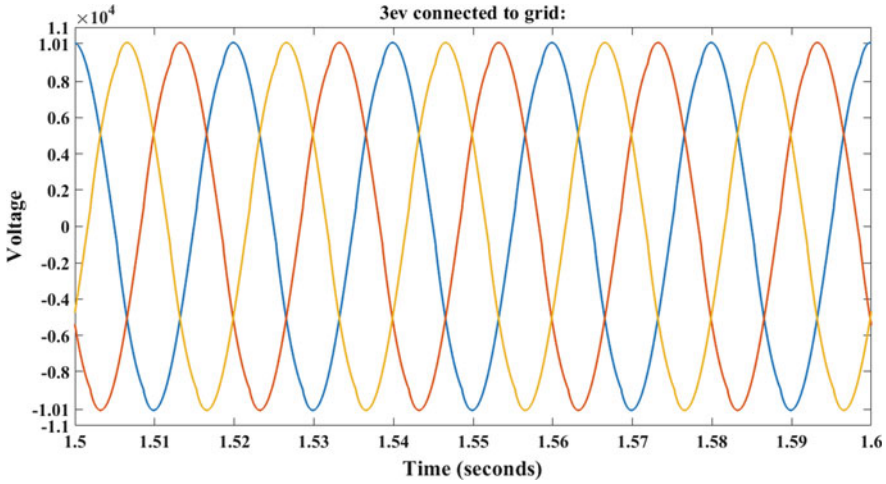

Fig. 7 Bus voltage waveform grid with EVC

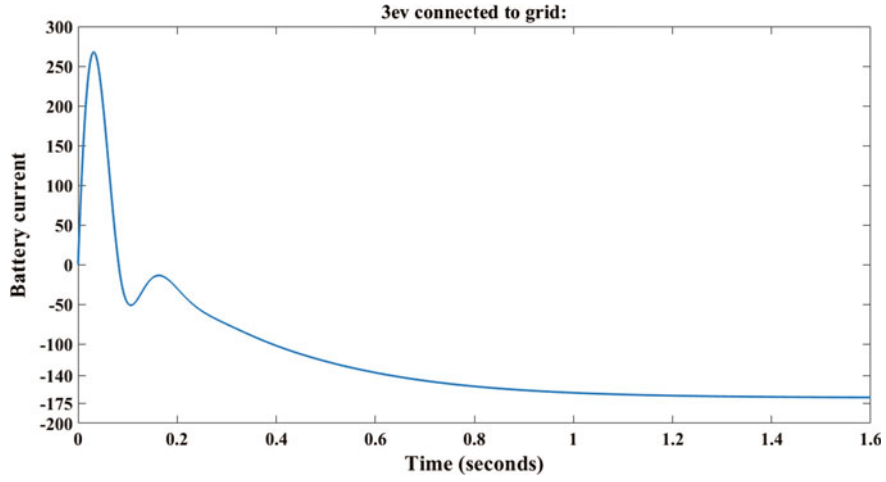

Fig. 8 Charging current of battery

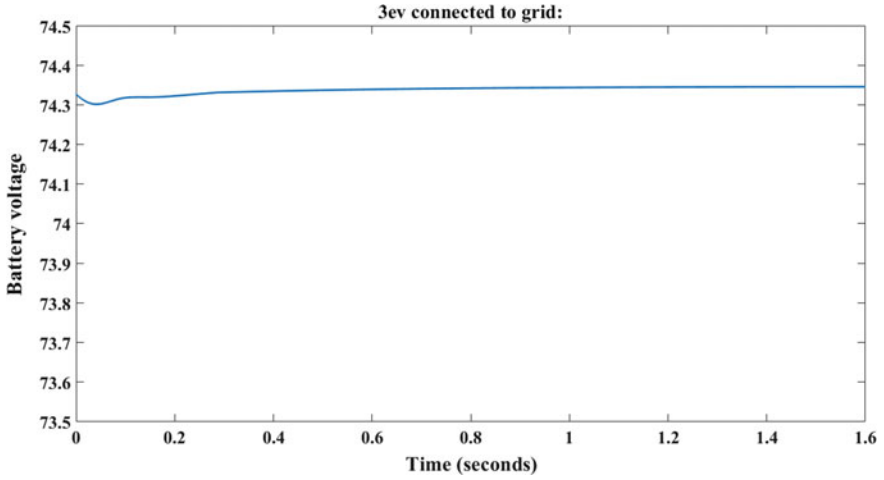

Fig. 9 Charging voltage of battery

Table 2 Total harmonic distortion voltage and current value

Distribution grid connected with EVC	
THDv	1.29%
THDi	2.26%

Simulation results from studies about voltage and current THD during EVC connected to Grid shown Table 2. Total Thad (1.29%) and THDi (2.26%) are inserted in the system.

3.3 Simulation of IEEE-15 Bus System With PV (Solar) as Distribution Generator

Now to analyze the effect of distributed generation on the feeder, a solar power plant rated 50 kW [15, 22] has been included in the simulated 15 bus distribution feeder. The PV has been implemented for a constant radiation of 1000 W/m^2. The solar delivers the power to the bus no 13. Other parameters of the PV system are as: Module: 1 Soltech 1 STH-215-P; Parallel string 0–4; Series-connected module per string-7; Irradiance-1000 W/m^2; Temperature-24 °C; Open circuit Voltage −36.3 V; Short circuit Current −7.84 A; Number of cell per module-60 (Fig. 10).

The topology used in this work uses buck type DC-DC converter to connect the PV with grid. The system was later simulated using simulation (MATLAB) software [19, 21]. With help of Phase Lock Loop (PLL) the output parameters of the inverter has been synchronized with the grid parameters. Harmonics in the output of the

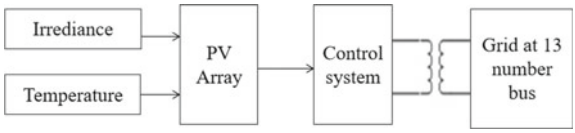

Fig. 10 Block diagram of grid with PV

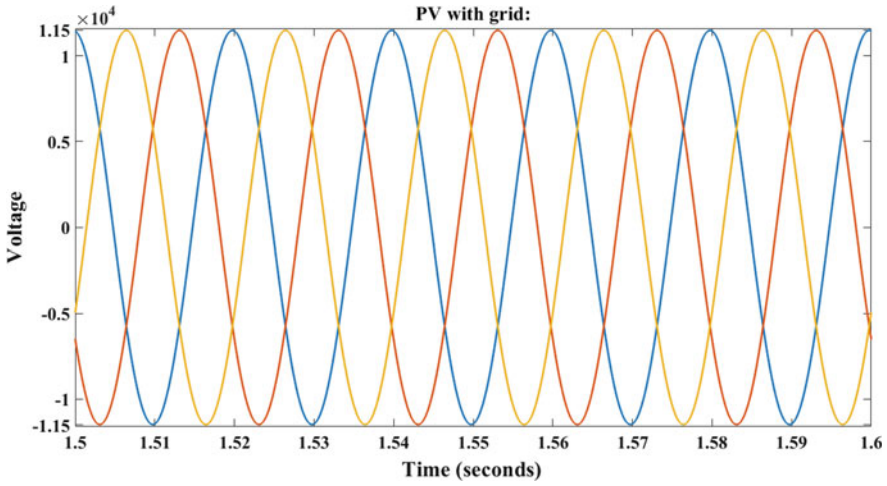

Fig. 11 Bus voltage waveform grid with PV

inverter will be taken care by inductive filters. To connect the 400 V output of the inverter, a step-up 400 V/11 kV transformer is used as interconnection to the grid.

With the inclusion of a PV generation with a constant irradiation on the IEEE-15 bus system. From Figs. 11 and 12, it can be noted that, voltage at bus 13 (11,450 V) has been increased and current at bus 13 (7.45 A) reduced. The PV is generating voltage (204 V), solar power (50 kW) with solar current (249 A). Total THD generated with proper filtration has been given in Table 3, respectively, THDv and THDi.

3.4 IEEE-15 Bus System with EVC and PV (DG)

The solar power plant is rated as 52 kW implemented with a constant radiation of 1000 W/m^2 and hence it provides constant output. The output of the PV is transformed to 11 kV with the help of a transformer. The PV is connected to bus no. 13 as in the previous case (Fig. 10).

An integration of the DG and EVC with IEEE-15 bus system is shown in Fig. 13. Figures 14 and 15 shows, time based variation in the voltage and current at Bus number 13.

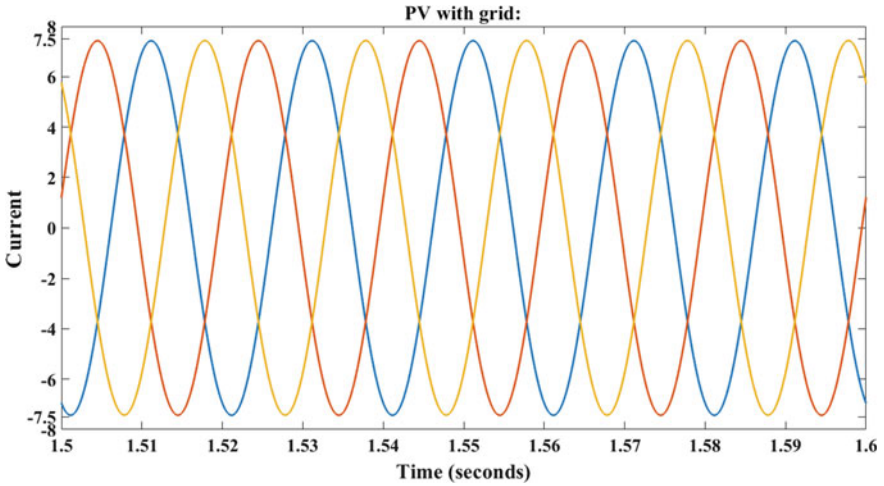

Fig. 12 Bus current waveform grid with PV

Table 3 Total harmonic distortion voltage and current value

Distribution grid connected with DG	
THDv	0.00%
THDi	0.01%

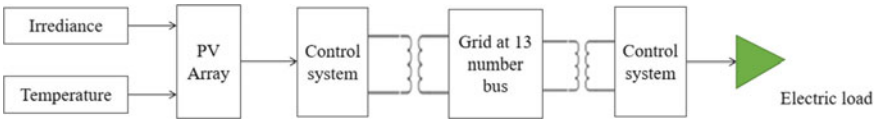

Fig. 13 Block diagram of grid connected EVC and PV

When the IEEE-15 bus standard distribution network is simulated with EV and PV simultaneously following observation are made.

- The bus voltage at bus 13 (10,850 V) remains almost constant when it is with any EV charging or PV generation
- The bus is handled much more current of (18.7 A)
- EV output voltage (204 V) with solar power (52 kW)
- Battery voltage (74.35 V) and battery current (200 A) waveform are shown below for 13 number bus.
- It can be observed from these results that voltage rating of the bus is increased and current rating decreases. It can be seen in Figs. 14 and 15 respectively. Therefore, an observation can be made that, the DG at bus number 13 is supporting the grid in case of the EV charging for better maintaining of the electrical parameters.

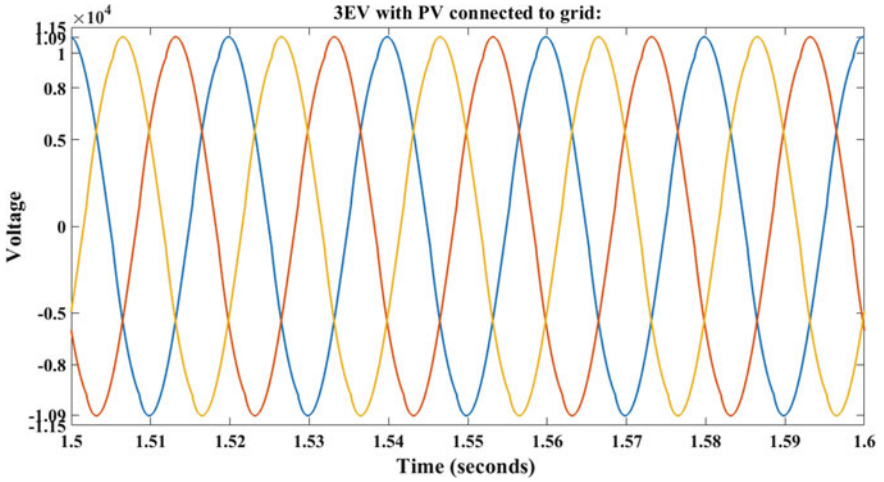

Fig. 14 Bus voltage waveform grid with EVC and PV

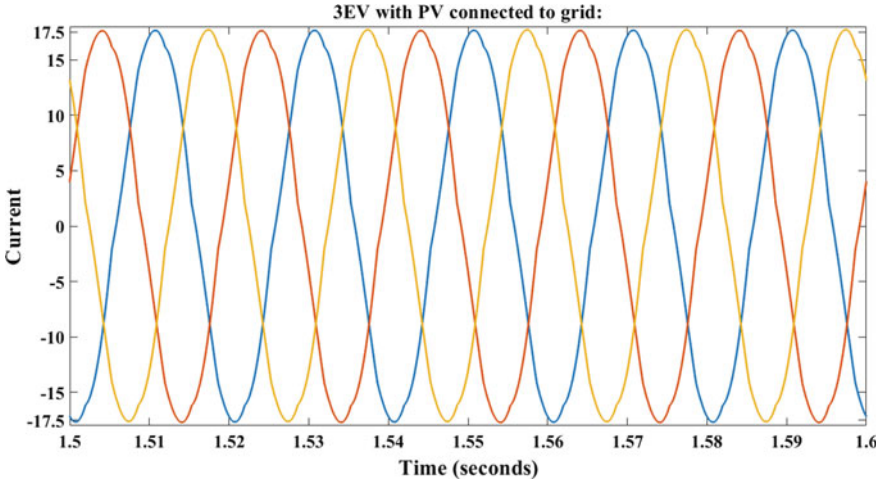

Fig. 15 Bus current waveform grid with EVC and PV

Like maintenance of the voltage level and by then reducing the requirement of current (Fig. 16).

Electrical Vehicles Charging current also increase from 167 A (EVC—Fig. 8) to 200 A (EVC with PV—Fig. 17).

Simulink system and observe THD value at bus shown Table 4 respectively with THDv and THDi. The current consumed THD is increasing from 2.26% (EVC) to 2.87% (EVC with PV) but it's within acceptable standard limit [14, 23]. A detailed

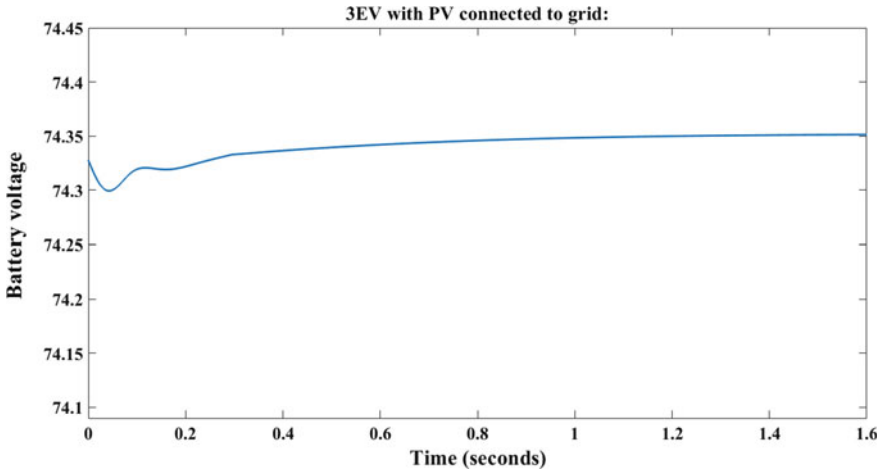

Fig. 16 Battery charging voltage

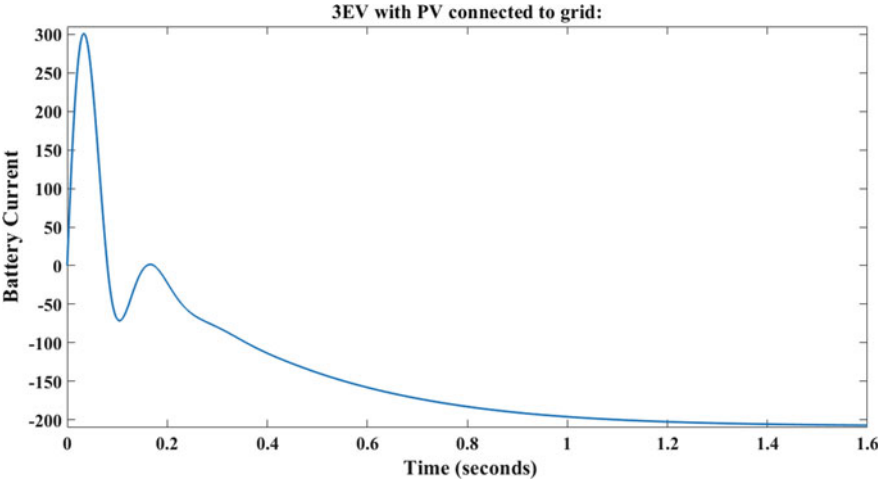

Fig. 17 Battery charging current

Table 4 Total harmonic distortion voltage and current value

Distribution grid connected with DG and EVC	
THDv	1.35%
THDi	2.87%

Table 5 Comparisons of grid with different cases

Distribution grid-bus parameter	Standard distribution-grid	Distribution grid with EVC charging	Distribution grid with PV Support	Distribution grid with EV charging and PV support
	$V = 10828$ V $I = 9.95$ A	$V = 10145$ V $I = 20$ A	$V = 11450$ V $I = 7.5$ A	$V = 10850$ V $I = 18.7$ A
Solar rating	NO PV connected	NO PV connected	$P = 50$ kW $V = 204$ V $I = 249$ A	$P = 52$ kW $V = 204$ V $I = 256$ A
EVC charging rating	NO EV connected	$V = 74.34$ V $I = 167$ A	NO EV connected	$V = 74.35$ V $I = 200$ A
THDV THDI	0% 0%	1.29% 2.26%	0% 0.01%	1.35% 2.87%

comparison of Voltage, current and THD variation for all considered four system variations has been provided in Table 5.

4 Conclusions

The distribution network affected adversely with increasing usage of electric vehicles (EV) chargers. These effects can be given as voltage deviation, power quality loss, increased losses, increased transformer loading, increasing current rating etc. This article investigates these effects of EV charging with standard charging points and observing its effect. To do so, a Simulink model of IEEE 15 bus distribution grid had been simulated. To evaluate the worst possible network condition, the EV charging station has been simulated on the weakest bus. This evaluation has been performed for the voltage, current and THD level.

To find out the solution to this problem, a solar DG has been implemented in the identical system. It can be observed from the obtained results that, with the inclusion of DG, a favorable change can be observed in the grid. The effect of EV charger will get reduced. It also proves that, the transformer rating can also be reduced with the help of DG.

Therefore, it can be reckoned that, difficulties observed during the implementation of the EV charging in distribution grid can be overcome by providing ancillary services like Distributed Generation (DG).

References

1. Encyclopedia.comcontent/Wikipedia
2. Jian, W., Zhizhen, L., Kuihua, W., Feng, W. and Yi, Z.: Impact of Plug-in Hybrid Electric Vehicles on Power Distribution Networks, IEEE ©2011
3. Clement, K., Haesen, E., Driesen, J.: The impact of charging plug-in hybrid electric vehicles on a residential distribution grid. IEEE Trans. Feb, 2010
4. Philip, P., de Mello, R.W.: Determining the Impact of Distributed Generation on Power Systems: Part 1—Radial Distribution Systems, IEEE ©2000
5. Hartmann, W.: Distributed Generation Protection and Control, IEEE/PES
6. Government of India ministry of power report Charging infrastructure for EV—Standards, 1 Oct 2019
7. Government of India Ministry of Heavy Industries & Public Enterprises Department of Heavy Industry, Standardization of protocol for charging Infrastructure—Comments Regarding 15 May 2017
8. Varun, C.K.: Problems in Electric Vehicles (IJARME)©2012
9. Automotive industry standard under central motor vehicles rules-technical standard committee (Department of road transport & highways) Jan 2018
10. Anna, R.J.: Impact of Plug-In Electric Vehicles on the Distribution Grid (IEEJ)
11. Putrus, G.A., Suwanapingkarl, P., Bentley, D., Narayana, E.C.: Impact of Electric Vehicles on Power Distribution Networks. Northumbria University, Newcastle upon Tyne, UK
12. Jiang, Z., Beshir, M.: Impact of electric vehicles on the IEEE 34 node distribution infrastructure. Int. J. Smart Grid Clean Energy ©2014
13. Monteiro, V., Gonçalves, H., Afonso, J.: Impact of Electric Vehicles on Power Quality in a Smart Grid Context', IEEE ©2011
14. Limits for harmonic in the electricity supply system, Abu Dhabi supply company for remote areas (RASCO) 30 Nov 2005
15. Government of India, Ministry of new and renewable energy, 26th Jun 2014
16. Central Electricity Authority (Construction of Electrical Plants & Electric Lines) Regulations, New Delhi (2009)
17. Dakshin Haryana bijli vitrannigam for 11 kV outdoor technical Specification April 2008
18. Maharastra state electricity distribution co. in specification Oct 2017
19. Zheng, Y., Yang, Z., Luo, F.J., Meng, K., Qiu, J., Wong, K.P.: Optimal Allocation of Energy Storage System for Risk Mitigation of DISCOs with High Renewable Penetrations, IEEE Tran ©2013
20. Zhang, Y., Ren, S., Xu, D.Y.: Optimal Placement of Battery Energy Storage in Distribution Networks Considering Conservation Voltage Reduction and Stochastic Load Composition, IET Gener. ©2017
21. Masri, S., Mohamad, N., Mohamed, M.H.: Design and Development of DC–DC Buck Converter for Photovoltaic Application. In: IEEE Conference on Power Engineering and Renewable Energy © 2012
22. Analysis of Indian electricity distribution system for the integration of high shares of rooftop PV, Aug 2017
23. Henderson, R.D., Rose, P.J.: Harmonic: the Effect on the Power Quality and Transform ©1994

Renewable Power Generation Using Asynchronous Generator: A Review

Nagendra Singh, Ritesh Tirole, Shekh Kulsum Almas, and Dimpy Sood

1 Introduction

Wind power is the present quickest developing sustainable power source. In the recent year, installed capacity of wind power generation has increased rapidly in India. Wind power total installed capacity of 37.669 GW as of 29 Feb 2020, as shown in Fig. 1. India has fourth largest installed capacity in the word. Other developed countries like China, US, Germany and Spain has 221 GW, 96.4 GW, 59.3 GW and 23 GW installed capacity respectively up to March 2019 [1, 2].

Most of the power is generated about 58% by thermal power plant of total generated power. That clearly shows we are totally dependency on thermal power plant. Figure 2, shows the progress of power generation capacity in India. Early day's contribution of the wind power was very less about 2%, but now its installed capacity increased and reached 37,669 MW and about 10–12% power is generated by wind power plant.

N. Singh (✉)
Department of Electrical Engineering, Trinity College of Engineering and Technology, Karimnagar, Telangana, India
e-mail: nsingh007@rediffmail.com

R. Tirole
Department of Electrical Engineering, Sir Padampat Singhania University, Udaipur, India
e-mail: riteshtirole@gmail.com

S. K. Almas
Department of Electrical Engineering, SSSUTMS, Sihore, India
e-mail: kulsum.aslam@gmail.com

D. Sood
College of Technology and Agriculture, Udaipur, India
e-mail: sooddimpy@gmail.com

O. H. Gupta and V. K. Sood (eds.), *Recent Advances in Power Systems*, Lecture Notes in Electrical Engineering 699, https://doi.org/10.1007/978-981-15-7994-3_18

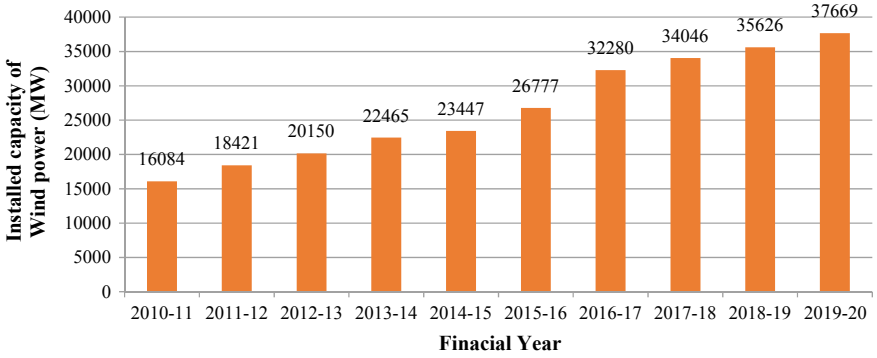

Fig. 1 Wind power installed capacity in India and other countries

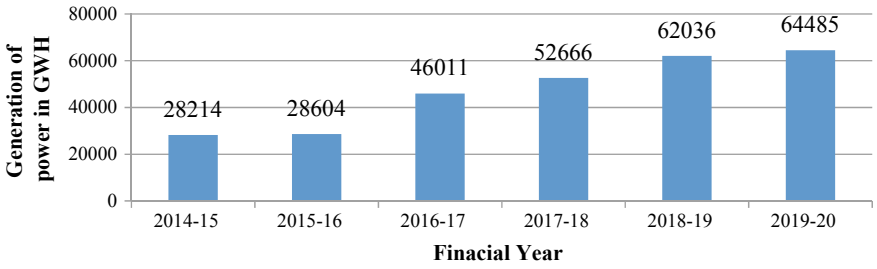

Fig. 2 Yearly generation of power in India

Almost in every country, 60–70% of electrical power is generated by coal, gas and oil. These are nonrenewable sources of energy and induce many harmful gases in the environment, which created health issues in human and living creatures, as well as increasing global warming [3].

Demand of electrical power increased in almost all developed countries day by day. This time demand is increased by 5.7% per year. And it is expected that in the upcoming ten to twenty years demand of electricity will increased four to five times than the present values [4].

For the conversion of wind energy into electrical energy mainly two methods are using one is called fixed or synchronous generation system and other is called asynchronous or variable speed conversion system. In synchronous generator conversion systems has many issues because of inherent condition of flow of wind such as voltage dip in bus bar, unbalance power supply and also affects the steady-state stability of the system [5].

Second system which is using over all word recently is the variable speed wind energy conversion system, are using two models. In one model induction generator is used with capacitor bank and power electronics converter as feedback system and FACTS controller used for switching the firing circuit of the power converter system. In second model of variable speed control system, with power electronics converter

and Pulse width modulation is used for firing pulse generation. It is more suitable and less complicated then first system and it is also economical then first system [6, 7]. Wind energy conversion system used as standalone system or it can used with grid-interconnected system.

2 Overview of Wind Conversion System and Used Control Techniques

Vector control technique, which is used for the speed control of synchronous generator, is explained by articles [8, 9]. Torque and excitation control of synchronous machine is carried out using vector control technique. A decoupled method is given by [10] for active and reactive power control of wind generation system. In this method rotor, side connected with grid using cyclo-converter and reference frame is taken as fixed quantity with respect to air gap flux.

Authors of article [11] proposed the new techniques of design of converter as well as control schemes for asynchronous generator system. A robust back-to-back pulse width of modulation technique with voltage source converters proposed for the control of rotor speed of doubly fed induction generator. Such control scheme is tested for grid connected wind generating system as well as standalone wind power generating system [12]. In the same article they proposed an adaptive system with model reference approximation [12].

The prompt situation of the rotor is required as for the stator, for decoupled control for active and reactive power. In ordinary field situated control conspires, the immediate rotor position is assessed by utilizing supreme encoder fitted to the rotor shaft. Since the cost of high resolution encoder is very high as compare to normal encoder and also not much reliable. Also mounting the sensor in the DFIG system is very hard work. So the authors of [13] proposed a sensor less control technique. This sensor less techniques is a vector control scheme used for control of rotor field and it is controlled by a sensor less algorithm.

In DFIG energy conversion system with grid-interconnected system proposed by article [14], they used advance techniques like maximum power point tracking system which help to extract more wind energy into electrical energy. They used such system for control of variable speed without change in frequency. So this system is very convenient for conversion of wind energy into electrical energy and also controls the active and reactive power of the electrical power.

When stator is connected to grid and rotor of induction generator is connected to the back-to-back converter system for speed control of rotor, such type of system may face problem when any symmetrical or asymmetrical fault arises in the grid side. If any fault arises in the grid side so for protection of wind turbine stator side is connoted through fault ride (FRT) [15, 16]. Such kind of connection protects the wind turbine system.

For the normal operation of grid connected DFIG system authors of [17–19] also proposed the FRT protection scheme with voltage frequency regulation which helps the flow of power from wind energy system to load without any interruption while any type of fault occurs in the grid side. So we can say that FRT system provide isolation operation during the fault in the grid system and wind energy system distribute the power without any interruption.

When operating the wind generating station and any fault arises in grid side we have to connect the DC link which protects the system and maintained stable condition and also it helps to control the flow of current in the stable limit. So DC link control strategy can help the system make stable during the abnormal condition of operation [20, 21], Some of articles describe the effectiveness of DC capacitor control and injection of current using fixed capacitor for grid connected wind generation system [22]. But it is seen that during heavy fault condition such type of control method is not sufficient for protection and control of grid connected wing generation system.

Be that as it may, proposed algorithm and innovations are clarified in the above writings so far don't deliver to all the prerequisites of VSCF doubly fed induction generator system. As of late, so as to improve the steady-state and transient strength, dynamic execution and power quality of the doubly fed induction generator system just as to create more output power, plenty of control systems have been proposed. Execution of such control algorithm requires quicker continuous calculations. Fast advanced digital signal processing are as of late acquainted with conquer such computational work. DSP-based execution approach has been depicted in the paper [23]. In the same work the presentation of three control technique in particular vector control, direct torque control and direct force control have been thought about.

Authors of [24] describe the robust control method namely called Sliding mode control procedure and articles [25], proposed the maximum power tracing scheme for extracting the maximum power from wind. In this methodology parametric vulnerability of the framework has been depicted and furthermore improved vector control system has been proposed [26, 27]. Various Model Predictive Control calculations has been recommended [28] for most extreme energy extraction from the wind turbine using torque control of rotor side. Article [29] proposed the vector control scheme which improved hysteresis-based current and also used conventional proportional and integral combined system for speed control of wind turbine and then they make a comparative performance analysis on steady-state and at transient condition.

3 DFIG Based Wind Energy Conversion System

3.1 DFIG Steady-State Mathematical Model

Mathematical model of DFIG system for steady-state operation can be obtained using the equivalent circuit diagram shown in Fig. 3. Rotor current is expressed in Eq. (1).

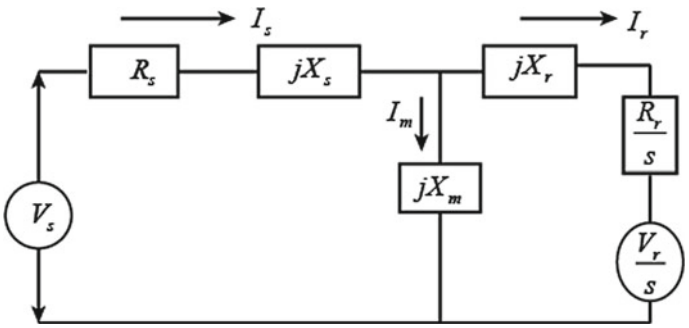

Fig. 3 Equivalent circuit of DFIG with injected rotor voltage

$$I_r = \frac{(V_S - V_r)/S_{\text{slip}}}{\left(R_s + \frac{R_r}{S_{\text{slip}}}\right) + j(X_{ls} + X_{lr})} \tag{1}$$

where V_s and V_r are stator and rotor steady-state voltages, X_{ls}, X_{lr} shows the leakage reactance of stator and rotor respectively, R_s and R_r are resistance of stator and rotor. S_{slip} is slip.

Induction machine torque is given as shown in Eq. (2).

$$T_e = \left(I_r^2\left(\frac{R_r}{S_{\text{slip}}}\right) + P_R\right) \tag{2}$$

where T_e is the electromechanical torque from stator side, P_R is the rotor fed real power.

Real power of rotor is given,

$$P_r = \frac{V_r I_r \cos\theta}{S_{\text{slip}}} \tag{3}$$

The magnetizing current is given as,

$$I_m = \frac{V_s}{X_m} \tag{4}$$

The total input stator current per/phase is as

$$I_s = I_m + I_r \tag{5}$$

Stator flux linkages are given by the relation as

$$\Psi_m = L_{ls} I_s + L_m(I_s - I_r) \tag{6}$$

The stators active power as,

$$P_s = V_s I_s \cos\theta \tag{7}$$

Whereas the stators reactive power is given by

$$Q_s = V_s I_s sin\theta \tag{8}$$

where L_m is the mutual inductance from stator side, θ is the power factor angle, ω_m being the angular velocity of the rotor in mechanical rad/s and is given by

$$\omega_m = \omega_{\text{syn}} 2/P \tag{9}$$

Alternatively, the electromagnetic torque is given as

$$T_s = \frac{3}{2}\frac{P R_r I_r^2}{S_{\text{slip}}\omega_{\text{syn}}} \tag{10}$$

3.2 Dynamic Model

The dynamic mathematical of DFIG system is represented in three phase system. The parameters are first presented in stationary vector form and the transform to the rotating vector form.

(1) *abc* to $\alpha\beta 0$ (stationary)

$$\begin{bmatrix} v_\alpha \\ v_\beta \\ v_0 \end{bmatrix} = \begin{bmatrix} \frac{2}{3} & -\frac{1}{3} & -\frac{1}{3} \\ 0 & \frac{1}{\sqrt{3}} & -\frac{1}{\sqrt{3}} \\ \frac{1}{3} & \frac{1}{3} & \frac{1}{3} \end{bmatrix} \begin{bmatrix} v_a \\ v_b \\ v_c \end{bmatrix} \tag{11}$$

(2) $\alpha\beta 0$ (stationary) to $dq0$ reference

$$\begin{bmatrix} v_d \\ v_q \\ v_0 \end{bmatrix} = \begin{bmatrix} \cos\omega t & \sin\omega t & 0 \\ -\sin\omega t & \cos\omega t & 0 \\ 0 & 0 & 1 \end{bmatrix} \begin{bmatrix} v_\alpha \\ v_\beta \\ v_0 \end{bmatrix} \tag{12}$$

(3) $dq0$ to *abc* reference

$$\begin{bmatrix} v_a \\ v_b \\ v_c \end{bmatrix} = \begin{bmatrix} \text{Cos}\omega t & -\sin\omega t & 1 \\ \text{Cos}\left(\omega t - \frac{2\pi}{3}\right) & -\sin\left(\omega t - \frac{2\pi}{3}\right) & 1 \\ \text{Cos}\left(\omega t - \frac{2\pi}{3}\right) & -\sin\left(\omega t - \frac{2\pi}{3}\right) & 1 \end{bmatrix} \begin{bmatrix} v_d \\ v_d \\ v_q \end{bmatrix} \tag{13}$$

4 DFIG Based Wind Energy Conversion System Issues and Controlling Strategies

So many issues arise during the operation of DFIG system, so as per the issues plenty of control techniques are proposed by the researchers. Here we considered only the recent techniques proposed by researches as follows:

4.1 Control of Regulation of Frequency

As we know that wind energy conversion system based on DFIG output directly connected with the grid system so it in not possible to regulate the frequency, also if using maximum power point tracking system then margin of reserve power is also very big problem to change the frequency. Using pitch control system we can regulate the frequency and control the speed of rotor as per the variation of the flow of wind [8].

4.2 Energy Storage Control Technique

Since the flow of wind is always uncertain so when it connected with grid required to operate on the constant output power. For controlling the fluctuated output power of wind generator system authors of [9] proposed a MPPT-based energy storage battery system. It helps to control the stable operation of wind system with grid connected system. This system is also helps to operate the system on unity power factor. Many researchers proposed DC link capacitor control scheme for stable operation of grid connected wind system, this is also replaced by battery system and it gives better operation system and for tuning of the wind system with grid the used bacterial foraging technique then dc link capacitor system [10]. A controller which work on the base of Eigen value is used for the controlling output generated power of wind system and an optimization technique particle swarm optimization proposed for tuning of wind power and battery storage systems [11, 12].

4.3 Harmonic Control of Generator Stator Current

Generation of harmonic in the stator of generator also influence the unstable operation of the system. For the elimination of 5th order negative sequence and 7th order positive sequence harmonics from the stator of generator current proposed a sixth order resonant circuit [13–15]. For the elimination of harmonic in the stator current a control winding is connected with the rotor current circuit. Some articles proposed

to use a resonant circuit which can help to achieved high bandwidth operation on the definite value of frequency and such kind of resonant circuit also prevent the harmonic generation in the three phase converter and inverter system [16, 20]. Articles [21, 24] also proposed controller based on the resonant frequency operation for the stable operation of the output current of the generator.

4.4 On the Basis of Fault in Grid Circuit

The wind generator when connected through the grid then it's a challenging task to synchronize and operate the system at stable condition when any fault arises and fault current traveling through the line. When any fault arises in the grid then doubly fed induction generator system overloaded if try for stability of the wind farm system. So it is required to check the capacity of the DFIG system whether it is capable to withstand such unstable condition which is arises due to fault and which type of equipment required protecting the system so it can work properly without loss of stability. For controlling such fault current in the DFIG system required a additional rotor current control with the help of DC link chopper controller connected to a braking resistor and one dynamic braking series resistor connected in the stator of the wind generator system [27, 28].

4.5 By Adjustment of Real and Reactive Power

For doubly fed induction generator system rotor voltage and pitch angle is consider as input quantities where as active and reactive power is considered as output quantities and some uncertain quantities like flow of air and mechanical parameter of wind turbine [30]. For maximization of reactive power article [31] proposed a controller with MPPT technique. Such controller helps to regulate the value of active power and also improve the power factor with suitable adjustment of reactive power. Authors of [32, 33] suggested some evolutionary techniques for optimum utilization of MPPT system for maximum generation of active power.

4.6 Control of Unbalance Voltage

The main disadvantages of wind energy generation system are its instable operation because of uncertain flow of wind. The unbalance output power cannot be easily connect with grid. The unbalance voltage if divided in positive and negative sequence magnitude and then stator voltage vector control used for dq and xq axis. This method used to control the flux of the stator in direct axis and quadrature axis. With help of PI controller it control stator flux and maintained constant output voltage [34, 35].

4.7 Direct Torque Control

For controlling the output power required to control the stator flux and rotor output voltage, vector controlled method is used. This method directly controls the rotor output constant and provides stable operation [36–38]. Article [39] proposed on anti jamming control techniques for direct torque control of DFIG system. For control of generator with inverter connected system a predictive control technique proposed by [40] and authors of [41] proposed long range predictive control technique for direct control of generator torque [42].

5 Conclusions

Wind power generation system is very popular renewable energy conversion system in these days. DFIG system has many advantages over synchronous generation system. Many researchers proposed so many techniques for smooth operation of DFIG system. After deep study of literature found following research gap,

- It is required to prepare the simulation model for DFIG system and explain the performance when apply different control techniques.
- For the variation of rotor speed required to add position sensor for increasing the stable operation of the system.
- Performance of the system should be checked with theoretical calculation for grid connected system when output voltage will stable and unstable.
- It is required to develop some good techniques which can measure the value of harmonics and protect from these harmonics.
- For the improvement of efficiency of the doubly fed induction generator required latest and fast optimization technique which can optimize the required active power.
- For controlling the value of active and reactive power efficient power electronics devices required.
- In general it is seen that during the theoretical study taken many assumptions so it is very difficult to find out actual performance of the system. That's why it is required to develop mathematical model which gives the actual performance of the DFIG system with variation of the different parameters.
- Need to develop more accurate fuzzy logic and fuzzy neural based controller for increasing the performance of DFIG system compare to other conventional controller.
- Some efficient controller required to control the speed of rotor especially when it is operated with grid connected system.
- For smooth and efficient operation of wind energy conversion system it is required to design compact and efficient wind turbine.

- Most of the articles neglected the leakage inductance of the rotor under unbalance voltage operation, so required to develop advance controller which can improve the performance when considered the leakage inductance of the rotor.
- Most of the cases for analysis of the performance the wind energy conversion system peoples taking assumed data so it's not give the accurate results especially when load is changing continuously. So for exact results required to perform the operation with real data.

References

1. Khan, I.: Dynamic modeling and robust controllers design for doubly fed induction generator-based wind turbines under unbalanced grid fault conditions. MDPI Energies **12**, 454 (2019). https://doi.org/10.3390/en12030454
2. https://en.wikipedia.org/wiki/Wind_power_in_India (2020)
3. Charles Rajesh Kumar, J.: Wind energy programme in India: emerging energy alternatives for sustainable growth. Energy Environ. SAGA Publication, April (2019)
4. Tazil, M.: Three-phase doubly fed induction generators: an overview. IET Electr. Power **4**(2), 75–89 (2010)
5. Michalke, G.: Variable Speed Wind Turbines-Modeling, Control, and Impact on Power Systems. Department of Renewable Energies at Darmstadt Technical University (Germany) (2008)
6. Choudhury, S.: Performance Analysis of Doubly-fed Induction Generator in Wind Energy Conversion System. A Thesis of Master of Technology in Electrical Engineering (Power Control & Drives, June National institute of technology Rourkela, (2011)
7. Hansen, D., Hasen, L.H.: Market penetration of wind turbine concepts over the years. Eur. Wind Energy, EWEA **10**, 81–97 (2007)
8. Berkani, A.: Sliding mode control of wind energy conversion system using dual star synchronous machine and three level converters. TECNICA ITALIANA-Italian J. Eng. Sci. **63**(2), 243–250 (2019)
9. Niasar, A.H.: Sensorless Direct Power Control of Induction Motor Drive Using Artificial Neural Network. Hindawi Publishing Corporation Advances in Artificial Neural Systems Volume (2015)
10. Kaloi, G.S.: Active and Reactive Power Control of the Doubly Fed Induction Generator Based on Wind Energy Conversion System. Energy Reports Elsevier, pp. 194–200 (2016)
11. Nora, Z., Hocine, L.: Active and reactive power control of a doubly fed induction generator. Int. J, Power Electr. Drive Syst. (IJPEDS) **5**(2), 244–251 (2014)
12. Pavan, D.: Pulgamkar: application of power electronics to power system. Int. J. Sci. Res. (IJSR) **3**, 1–8 (2017)
13. Luis, A.G.: Gomez: combined control of DFIG-based wind turbine and battery energy storage system for frequency response in microgrids. Energies **13**, 894 (2020). https://doi.org/10.3390/en13040894
14. Datta, R.: A simple position sensor less algorithm for rotor side field oriented control of wound rotor induction machine. IEEE Trans. Ind. Electron **48**(4), 710–718 (2001)
15. Cardenas, R.: MRAS observer for sensorless control of standalone doubly fed induction generators. IEEE Trans. Energy Convers. **20**, 4 (2005)
16. Sarkar, Dipu: An ab initio issues on renewable energy system integration to grid. Int. J. Sustain. Energy Plann. Manag. **23**, 27–38 (2019)
17. Amrane, F.: Design and implementation of high performance field oriented control for grid-connected doubly fed induction generator via hysteresis rotor current controller. Rev. Roum. Sci. Techn. Électrotechn. Énerg. **61**(4), 319–324 (2016)

18. Chen, B.A.: An analytical approach to maximum power tracking and loss minimization of a doubly fed induction generator considering core loss. IEEE Trans. Energy Convers. **27**(2), 449–456 (2012)
19. Wang, Z.: Magnitude and frequency control of grid connected doubly fed induction generator based on synchronized model for wind power generation. IET Renew. Power Gener. **4**(3), 232–241 (2010)
20. Xu, L., Wang, Y.: Dynamic modeling and control of DFIG-based wind turbines under unbalanced network conditions. IEEE Trans. Power Syst. **22**(1), 314–323 (2007)
21. Yao, J.: An improved control strategy of limiting the dc-link voltage fluctuation for doubly fed induction wind generator. IEEE Trans. Power Electr. **23**, 3 (2008)
22. In, H.C.: Design and control of small DC-link capacitor-based three-level inverter with neutral-point voltage balancing. MDPI Energies **11**, 1435 (2018). https://doi.org/10.3390/en11061435
23. Abo-Khalil, A.G.: Current injection-based dc-link capacitance estimation using support vector regression. IET Power Electr. **5** (2012)
24. Tremblay, E.: Comparative study of control strategies for the doubly fed induction generator in wind energy conversion systems: a DSP-based implementation approach. IEEE Trans. Sustain. Energy. **2**(3), 288–299 (2011)
25. Chen, S.Z.: Integral sliding-mode direct torque control of doubly-fed induction generators under unbalanced grid voltage. IEEE Trans. Energy Convers. **25**(2), 356–368 (2010)
26. Beltran, B.: Second order sliding mode control of a doubly fed induction generator driven wind turbine. IEEE Trans. Energy Convers. (2011)
27. Itsaso, M.: Control of DFIG wind turbine with direct current vector control configuration. IEEE Trans. Sustain. Energy **2**(3), 215–225 (2011)
28. Li, S.: Control of DFIG wind turbine with direct-current vector control configuration. IEEE Trans. Sustain. **3**(1), 1–11 (2012)
29. Soliman, M.: Multiple model predictive control for wind turbines with doubly fed induction generators. IEEE Trans. Sustain. Energy **2**(3), 215–225 (2011)
30. Mohensi, M.: Enhanced hysteresis-based current regulators in vector control of DFIG wind turbines. IEEE Trans. Power Electr. **26**(1), 223–234 (2011)
31. Yang, J.: A series dynamic resistor based converter protection schemes for doubly fed induction generator during various fault conditions. IEEE Tran. Energy Convers. **25**(2), 422–432 (2010)
32. Guo, Y.: Voltage/pitch control for maximization and regulation of active/reactive powers in wind turbines with uncertainties. IET Renew. Power Gen. **6**(2), 99–109 (2012)
33. Johnson, : Control of variable-speed wind turbines: standard and adaptive techniques for maximizing energy capture. IEEE Contr. Syst. Mag. **26**(3), 70–81 (2006)
34. Galdi, V.: Designing an adaptive fuzzy controller for maximum wind energy extraction. IEEE Trans. Energy Conversion **23**(2), 559–569 (2008)
35. Nian, H.: Dynamic modeling and improved control of DFIG under distorted grid voltage conditions. IEEE Trans. Energy Convers. **26**(1), 163–175 (2011)
36. El-Tawab S (2019) Hybrid DFIG driven wind turbine—grid systems modeling and control for reliable source. Int. J. Recent Techno. Eng. (IJRTE) **8**(4), November (2019). ISSN: 2277-3878
37. Wang, Fengxiang: Advanced control strategies of induction machine: field oriented control, direct torque control and model predictive control. MDPI Energ. **11**, 120 (2018). https://doi.org/10.3390/en11010120
38. Datta, R.: Direct power control of grid-connected wound rotor induction machine without rotor position sensors. IEEE Trans. Power Electronics **16**(3), 390–399 (2001)
39. de Alegria, I.: Novel power error vector control for wind turbine with doubly fed induction generator. IEEE Ind. Electron. Soc. **2**, 1218–1223 (2004)
40. Xiao-Ming, G.: Direct power control for wind-turbine driven doubly-fed induction generator with constant switch frequency. Electr. Mach. Syst. 253–258 (2007)
41. Kennel, R.: Generalized predictive control (GPC)-ready for use in drive applications. Proc. IEEE Power Electron. Special. Conf. (PESC) **4**, 1839–1844 (2001)
42. Wróbel, K.: Model predictive base direct speed control of induction motor drive—continuous and finite set approaches. MDPI Energies **13**, 1193 (2020). https://doi.org/10.3390/en13051193

Estimation of the Monthly Standard Diffuse and Universal Solar Eradiation for the City Varanasi, Uttar Pradesh, India

Munna Kumar, Nalini Singh, and Jitendra Kumar

1 Introduction

Daylight and Solar radiation are required for all living beings on the surface of planet. Solar light changes the planet climate movement that determines its essential climate. Its existence on the global area that is essential for the production of meal for creature beings. In addition, since solar energy is one of the promising sustainable energy sources, devices need to be developed and tested using solar radiation data. Thus it becomes necessary for us to figure out the nature of solar radiation and daylight, and in peculiar to regulate the amount of energy received on the entire area of earth surface [1, 2]. This information can be obtained from solar radiation data from various places. But unfortunately, solar radiation statics is not conveniently feasible for developing nations, because most of these regions cannot manage the techniques and measurement equipment [2]. Such countries need to use the various models and correlations developed after several investigations on the communication between the number of sunshine hours and solar radiation. This data is readily available in meteorological stations [3].

India's Ministry of New and Renewable energy has established 115 automatic solar and meteorological measurement stations called SRRA stations [4, 5]. In Uttar Pradesh, it has been set up in five districts namely Banda, Gorakhpur, Kanpur, Sultanpur and Moradabad [6, 7]. Data for Varanasi can be derived from Gorakhpur

M. Kumar (✉) · J. Kumar
Electrical Department, National Institute of Technology Jamshedpur, Jamshedpur, JH, India
e-mail: meakmunna@gmail.com

J. Kumar
e-mail: jitendra.ee@nitjsr.ac.in

N. Singh
Tata Motor, Pune, India
e-mail: nalini254@gmail.com

O. H. Gupta and V. K. Sood (eds.), *Recent Advances in Power Systems*, Lecture Notes in Electrical Engineering 699, https://doi.org/10.1007/978-981-15-7994-3_19

and Sultanpur as they lie quite close to the city. The data thus obtained can be used for working on the harnessing of solar energy in this area and also the development of several devices and their testing for the same purpose.

2 Methodology

Angstrom was the one who relate the sunshine received at a place by a linear equation. This relation is to date widely used as a reference for the assessment of universal solar radiation [8, 9]. The equation is given as:

$$\frac{\overline{H}_g}{\overline{H}_o} = +b\left(\frac{\overline{S}}{\overline{S}_o}\right) \tag{1}$$

where

$\overline{H}_g$ is the monthly standard regular universal solar radiation received on a straight plain (MJ m^{-2} day^{-1}), $\overline{H}_o$ is the monthly standard regular extra-terrestrial radiation on a straight plane (MJ m^{-2} day^{-1}), a and b are relapse constants,

$\overline{S}$ is the monthly standard regular statistic of hours of dazzling sunlight, a maximal statistics of hours of desirable sunlight.

The following formula given by Duffie and Beckman [10] is used to calculate the value of $\overline{H}_o$ used in Eq. (1):

$$\overline{H}_o = \frac{24}{\pi} I_{sc}\left(1 + 0.033\mathrm{Cos}\frac{360n}{365}\right)(\omega_s \mathrm{Sin}\phi \mathrm{Sin}\delta + \mathrm{Cos}\phi \mathrm{Cos}\delta \mathrm{Sin}\omega_s). \tag{2}$$

where

I_{sc} is the Solar constant having a value of 1367 W/m^2,
ϕ is the location's latitude, i.e., Varanasi,
δ is the angle of declination. That can be calculated as:

$$\delta = \left(\frac{(284+n)360}{365}\right)23.45\mathrm{Sin} \tag{3}$$

And ω_s can be the sunset hour angle given as:

$$\omega_s = \mathrm{Cos}^{-1}(-\tan\delta \tan\phi) \tag{4}$$

$$\overline{S}_o = \frac{2}{15}\omega_s \tag{5}$$

2.1 *Diffuse Solar Emission Flux Forcasting* ($\mathbf{H_d}$)

With the support of the regular total radiation amount $H_{o,}$ the diffusion solar radiation H_d can be used to conclude the value of diffuse solar radiation H_d. Correction for this reason, the equation developed by Krieth is widely used [11, 12]

$$\frac{H_d}{H_g} = 1.411 - \left[\frac{\overline{H}_g}{\overline{H}_o}\right] 1.696 \tag{6}$$

3 Results and Discussions

To conclude the monthly standard day-to-day solar radiation flux of Varanasi in Uttar Pradesh, MATLAB program requires some input parameters, such as latitude, longitude, regression constant monthly average sunshine hours and percentage of possible sunshine hours. The value to determine the regression constants of Prayagraj ($c = 0.27$ and $d = 0.50$) [12] as Varanasi, which is the closest city with data. The average monthly sunshine time for the whole year is shown in Fig. 1. Except for the monsoon season (June, July, August), as shown in Fig. 1, the possible hours of sunshine are more than 65%. Monthly mercury content as mentioned above, the daily average solar radiation can be calculated through several correlations (1)–(5) before. The values obtained from these equations are shown in Fig. 2.

Since the city of Varanasi [13] can obtain the measurement of solar radiation flux, so the values are different from these measured value is only different from the calculated value, so it can be used as a reference for the site under consideration. The

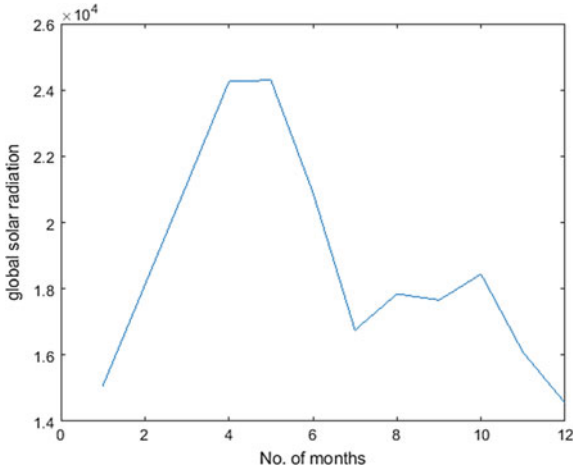

Fig. 1 Monthly deviation of overall solar radiation for Varanasi

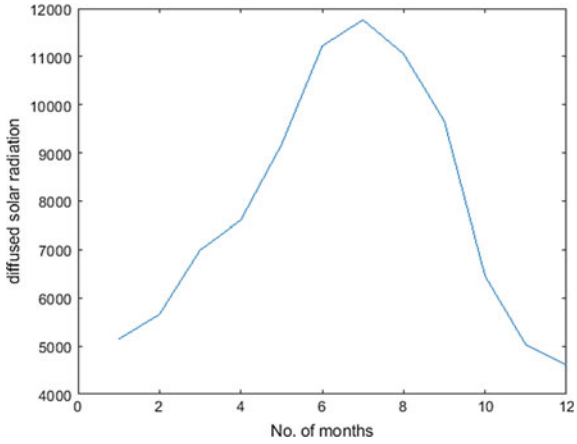

Fig. 2 Monthly deviation of diffused solar radiation for Varanasi

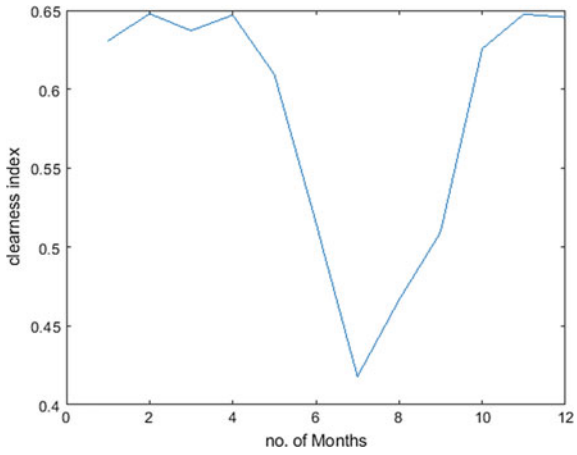

Fig. 3 Monthly deviation of clearness index for Varanasi

comparison between the calculated value and measured value can be observed. It is noted that during the monsoon season, the spread of solar radiation flux is very high, so during monsoon, i.e., June, July and August, the value of global solar radiation flux dropped significantly month (Fig. 3; Tables 1, 2 and 3)[14].

4 Conclusions

The aim of this work is to determine the value of solar radiation flux on the level ground of Varanasi to check the possibility of using solar energy. The calculated average global Angstrom equation and Liu and Jordan methods and diffuse the radiation flux. The calculated value shows that the solar radiation flux can be used for there

Table 1 n, δ and ω_s value for 12 months

Month	n (starting from 1st Jan)	δ (declination angle)	ω_s (radian)
January	16	−21.0964	1.3873
February	45	−13.6198	1.4559
March	75	−2.4177	1.5508
April	105	9.4149	1.6493
May	136	19.0306	1.7347
June	166	23.3144	1.7761
July	197	21.3537	1.7568
August	228	13.4550	1.6842
September	258	2.2169	1.5891
October	289	−9.9663	1.4876
November	319	−19.1478	1.4058
December	350	−23.3717	1.3649

Table 2 S, S_o and Ho value for 12 months

Month	S	S_o	H_o
January	7.6	11.4487	23.893
February	8.5	11.6535	27.957
March	8.7	11.9367	33.212
April	9.6	12.2337	37.487
May	8.8	12.4897	39.873
June	6.4	12.6128	40.550
July	4.2	12.5555	40.086
August	5	12.3385	38.244
September	5.6	12.0522	34.650
October	8	11.7461	29.482
November	8.2	11.5011	24.830
December	7.9	11.3794	22.540

are plenty of places under consideration, so you can use solar energy to relieve stress conventional energy. Although meteorological measurement results are not available at the following locations Varanasi, Uttar Pradesh, solar radiation flux is calculated based on sunshine hours. The available parameter and regression constants c and d for the most recent city. The calculated data can be further used to develop specific models for the considered location and other locations have the same climate conditions. The study aims to provide the required solar data radiation flux is for further study.

Table 3 H_g, H_d and K_T value for 12 months

Month	H_g	H_d	K_T
January	15.068	5.145	0.6306
February	18.111	5.657	0.6478
March	21.159	6.993	0.6371
April	24.254	7.608	0.6470
May	24.298	9.172	0.6094
June	20.901	11.220	0.5154
July	16.752	11.764	0.4179
August	17.846	11.057	0.4666
September	17.658	9.654	0.5096
October	18.443	6.456	0.6256
November	16.079	5.028	0.6476
December	14.550	4.601	0.6455

References

1. Muneer, T., Gueymard, C., Kambezidis, H.: Solar Radiation and Daylight Models, Elsevier (2004)
2. Chegaar, M., Chibani, A.: A simple method for computing global solar radiation. Rev. Energy Ren. Chemss, 54–66
3. Namrata, K., Sharma, S.P., Saxena, S.B.L.: Comparison of different models for estimation of global solar radiation in Jharkhand (India) region. Smart Grid Renew. Energy **4**, 348–352 (2013)
4. Rufuss, D.D.W., Rajkumar, V., Suganthi, L., Iniyan, S.: Studies on latent heat energy storage (LHES) materials for solar desalination application-focus on material properties, prioritization, selection and future research potential. Soalr Energy Mater. Solar Cells, 149–165 (2019)
5. Kumar, D.: Mapping Solar Energy Potential of Southern India through Geospatial Technology. Geocarto International (2018)
6. Giridhar, G., Das, P.K., Gomathinayagam, S.: Solar Radiation Resource Assessment Project in India-A New Initiative, Akshay urja Magazine, June 2014
7. http://niwe.res.in/department_srra_stations_phase1.php
8. Angstrom, A.: Solar and terrestrial radiation. Q. J. Royal Meteorol. Soc. **50**, 121–125 (1924)
9. Makade, R.G., Chakrabarti, S., Jamil, B.: Prediction of global solar radiation using a single empirical model for diversified locations across India. Urban Climate, 1–13 (2019)
10. Duffie, J.A., Beckman, W.A.: Solar Engineering of Thermal Processes. Wiley, New York (1991)
11. Kreith, F., Kreider, J.F.: Principles of Solar Engineering, Chapter 2. McGraw-Hill, New York (1978)
12. Solar Radiant Energy Over India, India Meteorological Department, Ministry of Earth Sciences, pp. 270–274 (2009)
13. George, A., Anto, R.: Analytical and experimental analysis of optimal tilt angle of solar photovoltaic systems. In: 2012 International Conference on Green Technologies (ICGT) (2012)
14. Mahajan, B., Namrata, K., Varshney, A: Estimation of Solar Radiation Flux using MATLAB for Amravati, Maharashtra, India, Carbon, pp. 34–38 (2018)

Evaluation of Residual Inductance of the Impulse Generator for the Generation of Lightning Impulse Voltage

Nidhi Chandrakar, Chadaram Chandra Sekhar, and K. Chandrasekaran

1 Introduction

Impulse voltage is a signal which is having a voltage of high value of amplitude for a very short period (micro or nano sec). Two types of impulse voltage waveform are there first is lightning impulse voltage waveform, switching impulse voltage waveform. The application of impulse voltage is to check the strength of electric power equipment in opposite to lightning and switching surges. In the field of electrical engineering, the main requirement of impulse voltages is for insulation testing of various components in the power system. This is why there is a need to generate high voltages in laboratories. An impulse generator is an electrical apparatus that makes very short high-voltage. The impulse generator produces high impulse voltage. In the field of the power system, the device should withstand not only high rated value but it should also put up with excess voltage, so because of this motive, it is necessary to take that equipment under high-voltage testing. Protection in the field of the power system is required to continue the facility of the electrical power system [1–4]. And protection is basically depending on insulation of the system because some situations will come due to lightning and switching application [5–8]. Transient over-voltage and sudden change in the status of a power system. Like switching operation and faults is called switching impulse voltage. And if this impulse voltage is coming because of lightening then it is called lightning impulse voltages and this voltage

N. Chandrakar (✉) · K. Chandrasekaran
Department of Electrical Engineering, NIT, Raipur, India
e-mail: chandrakarnidhi1996@gmail.com

K. Chandrasekaran
e-mail: kchandrasekaran.ee@nitrr.ac.in

C. C. Sekhar
Department of Electrical Engineering, NIT Warangal, JRF, Warangal, India
e-mail: cschandu.chandra@gmail.com

O. H. Gupta and V. K. Sood (eds.), *Recent Advances in Power Systems*, Lecture Notes in Electrical Engineering 699, https://doi.org/10.1007/978-981-15-7994-3_20

will affect the insulation on a high-voltage power system for voltage 300 kV and more than it [9, 10]. Therefore awareness is mandatory to these two kinds of over voltages. Lightning impulse voltage can be produced by using a Marx impulse generator, According to the rated voltage of specific apparatus magnitude and nature will change. The produced voltage by an impulse generator should assure the voltage's standards. This is the state by the International Electro Techno Commission to meet the criteria like standard impulse voltage; this can be applied for test analysis [6–8, 11, 12]. The standard way of calculation of high- voltage and essential way for a use for approximately every kind of device for alternating voltages, direct voltages, switching impulse voltages and lightning impulse voltages are laid down in the important national and international standards even though impulse voltage's wave shapes are taking place on a system that may vary widely. The standard numeric value of lightening impulse wave is 1.2/50 μs [5, 6, 13–15].

2 Analysis of Third-Order Impulse Generator Circuit

Third-order Equivalent Circuit with residual inductance for the Impulse Generator. An equivalent circuit, the circuit parameters are *Ls,* i.e., residual inductance, *Cs* is charging capacitor in the impulse generator circuit, *Co* is the load-part capacitor, where *Rs* and *Ro* is wave shaping resistor derivative terms are (Fig. 1);

$$\frac{\mathrm{d}^3 i_R}{\mathrm{d}t^3} + (Ls + RsRoCo)\frac{1}{LsRoCo}\frac{\mathrm{d}^2 i_R}{\mathrm{d}t^2} + (Cs(Rs + Ro) + RoCo)\frac{1}{LsRoCoCs}\frac{\mathrm{d}i_R}{\mathrm{d}t} + \frac{1}{LsRoCoCs} i_R = 0 \tag{1}$$

The following 3rd order derivative transfer function is shown Eq. (2) is found

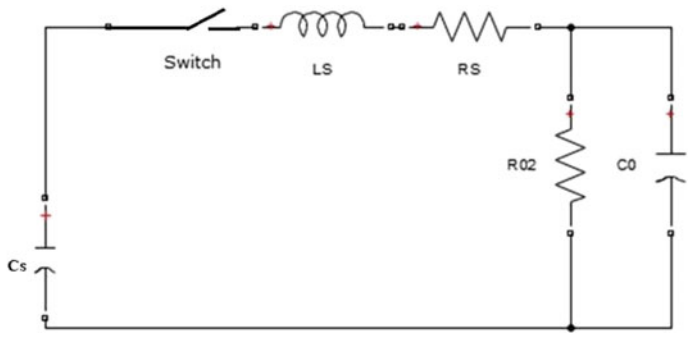

Fig. 1 Equivalent circuit for the impulse generator

$$v_{\text{out}}(s) = \frac{V/(LsCo)}{s^3 + (Ls + RsRoCo)\frac{1}{LsRoCo}s^2 + (Cs(Rs + Ro) + RoCo)\frac{1}{LsRoCoCs}s + \frac{1}{LsRoCoCs}} \tag{2}$$

The following third-order derivative equation is acquire when the constants of the expression is put back with the constants a, b, and c, respectively.

$$\frac{\mathrm{d}^3 i_R}{\mathrm{d}t^3} + a\frac{\mathrm{d}^2 i_R}{\mathrm{d}t^2} + b\frac{\mathrm{d}i_R}{\mathrm{d}t} + ci_R = 0 \tag{3}$$

$$a = \frac{(Ls + RsRoCo)}{(LsRoCo)} \tag{4}$$

$$b = (Cs(Rs + Ro) + RoCo)\frac{1}{LsRoCoCs} \tag{5}$$

$$c = \frac{1}{LsRoCoCs} \tag{6}$$

3 Optimization Method

For the third-order circuit which is having *Rs*, *Ls*, *Cs*, and *Co* circuit parameters finding the transfer function in *s*-domain, the transfer function is formed with a variable in terms of *Ls*, but in order find the *Ls* value, to select upper boundary and lower boundary range. In that selection of range will be like upper boundary and lower boundary, put 17.5, because according to IEC standard the maximum allowable overshoot is ±5%, and if *Ls* will not be present in the circuit then the standard *Vp* is 1, therefore 5% of 1 is to be calculated as 0.05–1.05 range of boundary values. So this is all about the selection of the range. Now after getting this, for the selecting range of *Ls*, find different transfer function and their responses. From those transfer functions responses need to find all the peak values of transfer functions. Those all the peak responses compare with the value of *Vp* is given in base paper [1]. So this known *Vp* compare with different *Vp* values which are coming from different transfer function according to *Ls* range. After comparison one peak values exactly matches with the base paper [1] peak value. Corresponding to that *vp* value respective response graph shows the *vp*, 0.9, 0.1, 0.5 *vp* and there (peak time) *tm*, *t*1, *t*2, and *t*3, from that particular response transfer function *Ls* value is shown (Fig. 2).

Algorithm for optimization method

Step 1 Selection of Ls range
Step 2 Finding the transfer function in the S domain with variable Ls.
Step 3 Getting different peak responses according to the Ls range.
Step 4 Vp ≤ U.B & Vp ≥ L.B.
Step 5 If no, go to step 4.

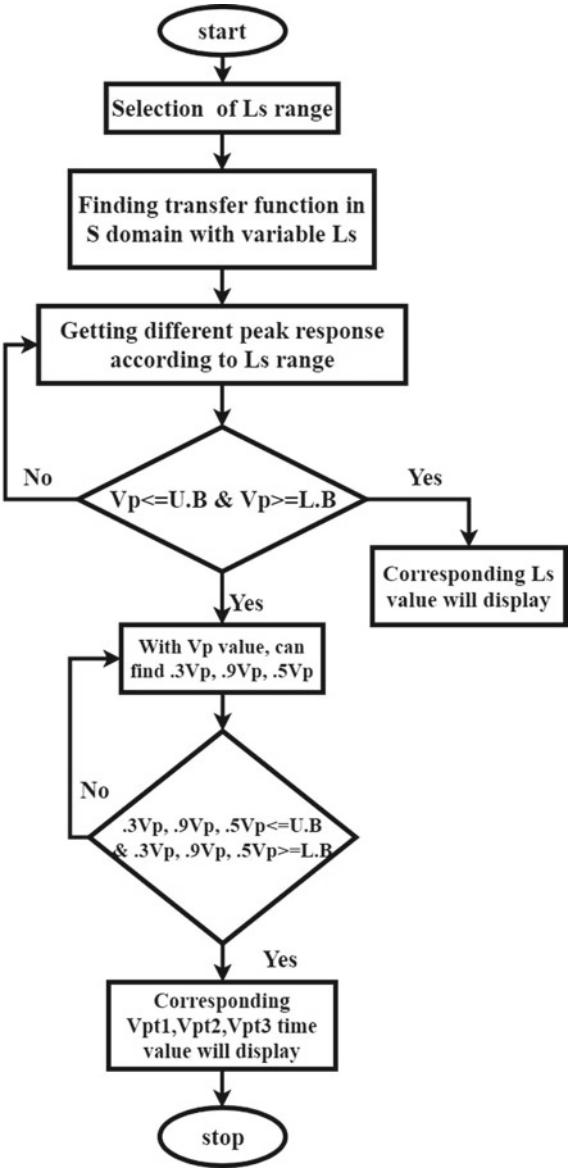

Fig. 2 Flow chart for optimization

Step 6 If yes, Corresponding Ls value will display and With Vp value, can find 0.3 Vp, 0.9 Vp, 0.5 Vp

Step 7 0.3 Vp, 0.9 Vp, 0.5 Vp $\leq$ U.B & 0.3 Vp, 0.9Vp, 0.5 Vp $\geq$ L.B.

Step 8 If no, go to step 6.

Step 9 If yes, Corresponding Vpt1, Vpt2, Vpt3 time value will display.

4 Simulation and Results

See Fig. 3.
Here,

Cs charging capacitor,
Rs wave shaping resistor,
Ro wave shaping resistor,
Co load-side capacitor,
Ls residual inductance.

This simulation is performed to get exact waveform shape and its data; according to variation in *Ls* (residual inductance), the peak overshoot will changes. This variation for a different value of inductance found by using the analytical method, in this method three values of residual inductance *Lsa*, *Lsb*, *Lsc* are the results for one value of inductance from base paper [1]. These three values are approximately equal to the exact value of inductance. From those three values, different time periods and overshoots make complexity to take one value from those three values. Therefore this analytical method is a complex method to select the correct *Ls* value. In order to overcome the difficulty, an optimization method is taken to find one value which is very near to the exact value. For example 1 circuit parameter $Cs = 0.5$ μf, $Co =$ 5000 pf, $Rs = 95.3$ Ω, $Ro = 1152$ Ω, $Vo = 1$ pu and $Vp = 1.08$ pu, the inductance value is 21.73 μH, $tm = 1.29$ μs, $t1 = 0.301$ μs, $t2 = 0.851$ μs, $t3 = 44.8$ μs results responses are shown in Fig. 4. Similarly example 2 circuit parameter $Cs = 0.5$ μf, Co $= 5000$ pf, $Rs = 95.3$ Ω, $Ro = 1152$ Ω, $Vo = 1$ pu and $Vp = 1.09$ pu, the inductance value is 23.7 μH, $tm = 1.294$ μs, $t1 = 0.322$ μs, $t2 = 0.862$ μs, $t3 = 44.3$, results responses is shown in Fig. 5.

Table 1 is a comparison between the optimization method and base paper [1–4, 9] data. For optimization technique took *Vp* value from the base paper, the above comparison table has the same value of *Vp*, so with the same value of *Vp*, the above data (parameter value) came. And all other remaining parameters are also approximately near to the base paper [1]. Comparison of waveforms for different values of $Ls = 30, 20, 10, 40$ μH.

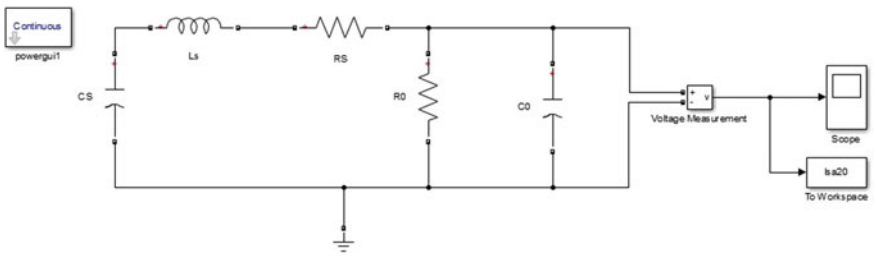

Fig. 3 Schematic diagram of a single-stage impulse voltage generator in MATLAB

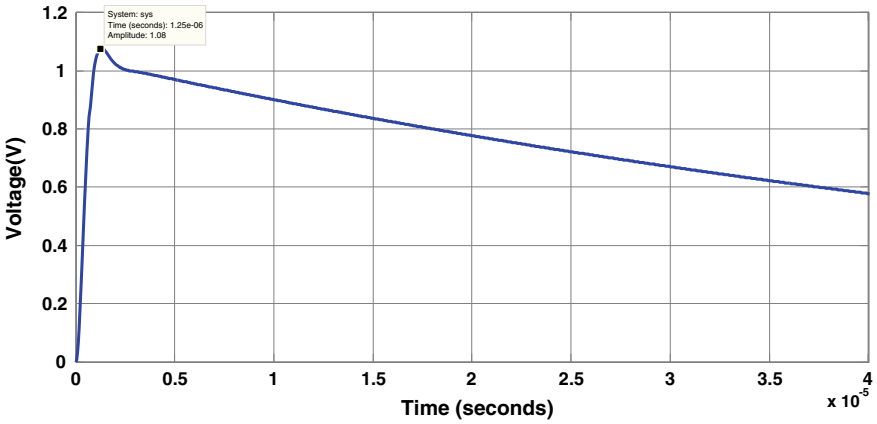

Fig. 4 Overshoot waveform for 1.08 peak value with $Ls = 21.7\ \mu H$

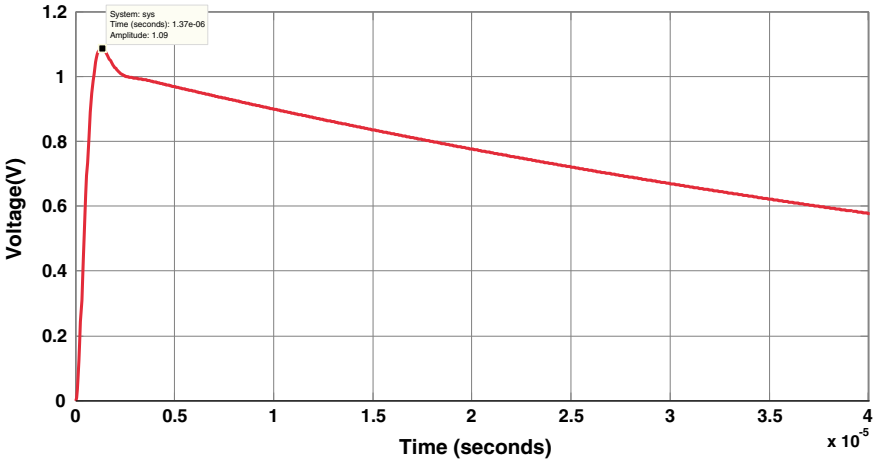

Fig. 5 Overshoot Waveform for 1.09 Peak value with $Ls = 23.7\mu H$

An analytical method is showing three different *Ls* values those values are analyzed by using base paper Cardino's solution and some of the numerical formulas were presented in base paper [1]. Based on the above graphs shown above optimization has only one *Ls* value it matches closely to standard *Ls* value.

Table 1 Summary for different values of *Vp* values

S. No.	Residual inductance (*Ls* μH) by base paper [1]					Residual inductance (*Ls* μH) by optimization method			
1	*Ls* (μH)	10	20	30	40	10.33	20	30.12	40.55
2	*Tf* (μs)	0.91	0.89	0.99	1.09	0.95	0.873	0.991	0.978
3	*Tt* (μs)	48.8	45.5	41.8	39	48.87	45.463	42.01	38.75
4	*tm* (μs)	1.62	1.29	1.38	1.5	1.59	1.27	1.38	1.54
5	*Vp* (pu)	1.01	1.06	1.12	1.17	1.016	1.06	1.12	1.17
6	*δ* (%)	0.97	5.88	11.8	16.6	0.99	5.66	10.7	14.52
7	*f* (kHz)	347	378	358	329	314.4	393.7	359.71	324.64
8	*t*1 (μs)	0.223	0.295	0.359	0.416	0.235	0.299	0.381	0.44
9	*t*2 (μs)	0.769	0.831	0.951	1.061	0.805	0.823	0.976	1.092
10	*t*3 (μs)	48.8	45.6	41.9	39.1	48.7	45.5	42.1	39.1

5 Conclusion

The idea of this project is to estimate the amount of inductance causing the overshoot when it is present into the system of impulse generator. The analysis is done with the basic third-order impulse circuits the circuit parameters are obtained by using the optimization method. Figures 6, 7 and 8 are showing the different *Ls* values corresponding to the base paper, Optimization method, and analytical methods. In this paper analytical analysis is done by using a third-order circuit with formulas are taken from the base paper [1–4]. Impulse circuit parameters are calculated for generating full lightning impulse voltage [7, 8]. By assuming the percentage overshoot the amount of inductance (*Ls*) causing the overshoot is calculated. *Ls* for the overshoot

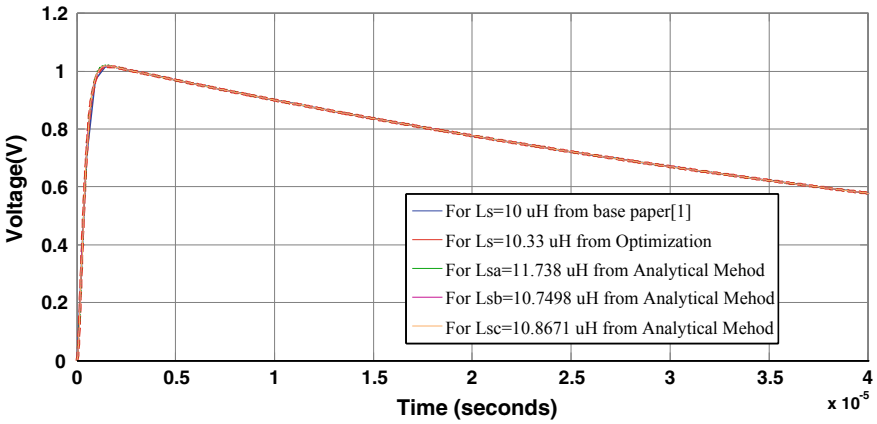

Fig. 6 Comparison of different *Ls* values for $R0 = 1152\ \Omega$, $RS = 95.3\ \Omega$, $CS = 0.05$ μf, $CO =$ 5000 pf, $Ls = 10$ μH, $V_o = 1$ p.u

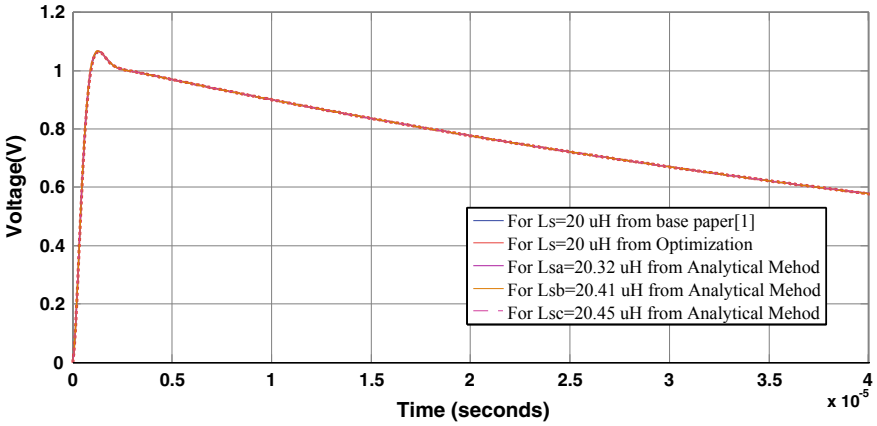

Fig. 7 Comparison of different Ls values for $R0 = 1152\ \Omega$, $RS = 95.3\ \Omega$, $CS = 0.05\ \mu$f, $CO =$ 5000 pf, $Ls = 20\ \mu$H, $V_o = 1$ p.u

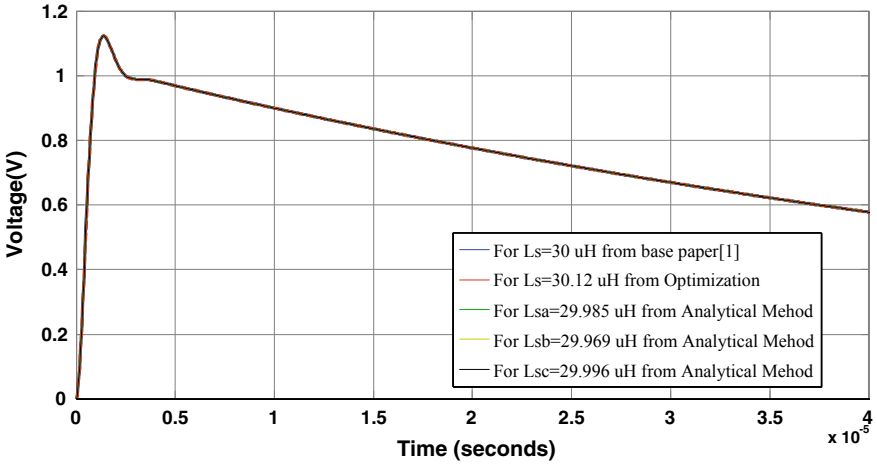

Fig. 8 Comparison of different Ls values for $R0 = 1152\ \Omega$, $RS = 95.3\ \Omega$, $CS = 0.05\ \mu$f, $CO =$ 5000 pf, $Ls = 30\ \mu$H, $V_o = 1$ p.u

is calculated, and the result is verified with the analytical expression. From the study, it is identified the limits of residual inductance, which is causing the overshoot in the generation, are identified. The calculated value of Ls through the optimization is compared with the analytical result [8, 11, 12]. The data of circuit and impulse wave parameters corresponding to different overshoot is generated and the results are discussed (Figs. 9 and 10).

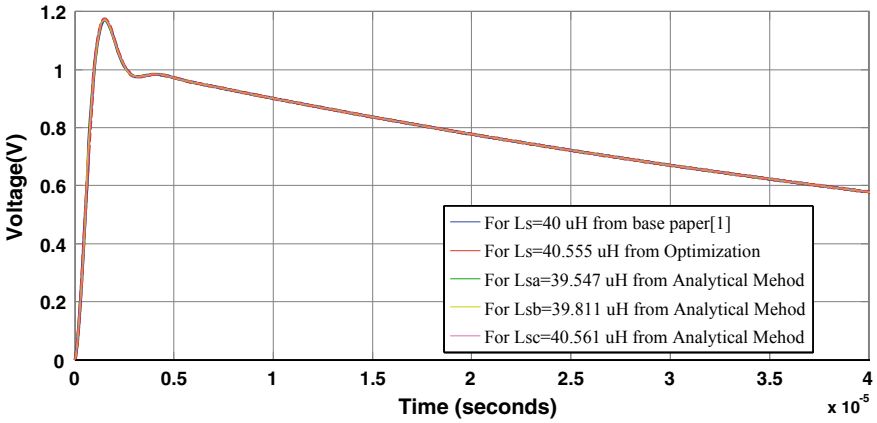

Fig. 9 Comparison of different Ls values for $R0 = 1152\ \Omega$, $RS = 95.3\ \Omega$, $CS = 0.05\ \mu$f, $CO =$ 5000 pf, $Ls = 40\ \mu$H, $V_o = 1$ p.u

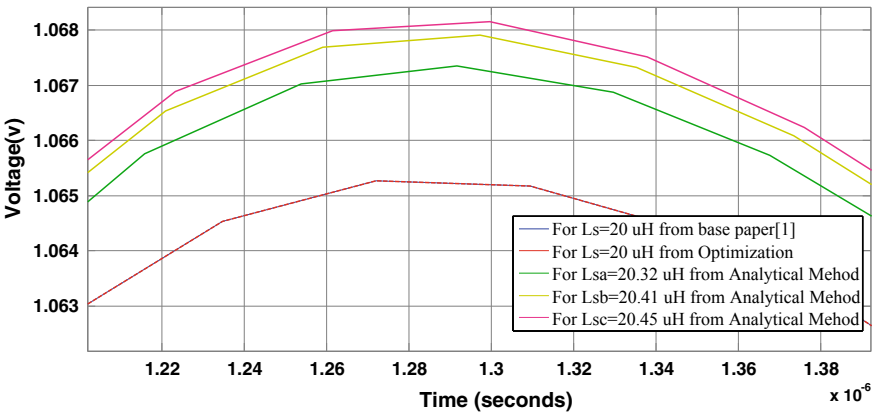

Fig. 10 Comparison of peak value for $Ls = 20\ \mu$H

References

1. Matsumoto, S.: Analysis and evaluation of waveform parameters for oscillating impulse voltage. Trans. Electr. Electron. Eng., IEEJ Trans. **2**(6), 651–656 (2007). Matsumoto, S.: Influence of the residual inductance of the impulse generator for the generation of the lightning impulse voltage. IEEJ Trans. Power Energy **127**(11), 1213–1218 (2007)
2. High-voltage test techniques Part 1 General definitions and test requirements IEC 60060-1 Ed.3.0 (2007)
3. Sato, S., Harada, T., Ebana, T., Hoshi, H., Sakaguchi, S.: Automatic determination of the circuit constants fulfilling the given impulse time parameters. IEEJ Trans. Fundam. Mater. **126**(9), 887–894 (2006). IEEJ. Handbook of High voltage testing (1983)

4. Hallstrom, J., Berlijn, S., Gamlin, M., Garnacho, F., Gockenbach, E., Kato, T., Li, Y., Rungis, J.¨Applicability of different implementations of K-factor filtering schemes for the revision of IEC60060-1 and 2. In International Symposium on High Voltage Engineering, Beijing, China, Paper No. B-32, pp. 1–6 (2005)
5. Basar, M.F.M., Jamaluddin, M.H., Zainuddin, H., Jidin, A., Aras, M.S.M.: Design and development of a small scale system for harvesting the lightning stroke using the impulse voltage generator at HV lab, UTeM. 2010 The 2nd International Conference on Computer and Automation Engineering (ICCAE), Singapore, pp. 161–165 (2010). https://doi.org/10.1109/iccae.2010.5451490
6. Rai, V., Pandey, K., Wadhwa, K.: Designing of multistage impulse voltage generator using ATP software. 2015 International Conference on Recent Developments in Control, Automation and Power Engineering (RDCAPE), Noida, pp. 276–279 (2015). https://doi.org/10.1109/rdcape.2015.7281409
7. Župan, T., Trkulja, B., Obrist, R., Franz, T., Cranganu-Cretu, B., Smajic, J.: Transformer windings' RLC parameters calculation and lightning impulse voltage distribution simulation. IEEE Trans. Magn. **52**, 1–4 (2016)
8. Smajic, J., Steinmetz, T., Rüegg, M., Tanasic, Z., Obrist, R., Tepper, J., Weber, B., Carlen, M.: Simulation and measurement of lightning-impulse voltage distributions over transformer windings. IEEE Trans. Magn. **50**, 553–556 (2014)
9. Naidu, M.S., Kamaraju, V.: High Voltage Engineering. Tata McGraw-Hill, New Delhi (1995)
10. Wadhwa, C.L.: High Voltage Engineering. New Age International Publishers, New Delhi (2007)
11. Bagheri, M., Hekmati, A., Heidarzadeh, R., Naderi, M.: 2009 Power and Energy Conference. Pecon 2008. IEEE, International (IEEE), pp. 387–392 (2008)
12. Jiang, T., Grzybowski, S.: Impact of lightning impulse voltage on polycrystalline silicon photovoltaic modules. 2013 International Symposium on Lightning Protection (XII SIPDA), Belo Horizonte, pp. 287–290 (2013). https://doi.org/10.1109/sipda.2013.6729225
13. Deaconu, et al.: Lightning Impulse Voltage Modeling for Transformer Windings Testing. In: 2019 11th International Symposium on Advanced Topics in Electrical Engineering (ATEE), Bucharest, Romania, pp. 1–6 (2019). https://doi.org/10.1109/atee.2019.8724942
14. Smajic, J. et al.: Simulation and Measurement of Lightning-Impulse Voltage Distributions Over Transformer Windings. IEEE Trans. Magnet. **50**(2), 553–556, Feb. 2014, Art no. 7013604. https://doi.org/10.1109/tmag.2013.2283061
15. Rodewald, A., Feser, K.: The Generation of Lightning and Switching Impulse Voltages in the UHV Region with an Improved Marx Circuit. IEEE Trans. Power Apparatus Syst. PAS-93(1), 414–420, Jan. 1974. https://doi.org/10.1109/tpas.1974.293962

Optimal Placement of PMUs for Kerala and Tamil Nadu State Level Regional Indian Power Grid

Chadaram Chandra Sekhar and P. Suresh Babu

1 Introduction

The power system is an interconnected network of several distribution networks, substations, transmission generating stations, and load centers over a large geographical distance. The network is always busy with power transmissions through the lines, power injections, etc. Since the system is so complex, the analysis of the operating condition of the network is even more complex and is so difficult [1, 2]. In the past, the power network was considered as a semi-static system where the system parameters like power injections and power transfer would not change significantly to time over short intervals. Nowadays, distributed generation with the addition of power electronic components and renewable sources made the power system more complex and it becomes dynamic [3]. Changes in the load are similar to transient characteristics due to the emergence of fast switches. For the balance between demand and supply consumption, the power network has to be monitored continuously such a way that power transfer becomes safe and secure [4]. Power system monitoring is normally done through the help of measurements from the system which are obtained using sensors located in the system. Generally, the sensors used in the power system are the current sensors (Current Transformers) and the voltage sensors (Potential Transformers) [5]. The monitoring of power network is done based on these voltage-current measurements such that whether these parameters are within the allowable limit or not. Power network is dynamic behavior; the system should be monitored continuously over small intervals of time. Normally, states of the power system are

C. C. Sekhar (✉)
JRF, Department of Electrical Engineering, NIT, Warangal, India
e-mail: cschandu.chandra@gmail.com

P. Suresh Babu
Assistant Professor Grade-I, Department of Electrical Engineering, NIT, Warangal, India
e-mail: drsureshperli@nitw.ac.in

O. H. Gupta and V. K. Sood (eds.), *Recent Advances in Power Systems*, Lecture Notes in Electrical Engineering 699, https://doi.org/10.1007/978-981-15-7994-3_21

monitored at every bus location [6, 7]. Power system states are defined as phase angles and magnitudes of voltage. Some states can be directly measured. In the power system, voltage magnitudes can be directly measured but phase angles at each bus cannot. Hence an emerging sensor called Phasor Measurement Unit (PMU) is used to measure voltage phase angles directly. For the monitoring purpose, states at each bus location have to be observed. Placing sensors at all the buses does not make sense, which is also economically impractical. So the sensors should be arranged in a system such a way that the number of sensors should be minimum in an economical point of view and with these minimum number of sensors, the system should be observable completely [8, 9]. A system becomes observable if the states of the system can be obtained from the measurements or outputs. So the sensors are placed at the most important bus locations called optimal bus locations which makes the system observable completely.

2 Optimization Based PMU Placement

(a) ***Objective function formulation and constraints***

The PMU placement issue for a P-bus network [10]:

$$\begin{aligned} &\min \sum_{i=1}^{p} w_i q_i \\ &s.t \quad F(Q)^3 d \end{aligned} \tag{1}$$

where Q represents the vector of binary decision variables whose rudiments are,

$$\begin{aligned} q_i \;&=\; 1 \quad \text{for } i\text{th bus having PMU.} \\ 0 \text{ Otherwise} \quad &\text{for } i \;=\; 1, \ldots, P \end{aligned}$$

d is a unity vector having length P, i.e. $d = \begin{bmatrix} 1 & 1 & 1 & 1 & 1 & 1 & 1 & 1 \end{bmatrix}^{\mathrm{T}}$ w_i represents the ith bus PMU cost. $F(Q)$ is function vector for observability by constraints. If the buses are observable for a given set of measurements, then the essentials of $F(Q)$ are nonzero and zero otherwise.

The optimal PMU placement location is identified below by pretentious w_i as unity [11],

$$\begin{aligned} &\min \sum_{i=1}^{p} q_i \\ &s.t \quad F(Q) \geq d \end{aligned} \tag{2}$$

Full network observability is guaranteed by a constraint vector function. A solution is to be set up that has to fulfill Eq. (2). The power network for bus matrix connectivity is A whose entries are in binary form. The vector function is constraint by using this matrix *A*. The matrix *A* denotes the connectivity in rank about the buses of a power network. Entries of matrix *A* is denoted as,

$$\begin{aligned} a_{m,p} = 1 \quad & \text{if } m = p \\ 1 \quad & \text{if } m \text{ and } p \text{ buses are linked} \\ 0 \quad & \text{if not} \end{aligned}$$

Equations (3) and (4) [11] shows an optimization problem as a constraint function at a specific bus '*i*' is given by:

$$F(Q) = AQ \geq d \tag{3}$$

$$f_i = a_{i,1}q_i + a_{i,2}q_i + \cdots + a_{i,p}q_p \tag{4}$$

I $a_{i,p}$ *t* is zero, the product a_i,*p* q_p will disappear from (4). If any of the q presents is nonzero in *fi*, Then *fi* is observable. The system is observable completely if all *fi* in *F* is non-zero.

(a) ***PMU placement by using Genetic Algorithm***

PMU placement in the system is framed as an optimization problem. In the optimization problem, for complete system observability, PMU is assumed to be placed at all the buses of the system. Here, the optimization technique used is the Genetic Algorithm (GA). In GA, the objective function showing the number of PMUs should be minimized. Finally, the output of GA will be the best optimal location or buses in the system for PMU.

Genetic Algorithm (GA) works on natural selection mechanics and natural genetics. It is one of the meta-heuristic search algorithms in optimization. GA used for the survival of the main suitable natural selection search method [11, 12]. The procedure of GA starts with representing design or decision variables for the population of random strings. To obtain fitness value each string is evaluated. To create a new population there are three main types of operations are follows as

Reproduction:

In search space Candidate solutions, created randomly with an initialized population, are used. By using fitness value the arrangement created by the population is set or the children population can evaluate using solutions of the candidate population. The continued existence of the candidate solutions fittest method is executed through conveying the collection procedure among superior fitness for additional copies of those solutions [13, 14]. The theory consideration of choosing favor superior results for more unfair results and several choosing methods comprise offered to get this attention with roulette-wheel selection.

Crossover:

To produce new two or more parental solutions combines parts Crossover or recombination, to obtain improved results solutions (offspring). The children in recombination won't be present the same from a particular parent, also, to slightly fix parental behavior in different methods [12, 14, 15].

Mutation:

Whereas the recombination mechanism compulsory parental chromosomes should be minimum two, transformation in the neighborhood however arbitrarily varies a solution. At this point, several varieties of changes occur, for the majority part, includes slightly one change being through to a person's superiority [10, 11, 14–16].

The iterative method is an evolution that starts population randomly to individuals created and gives a general population in each significance called a generation. Each individual is assessed in all generations in the population wellness. The opinion of the object effort is expected in the optimization of making fitness or wellness concerns finalized. By randomly varying gene properties and recombination each individual's chromosome new generation is formed by adjusting and by choosing more vigorous people. By candidate preparations, an iteration of the algorithm is followed by utilizing the after create a new population. Generally, the computation ends after every correct fitness stage has arrived in favor of the generation or the majority excessive number of generations has been created.

3 Implementation

For a better understanding of optimal PMU locations, a simple test IEEE 14 bus system is taken and connections between the bus can be done by using the connectivity matrix. Similarily for Tamil Nadu and Kerala state connectivity matrix is taken from a single line diagram is shown in Figs. 2 and 3 respectively. The current and voltage phasors can directly measure by using sensors are known as PMUs. PMUs are costlier so placing sensors is not possible for the entire bus system. Practically it is not possible so for that an optimization technique used to minimize numbers of PMUs in the entire system [11, 13]. The test system has five generating stations and corresponding bus locations are shown in Fig. 1. In those, all the buses connected either generator or load except bus 7 are not connected with any load or generator so bus 7 called zero injection bus (ZIB).

From Tables 1 and 2 bus names and their corresponding locations are mentioned by using serial numbers, this connectivity is taken from POWER GRID corporation 2013, all regional data maps.

Typically the Indian power grid has five regions, the northeastern region, eastern region, western region, northern region, and southern region [3]. In those five, the second largest region in the southern region and consists of five states Tamil Nadu, Kerala, and Karnataka, Telangana, Andhra Pradesh [3, 11, 15].

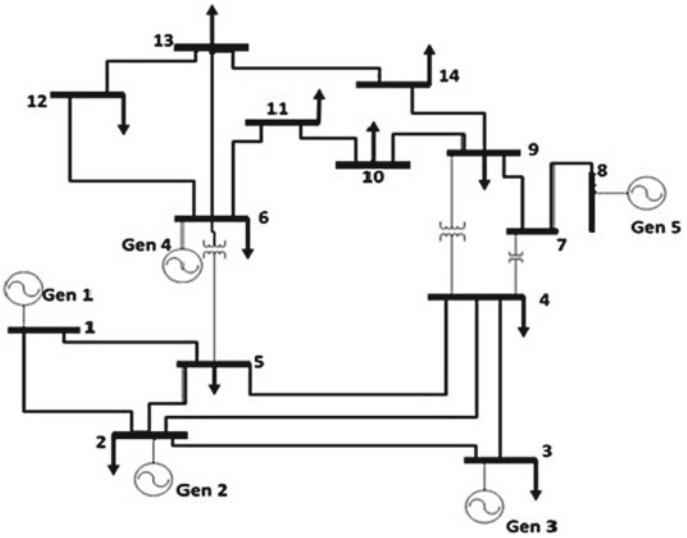

Fig. 1 IEEE 14 test bus system

A single line diagram can be drawn from the given data of the interconnection of the Power Grid Corporation of India Limited website. According to 2013 data from the power grid corporation Tamil Nadu power grid has 104 buses with an interconnection of 66, 110, 220, 400, 765 kV, and Kerala power grid has 31 buses with an interconnection of 66, 110, 220, 400, 765 kV [3, 11]. The connectivity of the bus system is shown in Figs. 2 and 3, and corresponding names are shown in Table 1.

4 Results

To completing of the confirmed method by placing PMUs and their corresponding bus locations should be minimum, in this paper a test IEEE-14bus, 104 bus, and 31-buses are used. All the results are obtained in a MATLAB software 13b version with 8 GB RAM and Intel i5 processor. The entire power system can be observed by using the optimal location of PMUs by using a genetic algorithm. This gives the superlative fitness function in the GA method [11, 14]. For example, an IEEE 14 bus test system is taken in Fig. 2. For that system, results are shown in Fig. 4. From that figure, a 10th bus has PMU it is stamping the data from 10, 11, 9 bus systems [11, 14, 17]. Similarly, remaining optimal PMU locating buses will take the data from corresponding connected buses to them. Similarly, for Tamil Nadu and Kerala state-level power grid optimal PMUs locations can be found by using GA are shown in Table 3 (Figs. 5 and 6).

Table 1 Bus locations for tamil nadu state power grid

S. No.	Bus locations	S. No.	Bus locations
1	SR Pudur	53	Deviarkurchi
2	Sankarneri	54	STCMC
3	Udayathur	55	Sail
4	Pasaumalai	56	Unjanar
5	Koodankulam	57	Pundanchandal
6	TTDS	58	Villianur
7	Auto	59	Cuddalore
8	Madurai	60	Eachengadu
9	Kayathal	61	Samaypurm
10	Tuticorin JV	62	Perambalur
11	Si Pcot	63	Janjavur
12	Indbharath	64	Thiruvarur
13	Udumalpet	65	PP Nallur
14	Veeranam	66	Karambayam
15	Kodikurchi	67	Paramalade
16	Amuthapuran	68	Vallathur
17	Thirunelveli	69	Alagarkoil
18	Nallamanaickerath	70	TV Malai
19	Paramakudi	71	Singarapetti
20	Arkay	72	Arani
21	Alagarkoil	73	Kalavindapattu
22	Karaikudi	74	Vinnamangalam
23	Sterlile	75	Bathoor
24	Karaikudi New	76	Villanur
25	Santhur	77	Thondamanatham
26	Trichy	78	SV Chatram
27	Theni	79	Oragadam
28	Pugalur	80	Korattur
29	Sembathi	81	Kalpakkam
30	Renganathapuram	82	KTS parli
31	Kadamparal	83	SP Budur
32	Aliyar	84	Kilpurk
33	Madukkarai	85	Manali
34	Anailkadava	86	Koyambeda
35	OK Madapam	87	Kaperi
36	Palladam	88	NCTPSTG2
37	Thudiyalur	89	TCPLGummdipoundi

(continued)

Table 1 (continued)

S. No.	Bus locations	S. No.	Bus locations
38	Sadayampalam	90	Almathy
39	Ponnapuram	91	Vallur
40	Kundah 2,3	92	Mosur
41	Suzlon	93	Emore
42	Thudiyalur	94	Tondiarpet
43	Gobi	95	Elephant gate
44	Ingur	96	Mylapore
45	MTPS	97	Thadamani
46	Salem	98	Hitech
47	Malco	99	Spkoil
48	Mettur tunnel	100	Chennai
49	Karimangalm	101	Mettur
50	Hosur	102	Mettur TPS
51	Arasur	103	Neyveli TSI
52	Neyvelli TS II	104	Kdalangudu

Table 2 bus locations for kerala state power grid

S. No.	Bus locations	S. No.	Bus locations
1	Kayamukulam	17	Kochi
2	Kundara	18	Bramhapram
3	Edappon	19	Palakkad
4	Edamon	20	Walayar
5	Pothencode	21	Shoranur
6	Trivandrum	22	Areakode
7	paruthipara	23	Kaniampet
8	parasala	24	Nallalam (Kozhikodde)
9	New palom	25	Vatakara
10	Idukki	26	Kanhikode
11	Pallom	27	Taliparamba
12	Ambalamugal	28	Kasarkode
13	Sabrigiri	29	Vidyanagar
14	Kalamassery	30	Kubanur
15	Unknown	31	Manjeshwar
16	Trichur		

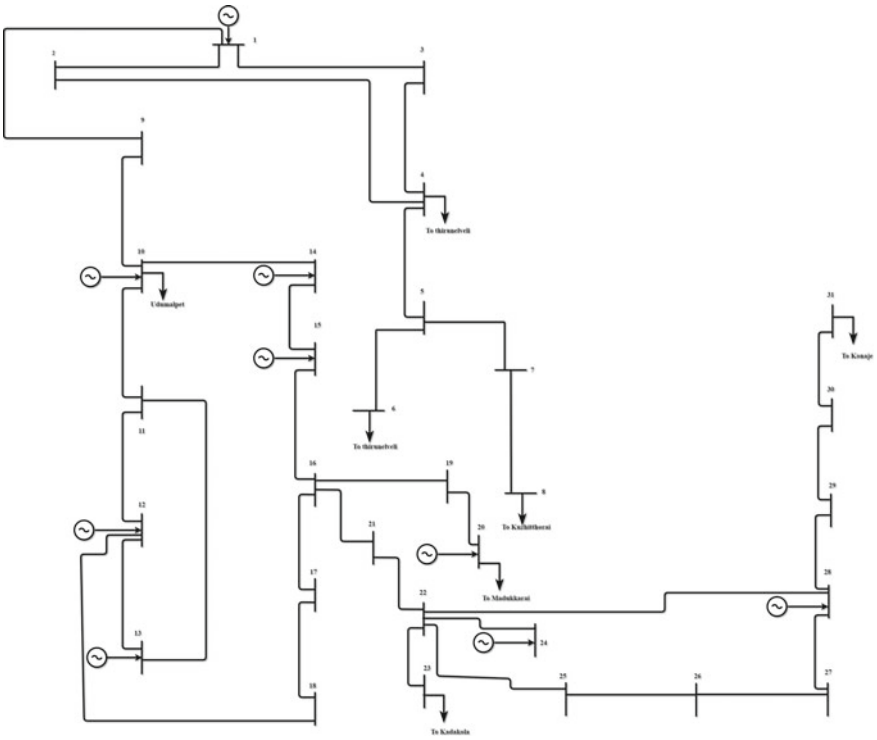

Fig. 2 Kerala power gird single line diagram

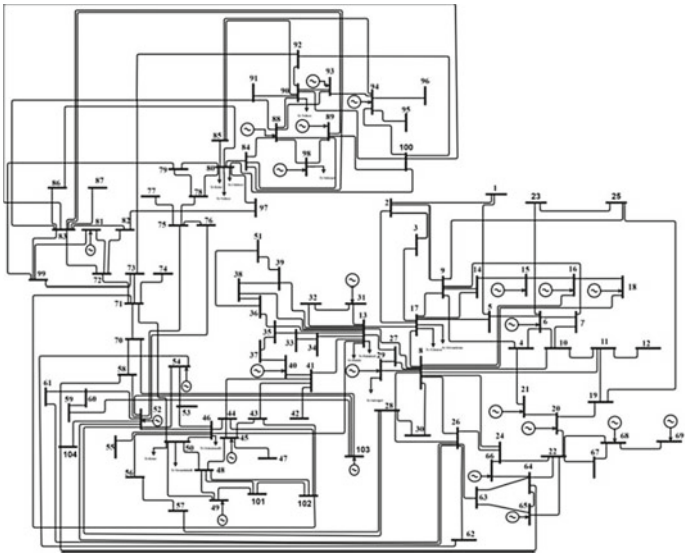

Fig. 3 Tamil Nadu power gird single line diagram

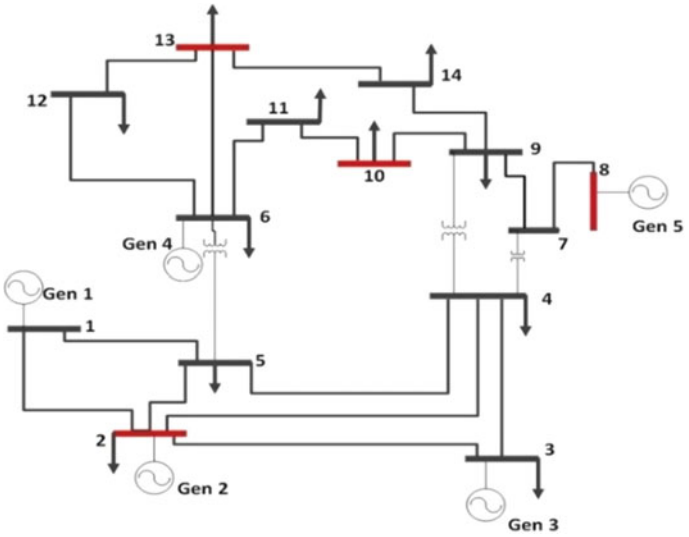

Fig. 4 IEEE 14 bus test system optimal PMU locations

Table 3 Details for IEEE 14 bus test system

System	No. of buses	No. of PMUs	PMU bus locations
IEEE 14 bus test system	14	4	13,10,8,2,

Table 6 clearly shows genetic algorithm 19 PMU is required for a total of 104 bus locations. As well as by using integer linear programming 20 PMUs are required for a total of 83 bus locations. By observing GA is required less number of optimal PMUs locations as compared to the ILP [3].

5 Conclusion

Formulation of locating placement of optimal PMU locations finding using darwin's theory of evolution [11]. Placing PMUs in the entire power system is not possible due to PMUs are costlier. By using optimization placing a PMUs is minimized as much as possible. This paper explains about Tamil Nadu power grid and Kerala PMUs locations. The optimal placement of the PMU locations has to be done by a Genetic Algorithm (GA) [17]. The idea is to facilitate the system in total observability and finding the minimum number of optimal locations to place PMUs. Tables 4 and 5 show Results for Kerala and Tamil Nadu regional level Indian power grid PMU optimal locations and corresponding bus names (Table 6).

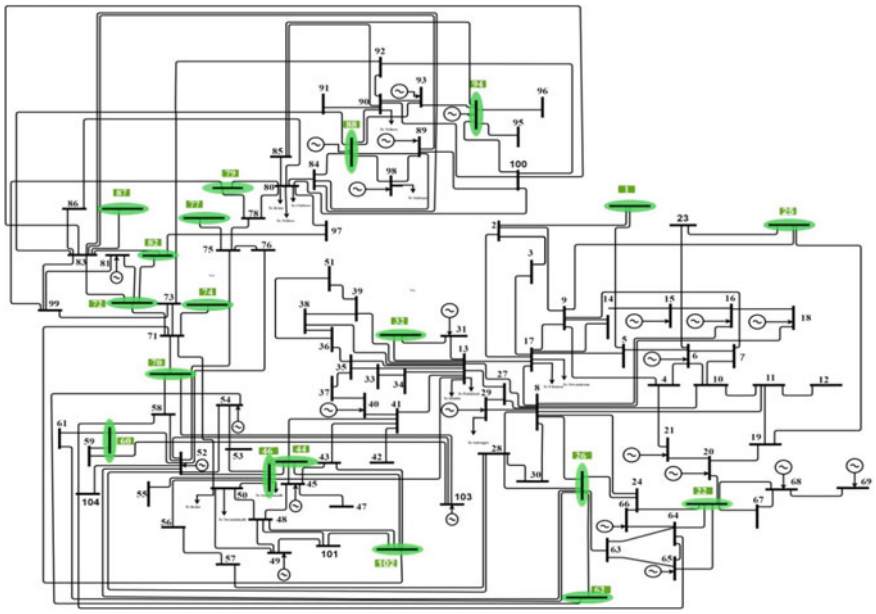

Fig. 5 Tamil Nadu power gird optimal PMU locations

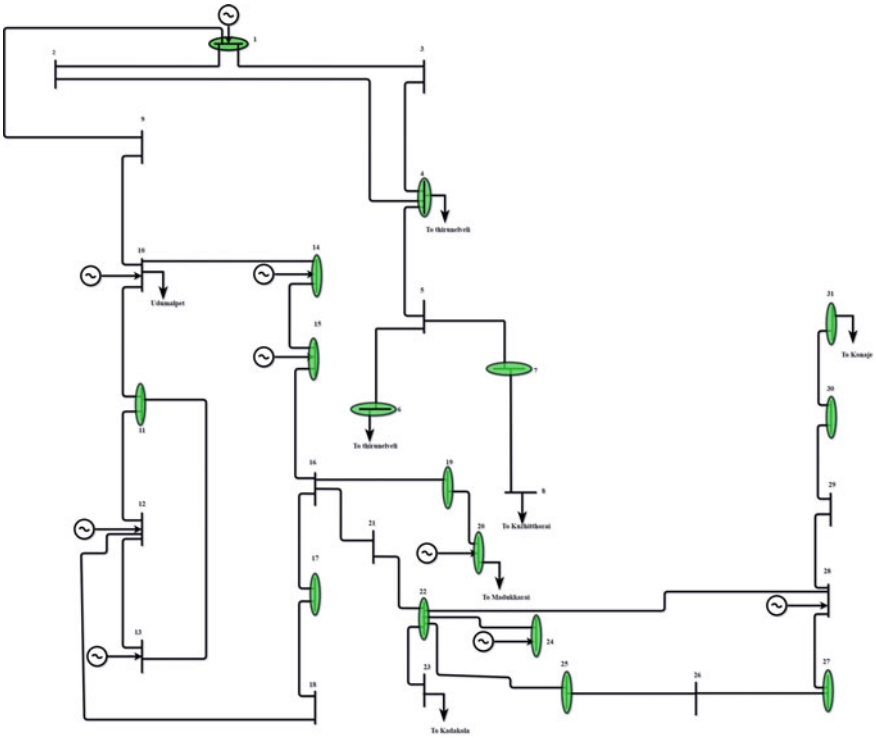

Fig. 6 Kerala power gird optimal PMU locations

Table 4 Optimal PMU location for complete observability for Tamil Nadu state power grid

S. No.	Bus locations
102	Mettur TPS
94	Tondiarpet
88	NCTPSTG2
87	Kaperi
82	KTS parli
79	Oragadam
77	Thondamanatham
74	Vinnamangalam
72	Arani
70	TV Malai
62	Perambalur
46	Salem
60	Eachengadu
44	Ingur
32	Aliyar
26	Trichy
25	Santhur
22	Karaikudi
1	SR Pudur

Table 5 Optimal PMU location for complete observability for Kerala state power grid

S. No.	Bus locations
31	Manjeshwar
30	Kubanur
27	Taliparamba
25	Vatakara
24	Nallalam (Kozhikodde)
22	Areakode
20	Walayar
19	Palakkad
17	Kochi
15	Unknown
14	Kalamassery
11	Pallom
7	paruthipara
6	Trivandrum
4	Edamon
1	Kayamukulam

Table 6 Comparison of the number of optimal PMUs required for ILP versus GA

S. No.	Tamil Nadu power grid	
	Several optimal PMUs required by using ILP [3]	Number of optimal PMUs required by using GA
1	20	19

References

1. Schweppe, F.C., Wildes, J.: Power system static-state estimation, part I: exact model. IEEE Trans Power Apparatus Syst PAS-89(1), January 1970
2. Larson, R.E., Tinney, W.F., Hajdu, L.P.: State estimation in power systems part ii: implementation and applications. IEEE Trans Power Apparatus Syst. 3, PAS-89 March 1970
3. Gopakumar, P.G., Chandra, S., Jaya Bharata Reddy, M.: Optimal placement of phasor measurement units for Tamil Nadu state of Indian power grid. In: 2012 11th International Conference on Environment and Electrical Engineering (2012)
4. Dy Liacco, T.E.: The role of state estimation in power system operation. ELSEVIER J. **15**(4), 1531–1533 June 1982
5. Monticelli, A.: State estimation in electric power systems: A generalized approach. Springer (2012)
6. Kamireddy, S., Schulz, N.N., Anurag, K.S.: Comparison of state estimation algorithms for extreme contingencies. In: 40th North American Power Symposium, Sept 2008. https://doi.org.10.1109/NAPS.2008.5307380
7. Jain, A., Shivakumar, N.R.: Impact of PMU in dynamic state estimation of power systems. In: 40th North American Power Symposium, September 2008. https://doi.org/10.1109/NAPS.2008.5307352
8. Aminifar, F., Shahidehpour, M., Fotuhi-Firuzabad, M., Kamalinia, S.: Power system dynamic state estimation with synchronized phasor measurements. IEEE Trans Instrum. Measur. **63**(2), 352–363, February 2014
9. Phadke, A.G., Thorp, J.S.: Synchronized Phasor Measurements and their Applications. Springer, New York, NY, USA (2008)
10. Meriem, N., Omar, S., Jamal, B., El Faissal. M.: Study of state estimation using weighted least squares method. Int. J. Adv. Eng. Res. Sci. (IJAERS), **3**(8), ISSN: 2349-6495(P)|2456-1908(O), Aug 2016
11. Akhlaghi, S., Zhou, N., Eva Wu, N.: PMU placement for state estimation considering measurement redundancy and controlled islanding. In: 2016 IEEE Power and Energy Society General Meeting (PESGM) (2016)
12. Saha Roy, B.K., Sinha, A.K., Pradhan, A.K.: An optimal PMU placement technique for power system observability. Electr. Power Energy Syst. **42**(1), 71–77, November 2. https://doi.org/10.1016/j.ijepes.2012.03.011
13. Yuill, W., Edwards, A., Chowdhury, S., Chowdhury, S.P.: Optimal PMU placement: a comprehensive literature review. In: IEEE Power and Energy Society General Meeting, pp. 1–8, October 2011
14. Korres, G.N., Manousakis, N.M., Theodorakatos, N.P.: Optimal placement of PMUS in power systems using binary integer programming and genetic algorithm. MedPower (2014)
15. IEEE Standard for Synchrophasor Measurements for Power Systems, IEEE Standard C37.118.1–2011, Dec 2011
16. Tebianian, H., Jeyasurya, B.: Dynamic state estimation in power systems: modelling and challenges. ELSEVIER J. Electr. Power Syst. Res. 109–114 (2015)
17. Gopakumar, P., Surya Chandra, G., Jaya Bharata Reddy, M., Mohanta, D.K.: Optimal redundant placement of PMUs in the Indian power grid—northern, eastern and northeastern regions. Front. Energy (2013)

Study of Phasor Measurement Unit and Its Applications

Shiv Shankar, K. B. Yadav, Alok Priyadarshi, and Vishal Rathore

1 Introduction

Electricity requirement is increasing day by day due to which demand is more than that of supply which leads to introduction of Renewable energy resources (RESs). Therefore, in Europe RESs provide two-third of energy sources by 2050 [1]. Occurrence of additional uncertainties in power system due to the RESs [2–7]. Overcapacity generation is one of the important challenges for using RESs [8]. For this case, Electrical Energy Storage (EES) is used for decreasing the problem of the system and increasing its performance [9]. The modern power system is complex in nature and it is divided in four categories: generation, transmission, distribution, utilization. Today due to this complexity it is very important to monitor power system network in real time [10].

Traditionally Supervisory Control and Data Acquisition (SCADA) is used for monitoring and controlling the PS network. Improper controlling creates electricity black out too many customers and losses in the economy [11]. These issues made it important to analyze the power system and hence synchrophasor technology come into the picture. Compared to SCADA system PMU is more accurate and faster. Moreover, PMU can be used to monitor and protection of many parts of power system. But due to its high cost it cannot widely used in system networks [12]. As

S. Shankar (✉) · K. B. Yadav · A. Priyadarshi · V. Rathore
Department of Electrical Engineering, NIT Jamshedpur, Jharkhand, India
e-mail: shiv.3122@gmail.com

K. B. Yadav
e-mail: kbyadav.ee@nitjsr.ac.in

A. Priyadarshi
e-mail: alokpriya4@gmail.com

V. Rathore
e-mail: vishalrathore01@gmail.com

O. H. Gupta and V. K. Sood (eds.), *Recent Advances in Power Systems*, Lecture Notes in Electrical Engineering 699, https://doi.org/10.1007/978-981-15-7994-3_22

requirement of PMUs decreases which will decrease the cost of power networks. Many research [13–16] have been done for finding the optimal location and many other optimization techniques have been introduced [17–19]. Each technique has its advantages and disadvantages, depending upon conditions and observability of use

2 PMU

An electronic element installed in Smart grid for estimating the magnitude and the phase angle of an electrical phasor quantity such as voltage and current. A synchrophasor refers to cosine wave magnitude and angle of different electrical components like voltages or current which is referred to the absolute value in time [20]. Figure 1 shows a sine wave with its phasor form is represented by:

$$y(t) = Y_m \cos(\omega(t) + \emptyset) \tag{1}$$

$$Y = \frac{Y_m}{\sqrt{2}} e^{j\emptyset} = \frac{Y_m}{\sqrt{2}} (\cos \emptyset + j \sin \emptyset) = Y_r + jY_i \tag{2}$$

By the help of current transformers and potential transformers the input data $V(t)$ and $I(t)$ of PMU are directly calculated. This voltage and current is passed through front-end anti-aliasing filter and then digitization using A/D converter. Synchronized Global Positioning System (GPS) clock [21] as describe in Fig. 2 at specified rate is coordinated for the digitization process. For tag time generating within the second a phase-locked oscillator is used [22]. To calculate different electrical phasors, the rate of change of frequency (ROCOF) and binary information the digital data is sent to the microprocessor.

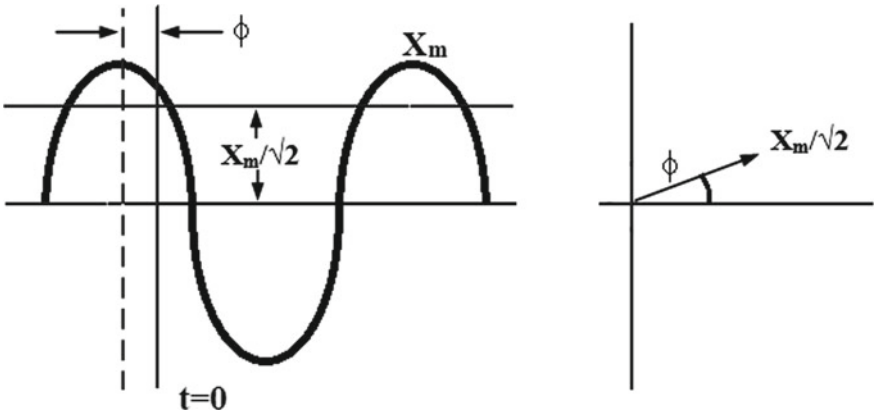

Fig. 1 Phasor representation of sine curve

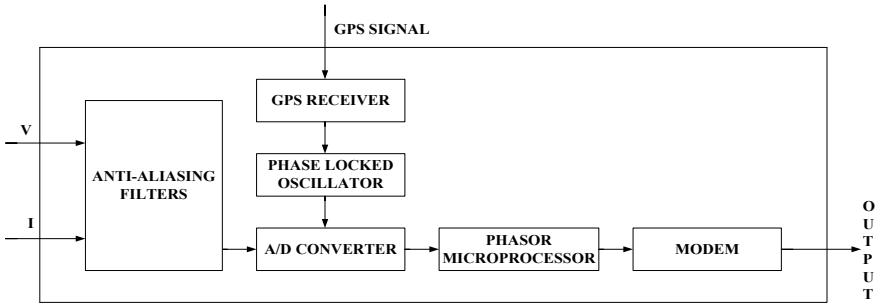

Fig. 2 PMU block representation

2.1 PMU Assessment Depends on Following Factors

- Availability in which phase data concentrators (PDC) receives the measured data by PMU in timely manner.
- Accuracy is refers to the difference between the true and the measured value. 1% total vector error (TVE) is the standard performance PMU. TVE is the accuracy index used in magnitude and angle.
- The time take to exchange data in between two points is defined as time delay or latency in a network. Latency of PMU is based on wide area which contains delays that are link with voltage/current transducers and actuators.
- Due to GPS signal loss PMU may lost its data. Therefore, data are dropped which does not arrive within specific time [23].

2.2 Communication

SCADA uses various types of communication such as coaxial cables, power line communication, satellites, fiber optics, telephone cable lines to transfer data. In WAMS communication is mainly categorized in two categories wired and wireless communication. Wired communication includes PLC and fiber optics whereas wireless includes Wi-Fi [24], WiMAX [25], cellular communication (5G, satellites), radio, microwaves [26] and ZigBee [27]. The merits and demerits are discussed in Table 1. Through electrical power lines PLC allowed to exchange data. Narrowband [28] (up to 500 kHz) and broadband [29] (2–50 MHz) are the two categories of PLC.

In future fifth generation(5G) mobile network is the best option for PMU communication. In comparison to 4G, 5G is 100 times faster with data transfer speed 50Gbps [30]. Combination of smart meters into the ZigBee network with other elements is done with the help of "ZigBee smart Energy" [31]. By the help of this application information are collected by smart meters from the integrated device.

Table 1 WAMS communication methods

Communication methods	Merits	Demerits
ZigBee	Smaller in size and it uses small bandwidth	Its lifetime is limited by small battery, low processing capability
PLC	Low cost and delay time, large coverage	High noise over power lines are created across discharge insulator
Wireless	Low cost, huge development across the world	For interference with other devices it requires high potential
Satellites	Availability of secure algorithms, data transfer at high rates	Depends on climate, it requires high initial and operational cost
5G	Time delay is less [32], network efficiency is high	latest technology and it requires high security assurance [33]
Microwave	Cost is medium and it does not required cables	Requires line of sight for operation and weather dependent technology

3 PMU Application in Power Distribution Network

Judging application in power system and monitoring in group is known as WAMS. SCADA is unable to find these information for the power grids as shown in Table 2. In both the system input data is analog of voltage and current. In SCADA these data are forwarded to Remote Terminal Unit (RTU) in digital form of voltage and current. With the norms IEC 61850 [23] and IEC 60870-5-104 the communication exists between RTU and SCADA control unit.

WAMSs consists PDC, super PDC, PMU and communication between these as shown in Fig. 3. Based upon IEEE C37.118.2 or IEC 61850-90-5 norms phasor value

Table 2 SCADA versus WAMS

Features	SCADA	WAMS
Angle measurement	Not possible	Possible
Measuremnt rate	One value in every one to few seconds	10–60 value in one seconds
Monitoring of oscillation	Not possible	Possible
Post fault analysis	Not possible in real time	Possible in real time
Resolution	Steady state observability	Dynamic/Transient observability
Total input/output channels	100 + analog and digital	16 + analog and digital, 10-phasor
Focus	Monitoring and control of local area	Monitoring and control over wide area

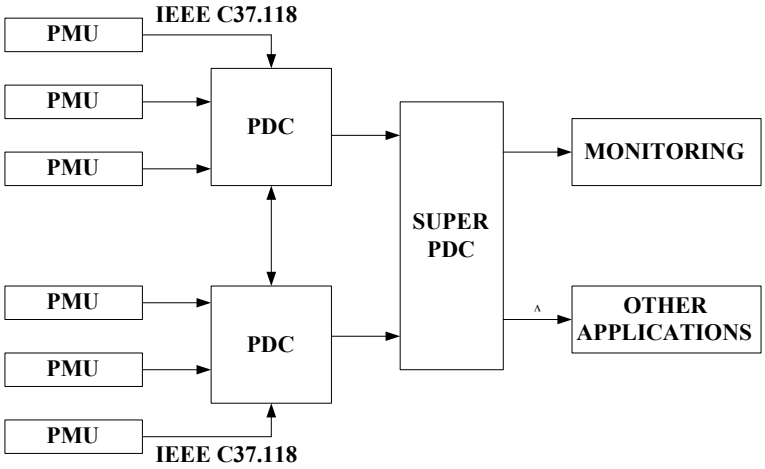

Fig. 3 Architecture of WAMS

Table 3 Classification of PMU in distribution system

Properties	Class A	Class B	Class C	Class D
Precision	4	2	4	1
Reliabiltiy	4	2	3	1
Low Latency	4	3	1	2
Message rate	4	2	4	2
Time align	4	4	1	2
Application	Automation	Reliability	Planning	Operation

of PMU will be sent PDC.PDC plays an important role in receiving data from PMUs and sent these data to other super PMU. The storing and monitoring of data with checking of errors is also the duty of PDC [34].

For fast communication the IEC61850-90-5 is taken in place of IEEE C37.118.2 protocol. Whereas the IEC61850 protocol is used for fast communication between the relays. As per the reports of North American Synchrophasor Initiative (NASPI) application of PMU in PS is mainly divided into four classes [35] as convey in Table 3.

3.1 Automation of Power System (Class a)

The advanced application which improves reliability, security and asset utilization are automatic controlled and protected by this type of PMUs in distribution system. Some of the application are listed below:

Microgrid operation—Resynchronization, balance between load and generation, islanding refers to micro grid operation. In absence of electrical power grid distributed generator continues to supply power to a location is known as islanding. Mainly islanding is classified into categories. Intentional islanding for maintenance of electrical network and during fault conditions another islanding called unintentional islanding occurs [36].

Location and Detection of Fault—Most of the faults are occurred at the distributed level of PS. The reduction of outage duration and cost is done by PMU. Synchronized measurement values of voltage and current will improve the accuracy of fault location. Both voltage and current phasors are used for the maximum accuracy [37].

Facts devices—Improvement of voltage profile is done by distributed FACTS (D-FACTS) devices. To control the distributed system instantly PMU are connected to FACTS devices.

3.2 Reliability or Coordination of Power System (Class B)

The factors which are considered in classification table of PMU Table 3 are important one. Improving reliability, situational awareness are the applications of Class B. due to lower voltage and higher customers traditionally many challenges are faced by distributed generator in achieving situational awareness.

3.3 Planning of Power System (Class C)

Reviewing of PS applications comes under this class. Latency is more important in comparison to accuracy. Some of the applications are as follows:

State Estimation (SE)—The present operating condition of a power system is known as State estimation. Previously without PMU, RTU done all the measurements and calculation of voltage, current, active/reactive power for the estimation of unknown variables under SCADA system which takes 2–5 s. but by using PMU we can reduce the capturing time to 30–40 ms as it directly observes the state variables [38].

Analysis of power qualitys—In distribution problems occurred due to power quality such as disturbances or interruption of voltage, waveforms quality issue. The expected TVE is 0.5–1% for the analysis of power quality [39].

Features of DG—Generation of power close to the customers is the advantage of DGs. However, changes occurred in power grid when different DGs are connected to the grid [40] such as short circuit levels will increase, voltage profiles changes, branches of system get crowded. Responses during faulty condition is done by online analyzing of active and reactive power.

Validation of model—Verification of line impedance, transformer, generators models, etc. of the power system network is called as validation of model. It's important for secure and reliable PS [41]. For the calculation of impedances of line segment and other variables accurate voltage and current phasor is needed which is provided by PMU application by enabling dynamic validation of model.

3.4 Operation of Power System (Class D)

Imagination and monitoring application comes under this category. Some of the application are as follows:

Detection of disturbance and topology—It helps in monitoring of voltage and frequency disturbance which is important for system stability after switching. In any power system location, the detection of switch position (open/close) is done by detection topology. Based on source impedance topology and disturbance are detected [40]. Algorithm Structure, Voting-based Detection Criteria are some of the methods for detection of topology using PMU [42].

Identification of phase—Maintenance, reconfiguration or changes in the DS cause further phase imbalance and these issues are not always monitored. Improper phase tagging is main reason of error in state estimation, detection of topology and location of fault [43]. Imbalance current results to imbalance voltage which lead to power loss, power failure. Therefore, phase identification is important to avoid phase imbalance.

4 Development and Placement of PMU

In early 1980s first PMU was introduced by power system researcher. After that many companies like Power Standards, Siemens, EATON etc. started to work on synchrophasor technology. The key aspects that supports for the development of PMU are given below:

4.1 Cost Vs Advantage

Cost of installation is more than its apparatus or PMU devices so, minimizing the cost is important as it reduces the overall cost of PMUs [44]. Synchronized monitoring of networks is done by distributed system operators(DSOs) which is enabled PMU measurement for the distributed energy resource(DER) management. And this a framework for future monitoring of Active distribution networks(AND) [45]

Table 4 Classification of OPP technique [47]

Heuristic method	Meta-heuristic method	Deterministic methods
Domination set [48] Greedy algorithm [49]	Genetic algorithms [50] Particle swarm optimization (PSO) [51]	Integer programming [52] Binary search method [53]

Note 4 refers to critically significant; 3 refers to significant; 2 refers to a bit significant; 1 refers to not quite significant

4.2 Sensing and Deployment Feasibility

The cost of installation of PMU is once justified as several other applications are sensed by this installation [45]. Once the PMU is installed at distribution network (DNs), the same PMU is used for monitoring conventional quantities with higher resolution [46].

4.3 Limited Covering Region

Lesser number of PMU is required to monitor DNs as DNs region is smaller when compared with transmission networks.

While the cost of installation is high so we have to reduce it. This reduction of cost is done by proper placement of PMU called optimal PMU placement (OPP). Mainly OPP is classified into three categories as per Table 4 with its examples.

Among many OPP methods integer programming is regularly used methods. It refers to programming technique used for calculating optimized value.

Some of the Research area in OPP are:

- Based on network constraints and topology evaluate the best results.
- OPP should provide more practical results by including the cost of installation and performance.
- Most of the OPP methods works for smaller PS so, implementation of method which is applicable for large PS networks.
- Work should be done in presence of DG for OPP for the distribution system.
- Hybrid method can be used by the combination of different methods.

5 Conclusions

This paper provides a compressive review of PMU with its optimal location and its application in power distribution system. The review also presents the future scope of OPP. Application described in this paper are presently practice in many of electric power plant. In academic publication some applications are being processed which will be later used by electric plant. For power system security these applications

used machine learning algorithm. For protection, monitoring and control application of PMU, it requires more accurate and fast communication. By introducing new technology as such 5G communication these problems are rectified. Far from PMU advantages it has some problems in distribution system like insufficient phasor precision and absence of networks that can support large amount of sensors. So by using single sensor model is an option for taking high precision phasors using PMU in distribution system. By using effective optimization method, the number of PMUs requirement is decreases which reduces the overall cost of the installation.

References

1. Oettinger, G.H.: Energy Roadmap 2050. Publications Once of the European Union, Brussels, Belgium (2011)
2. Jordehi, A.R.: How to deal with uncertainties in electric power systems—a review. Renew. Sustain. Ener. Rev. **96**, 145–155 (2018)
3. Hirth, Lion: The market value of variable renewables: the effect of solar wind power variability on their relative price. Energ. Econ. **38**, 218–236 (2013)
4. Edenhofer, O., Hirth, L., Knopf, B., Pahle, M., Schlömer, S., Schmid, E., Ueckerdt, F.: On the economics of renewable energy sources. Energ. Econ. **40**, S12–S23 (2013)
5. Ueckerdt, F., et al.: System LCOE: what are the costs of variable renewables? Energy **63**, 61–75 (2013)
6. Akrami, A., Doostizadeh, M., Aminifar, F.: Power system flexibility: an overview of emergence to evolution. J. Mod. Power Syst. Clean Energ. **7**(5), 987–1007 (2019)
7. Negnevitsky, M.: High renewable energy penetration and power system security: new challenges and opportunities. In: 10th International Scientific Symposium on Electrical Power Engineering, Elektroenergetika (2019)
8. Colmenar-Santos, A., et al.: Profitability analysis of grid-connected photovoltaic facilities for household electricity self-sufficiency. Energ. Policy **51**, 749–764 (2012)
9. Lai, C.S., McCulloch, M.D.: Levelized cost of electricity for solar photovoltaic and electrical energy storage. Appl. Energ. **190**, 191–203 (2017)
10. Saadat, H.: Power Systems Analysis, 2nd edn. PSA Publishing LLC, Portland (2002)
11. Baldick, R., Chowdhury, B., Dobson, I. et al: Initial review of methods for cascading failure analysis in electric power transmission systems IEEE PES CAMS task force on understanding, prediction, mitigation and restoration of cascading failures. In: Proceedings of IEEE PES General Meeting, Pittsburgh, USA, 20–24 July 2008, pp. 8 (2008)
12. Liu, Y., You, S., Yao, W., Cui, Y., Wu, L., Zhou, D., Zhao, J., Liu, H., Liu, Y.: A Distribution LevelWide area monitoring system for the electric power Grid-FNET/GridEye. IEEE Access **5**, 2329–2338 (2017)
13. Aminifar, F., Khodaei, A., Fotuhi-Firuzabad, M., Shahidehpour, M.: Contingency-constrained PMU placement in power networks. IEEE Trans. Power Syst. **25**, 516–523 (2010)
14. Akhlaghi, S.: Optimal PMU placement considering contingency-constraints for power system observability and measurement redundancy. In: Proceedings of the 2016 IEEE Power and Energy Conference at Illinois (PECI), Urbana, IL, USA, 19–20 February 2016, pp. 1–7 (2016)
15. Akhlaghi, S., Zhou, N., Wu, N.E.: PMU placement for state estimation considering measurement redundancy and controlled islanding. In: Proceedings of the 2016 IEEE Power and Energy Society General Meeting (PESGM), Boston, MA, USA, 17–21 July 2016, pp. 1–5 (2016)
16. Xie, N., Torelli, F., Bompard, E., Vaccaro, A.: A graph theory based methodology for optimal PMUs placement and multiarea power system state estimation. Electr. Power Syst. Res. **119**, 25–33 (2015)

17. Sarailoo, M., Wu, N.E.: A new PMU placement algorithm to meet a specified synchrophasor availability. In: Proceedings of the 2016 IEEE Power and Energy Society Innovative Smart Grid Technologies Conference (ISGT), Minneapolis, MN, USA, 6–9 September 2016, pp. 1–5 (2016)
18. Li, Q., Cui, T., Weng, Y., Negi, R., Franchetti, F., Ilic, M.D.: An information-theoretic approach to pmu placement in electric power systems. IEEE Trans. Smart Grid **4**, 446–456 (2013)
19. Zhang, C., Jia, Y., Xu, Z., Lai, L.L., Wong, K.P.: Optimal PMU placement considering state estimation uncertainty and voltage controllability. IET Gener. Transm. Distrib. **11**, 4465–4475 (2017)
20. IEEE: IEEE C37.118.1a-2014: IEEE standard for synchrophasor measurements for power system (2014)
21. Singh, B., Sharma, N., Tiwari, A., Verma, K., Singh, S.: Applications of phasor measurement units (PMUs) in electric power system networks incorporated with FACTS controllers. Int. J. Eng. Sci. Technol. **3**, 64–82 (2011)
22. Mini, S.T., McDonald, J.D.: Power System SCADA and Smart Grids, 1st edn. CRC Press, Boca Raton, FL, USA (2015)
23. Hojabri, M., et al.: A comprehensive survey on phasor measurement unit applications in distribution systems. Energies **12.23**, 4552 (2019)
24. Siow, L.K., So, P.L., Gooi, H.B., Luo, F.L., Gajanayake, C.J., Vo, Q.N.: Wi-Fi based server in microgrid energy management system. In: Proceedings of the TENCON 2009–2009 IEEE Region 10 Conference, Singapore, 23–26 January 2009, pp. 1–5 (2009)
25. Eissa, M.M.: New protection principle for smart grid with renewable energy sources integration using WiMAX centralized scheduling technology. Int. J. Electr. Power Energy Syst. **97**, 372–384 (2018)
26. Chin, W.L., Li, W., Chen, H.H.: Energy big data security threats in IoT-based smart grid communications. IEEE Commun. Mag. **55**, 70–75 (2017)
27. Batista, N.C., Melício, R., Matias, J.C.O., Catalão, J.P.S.: Photovoltaic and wind energy systems monitoring and building/home energy management using ZigBee devices within a smart grid. Energy **49**, 306–315 (2013)
28. Lampe, L., Andrea, T.T., Swart, G. (eds.): Power line communications: principles, standards and applications from multimedia to smart grid, 2nd edn. Wiley, Hoboken, NJ, USA (2016)
29. Dominiak, S., Dersch, U.: Precise time synchronization of phasor measurement units with broadband power line communications. Swiss Federal Oce of Energy SFOE, Bern, Switaerland (2017)
30. Heuzeroth, T.: Die GanzeWahrheitÜber die NächsteMobilfunk-Generation. Available online https://www.welt.de/wirtschaft/webwelt/article189459047/5G-Die-ganze-Wahrheit-ueber-die naechsteMobilfunk-Generation.html. Accessed on 28 Nov 2019
31. Luan, S.W., Teng, J.H., Chan, S.Y., Hwang, L.C.: Development of a smart power meter for AMI based on ZigBee communication. In: International Conference on Power Electronics and Drive Systems (PEDS), Taipei, 2–5 November 2009, pp. 661–665 (2009). http://dx.doi.org/10.1109/PEDS.2009.5385726
32. Cosovic, M., Tsitsimelis, A., Vukobratovic, D., Matamoros, J., Anton-Haro, C.: 5G mobile cellular networks: enabling distributed state estimation for smart grids. IEEE Commun. Mag. **55**, 62–69 (2017)
33. 5G Americas White Paper: 5G The Future of IoT. Available online https://www.5gamericas:5g-the-future-of-iot. Accessed on 28 Nov 2019
34. Martínez, C., Parashar, M., Dyer, J., Coroas, J.: Real time monitoring, control and protection. Phasor data requirements for real time wide-area monitoring, control and protection applications. Consort. Electr. Reliab. Technol. Solut. **26**, 8 (2005)
35. Huang, C., Li, F., Zhou, D., Guo, J., Pan, Z., Liu, Y., Liu, Y.: Data quality issues for Synchrophasor applications part I: a review. J. Mod. Power Syst. Clean. **4**, 342–352 (2016)
36. Almas, M.S., Vanfretti, L.: RT-HIL Implementation of the hybrid Synchrophasor and GOOSE-based passive islanding schemes. IEEE Trans. Power Deliv. **31**, 1299–1309 (2016)

37. Von Meier, A., Berkeley, U.C., Brady, K., Berkeley, U.C., Brown, M., Berkeley, U.C., Cotter, G.R., Llc, I.: Synchrophasor Monitoring for Distribution Systems: Technical Foundations and Applications A White Paper by the NASPI Distribution Task Team. NASPI: Berkeley, CA, USA (2018)
38. Kong, X., Chen, Y., Xu, T., Wang, C., Yong, C., Li, P., Yu, L.: A hybrid state estimator based on SCADA and PMU measurements for medium voltage distribution system. Appl. Sci. **8**, 1527 (2018)
39. Kumar, S., Soni, M.K., Jain, D.K.: Monitoring of wide area power system network with phasor data concentrator (PDC). Int. J. Inf. Eng. Electron. Bus. **7**, 20–26 (2015)
40. Dulau, L.I., Abrudean, M., Bica, D.: Eects of distributed generation on electric power systems. Procedia Technol. **12**, 681–686 (2014)
41. Allen, E., Kosterev, D., Pourbeik, P.: Validation of power system models. In: Proceedings of the IEEE PES General Meeting, Providence, RI, USA, 25–29 July 2010, pp. 1–7 (2010)
42. Arghandeh, R., Cavraro, G.: Renewable N. topology detection in microgridswith micro-synchrophasors. In: Proceedings of the IEEE Power and Energy Society General Meeting, Denver, CO, USA, 26–30 July (2015)
43. Von Meier, A., Arghandeh, R.: Every moment counts: synchrophasors for distribution networks with variable resources. In: Renewable Energy Integration, pp. 435–444. Academic Press, Cambridge, MA, USA (2017)
44. "Factors affecting PMU Installation Costs: U.S. Department of Energy Office of Electricity Delivery and Energy Reliability, Smart Grid Investment Grant Program (2014)
45. Joseph, H.E. et al.: Scoping study on research and development priorities for distribution-system phasor measurement units. Lawrence Berkeley National Laboratory, SAND2016–3546R (2016)
46. North American SynchroPhasor Initiative: Synchrophasor monitoring for distribution systems -technical foundations and applications (A white paper by the NASPI distribution task team)" (2018)
47. Manousakis, N.M., Korres, G.N., Georgilakis, P.S.: Optimal placement of phasor measurement units: a literature review, intelligent system application to power systems (ISAP). In: 16th International Conference on 25–28 Sept 2011, pp. 1–6 (2011)
48. Yuan, X.A.: A linear algorithm for minimum Phasor measurement units placement. Innov. Smart Grid Technol. (ISGT) pp. 1–3. 19–21 Jan (2010)
49. Zhou, M., Centeno, V.A., Phadke, A.G., Yi, H., Novosel, D., Volskis, H.A.R.: A preprocessing method for effective PMU placement studies. In: Proceedings 3rd International Conference Electric Utility Deregulation and Restructuring and Power Technologies (DRPT 2008), pp. 2862–2867. 6–9 Apr (2008)
50. Milosevic, B., Begovic, M.: Nondominated sorting genetic algorithm for optimal phasor measurement placement. Power Syst. IEEE Trans. **18**(1), 69–75 (2003)
51. Ahmadi, A., Alinejad-Beromi, Y., Moradi, M.: Optimal PMU placement for power system observability using binary particle swarm optimization and considering measurement redundancy. Expert Syst. Appl. **38**, 7263–7269 (2011)
52. Aminifar, F., Khodaei, A., Fotuhi-Firuzabad, M., Shahidehpour, M.: Contingency constrained PMU placement in power networks. In: IEEE Transaction Power System, pp. 516–523. (2010)
53. Chakrabarti, S., Kyriakides, E.: Optimal placement of phasor measurement units for power system observability. IEEE Trans. Power Syst. **23**(3), 1433–1440 (2008)

Optimal Placement of Electric Vehicle Charging Stations Using JAYA Algorithm

Ajit Kumar Mohanty and P. Suresh Babu

1 Introduction

In recent times, the people have understood that our planet suffers through the significance of climatic change and different issues triggered by a lack associated with responsibility. Conventional engine is regarded as the prime factor in the transportation sector which creates issues through carbon dioxide [1]. Most of the countries focus on EV markets, so various researches are done by scientist to obtain the optimal size and location of the CS.

The literature [2–4] tells about different methodologies and approaches to achieve optimal placement of CS. In [2], use the grid partition method to reduce power loss. In [3], adaptive PSO method is used to obtain the optimal placement of CS. In [4], IEEE 33 bus distribution network is used to find optimal placement by using a genetic algorithm (GA).

This work provides a technique locating charging stations on IEEE 33 bus distribution networks. Section 2 elaborates on the mathematical approach to formulating the objective function. Section 3 explains the optimization algorithm required for the solution. Section 4 results are discussed. Section 5 summaries the work.

A. K. Mohanty (✉) · P. S. Babu
Department of Electrical Engineering, NIT Warangal, Warangal, India
e-mail: ajitchinu@student.nitw.ac.in

P. S. Babu
e-mail: drsureshperli@nitw.ac.in

O. H. Gupta and V. K. Sood (eds.), *Recent Advances in Power Systems*, Lecture Notes in Electrical Engineering 699, https://doi.org/10.1007/978-981-15-7994-3_23

2 Objective Function

The prime objective function for the location of CS includes the economic aspects, i.e., minimization of cost and minimization of power grid loss. Cost: Optimization is done to minimize installation cost and minimization operation cost of charging station [5].

Total cost = Installation cost +operation cost

$$IC = X_f \times IC_f + Y_s \times IC_s \tag{1}$$

$$OC = (X_f \times OC_f + Y_s \times OC_s) \times E_p \times T \tag{2}$$

X_f = No. of fast charging station in distribution network
Y_s = No. of slow charging station in distribution network
IC_f = Installation cost required for fast charger
IC_s = Installation cost required for slow charger
OC_f = Power consumed by fast charger
OC_s = Power consumed by slow charger
T = Time frame

$$X_f = \sum_{k=1}^{b} X_k \times x_k \tag{3}$$

$$Y_s = \sum_{k=1}^{b} Y_k \times y_k \tag{4}$$

x_k = no. of fast charging point at kth bus
y_k = no. of slow charging point at kth bus
b = max. no. of location of charging station

Power loss: Whenever CS has placed in distribution network power flow pattern changes so the losses in the distribution network. Power loss has to minimize.

$$P_{\text{loss}} = \sum_{j=1}^{N_b} i_j^2 r_i \tag{5}$$

N_b = No. of buses

The above discussed objective function is subjected to various constraints which are as follow

$$0 < X_b < X_{\max} \text{ and } 0 < x_b < x_{\max} \tag{6}$$

$$0 < Y_b < Y_{\max} \text{ and } 0 < Y_b < Y_{\max} \tag{7}$$

$$P_k^{\min} \leq P_k \leq P_k^{\max} \tag{8}$$

$$Q_k^{\min} \leq Q_k \leq Q_k^{\max} \tag{9}$$

$$P_{gk} - P_{dk} - U_k \sum_{j=1}^{N_b} U_j Y_{kj} \cos(\delta_k - \delta_j - \theta_{kj}) = 0 \tag{10}$$

$$Q_{gk} - Q_{dk} - U_k \sum_{j=1}^{N_b} U_j Y_{kj} \sin(\delta_k - \delta_j - \theta_{kj}) = 0 \tag{11}$$

Equation (6) represents maximum number of fast CS and fast charging points. Equation (7) represents maximum number of slow CS and slow charging points. Equations (8) and (9) show the upper limit and lower limit of active power and reactive power. Equations (11) and (12) represent power balance equations so that there should be no mismatch between generation and load power when electric vehicles are used in the distribution network.

3 Algorithm

A brief review of PSO and JAYA algorithm are discussed. PSO [6] is an evolutionary algorithm based on the population search method, in which each particle continuously changes its position and time. It is a multidimensional search method. Velocity and position of each candidate are:

$$u_{m+1} = w \cdot u_m + c_1 \cdot rand_1(p_{\text{bestm}} - x_m) + c_2 \times rand_2(g_{\text{bestm}} - x_m) \tag{12}$$

$$x_{m+1} = x_m + u_t \tag{13}$$

JAYA algorithm [7] is a population-based method that continuously modifies a population of individual solutions. This concept is based where the given problem solution move forward to the best solution and worst solution is discarded. It includes basic controlling parameters, example size of the population, generation required, size of the elite, etc. However, it does not have algorithm-specific control parameters. This algorithm is easy to apply, and it has only one stage.

Let $\varphi(c)$ is the objective function and subjected to minimization (or maximization) having "t" iterations, design variables "l" (i.e., $p = 1, 2, 3\ldots$.l), size of population "n" ($q = 1, 2, 3\ldots n$). For pth variable, kth candidate, "t" iteration the value is $C_{p,q,t}$

and modified value will be:

$$C'_{p,q,t} = C_{p,q,t} + r_{1p,q} \times \left(C_{p,\text{best},t} - \left|C_{p,q,t}\right|\right) - r_{2p,q} \times \left(C_{p,\text{worst},t} - \left|C_{p,q,t}\right|\right) \tag{14}$$

where the best candidate value is $C_{p,\text{best},t}$ for the variable "p," and the worst candidate value is $Z_{p,\text{worst},t}$ for the variable "p," $r_{1p,q}$ and $r_{2p,q}$ are the two random variables for the pth variable at tth iteration within the range [0, 1]. Term "$r_{1p,q} \times \left(C_{p,\text{best},t} - \left|C_{p,q,t}\right|\right)$" illustrates solution move close to the best solution, and term "$-r_{2p,q} \times \left(C_{p,\text{worst},t} - \left|C_{p,q,t}\right|\right)$" illustrates solution avoids the worst solutions. Figure 1 shows the flow chart of JAYA algorithm.

To find the solution following steps are used:

Step 1: Load the input data of the given distribution network.
Step 2: Run the load flow and it should satisfy different constrained and calculate all the required parameters.
Step 3: Use optimized algorithm (PSO/JAYA).
Step 4: Compute the objective function cost, power grid loss, and voltage deviation.
Step 5: Iteration count is updated.
Step 6: If optimum solution is reached, then print the data.

The optimal location of CS is evaluated by PSO and JAYA algorithm with the help of IEEE 33 test bus system. Results of PSO algorithm is compared with JAYA algorithm.

4 Results Analysis

Table 1 shows the value of input parameters [8] which is essential for mathematical analysis. Table 2 depicts the result of the optimal location of CS obtained by the PSO algorithm and JAYA algorithm.

With the help of the PSO algorithm, CS is placed optimally as visible in Fig. 2 in IEEE 33 bus test system [9]. Similarly, from the JAYA algorithm, CS is placed optimally as depicted in Fig. 3.

With the help of the PSO algorithm, the optimal location of CS is identified at bus 3, 23, 28 in the distribution network with a power loss of 72.99 MW in the distribution network. Whereas number of fast charger connected to buses 3, 23, 28 is 1 and number of slow charger connected to these buses are 3, 3, and 2. Similarly, with the help of the JAYA algorithm, the optimal location of CS is identified at bus 6, 23, 3 in the distribution network with a power loss of 61.32 MW in the distribution network. Whereas number of fast charger connected to buses 6, 23, 3 is 1 and number of slow charger connected to these buses are 2, 3, and 3.

From the above result, the JAYA algorithm is superior to the PSO algorithm. Figure 4 gives the graphical view of power grid loss and the deviations in voltage.

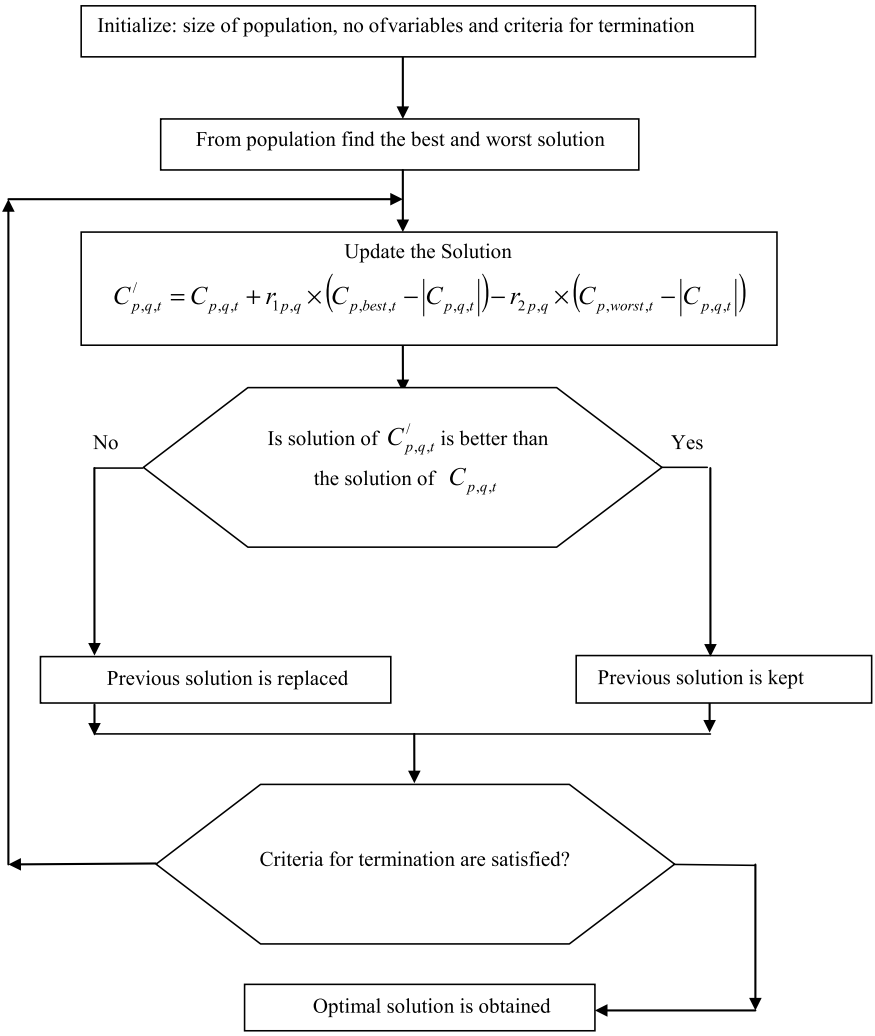

Fig. 1 JAYA algorithm flow chart

5 Conclusion

Since there is rapid growth in EVs, therefore the optimal placement of CS is essential. In this context, the JAYA algorithm is utilized for optimal placement of electrical CS, which shows better results with less number of iteration from PSO. Power loss and voltage profile have remained within an acceptable range after the placement of CS with optimally. Future work will deal with other multi-objective functions.

Table 1 Input parameters

Parameter	Value
IC_f	3000 $
IC_s	2500 $
OC_f	50 kW
OC_s	19.2 kW
E_p	65 $/MWhr
B	3
$X_{\max}$	2
$x_{\max}$	6
$Y_{\max}$	3
$y_{\max}$	10

Table 2 Optimal location of CS

Type of optimization algorithm	Power loss(MW)	B	X_{Fb}	Y_{sb}
PSO	72.99	3	1	3
		23	1	3
		28	1	2
JAYA	63.11	6	1	2
		3	1	3
		23	1	3

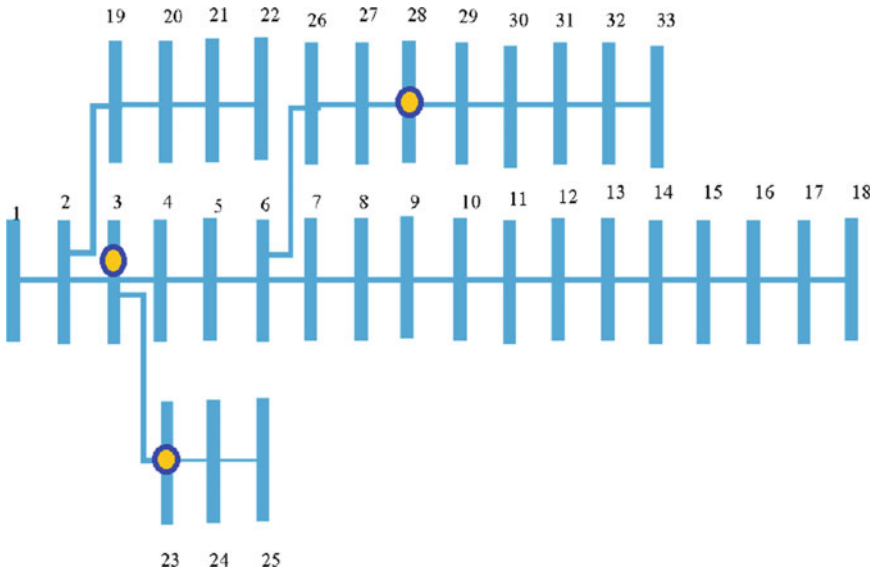

Fig. 2 CS placement in IEEE 33 bus test system by PSO

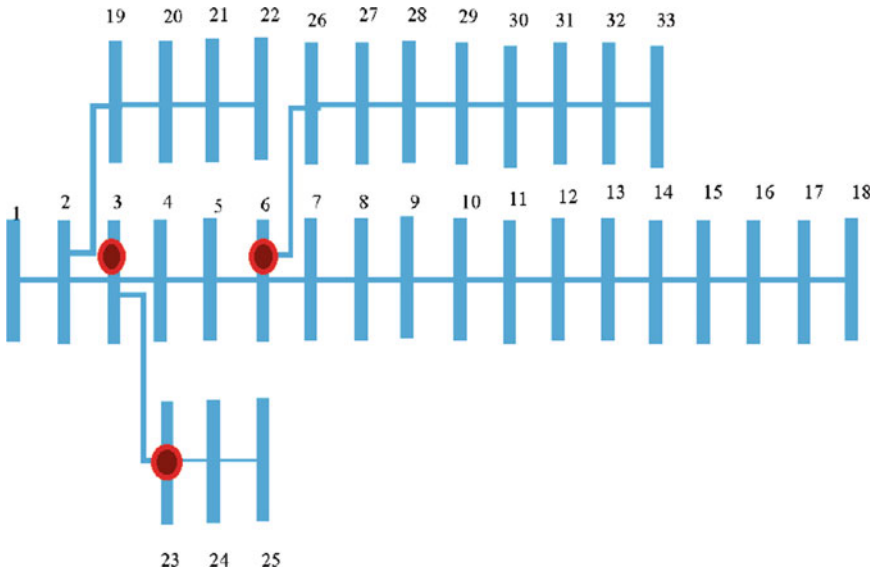

Fig. 3 CS placement in IEEE 33 bus test system by JAYA

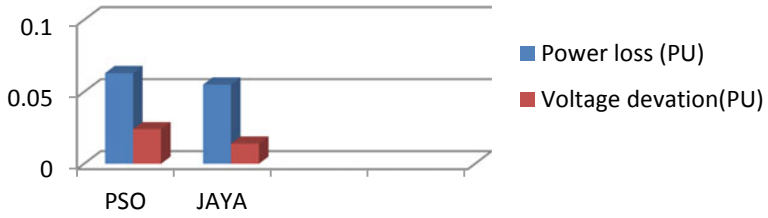

Fig. 4 Power loss and deviation in voltage of distribution network for optimal location of CS

References

1. Kavousi-Fard, A., Abunasri, A., Zare, A., Hoseinzadeh, R.: Impact of plug-in hybrid electric vehicles charging demand on the optimal energy management of renewable micro-grids. Energy 78:904e15 (2014)
2. Ge, S., Feng, L., Liu, H.: The planning of electric vehicle charging station based on Grid partition method. In: 2011 International Conference on Electrical and Control Engineering, Yichang, pp. 2726-2730 (2011)
3. Liu, Z.f., Zhang, W., Ji, X., Li, K.: Optimal Planning of charging station for electric vehicle based on particle swarm optimization. In: IEEE PES Innovative Smart Grid Technologies, Tianjin, pp. 1–5 (2012)
4. Yan, X., Duan, C., Chen, X., Duan, Z.: Planning of electric vehicle charging station based on hierarchic genetic algorithm. In: 2014 IEEE Conference and Expo Transportation Electrification Asia-Pacific (ITEC Asia-Pacific), Beijing, pp. 1–5 (2014)
5. Deb, S., Kalita, K., Gao, X.-Z., Tammi, K., Mahanta, P.: Optimal placement of charging stations using CSO-TLBO algorithm. In: Proceedings 3rd International Conference Research Computing

Intelligence Communications Network. (ICRCICN), pp. 84-89 (2017)
6. Cruz-Zambrano, M., Corchero, C., Igualada-Gonzalez, L., Bernardo, V.: Optimal location of fast charging stations in Barcelona: a flow-capturing approach. In: 2013 10th International Conference on the European Energy Market (EEM), Stockholm, pp. 1–6 (2013)
7. Venkata Rao, R., Saroj, R.A.: A self-adaptive multi-population based jaya algorithm for engineering optimization. Swarm Evolution. Comput. **37**, 1–26 (2017)
8. Shojaabadi, S., Abapour, S., Abapour, M., Nahavandi, A.: Optimal planning of plug-in hybrid electric vehicle charging station in distribution network considering demand response programs and uncertainties. IET Gener. Trans. Distrib. **10**(13), 3330–3340 (2016)
9. Wei, R., Liu, X., Ou, Y., Kiavash Fayyaz, S.:"Optimizing the spatio-temporal deployment of battery electric bus system. J. Trans. Geograph 68 (April) Pergamon: 160–168 (2018)

PSO Based Optimal Reactive Power Dispatch for the Enrichment of Power System Performance

K. Manasvi, B. Venkateswararao, Ramesh Devarapalli, and Upendra Prasad

1 Introduction

Electrical power system network is a modern-day issue with a lot of complexities. Therefore its operation and control have become a significant challenge to system operators. For proper and efficient working of a system voltage and the losses must be within limits. ORPD is a well familiar nonlinear optimization problem involving control variables that are both discrete as well as continuous. The formulation of ORPD problem differs depending on the assortment of variables, objectives and constraints [1]. ORPD shows a significant role in refining the economy and security in the process of the power system. Instead of dealing with the generation of additional power, minimizing the losses can be considered a reasonably good scheme.

Many methods are implemented for ORPD. There are several conventional techniques like differential evolutionary (DE), Dual linear programming and Quadratic programming [2]. Besides, these traditional methods modern optimization techniques are also developed for reactive power dispatch such as Genetic algorithm and self-adaptive Genetic algorithm, which are discussed in the sections below.

In early 1960, Carpentier [3] was the first to introduce optimal power flow. Thereafter OPF took the researchers by storm, and different methodologies were developed. ORPD is nonlinear in nature and is multi-objective, Varadarajan and Swarup [4] developed a DE based technique for diminution of active power transmission losses. The objective function of reducing the losses is amalgamated with penalty factors and is tested on IEEE systems. Manmundur and Chenoweth [5] used dual

K. Manasvi · B. Venkateswararao
Department of EEE, V. R. Siddhartha Engineering College, Kanuru, AP, India

R. Devarapalli (✉) · U. Prasad
Department of Electrical Engineering, B. I. T. Sindri, Dhanbad 828123, India
e-mail: ramesh.ee@bitsindri.ac.in

O. H. Gupta and V. K. Sood (eds.), *Recent Advances in Power Systems*, Lecture Notes in Electrical Engineering 699, https://doi.org/10.1007/978-981-15-7994-3_24

linear programming, which is very suitable for the reduction of losses under operating circumstances. In this ORPD control variables are optimally tuned, satisfying all the constraints.

Burchett et al. [6] proposed Quadratic programming for optimal power flow, it is suitable for divergent starting points or infeasible solutions. The optimal solution is attained by considering the second derivatives of the objective function. Zhang and Zhang [7] developed a genetic algorithm to supply reactive power effectively. The genetic algorithm comprises natural selection and genetics. Its rudimentary operators include selection, crossover and mutation. The outcomes of GA are proven to be better than conventional methods.

Subbaraj and Rajnarayanan [8] modified the GA with Self adaptive real coded GA for ORPD. This paper targets to enhance the enactment of GA with self-adaptation by considering continuous, discrete and binary variables. Abbasy and Hosseini [9] applied the Ant Colony Optimization procedure for resolving the ORPD problem. This methodology deals with the representing of elucidation space on an exploration graph, everyplace non-natural ants walk, and position approaches given to the elementary ant system boosts the algorithm's enactment in every position. Li et al. [10] developed the hybridization algorithm by using DE and ABC methods.ABC individually was found better than DE and the hybridization of two methods DE-ABC was found better than individual applied techniques. The ORPD is identified as an emerging research problem, and a variety of algorithms have been proposed by the various researchers to obtain the optimal parameters [11–17]. And it has been found that the application of metaheuristics [18, 19], its hybrid versions [20], and robust control techniques [21] became popular in getting optimal solution of a power system research problems.

This paper presents the well familiar algorithm, PSO. By using this method, the convergence characteristics of the system are improved, thereby leading to an increase in system performance by reducing losses.

2 ORPD Problem Construction

Reactive power flow can be categorized into different classes. In the economic point of view, network active power losses reduction is deliberated as the primary objective.

2.1 True Power Losses Minimization

The ORPD problem for reduction of active power losses is formulated as

$$F_L = \text{Min}(P_L) = \sum_{k=1}^{N_l} G_K [V_m^2 + V_n^2 - 2V_m V_n \cos(\delta_m - \delta_n)] \tag{1}$$

G_K Represents the conductance of the line coupled between m and n. Buses are denoted with m, n. Voltage levels at the buses are represented as $V_m, V_n . \delta_m, \delta_n$ are the angles at the buses m, n respectively. N_l, N_b, N_g represents number of transmission lines, buses and generators present in the system respectively.

2.2 Constraints

The equality constraint for solving the problem of ORPD is given as

$$P_{Gm} - P_{Dm} - V_m(G_{mn}\cos(\delta_m - \delta_n) + B_{mn}\sin(\delta_m - \delta_n)) = 0 \tag{2}$$

$$Q_{Gm} - Q_{Dm} - V_m(G_{mn}\sin(\delta_m - \delta_n) + B_{mn}\cos(\delta_m - \delta_n)) = 0 \tag{3}$$

Inequality restrictions given below,

Generator limitations:

True power, wattless power and voltage at the generator buses must be within limits.

$$P_{Gm,\min} \leq P_{Gm} \leq P_{Gm,\max} \quad m = 1 \ldots N_G \tag{4}$$

$$Q_{Gm,\min} \leq Q_{Gm} \leq Q_{Gm,\max} \quad m = 1 \ldots N_G \tag{5}$$

$$V_{Gm,\min} \leq V_{Gm} \leq V_{Gm,\max} \quad m = 1 \ldots N_G \tag{6}$$

N_G is the no.of generators.

Transformers tap setting limitations:

Tap locations of the transformer must be within the permissible limits

$$T_{m,\min} \leq T_m \leq T_{m,\max} \quad m = 1 \ldots N_i \tag{7}$$

N_t is the number of transformers.

Upper and lower limits restrict the reactive power offered by switchable VAR sources are given as,

$$Q_{cm,\min} \leq Q_{cm} \leq Q_{cm,\max} \quad m = 1 \ldots N_c \tag{8}$$

N_c is the no.of capacitors

3 Particle Swarm Optimization

PSO algorithm is replicated from the natural behaviour of animals like birds flocking and schooling generally practised by fish. Eberhart and Kennedy [22] were the proposals of this algorithm during the year 1995. Because of its intrinsic properties, it is very fast, easy to access and requires less storage. This algorithm effectively optimizes the problem by iteratively enhancing the quality of the solution. Each particle is assumed having velocity and position which are given by

$$V_{ij}^{k+1} = w \times V_{ij}^{k} + c_1 \times r_1 \times \left(P\text{best}_{ij}^{k} - Z_{ij}^{k}\right) + c_2 \times r_2 \times \left(G\text{best}_{j}^{k} - Z_{ij}^{k}\right) \quad (9)$$

$$Z_{ij}(k+1) = Z_{ij}(k) + V_{ij}(k+1) \quad (10)$$

Eberhart and Shi prefaced the weight factor w used in this method in 1999. This enables quick convergence by damping the calculated velocities through iterations stated. The acceleration constant c_1 is called as cognitive rate and c_2 as social rate. The random numbers r_1 and r_2 have range from 0 to 1. Flow chart of PSO provided in Fig. 1.

3.1 Implementation of ORPD Using PSO

In general, PSO converges quickly and nearer to the global solution. The steps for the implementation of ORPD using PSO are as follows:

- Random control variables (stated in Table 1) are generated in between the given limits.
- Fitness function is calculated, and the present particles are assigned as the Pbest (Present best)
- Gbest is determined by substituting all Pbest values in the given objective function.
- By using Pbest and Gbest values velocity is calculated, and the corresponding position of the particle gets updated.
- The objective function of each particle is compared with its Pbest. Previous values are compared with the present values, and values are replaced with the best values.
- Find the Gbest value and repeat the steps (2) to (6) till the iterations are satisfied.

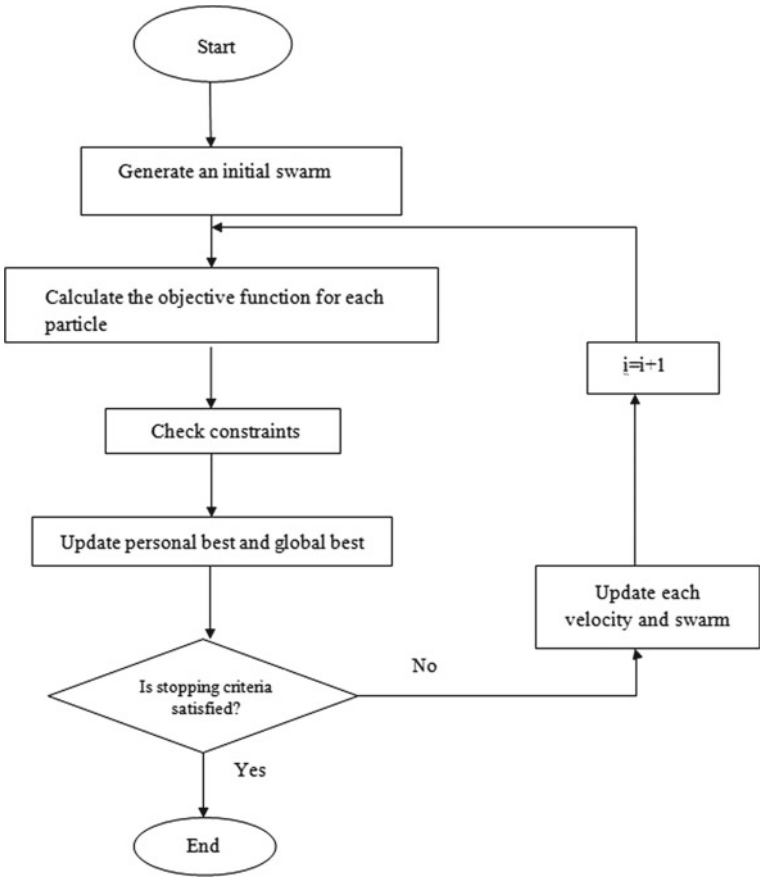

Fig. 1 Implementation of PSO

Table 1 Limits of control variables

Variables	Min in p.u	Max in p.u
Voltages of generator buses	0.90	1.10
Transformers tap locations	0.95	1.05
Size of shunt capacitors	0.0	0.2

4 Simulation Results

4.1 Minimizing True Power Loss

Table 1, minimum and maximum limits of the control variables of IEEE 14 and IEEE 30 bus system are shown. These limits are represented in p.u.

Table 2 Optimal values with PSO

Control variables	Control variable value with PSO
VG1	1.1098
VG2	1.0824
VG3	1.0225
VG6	1.0293
VG8	1.0140
T4-7	0.9971
T4-9	0.9906
T5-6	1.0123
QC9 in MVAR	14.7614
QC14 in MVAR	5.4675
Power loss in MW	**12.6107**
Voltage deviation in p.u	0.722

[a]Voltages and Transformers values are represented in p.u

4.1.1 IEEE 14 Bus System

This system comprises of 14 buses with 5 generator and 9 load buses. Transformers with tap changers are connected between 4–7,4–9, 5–6 and 9, 14 are the buses where the capacitors are connected. This addition of capacitors helps in increasing the bus voltage, which ultimately leads to efficient achievement of the considered objective function. So, totally there are ten control variables in this system.

The main objective here is the diminution of active power loss. The output of control variables are tuned using PSO such that the total losses in the system are low, and the results for the IEEE system 14 is shown in Table 2. The curve representing the convergence characteristics is shown in Fig. 2. The mean value and its SD are revealed in Table 3.

The evaluation made with altered optimization procedures is displayed in Table 4, where the losses are minimized to a greater extent which concludes the effectiveness of PSO over other conventional methods and Genetic algorithm.

4.1.2 IEEE 30 Bus System

This system comprises of 30 buses with 6 generators and 24 load buses. Tap changing transformers are connected between lines 4-12, 6-9, 6-10, 27-28. Reactive power compensators (capacitors) are placed at 3, 10 and 24 bus such that the total voltages are boosted. So, totally there are 13 control variables in this system.

The result of the control variables that are tuned in order to achieve the best of the objective function are given in Table 5, and its convergence characteristics are shown in Fig. 3.The mean and the standard deviation achieved for this system are shown in Table 6. The voltages are represented in p.u, and the angles are given in degrees.

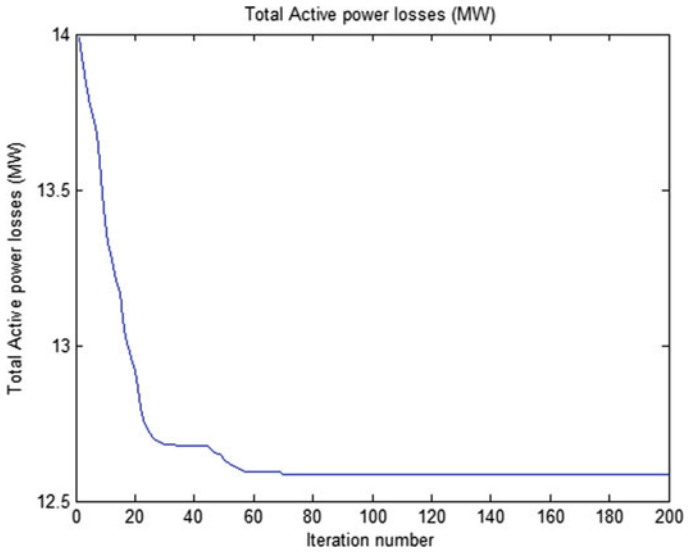

Fig. 2 Graph of convergence for minimization of losses for IEEE14 bus system

Table 3 Mean and standard deviation of IEEE 14 bus system

Technique	Mean value in MW	Standard deviation
PSO	12.6107	0.03459

Table 4 Comparison with different optimization techniques

Technique	EP[08]	SGA[08]	PSO
Power loss(MW)	13.34620	13.21643	12.6107

Penalty factor is imposed when control variables exceed their limits, and the value for the penalty is chosen based on the violated factor. The losses obtained in PSO is compared with different methods in Table 7 and found that the reactive power is dispatched optimally with a minimum amount of losses with the implementation of PSO.

5 Conclusion

In this paper, ORPD, which is a non-linear and non-convex optimization technique, is optimized for the objective functions of reduction of true power loss. The nature-inspired algorithm, which is PSO is used for this optimization and found effective when compared to the other conventional techniques like EP, DE, ABC and SGA, due to its random probability and quick convergence. Through these losses are reduced

Table 5 Optimal values with PSO

Control variables	PSO
Vg_1	1.1154
Vg_2	1.0841
Vg_5	1.0428
Vg_8	1.0429
Vg_{11}	1.0681
Vg_{13}	1.0085
$T_{4–12}$	1.0066
$T_{6–9}$	1.0167
$T_{6–10}$	0.9878
$T_{27–28}$	0.9876
QC3in MVAR	19.3599
QC10in MVAR	15.1235
QC24in MVAR	15.3625
Power loss in MW	**16.0494**
Voltage deviation in p.u	1.1023

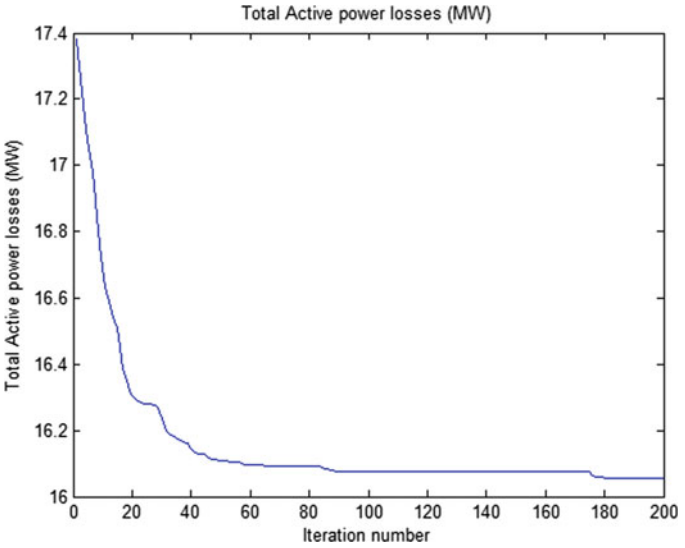

Fig. 3 Graph of convergence for minimization of losses for IEEE30 bus system

Table 6 Mean and standard deviation of IEEE30 bus system

Technique	Mean value in MW	Standard deviation
PSO	16.0494	0.0360042

Table 7 Relationship of true power loss with altered optimization methods

Method	True Power loss(MW)	Standard deviation
EP[08]	16.38962	0.09895
DE[10]	16.2187	0.4052
ABC[10]	16.2691	0.51401
DE-ABC[10]	16.2163	0.01098
SGA[08]	16.0929	0.01625
PSO	**16.0494**	0.0360042

and is executed for the IEEE14 and 30 bus systems. Authors implement the PSO for ORPD as a preliminary study, in future authors plan to use hybrid algorithm's like PSO along with BAT algorithm for ORPD problem, which my provide better results.

References

1. Anbarasan, P., Jaya bharathi, T.: ORPD solved by symbiotic organism search algorithm. In: International Conferences on Innovations in Power and Advanced Computing Technologies (2017)
2. Vijay, B.D., Karthik, S.P.: ORPD in highly stressed system-a comparitive study using DE and BAT algorithm. IJEDR **5**(2), 2061–2067 (2017)
3. Carpentier, J.: Contribution to economic dispatch problem. Bullentin de la Societe Francoise des Electricien. **3**(8), 431–447 (1962)
4. Varadarajan, M., Swarup, K.: Differential evolutionary algorithm for optimal reactive power dispatch. Electr. Power Energ. Syst. **30**, 435–441 (2008)
5. Mamandur, C., Chenowet, D.: Optimal control of reactive power flow for improvements in voltage profiles and for real power loss minimization. IEEE Trans. PAS **100**(7), 3185–3194 (1981)
6. Burchett, R., Happ, Vierat, D.R.: Quadratically convergent optimal power flow. IEEE Trans. Power Apparatus Syst. **103**(11), 3267–3276 (1984)
7. Zhang, H., Zhang, L.: Reactive power optimization based on genetic algorithm. In: POWERCON'98, International Conference on Power System Proceedings (1998)
8. Subbaraj, P., Narayana, P.R.: Optimal reactive power dispatch using self-adaptive real coded genetic algorithm. Electr. Power Syst. Res. **79**, 374–381 (2009)
9. Abbasy, Hosseini.: Ant colony optimization-based approach to optimal reactive power dispatch: a comparison of various ant systems. In: IEEE Power Engineering Society Conference and Exposition in Africa—PowerAfrica, Johannesburg, pp. 1–8 (2007)
10. Li Wang, Y., Li, B.: A hybrid Artificial Bee Colony assisted Differential Evolution algorithm for optimal reactive power flow. Electr. Power Energ. Syst. **52**, 25–33 (2013)
11. Wu, Q., Ma, T.: Power systems optimal reactive power dispatch using evolutionary programming. IEEE Trans. Power Syst. **10**, 1243–1249 (1995)
12. Das, T., Roy, R., Mandal, K.K.: Comparative performance analysis of variants of particle swarm optimization of optimal reactive power dispatch. Power Res. **15**(1), 16–24 (2019). https://doi.org/10.33686/pwj.v15i1.144733
13. Saddique, M.S., et al.: Solution to optimal reactive power dispatch in transmission sys-tem using meta-heuristic techniques-Status and technological review. Electr. Power Syst. Res. **178**, 106031 (2020). https://doi.org/10.1016/j.epsr.2019.106031

14. Nguyen, T.T., Vo, D.N.: Improved social spider optimization algorithm for opti-mal reactive power dispatch problem with different objectives. Neural Comput. Appl. **32**(10), 5919–5950 (2020). https://doi.org/10.1007/s00521-019-04073-4
15. Kanata, S., Suwarno, Sianipar, G.H., Maulidevi, N.U.: Hybrid time varying particle swarm optimization and genetic algorithm to solve optimal reactive power dispatch problem. In: 2019 International Conference on Electrical Engineering and Informatics (ICEEI), July 2019, pp. 580–585 (2019). https://doi.org/10.1109/iceei47359.2019.8988864
16. Kunapareddy, M., Rao, B.V.: Hybridization of particle swarm optimization with firefly algorithm for multi-objective optimal reactive power dispatch. In: Innovative Product Design and Intelligent Manufacturing Systems, Singapore, 2020, pp. 673–682 (2020). https://doi.org/10.1007/978-981-15-2696-1_64
17. Jiang, F., Zhang, Y., Zhang, Y., Liu, X., Chen, C.: An adaptive particle swarm optimization algorithm based on guiding strategy and its application in reactive power optimization. Energies **12**(9), 1690 (2019). https://doi.org/10.3390/en12091690
18. Devarapalli, R., Bhattacharyya, B.: Application of modified harris hawks optimization in power system oscillations damping controller design. In: 2019 8th International Conference on Power Systems (ICPS), December 2019, pp. 1–6 (2019). https://doi.org/10.1109/icps48983.2019.9067679
19. Devarapalli, R., Bhattacharyya, B.: Optimal parameter tuning of power oscillation damper by MHHO algorithm. In: 2019 20th International Conference on Intelligent System Application to Power Systems (ISAP), December 2019, pp. 1–7. (2019). https://doi.org/10.1109/isap48318.2019.9065988
20. Devarapalli, R., Bhattacharyya, B.: A hybrid modified grey wolf optimization-sine cosine algorithm-based power system stabilizer parameter tuning in a multimachine power system,. Opt. Control Appl. Methods. **n/a**(n/a). https://doi.org/10.1002/oca.2591
21. Devarapalli, R., Bhattacharyya, B.: A framework for H_2/H_∞ synthesis in damping power network oscillations with STATCOM. Iran J. Sci. Technol. Trans. Electr. Eng. **44**(2), 927–948 (2020). https://doi.org/10.1007/s40998-019-00278-4
22. Kennedy, J., Eberhart, R.: Particle swarm optimization. In: Proceedings IEEE International Conference on Neural Networks, vol. 4, pp. 1942–1948 (1995)

Design of Adaptive Distance Relay for Transmission Line Protection with Wind Power Integration

Venkata Rao Nikhil Garlapati, Sujo Palamoottil George, and Ashok Sankar

1 Introduction

Power systems, nowadays, are expanding at a faster rate. With the decentralization of power systems and evolution of microgrids and renewable penetration, anyone can export and import power. Therefore, power flow is not unidirectional any more, rather power flows in both ways, and hence, it is a bidirectional power system, so it is of great importance to maintain proper relay coordination. Therefore, the relaying scheme has to sense the changes in the environment and has to adjust its characteristics automatically. So designing a proper relaying scheme is of great significance for the reliability of the system.

Electrical power system is an interconnection of huge networks and spread over a wide area. As it is spread over a wide area, it is prone to different types of faults. Most of the transmission lines are overhead ones. There are different methods of protection for the overhead transmission lines, out of which distance protection is the widely used one [1, 2].

In the recent years, the penetration of renewable energy sources has increased drastically. In India, wind generation holds the highest percentage share of renewable energy. In the conventional protection of transmission line or feeder, fixed settings in the distance relay are sufficient for the proper operation of relay during fault condition; whereas in the systems with renewable penetration, the conventional settings for the distance relays does not hold good.

V. R. N. Garlapati (✉) · S. P. George · A. Sankar
National Institute of Technology, Calicut, Kerala 673601, India
e-mail: gvrnikhil123@gmail.com

S. P. George
e-mail: sujop709@gmail.com

A. Sankar
e-mail: ashoks@nitc.ac.in

O. H. Gupta and V. K. Sood (eds.), *Recent Advances in Power Systems*, Lecture Notes in Electrical Engineering 699, https://doi.org/10.1007/978-981-15-7994-3_25

The wind speed is not constant all the time. The power output of a wind generating unit changes with change in wind speed, and when the speed is beyond the set conditions, the farm cannot supply power to the grid and is cut off from the system [3, 4]. This leads to continuous change in the system environment [5]. Therefore, the impedance seen by the relay is continuously changing throughout the day.

Digital relays have gained quite popularity in the recent years because of their flexibility and ease of operation. Digital relay has wide range of advantages compared to conventional electromechanical relays. When renewable energy sources are integrated into the system, the fault trajectory varies according to the no. of wind generators connected to the system and type of fault occurred in the system. Based on this trajectory, the boundary of the relay settings has to be set [6, 7].

Quadrilateral characteristics are preferred to handle high fault resistance [8–11] with ground faults in relaying scheme. As the fault trajectory varies for different system configuration and for different types of faults, it is necessary to propose optimum quadrilateral settings [12–14].

Whenever there is an external fault, there is a chance that the relay may maloperate. Hence to prevent such conditions, there is a necessity for the relay to automatically adjust its characteristics based on the type of fault. To do so, an adaptive logic [15] has to be proposed so that the relay can automatically adjust its characteristics based upon the changes in the system environment and fault condition. Based on the algorithm, the expansion and contraction of the relay can take place.

This paper proposes a scheme for adaptive settings of the distance relay for a wind integrated system for the protection of transmission line. Simulations are conducted for different WG configurations and for internal and external LG faults with a fixed fault resistance. From the fault trajectories, different patterns are observed and ideal trip characteristics are observed. When wind penetration is high, some external fault trajectories may come inside the quadrilateral area. An adaptive setting scheme is proposed based on the information of current and number of wind generators in service so that the relay does not operate for the external fault. The proposed scheme is tested for an LG fault using PSCAD/EMTDC software.

2 Issues of Conventional Distance Protection

2.1 Effect of Wind Generators in Service on the Conventional Quadrilateral Settings

The wind speed is not constant throughout the day, and it depends upon several factors like weather conditions, geographical locations, etc. So depending on the velocity of the wind, the output of the wind generator varies continuously. The power output of the wind turbine is given by Eq. 1.

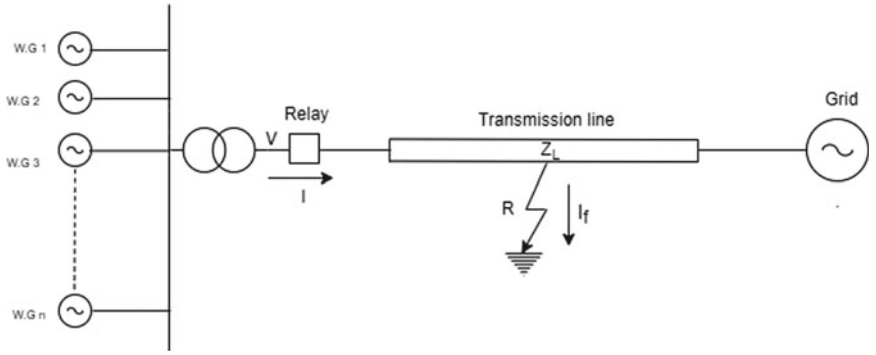

Fig. 1 Wind integrated power system

$$P_{\text{out}} = \frac{1}{2.10^6} \cdot \rho_{\text{air}} \cdot A \ldots C_P \cdot V_W^3 \cdot \eta_{\text{GB}}(M \cdot W) \tag{1}$$

C_p = power coefficient, $_{\text{air}}$ = air density (kg/m^3), A = rotor area of the wind turbine (m^2), V_W = wind speed (m/sec) and η_{GB} = gear box efficiency.

The wind speed should be within the limits for their contribution to the grid. As the wind speed changes, the WGs in service also change. This leads to the continuous change in the environment.

The distance relays measure the voltage to the current ratio. When the WGs in service vary, the amount of current injected by the generators varies, and as a result of this the V/I ratio changes (provided the change in the voltage is small). So the impedance seen by the relay varies continuously. Consider a distance relay monitoring a transmission line as shown in Fig. 1.

The vertical boundary for the quadrilateral setting is based on the transmission line length and its parameters while the horizontal boundary is based on the in feed effect for a constant fault resistance of one ohm. Because of the in feed effect, the magnitude of the fault resistance appears larger even though it is of smaller value. Figure 2 shows quadrilateral boundaries, and these values can be found using Eqs. 2 and 3. Under rated conditions, the current contributed by the WGs in service is much higher compared to the less number of WGs in service. When the speed is not in the limits, some of WGs in services are cut off; hence, the impedance seen by the relay changes (i.e. the impedance seen by the relay increases). The area of the quadrilateral is more for the lowest WG configuration when compared to the highest WGs in service, and this configuration is used for the quadrilateral settings such that the relay satisfactorily operates for all kinds of internal faults, for all types of wind generator configurations.

$$V = I Z_L + I_f R \tag{2}$$

$$Z = \frac{V}{I} = Z_L + \frac{I_f}{I} R \tag{3}$$

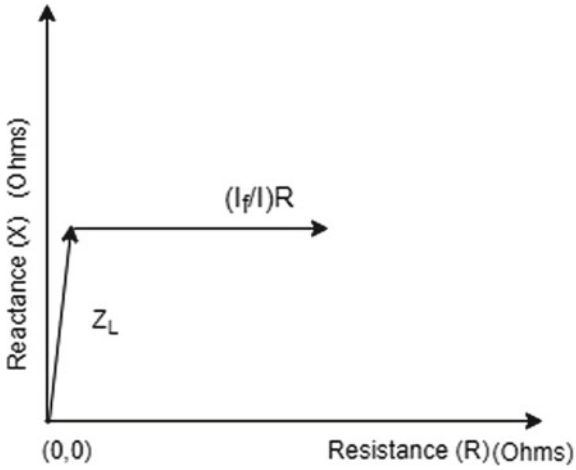

Fig. 2 Quadrilateral boundary settings

Z = impedance seen by the relay, Z_L = impedance of the transmission line, I_f = fault current and R = fault resistance.

As the area of quadrilateral is fixed and is set for a maximum area, there is a chance for the external fault trajectory to come inside the quadrilateral region as shown in Fig. 3. This leads to the security issue in the power systems.

To avoid the unnecessary operation, the relay has to modify its characteristics based on WGs in service and has to adapt to the changes in the environment such that it operates only for internal faults and does not operate for external fault.

This paper proposes a method to obtain the adaptive characteristics of a distance relay.

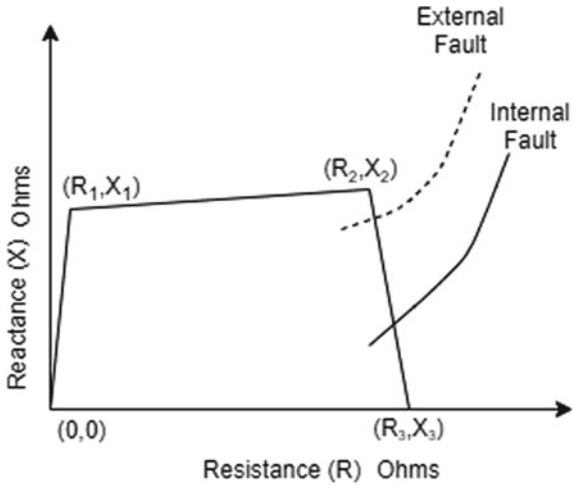

Fig. 3 Internal and external fault trajectories with conventional quadrilateral settings

3 Proposed Scheme

When the number of WGs in service increases, the system impedance decreases. For fixed quadrilateral settings, set for the rated conditions some of the external fault trajectories may come inside the quadrilateral region as shown in Fig. 3. So the quadrilateral has to shrink its area as shown in Fig. 4 to avoid unnecessary tripping.

Similarly, when WGs in service decrease, the quadrilateral has to expand its area to properly operate for the internal faults. This process of adjusting its characteristics based on number of WGs in service is nothing but adaptability.

When the wind generators in service increase, the current injected into the system increases. The current has a direct relationship with number of wind generators in service, since the horizontal boundary is set based on the wind generators in service; hence, current is chosen as reference quantity. To extend this logic to a balanced fault, we need to have a quantity which is present in the system during balanced and unbalanced situations and the positive sequence component of the current is present during all the conditions.

Based on the WG configurations, switching between the quadrilaterals is done. The flow chart shown in Fig. 5 gives an overall idea of the logic proposed in this paper. The generators take some of the amount of time to develop the rated voltage and current, and these rated values after the transients have died out are nothing but steady-state values. The steps for the flow chart are as follows.

Step 1: Read the predetermined positive sequence current values S_i, $S_{i+1} \ldots S_n$ for different WGs in service. (Example: S_i is the predetermined positive sequence current value when 1WG in service and so on…..)

Step 2: Measure the instantaneous voltage and current values of all the three phases.

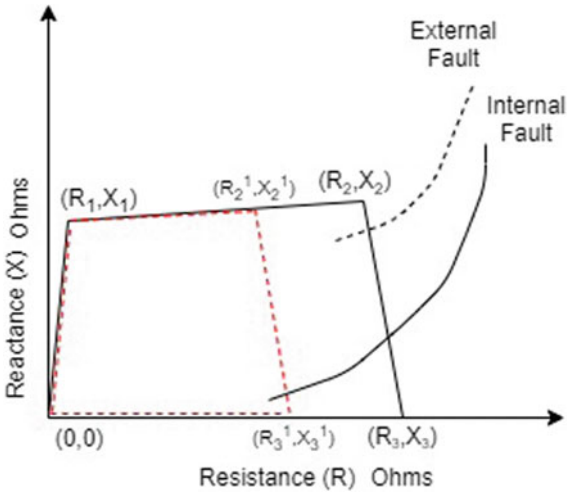

Fig. 4 Shrink in quadrilateral area for increase in WGs in service

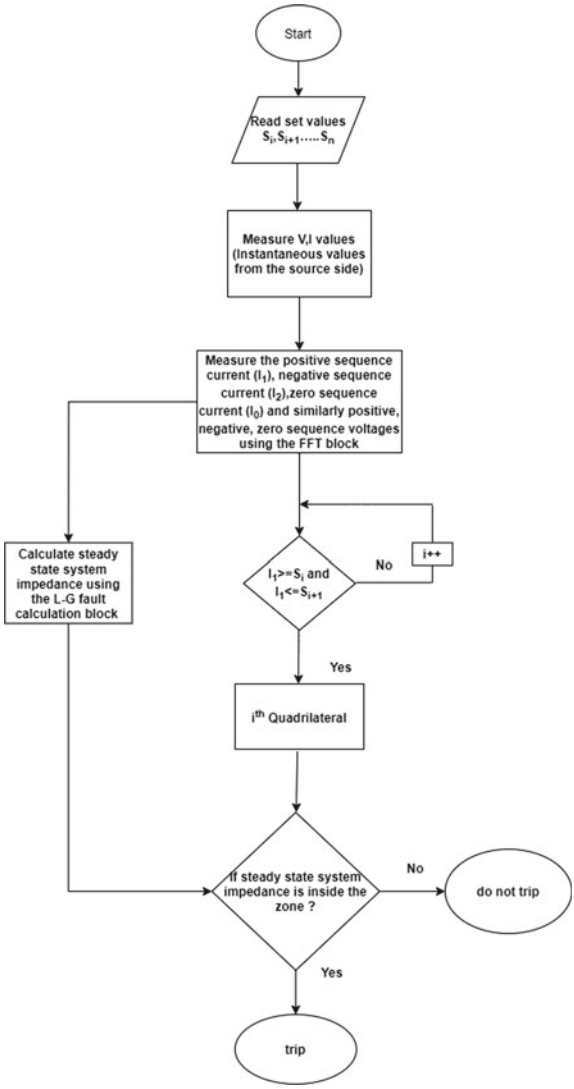

Fig. 5 Flow chart for the adaptive method proposed

Step 3: The measured values are sampled and decomposed into harmonic constitutes using the fast Fourier transform technique. The magnitude and phase angle of each signal are found, and using the sequence filter all the magnitudes and phase angles of the positive, negative, zero sequence components of voltage and currents are found.

Step 4: Based on the positive sequence, component of current appropriate quadrilateral is selected from the available set by comparing it with the predetermined values.

Step 5: Calculate the impedance seen by the relay using Eqs. 2 and 3.

Step 6: If the calculated impedance falls inside the quadrilateral area, then trip signal is issued by the relay else no trip.

4 Simulation Results and Analysis

To verify the proposed scheme validity for adaptive characteristics, a simulation study for LG internal fault on transmission line 1 and LG external fault at the bus 1 with a fault resistance of one ohm is carried on the system which is shown in Fig. 6 with system data given in the appendix [16].

The system is developed and tested using PSCAD/EMTDC software. The WGs attached to the bus 2 are fixed and are always in operation. The numbers of wind generators in service are modified only on the bus 1. An LG fault is simulated at the end of the transmission line 1 for different WGs in service. From the simulated data, the fault trajectories are plotted and corresponding quadrilateral settings are found. The simulated results are shown in Fig. 7.

From Fig. 7a, it is clear that as the number of WGs in service increases, the fault trajectory moves closer towards the origin, i.e. for the 1 WG configuration the fault trajectory is farther compared to the 16 WGs configuration.

Figure 7b–d, it is clear that as the WGs in service decrease, area of the quadrilateral is getting increased. So the quadrilateral setting for 1 WG configuration occupies large area in the R–X plane. So out of all the quadrilateral characteristics, quadrilateral with larger area is considered for fixed settings such that all the internal faults for any type of wind configuration come inside the quadrilateral area.

Figure 8, it is clear that if we consider the quadrilateral with larger area, the relay detects all kinds of internal faults as all the internal faults come inside the zone of protection. From Fig. 8, it is also clear that when the system is operating under rated condition, i.e. 16 WGs in service and if an external fault with fault resistance of one ohm occurs on the grid side bus, i.e. bus 1, then the external fault trajectory

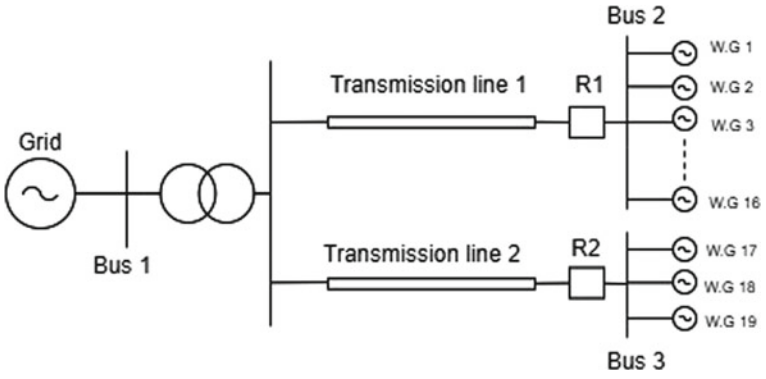

Fig. 6 Single line diagram of the wind integrated system

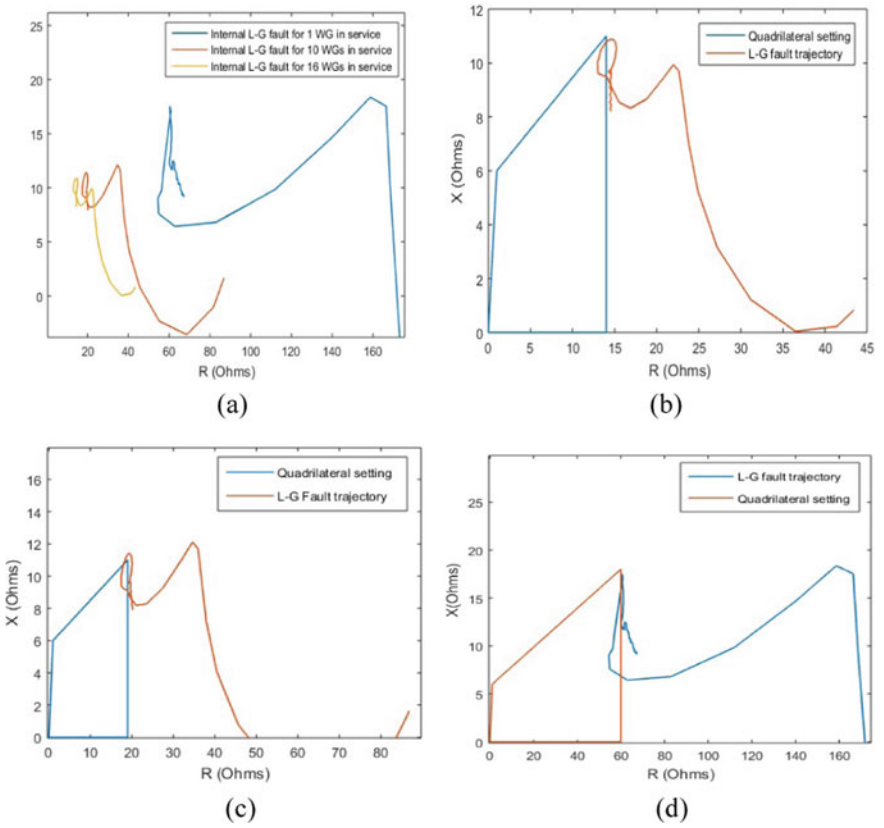

Fig. 7 **a** Internal LG fault trajectories for 1, 10, 16 WGs in service, quadrilateral settings and LG fault trajectory for **b** 16 WGs in service. **c** 10 WGs in service. **d** 1 WG in service

also comes inside the zone of protection which leads to the mal-operation of the relay nothing but security issue. To avoid the unnecessary operation, the relay has to shrink its characteristics, i.e. instead of fixed setting, the relay has to adjust its characteristics based on the number of WGs in service. So the relay with more WGs in service has to have smaller area in the R–X plane and larger area for less number of WGs in service.

5 Validation of Adaptive Relay Logic Under Simulated Environment

To avoid unnecessary operation for external faults, the relay automatically has to expand or shrink its area according to the changes in the system.

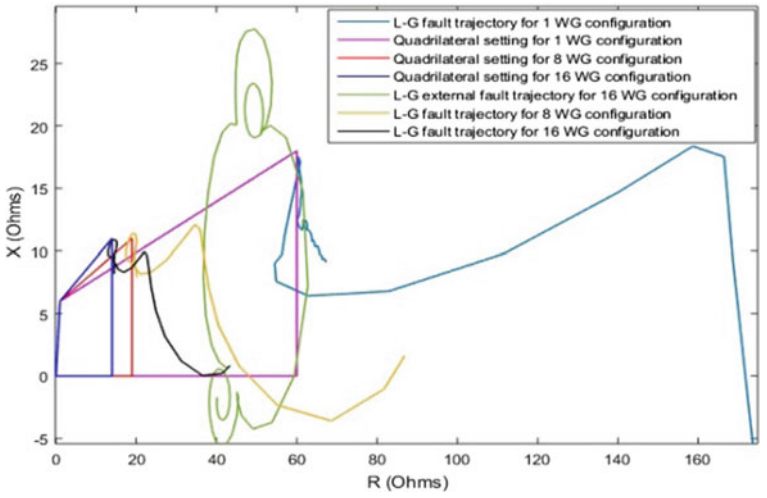

Fig. 8 Quadrilateral settings, internal LG fault trajectories for 1, 10, 16 WG configurations along with external LG fault trajectory for 16 WG configuration

The adaptive logic is implemented in the simulation environment using multiplexers and comparators as shown in Fig. 9 The positive sequence component of the current is obtained from the FFT block and given as one of the input to the comparator and is compared with the set value which is given to the other input. The set value is a predetermined +ve sequence current value for different WG configurations. The

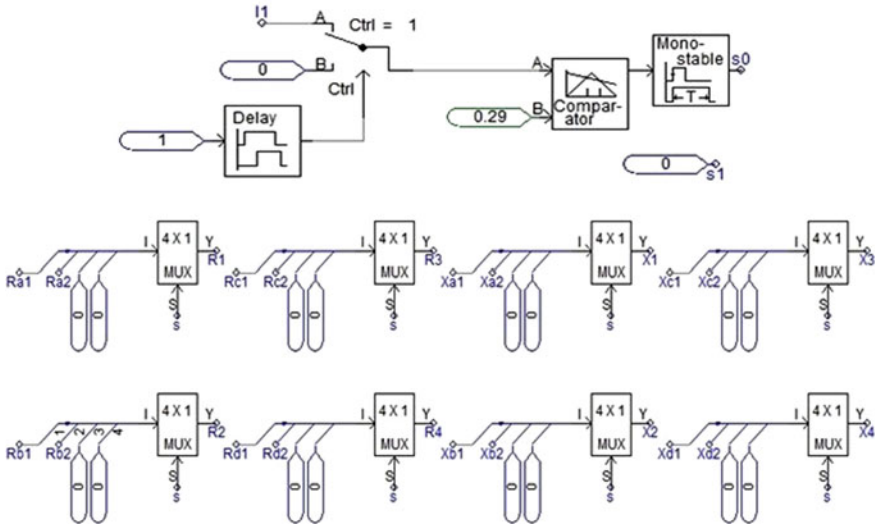

Fig. 9 Adaptive logic for distance relay using logical switching

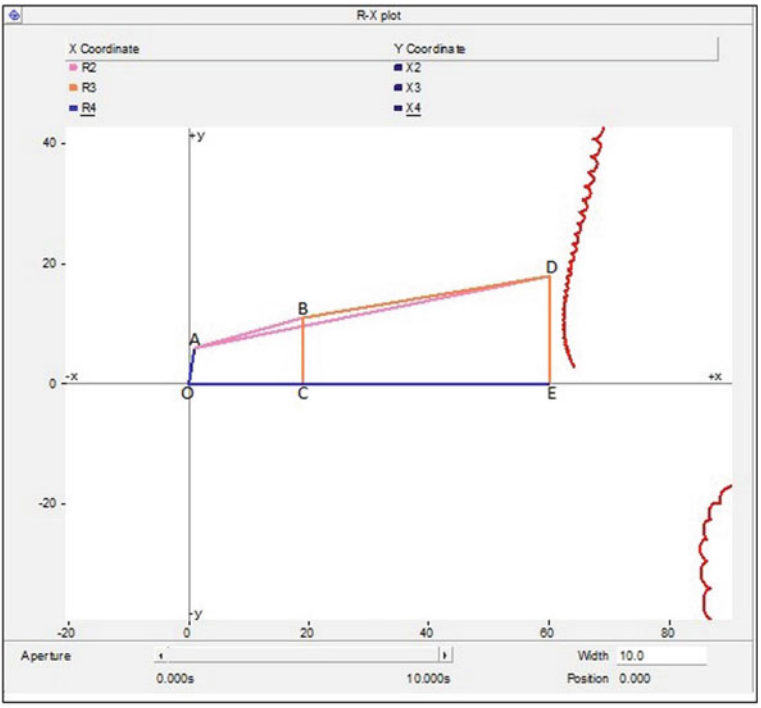

Fig. 10 Adaptive quadrilateral characteristics plot in PSCAD/EMTDC software

comparator outputs either logic high or low based on the input values, and the output of the comparator is given as input to the selection lines of a multiplexer. Based on the selection lines, the quadrilateral points O, A, B, C, D, E are selected which are shown in Fig. 10 which give a visual idea of shift in quadrilateral area based on the WGs in service.

OADE is the quadrilateral when 1 WG is in service. When the WGs number is increased from 1 to 16, the magnitude of current changes and as per the logic new quadrilateral points are chosen. From Fig. 10, it is clear that when the number of WGs in service is getting increased, the quadrilateral area is getting shrunk from OADE to OABC (nothing but the quadrilateral area for 16 WGs). Based on the WGs in service, the quadrilateral was able to adapt its characteristics.

6 Conclusion

The WGs in service affect the impedance seen by the relay during fault conditions. To avoid the unnecessary operation of the relay for external fault, the relay has to adjust its characteristics automatically. An adaptive distance protection scheme is proposed to prevent the unnecessary operation of the relay for an external fault. The

Table 1 Wind system data [16]

No of units	19
Generator unit	SCIG, 690V, 2MVA, 50Hz
Transformers	Δ/Υ, 690/33 KV, 2 MVA, 50 Hz
Main transformer	Y/Δ, 33/66 KV, 50 MVA, 50 Hz
Transmission line	30 Km (frequency-dependent model)

adaptive logic is verified under simulation environment. Compared to the conventional distance protection, the adaptive scheme implemented in this paper prevents the relay from mal-operating for the external faults. The implemented scheme is able to overcome the security issues in the wind integrated power system which is not possible in conventional distance protection.

Appendix

(See Table 1).

References

1. Eremia, M., Shahidehpour, M.: Major grid blackouts: analysis, classification, and prevention. Wiley, Hoboken, NJ, USA, pp. 789–863 (2013)
2. Horowitz, S., Phadke, A.: Blackouts and relaying considerations, relaying philosophies and the future of relay systems. IEEE Power Energ. Mag. **4**(5), 60–67 (2006)
3. Pradhan, A.K., Joos, G.: Adaptive distance relay setting for lines connecting wind farms. IEEE Trans. Energ. Convers. **22**(1), 206–213 (2007)
4. Eriksen, P., et al.: System operation with high wind generation. IEEE Power Energ. Mag. **3**(6), 65–74 (2005)
5. Sadeghi, Hadi: A novel method for adaptive distance protection of transmission line connected to wind farms. Int. J. Electr. Power Energ. Sys. **43**(1), 1376–1382 (2012)
6. El-Arroudi, K., Joós, G.: Performance of interconnection protection based on distance relaying for wind power distributed generation. IEEE Trans. Power Del. **33**(2), 620–629 (2018)
7. Stedall, B., Moore, P., Johns, A., Goody, J., Burt, M.: An investigation into the use of adaptive setting techniques for improved distance back-up protection. IEEE Trans. Power Del. **11**(2), 757–762 (1996)
8. Xia, Y., Li, K., David, A.: Adaptive relay setting for stand-alone digital distance protection. IEEE Trans. Power Del. **9**(1), 480–491 (1994)
9. Li, K., Lai, L., David, A.: Stand alone intelligent digital distance relay. IEEE Trans. Power Syst. **15**(1), 137–142 (2000)
10. Upendar, J., Gupta, C., Singh, G.: Comprehensive adaptive distance relaying scheme for parallel transmission lines. IEEE Trans. Power Del. **26**(2), 1039–1052 (2011)
11. Makwana, V., Bhalja, B.: A new digital distance relaying scheme for compensation of high-resistance faults on transmission line. IEEE Trans. Power Del. **27**(4), 2133–2140 (2012)
12. Mohajeri, A., Seyedi, H., Sabahi, M.: Optimal setting of distance relays quadrilateral characteristic considering the uncertain effective parameters. Int. J. Electr. Power Energ. Sys. **73**, 1051–1059 (2015)

13. Biswal, M., Pati, B.B., Pradhan, A.K.: Adaptive distance relay setting for series compensated line. Int. J. Electr. Power Energ. Sys. **52**(1), 198–206 (2013)
14. Biswal, M.: Adaptive distance relay algorithm for double circuit line with series compensation. Meas. J. Int. Meas. Confed. **53**, 206–214 (2014)
15. Paladhi, S., Pradhan, A.K.: Adaptive zone-1 setting following structural and operational changes in power system. IEEE Trans. Power Del. **33**(2), 560–569 (2018)
16. Data collected from wind integrated system—Ramakkalmedu (Idukki) in Kerala, India

Superimposed Components Based Directional Relaying During Power Swing

Shashi Bhushan Chandel, Lakshman Saroj, Kumar Harshavardhana, Himanshu Shekhar, and Jitendra Kumar

1 Introduction

When fault occurs in transmission line of power system, then after clearance of fault, power swing occurs in other healthy part of transmission line. Power swing can be of two types based on stability: stable and unstable. If power swing is stable, then circuit breaker should not operate that is why power swing is necessary to be distinguished whether it is stable or unstable. Due to incorrect measurements of relay signals within PSP, unintended trip takes place and it causes power system failure. To prevent this unintended trip, power swing blocking elements (PSB) generates the signal to block the distance relay. During such blocking period, detection and directional relaying are essential to disconnect the fault.

For power swing detection, there are many conventional methods which are used. These detection schemes of power swing are variation in resistance and swing center voltage (SCV) [1]. Within PSP, it is very difficult to detect a fault. In fault condition, the fault detection can be done using cumulative sum of NS current scheme but it is difficult to adjust drift and threshold variables in non-identical fault cases [2].Using prony and mathematical morphological methods, decaying DC is calculated which

S. B. Chandel (✉) · L. Saroj · K. Harshavardhana · H. Shekhar · J. Kumar
National Institute of Technology, Jamshedpur, Jharkhand, India
e-mail: chandelshashi77@gmail.com

L. Saroj
e-mail: nitjsrlakshman0@gmail.com

K. Harshavardhana
e-mail: kmrharshavardhana66@gmail.com

H. Shekhar
e-mail: 2018rsee004@nitjsr.ac.in

J. Kumar
e-mail: jitendra.ee@nitjsr.ac.in

O. H. Gupta and V. K. Sood (eds.), *Recent Advances in Power Systems*, Lecture Notes in Electrical Engineering 699, https://doi.org/10.1007/978-981-15-7994-3_26

is used for symmetrical fault detection [3, 4]. Conventional method of calculating phase angle of PS voltage and current cannot give accurate sense fault direction during PSP because it continuously fluctuates [5].

Then even fault direction estimation cannot be done using above-mentioned schemes. Since breaker operation depends upon FDE, it is very important to detect the direction in which fault is occurred. An FDE scheme is suggested based on superimposed components of voltage and current in this paper.

Therefore, proposed ideology is to introduce a technique which helps FDE.

Objective:

1. To estimate fault direction using proposed ideology
2. Testing the proposed technique in symmetrical fault condition and obtaining results in 'abc phase'
3. Testing the proposed technique in unsymmetrical fault condition.
4. Comparing the results with conventional methods

Some short names are used in paper as given here:

Fault directional estimation (FDE), power swing period (PSP), positive sequence (PS), negative sequence (NS), forward fault (FF), and reverse fault (RF).

1.1 Pscad Simulation of 9-Bus Power System

In this method, we have used 400 kV, 50 Hz system as shown in Fig. 1 with three synchronous generators. For power swing generation, a fault of duration 0.2 s is applied in line B2-B4and fault cleared using CB6 and CB5 which causes power swing in line B2-B8 and the data is taken from the B9. Using Fourier transform (DFT) technique, current and voltage phasors are obtained. To detect the fault direction, we have taken data by creating fault in **FF** and **RF** direction. Phase angle difference between superimposed PS and NS current and voltage. We have analyzed symmetrical as well as unsymmetrical faults and found some useful results that are working.

A three-phase fault is simulated within PSP at sampling frequency 1 kHz. Current and voltage at sampling frequency 1 kHz are plotted using PSCAD which can be seen in Figs. 2 and 3. Symmetrical as well as unsymmetrical faults of duration 0.2 s have been applied at 2.6 s and cleared at 2.8 s in FF to analyze the FDE scheme in PSP. Same process has also been tested for RF. Results of these tests have been mentioned in results section.

In Figs. 2 and 3, *x*-axis represents time (in second) whereas *y*-axis represents current (in kA) and voltage (in kV) at 50 Hz, respectively.

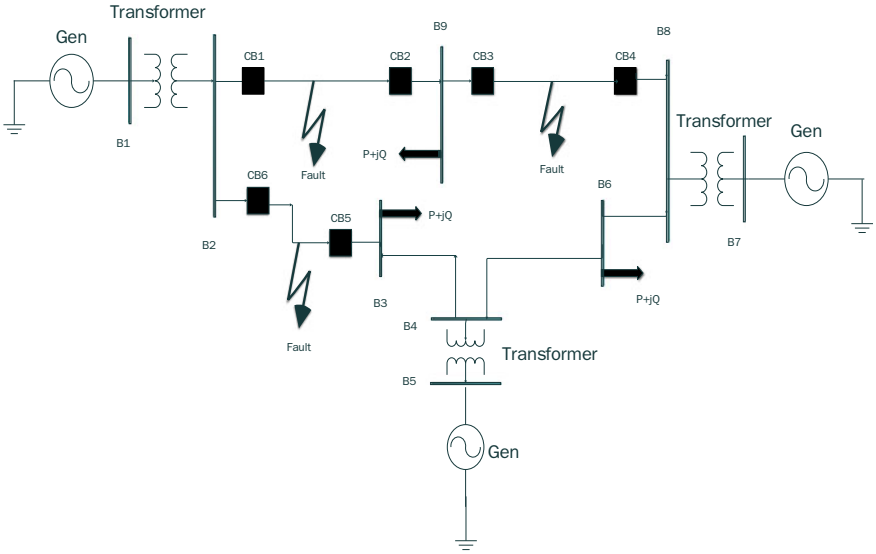

Fig. 1 400 kV, 50 Hz system

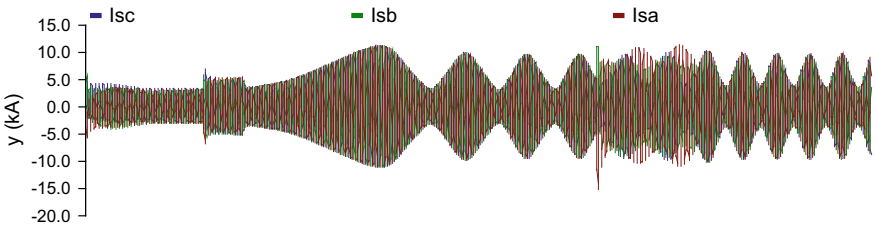

Fig. 2 Current in fault condition during PSP

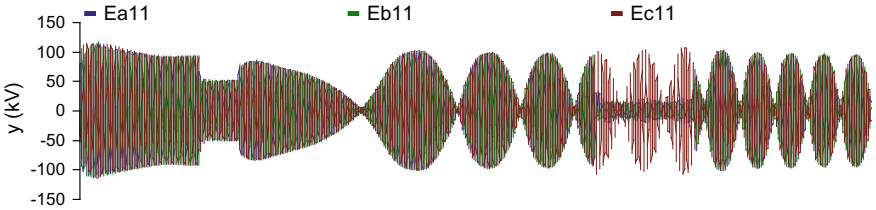

Fig. 3 Voltage in fault condition during PSP

2 Proposed Scheme for Fde During Psp

This scheme is dependent on phase difference between superimposed PS and NS current and voltage. In case of FF, the phase difference between superimposed PS voltage and current can be defined as

$$\alpha_1 = L\Delta \mathrm{V_{f1}} - L\Delta \mathrm{I_{f1}} \tag{1}$$

In similar way, in case of RF

$$\beta_1 = L\Delta V_{b1} - L\Delta \mathrm{I}_{b1} \tag{2}$$

where

$$\begin{aligned}
\Delta V_{f1} &= V_{f1-} V_{p1} \\
\Delta V_{b1} &= V_{b1} - V_{p1} \\
\Delta I_{f1} &= I_{f1} - I_{p1} \\
\Delta I_{b1} &= I_{b1} - I_{p1}
\end{aligned}$$

Here, V and I represent the voltage and current whereas subscripts f_1 and b_1 represent *PS* of *FF* and *RF* parameters, whereas p_1 represents prefault parameters. V_{f1} and V_{p1} represent *FF* value and prefault value of voltage in *PS*, respectively. ΔV_{f1} represents superimposed voltage of *PS* in *FF*.

In similar way, for superimposed NS

$$\alpha_2 = L\Delta V_{f2} - L\Delta I_{f2} \tag{3}$$

$$\beta_2 = L\Delta V_{b2} - L\Delta I_{b2} \tag{4}$$

where

$$\begin{aligned}
\Delta V_{f2} &= V_{f2} - V_{p2} \\
\Delta V_{b2} &= V_{b2} - V_{p2} \\
\Delta I_{f2} &= I_{f2} - I_{p2} \\
\Delta I_{b2} &= I_{b2} - I_{p2}
\end{aligned}$$

Here, V and I represent the voltage and current whereas subscripts $f2$ and $b2$ represent *NS* of *FF* and *RF* parameters, whereas $p2$ represents prefault parameters. Like V_{f2} and V_{p2} represent *FF* value and prefault value of voltage in *NS*, respectively. ΔV_{f2} represents superimposed voltage of *NS* in *FF*.

Since $\Delta\alpha_1$ and $\Delta\beta_1$ are opposite in sign; hence, this scheme helps in FDE. Similarly, $\Delta\alpha_2$ and $\Delta\beta_2$ are also opposite.

Here,

V_1 = Superimposed PS voltage
I_1 = Superimposed PS voltage
V_2 = Superimposed NS voltage
I_2 = Superimposed NS voltage

Implementation of proposed FDE is provided in flowcharts of Fig. 4. First superimposed NS current-based scheme is applied to any fault. If it fails, then second scheme is applied to the fault. Generally, most of the faults are unbalanced in power system. Then, superimposed NS current-based scheme is applied and it provides error in FDE for three-phase fault. Therefore, Superimposed PS technique is applied for balanced fault condition. However, superimposed PS technique works for all types of fault cases. With the help of calculated phase angle, fault direction can easily be estimated and trip decision by relay is taken place.

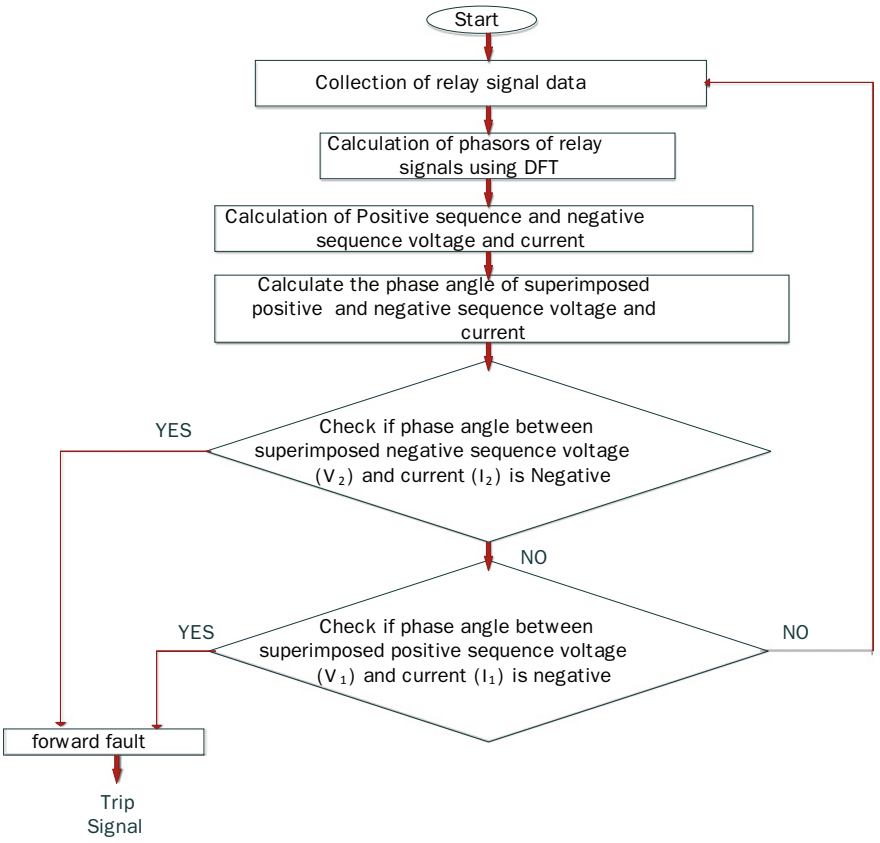

Fig. 4 Flowchart for execution of proposed algorithm for FF

3 Simulation Result and Discussion

In this part, the results obtained from proposed FDE algorithm are discussed for diverse types of fault during PSP. FF occurred at line between B8 and B9 and RF occurred at line between B9 and B2. Relay is placed at bus-9. Relay memory is used to store the prefault data. This algorithm works for both symmetrical as well as unsymmetrical faults. ABCG—type and ABG—type faults are applied at 100 km with $R_f = 10\ \Omega$ in forward as well as backward direction so that the operation of the proposed algorithm can be tested. The corresponding results of the proposed FDE algorithm are revealed in Fig. 5.

As shown in Fig. 5a, ABCG-type fault of duration 0.2 s has been occurred at time 2.6 s and cleared at 2.8 s. Here, it can be seen that the direction of the wave form of phase difference (α_1) is negative for FF, whereas phase difference (β_1) is positive for RF.

As shown in Fig. 5b, ABG—type fault of duration 0.2 s has been occurred at 2.6 s and cleared at 2.8 s. Here, there is a peak in α_2 which is positive for a very little time (approx. 0.003 s), which can be neglected and FDE can be done after that peak since the sign of angle is opposite in nature. Phase difference (α_2) is negative for FF, whereas phase difference (β_2) is positive for RF.

Since opposite signs of angles indicate direction estimation, i.e., FF and RF hence proposed scheme works accurate in both conditions.

4 Comparative Study

The conventional method [6] consists of phase angle between PS and NS voltage and current. An ABCG-type fault (at the 100 km with $R_f = 10\ \Omega$) within PSP is occurred at 2.6 s in the transmission line in both direction of relay consequently. The individual phase angle of PS voltage and current in symmetrical fault condition is shown below (Fig. 6).

This conventional method does not provide any information of fault direction but the proposed scheme is successful to do so. Further for testing purpose, an ABG-type fault ($R_f = 10\ \Omega$) is occurred at 2.6 s in the transmission line at distance of 100 km in both direction of relay, consequently. The results of conventional method and proposed scheme have been shown in Fig. 7. Figure 7a shows the characteristics of conventional method whereas Fig. 7b shows that of proposed scheme.

5 Conclusion

FDE issue is discussed in this paper. The proposed FDE technique is accurate for symmetrical as well as unsymmetrical faults during PSP. A comparison between

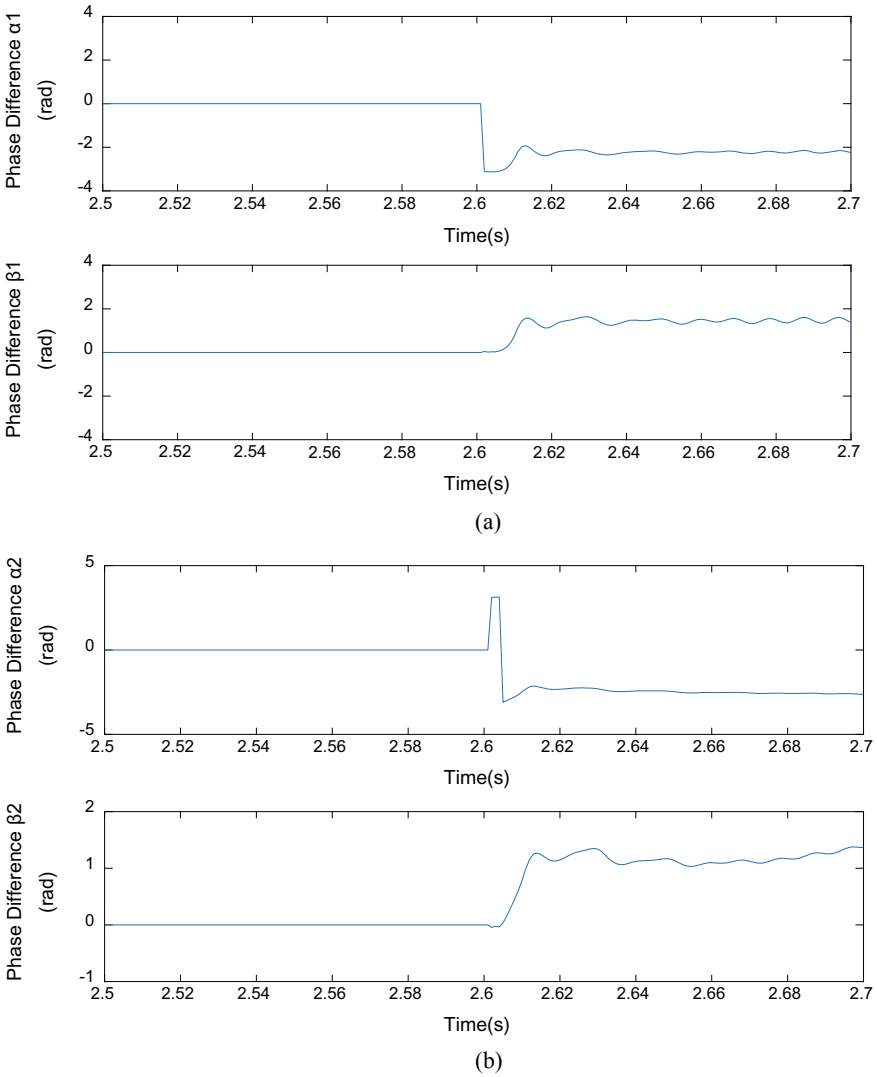

Fig. 5 Revealed results of proposed scheme **a**.$\alpha 1$ and $\beta 1$ in symmetrical (ABCG) fault **b**. $\alpha 2$ and $\beta 2$ in unsymmetrical (ABG) fault (Neglecting small interval of time)

conventional method and proposed scheme is made which infers that proposed scheme is dedicated to FDE and easy to implement.

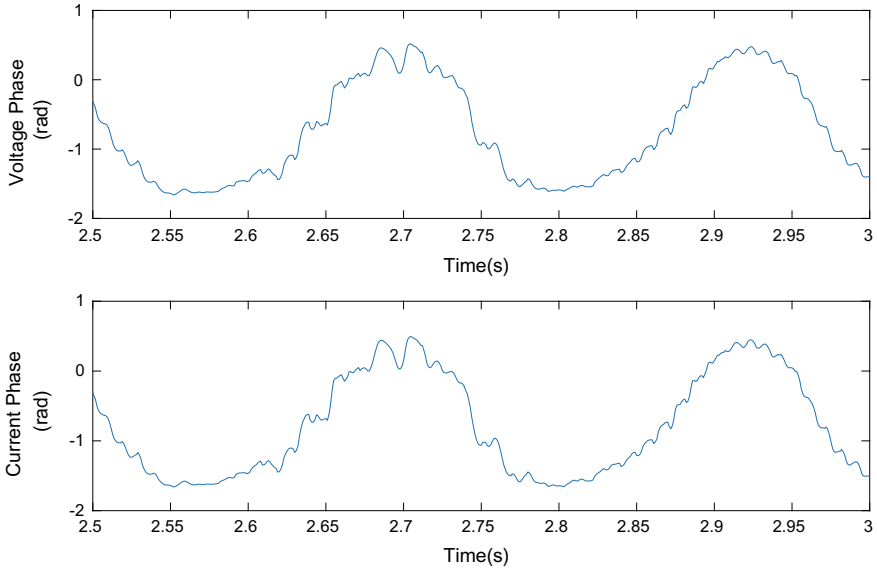

Fig. 6 Voltage phase and current phase angles, respectively, during symmetrical fault

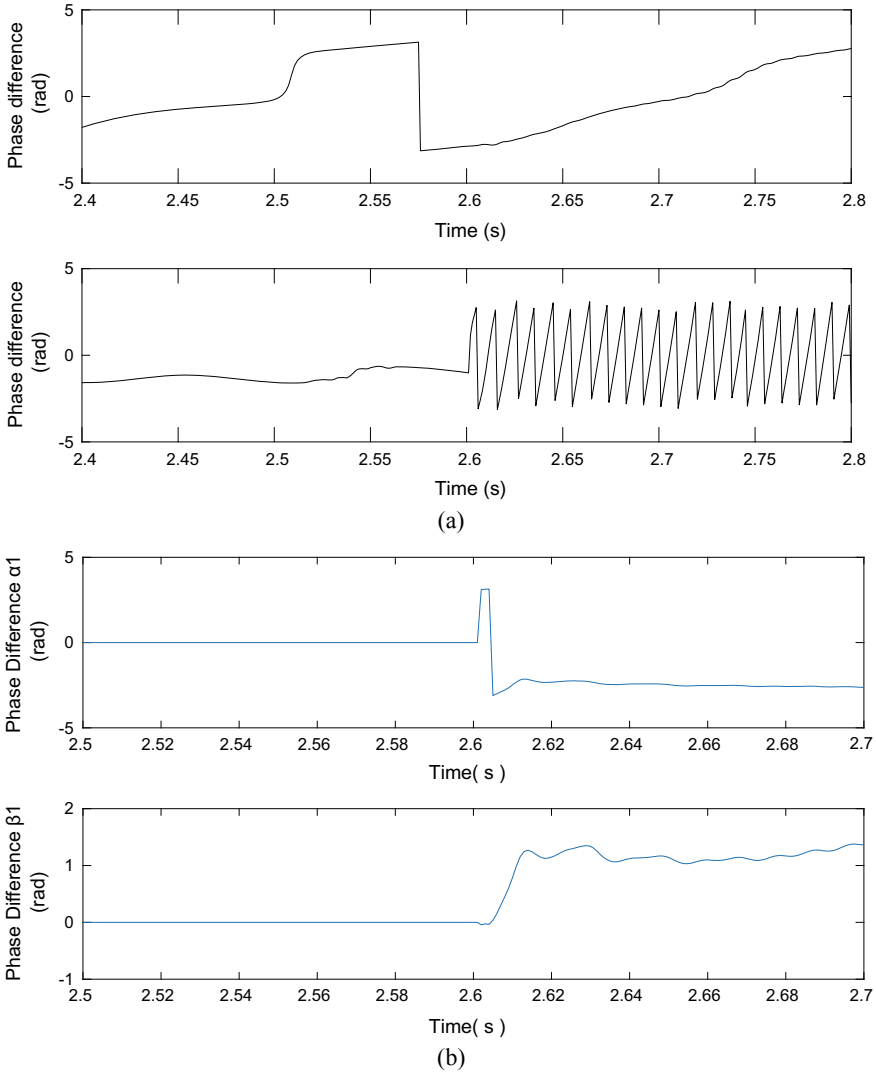

Fig. 7 Comparing proposed FDE scheme with conventional method [6] during FF and RF in ABG-type faults **a** Conventional method **b** α_1 and β_1 in Proposed scheme

References

1. Kumar, J., Jena, P.: Fault detection in a series compensated line during power swing using superimposed apparent power. In: 2015 IEEE Power and Energy Society General Meeting, Denver, CO, pp. 1–6 (2015)
2. Nayak, P.K., Pradhan, A.K., Bajpai, P.: A fault detection technique for the series-compensated line during power swing. IEEE Trans. Power Delivery **28**(2), 714–722 (2013)

3. Lotfifard, S., Faiz, L., Kezunovic, M.: Detection of symmetrical faults by distance relays during power swings. IEEE Trans. PowerDeliv. **25**(I), 81–87 (2010)
4. Morais, A.P., Junior, G.C., Moriotto, L., Marchesan, G.: Amorphological filtering algorithm for fault detection in transmission lines during power swings. Electric Power Syst. Res. **122**, 10–18 (2015)
5. Jena, P., Pradhan, A.K.: An integrated approach for directional relaying of the double-circuit line. IEEE Trans. Power Deliv. **26**(3), 1783–1792 (2011)
6. IEEE Power System Relaying Committee Working Group D6: Power swing and out-of-step consideration on transmission lines. (IEEE PSRC Report, 2005), pp. 1–59. [Online] Available www.pes-psrc.org
7. Patel, T.K., Mohanty, S.K., Mohapatra, S.: Fault detection during power swing by phase difference technique. In: 2017 Innovations in Power and Advanced Computing Technologies (i-PACT), Vellore, pp. 1–6 (2017); Eason, G., Noble, B., Sneddon, I.N.: On certain integrals of Lipschitz-Hankel type involving products of Bessel functions. Phil. Trans. Roy. Soc. London. A247, 529–551 (1955)
8. Gajbhiye, R.K., Gopi, B., Kulkarni, P., Soman, S.A.: Computationally efficient methodology for analysis of faulted power systems with series-compensated transmission lines: a phase coordinate approach. IEEE Trans. Power Delivery **23**(2), 873–880 (2008)
9. Roy, S., Babu, P.S.: Power swing protection of series compensated transmission line with novel fault detection technique. In: 2014 International Conference on Green Computing Communication and Electrical Engineering (ICGCCEE), Coimbatore, pp. 1–6 (2014)
10. Pradhan, A., Jena, P.: An integrated approach for directional relaying of the double-circuit line. In: 2012 IEEE Power and Energy Society General Meeting, San Diego, CA, pp. 1–1 (2012)

Energy Audit of Hybrid (Grid, Solar Rooftop Photovoltaic System and Diesel Generator) Electric Power Supply System: A Case Study of Commercial Building

Abhishek Pratap Singh, Aditya Singhal, Akanksha Athaya, Saurabh Kumar Rajput, Laxmi Srivastava, and Vikas Sharma

1 Introduction

Availability of energy contributes a crucial part in economical and sustainable development of any country. Categorization of energy is done on the basis of usage like fossil energy has the highest share in the electricity production of India around 79.80%. International research reports predict that coal electricity in India would reach 400 TW in 2033 if fossil energy generation is favored and 220 TW if renewable energy and gas are favored. Viewing these reports, energy conservation is the only effective, economical method to handle such issues which is achievable through energy audit. Energy conservation means to provide sustainable and economical approaches that can reduce energy wastage to minimum level. Energy audit assists

A. P. Singh (✉) · A. Singhal · A. Athaya · S. K. Rajput · L. Srivastava
Electrical Engineering Department, MITS, Gwalior, M.P, India
e-mail: apratap1689985@gmail.com

A. Singhal
e-mail: adityasinghal97@gmail.com

A. Athaya
e-mail: akanksha.athaya17@gmail.com

S. K. Rajput
e-mail: saurabh9march@mitsgwalior.in

L. Srivastava
e-mail: srivastaval@mitsgwalior.in

V. Sharma
NITRA, Ghaziabad, U.P, India
e-mail: vikassharma@nitratextile.org

O. H. Gupta and V. K. Sood (eds.), *Recent Advances in Power Systems*, Lecture Notes in Electrical Engineering 699, https://doi.org/10.1007/978-981-15-7994-3_27

in determining efficient energy options, identifying energy conservation opportunities, and also helps in planning and implementation of energy conservation projects. [1] Audit mainly focuses on lighting, power load, and harmonic analysis and replacement of several equipments as they were less efficient. [2] Energy efficient equipment like 300Amp IGBT inverter welding sets, etc., saves energy in industries. Software like ETAP [3] can be used to unplug and switch off the high-power appliances to minimize no-load losses. Sachin and Takshashila [4, 5] suggested replacement in the lighting system with energy efficient LEDs. [6] Aldona focuses on the enhanced efficiency of industrial processes by using various techniques, tools, measures like usage of standard meters, loggers, etc. [7]. Digambar focused on power factor controlling through static capacitor, phase advancer, etc., and machine maintenance. [8] Amit suggested to use maximum of the day light, LEDs in place of fluorescent lamps, rooftop solar panels and reduce the contracted demand to reduce tariff charges. [9] D.C. Maheepala gives an idea of working with "IOT" that will analyze the system and provides real-time data and remote monitoring. [10] O.E. Atiba provided energy saving by adjusting the motor drive speed and increase in building envelope insulation during the operating hours. [11] Elizabeth used the database of energy survey in residents to find out factors which helps in taking the decision of an audit. In today's scenario, hybrid electric power supply system [12] is used in industries/commercial buildings for improving energy efficiency. Till now, the energy conservation opportunities are not figured out in a hybrid electric power-based system. After seeing this urgent need and relevance of energy conservation, we performed an energy audit in a commercial building of NITRA. This paper is mainly focused on finding energy conservation opportunities in hybrid electric power supply system by analyzing Electricity bills, Voltage profile, Harmonics profile, Transformer loading/efficiency, DG set, and Solar RPVS [13]. This paper would help commercial buildings, industries, and individuals to analyze their hybrid electrical system.

2 Description of System Under Audit Study

NITRA is a textile research institute and textile commercial that uses hybrid based electric power supply system (see Fig. 1).

3 Energy Audit Study

Following the BEE guidelines [14], numerous data has been collected during the audit through manual inspection and metering at distribution transformer low tension (LT) panel with the help of power quality analyzer Chauvin Arnoux CA8331 QualistarPlus. We have classified energy audit study into six different parts, namely electricity bill analysis, voltage profile, harmonics analysis, transformer loading and efficiency, DG set, and solar RPVS.

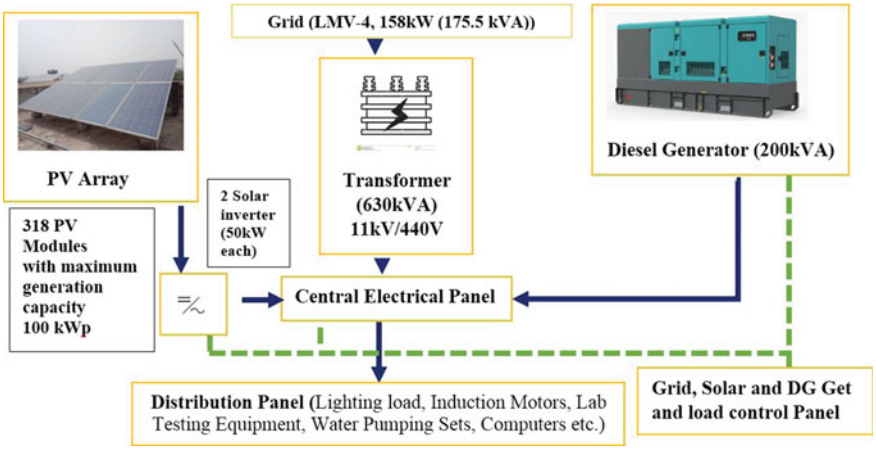

Fig. 1 Schematics of hybrid (grid, solar rpvs, diesel generator) based electric power system

3.1 Electricity Bill Analysis

Every energy bill contains lot of information and a good insight to our electricity consumption patterns. Analysis of various electricity bills can help one plan for money and energy savings. If consumer is having a high tension supply, then bill is divided into two parts. First one is demand charges, and second one is energy (kVAh/kWh) supplied from electricity board on monthly basis (see Table 1).

Table 1 Month wise electricity bills of one year

Month	Total units kVAh	Max. demand (kVA)	Avg. power factor	Total bill (Rs.)	Avg. cost Rs./ kVAh	Total demand charges (Rs.)	Over charges due to (MD)
Apr-19	21,692	96.44	0.94	211,656	9.75	35,550.90	9512.10
May-19	26,300	94.76	0.96	248,660	9.45	35,550.90	9965.70
Jun-19	34,684	125.76	0.96	313,673	9.04	35,550.90	1595.70
Jul-19	30,668	143.76	0.95	287,245	9.36	38,815.20	0.00
Aug-19	26,564	113.60	0.96	250,133	9.41	35,550.90	4878.90
Sep-19	27,572	103.24	0.97	257,385	9.33	35,550.90	7676.10
Oct-19	34,964	125.04	0.97	329,623	9.42	35,550.90	1520.10
Nov-19	25,372	102.64	0.95	252,331	9.94	35,550.90	7784.10
Dec-19	22,428	78.56	0.96	225,046	10.03	35,550.90	14,339.70
Jan-20	37,892	152.88	0.97	363,336	9.58	41,277.60	0.00
Feb-20	40,692	135.16	0.96	395,330	9.71	36,493.20	0.00
Mar-20	27,280	104.88	0.94	268,543	9.84	35,550.90	7233.30

Generally, monthly bill has parameters that are to be used for the analysis, like Contracted Demand, Minimum Billable Demand (MD), Time of Day (TOD) rates imposed by the Electricity Board, Total kVAh consumed during the month, Fixed Charges and Total Energy Charges imposed, Electricity Duties and other miscellaneous charges, Net payable amount, etc. By analyzing month wise electricity bills of a plant, we can find the provision in the tariff structure for reducing the amount of bill.

Tariff Details

Supply Company	: Paschimanchal Vidut Vitran Nigam Ltd.
Tariff Code	: LMV-4
Supply	: 11 kV
Demand Charges	: Rs.270 per kVA
Contracted Demand	: 175.50 kVA
Minimum Billable Demand	: 131.60 kVA

Unit Charges (TOD)

For first 1111 kVAh/month	: Rs. 7.43/kVAh
For next 1111 kVAh/month	: Rs. 7.65/kVAh
Above 2222 kVAh/month	: Rs. 7.88/kVAh

Electricity Bill Analysis (from April 2019 to March 2020).

Total demand charges paid are Rs. 2,73,013 per annum, minimum recorded demand is 78.56 kVA, maximum recorded demand 152.88 kVA, average recorded demand is 114.81 kVA (see Fig. 2), and total over charges paid Rs. 64,505.

Observation and Recommendation

- Installation of maximum demand controller (EM3460) [15] is recommended. It is an energy efficient device used to control the maximum demand by automatically shedding the load when in the condition of crossing the permissible limit of maximum demand preset in it.

Saving Anticipated.

$$\text{Recent Maximum Demandmeterset value} = 175.60\,\text{kVA},$$

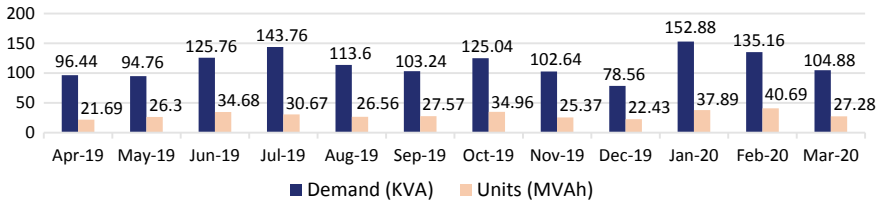

Fig. 2 Month wise maximum demand (kVA) and energy/units (MVAh) consumed in one year

Average maximum demand = 114.81 kVA, if maximum demand = 125.60 kVA
i.e. saving in maximum demand = (175.60 − 125.60)kVA × 270
= Rs. 13, 500 per month

Total Annual Savings = 13500 × 12 = Rs. 1, 62, 000 per year
Investment: Demand controller costs around Rs. 70, 000
Payback Period = 70000/13500 i.e. approximately 6 months

- Reduce maximum demand (no investment needed). Since, maximum demand is much more than required maximum demand. So it is advisable to set maximum demand to 135.60 kVA to get reduce bill amount.

  Savings Anticipated.

  Recent Maximum Demand value = 175.60 kVA
  Advisable Maximum Demand value = 135.60 kVA
  Saving in Maximum demand cost per month = (175.60 − 135.60) × 150
  = Rs.10, 800 per month
  Annual Savings = 10800 × 12 = Rs.1, 29, 600 per year

  So, reduce set maximum demand to 135.60 kVA.

3.2 Voltage Profile

Availability of nearly constant rated voltage is the requirement of any electrical machine. So, we have taken that fact in account and have analyzed phase 1,2,3 voltages at distribution transformer LT panel using three-phase power analyzer for a duration of 21 h 35 min (see Table 2).

Observation and Recommendation

Since, rated line voltage = 440 V, rated phase voltage = $440/\sqrt{3} = 254.03$ V

Table 2 Voltages phase 1, phase 2, and phase 3

Voltage	Avg. (V)	Min. (V)	Max. (V)	Duration (h:min:s)
V1 rms	244.86	0.00	258.10	21:35:00
V2 rms	243.38	0.00	254.60	21:35:00
V3 rms	243.93	0.00	257.20	21:35:00

But here voltage is varying, i.e., 258.10 V maximum and 0.00 V minimum. To maintain nearly constant voltage profile, application of three-phase voltage stabilizer is recommended.

3.3 Harmonic Analysis

Existence of non-ideal and nonlinear devices in an electrical system introduces harmonics in the system and original waveforms (current and voltage) get distorted from its fundamental frequency. Total harmonic distortion (*THD*) is measure of distortion present in the waveforms. Generally, *THD* is given in % (percentage) or in dB (decibel). Presently, two variant definitions of *THD* are used for harmonics analysis, i.e., THD_f (fundamental) and THD_r (RMS).

$$THD_f = \frac{\sqrt{V_2^2 + V_3^2 + V_4^2 + \ldots}}{V_1} \quad THD_r = \frac{\sqrt{V_2^2 + V_3^2 + V_4^2 + \ldots}}{\sqrt{V_1^2 + V_2^2 + V_3^2 + \ldots}}$$

Here, $V_{n=}$ Voltage (in rms) of nth harmonic, and $n = 1$ implies frequency of fundamental

For signals having low harmonic distortions, the *THD* obtained from both methods are similar, e.g., if the signal has THD_f of 10%, then it will have THD_r of 9.95%. But, when signal possess higher distortions then difference between the two becomes huge, e.g., if the signal has THD_f of 266%, then it will have THD_r of 94%. Thus, THD_f is preferred for measuring harmonic content as THD_r contributes a significant error when it comes to measure higher distortion level signals. THD_f and THD_r in voltage and current are measured with the help of three-phase power analyzer for a duration of 21 h 35 min (see Table 3).

Observation and Recommendation

Table 3 Total harmonic distortion (THD_f and THD_r) in voltage and current

Name	THD_f			THD_r		
	Avg. (in % f)	Min. (in % f)	Max. (in % f)	Avg. (in % r)	Min. (in % r)	Max. (in % r)
A1 THD	37.23	13.30	267.60	31.66	13.20	81.40
A2 THD	36.97	8.70	296.10	30.06	8.60	93.70
A3 THD	61.96	19.80	341.20	47.10	19.40	95.60
V1 THD	1.01	0.60	1.90	1.01	0.60	1.90
V2 THD	1.40	0.90	2.10	1.40	0.90	2.10
V3 THD	1.28	0.70	2.00	1.28	0.70	2.00

- As seen from the Table 3, voltage contains very low distortion level (Max. THD_f or $THD_r = 2.10\%$). Therefore, voltage harmonics reduction is not required.
- Current has high distortion level (Max. $THD_f = 341.20\%$ and Max. $THD_r = 95.60\%$). Also the average value for current contains higher distortion ($THD_f = 61.96\%$ and $THD_r = 47.10\%$). Therefore, current harmonics reduction is required.
- The harmful effect of harmonics is overheating of electrical equipment. This causes abnormal thermal tripping of circuit breakers, relays, and other protecting equipment. Major disadvantage of harmonics is that it can cause logical faults in digital devices and errors in the metering of voltage and current.
- It is recommended to reduce current harmonics by using techniques like harmonic filtering (passive, active, and hybrid) and through power factor improvement (static capacitors, synchronous condenser, and phase advances).

3.4 Transformer Loading and Efficiency

Transformer loading is defined as the ratio of average load (kVA) to rated load (kVA). We have recorded load variation data (one-day metering at transformer panel) through three-phase power analyzer (Fig. 3). For heavy power transmission, power transformer is employed that operates continuously with minimal load variation. But distribution transformer has been installed at NITRA. As seen from Fig. 3, load variation is significant, so we'll use last year electricity bills and calculate average load on the basis units (kVAh) consumed. From Table 1, following calculation can be done.

Actual kVAh consumed in year 2019–2020: 3,56,108 kVAh

$$\text{kVAh consumed as per transformer rating in 1 year} : 630 \times 24 \times 365$$
$$= 55, 18, 800 \text{ kVAh}$$

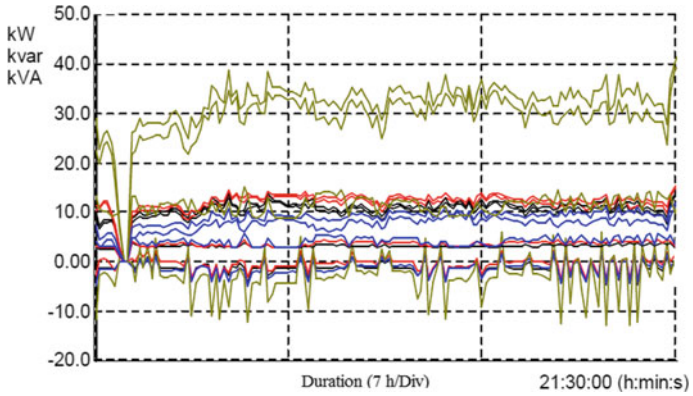

Fig. 3 Power variation curve (metering at transformer LT panel using power analyzer)

$$\%\,\text{Loading}(\text{Actual kVAh}/\text{Rated kVAh}) \times 100\% : (356108/5518800) \times 100\% = 6.45\%$$

Transformers Losses and Efficiency

Two types of losses are present in transformer, i.e., Core Loss (Iron loss) and Copper Loss. Transformer efficiency is given as

Efficiency = Power (Output in kW)/Power (Input in kW)

Transformers are most highly efficient machines present today. As seen from Table 1, average power factor is approximately 0.95.

Calculation

$$P_{(\text{total loss})} = P_{(\text{No load loss})} + (\text{loading})^2 \times P_{\text{Full load}},\ P_{\text{No load}} = 1.20\,\text{kW},\ P_{\text{Full load}} = 7.50\,\text{kW},$$
$$P_{\text{Total loss}} = 1.20\,\text{kW} + (0.0645)^2 \times 7.50\,\text{kW} = 1.23\,\text{kW}(\text{Since},\ \%\,\text{loading} = 6.45\%)$$
$$P_{\text{out}} = (\text{kVA rating}) \times (P.F) \times (\text{loading}) = 630 \times 0.95 \times 0.0645 = 38.60\,\text{kW}$$
$$\text{Transformer Efficiency} = P_{\text{Out}}/(P_{\text{Out}} + P_{\text{Total loss}}) \times 100\% = 96.91\%$$

Condition for obtaining maximum efficiency

$$\text{Loading} = (P_{\text{no load loss}}/P_{\text{Full load}})^{1/2} = (1.2/7.5)^{1/2} = 0.40 \text{ and } \%\text{Loading} = 40\%$$

Therefore, in our case maximum efficiency is achieved at 40% loading.

$$P_{(\text{total loss})} = 1.20 + (0.40)^2 \times (7.50) = 2.40\,\text{kW},\ P_{\text{out}} = 630 \times 0.95 \times 0.40 = 239.40\,\text{kW}$$
$$\eta\text{max} = P_{\text{Out}}/(P_{\text{Out}} + P_{\text{Total loss}}) \times 100\% = 239.40/(239.40 + 2.40) \times 100\% = 99.01\%$$

In the similar way, transformer efficiency versus loading curve can be plotted by finding efficiency at different loading profile (see Fig. 4). As per Fig. 4, transformer efficiency lies in the range of 96.91%–99.10%, i.e., nearly flat curve showing constant efficiency (apprx. 99%) between 40–50% loading profile.

Observation and Recommendation

% loading found to be poor (6.45%) and further efficiency (96.91%) also needs improvement. Hence, it is suggested to maintain loading in the range 40–50% for getting most efficient operation of transformer. Two methods can be employed for achieving maximum efficiency:

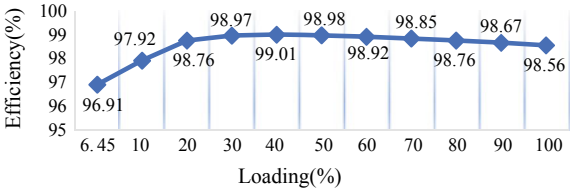

Fig. 4 Efficiency versus loading curve at different loading profile

- Average load was 38.60 kW which was resulting in poor loading and efficiency. So it is suggested to maintain average load in the range of 240–250 kW which will give 40–50% loading and 99.10% efficiency.
- If above suggestion is not achievable, then replace existing transformer with a low kVA rated transformer around 100–150kVA range so that your average load will remain same at 38.60 kW, i.e., nearly 40% loading and efficiency will maximum around 99%.

3.5 Diesel Generator Set

DG sets are often used as a backup power source when the grid fails to supply continuous power. NITRA has installed one diesel generator of capacity 200kVA (make Kirloskar) as backup power source. Regular energy efficient evaluation [16] of DG sets can be done through conducting 1- or 2-hour trial in steady load condition and the parameters, e.g., total fuel used by the help of dip level, current, voltage, power and energy generated, temperature of air and cooling water, and relative humidity are measured at a regular interval (15 min) of time. Evaluation of DG set performance is carried out in our study. Recorded data has been enclosed here for the reference (Table 4).

Observation and Recommendation

It can be seen from Table 4 that the unit cost of electricity has come out to be Rs. 21.52, which is very high as compared with grid supply cost, but the DG set is used as a backup power source in the plant and used for a limited period of time, so the high cost value is not affecting that much and can be reduced by making the load steady in nature, use of dust free air, maintenance of air filters, use of oil additives, etc.

Table 4 Diesel generator set parameters (metering at DG set using power analyzer for unit consumption and oil volume measurement)

Parameters	Value
Capacity	200 kVA
Average load (kVA)	50.23
Maximum load (kVA)	64.48
Average % loading	25%
Trial starting time	13:10:00
Trial ending time	14:50:00
Diesel consumption	25 Liters
Units generated	81.29 kWh
Unit cost (Rs.)	21.52
SFC (kWh/Liter)	3.25

3.6 Solar Rooftop Photovoltaic System

Total 318 PV solar panels were installed at NITRA's rooftop with installed capacity of 100Kwp DC capacity. Energy generation through solar RPVS is depending on various environmental parameters like sun light, time of the day, ambient temperature, module temperature, etc. Panel specifications of the installed panel at NITRA; maximum power output 320 W, voltage at open circuit 46.00 V, current at short circuit 9.03A, voltage rating 37.70 V, current rating 8.50A, fill factor 77.04%, efficiency 16.67%, maximum system operating voltage 1000V (IEC). For the analysis of RPVS, we installed a three-phase power analyzer at the common coupling point of hybrid supply system and recorded the parameters for the 24 h duration. We had also preferred DATAGLEN [17] online software system for real-time monitoring of RPVS on daily and monthly basis.

Recorded Information through DATAGLEN system on daily basis

- Energy (units) generated from the plant on 14, 15 July, 2019:

  3.70 kWh/kWp, 2.63 kWh/kWp and units 369.60 kWh, 263.10 kWh, respectively,

- Carbon emission saved on 14, 15 July, 2019:187.89 Tons, 188.08 Tons, respectively.
- Trees planed or saved on 14, 15 July, 2019: 27 k, 27 k, respectively.

Observation and Recommendation

- RPVS helps in reducing the maximum demand of the plant. A part of the load requirements is fulfilled by the RPVS plant, and hence, it supports the plant in energy savings as well as electricity bill savings.
- RPVS reduces the percentage loading on the transformer. So a smaller size (kVA) transformer may be used with solar plant. Hence, the RPV system not only improves the life of transformer but also it provides the economic support to the hybrid system.
- The operation of on-load tap changer (OLTC) system increases with RPVS. So an additional preventive maintenance is required at this part.

4 Conclusions

In this energy audit study, we have seen that renewable generation and environment concern have been taken care in hybrid electric power supply system but it is also responsible for poor power quality which can be troublesome for plant equipment. So, it is necessary to conduct energy audits in hybrid power supply systems for improving energy efficiency, power quality, and overall life of plant. Purpose of any energy audit is to cut down the excessive consumption of energy and cost saving which has been achieved in this particular audit. After implementing all the recommendations given

in this paper, i.e., replacement and addition of some low cost, effective, and efficient methods enable the consumer to get optimum performance, low cost backup power security, renewable generation, and green environment.

Acknowledgements The authors are indebted to acknowledge the assistance and encouragement provided by NITRA. for this audit especially Mr. Rajkumar Saini.

References

1. Kulkarni, S., Patil, K.: Energy audit of an Industrial unit—a case study. Int. J. Emerg. Sci. Eng. **2**(1), 22–26 (2013)
2. Saini, M., Chatterji, S., Mathew, L. et al.: Energy audit of an industry. Int. J. Sci. Technol. Res. **3**(12) (2014)
3. Kumar, A., Ranjan, S., Singh, M., et al.: Electrical energy audit in residential house. Procedia Technol. **21**, 652–630 (2015). https://doi.org/10.1016/j.proctcy.2015.10.074
4. Parthe, S., Kompeli, S.: Energy audit and conservation tool for energy efficiency. Int. Res. J. Eng. Technol. (IRJET) 2(08) (2015)
5. Bhandari, T., Thosar, A., Bachawad, M., Bhakre, P. et al.: Energy audit: a case study of an academic building. Int. J. Ind. Electron. Electr. Eng. 4(11) (2016)
6. Kluczek, A., Olszewski, P.: Energy audits in industrial processes. J. Clean. Prod. **142**, 3437–3453 (2017). https://doi.org/10.1016/j.jclepro.2016.10.123
7. Mane, D.B., Jadhav, A.B., Shinde, A. et al.: Electrical energy audit for riddhim siddhim steel india Pvt. Ltd. In: 2018 Internat 2018 International Conference on Computation of Power Energy Information and Communication (ICCPEIC), Khopoli. https://doi.org/10.1109/iccpeic.2018.8525156
8. Chakraborty, A., Dey, D., Das, P.: Investigation of energy consumption and reservation scheme using energy auditing techniques. In: 2018 International Conference on Smart Systems and Inventive Technology (ICSSIT) (2018). https://doi.org/10.1109/icssit.2018.8748724
9. Maheepala, D., Nayanajith, R., Somarathna, M. et al.: Designing an energy monitoring, analysing and solution providing system for energy auditing. In: 2018 Fourth International Conference on Advances in Electrical Electronics Information Communication and Bio-informatics (AEEICB) (2018). https://doi.org/10.1109/aeeicb.2018.8480953
10. Atiba, O., Efemwenkiekie, U., Olatunji, R., et al.: Walk-through energy audit of an institutional building. J. Phys: Conf. Ser. **1378**, 032051 (2019). https://doi.org/10.1088/1742-6596/1378/3/032051
11. Hewitt, E., Wang, Y.: Understanding the drivers of national-level energy audit behavior: demographics and socioeconomic characteristics. Sustainability **12**, 2059 (2020). https://doi.org/10.3390/su12052059
12. Hasan, K,. Fatima, K,. Sohel mahmood, M.: Feasibility of hybrid power generation over wind and solar standalone system. In: 2011 5th International Power Engineering and Optimization Conference (2011). https://doi.org/10.1109/peoco.2011.5970430
13. Rajput, S.: Solar energy: fundamental, economic and energy analysis, 1st edn. NITRA Publication (2017). ISBN: 978–93-81125-23-6
14. General aspects of energy management and audit: Guide book 1 for national certification examination for energy managers and auditors, bureau of energy efficiency, India 2005. Available on www.bee-india.nic.in
15. Patel, P., Patel, A., Patel, D., Patel, V., Solanki, D., Chudasama, P. et al.: Energy audit: utility bill analysis in an institute. Int. J. Electron. Electri. Comput. Syst. (IJEECS) **6**(11) (2017)

16. Energy efficiency in electrical utilities: Guide book 3 for national certification examination for energy managers and auditors, bureau of energy efficiency, India (2005). Available on www.bee-india.nic.in
17. inc d (2020) Solar Monitoring| Dataglen. In: Dataglen.com. http://www.dataglen.com. Accessed 20 May 2020

A Comparative Analysis of EVs Scheduling Strategies to Accomplish Valley Filling

Tanuj Rawat, K. R. Niazi, Nikhil Gupta, and Sachin Sharma

Nomenclature

Indices	
n	Index for EV
t	Index for time
Parameters	
N	Total number of EVs
T	Total number of time intervals
t^n_{arr}	Arrival time of EV
t^n_{dpt}	Departure time of EV
t^n_{char}	Charging duration of EV
$P_{\text{ev},n,t}$	Charging rate of EV
cost^t	Cost of EV charging
BL	Base load
En^n	Energy required by EV
Variables	
TL_t	Total demand after integration of EVs
t_{v}	Time instant when load is minimum
t^n_{st}	Start time of EV charging
t^n_{ed}	End time of EV charging

1 Introduction

Due to increasing environmental issues, depleting reserves of natural oil and rising prices of transportation fuel, electric vehicles (EVs) are reaping popularity. Even government across the world is making policies to replace conventional vehicles

T. Rawat (✉) · K. R. Niazi · N. Gupta · S. Sharma
Malaviya National Institute of Technology, Jaipur 302017, India
e-mail: tanujsometime@gmail.com

O. H. Gupta and V. K. Sood (eds.), *Recent Advances in Power Systems*, Lecture Notes in Electrical Engineering 699, https://doi.org/10.1007/978-981-15-7994-3_28

by EVs. Therefore, it is likely that the future distribution system will have large proliferation of EVs. The operation of EVs will require electrical energy as they are propelled by electric motors. The additional demand due to EVs will stress the grid if not managed properly. It has been shown that uncontrolled charging of EVs can cause increase in energy losses and peak demand paired with voltage limit violations and line congestions [9].

The negative impacts of uncontrolled EVs charging can be mitigated by coordinated scheduling of EVs [3, 12]. The idea behind coordinated scheduling is that EVs are idle for most of the time, therefore, their load is flexible and can be shifted in time. In coordinated scheduling, the flexibility of EVs is exploited and they are charged such that grid assets are utilized efficiently. The aim of coordinated scheduling of EVs is to determine optimal charging/discharging of EVs such that some objective is fulfilled. The objective for coordinated scheduling of EVs can be developed from different stakeholder's perspective [6].

Coordinated scheduling of EVs to fulfill the interest of system operator is widely studied in literature. In this context, different objectives such as minimization of energy losses [13], minimization of load variance [10, 11], maximization of load factor [4], minimization of load deviation [1] and minimization of EVs charging cost [2, 6, 8] are adopted in past by researchers. It is shown that each of these objectives results in valley filling of load demand profile. However, a comprehensive study comparing the impact of different EV charging strategies designed to directly/indirectly shift EVs demand to valley periods on distribution grid load curve has not been addressed in literature. Therefore, the main contribution of this work is to assess the impact of different EV charging strategies which results in valley filling of load demand profile of distribution system. For this purpose, firstly, EVs charging profile is obtained under minimum load variations model (MLVM), maximum load factor model (MLFM), valley search charging model (VSCM) and minimum charging cost model (MCCM), respectively. Thereafter, the impact of these charging strategies on average load, valley load, peak load, peak-valley difference and load factor of grid demand profile for different EV penetrations is investigated. Moreover, the impact on charging cost is also compared to these EV charging strategies.

2 Problem Formulation

2.1 Minimum Load Variation Model (MLVM)

In this strategy, EVs are charged such that variations in the load curve are minimized. Variations in demand profile are minimum when sum of differences between load demand of two consecutive time intervals is minimum. Mathematically, the objective function for charging of EVs under MLVM is expressed as

$$\min \sum_{t=2}^{T} |\mathrm{TL}_t - TL_{t-1}| \tag{1}$$

2.2 Maximum Load Factor Model (MLFM)

Under MLFM, EVs are charged in order to maximize load factor of grid demand. Load factor is defined as the ratio of average load to peak load of system for a given time interval. Therefore, the objective function under MLFM is calculated as

$$\max \left(\frac{\sum_{t=1}^{T} \mathrm{TL}_t}{max(\mathrm{TL}_t) \times T} \right) \tag{2}$$

2.3 Valley Search Charging Model (VSCM)

In VSCM, for any EV n, firstly, time period between its arrival and departure when load demand is minimum is determined according to Eq. (3) [14].

$$\mathrm{TL}_{t_\mathrm{v}}^{n-1} = min\ \mathrm{TL}_t^{n-1} \quad t \in [t_{\mathrm{arr}}^n, t_{\mathrm{dpt}}^n] \tag{3}$$

Then starting time for charging of EVs is obtained according to Eq. (4)

$$t_{\mathrm{st}}^n = \begin{cases} t_{\mathrm{arr}}^n & t_\mathrm{v} - t_{char}^n/2 < t_{\mathrm{arr}}^n \\ t_{\mathrm{dpt}}^n - t_{\mathrm{char}}^n & t_\mathrm{v} + t_{\mathrm{char}}^n/2 > t_{\mathrm{dpt}}^n \\ t_\mathrm{v} - t_{\mathrm{char}}^n/2 & \text{other} \end{cases} \tag{4}$$

The end time for EV charging is obtained as

$$t_{\mathrm{ed}}^n = t_{\mathrm{st}}^n + t_{\mathrm{char}}^n \tag{5}$$

2.4 Minimum Charging Cost Model (MCCM)

In the context of smart grid, dynamic pricing will be utilized to shift flexible demand such as demand of EVs. The pricing will be designed such that flexible demand is shifted toward valley periods and flat load profile is obtained. It is to be noted that using dynamic pricing both utility and EV owners will be benefitted. The utility will obtain an improved load profile while the customer will operate their load with less energy cost. Therefore, in MCCM, EVs will charge such that its charging cost is minimized while indirectly will also result in flat load profile. The fitness function for MCCM is expressed as

$$Min \sum_{n=1}^{N} \sum_{t=t_{\mathrm{st}}^n}^{t_{\mathrm{st}}^n + t_{\mathrm{char}}^n} P_{\mathrm{ev},n,t} \times cost_t \tag{6}$$

The steps for evaluating the optimal load profile of EVs are as follows:

1. Input BL, cost, number of EVs with their t_{arr}, t_{dpt}, En, P_{ev} and t_{char}
2. set $n = 1$ and $TL = BL$
3. Determine t_{st}^{n} lying between t_{arr}^{n} and t_{dpt}^{n} which optimizes the considered objective function
4. Add EV charging load obtained using step 3 to TL.
5. If $n < N$, $n = n + 1$ and go to step 3.
6. end

3 Numerical Simulation

The input parameters such as arrival time, departure time, initial state of charge and maximum charging rate of EVs are obtained from [5]. The residential demand profile of one day and dynamic electricity price which is utilized for evaluating charging cost of EVs is extracted from [7]. In this work, scheduling of EVs is carried out one by one. Total time of one day is partitioned into 1440 intervals. The results of four EV charging strategies are compared on the basis of average load, valley load, peak load, peak-valley difference, load factor and EV charging cost. Moreover, the impact on these parameters is analyzed for 20 EVs, 40 EVs, 60 EVs and 80 EVs, respectively. The parameters of base demand profile is depicted in Table 1 and the simulation results are summarized in Tables 2, 3, 4 and 5, respectively. The load profile of distribution grid with different charging strategies and for varying penetration of EVs is presented in Figs.1, 2, 3 and 4, respectively.

From results, it is observed that the average demand for any particular penetration of EVs remains same for all charging strategies. Further, as the penetration of EVs increase average demand increases. This is because higher number of EVs result in more EV's charging load that will be added to the base case load profile.

For MLVM, MLFM and VSCM, the load factor remains same for any particular penetration of EVs. It is because load factor is the ratio of average demand to peak demand and as only charging is considered, the peak demand in these three strategies remains same as that of base case. Also, increasing the number of EVs in the system increases average demand which consequently improvises load factor. In case of

Table 1 Load profile parameters in base case

Parameters	Value
Average load (kW)	134.88
Valley load (kW)	50.00
Peak load (kW)	258.00
Peak-valley difference (kW)	208.00
Load factor (%)	52.28

Table 2 Load profile parameters in MLVM

Number of EVs	20	40	60	80
Average load (kW)	137.55	141.28	144.40	148.49
Valley load (kW)	59.90	73.10	86.30	101.10
Peak load (kW)	258.00	258.00	258.00	258.00
Peak-valley difference (kW)	198.10	184.90	171.70	156.90
Load factor (%)	53.31	54.76	55.97	57.55
Charging cost (Rs)	29.23	70.17	103.90	147.88

Table 3 Load profile parameters in MLFM

Number of EVs	20	40	60	80
Average load (kW)	137.55	141.28	144.40	148.49
Valley load (kW)	52.37	60.07	66.67	69.97
Peak load (kW)	258.00	258.00	258.00	258.00
Peak-valley difference (kW)	205.63	197.93	191.33	188.03
Load factor (%)	53.31	54.76	55.97	57.55
Charging cost (Rs)	29.68	70.56	105.04	149.82

Table 4 Load profile parameters in VSCM

Number of EVs	20	40	60	80
Average load (kW)	137.55	141.28	144.40	148.49
Valley load (kW)	69.24	84.69	96.30	106.00
Peak load (kW)	258.00	258.00	258.00	258.00
Peak-valley difference (kW)	188.76	173.31	161.70	152.00
Load factor (%)	53.31	54.76	55.97	57.55
Charging cost (Rs)	28.08	68.45	102.43	147.45

Table 5 Load profile parameters in MCCM

Number of EVs	20	40	60	80
Average load (kW)	137.55	141.28	144.40	148.49
Valley load (kW)	56.94	69.04	69.38	74.94
Peak load (kW)	258.00	258.00	258.00	314.34
Peak-valley difference (kW)	201.06	188.96	188.62	239.40
Load factor (%)	53.31	54.76	55.97	47.24
Charging cost (Rs)	27.57	66.53	98.63	140.85

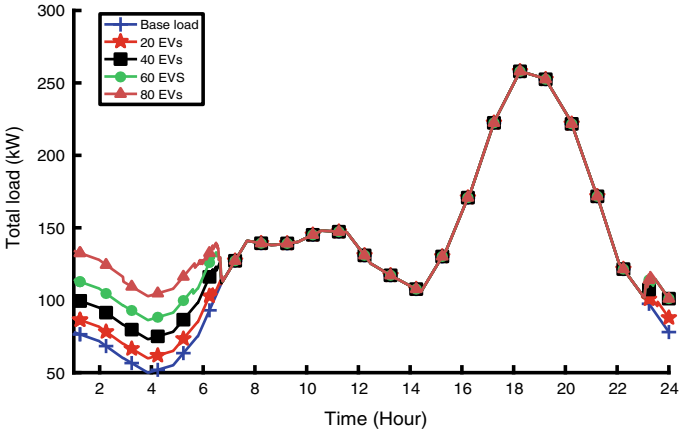

Fig. 1 Load profiles under MLVM

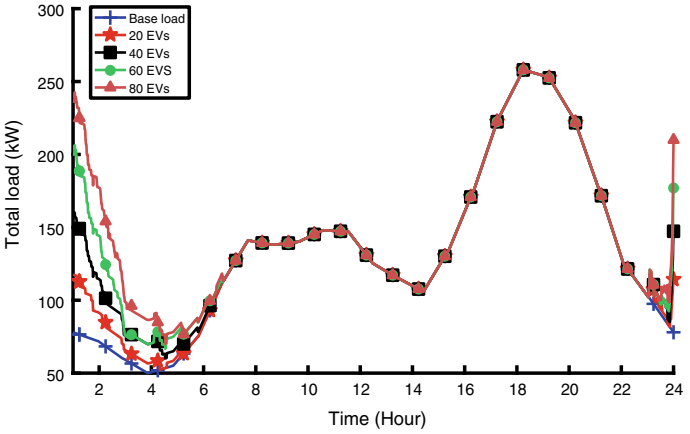

Fig. 2 Load profiles under MLFM

MCCM, the load factor is identical to other strategies for 20 EVs, 40 EVs and 60 EVs, respectively. Contrary, when a number of EVs are 80, the charging demand of EVs creates a new peak which is higher than original peak demand for MCCM. Due to increase in peak demand, the load factor when a number of EVs are 80 is less in MCCM as compared to other strategies. In case of MCCM, the peak demand when 80 EVs are present in the system is 21.83 % more as compared to peak demand of base case. It is important to note that MCCM creates a new peak demand because all EVs charges within a narrow time interval to minimize charging cost.

It is found that the maximum valley is filled in case of VSCM followed by MLVM. Similarly, the peak-valley different is minimum in case of VSCM. This is because VSCM specifically searches for valley period and then charges EVs to fill valley. For

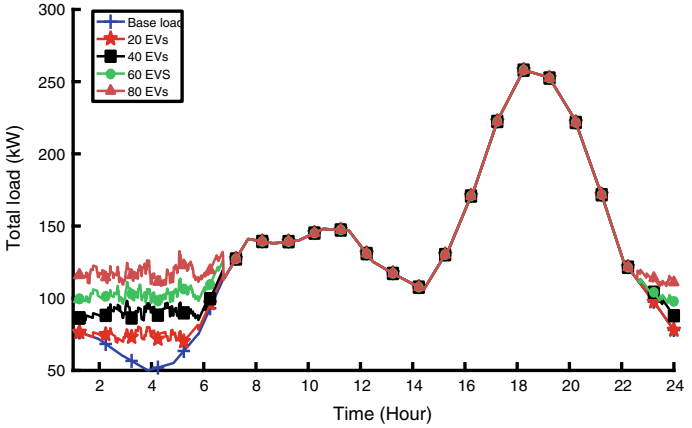

Fig. 3 Load profiles under VSCM

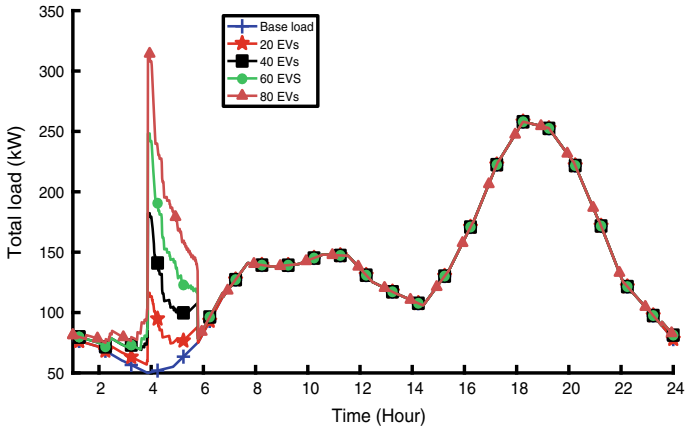

Fig. 4 Load profiles under MCCM

MLVM, MLFM and VSCM, the valley demand increases and peak-valley difference decreases as more number of EVs is added. But in case of MCCM, although valley is filled but peak-valley demand first decreases then increases as penetration of EVs increases. For example, the peak-valley demand continues to decreases as EVs are added from 20 to 60. But when a number of EVs are 80, the peak-valley difference increases. This is due to the introduction of new peak when higher number of EVs is present. It can also be seen from simulation results that MCCM results in minimum charging cost among all EV charging strategies. It is due to the design of fitness function in case of MCCM.

4 Conclusions

In this work, the impact of four different EV charging strategies, namely MLVM, MLFM, VSCM and MCCM on average demand, peak demand, valley demand, peak-valley difference and load factor on grid demand profile is investigated. Results show that the maximum valley filling is obtained in case of VSCM followed by MLVM. The valley filling for all strategies improvises on increasing the penetration of EVs. Moreover, MCCM results in minimum EV charging cost among all four strategies. In respect to future work, impact of these strategies can be examined on network losses and voltages by incorporating network constraints.

References

1. Crow, M.L., et al.: Economic scheduling of residential plug-in (hybrid) electric vehicle (phev) charging. Energies **7**(4), 1876–1898 (2014)
2. Leou, R.C.: Optimal charging/discharging control for electric vehicles considering power system constraints and operation costs. IEEE Trans. Power Syst. **31**(3), 1854–1860 (2015)
3. Mehta, R., Verma, P., Srinivasan, D., Yang, J.: Double-layered intelligent energy management for optimal integration of plug-in electric vehicles into distribution systems. Appl. Energy **233**, 146–155 (2019)
4. Mehta, R., Srinivasan, D., Khambadkone, A.M., Yang, J., Trivedi, A.: Smart charging strategies for optimal integration of plug-in electric vehicles within existing distribution system infrastructure. IEEE Trans. Smart Grid **9**(1), 299–312 (2016)
5. Rawat, T., Niazi, K.R., Gupta, N., Sharma, S.: Impact assessment of electric vehicle charging/discharging strategies on the operation management of grid accessible and remote microgrids. Int. J. Energy Res. **43**(15), 9034–9048 (2019)
6. Rawat, T., Niazi, K.R.: Comparison of EV smart charging strategies from multiple stakeholders' perception. J. Eng. **2017**(13), 1356–1361 (2017)
7. Rawat, T., Niazi, K.R.: Impact of EV charging/discharging strategies on the optimal operation of islanded microgrid. J. Eng. **2019**(18), 4819–4823 (2019)
8. Rawat, T., Niazi, K.: Coordinated charging of electric vehicles for reducing operation cost under tou electricity prices. In: 2018 20th National Power Systems Conference (NPSC), pp. 1–5. IEEE (2018)
9. Singh, J., Tiwari, R.: Cost benefit analysis for v2g implementation of electric vehicles in distribution system. IEEE Trans. Ind. Appl. 1 (2020)
10. Singh, J., Tiwari, R.: Multi-objective optimal scheduling of electric vehicles in distribution system. In: 2018 20th National Power Systems Conference (NPSC), pp. 1–6. IEEE (2018)
11. Singh, J., Tiwari, R.: Impact analysis of different charging models for optimal integration of plug-in electric vehicles in distribution system. J. Eng. **2019**(18), 4728–4733 (2019)
12. Singh, J., Tiwari, R.: Real power loss minimisation of smart grid with electric vehicles using distribution feeder reconfiguration. IET Gener. Transmiss. Distrib. **13**(18), 4249–4261 (2019)
13. Sortomme, E., Hindi, M.M., MacPherson, S.J., Venkata, S.: Coordinated charging of plug-in hybrid electric vehicles to minimize distribution system losses. IEEE Trans. Smart Grid **2**(1), 198–205 (2010)
14. Wu, T., Wu, G., Bao, Z., Yang, Q., Yan, W.: Demand dispatch of smart charging for plug-in electric vehicles. In: 2012 International Conference on Control Engineering and Communication Technology, pp. 803–806. IEEE (2012)

Islanding Detection Through Mean of Superimposed Voltage

Kanak Bhengra, Munna Kumar, and Jitendra Kumar

1 Introduction

In a microgrid, islanding detection is essential to ensure the security and effective performance of power system. Since a microgrid involves renewable energy sources as well as main utility grid, the power flow observed is from both the ends. So, whenever there is absence of main utility grid because of fault like situation, it is necessary to isolate the part of the microgrid to supply the local loads connected [1]. Therefore, it is required to identify islanding condition and isolate the distributed generators connected within the standard specified time as per IEEE STD 1547-2018 [2]. It is also required to prevent unintentional islanding as it may hazardous to the safety personnel and equipment. There should be appropriate distinction between islanding and non-islanding conditions.

Several passive, active, communication channel-based and hybrid techniques for islanding detection have been presented by researchers. Passive techniques determine islanding condition through comparison of system parameters: current THD, frequency, voltage, or system impedance with the set threshold. Though the passive techniques can be easily implemented, there is dependency on threshold. Lower threshold sometimes may lead to unnecessary tripping during non-islanding condition, whereas with higher threshold, islanding condition may not be traced. Over or under-voltage, over or under frequency [3], ROCOF, i.e., rate of change of frequency

K. Bhengra (✉) · M. Kumar · J. Kumar
EE Department, National Institute of Technology, Jamshedpur, Jamshedpur, Jharkhand 831014, India
e-mail: saumyakanak@gmail.com

M. Kumar
e-mail: 2019rsee004@nitjsr.ac.in

J. Kumar
e-mail: jitendra.ee@nitjsr.ac.in

O. H. Gupta and V. K. Sood (eds.), *Recent Advances in Power Systems*, Lecture Notes in Electrical Engineering 699, https://doi.org/10.1007/978-981-15-7994-3_29

[4], ROCOP, i.e., rate of change of power [5], and THD of current [6] are some passive techniques observed so far. Some active techniques are drift of active frequency [7], measurement of impedance [8], injection of current [9], and slip-mode frequency shift [10]. Active techniques determine islanding condition by varying system parameters intentionally through disturbing signal, thus deteriorating the power quality to some extent but having the advantage of lower non-detection zone. Communication techniques detect islanding through communication channels between grid and distributed generators. With high possibility of accuracy, the technique is costly.

A passive technique for islanding detection is proposed in this paper using the mean of Fourier transformed phase 'a' voltage at the desired location at the time of islanding. At the frequency of 1 kHz, three-phase voltage data are obtained. Mean of superimposed Fourier transformed phase 'a' voltage provides the accurate islanding detection.

2 Model Specification

The grid-connected microgrid model under consideration is presented in Fig. 1, which is modeled using MATLAB R2016a. Three PV-based distributed generators, 15 kW each, are connected through 0.380/25 kV transformers to a distribution system. Sampling frequency of the system is 1 kHz, and the system frequency is 50 Hz (Fig. 1).

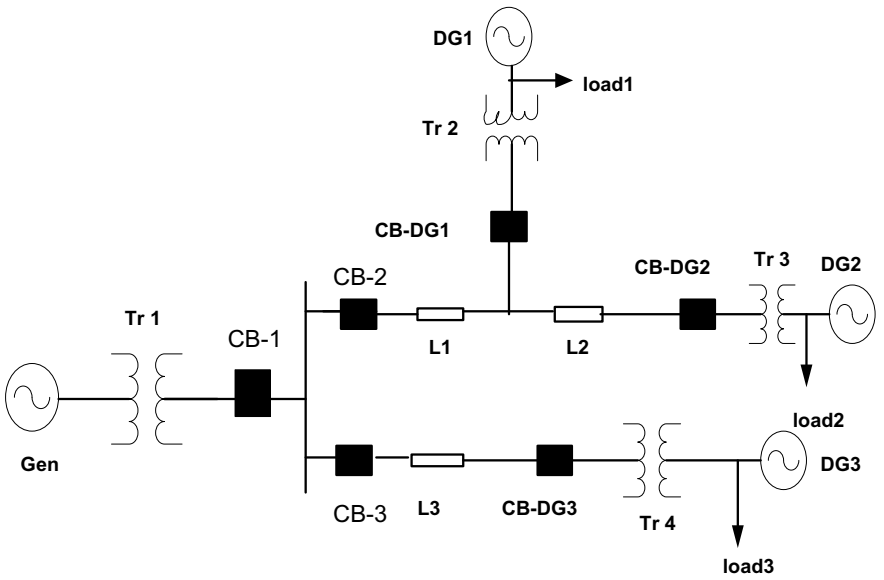

Fig. 1 Model for testing MSPV technique

3 Technique Proposed

The technique which is proposed in this paper uses phase 'a' voltage (or any phase voltage) to identify islanding condition. Superimposed component of Fourier transformed phase 'a' voltage through mean provides well-defined discrimination between islanding and non-islanding conditions. The necessary condition is checked at point of common coupling (PCC). Phase 'a' voltage is taken out from the three-phase voltage obtained. The Fourier transformation of phase a voltage is done. Superimposed component of phase 'a' provides the necessary islanding condition through its mean value.

Here, superimposed phase 'a' voltage is given as;

$$Va\mathbf{sup} = Va\mathbf{pos} - Va\mathbf{pre} \tag{1}$$

Through the mean of this superimposed phase 'a' voltage (MSPV), islanding condition is determined. The MSPV value becomes greater than zero during islanding condition, and this sufficiently distinguishes between islanding and non-islanding conditions. If MSPV remains greater than zero for 0.1 s, after 0.1 s of MSPV being greater than zero, trip signal is generated to isolate the remaining of system.

3.1 Algorithm for MSPV

The MSPV technique is implemented using the algorithm which is presented in Fig. 2. Out of three-phase voltage, phase a voltage is taken out at any desired location. After Fourier transformation, mean of superimposed component determines the islanding condition. If MSPV remains greater than zero for 0.1 s, the islanding condition is detected.

4 Results and Discussion

When there is 50% mismatch of active power (MAP), islanding condition is generated at 0.6 s, by opening the circuit breaker (CB1), the three-phase voltage is acquired at PCC. Phase 'a' voltage is taken out from the three-phase voltage. For non-islanding condition, MSPV becomes zero within 0.1 s from the non-islanding event, and for islanding, MSPV is nonzero throughout the simulation. The islanding detection is done as MSPV remains nonzero for 0.1 s. In Fig. 3, the performance analysis of MSPV technique at PCC is shown, and it is observed that at 0.6 s, when CB1 is tripped, MSPV became nonzero, and after 0.1 s trip signal is initiated. Islanding condition is detected at 0.7 s, and trip signal is initiated. Now the islanding event

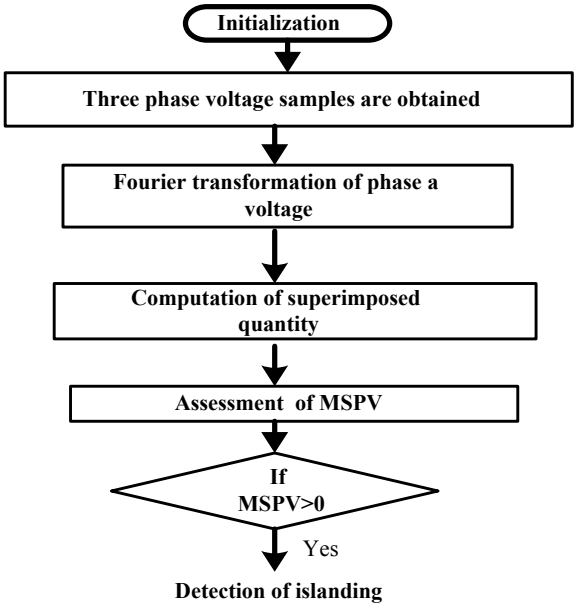

Fig. 2 Flow diagram for MSPV

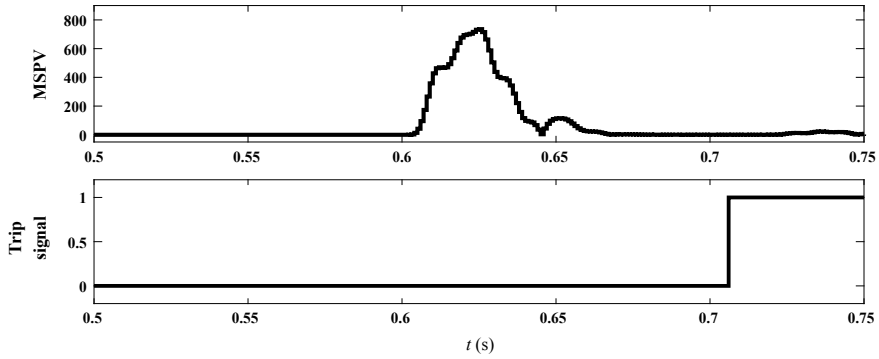

Fig. 3 MSPV technique of islanding at PCC with MAP of 50%

with 0% MAP is created by opening the CB1. The estimated MSPV at PCC where the islanding detection is done is shown in Fig. 4.

Capacitor switching which is a non-islanding event, when tested at PCC, there is no significant change, and it is observed that the MSPV remained zero throughout the testing period Fig. 5a.

A non-islanding condition, L-G fault, with high resistance (Ω) at PCC is initiated at 0.6 s, and it is found that trip signal is not generated because MSPV becomes zero within 0.1 s, Fig. 5b.

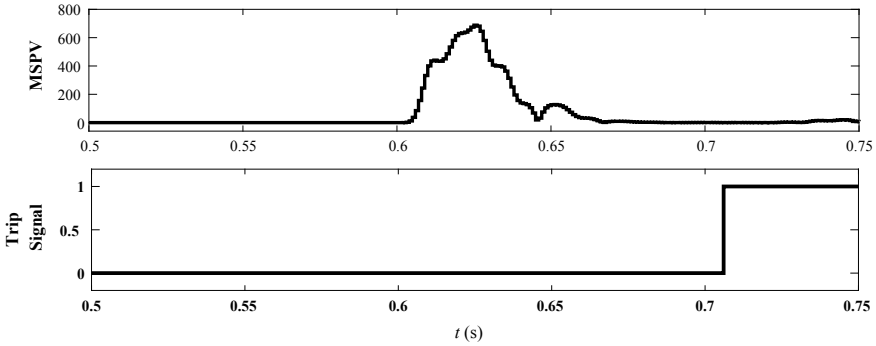

Fig. 4 MSPV technique of islanding at PCC with MAP of 0%

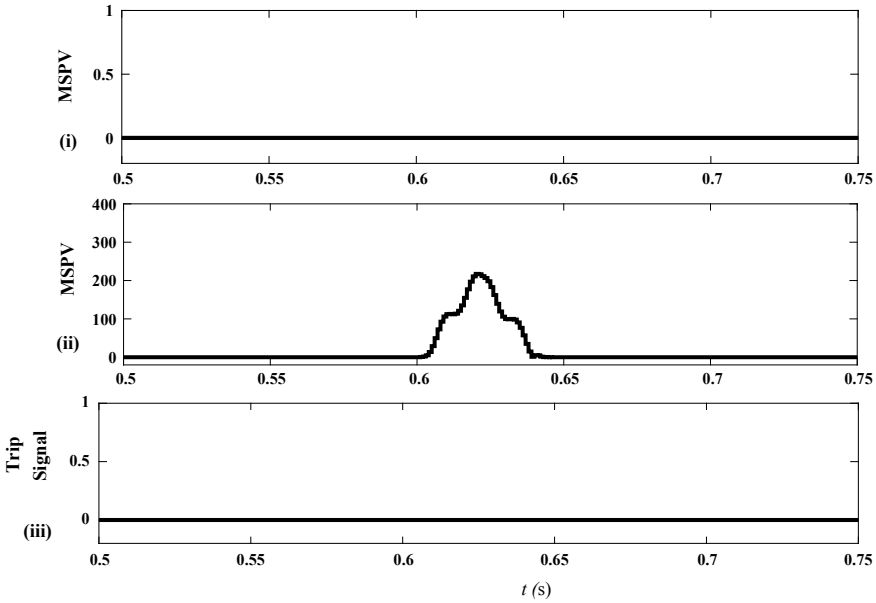

Fig. 5 MSPV technique of islanding during **a** capacitor switching at PCC, **b** L-G fault, **c** trip signal characteristic for mentioned non-islanding events

The trip signal for circuit breakers situated did not generate for any aforementioned non-islanding conditions. The behavior of circuit breakers during these non-islanding conditions can be observed from Fig. 5c which are closed throughout.

5 Comparative Study

For comparative study, an islanding detection based on active method is taken into account [11]. In the considered method, an alert signal (**As**) is generated to variate the system and determines islanding condition by measuring impedance. As it as an active method of detection, it lowers the power quality, and detection period taken is a bit more. MSPV technique can detect islanding without disturbing the power output. In Fig. 6, the comparison between the proposed technique and active method [11] is featured.

Islanding situation at 0.6 s is generated by tripping circuit breaker CB 1, and dV_{neg}/dt is calculated, Fig. 6a. When dVneg/dt crosses the set threshold, after 0.14 s, **As** is generated to inject the disturbing signal, Fig. 6b. Superimposed impedance ΔZ is calculated when there is injection of disturbing signal as shown in Fig. 6c. For islanding condition to be detected, it is checked if ΔZ remained greater than the set threshold for 0.1 s or not, if yes, then trip signal is generated to identify this islanding condition as shown in Fig. 6d. The total detection time taken by this method is almost 0.24 s after the islanding condition. However, if MSPV remains nonzero for 0.1 s, trip signal is generated and provides the correct information of islanding within 0.1 s. The proposed MSPV technique operates with the delay of only 0.1 s in an islanding condition, Fig. 6e, f.

As it is seen that active methods have nearly zero non-detection zone, the proposed MSPV technique also have almost zero of non-detection zone.

6 Conclusion

An islanding detection technique is presented based on mean of superimposed phase a voltage. The technique is fast and differentiates islanding and different non-islanding conditions well. The technique works satisfactorily even in 0% mismatch of active power. The technique is checked for different non-islanding conditions also- and it is observed that relay performs effectively without any unwanted tripping. There is a requirement of sensitive relay as during L-G fault, threshold zero plays significant character to identify this non-islanding condition.

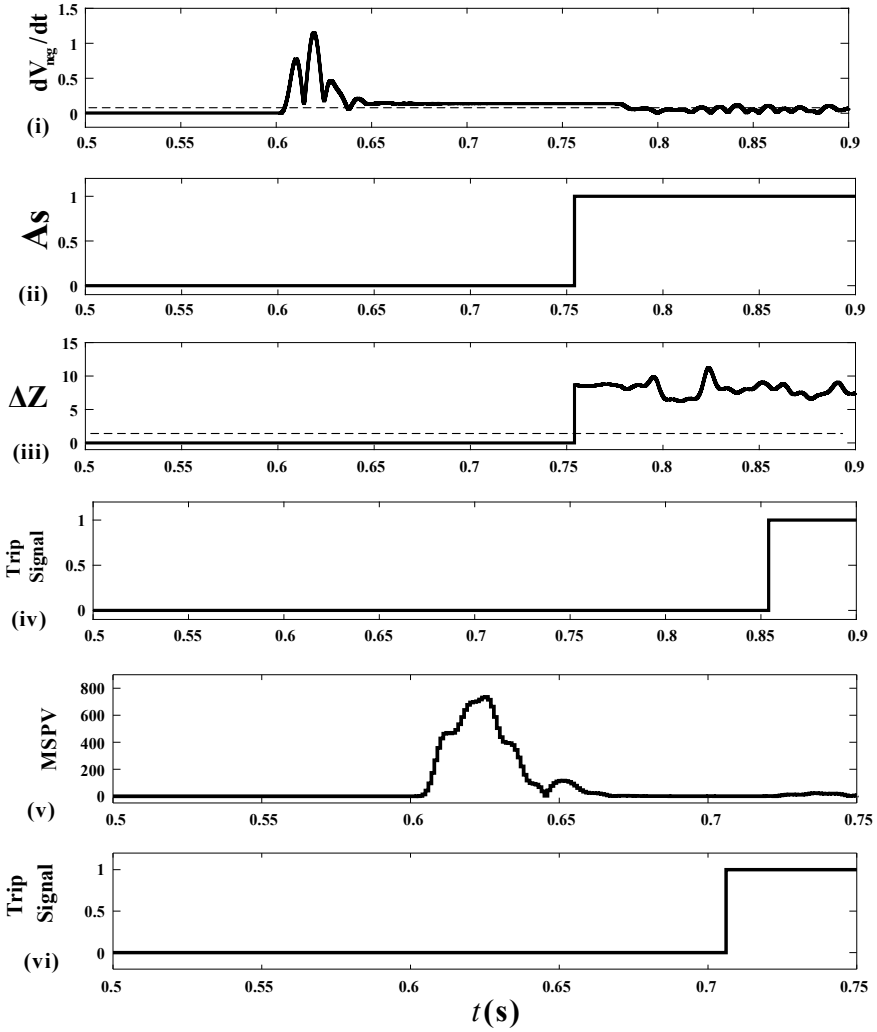

Fig. 6 Performances of technique [11] and MSPV during islanding **a** dV_{neg}/dt at PCC, **b As** generation at 0.14 s, **c** calculation of ΔZ after perturbation, **d** detection of islanding after 0.1 s, **e** MSPV technique of islanding, **f** islanding detection of islanding for MSPV

References

1. Zeineldin, H.H., Kirtley, J.L.: A simple technique for islanding detection with negligible nondetection zone. IEEE Trans. Power Delivery **24**(2), 779–786 (2009)
2. IEEE standard for interconnection and interoperability of distributed energy resources with associated electric power systems interfaces. In: IEEE Std, 1547-2018 (2018)
3. Zeineldin, H.H., Kirtley Jr., J.L.: Performance of the OVP/UVP and OFP/UFP method with voltage and frequency dependent loads. IEEE Trans. Power Delivery **24**(2), 772–778 (2009)

4. Chan, C.Y., Lau, T.K., Ng, S.K.: An impact study of ROCOF relays for islanding detection (2015)
5. Ropp, M.E., Begovic, M., Rohatgi, A., Kern, G.A., Bonn, R.H., Gonzalez, S.: Determining the relative effectiveness of islanding detection methods using phase criteria and nondetection zones. IEEE Trans. Energy Convers. **15**(3), 290–296 (2000)
6. Jang, S.I., Kim, K.H.: An islanding detection method for distributed generations using voltage unbalance and total harmonic distortion of current. IEEE Trans. Power Delivery **19**(2), 745–752 (2004)
7. Yafaoui, A., Wu, B., Kouro, S.: Improved active frequency drift anti-islanding detection method for grid connected photovoltaic systems. IEEE Trans. Power Electron. **27**(5), 2367–2375 (2011)
8. de Oliveira, R.R.S., Monteiro, H.M., Aleixo, R.R., Silva, L.R.M., Duque, C.A.: Islanding detection using impedance measurements techniques based on wavelet injection. In: 2017 Brazilian Power Electronics Conference (COBEP), pp. 1–5. IEEE (2017)
9. Lopes, L.A., Sun, H.: Performance assessment of active frequency drifting islanding detection methods. IEEE Trans. Energy Convers. **21**(1), 171–180 (2006)
10. Zeineldin, H.H., Salama, M.M.: Impact of load frequency dependence on the NDZ and performance of the SFS islanding detection method. IEEE Trans. Industr. Electron. **58**(1), 139–146 (2009)
11. Gupta, O.H., Tripathy, M., Sood, V.K.: Islanding detection scheme for converter-based DGs with nearly zero non-detectable zone. IET Gener. Transm. Distrib. **13**(23), 5365–5374 (2019)
12. Bashir, J., Jena, P., Pradhan, A.K.: Islanding detection of a distributed generation system using angle between negative sequence voltage and current. In: 2014 Eighteenth National Power Systems Conference (NPSC), pp. 1–5. IEEE (2014)

Application of Admittance-Based Relaying Scheme Under Dynamic Shunt Compensation

Jai Prakash Sharma, Shaili Shaw, and Om Hari Gupta

1 Introduction

Nowadays, in most parts of the world, power producers and power providers face the challenge of higher demand of power flow, reduced cost delivery of the power, and increase in reliability. There has also been a rise in alternative and renewable energy systems that has led to the rise in installation capacity of power production in the world. The continuous rise in the demand of electrical power has led to compound linkage among the power utilities to enhance the transferring of electrical power. Also due to strong economic and statutory policies, contriving the new TLs and expansion of old ones are becoming quite difficult day by day. Hence, the power systems are made to be operated close to their stability limits (including both transient and dynamic).

In these cases, the power system has greater chances of losing its stability even for minute interferences. To enhance the system stability, Flexible AC transmission systems (FACTS) are widely used to control power flow, voltage profile, and giving adequate damping of inter-area oscillations [1]. The most frequently used FACTS devices with respect to its application are the static VAR compensator (SVC).

SVC is a "primordial" FACTS device that uses thyristor as its controllers [2]. An SVC is high voltage system that maintains the system voltage effectively at its coupling point, to keep the system voltage invariant at its desired value. It is a shunt device that controls and compensates the reactive power flow with the help of a fixed

J. P. Sharma (✉) · S. Shaw · O. H. Gupta
National Institute of Technology, Jamshedpur, Jharkhand 831014, India
e-mail: 2018rsee010@nitjsr.ac.in

S. Shaw
e-mail: shailishaw1995@gmail.com

O. H. Gupta
e-mail: omhari.ee@nitjsr.ac.in

O. H. Gupta and V. K. Sood (eds.), *Recent Advances in Power Systems*, Lecture Notes in Electrical Engineering 699, https://doi.org/10.1007/978-981-15-7994-3_30

capacitor or thyristor-switched capacitor in combination with thyristor-controlled reactor [3].

The SVC injects VAr (inductively or capacitive) into the grid [4]. SVCs are used to control the phases of the voltages of the buses, the deviations in voltage(both negative and positive sequence), additional signal stabilizing, oscillation damping, and supplementary control.

Thus, SVCs are optimally tailored to suit wide range of requirements [5]:

- Increase in the grid reliability by assisting fault recovery and reducing the risk of blackouts.
- Improving the power factor by dynamically providing reactive power.
- Symmetrizing the unbalance between the phases.
- Reduces the flicker of large industrial consumers like electric arc furnaces.
- Helps the industrial customers to achieve more efficient operation by stabilizing the voltage that supplies the plant.

However, the conventional protective relays and fault locators for TL with SVC compensation can have some problems due to the control actions involved to control the SVC [6, 7]. The apparent line impedances measured by the traditional distance relays at the SVC location are contrived due to variation in voltage. When a one-phase fault occurs in a TL where SVC is used for compensation, the voltage of the system decreases. Hence, in order to achieve the reference value of the voltage value, SVC takes mitigating actions. This is how SVC injects the reactive current which is capacitive in nature which may cause mal-operation of protective scheme [8].

The influence of SVC on the operation of TLs distance relays and along with the impact of location variation of SVC is discussed [9]. In presence of SVC on a double circuit line, impedance measured at the relaying point; in the case of inter phase, LL fault and LLL faults are presented in [10]. A distance relay with zone setting tripping characteristics proposed in [11] for a varieties of fault along with load angle variation. In [12], optimization of power flow with the mid-point SVC is observed. The results in the paper [13] manifests that in presence of SVC, zero sequential component of the injected voltage is increasing during fault and may lead to relays under-reach during L-G fault.

A differential admittance (DA)-based relaying scheme for a fixed compensated TL has been proposed in [14]. The scheme shows promising performance. Since there is no discussion about its performance in presence of shunt compensation, the method proposed in [14] has been applied in this study for TLs with dynamic shunt compensation.

2 DA-Based Method

Consider a TL with mid-point compensation provided by SVC between two areas, i.e., Area-1 and Area-2 as shown in Fig. 1. Fault F_i is considered as internal fault while faults F_s and F_r are external faults. Admittance seen by Area-s and Area-r are

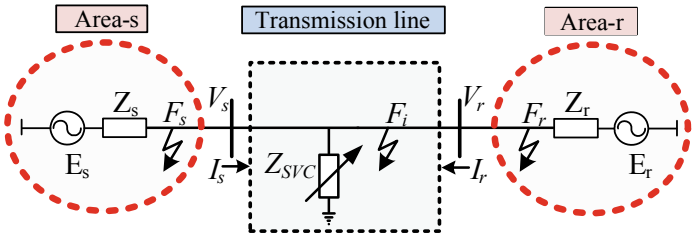

Fig. 1 Schematic diagram of a mid-point SVC compensated two area system

given in Eqs. (1) and (2), respectively.

$$Y_{\mathrm{sx}} = \frac{V_{\mathrm{sx}}}{I_{\mathrm{sx}}} \tag{1}$$

$$Y_{\mathrm{rx}} = \frac{V_{\mathrm{rx}}}{I_{\mathrm{rx}}} \tag{2}$$

where, x is a, b, and c for phase-a, b, and c, respectively, s and r denotes that parameter is measured at bus-s and r, respectively, Y_{sx} and Y_{rx} are the admittances of phase-x, V_{sx} and V_{rx} are the measured voltages of phase-x, and I_{sx} and I_{rx} are the measured currents of phase-x at bus-s and r, correspondingly.

Under normal operating condition (neglecting current through shunt parameters of the TL and current through SVC), absolute value of differential admittance as given by Eq. (3) of any phase is zero, i.e., $\mathrm{DA}_a = \mathrm{DA}_b = \mathrm{DA}_c = 0$, as $I_{\mathrm{sx}} = -I_{\mathrm{rx}}$ and $|V_{\mathrm{sx}}| = |V_{\mathrm{rx}}|$. However, practically, the differential admittances of all 3 phases are not equal to zero, as a portion of current I_{s} is flowing through shunt capacitance of TL and through SVC.

$$\mathrm{DA}_x = \left| \frac{I_{\mathrm{sx}}}{V_{\mathrm{sx}}} + \frac{I_{\mathrm{rx}}}{V_{\mathrm{rx}}} \right| \tag{3}$$

where DA_x = Differential admittance per phase.

During faulty condition, the value of differential admittance increases more significantly as compared to differential impedance across faulty phase/phases (its behavior is just opposite to differential impedance) as current in the system increases in presence of fault. Hence with proper selected threshold value, internal fault detection and classification can be achieved in presence of SVC in the system.

2.1 Relaying Criterion

At first, current and voltage data are acquired from both ends and per phase admittance has been calculated by using (1) and (2). DA is calculated by using (3). After that, per

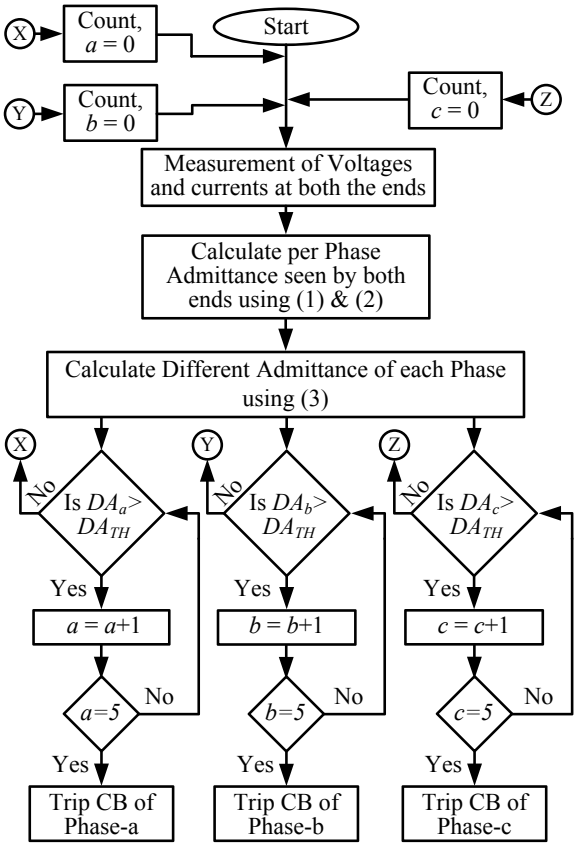

Fig. 2 Flowchart of DA-based scheme

phase DA is compared with threshold (DA_{TH}), if $DA > DA_{TH}$, then count is increased by one. If count ≥ 5, then the phase corresponding to that count declared as faulty phase and circuit breaker (CB) of the phase is tripped else count reset to zero and whole process starts again as manifested in Fig. 2. Count *a*, *b*, and *c* are assigned to phase *a*, *b*, and *c*, respectively.

2.2 Threshold Selection

On the basis of rigorous simulation studies, the threshold for the proposed scheme has been selected as $DA_{TH} = 0.02$ (mho), in order to make algorithm valid for the fault detection and classification.

3 Result

The response of the proposed scheme has been investigated on a 4-bus, 400 kV, 50 Hz test system model with mid-point 100/167 MVAr SVC compensation in Line-2 as manifested in Fig. 3. The system is simulated in PSCAD/EMTDC software in order to acquire data for algorithm. Line-1, Line-2, and Line-3 is 300 km, 400 km, and 300 km long in length ,respectively. F_1 and F_4 are external fault while F_2 and F_3 are internal fault locations correspondingly. With 1 kHz sampling frequency, the relaying algorithm is developed in MATLAB domain. The proposed method is investigated for different types of fault with different fault location (F_L) and fault resistance (R_f), different inception angle, cross-country fault, evolving fault, and high resistance fault. The acquired results of aforementioned scenarios are discussed next.

3.1 Investigation Under Various Types of Fault with Different $\mathbf{F_L}$ *and* $\mathbf{R_f}$

Various types of faults are introduced at 2.6 s with different F_L and R_f and corresponding acquired results are listed in Table 1. Figure 4a manifests per phase DA during AB-G fault and it can be observed that only DA_a and DA_b have crossed threshold and phase *a* and *b* are identified as faulty phase for an internal fault. In case of an external B-G fault at 00 km (F_1) from end-s, it can be perceived from Fig. 4b that neither of DA_a, DA_b nor DA_c have crossed threshold and B-G fault is detected as an external fault, the proposed scheme found to be selective.

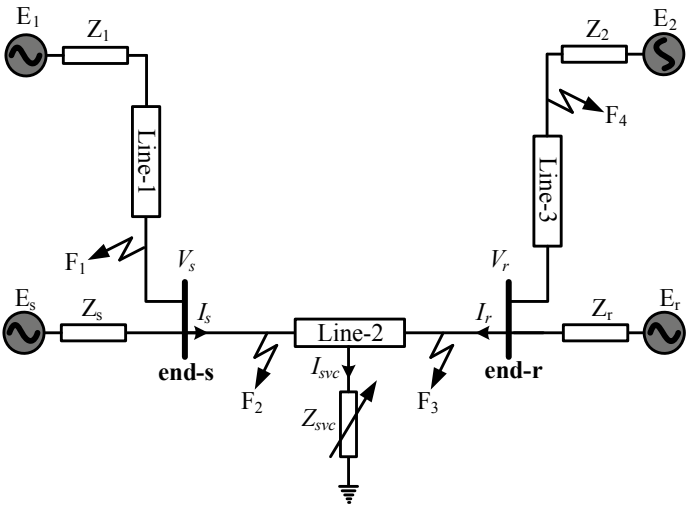

Fig. 3 Schematic diagram of a mid-point SVC compensated system

Table 1 Acquired result for various fault types with different F_L and R_f

Fault type	Distance from end-s (in km)	R_f (Ω)	DA$_a$ (mho)	DA$_b$ (mho)	DA$_c$ (mho)	Detection time (ms)		
						T_a	T_b	T_c
BC	00 (F_2)	10	–	0.039	0.039	–	8	8
A-G	00 (F_2)	25	0.020	–	–	8	–	–
ABC	100 (F_2)	0.01	0.049	0.029	0.049	13	13	17
C-G	200 (F_2)	10	–	–	0.029	–	–	25
CA	200 (F_2)	5	0.028	–	0.028	17	–	17
AB-G	300 (F_3)	25	0.027	0.027	–	22	21	–
BC-G	300 (F_3)	15	–	0.029	0.026	–	20	20
CA	400 (F_3)	5	0.097	0.097	0.153	8	–	8
A-G	400 (F_3)	10	0.050	–	–	11	–	–
B-G	−00 (F_1)	0.01	–	–	–	–	–	–
BC	−00 (F_1)	10	–	–	–	–	–	–
C-G	−00 (F_1)	00	–	–	–	–	–	–
ABC	700 (F_4)	0.01	–	–	–	–	–	–
A-G	700 (F_4)	00	–	–	–	–	–	–

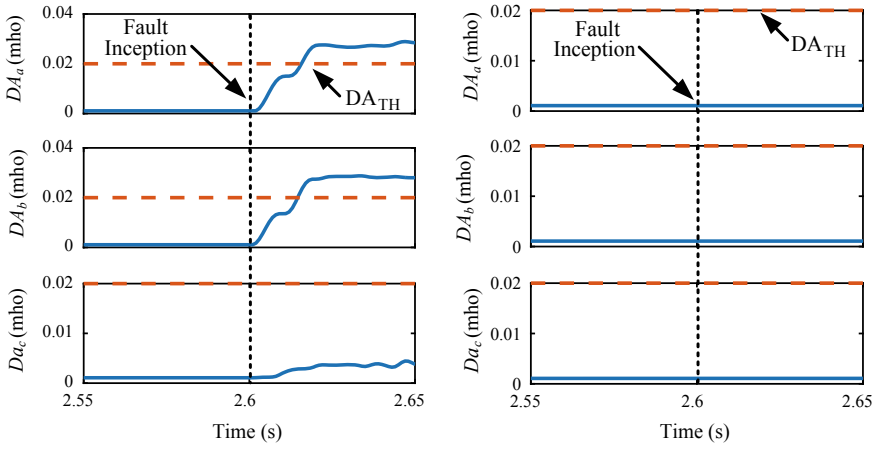

Fig. 4 Per phase DA for **a** an AB-G fault with $R_f = 25$ Ω at 300 km (F_3) and **b** an external B-G fault with $R_f = 0.01$ Ω at 00 km (F_1) from end-s, respectively

3.2 Investigation Under Different Inception Angles

An internal A-G fault with $R_f = 10\Omega$ is introduced at 300 km (F_3) from end-s with inception angle varied in range of 0°–360° with step size of 45° (i.e., fault inception time is varied in range of 2.6–2.8 s with step size of 0.0025 s) and corresponding responses are recorded in Table 2. It can be perceived that there is negligible effect of variation of inception angle on the proposed scheme. Figure 5a manifests per phase DA for A-G fault with 180° of inception angle.

Table 2 Results for different inception angles

Inception angle (°)	DA_a (mho)	DA_b (mho)	DA_c (mho)	Detection time (ms)		
				T_a	T_b	T_c
45	0.026	–	–	22.5	–	–
90	0.023	–	–	23	–	–
135	0.279	–	–	26.5	–	–
180	0.028	–	–	24	–	–
225	0.026	–	–	22.5	–	–
270	0.023	–	–	23	–	–
315	0.027	–	–	26.5	–	–
0	0.028	–	–	24	–	–

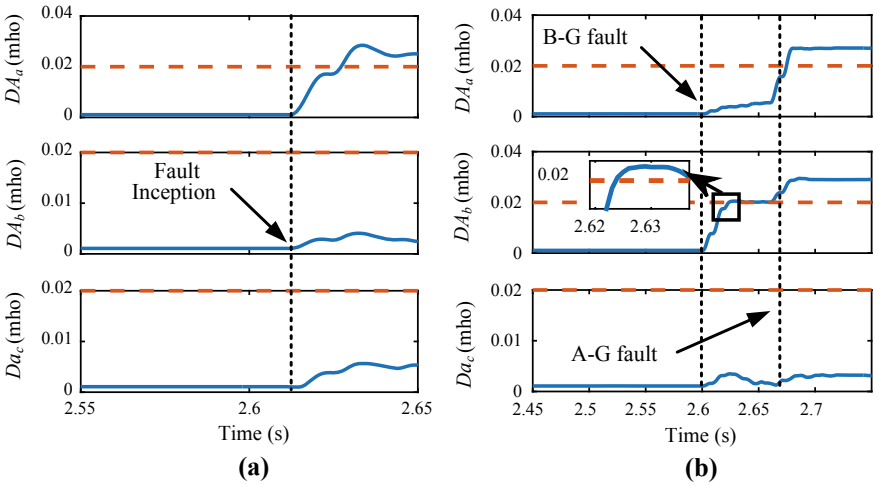

Fig. 5 Per phase DA for **a** an A-G fault with 180° of inception angle and **b** evolving fault

3.3 Investigation Under Evolving Fault

When the number of phase/phases involved in a fault changes with time, such type of fault is termed as evolving fault as per [15] and may create vagueness in relaying operation. To have an evolving fault, a B-G fault is introduced at 2.6 s and after 0.06 s, an A-G fault is incepted at the same location, i.e., at 100 km (F_2) from end-s with R_f = 25 Ω and corresponding result is manifested in Fig. 5b. It can be perceived from Fig. 5b, DA_a and DA_b have crossed threshold after the fault inception. Hence, the proposed scheme remains selective in case of evolving fault except in case of bolted fault.

3.4 Investigation Under Cross-Country Faults

Cross-country fault is defined as the situation of having two different faults affecting different phases at different line location at the same time. In order to have cross-country fault, a C-G fault at 00 km (F_2) and a B-G fault at 300 km (F_3) from end-s, respectively, are applied. Figure 6a portraits 3-phase DA for cross-country fault.

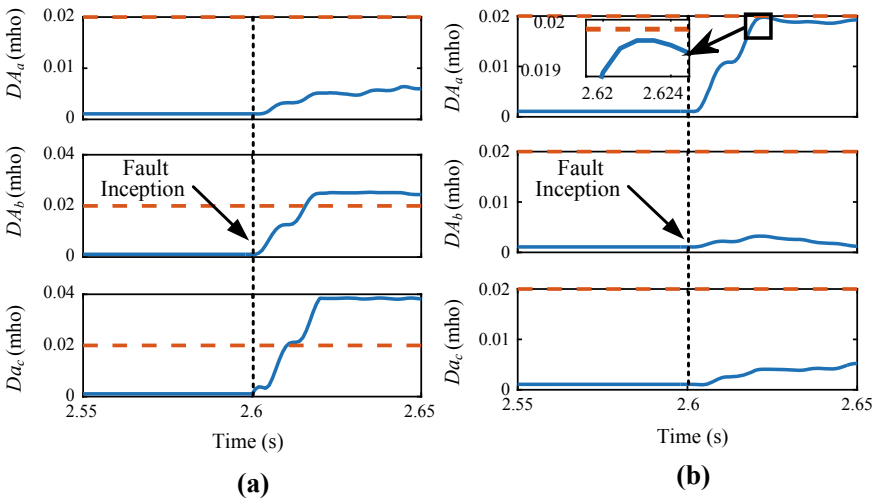

Fig. 6 Per phase DA for **a** a cross-country fault and **b** an A-G fault at 300 km (F_3) with $R_f = 30$ Ω

3.5 Investigation Under High Fault Resistance

With SVC in TL, the proposed scheme effectively performs for faults below 30 Ω fault resistance. Above 30 Ω, the impact of SVC variations create nuisance and since with increase in R_f, the current through fault decreases, with SVC voltage remains constant due to which overall admittance decreased below DA_{TH} and this may cause inaction of DA method in case of an internal fault. At 300 km (F_3) from end-s with $R_F = 30$ Ω, an A-G fault is incepted and acquired result is manifested in Fig. 6b.

4 Conclusion

The application of differential admittance-based relaying scheme under dynamic shunt compensation is included. A 4-bus, 400 kV, 50 Hz test system has been used with 100/167 MVAr SVC compensation in Line-2. DA-based scheme is tested against various types of fault with different F_L and R_f, variation in inception angle, evolving fault, cross-country fault, and high resistance fault. Based on the investigation, it is found that the scheme is selective, accurate, and fast in operation; however, SVC may cause inaction of DA method in case of high fault resistance.

References

1. Hoseynpoor, M., Najafi, M., Ebrahimi, R., Davoodi, M.: Power system stability improvement using comprehensive FACTS devices. Int. Rev. Model. Simul. **4**(4), 1660–1665 (2011)
2. Kumari, R.: Brief study on TSCS, SSSC, SVC Facts, pp. 7053–7060 (2016)
3. Noroozian, M., Petersson, Å.N., Thorvaldson, B., Nilsson, B.A., Taylor, C.W.: Benefits of SVC and STATCOM for electric utility application. In: Proceedings of IEEE Power Engineering Society Transmission and Distribution Conference, vol. 3, pp. 1143–1150 (2003)
4. Suyono, H., Hasanah, R.N., Astuti, K.N.: Optimization of the reactive power injection to control voltage profile by using artificial bee colony algorithm. In: Proceeding—2016 International Seminar on Sensors, Instrumentation, Measurement and Metrology (ISSIMM 2016), pp. 18–23 (2017)
5. Szabo, D., Regul'A, M., Bodnar, R., Altus, J.: Control of a SVC for power factor correction. In: 10th International Conference on ELEKTRO 2014, pp. 379–382 (2014)
6. Abedi, E., Aakarian Abyaneh, H., Asgari, R., Sadeghi, S., Shafiee, M.: Analysis of the SVC impact on distance relays performance. In: INTELEC, International Telecommunications Energy Conference (Proceedings) (2009)
7. Zellagui, M., Chaghi, A.: Impact of SVC devices on distance protection setting zones in 400 kV transmission line. UPB Sci. Bull. Ser. C Electr. Eng. **75**(2), 249–262 (2013)
8. Ghorbani, A., Khederzadeh, M., Mozafari, B.: Impact of SVC on the protection of transmission lines. Int. J. Electr. Power Energy Syst. **42**(1), 702–709 (2012)
9. Khederzadeh, M., Ghorbani, A.: Impact of VSC-based multiline FACTS controllers on distance protection of transmission lines. IEEE Trans. Power Deliv. **27**(1), 32–39 (2012)
10. Kazemi, A., Jamali, S., Shateri, H.: Measured impedance by distance relay in presence of SVC on transmission line. In: IECON Proceedings (Industrial Electronics Conference), pp. 2214–2219 (2006)

11. Khoa, N., Tung, D.: Locating fault on transmission line with static var compensator based on phasor measurement unit. Energies **11**(9), 2380 (2018)
12. Behera, S., Raja, P., Moorthi, S.: Modelling and simulation of the impact of SVC on existing distance relay for transmission line protection. In: 2015 International Conference on Condition Assessment Techniques in Electrical Systems, CATCON 2015—Proceedings, pp. 151–156 (2016)
13. Khoa, N.M., Hieu, N.H., Viet, D.T.: A study of SVC's impact simulation and analysis for distance protection relay on transmission lines. Int. J. Electr. Comput. Eng. **7**(4), 1686–1695 (2017)
14. Khadke, P., Patne, N., Singh, A., Shinde, G.: Pilot relaying scheme based on differential admittance concept for FSC-compensated EHV transmission line. Iran. J. Sci. Technol. Trans. Electr. Eng. **3** (2019)
15. Jiao, X., Liao, Y.: Accurate location of evolving faults on transmission lines using sparse wide area measurements. Int. J. Emerg. Electr. Power Syst. **19**(1), 1–11 (2018)

Wind Potential Assessment for Micropower Generation in Tropical Wet Climate of India

Santoshkumar Hampannavar, K. N. Patil, Swapna Manasani, R. Yaragatti Udaykumar, Rajashekar P. Mandi, and C. Nandakumar

1 Introduction

Large carbon emissions, serious environment concerns and depleting fossil fuels have promoted the concept of generation of power using green and renewable energy sources. Photovoltaics (PV) and wind energy are preferred sources of renewable energy as they are freely available in nature. India is ranked at fifth position globally for overall installed renewable energy capacity and shares 23.39% of the total installed generation capacity, i.e. 368.98 GW up to end of February 2020. India is working on world's largest renewable energy expansion programme of 175 GW by 2022 (Source: MNRE, India) [1]. Wind is a prominent player in renewable energy generation and wind speed assessment provides the information of amount of energy which can be extracted form from wind. Figure 1 shows geographical location of Goa wind site located at latitude of 15.2993° N and longitude of 74.1240° E in Indian state of Goa.

Due to intermittent and stochastic nature of wind, speed and energy potential are assessed using statistical distribution functions. In this paper, Rayleigh and Weibull distribution were used for wind speed assessment. The wind rose diagram was plotted for one complete TMY year data to portrait wind velocity and direction [2–7]. The

S. Hampannavar (✉) · R. P. Mandi
REVA University, Bengaluru 560064, India
e-mail: santoshkumar.sh@ieee.org

K. N. Patil · C. Nandakumar
SDM College of Engineering and Technology, Dharwad 580002, India

S. Manasani
National Institute of Technology, Silchar 788010, India

R. Y. Udaykumar
Malaviya National Institute of Technology, Jaipur 302017, India

O. H. Gupta and V. K. Sood (eds.), *Recent Advances in Power Systems*, Lecture Notes in Electrical Engineering 699, https://doi.org/10.1007/978-981-15-7994-3_31

Fig. 1 Geographical location of Goa wind site. *Source:* 2014 Encylopedia Britannica Inc

study was carried out using real-time data obtained from a wind site that helps in future expansion of wind system in a specific location.

2 Statistical Models for Wind Speed

To describe the wind speed distributions, many probability density functions (PDF) have been used such as beta, gamma, lognormal, Rayleigh and Weibull functions. Rayleigh and Weibull models are widely accepted according to the literature studies. Weibull function is preferred due to its flexibility in terms of shape factor and scale factor but suffers from the problem that cannot be used for calm wind speeds [8].

Two parameters of Weibull probability density function (PDF) are given by

$$f(v) = \frac{k}{c}\left(\frac{v}{c}\right)^{k-1} \mathrm{e}^{-\left(\frac{v}{c}\right)^{k}} \tag{1}$$

Weibull cumulative distribution function (CDF) is given by

$$F(v) = \int_{0}^{v} f(v)\,\mathrm{d}v = 1 - \mathrm{e}^{-\left(\frac{v}{c}\right)^{k}} \tag{2}$$

where v is the wind speed, k is shape parameter and c is scale parameter [9–19]. The value of the shape factor relates it to other probability distribution function, i.e. if $k = 2$, it becomes Rayleigh distribution.

Rayleigh PDF is given by

$$f(v) = \frac{\pi}{2}\left(\frac{v}{v_m^2}\right) \mathrm{e}^{-\left(\frac{\pi}{4}\left(\frac{v}{v_m}\right)^2\right)} \tag{3}$$

where v_m is mean wind speed.

Rayleigh CDF is given by

$$F(v) = 1 - \mathrm{e}^{\left(-\frac{\pi}{4}\left(\frac{v}{v_m}\right)^2\right)} \tag{4}$$

Energy pattern factor method (EPF) is used to determine the Weibull distribution parameters. Monthly mean power density (MMD) is given by

$$P = 0.5A\rho \sum_{i=0}^{n} \frac{v_i^3}{n} \tag{5}$$

$$\mathrm{MMD} = \frac{P}{A} = 0.5\rho \sum_{i=0}^{n} \frac{v_i^3}{n} \tag{6}$$

where A is swept area, v_i is wind speed in the sample measured at instant i, n is total days in the month and ρ is air density.

Energy pattern factor is given by

$$\mathrm{EPF} = \frac{\sum_1^n \frac{v_i^3}{n}}{\left(\sum_1^n \frac{v_i}{n}\right)^3} = \frac{\left(\frac{\mathrm{MMD}}{0.5\rho}\right)}{v_m^3} \tag{7}$$

According to the shape factor, Weibull distribution is described as

$$k = 1 + \frac{3.69}{\mathrm{EPF}^2} \tag{8}$$

The scaling factor is given as

$$c = \frac{v_m}{\Gamma\left(1 + \frac{1}{a}\right)} \tag{9}$$

For gamma function

$$\Gamma(k) = \int_0^\infty x^{k-1} \mathrm{e}^{-x} \mathrm{d}x \quad \text{and} \quad \Gamma(1+k) = k\,\Gamma(k) \tag{10}$$

Weibull power density is given by

$$\begin{aligned} \frac{P_{\text{Weibull}}}{A} &= 0.5\rho v_m^3 = 0.5\rho\left(c\Gamma(1+\frac{1}{k})\right)^3 \\ &= 0.5\rho c^3 \Gamma\left(1+\frac{3}{k}\right) \end{aligned} \tag{11}$$

Rayleigh power density is given by

$$\frac{P_{\text{R}}}{A} = \frac{3}{\pi}\rho v_m^3 = \frac{3}{\pi}\rho c^3 \tag{12}$$

3 Methodology

Real-time wind speed samples were collected for one complete year at 10 m height from Goa wind site. The site is located at latitude of 15.2993° N and longitude of 74.1240° E of Indian state GOA. Samples were collected every 10 min, and a total of 144 samples were obtained for one day. Daily and monthly mean wind speed were calculated for one year. Figure 2 shows the daily mean wind speed for complete one year.

4 Results and Discussion

The calculated monthly mean wind speed and Weibull distribution parameters were tabulated in Table 1. The mean wind speed was highest in the month of July, i.e. 3.5974 m/s, and lowest of 1.7020 m/s in November. The parameters determined using EPF for Weibull were tabulated in Table 1. For some months, the scale factor is greater than the shape factor and is nearly equal to the mean wind speed. It is inferred from Table 1 that most probable wind speed (V_{probp}) is less than the mean

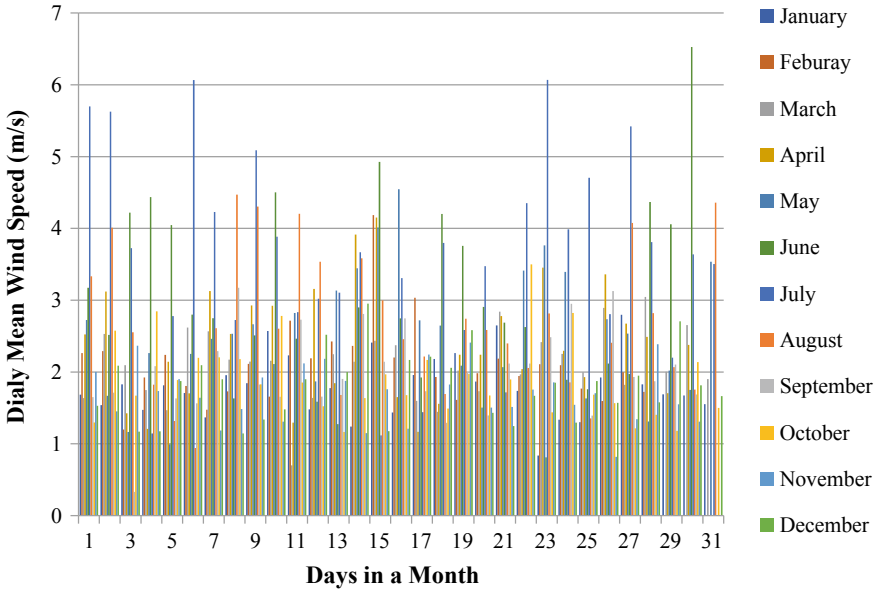

Fig. 2 Daily mean wind speed for complete one year

speed, whereas the wind speed carrying maximum power (V_{max}) is greater than the mean wind speed. It implies that there is a possibility of capturing more wind power than the calculated mean value.

These parameters in combination to the required gamma functions were used to compute the wind power densities , maximum wind speed, Weibull and Rayleigh models as shown in Table 2. For the month of July, wind speed was grouped into bins as shown in Table 3. Mean wind speed, frequency of each speed and corresponding probability distribution are also listed. The total monthly power density was 39.2712 W/m^2.

PDFs of Weibull and Rayleigh are shown in Figs. 3 and 4, respectively. Weibull PDF portraits that the mean speed is shifted to the right side, whereas in case of Rayleigh PDF mean is centred around or above monthly wind speed.

Weibull and Rayleigh CDF are plotted, and it is interesting to note that the mean wind speed was greater than the calculated as shown in Figs. 5 and 6, respectively. Wind power densities using different models are tabulated in Table 3 which are crucial to define the feasibility of a wind site. Rayleigh model is found to be superior as compared to the Weibull model in terms of mean power and power density. Goa site produces 59.77 W/m^2, 45.13 W/m^2 and 39.27 W/m^2 maximum, Rayleigh and mean power densities for the month of July, respectively (multiplying by 2). The average power densities are 13.74 and 10.43 W/m^2 for Rayleigh and Weibull models. Wind rose diagram is plotted for typical meteorological year (TMY) data in Fig. 7 and it shows that the wind blows above the velocity of 8 m/s in east and north-east, in

Table 1 Monthly mean wind speeds and Weibull distribution function for one year

Parameters	January	February	March	April	May	June	July	August	September	October	November	December
Mean wind speed (m/s)	1.804906	2.098289	2.105309	2.398333	2.508804	3.003056	3.597446	2.697581	2.00326393	1.901277	1.702013909	1.8063172
Energy pattern factor	1.174967	1.237161	1.1538	1.323799	1.352931	1.564223	1.419188	1.398983	1.26445325	1.268152	1.160351417	1.2092646
Shape factor	3.672852	3.410872	3.771822	3.10563	3.015927	2.508097	2.832088	2.88539	3.30792033	3.294477	3.740610342	3.5233859
Scale factor	1.878104	2.200044	2.184574	2.537819	2.662009	3.236072	3.838767	2.873821	2.10684988	2.000394	1.767644509	1.8876757
V_{probp} (m/s)	1.722419	1.987246	2.013247	2.23933	2.329175	2.642028	3.291545	2.479772	1.88961363	1.792375	1.626593817	1.7170401
V_{max} (m/s)	2.114089	2.518751	2.445409	2.978375	3.151114	4.088358	4.63575	3.449208	2.43062366	2.310232	1.982091067	2.1445761
x	1.816804	1.879541	1.795372	1.965987	1.994719	2.196126	2.059289	2.039721	1.90691422	1.910615	1.802008155	1.8514537
$\Gamma(1+3/a)$ or $\Gamma(x)$	0.935952	0.954921	0.930163	0.986093	0.997779	1.099486	1.026532	1.017448	0.96415316	0.965446	0.931918345	0.9460535

Table 2 Monthly mean wind speedsand Weibull distribution function for one year

Bins	V_i	V_{mni} (m/s)	Freq.	f (vi)	$f_{Weibull}$ (vi)	$f_{Rayleigh}$ (vi)	P/A (W/m)
	0–1	0	0	0	0	0	0
	1–2	1.354166689	4	0.129032258	0.158232087	0.194953419	0.192249813
	2–3	2.654861159	6	0.193548387	0.2946451	0.246689344	2.173032633
	3–4	3.576909789	12	0.387096774	0.260927279	0.205156785	10.62905769
	4–5	4.428472306	3	0.096774194	0.164450461	0.143299079	5.04281006
	5–6	5.457812584	4	0.129032258	0.06025992	0.075148831	12.58651225
	6–7	6.067708453	2	0.064516129	0.026217386	0.046301902	8.647561668
	Sum		31	1	0.9647322	0.9115494	39.271224

south-west it blows more than 4 m/s. In east and north-east, 25% of the wind blows above 8 m/s [20–22].

5 Conclusion

In this paper, wind speed potential assessment of Goa wind site located in Indian state using statistical distribution functions such as Weibull and Rayleigh is presented found that the Rayleigh model is most appropriate for the Goa wind site. The average power densities obtained were 13.74 W/m^2 and 10.43 W/m^2 for Rayleigh and Weibull models respectively. Also, the wind rose diagram was plotted which demonstrated that the maximum wind blows in east and north-east direction with a velocity of more than 8 m/s. This study helps to estimate and assess the amount of power which can be extracted from the respective wind site.

Table 3 One year wind power densities (W/m^2)

Parameters	January	February	March	April	May	June	July	August	September	October	November	December
Mean power density (W/m^2)	3.997021	6.737873	6.249781	10.65299	12.55101	25.11123	39.27122	16.25825	5.87207247	4.997937	3.295452332	3.996563
Most probable wind power density (W/m^2)	3.06597	4.708756	4.89601	6.737607	7.581545	11.06531	21.3969	9.149275	4.04827764	3.454919	2.582192417	3.037334
Maximum power density (W/m^2)	5.669191	9.587532	8.774169	15.85219	18.77343	41.00135	59.77387	24.6212	8.61597468	7.398062	4.672206865	5.918009
$P_{Weibull}/A$ (W/m^2)	3.720177	6.101162	5.8185	9.670548	11.29313	22.35609	34.84167	14.48915	5.41000982	4.636883	3.088260289	3.818116
$P_{Rayleigh}/A$ (W/m^2)	5.286212	8.497275	8.319288	13.0427	15.0527	27.0421	45.13993	18.93935	7.46253602	6.387522	4.407278053	5.367448

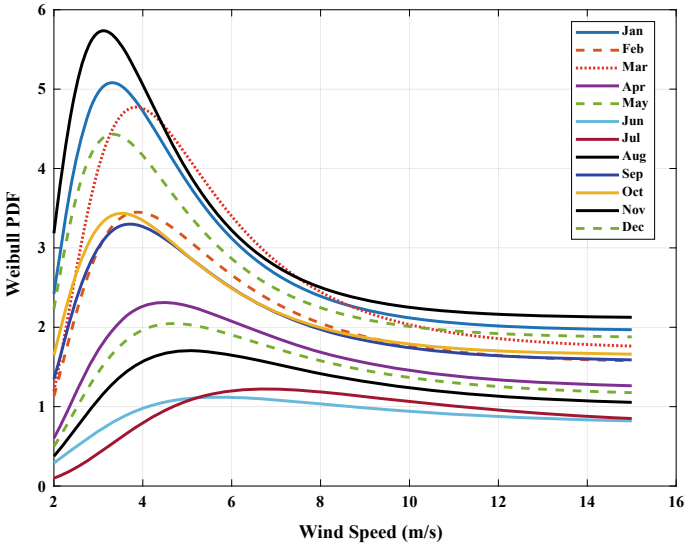

Fig. 3 Weibull PDF for one year

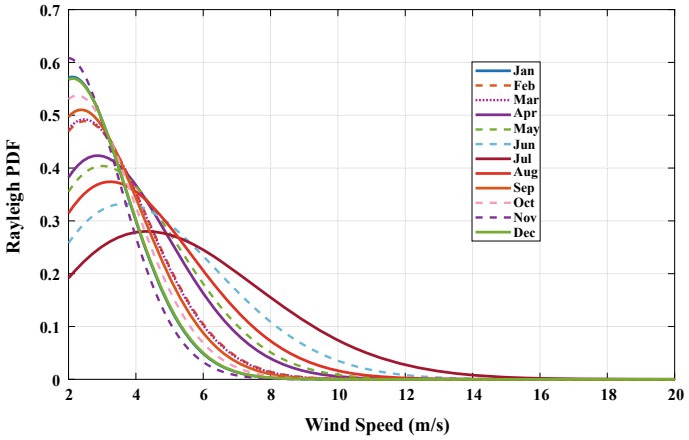

Fig. 4 Rayleigh PDF for one year

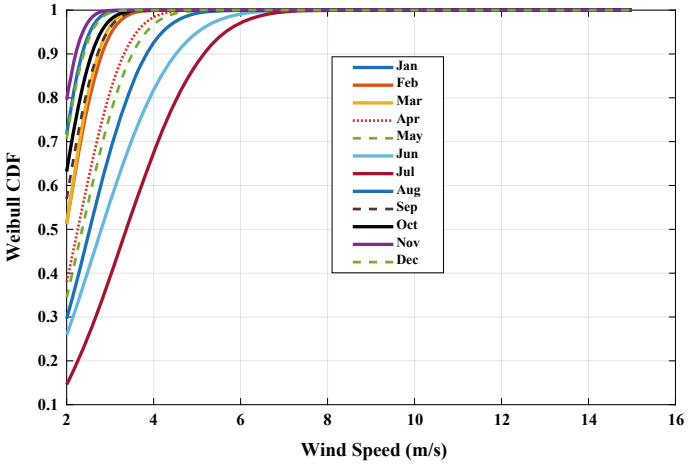

Fig. 5 Weibull CDF for one year

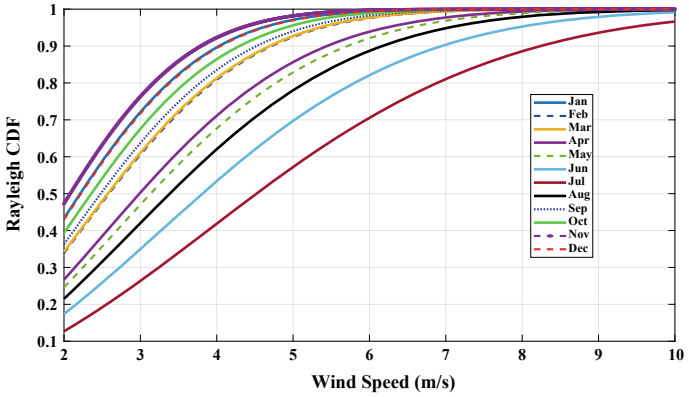

Fig. 6 Rayleigh CDF for one year

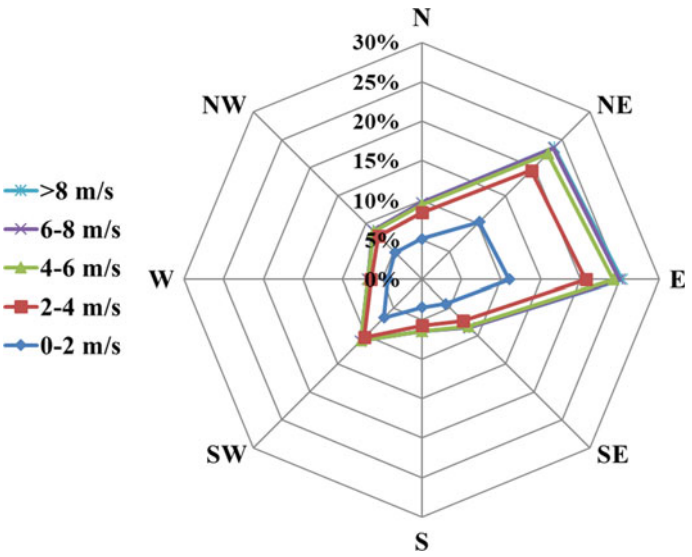

Fig. 7 Wind rose diagram for complete one year

References

1. Ministry of Renewable Energy (MNRE), Report (2019)
2. Mathew, S.: Wind Energy: Fundamentals Resource Analysis and Economics. Springer, Berlin (2006)
3. Manwell, J.F., Mcgowan, J.G., Rogers, A.L.: Wind Energy Explained: Theory, Design and Application, 2nd ed. Wiley, New (2009)
4. Nelson, V.: Wind Energy Renewable Energy and the Environment, 2nd ed. Taylor & Francis Group, LLC, Boca Raton (2014)
5. Twidell, J.W., Weir, A. D.: Renewable Energy Resources, 2nd ed. Taylor & Francis, Boca Raton (2006)
6. Li, X.: Green Energy, Basic Concepts and Fundamentals. Springer, London (2011)
7. Centre for Wind Energy Technology: Course Material: Seventh International Training Course on Wind Turbine Technology and Applications, pp. 3–26. Chennai: C-WET (2011)
8. Carta, J.A., Ramirez, P.: Use of finite mixture distribution models in the analysis of wind energy in the Canarian Archipelago. Energy Convers. Manage. **48**, 281–91 (2007)
9. Premono, B.S., Tjahjana, D.D.D.P. Hadi, S.: Wind energy potential assessment to estimate performance of selected wind turbine in northern coastal region of Semarang-Indonesia. In: International Conference on Engineering, Science and Nanotechnology 2016 (ICESNANO 2016), AIP Conference Proceedings 1788, pp. 030026-1–030026-10 (2016)
10. Altunkaynak., A., Erdik, T., Dabanlı, T., Sen, Z.: Theoretical derivation of wind power probability distribution function and applications. Appl. Energy **92**, 809–814 (2012)
11. Rajapaksha, K., Perera, K.: Wind speed analysis and energy calculation based on mixture distribution in Narakkalliya, Sir Lanka. J. Natl. Sci. Foundation **44**(4), 409–416 (2016)
12. Carta, J.A., Ramirez, P.: Use of finite mixture distribution models in the analysis of wind power in the Canarian archipelago. Energy Convers. Manage. **48**(1), 281–291 (2007)
13. Kollu, R., Rayapudi, S.R., Narasimham, S.V.L., Pakkurthi, K.M.: Mixture probability distribution functions to model wind speed distributions. Int. J. Energy Environ. Eng. **3**, 27 (2012)

14. Dahmouni, A.W., Ben Salah, M., Askri, F., Aloui, F., Ben Nasrallah, S.: Wind energy potential in the site of Borj-Cedria in Tunisia. In: CICME'08 (2008)
15. Chang, T.P.: Estimation of wind energy potential using different probability density functions. Appl. Energy **88**, 1848–1856 (2011)
16. Chang, T.P.: Performance comparison of six numerical methods in estimating Weibull parameters for wind energy application. Appl. Energy **88**, 272–282 (2011)
17. Akdag, S.A., Dinler, A.: A new method to estimate Weibull parameters for wind energy applications. Energy Convers. Manage. **50**, 1761–1766 (2009)
18. Rocha, P.A.C., de Sousa, R.C., de Andrade, C.F., da Silva, M.E.V.: Comparison of seven numerical methods for determining Weibull parameters for wind energy generation in the northeast region of Brazil. Appl. Energy **89**(1), 395–400 (2012)
19. Balouktsis, A., Chassapis, D., Karapantsios, T.D.: A nomogram method for estimating the energy produced by wind turbine generators. Solar Energy **72**, 251–259 (2002)
20. Patil, K.N., Kaushik, S.C.: Study of climatic potential for natural ventilation in buildings for typical Indian cities. Int. J. Ventil. **13**(4), 369–380 (2015)
21. Patil, K.N., Kaushik, S.C., Garg, S.N.: Performance prediction and assessment of energy conservation potential for a light pipe system in Indian composite climate of New Delhi. ASME J. Sol. Energy Eng. (2018)
22. Patil, K.N., Kaushik, S.C., Aggarwal, A.: Evaluation of natural ventilation potential for indoor thermal comfort in a low-rise building in arid and semi-arid climates of India. In: Zhang, G., Kaushika, N., Kaushik, S., Tomar, R. (eds) Advances in Energy and Built Environment. Lecture Notes in Civil Engineering, vol 36. Springer, Singapore (2020)

Analysis of a Grid-Connected PV System Located in Educational Institution

Sunil Kumar Singh, Shikha Singh, and Yashwant Singh

1 Introduction

Over the past few decades, renewable power generations have been preferred as it effectively outperforms the critical constraints of conventional power resources. It not only enhances the power generation but also mitigates the carbon emission. Hence, the share of renewable energy (Solar, wind, geo thermal, etc.) in overall generated electricity over the globe has been significantly improved. As India being the subtropical country, the availability of solar energy/insolation and the average number of sunny days are more than 70% over a year. The total solar-installed capacity of India is about 37.627 GW, out of which the contribution of different regions: North, West, South, East, and North East are 21.43%, 21.67%, 54.42%, 2.27%, and 0.13%, respectively [1]. During the session April 2018 to March 2019, the total generated solar energy was 39268.2 GWh and the respective share of aforementioned regions is 21, 20.26, 57.35, 1.3, 0.04% [2].

For generating solar energy, PV stand-alone system, rooftop system, and building integration are widely used. PV stand-alone system requires land for the installation of the system. But in India, due to the shortage of free land, the government now giving the importance of either a rooftop-based PV system or a building-integrated PV system. The overall temperature of a building-integrated PV system has higher in comparison to the rooftop system. Due to which the efficiency of the building-integrated PV system is low. However, it is preferred where the roof area

S. K. Singh (✉) · S. Singh · Y. Singh
Shri Ramswroop Memorial University, Deva Road, Lucknow, Uttar Pradesh, India
e-mail: sksingh.rs.eee13@itbhu.ac.in

S. Singh
e-mail: ishikha.singh@gmail.com

Y. Singh
e-mail: yashwant.y.p@gmail.com

O. H. Gupta and V. K. Sood (eds.), *Recent Advances in Power Systems*, Lecture Notes in Electrical Engineering 699, https://doi.org/10.1007/978-981-15-7994-3_32

is not available and sufficient for PV installation. When the roof area is available, rooftop systems are preferred. The efficiency of a rooftop system is high as the module temperature is low [3–5]. Majorly, two configurations of a rooftop system are frequently used to generate energy, i.e., grid-connected rooftop system and grid-less rooftop system [6–10]. Comparative efficiency analysis of multiple PV modules such as polycrystalline (pc-Si), amorphous silicon, hetero-junction film (HIT), etc., has been presented. It has been reported that the HIT-based system is more suitable in soppy areas where lesser roof area is available [6]. Polycrystalline and mono-crystalline cell types are generally used while making solar modules. Mono-crystalline cell type offers high efficiency and compact in size; however, the cost is high in comparison to polycrystalline cells. During the recent few years, multifarious authors have reported the performance analysis of on-grid and off-grid solar system based on various parameters such as cost benefit analysis, payback time based on the rating, and cost of the system [11–13].

The performance analysis of a grid-connected solar rooftop system of 56.7 kW is carried out which installed at Block-B1 of SRMU. Throughout the year, a monthly comparative analysis is performed to demonstrate the variation in real and approximated generated solar energy. A payback time is also carried out with environmental impact analysis to show the merits of the installed system. The outcomes of this analysis will be beneficial in calculating the payback time as well as provides guidelines for a rooftop grid-connected PV system installed with similar climatic conditions.

2 Geographical Location and System Description

A 56.7 kW_p rooftop on-grid PV system has been installed on the top of B-1 building of SRMU consisting 180 number of PV modules as shown in Fig. 1. Each module has a capacity of 330 W_p. These modules are aligned at 22° facing south direction. The

Fig. 1 Installed grid-connected rooftop system

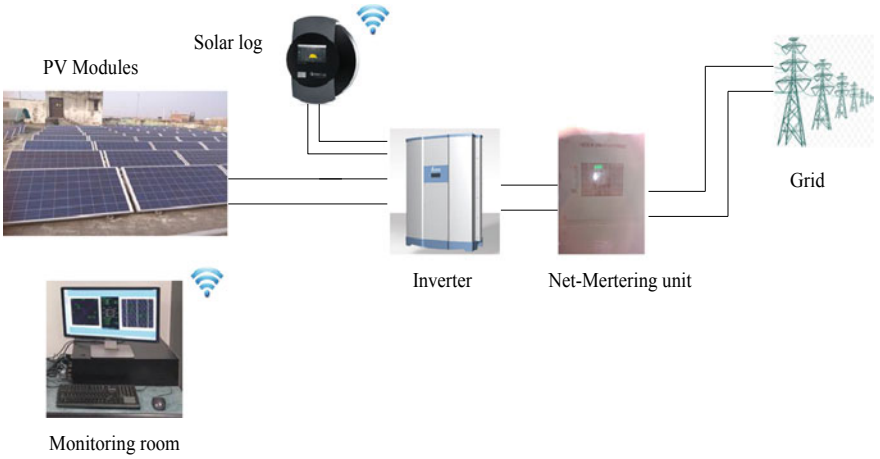

Fig. 2 System configuration of solar roof top system

system was installed in the year 2017. SRMU is located at 26° 85′ N and 80° 95′ S in Barabanki, Uttar Pradesh. The polycrystalline modules are manufactured by Tata Power with 16% efficiency during standard test conditions. The output of this rooftop on-grid solar PV system is fed in the inverter, which converts generated DC in AC as shown in Fig. 2. The generated power is directly fed to the grid after synchronization. For monitor and automation of generated energy, the data acquisition system (Solar log) has been utilized which logs and monitor data on a regular interval. The details of the solar module and inverter have been given in Table 1.

3 Performance Analysis

The actual performance of on-grid rooftop PV system is compared with the expected performance for analyzing the efficacy of the installed system. To analyze the theoretical performance, it has been assumed that in one complete year, 200 days will have bright sunlight (about 7 h), 120 days will have average radiation (about 5 h), and rest of the days will have rainy and cloudy conditions (about 2 h solar radiation) at the current location. As the solar irradiation is variable over the sunshine hours, it is assumed that around 60% electrical energy is being obtained from the maximum watt-peak rating of the installed on-grid rooftop PV system. Therefore, the total energy produced in one complete year is calculated as 34.02 kW * 7 h * 200 days + 34.02 kW * 5 h * 120 days + 34.02 kW * 2 h * 45 days = 71,101 kWh.

The actual energy produced by the installed system = 72,845 kWh. The variation in actual and assumed generated energy is due to the variation in solar intensity and sunshine hours. The month-wise actual produced energy is shown in Fig. 3. It is clear from Fig. 3 that the generation of energy is high in summer months (April, May, June,

Table 1 Parameters of the installed on-grid roof top PV system

S. No.	Parameters	Specifications
1.	Rooftop module	Polycrystalline
2.	Manufacturer of solar modules	Tata Power Solar System Limited
3.	Model number	TP315LBZ, H
4.	Maximum power	330 W_p
5.	V_{oc}	45.7 V
6.	I_{sc}	9.06 A
7.	V_{mpp}	36.85 V
8.	I_{mpp}	8.95 A
9.	Number of modules	180
10.	Efficiency of module	16%
11.	Manufacturer of inverter	Tata Power Solar System Limited
12.	Rating of inverter	50 kW
13.	Number of phase	3

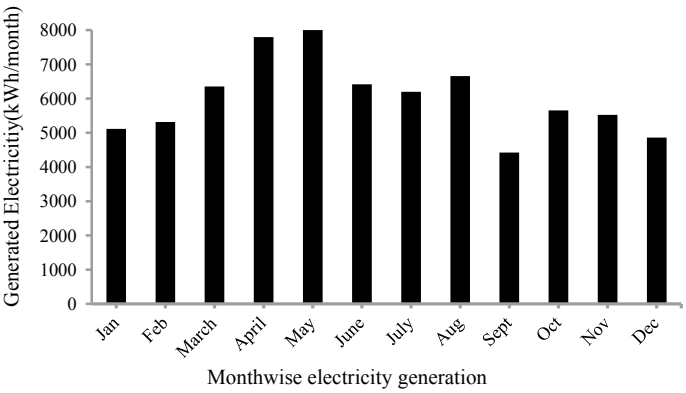

Fig. 3 Month-wise generated electricity of the installed solar rooftop system

July, and August) while low on rainy days such as September. Figure 4 represents the detailed electricity generation of installed grid-connected solar rooftop system. Due to the low/no sunshine, the generation is almost zero on 2nd and the 30th day of December month. The variation in the generation is due to the variation of solar irradiation and the number of hours.

The payback time is a very important factor that relates to the financial viability as well as for the recovery of total invested income. When the total cost invested in the project is negative and money coming back from the project as positive, that period is called payback time. It is considered as one of the major criteria. As the

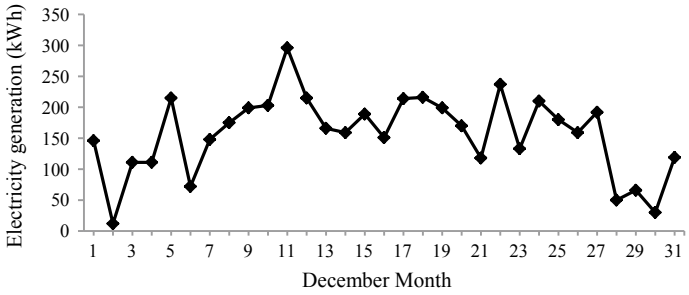

Fig. 4 Day-wise electricity generation in kWh of month December

government is encouraging to install solar PV systems, the costs of the PV modules are decreasing day by day while per-unit cost of electricity is increasing.

As the generation of the installed solar-based rooftop system is 72,845 kWh/year. Considering the inverter efficiency, the total generation of electricity is 65,560.5 units.

$$\text{Yearly cash flow of the installed solar rooftop system} = \sum_{i=0}^{t} \frac{E_g}{(1+d)^i} * \text{COE} \quad (1)$$

where COE refers cost of electricity, E_g is generated electricity.

The cost of 1 unit electricity is taken as 10 Rs. Therefore, the total cost of the generated electricity of the installed solar rooftop system for one year is 655,605 Rs.

Criteria used to calculate payback time: Taking the degradation factor of 1% per year, life of the installed rooftop PV system is considered as 25 years, it is considered to take the load from the bank for 10 years at 10.5% interest rate. Therefore, the financial analysis of the installed system is carried out for ten years. Table 2 shows the payback period calculation of the installed solar rooftop system.

Table 2 Payback period analysis without subsidy

Year	Amount in flow (Rs)	Cumulative amount outflow (Rs)
0	–	−4,987200
1	+655,605	−4,331,595
2	+649,054	−3,682,540
3	+642,564	−3,039,976
4	+638,838	−2,401,138
5	+632449	−1,768,688
6	+626,125	−1,142,563
7	+619,864	−522,699
8	+613,665	0
9	+607,528	0

Table 3 Payback period analysis with a subsidy of 30%

Year	Amount in flow (Rs)	Cumulative amount outflow (Rs)
0	–	−4,987200
1	+655,605	−4,331,595
2	+649,054	−3,682,540
3	+642,564	−3,039,976
4	+638,838	−2,401,138
5	+632,449	-1,768,688
6	+626,125	-1,142,563
7	+619,864	−522,699
8	+613,665	0
9	+607,528	0

Therefore, the total payback period is calculated as, $7\ years + \frac{522,699}{613,665} = 7.85$ years after that period, the cost of the system comes to zero. Therefore, the financial viability of the installed solar rooftop system is very beneficial. Now, a 30% subsidy has been taken on the overall cost of the installed solar rooftop system to calculate the payback period which is given in Table 3.

Therefore, the total payback period is calculated as $6\,year + \frac{218,565}{619,864} = 6.353\ years$. It is clearly seen from the payback time analysis that the significant reduction in the time is due to the government subsidy and it comes around 6.3 years.

4 Environmental Impact

In the current scenario, environmental pollution is a burning issue. After the implications of the Kyoto protocol, Chicago climate Exchange, etc., the rate of carbon emission has been thoroughly monitored by different nations. Hence, to mitigate the carbon emission is a prime concern for every nation. It has been calculated that the considered grid-connected PV system installed at SRMU reduces 1584 Tons [14] of carbon emission, which is almost equal to transplant 2535 trees. Therefore, it has been reaffirmed that the installed system not only economically viable but also mitigates carbon emission which improves the current environmental condition.

5 Conclusion

A comprehensive performance analysis has been carried out of a grid-connected solar PV system (56.7 kWp) installed in the SRMU campus, Barabanki. The approximated performance and the actual performance of the installed system are in line.

The slight variation in performance is due to the variation in solar irradiation. The payback period of the installed system without subsidy is 7.9 years and 6.3 year with subsidy which is quite satisfactory. The performance analysis also reaffirms that the installed system is economically viable and it also effectively mitigates the net carbon emission.

References

1. Physical Progress (Achievement): Ministry of New and Renewable Energy. Retrieved 18 July 2019
2. http://www.cea.nic.in/reports/monthly/executivesummary/2020/exe_summary-01.pdf
3. Tiwari, G.N.: Solar Energy: Fundamentals, Design, Modeling and Applications. Narosa Publishing House (2013)
4. Tekumalla, D.V., Pal, D., Bajpai, P.: Comprehensive Performance evaluation of various solar PV system configurations. IET Renew. Power Gener. 13(8), 1261–1270 (2019)
5. Balaras, C.A., Droutsa, K., Argiriou, A.A., Asimakopoulos, D.N.: Potential for energy conservation in apartment buildings. Energy Build. **31**(2), 143–154 (2000)
6. Quansah, D.A., Adaramola, M.S., Appiah, G.K., Edwin, I. A.: Performance analysis of different grid-connected solar photovoltaic (PV) system technologies with combined capacity of 20 kW located in humid tropical climate. Int. J. Hydrogen Energy **42**, 4626–4635 (2017)
7. Ueda, Y., Kurokawa, K., Kitamura, K., Yokota, M., Akanuma, K., Sugihara, H.: Performance analysis of various system configurations on grid-connected residential PV systems. Solar Energy Mater. Solar Cells **93**(6–7), 945–949 (2009)
8. Sharma, R., Goel, S.: Performance analysis of a 11.3 kWp roof top grid-connected PV system in Eastern India. Energy Rep. **3**, 76–84 (2017)
9. Kazem, H.A., Khatib, T., Sopian, K., Elmenreich, W.: Performance and feasibility assessment of a 1.4 kW roof top grid-connected photovoltaic power system under desertic weather conditions. Energy Build. **82**, 123–129 (2014)
10. Yadav, S.K., Bajpai, U.: Energy, economic and environmental performance of a solar rooftop photovoltaic system in India. International J. Sustain. Energy 51–66 (2019)
11. Saker, N., Al-Qattan, A., Al-Otaibi, A., Al-Mulla, A.: Cost-benefit analysis of rooftop photovoltaic systems based on climate condition of gulf cooperation Council countries. IET Renew. Power Gener. **12**(9), 107 (2018)
12. Barnwal, P., Tiwari, G.N.: Life cycle energy metric and CO_2 credit analysis of a hybrid photovoltaic/thermal greenhouse dryer. Int. J. Low Carbon Technol. **3**(3), 203–220 (2008)
13. Papadopoulos, A.M., Oxizidis, S., Papandritsas, G.: Energy, economic and environmental performance of heating systems in Greek buildings. Energy Build. **40**, 224–230 (2008)
14. https://mnre.gov.in

Reduction in Bill Using Time of Usage Pricing in a Smart Grid

Saurabh Pranjale, Tharun Balaji, Soumya Mudgal, Syed Aamir Ahmed, Praveen K. Gupta, Neeraj K. Singh, and Vasundhara Mahajan

1 Introduction

Ever-increasing electricity demand has resulted in the overburdening of traditional power systems. In recent years, scientists are utilizing the significant progress in information and communication technology and merging it with the regular electricity grid to form the smart grid. The main target of this incorporation is to connect the components of the grid via communication networks, such as Internet or sensor networks, to gather data about the grid's conditions and consumers' requirements [1].

A smart grid uses the idea of 'Internet of Things' to establish communications between all its components [8]. The most important advantage of the IoT smart grid is that with the help of two-way communication, data is transmitted wirelessly

S. Pranjale · T. Balaji · S. Mudgal (✉) · S. Aamir Ahmed · P. K. Gupta · N. K. Singh · V. Mahajan
Electrical Engineering Department, Sardar Vallabhbhai National Institute of Technology, Surat, Gujarat 395007, India
e-mail: mudgalsoumya@gmail.com

S. Pranjale
e-mail: saurabhpranjale@gmail.com

T. Balaji
e-mail: tharunbalaji@gmail.com

S. Aamir Ahmed
e-mail: syedaamir0801@gmail.com

P. K. Gupta
e-mail: praveenpragati12@gmail.com

N. K. Singh
e-mail: neerajksssingh@gmail.com

V. Mahajan
e-mail: vasu.daygood@gmail.com

O. H. Gupta and V. K. Sood (eds.), *Recent Advances in Power Systems*, Lecture Notes in Electrical Engineering 699, https://doi.org/10.1007/978-981-15-7994-3_33

between any two components with the help of the Internet, which makes the grid more resilient than the traditional power grid.

The components of a smart grid are connected via a common server. There is a multi-directional transfer of energy and data via this communication network. Monitoring information from a distant location becomes easy as it can be accessed through the common server. In an appliance to appliance (A2A) communication system, the compatibility between different component improves due to communication.

The communication system is essential for a smart grid, as discussed. Its uses can be further extended to a wireless sensor network that is used to reduce the bill of the consumer. Billing from the grid depends upon the load demand, rates varying between peak, moderate peak and off-peak durations. Flattening the load demand curve has been the motive behind minimizing the bills of consumers. The solution to this is time of use (TOU) pricing.

In TOU pricing, the load demand from the consumer is adjusted in a way to reduce the overall bill. To get a better idea, consider a fixed marginal production cost. During the peak durations, the demand increases. To fulfill it, even the units producing energy with lower efficiency are used, thereby increasing the cost corresponding to losses in the system. Contrary to this, at off-peak, the demand is fulfilled just by a few higher efficiency units. The cost decreases substantially. Therefore, if some adjustments are made by shifting some load from peak to off-peak durations, the overall price of energy is reduced and gets reflected in the bill.

In the past, there has been discussion upon several communication models for a smart grid [2, 9, 10, 15]. With communication comes the risk of vulnerability to cyberattack [16–21]. This aspect has not been discussed in this paper. The inclusion WSN is also shown in the literature [4, 6, 13]. The impact of TOU pricing can be referred from several sources [7, 11].

In the presented paper, the main emphasis is on focusing on the features of a smart grid based on communication between different components, load detection and reduction of prices. The first part discusses the communication between the different components of the grid. These components interchange physical and cyberdata in the form of energy and information, respectively. In the second part of the paper, the load demand at the consumer's side is detected using a wireless sensor network (WSN) and smart meters. This load data gets stored in the common server connecting all the components of the grid. The last part of the paper focuses on a method to reduce the bill of the consumer using TOU Pricing and the data stored in the server.

2 Component Communication

The communication in a smart grid is dependent on the following six components.

1. **Data acquisition (Energy Meter)**
   - To measure the real-time load value, the IC-ADE7758 is used. It is a three-phase electrical measuring IC with very high accuracy that consists of ADCs and integrators and can perform active, reactive and apparent energy measurement.

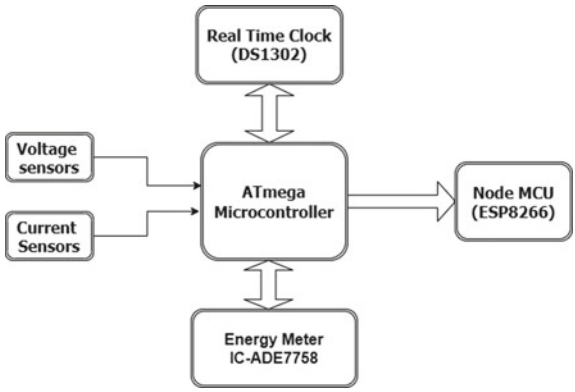

Fig. 1 Data acquisition

- A real-time clock (RTC) is also incorporated with this to put an exact time stamp for each reading taken from the load.
- To get the current and voltage levels from the load, ATmega microcontroller is used as the arbitrator [5]. The detected analog values from the load are converted into equivalent digital values forwarded for transmission.
- This value is given as an input to NodeMCU

This can be seen in Fig. 1.

2. **Transmission (NodeMCU)**
   To transmit the data collected from the meter in digital form, Arduino-based nodeMCU ESP8266 is used. It is a 32-bit microcontroller with built-in wifi. With 16 GPIO pins, 32KB instruction and 80KB user data space and a CPU clocked at 80MHz; it is an ideal device to send data over the Internet for this application. As it has complete TCP/IP stack capability, data can be sent as well as received over the Internet.
3. **Reception (Raspberry Pi 3B+)**
   The server receives the data transmitted by the NodeMCU. Raspberry 3 B+ which comes with 1.4 GHz 64-bit quad-core ARM Cortex-A53 CPU and 1GB RAM is used as the server. It also equips dual-band 802.11ac wireless LAN (2.4 and 5 GHz) which makes it possible to connect to the Internet, wirelessly which is an added advantage. The data received is stored in a database. This database is created using MySQL, which is an open-source database management system. Every data received from the node consists of the following entries: name of the node, load value and time of reading. This is entered into the database. While doing this, Raspberry Pi also acts as a Web server for the energy company. It hosts a web page which shows a real-time dashboard of load at each energy meter. It also uses the data from the database to make a load profile of each load and plots a graph in real time.

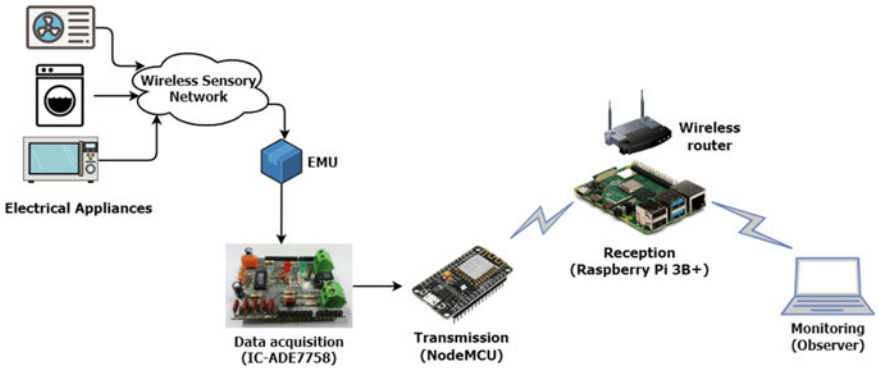

Fig. 2 Data flow

4. **Monitoring (Energy company)**
   The live dashboard hosted by the Raspberry Pi should be accessed only by the authorized people. For this, we created a secured login mechanism. This has a username and password which is encrypted for higher security. On successful login, data from all the energy meters can be monitored remotely.
5. **Wireless Sensor Network (WSN)**
   An arrangement of various sensors (between tens and thousands) that can detect the flow of data between the components and make decisions accordingly is called wireless sensor network. They are further discussed in Sect. 3.
6. **Energy Management Unit (EMU)**
   Energy management units are connected to WSNs to control the load of the appliances in use. They are further discussed in Sect. 3.

For the communication discussed above, the flow of data follows a path shown in Fig. 2. The WSN acts as a relay between the EMU and appliances. EMU communicates with the energy meter to amend the energy price and peak hour information. The load value is forwarded in digital form to the NodeMCU. For this modeling purpose, a wireless network created using a wifi router is used. All the components, NodeMCU, Raspberry Pi and end user are connected to this network. The data sent by NodeMCU is collected by the Raspberry Pi and stored in a database. Raspberry Pi hosts this database on a web page which can be viewed by the end user.

3 Load Detection

With the advancement in communication systems, there has been an increment in the use of smart sensors. As compared to the traditional sensors, these sensors are cheaper and less bulky [22]. They follow a series of local decision processes that sense and measure the data from their environment by forming a wireless network.

Thus, they are an essential part of the energy management system [3]. WSNs have integral roles in military surveillance systems, biomedical monitoring, exploring the environment for hazards and natural disaster reliefs [22]. For the given setup, the WSN takes input signals from several home appliances. It sends these signals to the energy management unit (EMU).

To coordinate between the consumer demands, the energy management unit is used. Its functions are twofold. It communicates with the smart meter to modify the peak load data and the price of electricity. Along with WSN, it collects the sensory information to communicate the load demand of consumer and reduce the bill. In the communication process, the Industrial, Scientific and Medical channel (ISM channel) is used as a radio band. Overcrowding the band during peak duration results in interference of the signal. This is a challenge faced by the wireless network. The issue of interference is resolved by improving the coordination between the nodes that have the appliances attached to them.

4 Price Reduction

The TOU pricing benefits the consumer by savings in terms of cost of energy. TOU pricing is a tool for load management. It is based upon the concept of flattening of the load curve. The users are encouraged to shift their load demands from peak hours to off-peak hours. This results in a shift from more expensive to a cheaper cost of energy. Although TOU pricing is beneficial for the user, it faces issues due to dynamic pricing. Being aware of the most recent rate of energy is essential. Therefore, the smart meters and sensors need to be modified for the same.

4.1 Case Study for a Smart Household

Consider the case of a typical household. Table 1 shows the energy consumption data and duration of use of different appliances in the household for a day. Depending upon the load duration curve for the day, peak hours are taken in two slots, 09:00–12:00 hrs and 18:00–22:00 hrs, and non-peak hours are taken from 06:00–09:00 h and 12:00–18:00 h [12, 14]. So two cases are analyzed:

- **Case 1**:
  This refers to the peak hours of the load curve. Additional to the base charges of energy generation, there are charges corresponding to losses as well. For the calculations, take the cost per unit at peak hours as Rs. 7.41 per kWh [14].
- **Case 2**:
  This refers to the off-peak hours of the load curve. Thus, very negligible charge corresponding to losses gets added up to base charge. For the calculations, take the cost per unit at off-peak hours as Rs. 4.59 per kWh [14].

Table 1 Power ratings and duration of operation for different appliances in use

Appliance	Energy consumption (kW)	Duration (h)
Automatic cleaning system	0.8	1
AC (1 tonne)	3.517	2
Washing machine	1.3	1
Microwave	1	1
Hair dryer	0.6	0.5

To calculate the cost corresponding to an automatic cleaning system for the case I:

Given,
Energy consumed = 0.8 kW
Duration = 1 h
Cost per kWh = Rs. 7.41

Power consumed (kWh) = energy consumed × duration = 0.8 × 1
Power consumed = 0.8 kWh

Cost = Power consumed × cost per kWh = 0.8 × 7.41
Cost = Rs 5.928

To calculate the cost corresponding to automatic cleaning system for case II:

Given,
Energy consumed = 0.8 kW
Duration = 1 h
Cost per kWh = Rs. 4.59

Power consumed (kWh) = energy consumed × duration = 0.8 × 1
Power consumed = 0.8 kWh

Cost = Power consumed × cost per kWh = 0.8 × 4.59
Cost = Rs 3.672

The cost corresponding to the other appliances, for both the cases, can be seen in Table 2. From this, the total cost during peak hours is obtained to be Rs. 77.31 and total cost during off-peak hours is Rs. 47.89.

To calculate the difference in the cost for the two cases
Difference in cost = Cost for case I − Cost for case II = 5.928 − 3.672
Difference in cost = Rs. 2.256

Similarly on calculating for other appliances, a saving of Rs. 29.42 or 38.04 % per day is seen for operating during off-peak hours. Figure 3 compares the cost per day of the given appliances during the peak and off-peak hours and highlights the savings from each appliance. This approach can be further extended for different categories of load such as agricultural, commercial and industrial.

Table 2 Cost corresponding to peak and off-peak load

Appliance	Cost for case I (Rs.)	Cost for case II (Rs.)
Automatic cleaning system	5.928	3.672
AC (1 tonne)	52.12194	32.28606
Washing machine	9.63	5.97
Microwave	7.41	4.59
Hair dryer	2.22	1.38

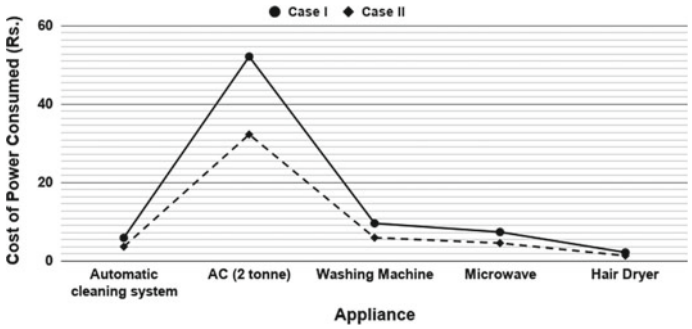

Fig. 3 Difference in cost for the two cases

5 Conclusion

In this paper, a communication system between components of a smart network is established to calculate the total cost of energy for the consumer using TOU pricing. The collected energy usage data is transmitted to the Raspberry 3 B+ via NodeMCU. TOU pricing encourages consumers to decrease their usage during peak hours and shift it to off-peak hours. It is preferred over real-time pricing (RTP) because of its static prices for peak and non-peak hours. In RTP tariffs, the cost per unit varies throughout the day. Operating the load (appliances) during non-peak hours reduces the energy costs. WSN and EMU are used in coordination to decrease the cost to consumers. To calculate savings for a month or year, we require a load curve corresponding to the entire month or year. This load curve will vary seasonally. The above work can be extended to larger systems, industries or entire smart grid networks.

References

1. Abdallah, A.: Security and privacy in smart grid. In: Electrical and Computer Engineering, University of Waterloo, Canada, Thesis, Submitted (2016)
2. Dr. Chafic BouSaba, M.T.K., Pizio, D.W.C.: Wireless network security using Raspberry Pi. In: ASEE Annual Conference & Exposition, vol. 25, pp. 24–29 (2016)

3. Erol-Kantarci, M., Mouftah, H.T.: Wireless sensor networks for domestic energy management in smart grids. In: 25th Biennial Symposium on Communications, pp. 63–66 (2010)
4. Erol-Kantarci, M., Mouftah, H.T.: Wireless sensor networks for cost-efficient residential energy management in the smart grid. IEEE Trans. Smart Grid **2**, 314–325 (2011)
5. Guimarães, A.M.F., Freitas, T.T., Griner, H., de Almeida, T.H.S.: Smart energy monitoring system with ade7758 ic. In: 5th International Youth Conference on Energy (IYCE), pp. 1–5 (2015)
6. Gungor, V.C., Lu, B., Hancke, G.P.: Opportunities and challenges of wireless sensor networks in smart grid. IEEE Trans. Ind. Electron. **57**, 3557–3564 (2010)
7. Hussin, N.S., Abdullah, M.P., Ali, A.I.M., Hassan, M.Y., Hussin, F.: Residential electricity time of use (tou) pricing for malaysia. In: 2014 IEEE Conference on Energy Conversion (CENCON), pp. 429–433 (2014)
8. Kimani, K., Oduol, V., Langat, K.: Cyber security challenges for iot-based smart grid networks. Int. J. Crit. Infrastruct. Protect. **25**, 36–49 (2019)
9. Liu, S., Chen, B., Zourntos, T., Kundur, D., Butler-purry, K.: A coordinated multi-switch attack for cascading failures in smart grid. IEEE Trans. Smart Grid 2682–2688 (2014)
10. Mazloomzadeh, A., Mohammed, O.A., Zonouzsaman, S.: Empirical development of a trusted sensing base for power system infrastructures. IEEE Trans. Smart Grid **6**, 2454–2463 (2015)
11. Nazar, N.S.M., Abdullah, M.P., Hassan, M.Y., Hussin, F.: Time-based electricity pricing for demand response implementation in monopolized electricity market. In: 2012 IEEE Student Conference on Research and Development (SCOReD), pp. 178–181 (2012)
12. Nicolson, M.L., Fell, M.J., Huebner, G.M.: Consumer demand for time of use electricity tariffs: a systematized review of the empirical evidence. Renew. Sustaina. Energy Rev. **97**, 276–289 (2018)
13. Patel, K., Khosla, A.: Home energy management systems in future smart grid networks : a systematic review. In: 2015 1st International Conference on Next Generation Computing Technologies (NGCT), pp. 479–483 (2015)
14. Shaikh, S.K.M., Dharme, A.A.: Time of use pricing—India, a case study. In: 2009 International Conference on Power Systems, pp. 1–6 (2009)
15. Sheshai, S.S.: Raspberry pi based security system. Report, Submitted: Department of Electrical and Information Engineering, University of Nairobi, pp. 268–273 (2016)
16. Singh, N.K., Gupta, P.K., Mahajan, V.: Cyber intrusion detection in smart grid using KPCA and novel trust method. In: IEEE International Conference on Emerging Trends for Smart Grid Automation and Industry 4.0 (ICETSGAI4.0), Birla Institute of Technology (BIT), Mesra, Ranchi (2019)
17. Singh, N.K., Mahajan, V.: Cyber attack detection in smart grid substation using virtual range increment and trust weight. In: 8th International Conference on Power Systems, (ICPS), Malaviya National Institute of Technology Jaipur (MNIT), Jaipur, Rajasthan, India (2019)
18. Singh, N.K., Mahajan, V.: Fuzzy logic for reducing data loss during cyber intrusion in smart grid wireless network. IEEE Student Conference on Research and Development (SCOReD), Universiti Teknologi PETRONAS, Perak, Malaysia, pp. 192–197 (2019)
19. Singh, N.K., Mahajan, V.: Mathematical model of cyber intrusion in smart grid. In: IEEE PES GTD Grand International Conference and Exposition Asia (GTD Asia), Bangkok, pp. 965–969 (2019)
20. Singh, N.K., Mahajan, V.: Smart grid: Cyber attack identification and recovery approach. In: IEEE 2nd International Conference on Innovations in Electronics, Signal Processing and Communication (IESC), NIT Meghalaya, pp. 1–5 (2019)
21. Singh, N.K., Mahajan, V., Aniket, A., Pandya, S., Panchal, R.,Mudgal, U.: Identification and prevention of cyber attack in smart grid communication network. In: International Conference on Information and Communications Technology (ICOIACT) Yogyakarta, Indonesia, pp. 5–10 (2019)
22. Yick, J., Mukherjee, B., Ghosal, D.: Wireless sensor network survey. Comput. Networks **52**, 2292–2330 (2008)

Congestion Management Based on Real Power Rescheduling Using Moth Flame Optimization

Kaushik Paul, Niranjan Kumar, Debolina Hati, and Anumeha

1 Introduction

The process of deregulation has brought significant variations in the performance of power system utilities. The independent system operator (ISO) has to coordinate to ensure proper allocation of the power generation and load demand to guarantee healthy operation of the system [14]. In certain situations, the transmission channels may function dissatisfying the thermal limits which give rise to the congestion problem. The congestion leads to the overloading of the transmission corridors. Thus, to restore the power system to normal state while attenuating congestion, appropriate techniques must be incorporated for congestion management (CM) [15]. Some of the techniques that are readily in practice are generator rescheduling (GR), installation of FACTS devices, load management, etc. In this manuscript, a CM initiative has been modelled with GR approach.

The influence of deregulation on the restructuring of power industries and its problems with transmission congestion are listed in [17]. Methods to address the congestion elimination are discussed in [16]. The influence of market flow strategies and its economical aspects dealing with CM have been discussed in [11]. A model based on the pool and bilateral framework has been used by Fang et al. to encourage the willingness to pay for CM [6]. Conejo et al. adopted measures to circumvent

K. Paul (✉)
BIT Sindri, Department of Electrical Engineering, Dhanbad, Jharkhand 828123, India
e-mail: kaushiksunnypaul@gmail.com

N. Kumar
National Institute of Technology, Jamshedpur, Jamshedpur, Jharkhand 831014, India

D. Hati
University of South Carolina, Columbia, SC 29208, USA

Anumeha
Government Womens' Polytechnic Jamshedpur, Jamshedpur, Jharkhand 831013, India

O. H. Gupta and V. K. Sood (eds.), *Recent Advances in Power Systems*, Lecture Notes in Electrical Engineering 699, https://doi.org/10.1007/978-981-15-7994-3_34

the congestion problem and worked towards rectifying the voltage stability issues occurring due the CM problem [2].

The CM conducted with the power rescheduling process by the generators has been one of the primary strategies implemented by ISO during congestion. Kumar et al. in their work implemented CM on a zonal model and performed GR for the specified zone to relive the congestion [10]. Selecting generators based upon the relative electrical distance (RED) for power management with GR to attenuate over-burdening of the transmission paths have been developed in [19]. In [1], a power flow tracing model for CM has been formulated with GR of real power confined to the congested zones. In [9], the hybrid model for electricity market has been taken to evaluate the congestion pricing with Sen transformer application and GR method. A sensitivity approach has been formulated by Venkaiah et al. to reschedule the real power with the fuzzy adaptive mechanism for CM [18].

In the recent times, there has been a drift towards the evaluation of CM problem with the metaheuristic algorithms. In [4], sensitivity indices were computed termed as generator sensitivity factor (GSF) to be brought in the most effective generators for CM, and particle swarm optimization (PSO) was used to achieve the optimal real power generation with GR. In another research, Deb et al. in [3] performed GR to achieve the minimum congestion cost with artificial bee colony (ABC) algorithm. In [7], CM was done to shed out the power flow in congested line with GR procedure with cuckoo search algorithm. In [14], GR has been done with gravitational search algorithm (GSA) considering the optimal positioning and effect of wind farm for CM. The persistent progress and incredible advancements of metaheuristic computational algorithms have encouraged the application of such efficient techniques for CM with GR of real power. Thus, a metaheuristic procedure based on the navigating phenomenon of moths termed as moth–flame optimization (MFO) has been applied to the proposed CM problem with GR. MFO has shown significant improvement in results with application in various domain of optimization problem [13]. In [20], MFO has been applied to the manufacturing process to fetch the optimal machine parameters. Multilevel image processing with MFO has been discussed in [5]. In [8], Khalilpourazari et al. have implemented MFO to solve constrained engineering problem related to optimization. MFO has also provided encouraging output for loss minimization in case of reactive power dispatch problem [12]. Thus, MFO has been opted to provide significant improved results for the CM problem.

This manuscript portrays a CM problem with the implementation of MFO to achieve minimized congestion cost with optimal values of real power adjusted by GR process.The generators exercised for power rescheduling are made to involve in the CM process based on GSF. The 39-bus system based on the New England framework has been adopted to validate and analyse the efficacy of the proposed CM problem.

2 Problem Formulation

The term GSF can be understood as the sensitivity indices that signify the quantity of power flow change (ΔP_{lm}) in the transmission corridors when a minor change occurs in generator power output (ΔP_{g}). Equation (1) shows the mathematical description of GSF.

$$\mathrm{GSF_g} = \frac{\Delta P_{\mathrm{lm}}}{\Delta P_{\mathrm{g}}} \tag{1}$$

The real power flowing in the transmission channel (here through congested line) is represented by load flow analysis as follows:

$$P_{\mathrm{lm}} = -V_l^2 G_{\mathrm{lm}} + V_{\mathrm{l}} V_{\mathrm{m}} G_{\mathrm{lm}} cos(\theta_{\mathrm{l}} - \theta_{\mathrm{m}}) + V_{\mathrm{l}} V_{\mathrm{m}} B_{\mathrm{lm}} sin(\theta_{\mathrm{l}} - \theta_{\mathrm{m}}) \tag{2}$$

Here V_{l} and V_{m} signify lth and mth bus voltages, respectively. The conductance is designated as G_{lm} and susceptance as B_{lm} of the transmission channel existing between the buses '$textl$' and 'm'. The phase angle magnitudes are given by θ_{l} and θ_{m}.

Equation (1) can be mathematically modelled to be represented as follows [4]:

$$\mathrm{GSF}_g = \frac{\delta P_{\mathrm{lm}}}{\delta \theta_{\mathrm{l}}} \cdot \frac{\delta \theta_l}{\delta P_g} + \frac{\delta P_{\mathrm{lm}}}{\delta \theta_{\mathrm{m}}} \cdot \frac{\delta \theta_{\mathrm{m}}}{\delta P_g} \tag{3}$$

The complete sequential steps related to the derivation of GSF portrayed in Eq. (3) have been illustrated in [4].

The congestion cost minimization in relation to the optimal generation of real power is represented in Eq. (4) as follows:

$$\min\ \mathcal{C} = \min \sum_{g=1}^{N_g} C_g(\Delta P_g) \Delta P_g \tag{4}$$

Here the price bids of the generators are denoted as C_{g} and real power adjusted with GR is ΔP_{g}. The optimization problem for the CM has been evaluated based on the following constraints:

$$\sum_{g=1}^{N_g} ((\mathrm{GSF}_g) * \Delta P_g) + PF_k^0 \leq PF_k^{\max} \tag{5}$$

$$\Delta P_g^{\min} \leq \Delta P_g \leq \Delta P_g^{\max} \tag{6}$$

$$\Delta P_g^{\min} = P_g - P_g^{\min} \tag{7}$$

$$\Delta P_g^{\max} = P_g^{\max} - P_g \tag{8}$$

$$\sum_{g=1}^{N_g} \Delta P_g = 0 \tag{9}$$

Here Equations (5) and (6) represent the inequality constraints with PF_k^0,$PF_k^{\max}$, $P_g^{\max}$,$P_g^{\min}$ as the current power flow status and maximum power flow limit, change in the upper and lower generation limit, respectively. Equations (7) and (8) show the minimum and maximum generation limits based on the initial generation. Equation (9) is the equality constraints which signifies the power balance in the CM process.

The fitness function for the CM has been developed with the penalty multiplier for cost minimization is shown in Equation (10):

$$\sum_{g=1}^{N_g} C_g(\Delta P_g)\Delta P_g + \mathcal{P}_{\mathbf{M}} * [(\sum_{g=1}^{N_g}((\mathrm{GSF}_g) * \Delta P_g) + \mathrm{PF}_k^0 \leq \mathrm{PF}_k^{\max}) + P_g - P_g^{min} + \sum_{g=1}^{N_g} \Delta P_g = 0)] \tag{10}$$

The penalty multiplier $\mathcal{P}_{\mathbf{M}}$ is taken as 500 [3].

3 Moth–Flame Optimization

Mirjalili in the year 2015 came up with a heuristic algorithm based on the phenomenon of transverse orientation which is the navigation technique adopted by the moths [13]. The moths use transverse orientation which makes it fly in a straight path at night keeping a constant angle in relation to the position of the moon. When the moths discover the light source (flame) to be in a measurable distance, they converge towards maintaining a spiral path.

3.1 MFO Algorithm

In MFO, the two most primary components are the moths and the flames in which both of them are considered as solution set. The moths are treated as the search agents. The boundary of the region/space where they move is marked as the search region. The flames are treated as the best position. The moth on finding a flame updates it when turns out to be a better solution.

In MFO, the group of moths can be represented in matrix form which is given as follows:

$$B = \begin{bmatrix} b_{1,1} & b_{1,2} & b_{1,3} & \dots & b_{1,d} \\ b_{2,1} & b_{2,2} & b_{2,3} & \dots & b_{2,d} \\ \vdots & \vdots & \vdots & \ddots & \vdots \\ b_{n,1} & b_{n,2} & b_{n,3} & \dots & b_{n,d} \end{bmatrix} \tag{11}$$

The fitness function data are taken into matrix represented as follows:

$$OB = \begin{bmatrix} \mathrm{OB}_1 & \mathrm{OB}_2 & \mathrm{OB}_3 & \dots & \mathrm{OB}_n \end{bmatrix}^T \tag{12}$$

here n, d and T are the number of moths, dimension/variable of the problem and transpose of the matrix, respectively.

In the similar manner, the flames are also represented in matrix as follows:

$$C = \begin{bmatrix} C_{1,1} & C_{1,2} & C_{1,3} & \dots & C_{1,d} \\ C_{2,1} & C_{2,2} & C_{2,3} & \dots & C_{2,d} \\ \vdots & \vdots & \vdots & \ddots & \vdots \\ C_{n,1} & C_{n,2} & C_{n,3} & \dots & C_{n,d} \end{bmatrix} \tag{13}$$

The fitness data based on the flames are confined as shown below [13]:

$$OC = \begin{bmatrix} \mathrm{OC}_{1,1} & \mathrm{OC}_{1,2} & \mathrm{OC}_{1,3} & \dots & \mathrm{OC}_{1,d} \end{bmatrix}^{\mathrm{T}} \tag{14}$$

The MFO is comprised of three-tuple approximation functions given in Equation (15) :

$$MFO = (I, P, T) \tag{15}$$

here I is utilized to generate random population for the moths and the fitness values corresponding to each of them are represented as follows [13]:

$$B(i, j) = (zu(i) - zb(i) * \varphi_{\mathrm{rand}} + lb(i)) \tag{16}$$

$$\mathrm{OB} = \text{Fitness Function}(B) \tag{17}$$

here zu is the upper limit and zb is the lower limit designated for the considered variables.

Once the initialization has been done, the operation of the function P is done as long as a condition is reached where the termination function T is satisfied. The navigation of the moth is governed by the P function in search region. The method of updating the position of the moth is performed based on the flame and is updated with Equation (18)

$$B_i = S(B_i, C_j) \tag{18}$$

Due to the moths' transverse movement, the mathematical description for spiral function is given in Eq. (19):

$$S(B_i, C_j) = D_i.e^{kt}.\cos(2\pi t) + C_j \tag{19}$$

here S denotes the spiral function, and B_i and C_j represent the moth and flame, respectively. The measurement of the distance existing between the i^{th} and j^{th} position moth is taken as D_i. k is the constant for the logarithmic spiral, and t ranges from $[r, 1]$ in random manner. r denotes the adaptive convergence constant that reduces in a linear manner from the range -1 to -2 during the iteration in order to accelerate the convergence within the vicinity of the flame. The expression to determine D_i is given as in Eq. (20)

$$D_i = |C_j - B_i| \tag{20}$$

The balance between the operation of exploration and exploitation is maintained with the reduction in the flame number with the increase in the iterations shown in Equation (21).

$$\text{Flame No} = \text{round}(N - l \times \frac{N-1}{t}) \tag{21}$$

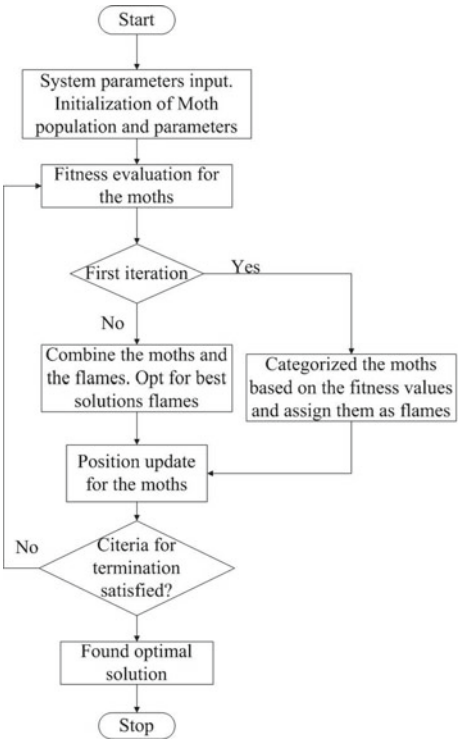

Fig. 1 MFO flow chart for CM

here N is the maximum count of flames, l is the iteration count, and t stands for maximum count of iteration. Here population size 40 is considered for the CM problem with MFO. The MFO-based flow chart for CM is given in Fig. 1.

4 Results and Discussions

In this work, MFO approach has been implied to GR process to get optimal real power generations in order to achieve minimum congestion cost. The simulation has been performed on MATLAB 2016b. The 39-bus framework of New England system has been taken to evaluate the proposed CM problem which is shown in Fig. 2. The results achieved from this research output are compared with RED [19], PSO [4] and ABC [3] to analyse the potency of the MFO for the CM.

In this proposed approach, the line outage has been considered to generate congestion in the system. The line L_{14-34} has a normal power flow of 262.3 MW, where its maximum line limit is 600 MW. This line has been tripped which results in congestion in line L_{15-16}. The power flow in it has been raised to 628.4 MW for line L_{15-16} whose maximum flow limit was 500 MW. In this case, L_{14-34} has been tripped to establish a comparative description with the reported results in [19], PSO [4] and ABC [3].

In the MFO approach for CM, the GR process is carried out with most significant generators based on the GSFs. The GSFs are determined considering the line L_{15-16} in Table 1.

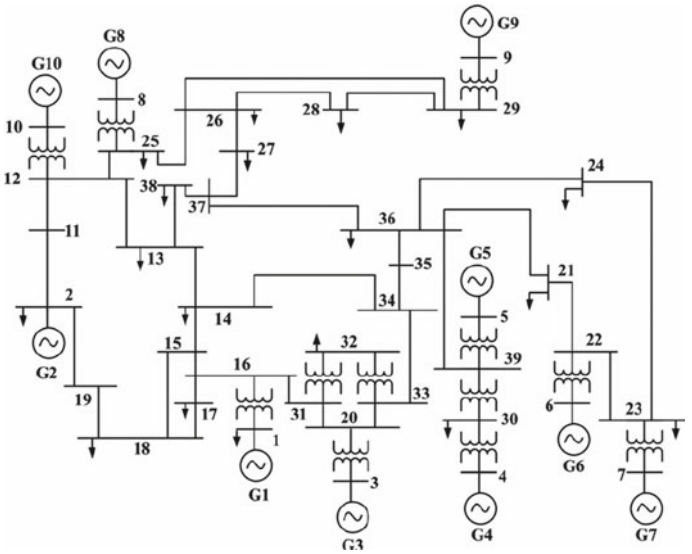

Fig. 2 39-bus New England framework

Table 1 Generator sensitivity factor data for 39-bus

Gn. No.	1	2	3	4	5	6	7	8	9	10
GSF	0.00	−0.49	−0.12	−0.35	−0.35	−0.35	−0.35	−0.53	−0.46	−0.58

The generators 4, 5, 6, 7 in Table 1 are holding uniform values for GSF. Thus, their influence to modulate the power flow in congested line is not significant. Again for the same CM problem, the generators 2, 3, 8, 9, 10 are holding most negative and deviated GSF values which makes them most eligible to provide significant modulation in the power management in congested line. Therefore, these generators are made to involve in the GR process. The generator price bids for congestion cost determination are given in Table 2.

The comparative performance analysis for the CM problem with MFO and RED [19], PSO [4] and ABC [3] has been represented in Table 3. The MFO has been successful to relive the congested line from over loading. The current power flow of the line L_{15-16} is 497.90 MW (maximum limit 500 MW) with MFO after GR. The

Table 2 Generator price bids for 39 bus

Gn. No.	1	2	3	4	5	6	7	8	9	10
Bids($/MWh)	15	20	17	16	12	17	13	11	14	19

Table 3 Comparative evaluation of results with MFO for 39-bus

	RED [19]	PSO [4]	ABC [3]	MFO [proposed]
Rescheduling cost ($/h)	8640.2	8873.1	8451.8	8179.78
Power flow of L_{15-16} (MW) after CM	510	490	499.50	497.90
$\Delta\mathbf{P_1}$ (MW)	−99.59	−149.1	−131.0	−132.99
$\Delta\mathbf{P_2}$ (MW)	98.75	65.6	63.2	52.12
$\Delta\mathbf{P_3}$ (MW)	−159.64	−129	−132.0	−105.32
$\Delta\mathbf{P_4}$ (MW)	12.34	Not involve	Not involve	Not involve
$\Delta\mathbf{P_5}$ (MW)	24.69	Not involve	Not involve	Not involve
$\Delta\mathbf{P_6}$ (MW)	24.69	Not involve	Not involve	Not involve
$\Delta\mathbf{P_7}$ (MW)	12.34	Not involve	Not involve	Not involve
$\Delta\mathbf{P_8}$ (MW)	24.69	75.4	72.2	123.78
$\Delta\mathbf{P_9}$ (MW)	12.34	52.1	49.1	42.95
$\Delta\mathbf{P_{10}}$ (MW)	49.38	83.0	78.8	56.19
Total amount (MW)	518.45	554.2	526.3	513.35

generators involvement has been reduced to six generators with GSF application. The MFO has helped to achieve a congestion cost of 8179.78 $/h which is lower than the other costs with RED [19], PSO [4] and ABC [3]. The amount of the total rescheduled power in the GR process is also minimum than the other reported results. The levels of the rescheduled real power have been shown in Fig. 3.

Real power loss after GR with MFO is also reduced to 57.23 MW, and the voltage profile is conserved at 0.968 p.u. is highlighted in Table 4. It is observed that the system losses and voltage profile improvements are better than the reported results. Pictorial representation of voltages for each of the buses for the system with MFO is shown in Fig. 4. Table 5 shows the line overload factors after GR with MFO. The line overload factor after GR with MFO is 0.98 and comparatively appreciable.

The convergence graph with MFO for the CM problem is shown in Fig. 5. The optimization problem for the CM has converged successfully to reach the minimum cost. MFO has significantly performed better for the proposed CM problem with GR.

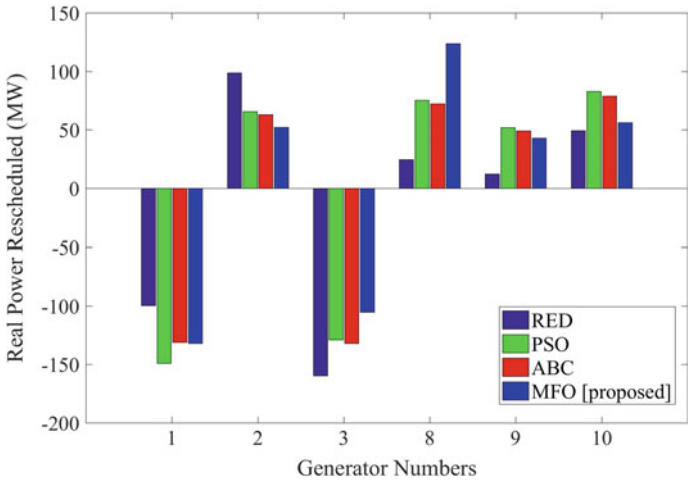

Fig. 3 Rescheduled active power with RED [19], PSO [4], ABC [3] and MFO [proposed]

Table 4 Comparative analysis of system parameters

System parameters	Before rescheduling	RED [19]	PSO [4]	ABC [3]	MFO [proposed]
P_{loss} (MW)	59.64	57.31	58.00	59.36	57.23
V_{min} (p.u)	0.941	0.945	0.932	0.940	0.968

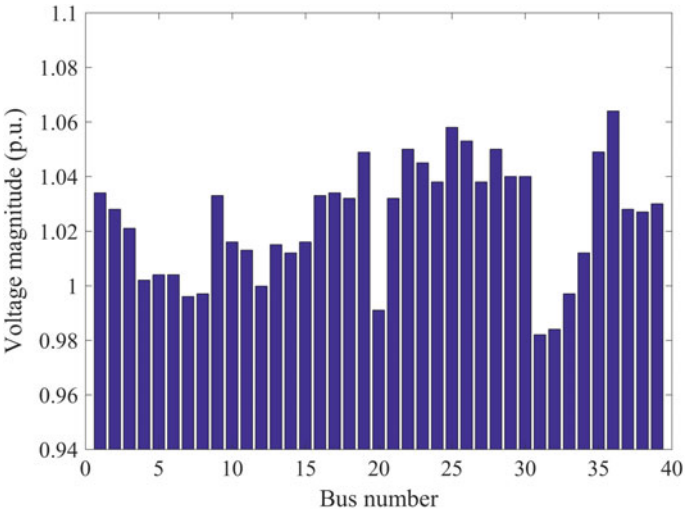

Fig. 4 Bus voltages after CM

Table 5 Comparative representation of Line overload factor

Line number	Before rescheduling	RED [19]	PSO [4]	ABC [3]	MFO [proposed]
L_{15-16}	1.25	1.02	0.98	0.99	0.98

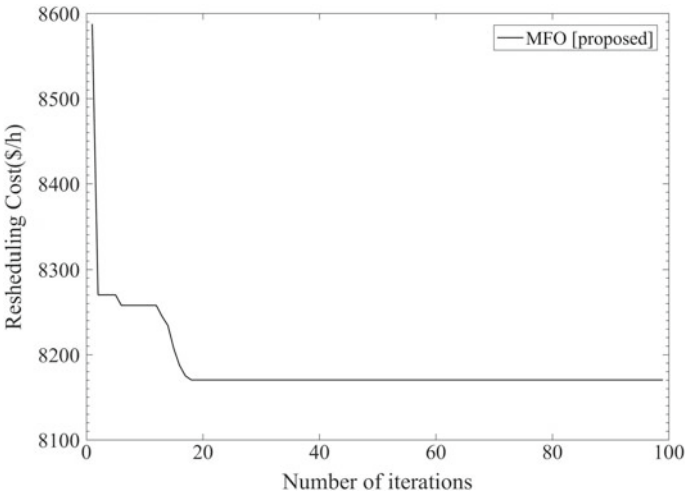

Fig. 5 MFO convergence profile for optimal congestion cost

5 Conclusion

This manuscript has presented MFO as an efficient optimization algorithm for CM problem. The GR method has been utilized involving the most sensitive generator to manage their power deliveries optimally for CM. The system parameters like real power losses and system voltages have also shown significant improvement with the MFO application.

References

1. Chellam, S., Kalyani, S.: Power flow tracing based transmission congestion pricing in deregulated power markets. Int. J. Electr. Power Energy Syst. **83**, 570–584 (2016)
2. Conejo, A.J., Milano, F., García-Bertrand, R.: Congestion management ensuring voltage stability. IEEE Trans. Power Syst. **21**(1), 357–364 (2006)
3. Deb S, Goswami AK (2012) Congestion management by generator rescheduling using artificial bee colony optimization technique. In: 2012 Annual IEEE India conference (INDICON). IEEE, pp 909–914
4. Dutta, S., Singh, S.: Optimal rescheduling of generators for congestion management based on particle swarm optimization. IEEE Trans. Power Syst. **23**(4), 1560–1569 (2008)
5. El Aziz, M.A., Ewees, A.A., Hassanien, A.E.: Whale optimization algorithm and moth-flame optimization for multilevel thresholding image segmentation. Expert Syst. Appl. **83**, 242–256 (2017)
6. Fang, R., David, A.: Transmission congestion management in an electricity market. IEEE Trans. Power Syst. **14**(3), 877–883 (1999)
7. Kaushik, P., Kumar, N.: Cuckoo search algorithm for congestion alleviation with incorporation of wind farm. Int. J Electr. Comput. Eng. **8**(6), 4871 (2018)
8. Khalilpourazari, S., Khalilpourazary, S.: An efficient hybrid algorithm based on water cycle and moth-flame optimization algorithms for solving numerical and constrained engineering optimization problems. Soft Comput. **23**(5), 1699–1722 (2019)
9. Kumar, A., Sekhar, C.: Comparison of sen transformer and UPFC for congestion management in hybrid electricity markets. Int. J. Electr. Power Energy Syst. **47**, 295–304 (2013)
10. Kumar, A., Srivastava, S., Singh, S.: A zonal congestion management approach using real and reactive power rescheduling. IEEE Trans. Power Syst. **19**(1), 554–562 (2004)
11. Luo, C., Hou, Y., Wen, J., Cheng, S.: Assessment of market flows for interregional congestion management in electricity markets. IEEE Trans. Power Syst. **29**(4), 1673–1682 (2014)
12. Mei, R.N.S., Sulaiman, M.H., Mustaffa, Z., Daniyal, H.: Optimal reactive power dispatch solution by loss minimization using moth-flame optimization technique. Appl. Soft. Comput. **59**, 210–222 (2017)
13. Mirjalili, S.: Moth-flame optimization algorithm: a novel nature-inspired heuristic paradigm. Knowl. Based Syst. **89**, 228–249 (2015)
14. Paul, K., Kumar, N., Agrawal, S.: Optimal rescheduling of real power to mitigate congestion with incorporation of wind farm using gravitational search algorithm in deregulated environment. Int. J. Renew. Energy Res. (IJRER) **7**(4), 1731–1740 (2017)
15. Paul, K., Kumar, N., Agrawal, S., Paul, K.: Optimal rescheduling of real power to mitigate congestion using gravitational search algorithm. Turk. J. Electr. Eng. Comput. Sci. **27**(3), 2213–2225 (2019)
16. Pillay, A., Karthikeyan, S.P., Kothari, D.: Congestion management in power systems—a review. Int. J. Electr. Power Energy Syst. **70**, 83–90 (2015)
17. Shahidehpour, M., Yamin, H., Li, Z.: Market Operations in Electric Power Systems: Forecasting, Scheduling, and Risk Management. Wiley, New York (2003)

18. Venkaiah, C., Kumar, D.V.: Fuzzy adaptive bacterial foraging congestion management using sensitivity based optimal active power re-scheduling of generators. Appl. Soft Comput. **11**(8), 4921–4930 (2011)
19. Yesuratnam, G., Thukaram, D.: Congestion management in open access based on relative electrical distances using voltage stability criteria. Electric Power Syst. Res. **77**(12), 1608–1618 (2007)
20. Yıldız, B.S., Yıldız, A.R.: Moth-flame optimization algorithm to determine optimal machining parameters in manufacturing processes. Mater. Test. **59**(5), 425–429 (2017)

Transmission Line Outage Estimation Through Bus Current Comparison Utilizing Current Phasor of PMU

Mehebub Alam, Shubhrajyoti Kundu, Siddhartha Sankar Thakur, and Sumit Banerjee

1 Introduction

The modern power system is operating in a very stressed condition due to various reasons like penetration of renewable energy which is intermittent in nature. Further, the introduction of various power electronic devices has made the power system more and more complex. To this end, any deviation of system parameter may lead to the unstable operation of the system. In past few decades, several blackout events have occurred across the whole world. Researchers reported that the deficiency of monitoring and lack of situational awareness caused these blackout events. In this context, the monitoring of the system parameter in continuous basis is essential to maintain the reliable operation of the power system. The real-time monitoring of the power system can be done through the time-synchronized measurements of phasor measurement units (PMUs). The transmission line outage estimation (TLOE) is one of the key factors in this regard. In past few decades, a number of blackout events have occurred across the globe. The investigations on the 2003 North American blackout and 2012 Indian blackout have pointed out the lack of situational awareness as the root cause of these blackouts. This fact indeed motivated the researchers to find out suitable scheme for accurate estimation of line outage.

M. Alam (✉) · S. Kundu · S. S. Thakur
Department of EE, NIT, Durgapur, Durgapur, West Bengal 713209, India
e-mail: mehebubjgec1990@gmail.com

S. Kundu
e-mail: sk.17ee1102@ee.nitdgp.ac.in

S. S. Thakur
e-mail: sst@ee.nitdgp.ac.in

S. Banerjee
Department of EE, Dr. B.C. Roy Engineering College, Durgapur, West Bengal 713206, India
e-mail: sumit_9999@rediffmail.com

O. H. Gupta and V. K. Sood (eds.), *Recent Advances in Power Systems*, Lecture Notes in Electrical Engineering 699, https://doi.org/10.1007/978-981-15-7994-3_35

A lot of methods related to TLOE topic have been reported in literature. The authors presented a compressive sensing (CS)-based method in [1]. The blockwise compressive sensing (BWCS)-based method has been presented in [2]. A dependency graph-based model is suggested in [3]. The single transmission line outage (STLO) is estimated in [4] by using the support vector machine (SVM)-based tool. The each topology was tested with different loading scenario in [4]. Three different models, viz. DC method (DCM), AC method including loss (ACMIL), and AC method excluding loss (ACMEL) are presented in [5]. Authors address two issues, viz. limited PMUs and computational speed in [6] by employing the ambiguity group theory. In [7], the bus admittance matrix-based model is presented using the phasor angle of PMUs, and the TLOE is performed by comparing the bus power. Data mining-based method is adopted in [8] to detect distribution line outage. The multilevel SVM [8] tool is used to identify the status of the line using customer smart meter data. The transient state of power system is considered during detection of outage in [9].

Most of the TLOE models utilize the voltage phasor of PMU. In transmission network, a bus is connected with single or multiple lines. Therefore, if a PMU is placed at any bus, then a single voltage phasors can be obtained and multiple current phasors can be obtained through PMU. It is clear that the number of observable voltage phasors is always less than the number of observable current phasors for the transmission network. To this end, it can be inferred that information available using current phasors will be more than using voltage phasors. In this work, current phasors of PMUs are utilized to develop the TLOE model.

2 Methodology

The bus currents can be simulated easily for each possible outage cases (OCs). These simulated bus currents (SBCs) are stored by case to case basis. Now, when actual outage happens, the line current measurements are available from PMUs. From these line currents, bus currents are calculated which are termed as measured bus currents (MBCs). The proposed methodology detects the line outage by comparing the SBCs for each OCs with MBCs calculated from PMU measurements after actual outage occurs. We assume that PMUs are located optimally and the current measurements are available through PMUs. It is also assumed that the post-outage system reaches to the quasi-stable state.

2.1 TLOE Model Without Bad Data

Let us proceed with a system having N buses and L lines. We can write the complex line current (I_{pq}) flowing between pth bus to qth bus as

$$I_{pq} = (V_p - V_q)y_{pq} + y_{p0}V_p \tag{1}$$

where V_p and V_q is the voltage phasor of pth bus and qth bus, respectively. y_{pq} is the admittance between pth and qth bus. Further, y_{p0} denotes the line charging admittance elements connected at pth bus. The bus currents can be computed by summing up the currents of the lines connected to that particular bus. Let the magnitude of SBCs for different OCs be represented by

$$I_{s,\text{bus}}^{k} = \left[I_s^1, I_s^2, \ldots, I_s^n\right] \tag{2}$$

Here $I_{s,\text{bus}}^{k}$ is the SBCs for kth OC and we can write $k = 1, 2, \ldots, n$; n represents the total OCs. Considering a specific simulated OC, i.e., for nth OC, the SBCs can be written as

$$I_s^n = \left[I_{s,1}, I_{s,2}, \ldots, I_{s,N}\right]^{\text{T}} \tag{3}$$

Here, I_s^n represents the SBCs for nth OC and its dimension is $N \times 1$. As the PMUs are installed around the network, the MBCs can be obtained from PMUs following the line outage. The MBCs (by summing up the current of lines connected to the specific bus) from PMU are denoted by

$$I_{m,\text{bus}} = \left[I_{m,1}, I_{m,2}, \ldots, I_{m,N}\right]^{\text{T}} \tag{4}$$

The mismatch between MBCs from PMUs and SBCs for OC-k can be expressed by

$$I_{m,\text{bus}} - I_{s,\text{bus}}^{k} = \begin{bmatrix} I_{m,1} - I_{s,1}^{k} \\ I_{m,2} - I_{s,2}^{k} \\ \vdots - \vdots \\ I_{m,N} - I_{s,N}^{k} \end{bmatrix} \tag{5}$$

The TLOE problem can be formulated by comparing the set of SBCs for various OCs with MBCs. Therefore, the TLOE problem can be expressed by

$$F1\left(k;\, I_{m,\text{bus}}, I_{s,\text{bus}}^{k}\right) = \left\| I_{m,\text{bus}} - I_{s,\text{bus}}^{k} \right\|_2^2 \tag{6}$$

However, this expression is applicable for ideal case only where measurements are considered to be noise-free and error-free. In real power system, measurements are subjected to noise addition. Therefore, we introduce a noise vector τ to reflect this noise into the mathematical model. Now, after including the noise vector, the TLOE problem is defined as

$$F2\left(k;\, I_{m,\text{bus}}, I_{s,\text{bus}}^{k}\right) = \left\| I_{m,\text{bus}} - I_{s,\text{bus}}^{k} + \tau \right\|_2^2 \tag{7}$$

Thereby, the outage of line can be estimated using the following expression

$$k = \text{index}\left(\min\left(F2\left(k;\, I_{m,\text{bus}},\, I^{k}_{s,\text{bus}}\right)\right)\right) \tag{8}$$

2.2 TLOE Model with Bad Data

It is worth noting that if all the current phasor measurements of PMUs are free from error, then the solution given by (7) and (8) will be correct. However, in real power network, some measurements may be erroneous which will affect the estimation procedure. Let, error in bus current measurements is to be added to the original measurements ($I_{m,\text{bus}}$) to get the final corrupted measurements. Mathematically, corrupted bus current measurements ($I_{mb,\text{bus}}$) due to bad data be represented by

$$I_{mb,\text{bus}} = I_{m,\text{bus}} + I_{b\text{bus}} \tag{9}$$

Now, considering the erroneous measurement of all line currents, we define *total error vector* (G) using the following expression

$$G = K\, I_{m,\text{bus}} \tag{10}$$

Here, the term K represents *error coefficient*. As per IEEE standard C.37.118-2011, PMU error is specified by the total vector error (TVE) which will be within 1%. It is to be noted that we have varied the value of K from 0.01 to 0.05 in this work to check the effectiveness of the proposed model for the error from 1% to 5%. Now, let us introduce the *final error vector* (h) which will basically add the error to the measurements. The *final error vector* is defined as

$$h_k = \begin{cases} G_k, \text{ if } k\text{th bus is connected with faulty PMU} \\ 0, \qquad\qquad\qquad \text{otherwise} \end{cases} \tag{11}$$

Now, the status of disconnected line is denoted by outage vector (OV) (s_0). Set of disconnected line is denoted by $\mathcal{L}_{\text{out}}$, and set of all line is denoted by $\mathcal{L}$. Now, the OV can be written as

$$s_0 = \begin{cases} 1, \text{ if } l \in \mathcal{L}_{\text{out}} \\ 0, \text{ otherwise} \end{cases} \tag{12}$$

Let the set of lines connected to the buses having faulty PMUs is denoted by $\mathcal{L}_b$ and we can write $\mathcal{L}_b \subset \mathcal{L}$. Now, we consider s_b be the binary vector which is defined as

$$s_b = \begin{cases} 1, & \text{if } l \in \mathcal{L}_b \\ 0, & \text{otherwise} \end{cases} \tag{13}$$

Now, including the bad data, the TLOE problem can be written as

$$F3\left(k;\, I_{m,\text{bus}},\, I^k_{s,\text{bus}},\, h\right) = \left\| I_{m,\text{bus}} - I^k_{s,\text{bus}} + h + \tau \right\|_2^2 \tag{14}$$

So, estimation of outages can be done using the following expression

$$k = \min\left(F3\left(k;\, I_{m,\text{bus}},\, I^k_{s,\text{bus}},\, h\right)\right) \tag{15}$$

The procedure of the developed TLOE algorithm is described step by step as follows:

Step 1: Read the system data, SD of noise, % error, etc.
Step 2: Conduct the load flow study for various OCs. Thereafter, store the SBCs $\left(I^k_{s,\text{bus}}\right)$ for various OCs.
Step 3: Take the measurements of the line currents from PMUs
Step 4: If any PMU is faulty, proceed to step 6 else proceed to step 5.
Step 5: For possible OCs, calculate L2-norm value (LNV) using (7) and proceed to step 8.
Step 6: Calculate the error (h)
Step 7: Calculate L2-norm value (LNV) using (14) for various OCs
Step 8: Find out the minimum LNV and its related index.
Step 9: Estimate the OC and form the OV.

3 Simulation Results

Simulation of the proposed TLOE algorithm was carried out in MATLAB 2013 version with Intel i-3 processor (2.4 GHz) and 4 GB RAM. The standard IEEE 5-, 14-, 57-bus systems [10] and Damodar Valley Corporation (DVC) 38-bus [11] Indian practical system were used as the test networks. The SD of noise was varied from 1 to 5%. The system loading is assumed to be base load.

3.1 IEEE 5-Bus Test Case

For IEEE 5-bus network, let outage occur at line no. 6 with faulty PMU at bus 2. Considering bad data error and noise SD 5%, the L2-norm value (LNV) obtained is given as:

$$\text{LNV} = [8.8044\ 1.6837\ 1.6099\ 1.3739\ 3.5271\ \mathbf{0.1252}\ 1.8284]$$
$$\text{Minimum LNV} = \mathbf{0.1252};\ \text{Index} = 6$$

The outage of line no. 6 is referred by the index 6. Hence, we can form OV as, $s_o = [0000010]^T$ and also we can write, $s_b = [1011100]^T$. The results for this case are represented by Fig. 1. The LNV for seven single line OCs are presented in Table 1.

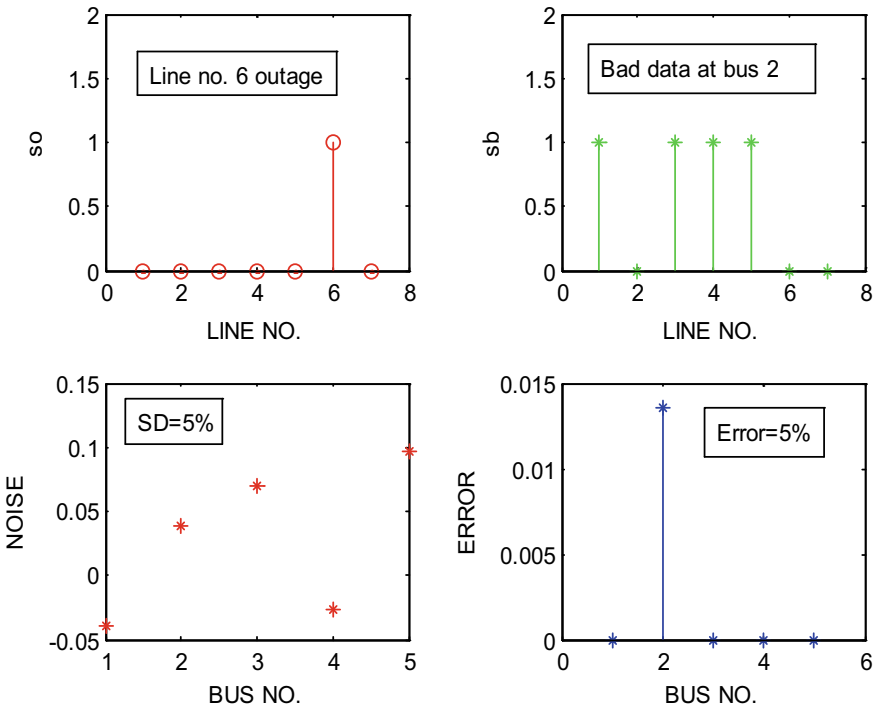

Fig. 1 Outage of line 6 (error, noise SD 5%)

Table 1 LNVs for seven OCs of IEEE 5-bus network

OC	Outage of line no.						
	1	2	3	4	5	6	7
1	**0.1981**	0.2262	0.2914	0.2533	0.1944	0.2611	0.2657
2	0.3407	**0.019**	0.0764	0.0507	0.1215	0.0412	0.0467
3	0.359	0.0272	**0.0605**	0.0448	0.1327	0.0244	0.0303
4	0.3575	0.0265	0.063	**0.0441**	0.131	0.0249	0.0322
5	0.3093	0.0857	0.1519	0.0961	**0.0713**	0.1057	0.1069
6	0.3651	0.0316	0.0616	0.0448	0.1331	**0.0199**	0.0277
7	0.367	0.0338	0.0619	0.045	0.1329	0.021	**0.0247**

For a particular OC, the seven LNV can be found considering STLO. Among these LNV, the minimum LNV will indicate the actual OC. Bold face value indicates the minimum LNV which refers to actual outage. For instance, in case of line 1 outage, the minimum LNV is found 0.1981 which basically represents the OC-1. Here, minimum LNV, i.e., 0.019, 0.0605, 0.0441, 0.0731, 0.0199, and 0.0247, indicates the outage of line 2, 3, 4, 5, 6, and 7, respectively. Further, the double transmission line outage (DTLO) at line no. 2 and 7 is considered. The noise SD and bad data error are assumed to be 5% with bad data at bus 5. The LNV obtained after simulation is given below:

$$\begin{aligned}\text{LNV} = [&35.8582\ 9.3363\ 8.5437\ 9.4567\ 207.4243\\ &9.3168\ 1.4810\ 1.0589\ 4.0368\ 0.7487\ \mathbf{0.1135}\\ &1.7315\ 4.4641\ 1.2847\ 0.7479\ 5.2631\ 9.8736\\ &1.0177\ 9.7460\ 1.6465]\\ \text{Minimum LNV} = &\mathbf{0.1135};\ \text{Index} = 11\end{aligned}$$

The index 11 refers to the outage of line 2, 7. In this case, OV can be written as,$s_o = [0100001]^T$ and also we can write,$s_b = [0000101]^T$. The simulation result for this case is illustrated in Fig. 2. It is clearly seen from Figs. 1 and 2 that the error is added only at bus 2, i.e., the bus at which the bad data is located. The line 1, 3, 4, 5 are connected with bus 2. Therefore, the s_b associated with these lines are denoted by "1" and other lines are denoted by "0".

3.2 IEEE 14-, 57-Bus and DVC 38-Bus Test Case

For IEEE 14-bus, single line outage (line 11) detection with faulty PMU at bus 6 is considered. The error and noise SD of 5% are assumed as shown in Fig. 3. The LNV for various single line OCs are highlighted in Fig. 4. For this system, 19 LNV can be found considering STLO. From this Fig. 4, it is clear that the minimum LNV (0.1296) obtained for OC no. 11 which corresponds to line no.11. The lines 10, 11, 12, and 13 are connected with bus 6. Hence, the s_b associated with these lines are denoted by "1" which can be seen from Fig. 3 and error is added at bus 6.

For IEEE 57-bus, the outage of line 40 is considered with faulty PMU at bus 29 (error and noise SD of 5% take into account). The obtained LNV for different single line OCs is displayed in Fig. 5, and this estimated case is represented in Fig. 6. For this system, 78 LNV can be found considering STLO. The minimum LNV (0.4408) obtained for OC no. 40 basically refers to the outage of line 40. The error is added at the bus 29 as the bad data is assumed at this bus.

The simulation results of few single line OCs of IEEE 14-bus test system are summarized in Table 2. The location of bad data is written in the bracket. For this system, 19 LNVs are found for each single line OC. The minimum LNV is marked with bold face value which refers to the actual OC. Here, minimum LNV, i.e., 0.6636,

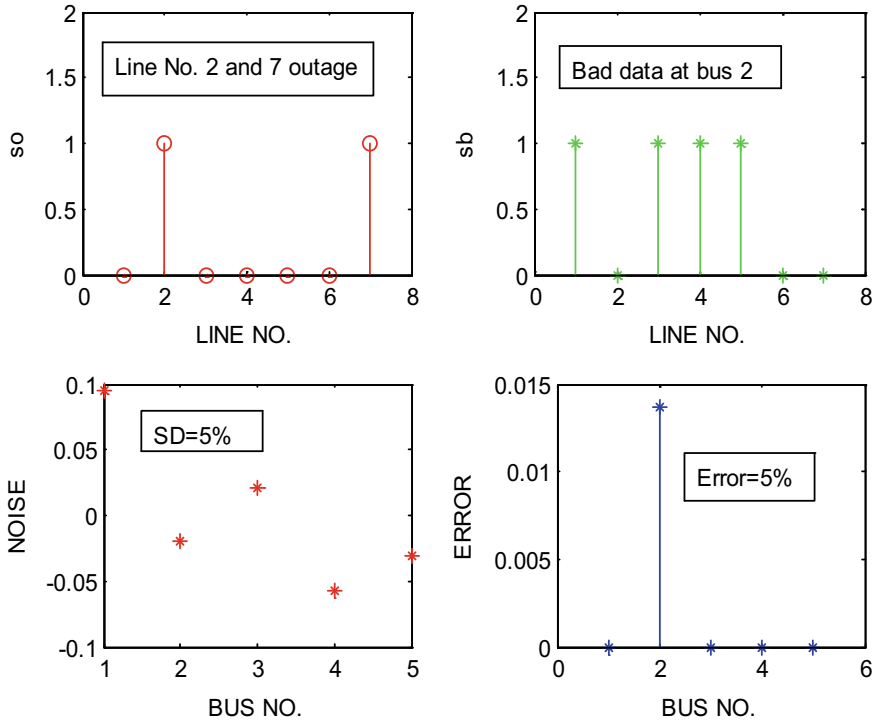

Fig. 2 Outage of line 2, 7 (error, noise SD 5%)

0.1546, 0.226, 0.1683, 0.1954, 0.1988, 0.192, and 0.185, indicates the outage of line 1, line 2, line 3, line 4, line 5, line 6, line 7, and line 10, respectively. The position of the bad data is also varied, and simulation test has been conducted. The different position of bad data is mentioned in the bracket of Table 2. We found that for different position of bad data, the estimation of line outage has been performed accurately. The DVC is a public sector utility under Ministry of Power Government of India. The transmission network of DVC basically covers two states West Bengal and Jharkhand. DVC network consists of 38 buses and 48 lines. The proposed TLOE scheme is also applied on this practical system. For this network, we consider 39 single contingencies. Therefore, 39 LNV can be obtained for each case of STLO.

4 Discussion

We have tested total 300 OCs (143 single line and 157 double line OCs) considering all the test systems. During simulation study, it has been found that some of the OCs lead to the divergence of power flow solution. These diverging cases (DCs) are beyond the scope of this study. The DCs for all STLO and few double transmission

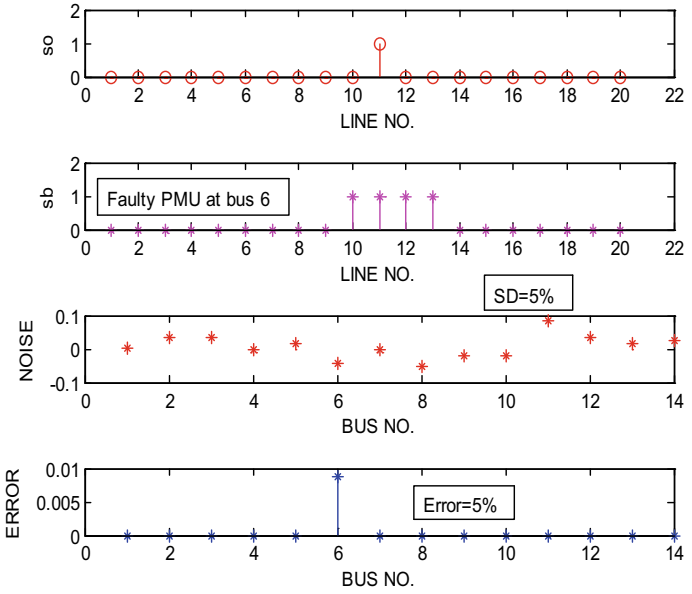

Fig. 3 Outage of line 11(noise SD 5%)

Fig. 4 NVs for various OCs of IEEE 14-bus network

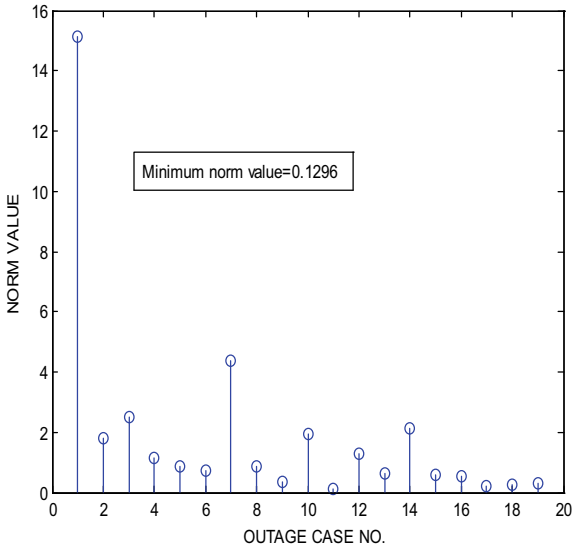

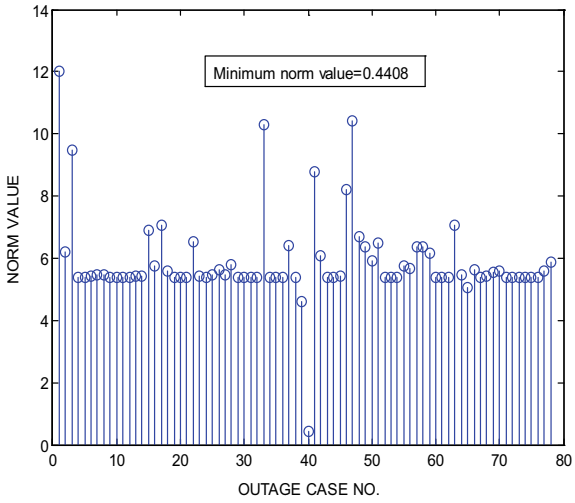

Fig. 5 NVs for various OCs of IEEE 57-bus network

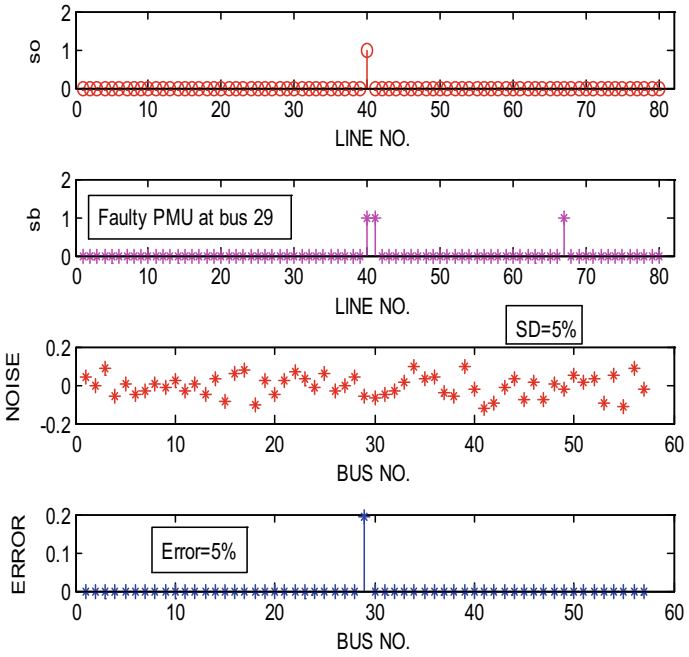

Fig. 6 Outage of line 40 noise SD 5%

Table 2 LNVs for few OCs of IEEE 14-bus network

Line outage (bus no. with bad data)							
1(2)	2(2)	3(6)	4(7)	5(6)	6(7)	7(9)	10(9)
0.6636	14.0868	14.0672	14.6302	14.6751	15.0996	15.6504	15.2394
13.6496	**0.1546**	2.9111	1.9769	1.3547	1.9182	3.8437	1.8956
13.7321	2.8519	**0.226**	2.2357	2.1784	2.0664	4.9234	3.1748
14.2634	2.0123	2.3228	**0.1683**	1.073	1.536	3.8238	2.2556
14.4022	1.392	2.3604	1.0422	**0.1954**	1.1169	3.959	1.6437
14.716	1.8749	2.1308	1.4538	1.0402	**0.1988**	4.5938	2.072
15.2812	3.8789	4.9987	3.8673	3.9446	4.6403	**0.192**	3.8352
14.7211	1.9161	2.6341	1.405	1.1553	0.9928	4.5089	2.1154
14.7217	1.7581	2.5674	1.2535	0.8907	0.6751	4.5105	1.9613
14.8353	1.8672	3.3006	2.2098	1.7372	2.1642	3.8185	**0.185**
14.7166	1.7763	2.5619	1.0902	0.8816	0.7793	4.3591	1.9237
14.6709	2.0839	2.7944	1.6719	1.5258	1.4421	4.5166	2.0748
14.7191	1.8418	2.6413	1.2417	1.0989	0.9843	4.398	1.755
14.8829	2.7066	3.2709	2.3733	2.2902	2.1606	4.8471	2.8711
14.7379	1.8296	2.6125	1.224	1.0755	0.9677	4.3786	1.9795
14.7293	1.8052	2.5965	1.1583	0.9418	0.8754	4.3758	1.9692
14.7202	1.7573	2.5528	1.0864	0.8722	0.7564	4.3502	1.9476
14.7224	1.7497	2.5566	1.0769	0.841	0.7241	4.3482	1.9434
14.7186	1.7601	2.5557	1.0858	0.8438	0.7561	4.3539	1.957

line outage (DTLO) are listed in Table 3. The efficiency of the proposed algorithm is determined through the estimation rate which is defined as follows.

$$\text{Estimation rate} = \frac{\text{Successfully estimated cases}}{\text{Total trials}}$$

For illustration, 7 single line OCs and 20 double line OCs are estimated successfully in case of IEEE 5-bus network. Therefore, the estimation rate (excluding DCs) will be $27/27 = 100\%$ and estimation rate (including DCs) will be $27/28 = 96.42\%$. The comparison of the estimation rate of the proposed scheme with some existing

Table 3 DCs for various test systems

Outage	IEEE network			DVC 38-bus
	5-bus	14-bus	57-bus	
STLO	–	14	45,48	8,9,33,34,42,43,44,46,47
DTLO	(5,7)	(14,20), (17,20	(29,30), (38,39), (39,40)	(7,8), (9,10), (32,33), (41,42), (44,45), (47,48)

Table 4 Comparison of estimation rate for various test networks

Method	IEEE networks			DVC 38-bus (%)
	5-bus	14-bus (%)	57-bus (%)	
Ref. [6] with PMU at 30% buses	–	80	65	
Ref. [5] ACMEL	–	–	91	–
Ref. [5] DCM	–	–	81	–
Ref. [5] ACMIL	–	–	93.5	–
Proposed (including DCs)	96.42	95.833	96.24	85.14
Proposed (excluding DCs)	100	100	100	100

schemes is shown in Table 4. The 30% PMU coverage is considered for the comparison with method [6], as we know that PMUs are to be located roughly at the 1/3 of total network buses. Table 4 clearly proves the supremacy of the proposed algorithm w.r.t estimation rate. The cases for which the system become islanded are not considered here.

5 Conclusion

A new model for TLOE is developed in this paper. The developed TLOE model utilizes the current phasors of PMUs. The developed scheme is based on AC power flow model, and hence, AC nature of the transmission system can be exploited through the proposed model. The efficiency of the proposed model is compared with two existing models, and the satisfactory results have been found. The estimation rate excluding DCs is found to be 100% for all the test networks. On the other hand, the estimation rate including DCs is found 96.42, 95.833, 96.24, and 85.14% in case of IEEE 5-, 14-, 57-bus and DVC 38-bus network, respectively. In view of this, the improvement in estimation rate is observed w.r.t the methods reported in [5, 6]. Therefore, the proposed model can be utilized for identification of network topology, so that the control actions can be taken in order to ensure the power system reliability and security. In this work, TLOE has been tested up to double contingency. The consideration of more than two line outages is left for future scope of this work. In near future, the reduction of required number of PMUs will open an area to the power system researchers.

References

1. Babakmehr, M., Harirchi, F., Al-Durra, A., Muyeen, S.M., Simões, M.G.: Compressive system identification for multiple line outage detection in smart grids. In: IEEE Trans. Ind. Appl. **55**(5), 4462–4473 (2019)

2. Yang, F., Tan, J., Song, J., Han, Z.: Block-wise compressive sensing based multiple line outage detection for smart grid. IEEE Access **6**, 50984–50993 (2018)
3. He, M., Zhang, J.: A dependency graph approach for fault detection and localization towards secure smart grid" IEEE Trans. Smart Grid **2**(2), 342–351 (2011)
4. Abdelaziz, A.Y., Mekhamer, S.F., Ezzat, M., El-Saadany, E.F.: Line outage detection using support vector machine (SVM) based on the phasor measurement units (PMUs) technology. In: IEEE PES General Meeting, pp. 1–8 (2012)
5. Arabali, A., Ghofrani, M., Farasat, M.: A new multiple line outage identification formulation using a sparse vector recovery technique. Electr. Power Syst. Res. **142**(3), 237–248 (2017)
6. Wu, J., Xiong, J., Shi, Y.: Efficient location identification of multiple line outages with limited PMUs in smart grids. IEEE Trans. Power Syst. **30**(4), 1659–1668 (2015)
7. Alam, M., Kundu, S., Thakur, S.S., Banerjee, S.: A new algorithm for single line outage estimation. In: 2019 Devices for Integrated Circuit (DevIC), Kalyani, India, pp. 113–117 (2019)
8. Hosseini, Z.S., Mahoor, M., Khodaei, A.: AMI-enabled distribution network line outage identification via multi-label SVM. IEEE Trans. Smart Grid **9**(5), 5470–5472 (2018)
9. Rovatsos, G., Jiang, X., Dominguez-Garcia, A.D., Veeravalli, V.V.: Statistical power system line outage detection under transient dynamics. IEEE Trans. Signal Process. **65**(11), 2787–2797 (2017)
10. 'Power Systems Test Case Archive'. https://labs.ece.uw.edu/pstca/
11. www.dvc.gov.in

Analysis of the Impacts on Power Flow After Introducing Renewable Energy Source in a Power System with HVDC Line

Md. Mehedi Hasan Tanim, Md. Feroz Ali, Md. Asaduzzaman Shobug, and A. A. Mamun

1 Introduction

With the increase of energy demand in this modern world due to many factors including industrialization and population growth, a number of power plants based on different energy sources are connected in a grid system which is also increasing [1]. For introducing various types of power plant needed a particular arrangement or design for power system stability. Because stability is concerned with voltage level in the grid, instability may result in voltage collapse as well as various connected components may shut down or damaged, and it will result in economic loss [2]. Determining voltage magnitude and voltage angle at each bus and as well as real and reactive power flows from bus to bus is an essential parameter for determining and analysing power system stability. So in a newly installed power system, it is necessary to study the power flow.

At [1, 2], stability condition of IEEE-21 bus and IEEE-14 bus system, respectively, has demonstrated under load changes, line outage or three-phase fault. But they have considered only variable speed wind turbines. They did not consider changing the transmission system; in this paper, a direct drive synchronized generator with wind turbine and HVDC transmission link has been considered for power flow studies. Two excellent software packages for power system analysis, i.e., UWPFLOW and PSAT, have described briefly with their advantages in [3–6]. These references use only IEEE standard power system as an example of using this software; in this paper, WSCC-9 bus system has taken as an example of study. A method of improving the dynamic

Md. M. H. Tanim (✉) · Md. F. Ali · Md. A. Shobug
Department of Electrical and Electronic Engineering, Pabna University of Science and Technology, Pabna 6600, Bangladesh
e-mail: mehedihasantanim@gmail.com

A. A. Mamun
Faculty of Engineering and Technology, Multimedia University, Melaka 75450, Malaysia

O. H. Gupta and V. K. Sood (eds.), *Recent Advances in Power Systems*, Lecture Notes in Electrical Engineering 699, https://doi.org/10.1007/978-981-15-7994-3_36

stability of an HVDC line has shown in [7], and it has also shown a comparison of performance in IEEE-14 bus and IEEE-9 bus system. In this research paper, a new power system has taken for showing HVDC transmission performance. Impacts of introducing wind turbine on power flow have been described in [9], effects on reactive power compensation on [10], whereas effects on transient stability have shown in [11–13]. This study adds a new method of power flow study with HVDC transmission and renewable energy sources together [14] and describes HVDC performance by calculating voltage and frequency in sending end in a practical power system (Hu-Liao DC project) with the thermal power plant and [15] demonstrates power flow study in the IEEE-57 bus system; in this research, we have focused on power flow because of HVDC and wind farm in a new power system.

For various advantages, renewable energy sources are getting popular day by day. Wind power station or wind farm is an example of a renewable energy source. In this paper WSCC-9 bus, three machine systems are used as a test power system because it was never used before for this type of study. On that system, HVDC transmission line and wind farm have been installed by using PSAT, and analysis has been done under reasonable operating condition.

This paper is organized as follows: Sect. 2 describes the methodology for power flow studies and test system design, Sect. 3 discusses on HVDC transmission link in the power system. Section 4 describes wind farm technology, and Sect. 5 simulates WSCC-9 bus three-machine power system without and with wind farm and HVDC transmission link; this section also illustrates the result of the simulation. Finally, Sect. 6 illustrates the conclusion.

2 Methodology

For power system analysis, commercial and educational/research aimed software's are available. It is not possible to change source code that means the user cannot add a new algorithm into commercial software (PSS/E, Simpow, and CYME) [1]. On the contrary, educational software allows user to do that like UMPFLOW [2]. PSAT is a toolbox for power system analysis; it distributes freely online; and it is based on MATLAB. It can run on GNU/Octave also [3, 4], and feature includes on PSAT

- Power flow analysis
- Optimal power flow analysis
- Time-domain analysis
- Continuation power flow analysis.

This package also provides a Simulink based one line network editor and a complete graphical interface for the setting system and routine parameters. It also includes a converter to convert data from one format into another. User can build their model and see command logs on this software [1, 5].

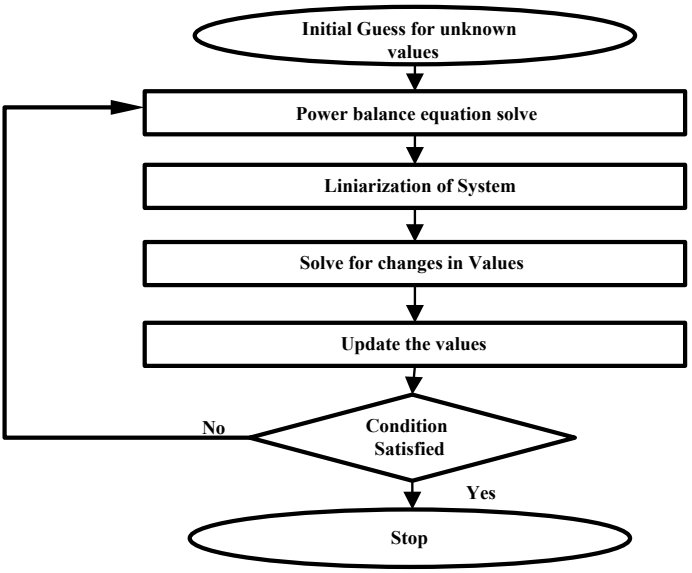

Fig. 1 Newton–Raphson method flow diagram

2.1 Power Flow Analysis

Power flow analysis in a power system is essential for designing, planning and economic scheduling. It involves numerical analysis in a power system. Various information can be found by this analysis as an example voltage magnitude and voltage angle at each bus in the system, real and reactive power flowing through each transmission line during simulation [4]. PSAT includes six types of power flow solver [6]; they are XB and BX fast decoupled method, Newton–Raphson (NR) method, Runge–Kutta method, Iwamoto method and simple robust method.

In this paper for power flow analysis, NR method is used. This analysis is also crucial for selecting transmission line priorities list if necessary, that means if a line is taken off for maintenance, this analysis can show whether other lines can operate without overload or not [5] (Fig. 1).

2.2 Test System Structure

Total of two cases has considered in this part. Case A, which is indicated here as the base power system, consists of three synchronous generators with three automatic voltage regulators, three transformers, three PQ loads, two PV buses and a slack bus. Some parameters are shown in Fig. 2. Detail parameters of WSCC-9 bus system can be found on reference [13]. Reason for using the WSCC system for simulation is its

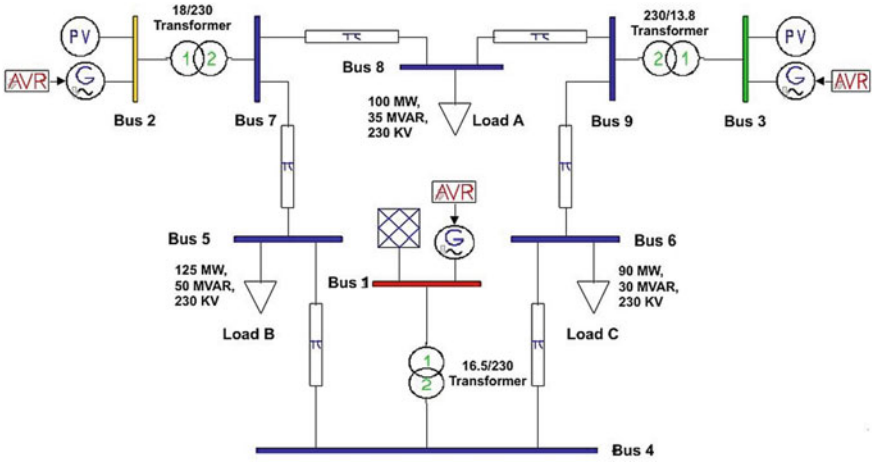

Fig. 2 WSCC-9 bus system as the base power system

effectiveness on planning studies and its simplicity. For the simulation of all cases in PSAT interface, base frequency was 50 Hz, power base was 100 MVA, maximum power flow (PF) and dynamic iteration was 20.

3 High Voltage Direct Current (HVDC) Transmission

HVDC transmission system is used because the DC system can operate in high voltage without significant current loss. So it can carry more power than the AC line, and power transfer between two systems operating at different frequencies is comparatively easy. This system uses inverter and rectifier for connecting in the AC network, as shown in Fig. 3 [7].

Both DC and AC system equations joint solutions are required for a power flow analysis of an HVDC system. Various methods are available for finding these solutions. There are two types of variables available for DC equations independent and dependent; both types of variables depend on control modes of converters, i.e., inverter and rectifier. By taking rectifier on constant current (CC), control modes and

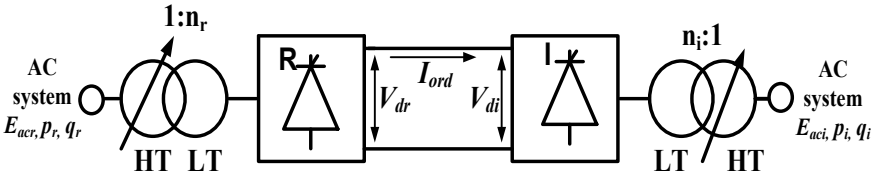

Fig. 3 HVDC transmission link

inverter on constant excitation angle (CEA) control mode following output equations have been found [8]. By taking subscript 'i' for inverter and 'r' for rectifier,

no-load direct voltage for inverter can be written as

$$V_{\text{doi}} = \frac{3\sqrt{2}}{\pi} B_i n_i E_{aci} \tag{1}$$

where B_i denotes series-connected bridge number, n_i denotes turns ration of a transformer, E_{aci} denotes RMS line to line voltage on high transmission (HT) side

Now, direct voltage per pole at DC system can be found from below equation

$$V_{\text{di}} = V_{\text{doi}}(\cos \gamma_{\min}) - \frac{3}{\pi} X_{\text{ci}} B_i I_{\text{ord}} \tag{2}$$

where X_{ci} indicates reactance for commutation per phase or per pole and $\gamma_{\min}$ is firing angle at the inverter. In Eq. (2), V_{doi} is known from the previous Eq. (1) so it can be easily calculated. Equations for finding real power at inverter side are –

$$P_i = V_{\text{di}} I_{\text{ord}} \tag{3}$$

Both terms for this calculation are already known from the previous two equations. For finding reactive power at inverter power factor angle needed which is a ration of direct voltage and no-load direct voltage as in below equation

$$\emptyset_i = \cos^{-1}\left(\frac{V_{\text{di}}}{V_{\text{doi}}}\right) \tag{4}$$

Now reactive power can be found by using

$$Q_i = P_i \tan \emptyset_i \tag{5}$$

where P_i is the real power in inverter as in Eq. (3) and $\emptyset_i$ is the power factor angle as in Eq. (4).

Now for the rectifier section, all equations above are the same just need to use subscript 'r' instead of 'i' [8]. In this paper, a current control with 230 kV at both side terminal buses and 300 kV, .3 kA DC rated HVDC transmission link used for simulation.

4 Wind Farm

A wind farm or wind power plant is a place which consists of multiple numbers of the wind turbine. Wind turbine generator can be classified into four groups [9]

- Doubly fed asynchronous generators of variable speed.

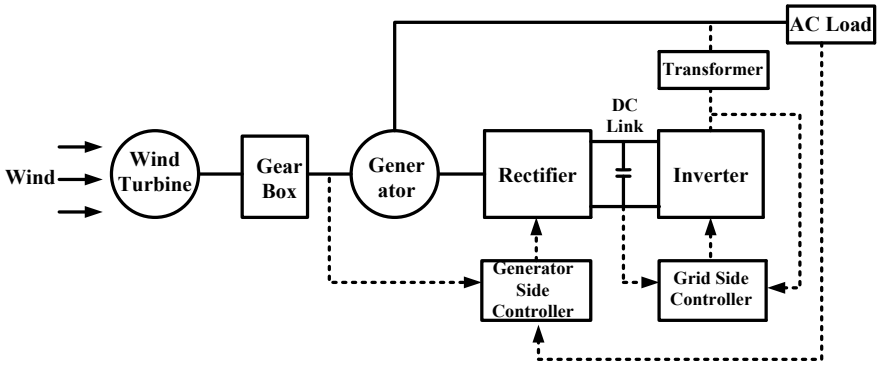

Fig. 4 Grid-connected wind power system

- Generator of variable speed and with full converter interface.
- Fixed speed squirrel cage induction generators
- Induction generators with variable slip and variable rotor resistance.

All these wind turbine generators consume a large amount of reactive power, so major difficulties that an existing grid will face if a wind farm is introduced is that, adjusting the sizeable reactive power consumption by that machines. Failure of adjusting reactive power may cause voltage stability problem. As a result, the local transmission network voltage may collapse [10, 11].

4.1 Wind Power System Modelling and Energy Calculation

Principle component for a grid-connected wind power system has shown below in Fig. 4. A wind turbine converts available kinetic energy of wind in the environment into electrical energy by using gearbox and generators, and this principle has been described in various references by using different types of aero-generators [11, 12]. The output mechanical power of a wind turbine can be modelled as

$$P_{\mathrm{m}} = \frac{A\rho V_{\mathrm{wind}}^{3}}{2} C_{\mathrm{p}}\lambda\beta \tag{6}$$

where A indicates surface area pick up by wind turbine, ρ denotes the density of air, $\mathrm{V}_{\mathrm{wind}}$ denotes the speed of wind, C_{p} represents the coefficient of power. Now tip ratio speed λ can be calculated from

$$\lambda = \frac{\Omega_{\mathrm{r}} R}{V_{\mathrm{wind}}} \tag{7}$$

where Ω_r is the turbine blade mechanical angular velocity, R represents the radius of the rotor blade. The gearbox can be modelled as follows

$$C_g = \frac{C_{aero}}{G} \tag{8}$$

PSAT Simulink library contains numerous types of wind turbine, both variable and constant speed. For this research, a direct drive synchronous generator with a variable speed wind turbine has been used. The wind park consists of 10 machines each rated 100 MVA, 16.5 kV, 60 Hz, and nominal wind speed measured 15 m/s with air density 1.22 kg/m^3.

5 Simulation Result and Analysis

After power flow analysis has been done for Case A, Fig. 5, 7, 9 and 11 indicate its result. Now transmission line from bus 7 to bus 8 is replaced by an HVDC transmission link as described in Sect. 3, and synchronous generator at bus 1 is replaced by a wind farm as modelled in Sect. 4. This combination is indicated as Case B in this paper. Now again, power flow analysis has been done on the Case B power system, and results have shown in Figs. 6, 8, 10 and 12. Buses 1, 2, 3 are synchronous generator bus, and buses 5, 6, 8 are load bus.

From the voltage magnitude profile in Figs. 5 and 6, it can be seen that after introducing HVDC and wind farm voltage level has slightly reduced in buses no. 7 and 8, which is a slight change but a significant change has happened in the voltage angle profile, and it can be observed from Figs. 7 and 8. Bus no. 1 is considered as reference bus. Hence, angle remains almost zero for both cases, but at bus no.1 synchronous generator is replaced by a direct driven synchronous generator with variable speed wind turbine, so at bus no. 3 voltage angle almost became double.

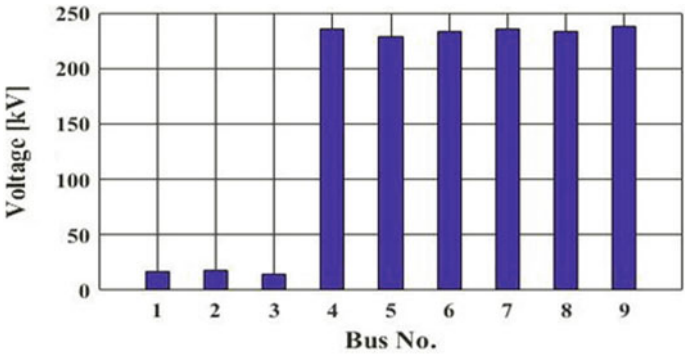

Fig. 5 Voltage magnitude profile for base power system

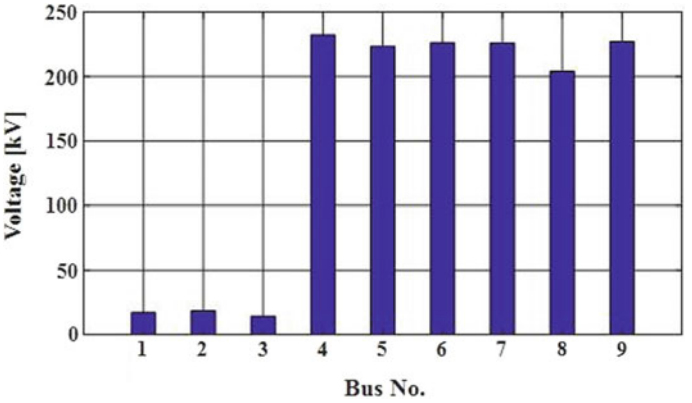

Fig. 6 Voltage magnitude profile with HVDC and wind farm

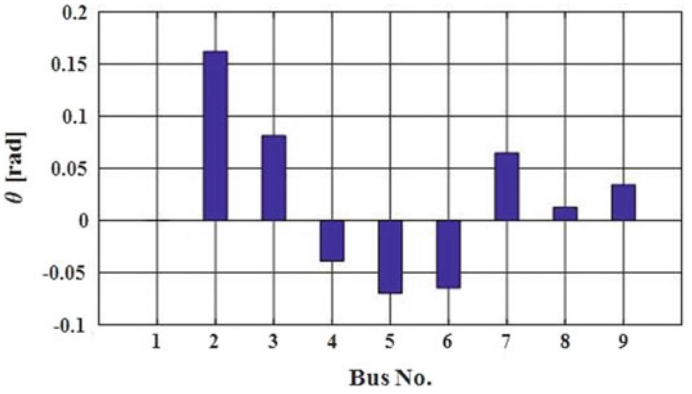

Fig. 7 Voltage angle profile for base power system

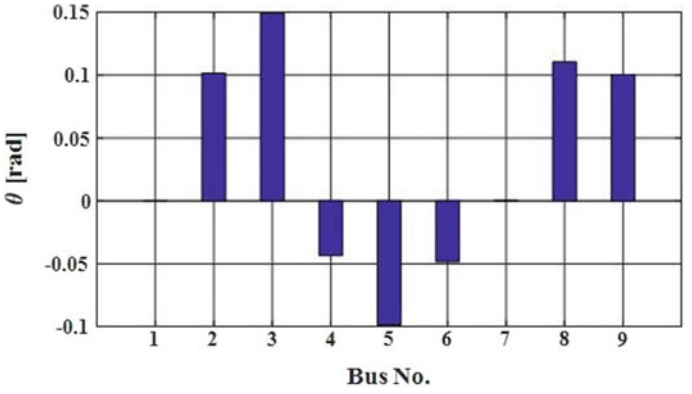

Fig. 8 Voltage angle profile with HVDC and wind farm

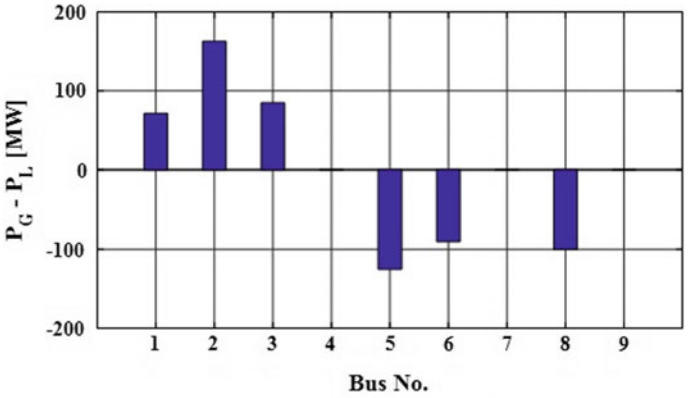

Fig. 9 Real power profile for base power system

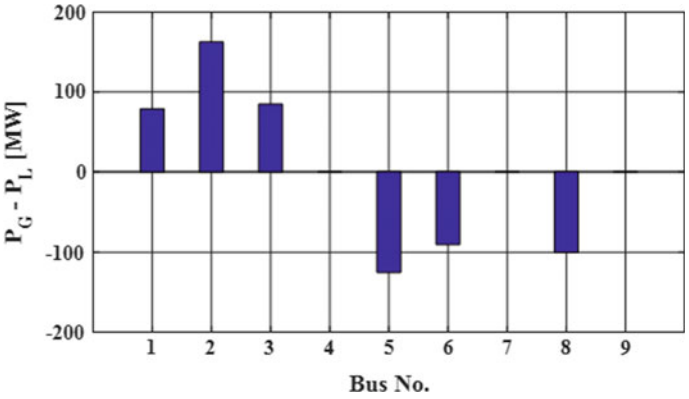

Fig. 10 Real power profile with HVDC and wind farm

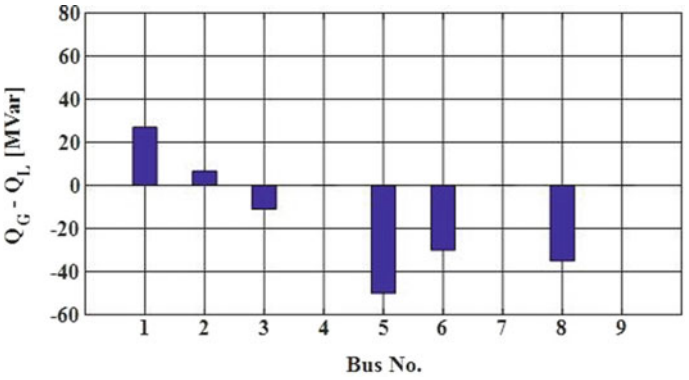

Fig. 11 Reactive power profile for the base power system

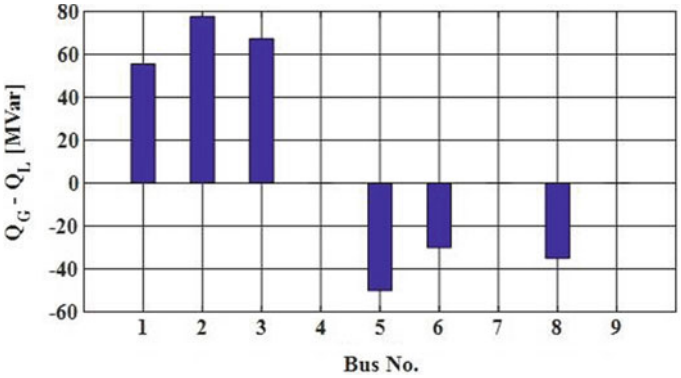

Fig. 12 Reactive power profile with HVDC and wind farm

Because of introducing DC transmission system in bus no. 7 its angle profile turns into zero from 0.07 rad. And AC load is connected in bus no. 8, so its positive angle profile increased approximately a value of 0.09 rad.

No considerable change has been found from real power reorientation in Figs. 9 and 10 for both cases. But reactive power has increased to a great extent at three generator bus after power flow analysis has done for Case B as in Fig. 12. It is mostly because of the nature of the variable speed wind turbine. More detail comparison of power flow can be seen in Tables 1 and 2. Now consider the line flows, from Table 1. It can be shown that before introducing HVDC on bus 7–8 real power was 76.38 Mw after that it became 104.76 Mw, whereas real power losses remain negligible. But reactive power generation and losses increased in a significant value. After introducing the wind farm at the bus no. 1, its reactive power flow increases a little bit. Still, for reducing its impacts on power system other two synchronous

Table 1 Line flows report

Bus from–to	Real power flow, P [Mw]		Real power loss, P_{loss} [Mw]		Reactive power flow, Q [Mvar]		Reactive power Loss, Q_{loss} [Mvar]	
	Case A	Case B	Case A	Case B	Case A	Case B	Case A	Case B
1-4	71.64	79.07	0	0	27.045	55.607	3.122	4.976
2-7	163	163	0	0	6.653	77.718	15.831	19.399
3-9	85	85	0	0	−10.86	67.408	4.095	6.565
7-8	76.38	104.76	0.475	6.25	−0.797	74.830	−11.501	136.461
7-5	86.62	98.24	2.3	1.125	−8.380	−16.51	−19.693	−23.546
5-4	−40.70	−67.88	0.257	0.615	−38.69	−42.96	−15.794	−12.047
6-4	−30.54	−10.42	0.166	0.147	−16.54	−34.61	−15.531	−14.90
9-6	60.816	82.325	1.353	2.75	−18.07	−27.39	−31.531	−22.777
9-8	24.183	2.674	0.088	1.182	3.119	88.235	−21.176	−8.395

Table 2 Global summary report from power flow analysis

Case	Power	Total generation	Total load	Total losses
Base power system (Case A)	Real power (Mw)	319.641	315	4.641
	Reactive power (Mvar)	22.8399	115	−92.1601
With wind farm and HVDC line (Case B)	Real power (Mw)	327.07	315	12.07
	Reactive power (Mvar)	200.734	115	85.734

generators at the buses no. 2 and 3 generate a massive value of reactive power compare to their primary value. A summary report in Table 2 indicates total power generation and losses for both cases at constant load value.

6 Conclusion

Principle objectives of this simulation-based study were to demonstrate the impacts on power flow because of introducing a renewable energy source along with HVDC transmission link in a power system. In WSCC-3 machine, nine bus system with or without integrating wind and HVDC line power flow analysis has done, and results have shown that power flow increase because of this installation as we have studied on theory. The global summary report has also shown that although load remains constant for both cases; reactive power generation and losses have increased in a significant manner. Before installation, these components on system reactive power generation was 22.84 Mvar, and after 200.74 Mvar, so reactive power flow increased approximately 900%. This immense value of reactive power could be a problem for an efficient power system and hampers its electrical component general operation so proper safety measure need to take.

References

1. Parker, B., Blevins, S., Facemire, M., Hatipoglu, K.: The effect of variable speed wind turbines on a 21 bus power system. In: SoutheastCon 2017. IEEE, Charlotte, pp. 1–8 (2017). https://doi.org/10.1109/secon.2017.7925362
2. Kumar, S., Kumar, A., Sharma, N. Analysis of power flow, continuous power flow and transient stability of IEEE-14 bus integrated wind farm using PSAT. In: 2015 International Conference on Energy Economics and environment (ICEEE), pp. 1–6. IEEE, Noida (2015). https://doi.org/10.1109/energyeconomics.2015.7235099
3. Milano, F.: An open source power system analysis toolbox. IEEE Trans. Power Syst. **20**(3), 1199–1206 (2005). https://doi.org/10.1109/TPWRS.2005.851911
4. Canizares, C., Alvarado, F., Zhang, S., Watson, M.U.: UWPFLOW: continuation and direct methods to locate fold bifurcations in AC/DC/FACTS power systems. In: UWPflow Free-Software (2004). Available at www.power.uwaterloo.ca, Electrical and Computer Engineering, University of Waterloo

5. Larsson, M.: Object Stab an educational tool for power system stability studies. IEEE Trans. Power Syst. **19**(1), 56–63 (2004)
6. Nitve, B., Naik, R.: Steady state analysis of IEEE-6 bus system using PSAT power toolbox. Int. J. Eng. Sci. Innov. Technol. (IJESIT) **3**(3), 197–203 (2014)
7. Thompson, L., Washington, C.: HVDC dynamic modeling (2016)
8. Kundur, P.: Power System Stability and Control. McGraw-Hill, New York (1994)
9. Bekri, O., Fellah, M., Benkhoris, M.: Impact of the wind generator on the power flow in the electric grid. In: 3rd International Symposium on Environmental Friendly Energies and Applications (EFEA). IEEE, St. Ouen, pp 1–6 (2014). https://doi.org/10.1109/efea.2014.7059945
10. Keshmiri, S.N., Jamehbozorg, A., Radman, G.: Optimum reactive power compensation regime for radial connected wind turbines. In: 2011 Proceedings of IEEE Southeastcon, pp 24–28. IEEE, Nashville (2010). https://doi.org/10.1109/secon.2011.5752898
11. Benseddik, A., Kouba, N., Boudour, M., Hasni, M., Menaa, M.: Wind farm integration intermittency impact on power system transient stability. In: 2018 international conference on electrical sciences and technologies in Maghreb (CISTEM), pp. 1–6. IEEE, Algiers (2018). https://doi.org/10.1109/cistem.2018.8613551
12. Bekri, O., Mekri, M.: Impact of the wind generator on voltage stability. In: International Conference on Wind Energy and Applications in Algeria (ICWEAA). IEEE, Algieris (2018). https://doi.org/10.1109/icweaa.2018.8605078
13. Sauer, P.W., Pai, M.A., Chow, J.H.: Multimachine simulation. In: Power System Dynamics and Stability: With Synchrophasor Measurement and Power System Toolbox, pp. 135–182. IEEE (2012). https://doi.org/10.1002/9781119355755.ch7
14. Song, Y., Zhang, J., Zhao, Y., Li, G., Li, S., Liu, Y., Yang, L., Zhou, Z., Zhao, C.: Sending end frequency and voltage under islanded operation mode of HVDC transmission system. In: 2017 IEEE Conference on Energy Internet and Energy System Integration (EI2), pp 1–6. IEEE, Beijing (2017). https://doi.org/10.1109/ei2.2017.8245266
15. Anand, R., Balaji, V.: Power flow analysis of simulink IEEE 57 bus test system model using PSAT. Ind. J. Sci. Technol. **8**(23), 1–7 (2015). https://doi.org/10.17485/ijst/2015/v8i23/79266

Techno-economic Assessments of Green Hybrid Microgrid

Sumit Sharma, Yog Raj Sood, and Ankur Maheshwari

Nomenclature

cost_{NPC}	Total net present cost (₹)
$\text{cost}_{\text{total}_{\text{annual}}}$	Total annual cost (₹)
$C_{\text{RF}}(\text{int}_{\text{annual}}, N_{\text{lifespan}})$	Capital recovery factor
$\text{int}_{\text{annual}}$	Annual interest rate
N_{lifespan}	Project lifespan (year)
$P_{\text{out}_{\text{PV}}}$	Solar power output (kW)
$P_{\text{rated}_{\text{PV}}}$	SPV rated power (kW)
$\text{d}F_{\text{PV}}$	SPV derating factor
$\text{Irr}_{\text{global}}$	Global solar irradiance (kW/m^2)
Irr_{STC}	$Radiation at STC (kW/m^2)$
C_{Temp}	Temperature coefficient
T_{cell}	Cell temperatue
T_{ref}	Cell temperature at STC
f_{DG}	Fuel consumption
C_{DG}	Coefficient of fuel consumption
$P_{\text{DG-rated}}$	DG nominal power
A_{DG}	Coefficient of fuel consumption
$P_{\text{DG-OUT}}$	Output power

S. Sharma (✉) · Y. R. Sood · A. Maheshwari
Electrical Engineering Department, National Institute of Technology, Hamirpur, Hamirpur, Himachal Pradesh 177005, India
e-mail: sumitsharma8882@nith.ac.in

Y. R. Sood
e-mail: yrsood@nith.ac.in

A. Maheshwari
e-mail: maheshwari.ankur@nith.ac.in

O. H. Gupta and V. K. Sood (eds.), *Recent Advances in Power Systems*, Lecture Notes in Electrical Engineering 699, https://doi.org/10.1007/978-981-15-7994-3_37

$S_{\text{B-Whr}}$	Battery storage capacity
E_{load}	Average daily load $\left(\frac{\text{kWh}}{\text{day}}\right)$
BA	Battery autonomy
eff_{inv}	Inverter efficiency
eff_{b}	Battery efficiency
B_{DOD}	Depth of discharge

1 Introduction

With oil prices reaching their highest point and expansion costs of the transmission line is increasing rapidly, along with a need to minimize greenhouse gas emissions, renewable energy has befitted a relevant solution as a power source. The cost of fossil fuel-based energy sources is lower than that of renewable energy, but a combination of renewable energy and diesel can lower energy costs. Energy consumption is increasing exponentially, necessitate energy resources to meet scheduled demands, resulting in an exponential rise in emissions from greenhouse gases. Renewable energies, which are clean and inexhaustible energy sources, are attracting energy producers these days. However, the assessment of the right system for renewable energies must be made within the framework of the optimization technique.

Consequently, renewable energy sources are progressively recognized as profitable, generating sources for off-grid power system networks. The high losses and transmission system costs are responsible for promoting the use of green sources of energy in sparsely populated areas. A H.E.S. offers a stable supply of energy in contrast with conventional energy. Much work has already been conducted to evaluate the optimal H.E.S. for isolated and remote communities. Upadhyay et al. discussed that energy produced from non-conventional sources has very less harmful impacts on the environment [1]. In reference [2], Aziz et al. presented the different behavior of H.E.S. with the sensitive parameters for a case study of a rural village in Iraq. Adam Hirsch et al., in reference [3], discussed all the characteristics of microgrids in detail. In reference [4], Kumar et al. discussed the integrated assessment of the rural village with a microgrid setup. In the previous analysis, Hafez et al. show that a diesel-renewable combined hybrid system has the lowest cost values and less emission as compared to the stand-alone diesel-based microgrid system [5]. The appropriate solution for electricity supply in rural and remote locations are green energy [6]. Garni et al. concluded that a H.E.S. could be more efficient, viable, and weather-friendly as compared to individual energy systems [7]. As compared to the autonomous D.G. that creates higher pollution, the hybrid system practically has zero emissions [8]. To plan microgrids in rural areas, the description of the viable energy sources to be used is required, including the ability of the sources to be used for renewable energy usage.

However, governments in many countries actively advocate microgrid developers to invest in the renewable energy sector. The two primary renewable energy sources

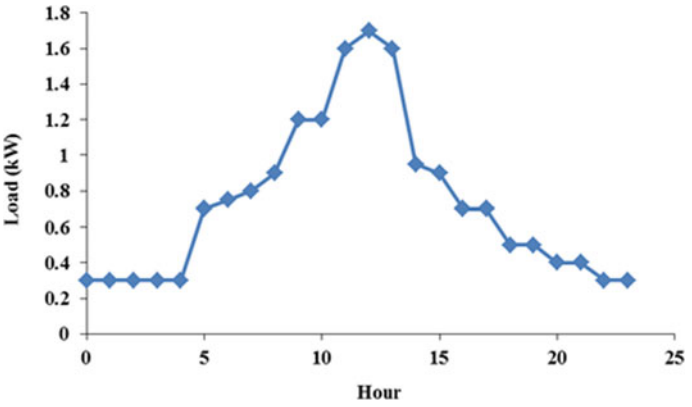

Fig. 1 Electrical load demand for 24 h

scrutinized at selected locations are SPV and wind energy. The potential of these sources at selected locations are studied in the previous study [9]. This research paper presents the analysis of the optimal solution of H.E.S. consisting of SPV, wind turbine, D.G., and battery.

2 Load Profile and Resource Description

The location chosen for the case study is a health clinic situated in district Iseyin in Nigeria. The average load was found to be 15 kWh per day. The peak load value is 2.7 kW with including day to day and time step to time step random variability. The solar power output is dependent on solar irradiance; therefore, the solar resource variable is considered in power calculated. The daily load demand for the chosen site is given in Fig. 1. Figures 2 and 3 show the daily solar radiations and wind speed profile for the site chosen in this research paper.

A H.E.S. is a combination of many sources like SPV, wind turbine, D.G., battery, etc. A converter is also used for the conversion of D.C. electrical power to the electrical A.C. power to meet the load demand. Figure 4 shows the structural diagram of the H.E.S.

The different input parameters and cost of different components like SPV, wind turbine, battery, D.G., and converter shown in Table 1 taken from reference [9].

3 Hybrid System Economic Evaluation

Optimal sizing and cost assessment of the selected location is carried out on the basis of the total N.P.V. of the system. The most appropriate solution is the lowest N.P.V.,

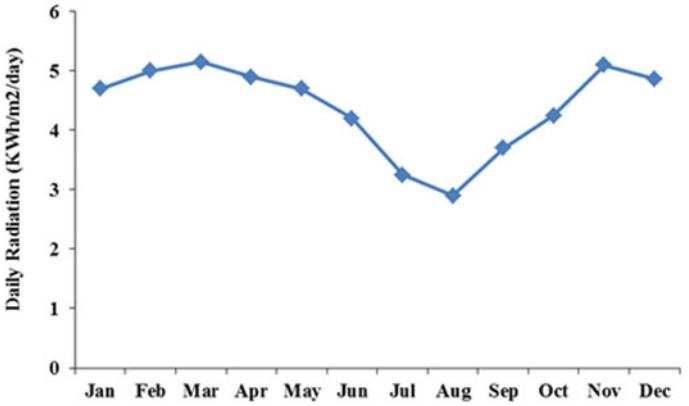

Fig. 2 Monthly average solar radiations

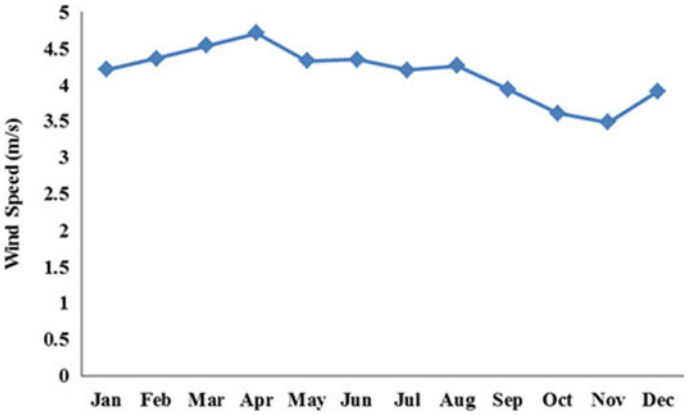

Fig. 3 Monthly average wind speed

and C.O.E. SPV panels produce D.C. electrical output power given by the relation [10]:

$$P_{\text{out}_{\text{PV}}} = P_{\text{rated}_{\text{PV}}} \text{d} F_{\text{PV}} \left(\frac{\text{Irr}_{\text{global}}}{\text{Irr}_{\text{STC}}} \right) \left[1 + C_{\text{Temp}} (T_{\text{cell}} - T_{\text{ref}}) \right] \tag{1}$$

For emergency power supply, a generator is used based on fuel exhaustion, and the battery is used in this hybrid energy system to store D.C. energy. The battery storage capacity is given as [11]:

$$f_{\text{DG}} = C_{\text{DG}} P_{\text{DG-rated}} + A_{\text{DG}} P_{\text{DG-OUT}} \tag{2}$$

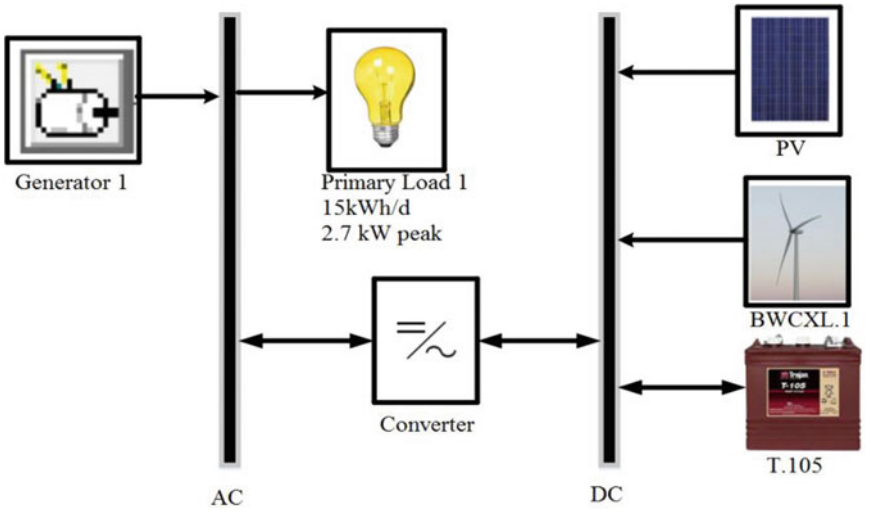

Fig. 4 Block diagram of the H.E.S

$$S_{\text{B-Whr}} = E_{\text{load}} * \text{BA}/\text{eff}_{\text{inv}} * \text{eff}_{\text{b}} * B_{\text{DOD}} \tag{3}$$

Total N.P.V. is the cost of H.E.S., which is the total cost of the system including maintenance, capital and replacement cost at the end of project completion minus total revenue at project lifetime, usually given as [10]:

$$\text{Cost}_{\text{NPC}} = \frac{\text{Cost}_{\text{total}_{\text{annual}}}}{C_{RF}(\text{int}_{\text{annual}}, N_{\text{lifespan}})} \tag{4}$$

System capital recovery factor is calculating based on the interest rate and lifespan, while the cost of energy is calculated as [10, 11]:

$$C_{\text{RF}}(\text{int}_{\text{annual}}, N_{\text{lifespan}}) = \frac{\text{int}_{\text{annual}}(1 + \text{int}_{\text{annual}})^{N_{\text{lifespan}}}}{(1 + \text{int}_{\text{annual}})^{N_{\text{lifespan}}} - 1} \tag{5}$$

$$\text{Cost}_{\text{Energy}} = \frac{\text{Cost}_{\text{total}_{\text{annual}}}}{\text{Load}_{\text{Served}}} \tag{6}$$

4 Result and Discussion

To determine the sizing and different cost parameters for H.E.S., the software employed is HOMER. All the input parameters in this research paper are taken from the case study of Nigeria [9]. The dispatch strategy used in this paper is cycle

Table 1 Cost assessment of the components for H.E.S

S. No.	Detail	SPV	Wind turbine	Battery	Converter	DG
1	Capital Cost	242,228.80 ₹	433,362.46 ₹	13,171.19₹	15,139.30 ₹	15,139.30 ₹
2	Replacement Cost	227,089.50₹	276,292.22 ₹	13,171.19 ₹	15,139.30 ₹	15,139.30 ₹
3	Maintenance Cost	756.97 ₹/year	7569.65 ₹/year	378.48 ₹/year	756.97 ₹/year	37.85₹/h
4	Lifetime (years/hour)	20	20	10	15	15,000
5	Model	Flat panel	BWC XL 1	Trojan T-105	Converter	Generator
6	Capacity/Quantity	1 kW	1 kW	1	1 kW	1 kW

charging dispatch strategy, where a generator is operating at its full capacity with 80% of the state of charge set point. Different combinations are obtained for the optimal configurations of H.E.S.

Table 2 shows the different combinations of a hybrid microgrid for the selected location in this research paper. From the 12 different cases, it has been found that case 5 is the optimal combination for the system having the lowest N.P.V. and C.O.E. As the initial capital cost is higher in comparison with other cases but the total N.P.V. is very less in this case; therefore, it is suggested that case 5 is the optimal sizing for the chosen site having total N.P.V. of ₹ 3355398.76 and C.O.E. is ₹/kWh 55.93. Since no wind turbine is used in this system configuration, the total load requirement is meet by SPV, D.G., and battery. Further, Tables 3 and 4 show the cost summary for the optimal solution and total electrical production of different components in the system.

H.E.S. is the combination of conventional and non-conventional energy sources with some backup supply source. A diesel generator is used for the backup supply so that some environmental emissions would occur to some extent. Table 5 shows the values of different environmental pollutants in H.E.S. having carbon dioxide emission is much higher as compared to other pollutants of value 335 kg/year.

5 Conclusion

This paper presents the systematized sizing and techno-economic practicability analysis for the selected site in rural villages. Different cases have been studied in the simulation environment, and results obtained revealed that H.E.S. consists of SPV, DG, and battery as the most cost profitable configuration having total N.P.V. ₹ 3,355,398.76 as compared to stand-alone diesel system has cost ₹ 90,414,739.02. The suggested approach may be profitable for policymakers in the planning of microgrids in India.

Table 2 Optimal sizing and cost assessment of H.E.S. for different combinations

S. No.	System configuration	SPV	Wind turbine	DG	Battery	Converter	Initial Capital Cost (₹)	Total NPV (₹)	COE (₹/kWh)	RF	Diesel (L)
1	Diesel alone	–	–	3	–	–	45,411	90,414,739.02	245.45	0	4275
2	SPV-wind-diesel-battery	5	1	1	64	4	2,562,769.79	3,646,730.35	60.78	1	–
3	SPV-wind-diesel-battery	4.5	1	5	64	2	2,471,947.79	4,146,175.67	69.10	0.9	242
4	SPV-wind-diesel-battery	4.5	2	3	64	4	2,905,244.41	40,78,740.33	67.97	1	–
5	SPV-diesel-battery	5	–	1	64	3	2,114,336.16	3,355,398.76	55.93	0.9	127
6	SPV-wind-diesel-battery	3.5	1	1	64	3	2,184,344.79	3,505,653.52	58.43	0.9	137
7	SPV-wind-diesel-battery	4.5	2	5	64	3	2,920,381.41	4,077,453.69	67.97	1	–
8	SPV-wind-diesel-battery	2	3	2	64	4	2,717,924.04	4,087,746.85	68.12	0.9	77
9	SPV-wind-diesel-battery	2	2	5	64	3	2,314,901.41	4103,,035.22	68.34	0.8	307
10	SPV-diesel	5	–	2	–	2	1,271,508	8,496,700.84	141.61	0.6	2076
11	SPV-diesel-battery	4	–	5	64	2	1,917,555.16	4,134,974.29	68.95	0.8	507
12	SPV-diesel-battery	4	–	4	64	3	1,917,555.16	3,655,055.71	60.93	0.8	369

Table 3 Cost summary of the different components in H.E.S

S. No.	Component	Capital cost (₹)	Replacement cost (₹)	Operation and maintenance cost (₹)	Fuel cost (₹)	Salvage value (₹)	Total cost (₹)
1	SPV	1,211,144.0	243,591.34	40,421.93	0	−124,369.35	1,370,787.92
2	DG	15,139.3	0	164,034.32	113,090.57	−681.27	291,507.22
3	Battery	842,956.22	571,281.49	258,579.24	0	−61,541.25	1,611,275.70
4	Converter	45417.9	14,306.64	24,222.88	0	−2195.20	81,752.22
5	System	2,114,657.42	829,255.16	487,258.37	113,090.57	−188,787.07	3,355,398.76

Table 4 Different Electrical Power Parameters of H.E.S

S. NO.	Electrical parameter	Components	kWh/year	%
1	Production	SPV	7258	95
		DG	379	5
		Total	7637	100
2	Consumption	A.C. primary load	5621	100
3	Quantity	Electricity excess load	908	11.9
		Unmet	0.283	0
		Shortage of capacity	1.33	0

Table 5 Environmental emissions pattern for the H.E.S

S. No.	Environmental Pollutant	Amount (kg/year)
1	Carbon dioxide	335
2	Carbon monoxide	0.827
3	Unburned hydrocarbon	0.0916
4	Particulate matter	0.0623
5	Sulfur dioxides	0.673
6	Nitrogen oxides	7.38

References

1. Upadhyay, S., Sharma, M.P.: A review on configurations, control and sizing methodologies of hybrid energy systems. Renew. Sustain. Energy Rev. **38**, 47–63 (2014). ISSN 1364-0321
2. Aziz, A.S., Tajuddin, M.F.N., Adzman, M.R., Azmi, A., Ramli, M.A.M.: Optimization and sensitivity analysis of stand-alone hybrid energy systems for rural electrification: a case study of Iraq. Renew. Energy **138**, 775–792 (2019). ISSN 0960-1481
3. Hirsch, A., Parag, Y., Guerrero, J.: Microgrids: a review of technologies, key drivers, and outstanding issues. Renew. Sustain. Energy Rev. **90**, 402–411 (2018). ISSN 1364-0321
4. Kumar, A., Singh, A.R., Deng, Y., He, X., Kumar, P., Bansal, R.C.: Integrated assessment of a sustainable microgrid for a remote village in hilly region. Energy Convers. Manage. **180**, 442–472 (2019). ISSN 0196-8904
5. Hafez, O., Bhattacharya, K.: Optimal planning and design of a renewable energy-based supply system for microgrids. Renew. Energy **45**, 7–15 (2012). ISSN 0960-1481
6. Halabi, L.M., Mekhilef, S., Olatomiwa, L., Hazelton, J.: Performance analysis of hybrid P.V./diesel/battery system using HOMER: a case study Sabah, Malaysia. Energy Convers. Manag. **144**, 322–339 (2017)
7. Garni, H.Z.A., Awasthi, A., Ramli, M.A.: Optimal design and analysis of gridconnected photovoltaic under different tracking systems using HOMER. Energy Convers. Manag. **155**, 42–57 (2018)
8. Aziz, A.S.: Techno-economic analysis using different types of hybrid energy generation for desert safari camps in U.A.E. Turk. J. Electr. Eng. Comput. Sci. **25**, 2122–2135 (2017)
9. Olatomiwa, L.: Optimal configuration assessments of hybrid renewable power supply for rural healthcare facilities. Energy Rep. **2**, 141–146 (2016). ISSN 2352-4847
10. Lambert, T., Gilman, P., Lilienthal, P.: Micropower system modeling with HOMER. Integr. Altern. Sources Energy **1**(1), 379–385 (2006)

11. Ismail, M., Moghavvemi, M., Mahlia, T.: Techno-economic analysis of an optimized photovoltaic and diesel generator hybrid power system for remote houses in a tropical climate. Energy Convers. Manage. **69**, 163–173 (2013)

Reduced the Fuel Cost by Using Renewable Energy-Based DG in Pool Electricity Market

Manish Kumar, Ashwani Kumar, and K. S. Sandhu

1 Introduction

In this World, a large portion of the research is focused on the conservation of energy and its better utilization. Some research also being focused on the development of the more robust and secure systems to extract energy from renewable energy resources (RER). In all, the renewable energy resources, the use of solar and wind resources have attained massive strides in the energy sector. These are environment friendly and freely available. The total installation of the photovoltaic (PV) is reached up to 39 GWe at the end of 2013 [1]. Along with that, the wind energy conversion system total generation has been reached up to 370 GWe by the end of 2014 [2].

RERs, like as solar and wind, are random in nature and changes according to the geographical and climatic conditions. But, there is many parts of the word where combine use of these two resources provide their complement use. Combined use of these two resources makes the system more robust, reliable and efficient and system cost decrease significantly. But, the sizing of the entire system and the energy management become more complex task as number of components increases.

Nowadays, the concepts of distributed generation (DG) are is getting more attention in researchers' point of view because it provides many advantages as compared to the tradition power system where all the generation points and load points are connected to common transmission lines. As per [2– 4] DG have many benefits, it improve the voltage profile, improved system reliability, minimizing transmission

M. Kumar (✉)
Department of Electrical Engineering, SOET, Central University of Haryana, Mahendergarh, Haryana 123031, India
e-mail: manish.kumar@cuh.ac.in

A. Kumar · K. S. Sandhu
Department of Electrical Engineering, NIT, Kurukshetra, Kurukshetra, India

O. H. Gupta and V. K. Sood (eds.), *Recent Advances in Power Systems*, Lecture Notes in Electrical Engineering 699, https://doi.org/10.1007/978-981-15-7994-3_38

losses of the system, save fuel cost and power quality of the system. For more, challengeable task of DGs is optimal placement and size in the system. When placement and size is not optimal thus benefits of DG is zero, thereby should be considered upmost priority. Number of DG technologic and method are proposed by researcher and scientists. The literature-based technologic and method are genetic algorithm (GA) with fuzzy, with particle swarm optimization (PSO), novel power stability index (PSI), ant colony optimization (ACO), Monte Carlo simulation (MCS), generation worth index (GWI), non-dominated sorting genetic algorithm-II (NSGA-II), artificial bee colony (ABC) algorithm, etc. [5–12].

The research related to the modeling and operation of hybrid renewable energy system has been reported in various [13, 14]. In [15–17], author purposed MLP approach for finding the optimal scheduling and power management of the hybrid system. The distribution network planning for reducing the total cost including investment and variable cost by obtaining the siting and optimal DG sizing was presented in [18, 19]. In [20, 21], decrease the cost of energy as well as loss occurring in the system using generation worth index (GWI) approach and novel index method for different type DGs.

This paper proposes a mixed integer nonlinear programming (MINLP) approach consists of reduced the total fuel cost of CG. The contribution of the present work is a comparison of two renewable energy-based DG (wind and PV) with the following main focus point are: (a) To find the optimal location of PV and WT-based DG, for reduction of fuel cost of conventional generator (CG). (b) To find the total reactive loss, voltage profile and active power loss. (c) To find the effect of constant PQ and zip load.

2 General OPF

Objective: Minimization fuel cost of conventional generations considering renewable energy-based cost.

$$\text{Min} \quad F\left(m, r, \xi^{\text{int}}\right) \tag{1}$$

Subject to equality and inequality constraints defined as

$$x\left(m, r, \xi^{\text{int}}\right) = 0 \tag{2}$$

$$u\left(m, r, \xi^{\text{int}}\right) \leq 0 \tag{3}$$

where

m is state vector of variables V, δ;
r is the control parameters, $P_{(\text{PV-WT})k}$, $Q_{(\text{PV-WT})k}$, P_{gk}, $Q_{gk;}$

ξ^{int} is an integer variable with values {0,1}. 0: absence of renewable energy-based DG and 1: presence of renewable energy-based DG.

$$F\left(m, r, p, \xi^{\text{int}}\right) = \left\{ \begin{array}{c} \sum_{k \in N_g} \left(a_{gk} + b_{gk} P_{gk} + c_{gk} P_{gk}^2\right) + \xi_k^{\text{int}} \\ * \sum_{k \in N_{(\text{PV-WT})}} \left(a_{(\text{PV-WT})k} + b_{(\text{PV-WT})k} P_{(\text{PV-WT})k} + c_{(\text{PV-WT})k} P_{(\text{PV-WT})k}^2\right) \end{array} \right\} \quad (4)$$

The equality and inequality constraints, cost function of the DG, ZIP load and modeling of PV and wind-based DG discussions in [17, 18]

3 Results and Discussion

A MINLP approach has been applied to IEEE 24-bus reliability test system for optimal distribution location (ODL) generation [13]. The fuel cost, losses, voltage profile and size of renewable resource-based DG has been obtained considering renewable resource-based DGs. Various cases are in order to minimize fuel cost. The results are also obtained with two different loads (constant and ZIP load). The flowing cases are characterized as:

Case 1: without participate renewable energy DG
Case 2: 1 renewable energy DG
Case 3: 2 renewable energy DG
Case 4: 3 renewable energy DG.

3.1 Comparison of Results with DGs (PV-Based DGs and WT-Based DGs) for Constant PQ and ZIP Load

The results with each renewable energy source-based DGs have been obtained and comparisons of results for a case with combined fuel cost for both load models are given in Table 1.

The results are also shown in Figs. 1 and 2. It is observed that the fuel cost is lower with wind turbine-based DGs for both types of loads. Average marginal price for real power is shown in Figs. 3 and 4. It is seen that the average marginal prices decreases with DGs.

Table 1 Results of different renewable energy-based DGs with combine fuel cost case at constant PQ and ZIP load

		Fuel cost + DG cost ($/h)		Average real power marginal cost ($/MWh)	
		PV-based DG	WT-based DG	PV-based DG	WT-based DG
Constant load	Case 1	14,624.9336	14,624.9336	31.6446	31.6446
	Case 2	14,628.5515	14,623.5884	31.5945	31.4193
	Case 3	14,631.9093	14,623.4338	31.4958	30.111
	Case 4	14,634.7096	14,624.3309	31.8742	30.5603
ZIP load	Case 1	14,620.0889	14,620.6059	32.0818	32.6588
	Case 2	14,621.6211	14,619.7105	32.0286	30.4126
	Case 3	14,625.3022	14,614.0025	29.7006	29.8095
	Case 4	14,628.0275	14,614.8947	29.5587	29.7524

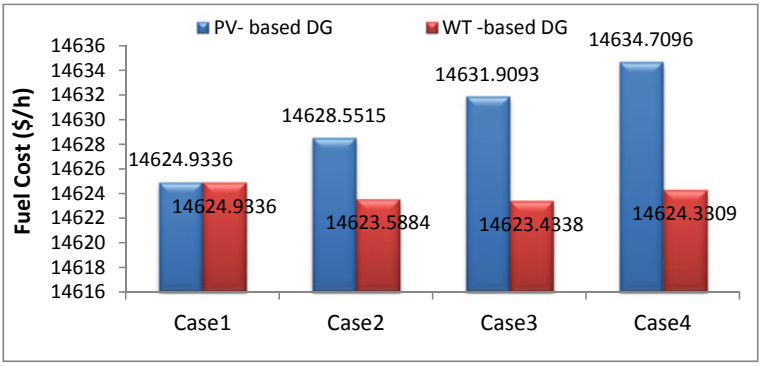

Fig. 1 Fuel cost ($/h) of different renewable energy-based DG for constant PQ load

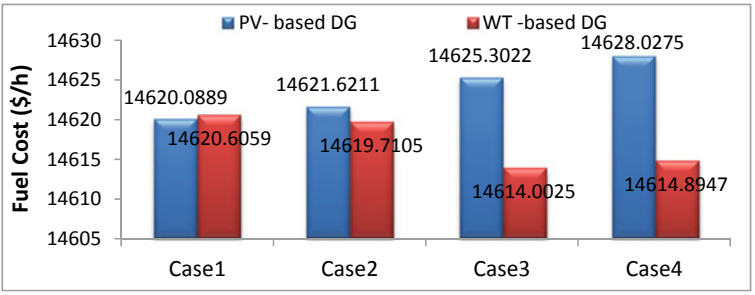

Fig. 2 Fuel cost ($/h) of different renewable energy-based DG for ZIP load

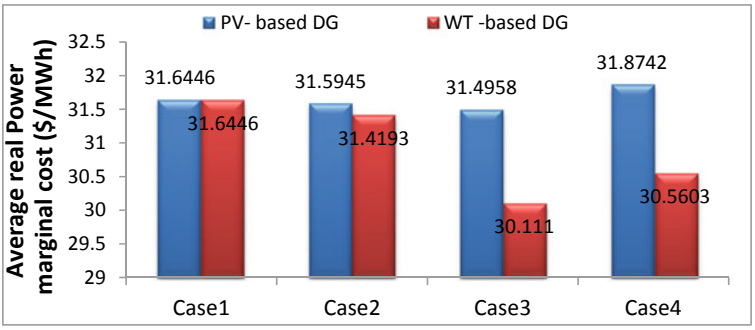

Fig. 3 Average real power marginal cost ($/MWh) of different renewable energy-based DG for constant PQ load

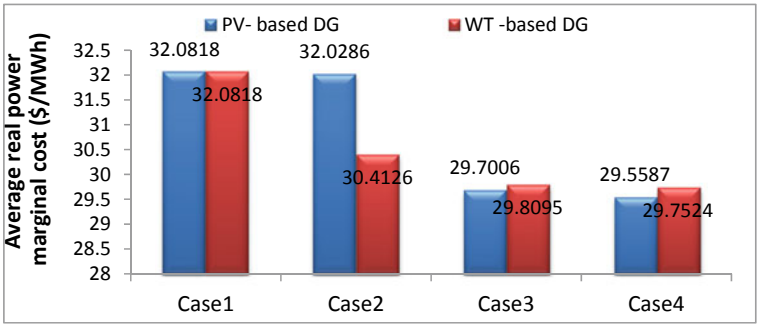

Fig. 4 Average real power marginal cost ($/MWh) of different renewable energy-based DG for ZIP load

3.2 Comparison of Results with DGs (PV-Based DGs, WT-Based DGs) with Constant PQ and ZIP Load Without Taking Cost Function of DGs

The results obtained for fuel cost and average marginal cost with DGs taking the two types of loads are given in Table 2. The average marginal cost reduces with DGs in all the cases. There is marginal change in the fuel cost. Figures 5 and 6 show the convectional generator (CG) fuel cost ($/h) at ZIP and PQ load with DGs. The average real power marginal cost (ARPMC) $/MWh with PQ and ZIP load at different renewable energy-based DGs have been shown in Figs. 7 and 8, respectively. The marginal prices decrease with the DGs. With ZIP load, the marginal prices are lower.

Table 2 Results of different renewable energy-based DGs with convectional generator fuel cost case at constant and ZIP load

		Fuel cost ($/h)		Average real power marginal cost ($/MWh)	
		PV-based DG	WT-based DG	PV-based DG	WT-based DG
Constant load	Case 1	14,624.9336	14,624.9336	31.6446	31.6446
	Case 2	14,613.3022	14620.9024	31.5433	31.4604
	Case 3	14,605.8036	14,603.4769	31.4825	31.4737
	Case 4	14,598.6728	14,599.1377	31.4328	31.4331
ZIP load	Case 1	14,620.0889	14,620.6059	32.0818	32.6588
	Case 2	14,610.8362	14,606.9227	32.0286	30.2465
	Case3	14,599.0372	14,591.6541	29.6633	30.1313
	Case 4	14,591.7042	14,589.2709	29.6051	30.0676

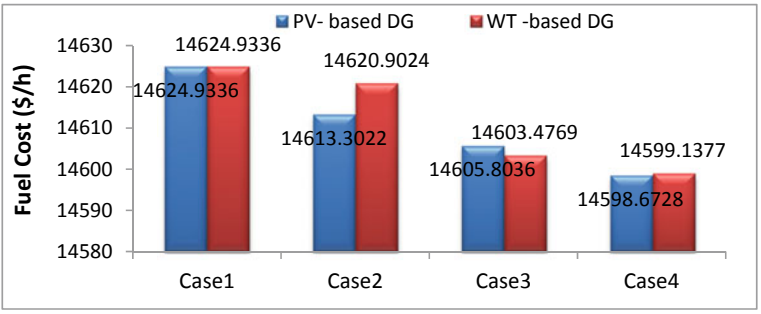

Fig. 5 Fuel cost ($/h) of convection generator with different renewable energy-based DG for constant PQ load

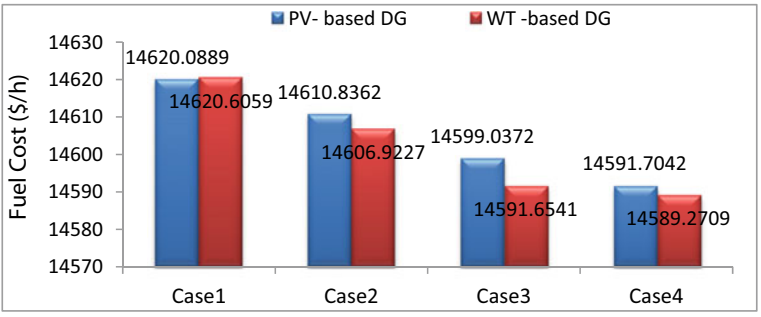

Fig. 6 Fuel cost ($/h) of convection generator with different renewable energy-based DG for ZIP load

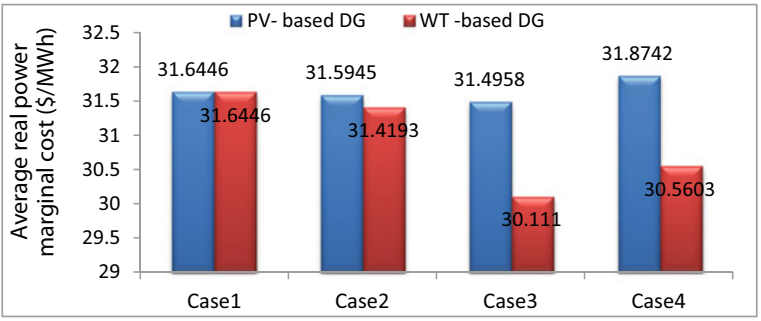

Fig. 7 ARPMC ($/MWh) with different renewable energy-based DG for constant P, Q load

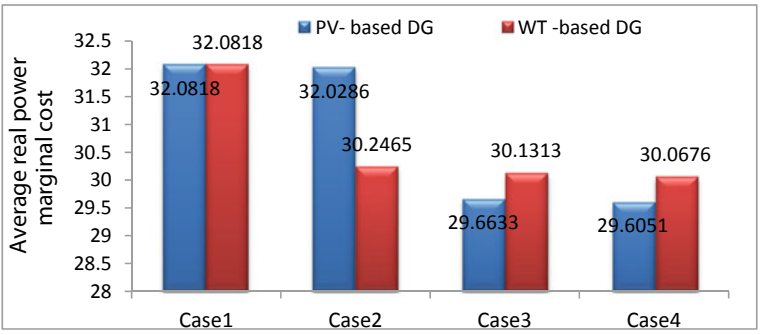

Fig. 8 ARPMC ($/MWh) of different renewable energy-based DG for ZIP load

4 Conclusion

In this paper, MINLP approach has been proposed to obtain number of DGs and optimal location for reduced the fuel cost of conventional generators (CG) with solar PV and wind-based DGs. The impacts of wind and solar integration on the nodal prices also have been obtained. Major observations as observed are:

(i) The marginal prices of real power decreases with the presence of both types DGs. The impact of wind-based DGs is dominant compared to solar PV-based DGs due to higher power availability of wind-based DGs.
(ii) The marginal prices of real power are lower for ZIP load case compared to the constant P,Q load case.
(iii) There is marginal change in the fuel cost when the cost functions of both the DGs are also taken into the objective function minimization. Without the cost functions of the DGs, there is reduction in the fuel cost due to power availability of DGs.

References

1. Prabhakar Karthikeyan, S., Jacob Ragled, I., Kothari, D.P.: A review on market power in deregulated electricity market. Electr. Power Energy Syst. **48**, 139–147 (2013)
2. Moradi, M.H., Abedini, M.: A combination of genetic algorithm and particle swarm optimization for optimal DG location and sizing in distribution systems. Int. J. Electr. Power Energy Syst. **34**(1), 66–74 (2012)
3. Kim, K., Song, K., Joo, S., Lee, Y., Kim, J.: Multi-objective distributed generation placement using fuzzy goal programming with genetic algorithm. Eur. Trans. Electric Power. **8**, 217–230 (2008)
4. Ghosh, S., Ghoshal, S.P.: Ghosh Sa,: optimal sizing and placement of distributed generation in a network system. Int. J. Electr. Power Syst. **32**, 849–856 (2010)
5. Porkar, S., Poure, P., Abbaspur-Tehrani-fard, A., Saadate, S.: A noval optimal distribution system planning framework implementing distributed generation in a deregulated electrical market. Int. J. Electr. Power Syst. **60**, 828–837 (2010)
6. Mohammadi, M.: Nafar M,: Optimal placement of multitype DG as independent private sector under pool/hybrid power market using GA-based Tabu Search method. Electr. Power Energy Syst. **51**, 43–53 (2013)
7. Kumar, S., Kumar Prema, N.: A noval approach to identify optimal access point and capacity of multiple DGs in a small, medium and large scale radial distribution systems. Electr. Power Energy Syst. **45**, 142–151 (2013)
8. Ugranli, F., Karatepe, E.: Multiple-distributed generation planning under load and different penetration levels. Int. J. Electr. Power Energy Syst. **46**, 132–144 (2013)
9. Hung, D.Q., Mithulananthan, N., Bansal, R.C.: Analytical strategies for renewable distributed generation integration considering energy loss minimization. Appl. Energy **105**, 75–85 (2013)
10. Hung, D.Q., Mithulananthan, N., Lee, K.Y.: Determining PV penetration for distribution systems with time-varying load model. IEEE Trans. Power Syst. **29**(6), 3048–3057 (2014)
11. Atwa, Y.M., El-Saadany, E.F., Salama, M.M.A., Seethapathy, R.: Optimal renewable resources mix for distribution system energy loss minimization. IEEE Trans. Power Syst. **25**, 360–370 (2010)
12. Kumar, M., Kumar, A., Sandhu, K.S.: Wind speed variation impact on transmission loss reduction in electricity market. Procedia Comput. Sci. **70**, 526–537 (2015)
13. Kumar, M., Kumar, A., Sandhu, K.S.: Impact of distributed generation on nodal prices in hybrid electricity market. Mater. Today Proc. **5**, 830–840 (2018)
14. Kusiak, A., Li, W.: Short-term prediction of wind power with a clustering approach. Renew. Energy **35**(10), 2362–2369 (2010)
15. Kusiak, A., Li, W.: Virtual models for prediction of wind turbine parameter. IEEE Trans. Energy Convers. **25**(1), 245–252 (2010)
16. Yang, X.-S.: Firefly algorithm, stochastic test functions and design optimization. Int. J. Bio-Inspir. Comput. **2**(2), 78–84 (2010)
17. Kumar, M., Kumar, A., Sandhu, K.S.: Optimal location of WT based distributed generation in pool based electricity market using mixed integer non linear. Mater. Today Proc. **5**, 445–457 (2018)
18. Kumar, M., Kumar, A., Sandhu, K.S.: WT based distributed generation location minimizing transmission loss using mixed integer non-linear programming in deregulated electrical market. In: Proceedings of the International Congress on Information and Communication Technology ICICT-2015, Advances in Intelligent System and Computing, vol. 438, pp. 443–358 (2015)
19. Kumar, M., Kumar, A., Sandhu, K.S.: PV-based distributed generation location using mixed integer non-linear programming in deregulated electricity market. Advanced Computing & Communication Technology ICACCT 2015, Advances in Intelligent System and Computing, vol. 452, pp. 535–547 (2015)

20. Crisostomi, E., Liu, M., Raugi, M., Shorten, R.: Plig and play distributed algorithms for optimized power generation in a micro grid. IEEE Trans. Smart Grid **5**(4), 2145–2154 (2014)
21. Krishan, O., Suhag, S.: Techno-economic analysis of a hybrid renewable energy system for an energy poor rural community. J. Energy Storage **23**, 305–319 (2019)

Congestion Management in Power System—A Review

Shaik Riyaz, Ramanaiah Upputuri, and Niranjan Kumar

1 Introduction

As the load demand is increasing and with the advancement of technology, the regulated monopoly public utilities are replaced with deregulated environment to provide competition in the market and to meet the public with affordable prices [1]. This led to the congestion in transmission network and causes system security and reliability issues [2]. The deregulated market has a lot of challenges which include selecting an electricity auction plan, reducing market power of competitors, relieving the transmission network congestion, spikes in locational price, maintaining reliability of the system, evaluating market equilibrium and power market efficiency [3]. Among this, congestion management is focused recently. There are several reasons for network congestion. The main reason for congestion is due to violation of system constraints and unable to facilitate all power flow transactions [4]. According to the market needs, transmission networks are not enough to supply the power during congestion. Congestion refers to transmission lines overloading due to violation of line capacities an thermal limits [5]. Congestion can also occur when there is unexpected generation outages, unpredicted increase in the demand, and failure of the equipment [6]. Power quality problem will occur during congestion, and it will damage the power system if outages occur frequently [7]. If this congestion is not considered for a long time, there will be a widespread outage of the entire power system. So,

S. Riyaz (✉) · R. Upputuri · N. Kumar
Department of Electrical Engineering, NIT Jamshedpur, Jamshedpur, India
e-mail: nitjsrriyaz@gmail.com

R. Upputuri
e-mail: 2018rsee005@nitjsr.ac.in

N. Kumar
e-mail: nkumar.ee@nitjsr.ac.in

O. H. Gupta and V. K. Sood (eds.), *Recent Advances in Power Systems*, Lecture Notes in Electrical Engineering 699, https://doi.org/10.1007/978-981-15-7994-3_39

this should be avoided quickly for proper power system operation. So, the significance of congestion management methods is vital to supply the power without violation of system constraint limits, for system security and reliability [8]. Several studies underwent to evaluate the best congestion management methods. Some of the methods are generators rescheduling, optimal power flow, by using FACTS devices, distributed generation and algorithms including particle swarm optimization, genetic algorithm, shuffled frog algorithm, mixed integer nonlinear programming, and fuzzy logic system approaches.

1.1 Congestion Management Methods

Congestion management methods are classified into technical solutions and non-technical solutions described in [9] shown in Fig. 1.

This paper reviews different methods and artificial intelligence techniques for avoiding network congestion. This paper is organized as follows: congestion management based on market demand, optimization techniques, and artificial intelligence techniques.

Based on market demand: There are various models for power market to avoid congestion. The well-known methods of power system congestion management

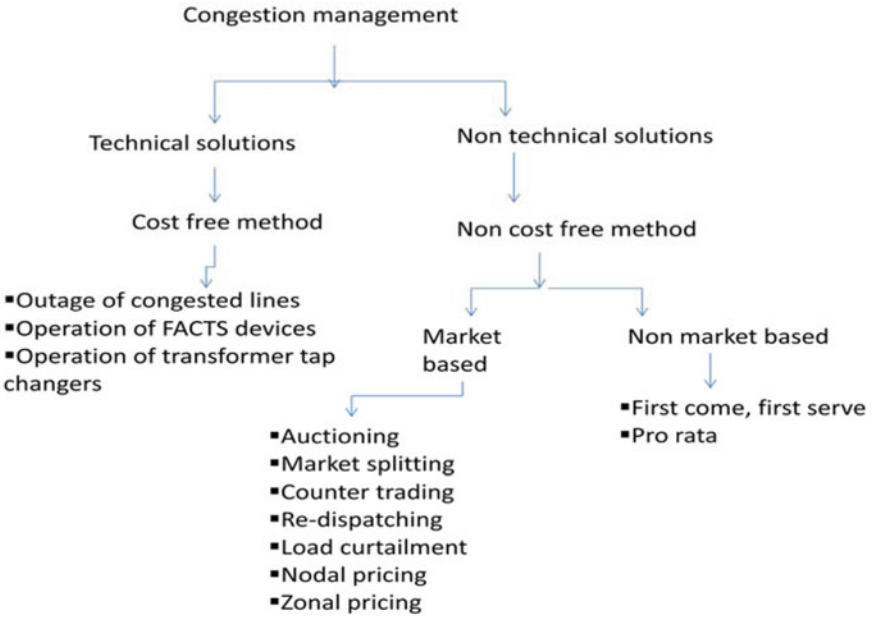

Fig. 1 Summary of congestion management methods

in market are generation rescheduling, nodal pricing, load shedding method, and distributed generation.

Generator rescheduling: The literature [10] described generator rescheduling method for avoiding congestion. It deals with reducing generation and load operational costs. From reference, [11] discussed about the generator rescheduling method as a ineffective and slow. Use of artificial intelligence techniques with generator rescheduling was described such as genetic algorithm [12, 13] and by using particle swarm optimization with generator rescheduling [14].

Nodal pricing: This nodal pricing method is described for effective utilization of transmission utility and generating utility to give correct economic signals. Nodal pricing is defined as providing next increment of power at a node. Every participant who associated in this management of congestion was imposed based on the nodal price obtained in the power system. Reference [15] depicts this method of pricing which is a market-based in which system cost changes based on nodal price selected.

Distributed generation: Reference [16] describes the congestion management method called distributed generation. Locational marginal price schemes are implemented for this management. This method of distribution generation relieves congestion as well as reducing generation costs.

$$I_{\mathrm{DIG}} = \frac{(P_B + TC_B) - (P_{\mathrm{DIG}} + TC_{\mathrm{DIG}})}{PC_{\mathrm{DIG}}} \tag{1}$$

I_{DIG} is distributed generation performance indicator, P_B is generation price with respect to base, TC_B = Total cost for congestion, P_{DIG} is generation price with respect to placement of distributed generation, TC_{DIG} is total cost for congestion with respect to placement of distributed generation, PC_{DIG} is distributed generation price characteristic.

$$RC_{ij} = \delta LP_{ij}.P_{ij} \tag{2}$$

$$ij = 1, 2, \ldots n$$

$$TC = \sum_{ij=1}^{n} \delta LP_{ij}.Pij \tag{3}$$

RC_{ij} is rental cost of congestion of i and j line, P_{ij} is flow of power in i & j line, δLP_{ij} is difference of locational marginal price of lines i & j.

Locational marginal price schemes are prominent method in deregulated market to avoid congestion price [17]. Locational marginal price schemes at all nodes of buses are evaluated to eliminate huge mismatch at the reference bus by considering distribution and concentrated model. The linear bids considered in distributed model compared to concentrated model show that there is significant decrease in generation

fuel cost. Literature [18] made a complete review on optimal location of distributed generation to resolve the problems associated to sizing and location of distributed generation by having different objective functions and explains the importance of optimal location of distributed generation. This paper conducted comprehensive study on loss minimization and voltage stability improvement by opting optimal location of distributed generation with multiobjective considerations.

Literature [19, 20] introduced a demand response methodology for relieving the congestion problem. The author imparts a chance to market players to engage in competitive market and by permitting them to modify their utilization based on benefits given. Literature [21, 22] proposed the programs related to demand response in reducing the network congestion. The authors of this described that demand response methodology is important in energy market to aid stable load demand and generation. Literature [23] introduced that PRDS form of auctioning of distribution companies has been considered for relieving the congestion by supervising the increase of locational marginal price in power market.

2 Optimization Methods

Literature [24] discussed about the congestion management when load demand is high. The author implemented FACTS technology devices to reduce the flows during heavy demand by controlling the line flow which results in increased loadability, low losses, and decreased cost of production. Sensitivity analysis also considered for most favorable location of FACTS devices. Management of congestion is done in steps: in first step, modeling of FACTS device, i.e., TCSC and UPFC modeling, and final step is implementing in optimal location of FACTS devices. Literature [25] extended the research work for management of congestion with improved results by implementing a new optimization methodology of harmony search algorithm heuristic method for most favorable location and setting of parameter for TCSC. This mainly depends on outage sensitivity factors and harmony search algorithm. The author points outage sensitivity factors to decrease the solution scope for proper location of TCSC.

Literature [26] discussed about the proper location and sensitivity of total system losses of UPFC by two approaches, namely pricing-based approach and sensitivity-based approach. Based on pricing approach makes usage of difference of Locational marginal price approach for optimal location of UPFC. The objective considered in congestion management is minimization of cost of rescheduling maintaining system limits. The author utilizes mathematical for nonlinear optimization for the problem.

Literature [27] discussed an improved performance by using FACTS devices and optimal location of TCSC and UPFC for congestion management. In this paper, author implemented a nonlinear objective function which can be solved by genetic algorithm for optimal generation schedule for social welfare maximizing. In this paper, with the help of spot pricing theory, congestion management is illustrated.

Literature [28] discussed the most favorable location of TCSC to diminish the installation cost and to remove the congestion problem. Literature [29] proposed

mixed integer nonlinear programming problem. Congestion management problem is conducted according to the market conditions. This programming problem is used for optimal location of TCSC. Maximization of social welfare function is the objective function used. Real power and reactive power procurement cost difference gives the social welfare function. The author concluded that mixed integer nonlinear programming problem gives effective result compared to other existing conventional methods.

3 Artificial Intelligence Approaches

Artificial intelligence techniques include fuzzy-based logic systems, different algorithms like simulated annealed algorithm, artificial bee colony algorithm, fish school optimization algorithm, flower pollination algorithm, multiobjective evolutionary algorithm, and Levy flight-based modified artificial wolf group technique.

Literatures [30, 31] introduced particle swarm optimization method for congestion management and reducing the generator rescheduling cost. Literature [32] proved that particle swarm optimization is proved to give better result at the end. System security of both line loading and bus voltage holds good with particle swarm optimization [30].

Literature [33, 34] discussed the main problem related to power transfer limit and generation capacity availability and introduced genetic algorithm to solve this issue for congestion management.

Literature [35] introduced fuzzy-based scheme with motive to control real power flow by using FACTS device for effective management of network congestion. Literature [36] discussed a fuzzy-based artificial intelligence approach to identify the most favorable location of TCSC for management of congestion problem as well as to control the real power flow.

Literature [36] proposed simulated annealed algorithm for optimal location of UPFC for congestion management. UPFC is having both shunt compensated and series compensated for effective stabilization of the system during management of congestion. Simulated annealed algorithm is very effective in locating the optimal location of UPFC and concluded that the result obtained is effective in congestion management

Literature [37] introduced a artificial intelligence technique artificial bee colony algorithm and fish school optimization algorithm for congestion management by considering both voltage and economical deviation aspects. These algorithms are proposed and implemented for having reduced deviation in voltage after disturbance in load demand. Based on the comparison of result, particle swarm optimization algorithm which gives fish school optimization algorithm gives less rescheduling cost compared to other techniques. So, the author concluded that the two algorithms are effective with economy of scale.

Literature [38] proposed a new heuristic approach, i.e., a Levy flight-based modified artificial wolf group for chasing tendency by wolves and step sizes. Hausdorff's quadratic cross-method decides the dimension. This algorithm is inspired from hunting the addiction of wolves inclusion with Levy flight sizes. It is mainly to evaluate the real power on the basis of contribution component accurately that decides the locality of placing distributed generation. The maximum social welfare objective decides the setting area of distributed generation, but for economical consideration, it is somewhat viable. The most desirable position of distributed generation leads to congestion management.

Literature [39] discussed the independent system operator responsible for market clearance price and maintains the system limits. The author proposed a hybrid algorithm with a combined gravitational search algorithm and fuzzy adaptive particle swarm optimization to solve for nonlinear congestion problem and to reduce congestion cost. This algorithm contains the advantages of having global search and linear search capability of conventional particle swarm optimization and gravitational search algorithm. This algorithm is implemented in bilateral and multilateral transactions and outage of the lines on IEEE different bus systems.

Literature [40] proposed a new hybrid algorithm of combined time-varying accelerating coefficients of particle swarm optimization and gravitational search algorithm. This algorithm will reduce the cost of rescheduling. This paper deals with management of congestion by active power rescheduling with the large selectivity factor.

Literature [41] proposed a new combination of machine learning and model-based scheme to easily identify before congestion in transmission lines. This does not require optimal power flow to know the branch loading. Here, the author introduced a trained model which predicts the optimal generation based on load information. To evaluate the power flows, shift factors are used. This algorithm is mainly based on nodal injection. It uses line outage distribution factors to predict loading of the branch. This technique is implemented on IEEE-118 and IEEE- 57 and EPRI 39 bus system. It is the latest technology which can identify before the congestion and after the congestion in transmission network.

4 Conclusion

A review on congestion management is presented in this paper. This paper focuses primarily on methods implemented for congestion management. From this paper, it is concluded that the optimization techniques and artificial intelligence techniques are very effective in relieving the congestion problem. Different authors came up with their optimization ideas to overcome this congestion. This congestion problem is current issue, and researchers are coming with new heuristic approaches to tackle this problem with minimum time for system security and reliability. In this paper, recent algorithms and advancements are discussed. This paper mainly attracts the power system engineers, and students and teachers should take up this issue and

work in this area. This can be further extended in the future for any new artificial techniques and methods for congestion management.

References

1. Pillay, A., Prabhakar Karthikeyan, A., Kothari, D.P.: Congestion management in power systems—a review. Int. J. Electri. Power Energy Syst. **70**, 83–90 (2015)
2. Tumuluru, V.K., Tsang, D.S.K.: A two-stage approach for network constrained unit commitment problem with demand response. IEEE Transactions on Smart Grid, pp. 1–9 (2016)
3. Prabhakar Karthikeyan, S., Jacob Ragle, I., Kothari, D.P.: A review on market power in deregulated electricity market. Electr. Power Energy Syst. **48**, 139–47 (2013)
4. Nandini, S., Suganya, P., Lakshmi, K.M.: Congestion management in transmission lines considering demand response and facts devices. Int. J. Inn. Res. Sci. Eng. Technol **3**(1), 682–688 (2014)
5. Chung, H.-M., Su, C.-L., Wen, C.-K.: Dispatch of generation and demand side response in regional grids. IEEE Transactions, pp. 1–5 (2015)
6. Yousefi, A., Nguyen, T.T., Zareipour, H., Malik, O.P.: Congestion management using demand response and facts devices. Int. J. Electri. Power Energy Syste. **37**(1), 78–85 (2012)
7. Srinivasa Rao, J., Amamath, J.: Transmission congestion management comparative studies in restructured power system. Int. J. Sci. Eng. Res. (IJSER) **4**(8), 177–182 (2013)
8. Emami, H., Sadri, J.A.: Congestion management of transmission lines in the market environment. Int. Res. J. Appl. Basic Sci. **3**, 2572–2580 (2012)
9. Mwanza, K., Shi, Y.: Congestion management: re-dispatch and application of facts in Department of Energy and Environment, pp. 1–16. Chalmers University of Technology, Goteborg, Sweden (2006)
10. Surender Reddy, S.: Multi-Objective based congestion management using generation rescheduling and load shedding. IEEE Transactions on Power Systems, pp. 1–12 (2016)
11. Retnamony, R., Jacob Raglend, I.: Congestion management is to enhance the transient stability in a deregulated power system using Facts devices. In: International Conference on Control, Instrumentation, Communication and Computational Technologies (ICCICCT), pp. 744–752 (2015)
12. Sivakumar, S.: Congestion management in deregulated power system by rescheduling of generators using Genetic Algorithm. In: International Conference on Power, Signals, Controls and Computation (EPSCICON), pp. 1–5 (2014)
13. Pal, S., Sen, S., Sengupta, S.: Power network reconfiguration for congestion management and loss minimization using Genetic Algorithm, in Michael Faraday IET International Summit: MFIIS-(2015). Kolkata, India, pp. 291–296 (2015)
14. Rajesh, R., Mutharasan, A., Rameshkumar, T., Senthilkumaran, B.: Congestion management in deregulated environment using Generation Rescheduling with an intelligent approach. Int. J. Appl. Eng. Res. **10**(20), 41665–41668 (2015)
15. Holmberg, P., Lazarczyk, E: Congestion management in electricity networks: nodal, zonal and discriminatory pricing. Research Institute of Industrial Economics (IFN), pp. 1–32 (2012)
16. Sarwar, M., Shahzad Siddiqui, A.: Congestion management in deregulated electricity market using Distributed Generation. IEEE Indicon, pp. 1–5 (2015)
17. Matcha, M., Matam, S.K., Maheswarpau. S.: LMP calculation with distributed loss using GA based DCOPF. J. Electric. Syst. (JES) **8**(3), 292–303 (2012)
18. Sultana, U., et al.: A review of optimum DG placement based on minimization of power losses and voltage stability enhancement of distribution system, Renew. Sustain. Energy Rev. **63**, 363–378 (2016)
19. Mohagheghi, S., Raji, N.: Intelligent demand response scheme for energy management of industrial systems. IEEE Transactions, pp. 1–9 (2012)

20. Vardakas, J.S., Zorba, N., Verikoukis, C.V.: Demand Response programs in smart grids: pricing and optimization. IEEE Commun. Surv. Tutorials **17**(1), 152–177 (2015)
21. Dehnavi, D., Abdi, H.: Determining optimal buses for implementing Demand Response as an effective congestion management method. IEEE Trans. Power Syst. pp 1–8 (2016)
22. Zhang, Z., Ren, Y., Zhou. M: A comprehensive decision model of optimal Demand Response program. In: 5th International Conference on Electric Utility Deregulation and Restructuring and Power Technologies pp. 121–126. Changsha, China (2015)
23. Singh, K., Padhy, N.P., Sharma, J.: Influence of price responsive demand shifting bidding on congestion and LMP in pool-based day-ahead electricity markets. IEEE Trans. Power Syst. **26**(2) 886–896 (2011)
24. Patel, H., Paliwal, R.: Congestion management in deregulated power system using Facts devices. Int. J. Adv. Eng. Technol. (IJAET), 175–184 (2015)
25. Javaheri, H., Goldoost-Soloot, R.: Locating and sizing of series Facts devices using line outage sensitivity factors and Harmony Search Algorithm. Energy Procedia **14** 1445–1450 (2012)
26. Kumar Reddy, K.A., Singh, S.P.: Congestion mitigation using UPFC, IET Generation. Trans. Distribut. **10**(10), 2433–2442 (2016)
27. Vijayakumar, K.: Optimal location of Facts devices for congestion management in deregulated power systems. Int. J. Comput. Appl. (0975–8887) **16**(6), pp. 29–37 (2016)
28. Khan, M.T., Siddiqui, A.S.:. Congestion management in deregulated power system using Facts devices. Int. J. Syst. Assur Eng Manag. pp. 1–7 (2014)
29. Singh, K., Yadav, V.K., Dhingra, A.: Congestion management using optimal placement of TCSC in deregulated power system. Int. J. Electri. Eng. Inform. **4**(4), 620–632 (2012)
30. Chanda, S., De, A..: Application of Particle Swarm Optimization for relieving congestion in deregulated power system. IEEE Transactions, pp. 837–840 (2011)
31. Kinhekar, N., Padhy, N.P., Gupta, H.O.: Particle Swarm Optimization based Demand Response for residential consumers. IEEE Transactions, pp. 1–5 (2015)
32. Adhip., Thukaram, D.: Congestion management based on virtual real power flows. Biennial International Conference on Power and Energy Systems: Towards Sustainable Energy (PESTSE), pp. 1–5, (2016)
33. Nabavi, S.M.H., Kazemi, A., Masoum, M.A.S.: Congestion management using Genetic Algorithm in deregulated power environments. Int. J. Comput. Appl. **18**(2) 19–23 (2011)
34. Singh, D., Verma, S.K.: GA-based congestion management in deregulated power system using Facts devices. IEEE Transactions, pp. 1–6, (2012)
35. Nirmalraj, P., Amsavalli, A.: Congestion management in a deregulated power system using Fuzzy Logic with IPFC. Int. J. Res. Appl. Sci. Eng. Technol. (IJRASET) **3**(4), 531–536 (2015)
36. Mahesh, H., Munisekhar Reddy, G., Kiran, S.R., Nanda Kumar, B.: Congestion management in transmission lines using fuzzy based optimal location of Thyristor Controlled Series Capacitor (TCSC). SSRG Int. J. Electric. Electron. Eng. (SSRG-IJEEE), **2**(8) (2015)
37. Thangalakshmi, S., Valsalal, P.: Congestion management in restructured power systems with economic and technical considerations. Asian J. Inf. Technol. **15**(12), 2079–2086 (2016)
38. Sharma, V., Walde, P., Saurabh, P:. A Levy flight based modified artificial wolf group technique for transmission line congestion management in deregulated environment. In: 2018 8th International Conference on Cloud Computing, Data Science & Environment (Confluence), pp. 100–105. Noida (2018)
39. Peesapati, R., Yadav, A., Yadav, V.K., Kumar, N.: GSA- FAPSO- Based Generators Active Power Rescheduling for Transmission Congestion Management. IEEE Syst. J. **13**(3), 3266–3273 (2019)
40. Sharma, V., Walde, P., Siddiqui, A.S.: A new hybrid pOOGSA-TVAC algorithm for transmission line congestion management in deregulated environment. In: 2019 6th Inernational Conference on Signal Processing and Integrated Networks (SPIN), pp. 1116–1121. Noida, India (2019)

41. Hasan, F., Kargarian, A.: Combined Learning and Analytical Model Based Early Warning Algorithm for Real- Time Congestion Management, 2020 IEEE Texas Power and Energy Conference (TPEC), pp. 1–6. College Station, TX, USA (2020)

Voltage Constrained Reactive Power Planning by Ameliorated HHO Technique

G. Swetha Shekarappa, Sheila Mahapatra, and Saurav Raj

1 Introduction

Today's world power system plays a very vital role in generation, transmission, and distribution. The present-day power system is majorly focusing on the RPP. Based on the location and size, the placement of var sources is done in reactive power planning. The allocation of the var sources is based on the methods in RPP or on the optimization techniques. The major objectives which are considered in RPP are as follows: reduction of real power loss, reactive power loss, operating cost, and improvement of voltage outline in each bus by controlling transformer tap-changing position, reactive power generated by generator buses, generated voltage, and shunt capacitors.

RPP is one of the compelling and confronting concern for minimizing congestion on transmission lines, true power loss, and overall operating costs with manageable voltage profile in defined limits [1]. Generally, the RPP solutions are developed applying analytical approaches, arithmetic programming, and most recently by metaheuristic algorithms. Metaheuristic algorithms are designed and implemented for handling numerous large scale, multimodal real-world problems owing to their simplicity and ease of implementation [2]. Kessel and Glavitch voltage stability index method is adopted in [3] to identify the weakest bus for the placement of reactive power sources. Numerous works using metaheuristics have been reported in [4]. A new method for reactive power management along with retaining voltage stability is presented by authors in [5]. The dynamic behavior of metaheuristic optimization algorithm of Harris Hawk technique is discussed in [6]. The reactive power planning

G. Swetha Shekarappa · S. Mahapatra
Alliance University, Banagalore 562106, India

S. Raj (✉)
Institute of Chemical Technology Mumbai, Marathwada Campus, Jalna 431203, India
e-mail: sauravsonusahu@ee.ism.ac.in

O. H. Gupta and V. K. Sood (eds.), *Recent Advances in Power Systems*, Lecture Notes in Electrical Engineering 699, https://doi.org/10.1007/978-981-15-7994-3_40

variables which have been optimized using several integrated strategies of differential evolution optimization technique in [7] are implemented for large standard test system. In this paper [8], genetic algorithm and particle swarm optimization are modified with kriging concept technique to improve the performance of evolutionary-based computation for solving optimal power flow. Authors have implemented black hole algorithm in [9] and glowworm swarm optimization [10] technique to solve the OPF problem. The author describes PSO [11] and GSA [12] for optimal reactive power flow considering single or multiobjective for real power loss minimization having secured generation schedule. A multilevel methodology is designed by incorporating fast voltage stability index device in [13] using differential search algorithm technique for reactive power planning. An ordinal optimization-based approach is described in [14] for reactive volt-ampere sources problem. The proposed method describes the comprehensive which is implemented for reduction of true power losses and progress in voltage. Reactive power planning is performed in [15–17] by controlling var sources like reactive power generation, shunt capacitors, and transformer tap positions by using evolutionary algorithms. By using general solution algorithm-based simulated annealing in [18], the optimal placement of capacitor is proposed. Voltage controlled series compensator has been adopted by authors in [19] for improving the voltage outline and diminishing the transmission loss. Loss sensitivity approach has been adopted in [20] for determining the locations for the positioning of reactive sources.

The research described in this article depicts the implementation of a new meta-heuristic algorithm of Harris hawk optimizer (HHO) applied to voltage constrained reactive power problem. The key idea of optimization is to diminish the true power loss, running costs and improving the voltage profile in each bus by monitoring the changing location of the transformer tapings, reactive power, voltage constrain, and shunt capacitors under variable loading conditions. The research paper initiates with the introduction, mathematical problem formulation and proposed Harris hawk algorithm work for better optimization of the objectives mentioned in the problem formulation, followed by simulation results and conclusion.

2 Mathematical Problem Formulation

The key to reactive power planning is the optimum location-based distribution of reactive power sources. Such positions are systematic approaches based on optimization using the var sources in recent works. The main purpose of the task undertaken is to diminish the transmission loss of connected power network. Optimization must also be rendered with running cost and boost the voltage profile in the system

2.1 Minimize True Power Loss

To diminish true power transmission loss given by:

$$\text{Minimize } P_L = \sum_{n=1}^{k} g_{mn}\left[V_m^2 + V_n^2 - 2V_m V_n \cos(\delta_{mn})\right] \tag{1}$$

where

P_L = Real power loss
g_{mn} = conductance between mth and nth bus,
V_m = Voltage magnitude of mth bus,
V_n = Voltage magnitude of nth bus,
δ_{mn} = Phase angle of voltage

2.2 Minimize Operating Cost

To diminish the operating cost in power lines, it can be formulated as below (2).

$$\text{Total operating cost } = S_{\text{Energy}} + S_{\text{Cap}} \tag{2}$$

where S_{Energy} is the cost because of loss of energy,
S_{Cap} is the cost of capacitors equipped at nodes which are weak.
$S_{\text{Energy}} = P_{\text{loss}} \times$ Energy rate
Energy price = 0.06$/kwh,
Capacitor price/KVar = 3$,
Price of capacitor installed = 1000$, some of the cost data is collected from [18].

$$\text{Energy rate } = 0.06 \times 100000 \times 8760 \tag{3}$$

The above-mentioned problem formulations needed to be optimized by satisfying all the constraints as mentioned below:

Equality constraints. The load flow equation for equality constraints is illustrated as follows:

$$P_{Gm} - P_{Dm} - V_m \sum_{N=1}^{N_b} V_n[G_{mn}\cos(\delta_{mn}) + B_{mn}\sin(\delta_{mn})] = 0,\ N = 1,\ 2,\ 3\ldots, N_b \tag{4}$$

$$Q_{Gm} - Q_{Dm} - V_m \sum_{N=1}^{N_b} V_n[G_{mn}\cos(\delta_{mn}) + B_{mn}\sin(\delta_{mn})] = 0,\ N = 1,\ 2,\ 3\ldots, N_b \tag{5}$$

where N_b = number of buses,

P_{Gm} = Real power generated,
Q_{Gm} = Reactive power generated,
P_{Dm} = Real power demand,
Q_{Dn} = Reactive power demand,
G_{mn} = Conductance,
B_{mn} = Susceptance.

Inequality constraints. It includes magnitude of var power output by generator buses, shunt capacitors, and location of transformer taps. The boundary limits of these constraints must be satisfied.

$$\left.\begin{array}{c} V_{gm}^{\min} \le V_g \le V_{gm}^{\max} \\ P_{Gm}^{\min} \le P_G \le P_{Gm}^{\max} \\ Q_{Gm}^{\min} \le Q_G \le Q_{Gm}^{\max} \\ Q_{Cm}^{\min} \le Q_C \le Q_{Cm}^{\max} \\ T_m^{\min} \le T_m \le T_m^{\max} \end{array}\right\} \tag{6}$$

3 Harris Hawk Algorithm for Proposed Work

From the work proposed and presented in this paper, Harris hawks optimizer is a speculative optimization algorithm which is implemented to generate optimized solution to the VCRPP problem. Heidari et al. propose this unique nature-inspired, population-based, gradient-free optimization algorithm which mimics Harris hawks behavior and manner of chasing the prey. The optimizer of Harris hawks can be modeled mathematically, where the activities of angling (hunting) can be modeled in two stages, namely exploratory and exploitative.

Exploration Phase. Harris hawks detect their prey with their powerful eyes depending upon the position of the prey and is given below:

$$Z(t+1) = (Z_c(t) - Z_a(t)) - r_3(LB + r_4(UB - LB)) \tag{7}$$

$$Z(t+1) = Z_{\text{rand}}(t) - r_1|Z_{\text{rand}}(t) - 2r_2\,Z(t)| \tag{8}$$

$Z\ (t+1)$ is the setting vector of hawks for the next iteration, and $Z\ (t)$ is the current setting represents the position of the prey. $Z_{\text{rand}}(t)$ is the randomly chosen location of the hawks from the current team. The random numbers r_1, r_2, r_3 and r_4 are used to intensify and diversify the exploration in the search space. UB and LB are the upper and lower bound of search space. The average position of current hawk population is given as $Z_a(t)$. The HHO technique can be incorporated from the process of exploration to the phase of exploitation based on its getaway energy. The getaway energy of the prey is modeled as

$$E = 2E_i(1 - \frac{t}{T})$$

where E_i is the starting energy stage of prey which lies in interval between −1 and 1, T is the maximum no. of iterations, and t is the current iteration.

Exploitation phase. The transformation from exploration to exploitation phase is to achieve the surprise pounce of Harris hawks by attacking its prey which was identified in the exploration phase. The hawks encircle the prey either hardly or softly depending upon the energy of the prey retained. The energy parameter E is categorized in for different steps as follows:

Step 1 ***Soft** Encircling*
When $r > 0.5$ and $|E| \geq 0.5$, where rabbit still has enough energy to run away by its misleading jumps, but it cannot escape finally.

Step 2 ***Hard** Encircling*
When $r \geq 0.5$ and $|E| < 0.5$, where rabbit is exhausted and has very less escaping energy.

Step 3 ***Soft** encircling **with progressive rapid dives***
When $r < 0.5$ and $|E| \geq 0.5$, the rabbit acknowledges to still have energy to escape strongly. So, the hawks make the move to quagmire it effectively and dive toward the rabbit.

Step 4 ***Hard** encircling **with progressive rapid dives***
When $r < 0.5$ and $|E| < 0.5$, the rabbit loses its complete energy to escape and the hawks construct a surprise pounce and reduces the distance between them and finally kill the rabbit.

The initialization process consists of generation of random population followed by fitness evaluation of hawks and the target through Eq. (9). The updating process is done in exploitation phase through steps 1–4. The process is terminated when maximum iteration or optimal solution has been reached.

4 Result and Discussion

For the objective of justifying the work and efficacy of the proposed AHHO and HHO algorithms, test and analysis are performed on IEEE 14 bus. The details about this network are adopted from [21]. The simulations and tests are performed using MATLAB 2019b and computed on core i7-3520 M CPU a 2.90 GHz with 8 GB RAM. A total of 30 independent trials are performed for the proposed AHHO and HHO.

The IEEE 14-bus system has 05 generator with 20 power lines and three tap-changing transformer. The load real and reactive power demand are 259.00 MW and 73.5 MVar on 100 MVA base, respectively. The boundary restrictions of the controlling parameters like magnitude of generated voltage, generator bus reactive power, shunt capacitors, and transformer tapping are presented in Table 1. Initially, shunt

Table 1 Optimal parameter settings of control variables under different loading conditions

		100% loading		110% loading		120% loading		
	Minimum	HHO	AHHO	HHO	AHHO	HHO	AHHO	Maximum
Generated voltage								
V_G (2)	0.94	0.9747	0.94	1.0562	0.94	0.94	0.9462	1.06
V_G (3)	0.94	0.9999	0.94	0.9470	0.94	0.94	0.9538	1.06
V_G (6)	0.94	0.9400	0.94	1.0041	0.9602	0.94	0.94	1.06
V_G (8)	0.94	0.9637	0.94	0.9718	0.94	0.94	0.94	1.06
Generation of reactive power by generator								
Q_{GEN} (2)	−0.40	0.2343	0.2453	0.3192	0.3565	0.3055	0.2373	0.50
Q_{GEN} (3)	0.0	0.2382	0.2215	0.3021	0.2024	0.1655	0.2853	0.40
Q_{GEN} (6)	−0.06	0.0417	0.0311	0.1691	0.0389	0.0298	0.1869	0.24
Q_{GEN} (8)	−0.06	0.1087	0.0270	−0.0498	0.0524	0.1244	0.0773	0.24
Shunt var capacitor								
Q_{CAP1}	0.0	0.1065	0.0928	0.1078	0.1107	0.0650	0.0644	0.15
Q_{CAP2}	0.0	0.0242	0.0631	0.0684	0.0642	0.0345	0.0947	0.15
Q_{CAP3}	0.0	0.0603	0.0964	0.0976	0.1343	0.0893	0.0624	0.15
Position of transformer								
TP (8)	0.9	0.9	0.9	0.9253	0.9	0.9	0.9	1.0
TP (9)	0.9	0.9	0.9	0.9175	0.9	0.9	0.9	1.0
TP (11)	0.9	0.9589	0.9	0.9097	0.9	0.9	0.9	1.0
Transmission loss (p.u)		0.1319	0.1318	1.1322	0.1321	0.1324	0.1323	
Operating cost ($\times 10^6$)		6.9331	6.9285	6.9502	6.9445	6.9582	6.9540	

var sources are placed at the buses as mentioned in [20] and transmission loss is 0.1337 p.u. Thereafter, HHO and AHHO techniques are implemented for transmission loss and operating cost minimization. Various settings of controlling parameters like generated voltage, reactive power by generator bus, shunt capacitors, and transformer tap positions have been closely set within the limits satisfying all the required inequality constraints. Table 1 shows the optimal setting for system constraints under different loading conditions, and it may also be observed that controlling parameters are within the permissible limit. Figure 1 provides the convergence curve for line losses under different reactive loading conditions using HHO and AHHO algorithm. The complete cost of operation under different reactive loading conditions using HHO and AHHO has been presented in Fig. 2. The comparative analysis of the VCRPP under base loading has been shown in Table 2. From these results, it can be noticed that proposed AHHO technique has been able to diminish transmission power loss to large extent which improves the transferring power capability.

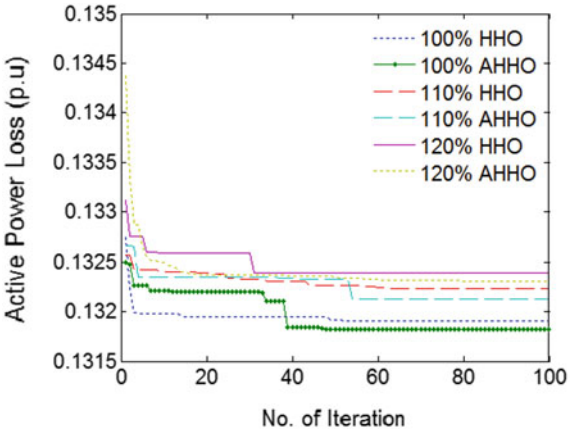

Fig. 1 Convergence curve of transmission loss reduction under different loading condition

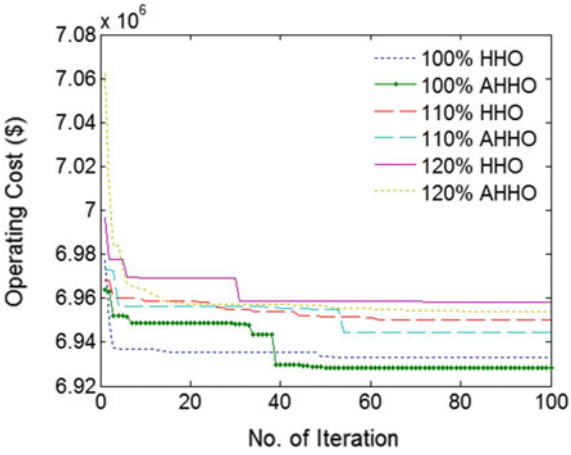

Fig. 2 Convergence curve of system operating cost different loading condition

5 Conclusion

In the proposed work, one of the recently improved heuristic algorithms, namely Harris hawks optimization, has been successfully applied to solve VCRPP issue in a given test system. The issue of optimization is defined as a nonlinear and dynamic problem of constrained optimization, characterized by both continuous and discrete control parameters. In this study, various objective functions were considered to improve the transmission capacity under enhanced reactive loadability. The AHHO and HHO approaches are inspected on IEEE 14 bus of interconnected power grid. The solution obtained from the proposed algorithm was contrasted with other methods previously published beforehand.

Table 2 Result verification for operating cost with other techniques

Unplanned cost of operation ($)	Algorithms	Planned operating cost ($)	Total cost reduction ($)
7.35314×10^6	GA [20]	6.9493×10^6	4.0384×10^5
	SA-GA [20]	6.9473×10^6	4.0584×10^5
	Sens-GA [20]	6.9470×10^6	4.06144×10^5
	DE [20]	6.9470×10^6	4.0614×10^5
	SA-DE [20]	6.9472×10^6	4.0594×10^5
	Sens-DE [20]	6.9472×10^6	$4.05{,}944 \times 10^5$
	PSO [20]	6.9477×10^6	4.0544×10^5
	SA-PSO [20]	6.9476×10^6	4.0554×10^5
	Sens-PSO [20]	6.9472×10^6	4.0594×10^5
	EPSO [15]	6.9477×10^6	4.0540×10^5
	SPSO [15]	6.9477×10^6	4.0544×10^5
	APSO [15]	6.9481×10^6	4.0500×10^5
	GWO [16]	6.9369×10^6	4.16244×10^5
	OGWO [16]	6.9361×10^6	4.17040×10^5
	HHO	6.9331×10^6	4.2004×10^5
	AHHO	6.9285×10^6	4.2464×10^5

References

1. Hemmati, R., Hooshmand, R.-A., Khodabakhshian, A.: Market based transmission expansion and reactive power planning with consideration of wind and load uncertainties. Renew. Sustain. Energy Rev. **29**, 1–10 (2014)
2. Birchfield, A.B., Ti, X., Overbye, T.J.: Power flow convergence and reactive power planning in the creation of large synthetic grids. IEEE Trans. Power Syst. **33**(6), 6667–6674 (2018)
3. Sekhane, H., Djamel, L.: Identification of the weakest buses to facilitate the search for optimal placement of var sources using "Kessel and Glavitch" Index. J. Electric. Eng. Technol 1–11 (2019)
4. Karami-Horestani, A.R., Golshan, M.E.H., Monsef, H.: Expected security constrained reactive power planning. IET Gener. Trans. Distrib. **10**(10), 2306–2315 (2016)
5. El-Araby, E.-S.E., Yorino, N.: Reactive power reserve management tool for voltage stability enhancement. IET Gener. Trans. Distrib. **12**(8), 1879–1888 (2018)
6. Heidari, A.A., Seyedali, M., Hossam F., Ibrahim, A., Majdi, M., Chen, H.: Harris Hawks optimization: Algorithm and applications. Fut. Gener. Comput. Syst. **97**, 849–872 (2019)
7. Shaheen, A.M., Ragab A.E.-S., Sobhy M.F.: A reactive power planning procedure considering iterative identification of VAR candidate buses. Neural Comput. Appl. **31**(3), 653–674 (2019)
8. Deng, Z., Mihai D.R., Jan K.S.: Kriging assisted surrogate evolutionary computation to solve optimal power flow problems. IEEE Transactions on Power Systems (2019)
9. Bouchekara, H.R.E.H.: Optimal power flow using black-hole-based optimization approach. Appl. Soft Comput. **24**, 879–888 (2014)
10. Reddy, S.S., Srinivasa, C.R.: Optimal power flow using glowworm swarm optimization. Int. J. Electri. Power Energy Syst. **80**, 128–139 (2016)
11. Singh, R.P., Mukherjee, V., Ghoshal, S.P.: Optimal reactive power dispatch by particle swarm optimization with an aging leader and challengers. Appl. Soft Comput. **29**, 298–309 (2015)

12. Rajan, A., Malakar, T.: Optimal reactive power dispatch using hybrid Nelder–Mead simplex based firefly algorithm. Int. J. Electri. Power Energy Syst. **66**, 9–24 (2015)
13. Amrane, Y., Mohamed, B., Messaoud, B.: A new optimal reactive power planning based on differential search algorithm. Int. J. Electric. Power Energy Syst. **64**, 551–561 (2015)
14. Lee, W.-T., Horng, S.-C., Lin, C.-F.: Application of ordinal optimization to reactive volt-ampere sources planning problems. Energies **12**(14), 2746 (2019)
15. Bhattacharyya, B., Raj, S.: PSO based bio inspired algorithms for reactive power planning. Int. J. Electr. Power Energy Syst. **74**, 396–402 (2016)
16. Raj, S., Bhattacharyya, B.: Reactive power planning by opposition-based grey wolf optimization method. Int. Trans. Electric. Energy Syst. **28**(6), e2551 (2018)
17. Bhattacharyya, B., Raj, S.: Differential evolution technique for the optimization of reactive power reserves. J. Circ. Syst. Comput. **26**(10), 1750155 (2017)
18. Chiang, H.D., Wang, J.C., Cockings, O., Shin, H.D.: Optimal capacitor placements in Distribution systems: part 2: solution algorithms and numerical results. IEEE Trans Power Deliv **5**(2) (1990)
19. Mahapatra, S., Jha, A.N., Panigrahi, B.K.: Hybrid technique for optimal location and cost sizing of thyristor controlled series compensator to upgrade voltage stability. IET Generat. Trans. Distribu. **10**(8), 1921–1927 (2016)
20. Bhattacharyya, B., Goswami, S.K., Bansal, R.C.: Loss sensitivity approach in evolutionary algorithms for reactive power planning. Electric Power Comp. Syst. **37**(3), 287–299 (2009)
21. Pai, M.A.: Computer Techniques in Power System Analysis, 3rd edn. Tata McGraw Hill Education Private Limited (2005)

Performance Evaluation of Solar PV Array Under Various Partial Shading Conditions

Karni Pratap Palawat, Vinod K. Yadav, and R. L. Meena

1 Introduction

In India, presently the total installed capacity of 37 0GW (central electricity authority (CEA) as of 30-03-2020), the highest share of fossil fuel-based energy generation approx. 62% (230.6 GW) [1]. Fossil fuel-based electricity generation is polluting in nature which has several negative impacts on humans and other forms of lives on earth. Some of those pollutants are SO_2 and NO_x, particulate matter (PM), and Hg [2]. In many, reports suggest that excessive exposure to these pollutants has life-threatening consequences [3], mostly respiratory type of diseases, etc. [3]. On the other hand, life without electricity is not imaginable, so for better development of clean and green energy, a shift is toward renewable energy sources. Scientists and policy makers around the globe are now shifting toward renewable energy sources, as an answer to this emergency with special emphasis on solar energy, in India sun radiation is most abundantly available energy source [4] which is renewable in nature and as moving toward technology revolutions such that using resources provided by mother earth. But without making judicious utilization of resources, it leads to depleting natural resources and abundant loss in environmental and ecological balance. As to move toward a technological revolution in balance with nature, it is beneficial overall by using material wisely and with the concept of sustainable development [5]. This document discusses the effective utilization of PV module

K. P. Palawat (✉) · V. K. Yadav · R. L. Meena
Department of Electrical Engineering, Delhi Technological University (DTU), New Delhi, Delhi, India
e-mail: karnipratappalawat@gmail.com

V. K. Yadav
e-mail: vinodkumar@dtu.ac.in

R. L. Meena
e-mail: meenarl@yahoo.com

O. H. Gupta and V. K. Sood (eds.), *Recent Advances in Power Systems*, Lecture Notes in Electrical Engineering 699, https://doi.org/10.1007/978-981-15-7994-3_41

and discusses about multiple maximum power points (MPPs) which are introduced due to partial shading and effects. [6–8]. To elaborate further, some are global and local maximum power points which makes it difficult for conventional algorithm to trace global maximum power point (GMPP). Thus, if it got stuck in local maximum power point (LMPP), it becomes difficult to retrieve it out of that zone. The output of the module is influenced mainly by the change in levels of irradiance, operating temperatures, or even shading many linked aspects and performance get impacted [9, 10]. Lots of improvements are required in MPP tracing conventional algorithms [11, 12]. Hence, the process of advance algorithms requires lots of data, which leads to making process bulky. Thus, system requires a heavier processing power which the conventional system is not able to handle, such that the system becomes more costlier and sophisticated to give reliable and stable output [8, 13, 14]. Several other parameters such as dust amassing on module and temperature intensification of module due to solar heating and hotspot creation also lead to bargain with efficiency [9]. To deal with such a situation, we have to make alterations in algorithms as well as circuit topologies to gain maximum power output [15]. And to trace such conditions, we can go by parameters such as form factor (FF), mismatching power loss (ΔL), and efficiency [16].

2 Description About Circuit Configuration Taken for the Experiment

In this experiment, setup consists of series–parallel circuit topology to be analyzed in which three PV modules are taken in series–parallel to get desired output voltage for inverter. Then, three different strings like that are connected in parallel to get the desired output current, and this makes series–parallel (SP) topology to get desired power output [6] as shown in Fig. 1. As this topology is mostly taken for generation

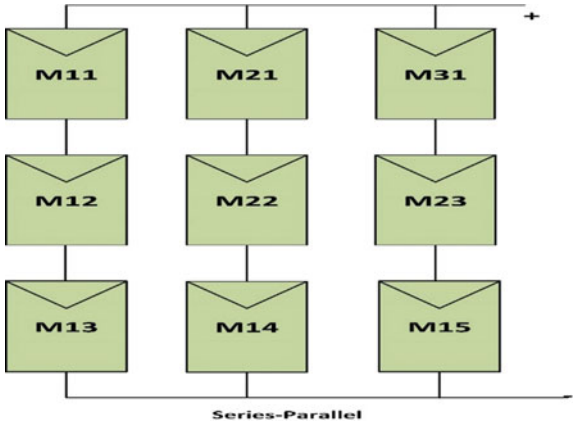

Fig. 1 3 × 3 PV array taken for experiment

due to incorporated simplicity and ease of connection and gives maximum power output which is at normal conditions, under partial shading total cross-tied (TCT) gives more determined performance as in comparison with series–parallel [17, 18]

2.1 Experimental Setup and Its Details

Experimental setup consists of the following apparatus as shown in picture (Fig. 2).

In this setup, two multimeters are used as voltmeter and as an ammeter, pyranometer which is used for measuring solar incident radiation, a variable load or rheostat (approx. 200 Ω), and nine solar panels are used of same ratings as given in Table 1 below. Here, in this document, most of the work is done in January on the days of clear sky, so that uniform irradiance is of 700–800 W/m^2.

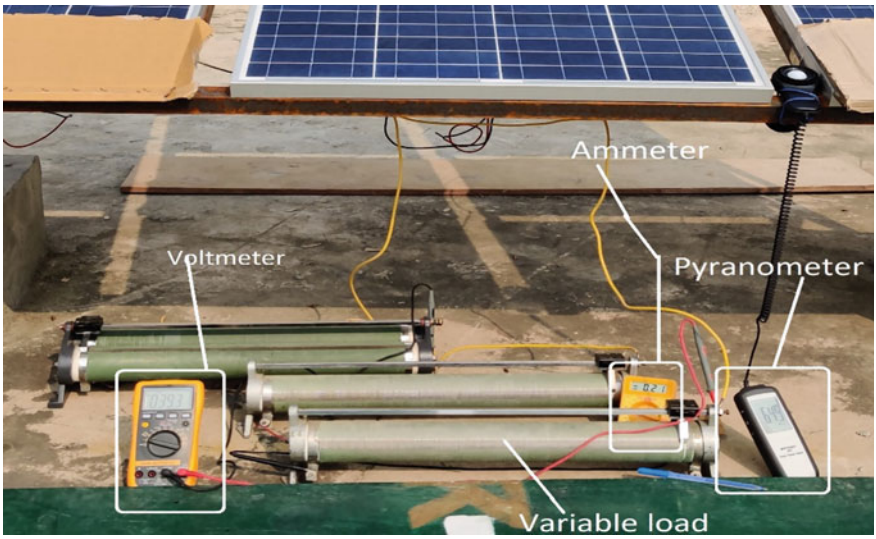

Fig. 2 Apparatus used for the experiment

Table 1 EIL 40, all given specification are at STC: – 1000 W/m^2 irradiance, AM 1.5, temp.25 °C

Maximum power (P^{max})	40 W (36 cells)
Voltage max. power (V^{mp})	18.00 V
Current at max. power (I^{mp})	2.22 A
Open-circuit voltage (V^{oc})	22.18 V
Short-circuit current (I^{sc})	2.40 A
Tolerance	+0–5 W

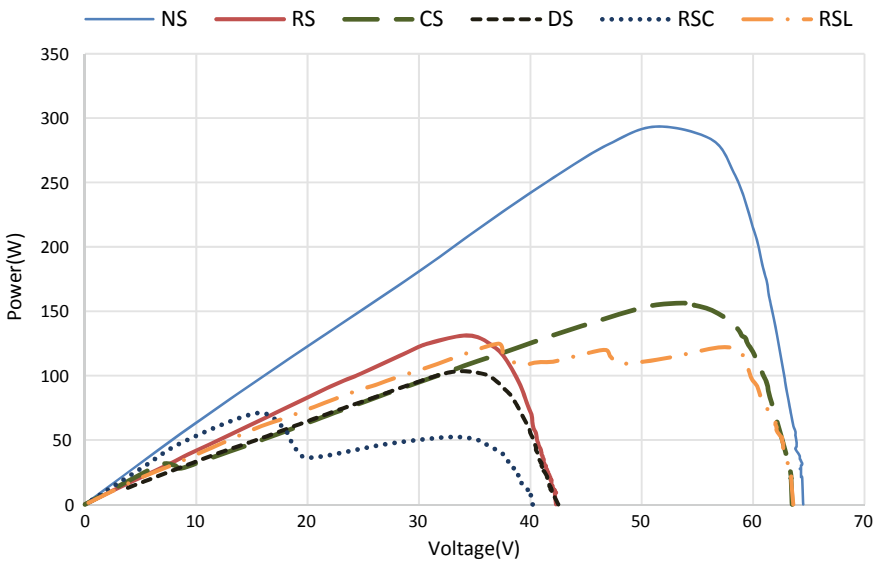

Fig. 3 PV plot for all partial shading conditions

2.2 *Partial Shading Conditions Are Taken for Experiment Purpose*

The name itself suggests that modules are partially shaded in nature generally by shadow, bird dropping, dry leaves, etc. For sake of experiment, the artificial apparatus are cardboards and fallen leaves which are used here to mimic the natural conditions. As many authors have suggested plethora of shading patterns [6, 7, 19], but for sake of experiment, the five different partial shading conditions are used namely non-shaded (NS), row shading (RS), column shading (CS), diagonal shading (DS), random shading using cardboard (RSC), and random shading using leaves (RSL). The last one is unique in this text. Here, these all PSCs are accomplished using 3 × 3 series–parallel circuit topology as shown in Figs. 3 and 4.

2.3 *Performance Assessment Under Different PSCs*

In general, as many authors suggest that assessment of PV array is done mainly by mismatching power loss (ΔP_L), efficiency (η), and form factor(FF). [6, 16], these are described as shown in below formulas

- *Mismatching power loss* ((ΔP_L) in percentage is given by Eq. (1) [20].

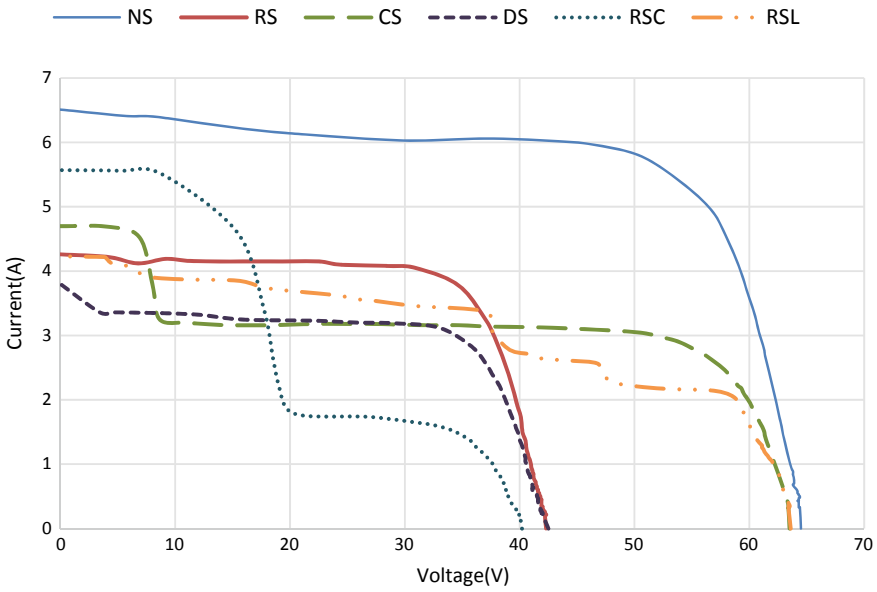

Fig. 4 IV plot for all partial shading conditions

$$\Delta P_L = \frac{P^{\mathrm{MPP}} - P^{\mathrm{PSC}}}{P^{\mathrm{MPP}}} \times 100 \tag{1}$$

where P^{MPP} is maximum power under uniform irradiance which is achieved by multiplying V^{mpp} and I^{mpp}. And P^{PSC} is maximum power under partial shading condition which is obtained by multiplying V^{oc} and I^{sc} generated. [6]

- *Efficiency* is defined as the ratio of output by input, whereas here input is considered as solar power input which is computed by multiplying solar intensity per meter square (I) and area of PV array '*A*' divided by output which is P^{MPP} which is a multiplication of V^{mpp} and I^{mpp}.
- *Fill-factor. (FF)* is derived from the IV plot by multiplying V^{mpp} and I^{mpp} and divided by V^{oc} and I^{sc}. As the form factor value is near to unity, performance is higher for the PV system [6].

$$FF = \frac{\mathrm{V}^{\mathrm{mpp}} * \mathrm{I}^{\mathrm{mpp}}}{\mathrm{V}^{\mathrm{oc}} * \mathrm{I}^{\mathrm{sc}}} \tag{2}$$

3 Graphs and Tables

Shown below is the process of analyzing the performance of PV array which is mainly done by using PV and IV plot, so as it is described below

4 Results and Observations

In this document, the circuit topology is considered in series-parallel. So on that topology, all these five PSC's are applied, and results are computed, which are summarized below.

- Drastic reduction in power output due to partial shading condition as in table or in PV plot (Fig. 3), we can see power generation due to non-shading is 293.376 W. And in PSC, such as row PSC power output is at 131.134 W. Reduction is more than 50% which makes system less beneficial for user.
- Multiple peaks are also being introduced, one is global maximum power point (GMPP), and rest others are local maximum power point (LMPP). For example, under row shading leaves, three maximum power point are seen among them, (124.8248,37.04) is GMPP, rest two (121.8,58;120.019,46.7) are LMPP, which further introduce complexities for conventional algorithms to trace maximum power point.
- When the partial shading conditions are performed using MATLAB/Simulink, modeling is done by reducing irradiance level of whole PV module, but in practice, this phenomena occurrence is rare, but irradiance is partially reduced by bird droppings, fallen leaves accumulation, shadow, etc.
- As we generally apply series–parallel topology for voltage which is most promising in column PSC, here in this PSC, power output is maximum among others as shown in Fig. 3 and Table 2.

Table 2 Various parameters for performance analysis of series–parallel under partial shading condition

Type of PSC	V^{mpp} (V)	I^{mpp} (A)	V^{oc} (V)	I^{sc} (A)	P^{mpp} (W)	Fill-factor (FF)
Non-shaded (NS)	51.2	5.73	64.5	6.51	293.376	0.6986
Row shaded (RS)	34.6	3.79	42.3	4.26	131.134	0.7277
Column shaded (CS)	53.9	2.9	63.5	4.7	156.31	0.5237
Diagonal shaded (DS)	33	3.12	42.5	3.8	102.96	0.6375
Random shaded cardboard (RSC)	15.41	4.6	40.2	5.57	70.886	0.3184
Random shading leaves (RSL)	37.04	3.37	63.6	4.23	12.48248	0.4639

- In practice, series–parallel circuit topology is generally used because due to ease in circuit configuration and is economical. As the results computed above suggests, during partial shading condition, power outcome is drastically reduced so for that user has to take a look in results of other circuit topologies such as honeycomb and total cross-tied.

References

1. All india installed capacity (MW) of power station installed capcity (MW) of power utilities in the states/UTs located in northern region. http://www.cea.nic.in/reports/monthly/installedcapacity/2020/installed_capacity-04.pdf (2020)
2. I. Brief, India' s Energy Transition . https://www.iisd.org/sites/default/files/publications/india-energy-transition-air-pollution-standards.pdf (2019)
3. Boningari, T., Smirniotis, T.G.: Science Direct Impact of nitrogen oxides on the environment and human health : Mn-based materials for the NO_x abatement. Curr Opin Chem Eng **13**(x), 133–141 (2016)
4. Ghosh, S., Yadav, V.K., Mukherjee, V., Yadav, P.: Evaluation of relative impact of aerosols on photovoltaic cells through combined Shannon's entropy and Data Envelopment Analysis (DEA). Renew. Energy **105**, 344–353 (2017)
5. S. Centre, "SDG 7: Ensuring access to affordable, reliable, sustainable and modern energy for all (2018, January)
6. Pendem, S.R., Mikkili, S.: Modelling and performance assessment of PV array topologies under partial shading conditions to mitigate the mismatching power losses. Sol. Energy **160**, 303–321 (2018)
7. Mishra, N., Yadav, A.S., Pachauri, R., Chauhan, Y.K., Yadav, V.K.: Performance enhancement of PV system using proposed array topologies under various shadow patterns. Sol. Energy **157**, 641–656 (2017)
8. Kumar, N., Hussain, I., Singh, B., Panigrahi, B.K.: Maximum power peak detection of partially shaded PV panel by using intelligent monkey king evolution algorithm. IEEE Trans. Ind. Appl. **53**(6), 5734–5743 (2017)
9. Singla, A., Singh, K., Yadav, V.K.: "nvironmental effects on performance of solar photovoltaic module. In: Biennial International Conference on Power & Energy Systems: Towards Sustainable Energy (PESTSE-2016) (2016)
10. Ghosh, S., Yadav, V.K., Mukherjee, V.: Impact of environmental factors on photovoltaic performance and their mitigation strategies–a holistic review. Renew. Energy Focus **28**(00), 153–172 (2019)
11. Sen, T., Pragallapati, N., Agarwal, V., Kumar, R.: Global Maximum Power Point Tracking of PV Arrays Under Partial Shading Conditions Using A Modified Particle Velocity-Based PSO Technique, pp. 555–564 (2018)
12. Bayrak, F., Ertürk, G., Oztop, H.F.: Effects of partial shading on energy and exergy ef fi ciencies for photovoltaic panels. J. Clean. Prod. **164**, 58–69 (2017)
13. Tang, S., Sun, Y., Chen, Y., Zhao, Y., Yang, Y., Szeto, W.: An enhanced MPPT method combining fractional-order and fuzzy logic control. IEEE J. Photovoltaics **7**(2), 640–650 (2017)
14. Liu, Y.H., Huang, S.C., Huang, J.W., Liang, W.C.: A particle swarm optimization-based maximum power point tracking algorithm for PV systems operating under partially shaded conditions. IEEE Trans. Energy Convers. **27**(4), 1027–1035 (2012)
15. Ishaque, K., Salam, Z.: A review of maximum power point tracking techniques of PV system for uniform insolation and partial shading condition. Renew. Sustain. Energy Rev. **19**, 475–488 (2013)

16. Bingöl, O., Özkaya, B.: Analysis and comparison of different PV array configurations under partial shading conditions. Sol. Energy **160**, 336–343 (2018)
17. Balato, M., Costanzo, L., Vitelli, M.: Series-Parallel PV array re-configuration: Maximization of the extraction of energy and much more. Appl. Energy **159**, 145–160 (2015)
18. Villa, L.F.L., Picault, D., Raison, B., Bacha, S., Labonne, A.: Maximizing the power output of partially shaded photovoltaic plants through optimization of the interconnections among its modules. IEEE J. Photovoltaics **2**(2), 154–163 (2012)
19. Prince, D., Winston, S., Kumaravel, B., Praveen K., Devakirubakaran, S.: Performance improvement of solar PV array topologies during various partial shading conditions. Sol. Energy **196**, 228–242 (2020)
20. Mäki, A., Valkealahti, S., Leppäaho, J.: Operation of Series—Connected Silicon—Based Photovoltaic Modules Under Partial Shading Conditions, pp. 298–309 (2012)

Environmental Impacts from the System of Solar Energy

Mukesh Kumar Nag, Parmanand Kumar, and Mani Kant Paswan

1 Introduction

Substantial fossil fuels are utilized by more or less every human on the earth directly or indirectly. This is often the cause for a few undesired phenomena along with atmospheric and environmental pollution, that have not been sensed before in recognized human history. Therefore, worldwide warming, climate change, effect of greenhouse, reduction of ozone layer, and terms of acid rain have commenced to looked inside the literature frequently. Since 1970, it is been known accurately with the aid of researches and experiments that those phenomena are closely associated with conventional sources of energy causes of hazardous gases such as dioxide of carbon (CO_2), mono-oxide of carbon (CO), inhalation general anesthetic gas (N_2O), and methane (CH_4). The ozone (O_3) layer which blocks sun's ultraviolet radiation is going to be depleted by these generated toxic gases, and so, troposphere of the planet turning hot day by day. To avoid similar effects of these occurrences, there are two options which are both to enhance the fossil-based fuel (Hydrocarbons) standard with minimizing in their dangerous emission into the environment or, greater scientifically, to fossil fuel interchange usage maximum expediency with environment benefit, i.e., energy sources which is renewable and clean. Among in these sources of energy get from solar is at topmost, because of its much and more even distribution in nature than other renewable energy available of this kind like hydro, wind, tidal, wave and geothermal [7].

M. K. Nag (✉) · P. Kumar · M. K. Paswan
Mechanical Engineering Department, NIT Jamshedpur, Jamshedpur, Jharkhand, India
e-mail: nag0859@gmail.com

P. Kumar
e-mail: pkumar.me@nitjsr.ac.in

M. K. Paswan
e-mail: mkpaswan.me@nitjsr.ac.in

O. H. Gupta and V. K. Sood (eds.), *Recent Advances in Power Systems*, Lecture Notes in Electrical Engineering 699, https://doi.org/10.1007/978-981-15-7994-3_42

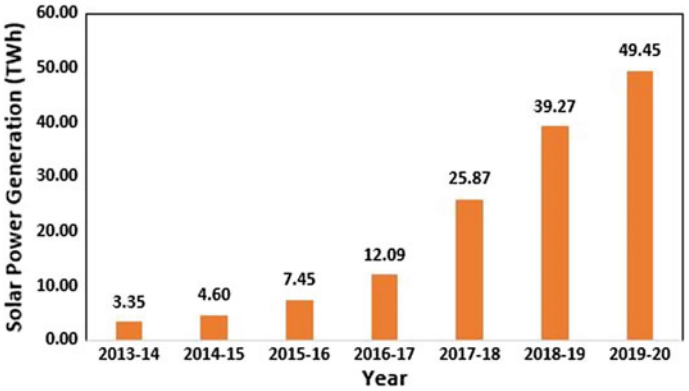

Fig. 1 Solar power generation growth in India [3]

In India, annual solar energy generation visiting increases, and it is up to 49.45 TWh year 2019–20 as shown in Fig. 1. Although energy got from sun power is a continual and long-life energy future, as soon as demand of these limited energy source boost, energy production and its harmful environmental effect will also be increased. As a consequence, the pollution in the environment became a world-wide challenge. Hence, we can see in these past years the seriousness dependency on the source of clean energy such as solar-based energy appliances that have been expanded.

But energy of solar-based technology has created some bad effect on the environment. We can see it by a simple example, such as colony solar tree or street light solar panel, that has some limited life cycle and after that it has become waste and this waste consists of many hazardous materials like lead, cadmium, cadmium telluride, gallium arsenide, copper–indium–gallium arsenide, and other toxic materials. During this whole study, we discussed positive and negative sides of the system of the solar energy to the environment.

2 Solar Energy

The energy which is gain from the sun light and converted into useful work by utilize using a number of ever-evolving technologies including appliances like solar heater, photovoltaic, solar based thermal power plant, and photosynthesis with artificial method. These are main tool and appliances of renewable energy and its broadly characterized technology as either active solar or passive solar relying upon how they collect and distribute solar energy or converted into electricity or power. Archimedes a Syracusian used concentrating solar mirrors to set fire to Roman ships in 214 B.C and Alexandrian Heron designed a simple water pump almost 2000 years back, sunlight plays a vital role in both of them invent [13].

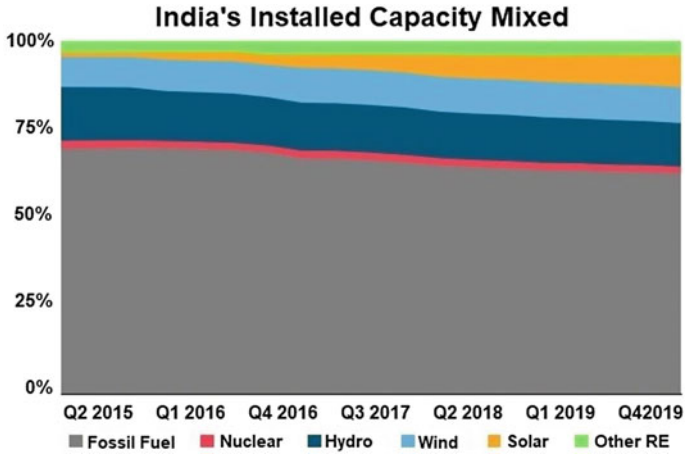

Fig. 2 Share of various energy sources capacity in India [6]

2.1 Comparative Assessment

The energy which is obtained from other sources like fossil fuel, nuclear, hydro, wind, solar, and other renewable energy in which solar-based energy has increased volume installation in India up to year 4th quarter 2019 is shown in Fig. 2.

2.2 Solar Tree

Solar tree is a structure and a concept in which a number of photovoltaic solar cell panels are arranged in such a way with the hanging arms of erected pillar that look like a structure of tree. All solar panels are mounted on the end of the arms and look as leaves of tree. Solar tree is an example of active solar system to generate electricity. The whole structure includes iron pillar, welded iron rods as branches, solar photovoltaic (PV) module, light-emitting diodes (LEDs), inverter and battery, sprinkler, lightening arrester, and earthing. Solar tree how it looks like is shown in Fig. 3. Solar PV module collects the radiant sunlight, and with the help of inverter, it charges the connected battery and uses the charged battery at night by switching on the LED bulb. Sprinkler is used for cleaning the solar PV module in evening, and lightening arrester and earthing are used for safety purposes. This solar tree concept saves 99% of land use compared to traditional arrangement of solar PV module with same amount of electricity generation [15].

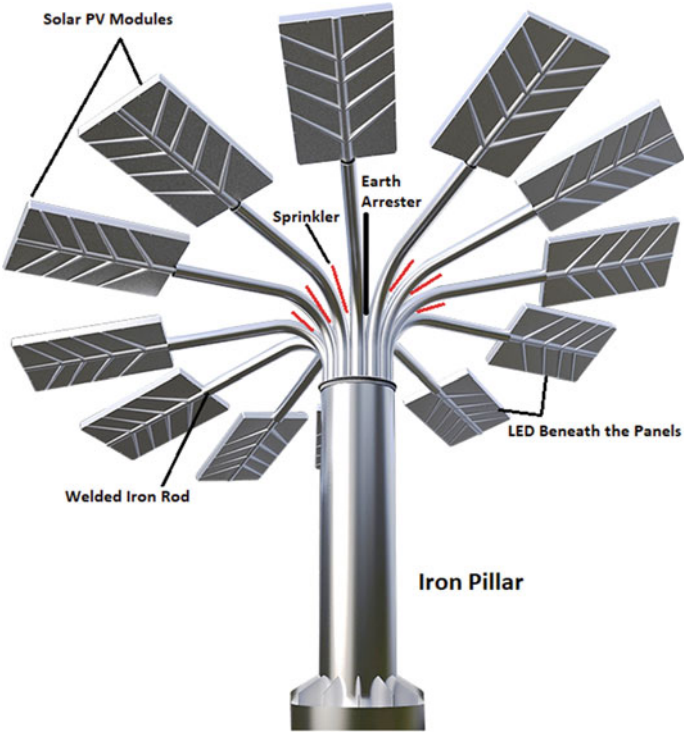

Fig. 3 Solar tree

3 Solar Energy Systems

3.1 Solar Collectors

A solar collector is an equipment that gathers and/or concentrates radiation of solar from the sun. There are basically two varieties of solar collectors that depend on temperature produced:

Low-temperature collector (i.e., flat plate and unglazed solar collectors).

High-temperature collector (i.e., collector based on evacuated tube, line focused, and point focused collectors) [5].

Flat-plate solar collectors: The basic working principle of these collectors depends on the conversion of the solar energy into the thermal energy. Flat-plate collectors are fabricated from a rigid frame having top side covered by tumbler/glass having absorbing and transparent property. Felled ray of the sun passed over the glass plate and hence tapped by the system. This tumbler/glass plate is covered with paints or unique coatings for excessive soaking up properties. The flat-plate collector parts are

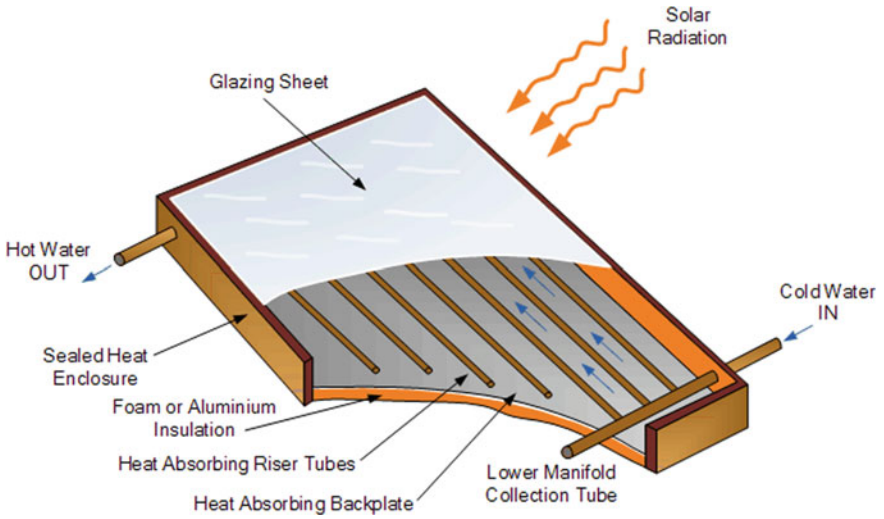

Fig. 4 Flat-plate solar collector (sectional view)

shown in Fig. 4. More or less ninety percent of the solar radiation felt at the surface are absorbed by these coating of plates.

Conversing solar collectors: A conversing solar collector is a type of high-temperature solar collector that concentrates the solar radiation with their parabolic dish concentrator as shown in Fig. 5. These convergent sunlight is collected on to a solar receiver Stirling engine, where it is captivated and transformed into heat energy or into the electricity.

The conversing type solar collector is used to achieve more than 140 °C temperature that is required to heat the water, and their significance is used in different types of mechanical cycles to generate electricity.

Fig. 5 Conversing solar collector

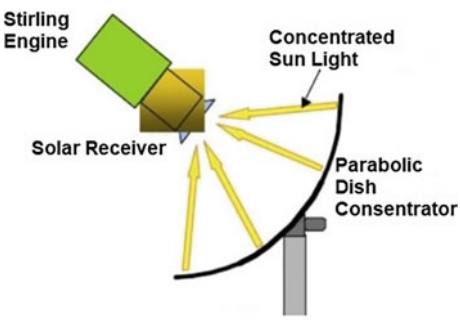

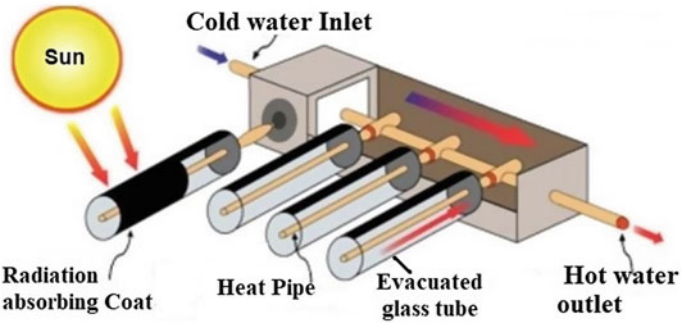

Fig. 6 Evacuated tube solar collector

Evacuated glass tube collectors: Evacuated glass tube collector is a type of solar collector through which we can get high degree range of temperature ~177 °C under the appropriate set of circumstances. It is little bit expensive approximately double that of flat-plate solar collectors when we consider unit area cost. This type of solar collector is used for domestic heating purpose mainly in cloudy weather region. It is also used in cooling application by regenerating refrigeration cycle. However, flat-plate solar collector is domestically fit, cheaper, and more suitable for heating the water in cold days as compared to evacuated glass tube collector. The construction of evacuated glass tube collector is shown in Fig. 6. Transparent, parallel evacuated glass tube has a heat pipe that is connected with a single header pipe in which 50% propylene glycol and 50% of water flow carry heat which is trapped by evacuated glass tube from the sun. Variety of evacuated tube has been already used and manufactured in UK, Germany, China, and Canada (Apricus, 2006) [14].

3.2 Electrical Energy Converters

Solar cells: It is also known as photovoltaic cell that converts sunlight energy into electricity through the photovoltaic effect. Working principle of solar cell is based on P-N junction diode as shown in Fig. 7. When solarlight falls on the transparent conducting electrode and reaches the P-N junction layer, then some of the sunlight photons develop a pair of electron and hole. The developed electron and hole cause current in the circuit.

Solar thermal power systems: In this, electric generation system gathers and intensifies sunlight to generate the high-temperature steam needed to generate electricity. Every solar thermal power system or electric generation system solar energy collector has two basic parts: solar dish concentrator and converter of power unit (engine/generator). In this system, concentrator causes boiling of water and generates the high-temperature steam and this steam goes to a thermal cycle (i.e., Rankine cycle, Brayton cycle, and Stirling cycle) and by engine or Stirling-type generator generates electricity. Rankine cycle is basic and mostly used.

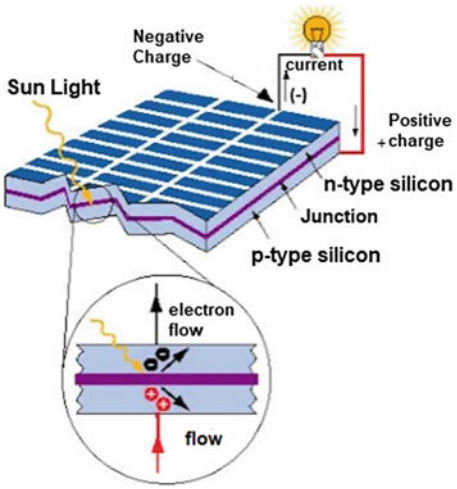

Fig. 7 Photovoltaic solar cell diagram

4 Environmental Impact Assessment

The sustainable improvement is now deeply embedded in each countrywide and worldwide state of affairs, and it is miles from an enormous international hassle; therefore, India has additionally keen problem at the protection of surrounding, improvement, and sustainable development. Concept of sustainable importance has been expanded in India too. As a result, some new rules put good that each one improvement initiative must be tuned with substantiate environmental norms.

An environmental impact assessment (EIA) looks into various problems and conflicts which will not affect the viability of an assignment, however also predicts if a mission may harm the humans or society, their land, livelihood, and environment more importantly. The EIA procedure identifies the measures to decrease those impacts and mitigation of dangerous affects and maximizes the useful impact, and this choice is made with a reason to protect and for the betterment of the most effective environment. The first ambition is to extend industrialization which maintains environmental pleasant. In this way, "sustainable development" will be possible by way of continuing the use and conservation balance among affordable improvement. Therefore, the environmental assurance is more crucial integral element of EIA.

The EIA policies in India are statutory sponsored by using the environmental protection Act in 1986 and were followed by the EIA policies of 1994 and 2006. Many amendments are completed within the past year. However, system of solar energy is still exposed to the EIA procedures and guided to reduce the bad ability influences on the environment [2]. Despite that, solar energy system is an environmental-friendly system.

5 Environmental Impacts from the System of Solar Energy (Mainly Photovoltaic Solar Cell)

Energy of solar may be the cleanest power source while compared with conventional power resources. System of solar energy has many great blessings because it is smaller amount expensive and most importantly does not produce any pollution for the duration of operation, and also has inexhaustible strength supply in comparison with conventional supply of energy, for instance, fossil fuels. However, solar energy appliances have certain bad effects on the environment very similar to other systems of energy appliances [4] and on utility-scale solar energy system [10].

5.1 Impact on Land and Biodiversity

Relying on the realm, big large service-scale solar appliances can enhance concern approximately on land deterioration and habitat distraction. Total required area is exceptional counting on the technology, the geomorphology of the net sites, and also the solar resources strength.

Roughly estimation of photovoltaic cell system taken for generation of one megawatt electricity is around ~3.5–10 acres [8]. Solar photovoltaic cell system structure on cultivable land can motive viable harm on the fertile areas [4]. Energy of solar on utility-scale also affects the direct and regional biodiversity. We can see from Fig. 8a and c [9] that the detailed death history has observed approximately 26 different kinds of birds in more than 280 days, along with effect of scavenger

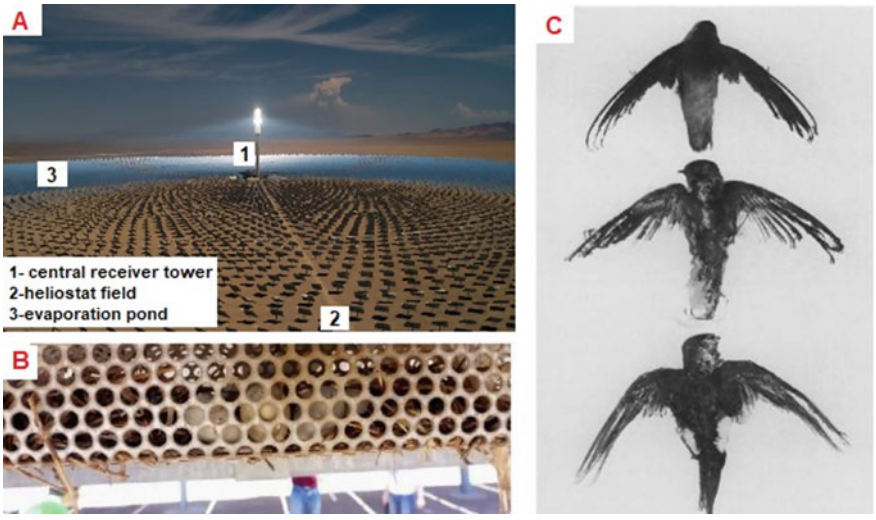

Fig. 8 Impact of utility-scale solar energy on biodiversity [9]

bias, which is arisen from the generation of ~10 megawatt concentric solar thermal energy. Approximately 81% death of birds is due to unfortunate direct strike with site framework, mainly with heliostat and due to scorching when heliostat was rotated toward central receiving point. In B picture segment, A few nests of birds were found on PV module infrastructure backside. This picture is taken from utility-scale solar energy (USSE) power plant California.

5.2 Impact on Human Health and Environment

The manufacturing process of photovoltaic cell constitutes a variety of toxic materials, which are mostly used to clean and purify the layer of semiconductors. These are the same chemicals which are used in the semiconductor-based industries and consist of hazardous acid based on sulfur, hydrogen, chlorine, fluorine, nitrogen, and other organic compounds as acetone and 1,1,1-trichloroethane. As per the silicon wafer size and cell, the amount of these hazardous chemicals used [12] silicon dust inhaling risk faced by the worker associated with the manufacturing unit. Thus, photovoltaic company must have to follow US laws to confirm that no harm from the company exposed manufacturing waste to working person associated with that company. Hazardous waste should be disposed properly so that it does not harm any people or environment. Thin-film PV cell as shown in Fig. 9 consists of a variety of harmful substances than using common silicon photovoltaic cells. Modern PV cells consist of copper–indium–gallium arsenide, cadmium telluride, copper–indium–gallium diselenide, and gallium arsenide (GaAs) [10]. If these do not seem to be handling properly, they could act very severely on public health and environmental threats.

Fig. 9 Thin-film PV cell

Fig. 10 **a** Poor **b** good **c** best aesthetic appearance of PV cell on the roof [1]

5.3 Visible Burdens

There are some visible influences as a burden while first look depends on the types of solar photovoltaic cells and its surrounding. If we propose to install the solar cell in our house, it is preplanned before constructing the design of house or buildings. This is why aesthetic appearance of the building is common dream. For this well-planned and well-screened solar panel, make this dream true without any visual burdens. Solar photovoltaic cells may be used as a skinning tiles that might be integrated into the roof of house or walls. Decent fitting and designing are fundamental factors for big photovoltaic solar cell application.

British renewable energy (BRE), planning and practice guidance for renewables, and Department of Energy and Climate Change (DECC) are some well-established guides for solar panel installment to solve the visual burdens. Figure 10 shows how visual burdens look with proper or without proper planning guidance [1]

Another most important factor about the improved aesthetic appearance is color of photovoltaic cells, opting sufficient care while color selection to set up the solar cell modules for the house[4].

5.4 Influences on Natural Assets

We are trying to fully depend on solar energy system because of limited fossil fuels on the earth. For continual requirement of energy for growing population, the solar energy systems are only and last option for us. During the production phase, some toxic chemical substances generate by-product. Specially, the photovoltaic cell acts as a curse on natural assets or resources because of its manufacturing that encompasses heavy metals like cadmium [4]. Water is also a natural resource which is consumed during the operation (e.g., photovoltaic energy systems that require 0.02 m^3/MWh and concentrated solar power (CSP) wet cooling 3.07 m^3/MWh) consumption of water only for dust-contaminated panel washing. Presently, common idea for dust removing is only to wash the panel or mirror with water. A latest search predicted by USSE (Utility Scale Solar Energy) installation in southwestern US that the water consumption for controlling dirt is a big issue that 60–90% intake of total water for each dry cooled CSP and PV setup [11].

5.5 Air Pollution Cause Global Warming

Solar appliances lifecycle stages produce some emission which includes manufacturing, material transporting, setup, decommissioning, dismantlement, and maintenance that estimated generated emission from life cycle of photovoltaic cell system within ranges ~(0.03–0.08) kg of CO_2 E/kWh. Emission produced by transportation ranges ~(0.1–1)% of the overall production emissions. The estimated emissions are in the range ~(2.76–3.85) kg of CO_2/kWp, ~(5.05–5.52) kg of SO_2/kWp, and ~(4.50–5.28) NOx/kWp in mono- and polycrystalline modules (kWp stands peak kilowatt) [4].

5.6 Noise Interference

Producing noise is negligible as compared to different power generating options from the traditional source of energy, gas turbine, and the wind power generation. Large-scale scheme power generating plant produces noise that rarely creates any unrest sound for people. However, at night when human being is greater touchy for any minor sound, the system is not able to function.

In parabolic dish system, attached Stirling engine may produce noise but not enough as compared to a stand by diesel generating sets. New technology constructed advanced Stirling engine that can operate noiselessly.

6 Discussion, Conclusions, and Recommendations

The solar which is alternative source of energy offers a really plentiful delivery of energy that is available to every person. This energy from the sun is totally under-used. The future of solar energy is highly demandable because of its environment-friendly behavior and abundant availability as compared to fossil fuel or hydrocarbons. These hydrocarbons emitted toxic greenhouse gases, and these gases cause global warming which melts the pole ice very quickly and causes a severe issue for world. This is the reason that we are trying to move very fast toward solar energy systems. Recently, a National Renewable Energy Laboratory (NREL) expects 175 GW renewable energy Indian electricity grid by 2022.

So far as economics related to solar energy in delivering power to customer is concerned, in India, the formation of Ministry of New and Renewable Energy (MNRE) and Solar Energy Corporation of India (SECI) brings India as 5th largest solar installer in the world and SECI made possible the per unit cost reduction. This is made possible by SECI because tariff-based bidding among SECI, state, and central government is taken. So, we can say in coming future our government incentives

and policies, land certainty, low-cost labor, and willing of solar energy equipment manufacturer company establishing in India make it cheaper in coming future.

The utility-scale-based system of solar energy grows internationally. This development happens due to changes of EIA policy, emerging hi-tech technologies, improving the emission system by vehicles and manufacturing like hybrid cars. "Tesla," Honda, Nissan, Mercedes, Toyota, and other automobile company introduced solar-based electrical passenger vehicles in market to reduce carbon-based limited fuels and their hazardous emission of greenhouse gases in the environment. In these days, every country focuses on their research and technology including scientist, solar energy developer, policymaker, and land manager to figure out the both positive and negative effects.

The wastage of solar panel/photovoltaic cell is called e-waste by directives of Waste Electrical and Electronic Equipment (WEEE). 96% wastes panels of solar can be reused to again manufacture the new solar panels by opting effective recycling process either silicon-based or thin-film-based solar panel. This recycling process also generates the opportunity of employment. This review consolidates sum of knowledge and experience, which conceptually spans multifold practices and crosses a pair of multidisciplinary barriers. However, the negative effects are usually smaller and should be decreased by means of convenient measures, which incorporate the usages of the cutting-edge available technology using air emission or odor control appliances, certified and best practices guidelines, design tool for superior design, and installation by considering the norm of EIA of every individual country.

References

1. Al, S. Visual impacts of the solar collectors and water tanks. in: Second National Congress of Engineering of Installation Announcement Book, vol. 2. Chamber of Mechanical Engineers Press, No: 176/1, Izmir (in Turkish) (1995)
2. EIA, Knight Frank Report on Environmental Impact Assesment, Nagalamadike Hobli, Pavagada Taluk, Tumkur in India (2016)
3. Executive summary on power sector January (2020)- Solar power in India http://www.cea.nic.in/
4. Tsoutsos, T., Frantzeskaki, N., Gekas, V.: Environmental impacts from the solar energy technologies. Energy Policy **33**, 289–296 (2005)
5. Atagunduz, G.: Fundamentals of the Solar Energy and Applications. Solar Energy Institute Publication No. 2. Bornova, Izmir: Ege University Press (in Turkish) (1989)
6. As per Government of India data between March 2015- Dec 2019 Clean technica
7. Sen, Z.: Solar energy in progress and future research trends. Progr. Energy Combust. Sci. **30**, 367–416 (2004)
8. National Renewable Energy Laboratory (NREL). 2012. Renewable Electricity Futures Study. Hand, M.M.; Baldwin, DeMeo, 4 vols. NREL/TP-6A20-52409
9. Millstein, D., Menon, S.: Regional climate consequences of large-scale cool roof and PV array deployment. Environ. Res. Lett. **6**(3), 034001 (2011)
10. Hernandez, R.R.: Environmental impact of utility-scale solar energy. https://escholarship.org/uc/item/62w112cg (2014)
11. Ravi, S., Lobell, D.B.: Tradeoffs and synergies between biofuel production and large-scale solar infracture in desert. Energy Environ. Sci (2015)

12. National Renewable Energy Laboratory. Best Research-Cell Efficiencies
13. Vanderhulst, P., Lanser, H., Bergmeyer, P., Foeth, F., Albers, R.: Solar energy: Small scale applications in developing countries. Stichting TOOL, Amsterdam, Holland. Retrieved December 11, 2006, Environmental Protection Agency (EPA). Renewable Energy at Mining SitesHh
14. Apricus. A new era in solar hot water. Retrieved December 11, 2006, from http://www.apricus.com/html/evacuated_tubes.htm
15. Pavan, G., Rajiv, S., Ravi, P.T., Ashutosh, K.S. Effective solar power harnessing using a few novel solar tree design and their performance assessment (2018). ISSN: 1556–7036

Impact of DGs in Competitive Deregulated Environment for Congestion Management

Dipu Sarkar, Kabita Kumari, and Rupali Brahmachary

1 Introduction

'Deregulation' of market in India was started to push the economic growth as electricity shares positive correlation with GDP growth by avoiding the problem associated with monopoly market. After the Electricity (Amendment) Bill 2014 passed by Government of India which introduced competitive market structure in the Indian Electricity sector, consumers can choose the supply by the way of perfect competition.

The major challenge of deregulated market includes the overloading of transmission line or network congestion which might occur if the selected transmission line or system is not fully equipped to transfer the necessary power according to the load demand, without violating system constraints. Congestion can lead to severe system damage and voltage instability, which further leads to system blackout.

In current time, due to rise in power demand and supply, it is difficult task to manage the generation and cost all together by a single party, one market, or one-handed [1]. Deregulation means opening of all components of power system (which are generation, transmission, and distribution), availability of components for sale and also forming new set of rules and regulations for operation, management, and sales of electricity [2]. The methods of congestion managements are: nodal pricing, load shedding, GR, market splitting, and DGs. [3]. Distributed generation refers to

D. Sarkar (✉) · K. Kumari · R. Brahmachary
Department of Electrical & Electronics Engineering, National Institute of Technology Nagaland, Dimapur 797103, India
e-mail: dipusarkar5@rediffmail.com

K. Kumari
e-mail: kabita0097@gmail.com

R. Brahmachary
e-mail: brahmachary.rupali29@gmail.com

O. H. Gupta and V. K. Sood (eds.), *Recent Advances in Power Systems*, Lecture Notes in Electrical Engineering 699, https://doi.org/10.1007/978-981-15-7994-3_43

the method that makes use of the small-scale expertise to produce electricity for the end users of power supply chain. It mostly consists of integrated generators, thus offers potential benefits such as easy in installation, less maintenance cost and provides maximum efficiency. Using DG method for congestion management is based on LMPs which are basically wind, solar, biomass, etc. [4]. 1960s were the era when optimal power flow was first came into attention [5] and its use still is playing an important role in the optimization problem for proper power systems analysis in deregulated electricity market. The main challenges faced in order to have the solution of OPF fall under the category of an operational level problem that is required to be solved after regular time interval, and the result of using large-scale power network ends in a non-convex optimization issues. Methods such as load shedding, generation rescheduling, nodal pricing cost, genetic algorithms, fuzzy logic system approaches, and use of renewable energy [6] have considered some of the congestion management (CM) techniques and help in minimizing operating costs. A real-time supervisor [7] is used to manage congestion, thus promoting a platform where redispatch is done using wind and conventional generators. Paper [8] suggests various methods to manage congestion in Indian grid system, including the present market scenario which can convert the present conventional grid to smart grid system using intelligent electronic devices and small-scale generation at load side. Mathematical model of optimal power flow in IEEE 14-bus test system is discussed in paper [9], and it has two DGs and a PV power plant. DG systems are becoming major alternative for power generation as discussed in [10], and the technical, economical, and operational effects of DG on distribution system are discussed here.

2 Congestion and Its Methods of Management

The violation of transmission network constraints such as voltage, stability, and thermal limits in order to meet the desired transaction leads to rise of congestion. Various limitations of the system and also the geographic limitations of transmission network are important factors for the occurrence of congestion on transmission lines. Thermal limitation includes transformer or transmission line congestion, and voltage limitation includes dynamic stability, reliability, and transient stability that also ultimately lead to congestion of the transmission network. So a proper method is required to manage the congestion. In this proposed work, the congestion has occurred due to line outage which is managed using distributed generators and OPF is done based on LMPs calculation using PSAT based MATLAB software.

3 Distribution Generators Based on LMP Calculation

Distributed generators (DGs) such as wind, biomass, and solar are used in optimal capacities in the transmission lines in order for congestion management. DGs help

in improving the real power loss, transmission congestion, voltages, and investment costs. One of the popular methods is the use of LMP calculation in deregulated electricity market to reduce the overall congestion cost. LMP is essential for the optimized DG placement keeping in consideration the power loss minimization, voltage stability improvement, and the overall upgrading of voltage profile. The expression of locational marginal pricing (LMP) is given by:

$$\text{LMP} = \lambda e - \tau LF + T\mu \tag{1}$$

where λe is the price for energy used, τ is the price estimate for system losses, LF is the loss sensitivity element, T is the constraint sensitivity matrix and μ price for transmission or congestion constraint.

Thus, the LMPs can be decomposed into these components:

$$\text{LMP}\big[\text{Energy}\big] = \lambda e \tag{2}$$

$$\text{LMP[Loss]} = -\tau LF \tag{3}$$

$$\text{LMP}\big[\text{Congestion}\big] = T\mu \tag{4}$$

4 Optimal Power Flow—Mathematical Model

In this work, NR-iterative method is used in order to determine the optimally distribution, generation, and transmission of the power network. Here, OPF is simulated in PSAT. The aim being the minimization of the generation cost function ($G(C)$) and the power loss function of the system (ΔS). Thus, the equations of the objective function are given by:

$$\text{Min}\{F = G(C) + \Delta(S)\} \tag{5}$$

where $G(C)$ is generation costs part and ΔS is power loss part of the system. The generation cost part $G(C)$ is further expressed as:

$$C(P) = \text{a}^* P_{Gi}^2 + \text{b}^* P_{Gi} + \text{c} \tag{6}$$

Here, P_{Gi} represents the output of generating unit and a, b, and c are constants. Power loss part of the system is expressed as:

$$\Delta S = P_L + jQ_k \tag{7}$$

The terms P_L and Q_L are denoting the active power loss and the reactive power loss of the system. The system constraints are:

$$Pi(V,\theta) = P_{Gi} - P_{Di} = \sum_{j=1}^{n} |Vi|||VI|||Yij|\cos(\delta i - \delta j + \theta ij) \tag{8}$$

$$Qi(v,\theta) = Q_{Gi} - Q_{Di} = -\sum_{j=1}^{n} |Vi|||VI|||Yij|\sin(\delta i - \delta j + \theta ij) \tag{9}$$

$$P_{G\,\min} \leq P_G \leq P_{G\,\max} \tag{10}$$

$$Q_{G\,\min} \leq Q_G \leq Q_{\mathrm{G}\,\max} \tag{11}$$

$$V_{\mathrm{i}\,\min} \leq V_i \leq V_{\mathrm{i}\,\max} \tag{12}$$

$$P_{L\,\min} \leq P_L \leq P_{L\,\max} \tag{13}$$

Equations (8) and (9) give the active (real) power flow and the reactive power flow equation, respectively, where V is the potential difference from bus i to bus j, Y is the admittance between bus i and bus j, δ is the angle between the respective buses, and θ is the angle of admittance, both these angles entirely compose the power factor of the node. Equations (10), (11), (12), and (13) denote the maximum and minimum system constraints.

5 Study of the Test Bus Model

The standard IEEE 14-bus test system network is modeled using MATLAB-based PSAT application software and is shown in Fig. 1. The network is composed of 16 transmission lines, 4 transformers, 5 generators, 5 supplies, 5 generator bus, 11 static loads, and 11 demands; the base MVA is taken as 100 MVA and the system is having 69 kV as the base voltage. Here, the network is first considered congestion free in order to check the performance of the system and then some line outage is caused in system to check the change in system parameters when it is subjected to congestion in the transmission line, and then congestion is managed using wind and solar plant at bus 1, bus 3, and bus 8.

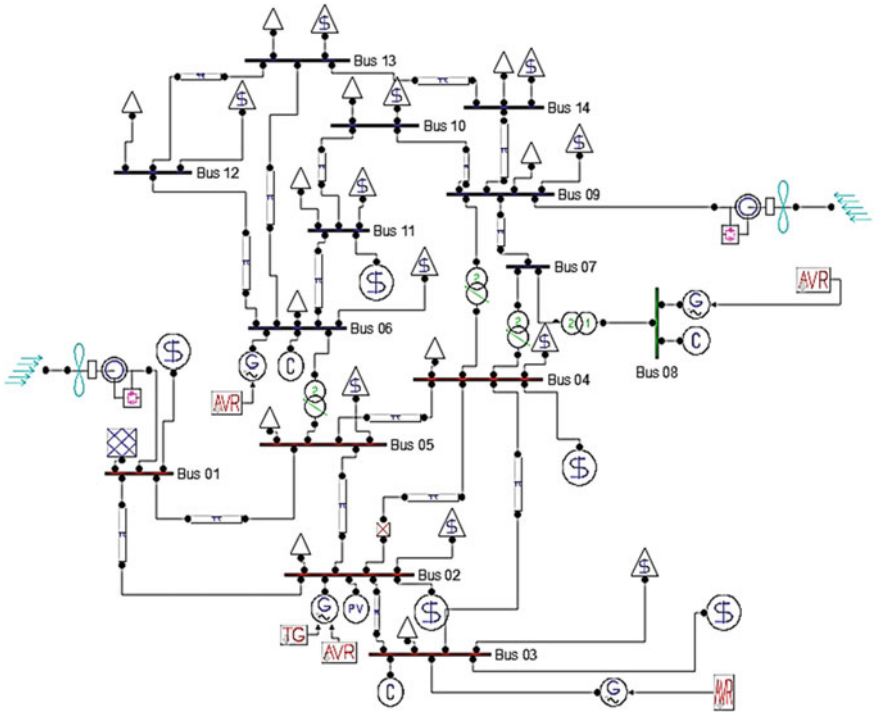

Fig. 1 IEEE 14-bus system before line outage

6 Result and Discussion

The proposed work has been done in MATLAB-based PSAT software in which the congestion is experienced in the line-by-line outage between bus 01 to bus 05, and wind power plant and solar power plant have been used as the non-conventional energy sources to mitigate this problem. The whole work has been divided into three parts which are—(1): **before congestion**, (2): **during congestion**, and (3): **after the congestion is managed using DGs**. Locational marginal price (LMP) is calculated at each bus, (where LMP = Marginal energy cost—Losses + Congestion cost).

Table 1 shows the locational marginal pricing of the test system. The table shows the locational prices before congestion (i.e. the normal case), during congestion, and after using the DGs to manage congestion. It is clearly seen that during congestion the locational marginal prices have increased drastically, but with use of DGs the price has reduced more than that of before congestion case. Thus, the use of DGs is an effective method for reducing the congestion price in deregulated environment.

Table 2 shows the load flow result before congestion, during congestion, and after using DGs to manage congestion. It is seen that the total real power generation has improved significantly from 8254.758 (during congestion) to 393.3113 (after

Table 1 Locational marginal pricing ($/MWh)

Sl. no.	Bus no.	Before congestion	During congestion	CM using DGs
1	Bus 01	0	0	0
2	Bus 02	0.42945	3,303,656,553	0.3582
3	Bus 03	0.98688	4,210,815,048	0.88814
4	Bus 04	0.83804	3,048,998,741	0.75157
5	Bus 05	0.73445	2,635,264,349	0.65704
6	Bus 06	1.2042	3,214,638,442	1.0969
7	Bus 07	1.0795	3,379,775,444	0.98102
8	Bus 08	1.0795	3,379,775,444	0.98102
9	Bus 09	1.2113	3,542,743,791	1.1065
10	Bus 10	1.2785	3,245,824,979	1.1689
11	Bus 11	1.2232	2,961,610,260	1.1156
12	Bus 12	1.3432	3,383,748,331	1.223
13	Bus 13	1.3258	3,450,030,177	1.2071
14	Bus 14	1.3859	3,739,394,490	1.2683

Table 2 Load flow result

Sl. no.		Before congestion	During congestion	CM using DGs
Total generation				
1	P [MW]	396.9559	8254.758	393.3113
2	Q [MVAr]	219.9545	25665.486	208.0883
Total load				
3	P [MW]	362.6	362.6	362.60
4	Q [MVAr]	11142	111.42	111.42
Total losses				
5	P [MW]	34.3559	7892.1582	30.7113
6	Q [MVAr]	108.5345	25554.0662	96.6683

managing congestion using DGs) and again in case of total real power losses from 7892.1582 (during congestion) to 30.7113 (after managing congestion using DGs).

Table 3 also has indicated that the cost per hour has decreased significantly from 312,190,757 (during congestion) to 225.2076 (CM using DGs). The LMP is associated mainly with the total real power generated from each bus and the marginal cost associated with the generated power. The LMP for all the three cases is shown in Table 1. Here, it can be noticed that when there is no congestion in system (Fig. 1), the LMP is the actual cost of the power, but when there is congestion present in the system, the LMP increases drastically (Table 1) which is not acceptable in competitive market. So, optimal placements of DGs, i.e., wind/solar plants are done near the load center (Fig. 1, bus 1, bus 2, and bus 8) to decrease the congestion cost as well

Table 3 Total final result

Sl no.	ELEMENTS	Before congestion	During congestion	After CM using DGs
1.	Total losses [MW]	26.032	5.762	22.897
2.	BID losses [MW]	– 8.324	– 1391.626	−7.814
3.	Total demand [MW]	78.8352	−0.12134	76.185
4.	TTL [MW]	441.4352	362.4787	438.785
5.	IMO pay [$/h]	256.2635	312190757	225.2076

to decrease transmission cost and losses. It helps in improvement of real and reactive power and voltage profiles to make system more reliable, palatable and provide benefit for suppliers and customers. The total losses, total demand, total transaction level [MW], total bid losses, and the IMO to be paid are described in Table 3. The power flow results including the total generations, total loads, and total losses are discussed in Table 2.

When congestion occurs in the system, the network does not converges (Fig. 2), and it is not possible to determine the operating specifications of the network and thus system is not operable, but when the system is not congested, operating points for all the parameters are obtained easily (Fig. 3) that shows the network is optimally scheduled and committed generators are working on maximum power generation at least cost. In the given convergence curve, the green and blue lines denote real and reactive power profile, red line denotes voltage profile, and yellow line denotes phase angle.

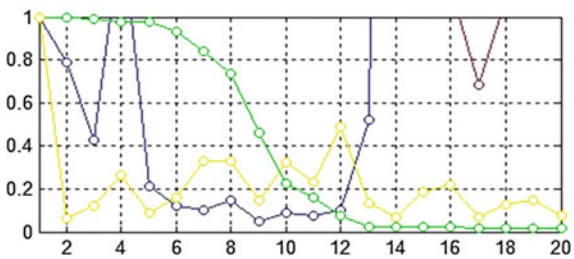

Fig. 2 Graph showing convergence curves of the standard IEEE 14-bus test system network during congestion

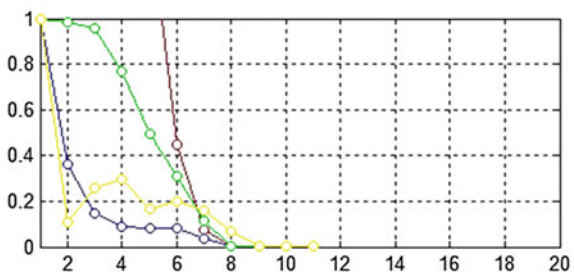

Fig. 3 Graph showing optimized convergence curves of the standard IEEE 14-bus test system network during no congestion

7 Conclusion

The standard IEEE 14-bus test system network is first analyzed in MATLAB-based PSAT software using Newton–Raphson (NR) iterative method for analysis and then various system parameters are noted, a prominent deviation is observed when congestion appears in the system, which resulted in huge increase in the generation and transmission cost and if persistent it may even cause the system blackout. Since we know, if a particular power supplier is giving the power at least and high quality that will earn more profit but it will harass the transmission line more. So, to save this, some amount has been fixed for the supplier, i.e., congestion cost which they have to pay to independent electricity market operator (IMO or ISO) to keep standing the market, and to drop this cost, DGs are used at the load side its self, where use of renewable energy is brought into focus since they can be installed directly on load side. There are some additional advantages of DGs like line losses and the cost involved in the system are less. DGs, such as wind and solar plant, produce small-scale generation, and it is modular, portable, and relocatable which makes its use widely accessible and introduces competition in market promoting deregulation. Hence, the issues in the network like congestion can be easily mitigated on the large scale using small-scale generating unit. Introducing the small-scale generating plant promoted pros-consumer ways for the people in power network, and at the same time, it also promotes the smart grid to be more flexible for both producers and consumers.

References

1. Dhanalakshmi, S., Kannan, S., Mahadevan, K.: Market modes for deregulated environment—a review. In: International Conference on Emerging Trends in Electrical and Computer Technology, pp. 82–87. Nagercoil (2011)
2. Barbulescu. C., Kilyeni. S., Mnerie. D., Cristian. D., Simo. A.: Deregulated power market congestion management. In: Melecon 2010–2010 15th IEEE Mediterranean Electrotechnical Conference, pp. 654–659. Valletta (2010)
3. Huang, S.: Congestion management of electric distribution networks through market based methods. Technical University of Denmark, Department of Electrical Engineering, IEEE (2017)
4. Yadav. A., Srivastava. L.: Optimal placement of distributed generation: An overview and key issues. In: 2014 International Conference on Power Signals Control and Computations (EPSCICON), pp. 1–6. Thrissur (2014)
5. Dawn. S.G., Mitra. S., Goswami. R., Tiwari. A., Prashant.: Transmission Congestion Relief with Integration of Photovoltaic Power Using Lion Optimization Algorithm. SocProS, 2017, vol. 1. https://doi.org/10.1007/978-981-13-1592-3_25 (2018)
6. Yusoff. I.N., Zin. M.A.A., Khairuddin. B.A.: Congestion management in power system: a review. In: 2017 3rd International Conference on Power Generation Systems and Renewable Energy Technologies (PGSRET), pp. 22–27. Johor Bahru (2017)
7. Vergnol., Sprooten. A., Robyns. J., Rious. B., Deuse. V., Jacques.: Real Time Grid Congestion Management in Presence of High Penetration of Wind Energy. HAL, Post-Print (2009)
8. Khan., Ahmad. Q., Imran. F., Mohd.: Congestion management in Indian Power Transmission System. Int. J. Eng. Technol (2017)

9. Dulau., Ioan. L.: Optimal power flow analysis of IEEE 14 system with distributed generators. J. Electri. Electron. Eng. (9), 9–12 (2016)
10. Bhadoria., Singh. V., Shrivastava. N., Vivek.: A review on distributed generation definitions and DG impacts on distribution system (2013)

Co-optimal PMU Placement for Complete Monitoring of Distributed Generations Installed System

Anik Tahabilder, A. A. Mamun, N. Rahman, and Pronob K. Ghosh

1 Introduction

Today, the electric power demand has reached to its topmost level. Therefore, the new generating stations are frequently being added to the existing grid. Considering the reliability and security of the power supply, distributed generations are the best solution [1]. Moreover, DGs provides significant amount of facilities including the opportunity to use as independent power source or penetrated to the main grid to the nearest as well as the remote consumers.

DGs are the good options to reduce to unexpected power losses if these resources are placed at the best locations with proper size [2]. Moreover, because of having the capability of efficient and quick control over reactive power response, the modern renewable, i.e., photovoltaic, wind power, etc., -based DGs can be used as reactive power compensator. These types of DGs can also be used as good solutions of the security issues of today's vulnerable and overstressed power grid [3].

DGs are good options of backup or reserved power supply can lead to an islanded condition when the complete system experiences large blackouts. This kind of islanded conditions can invoke a dangerous situation to the power system operators and workers. Angle measurement from the PMUs can be used here for fast identification of the unintentional islanded conditions. This research promotes an optimal

A. Tahabilder
School of Engineering + Technology, Western Carolina University, Cullowhee, NC 28723, USA

A. A. Mamun
Faculty of Engineering and Technology, Multimedia University, Bukit Beruang, Malaysia

N. Rahman
Department of EEE, University of Asia Pacific, Dhaka, Bangladesh

P. K. Ghosh (✉)
Department of Electrical Engineering, NIT Agartala, Agartala, Tripura, India
e-mail: 4ghosh.k.pronob@gmail.com

O. H. Gupta and V. K. Sood (eds.), *Recent Advances in Power Systems*, Lecture Notes in Electrical Engineering 699, https://doi.org/10.1007/978-981-15-7994-3_44

PMU placement for observing the system completely when single or multiple DGs are installed in the system.

A lot of researches on optimal PMU placement that have been done by the researchers form the past several years. Some researchers have used optimizations techniques to solve the problem of PMU allocations for complete observability. For instance, binary cuckoo algorithm was used after necessary modifications in [4]. In [5], modification of BPSO technique was also carried out for solving OPP. One of the common optimization techniques, MILP, was applied to solve the PMU problem in [6]; whereas, some researchers used generalized integer linear programming (GILP) in [7]. However, optimizations techniques are computationally burden and involve a huge number of iterations to solve the problems.

Graph theory, combining with multi-criteria decision-making approach was applied in [8]; whereas, multi-criteria decision support was used in [9] to monitor the critical power system elements by PMU. However, these techniques targeted to optimize the total number of PMU requirements considering the conventional strategies. This research added the DG installed for PMU locations considering the power system security issues.

The complete paper organization has been done as follows: Sect. 2 deals with the problem formulation for optimal PMU placement. Section 3 discusses the proposed method. Section 4 elaborates the results of the proposed method. Then, Sect. 5 is used for conclusion remarks.

2 PMU Placement Formulation

Complete observability utilizing minimum number of PMUs can be achieved as follows:

$$\text{Min} \sum_{i=1}^{M} Fi\,Ai$$
$$\text{s.t.} F(m) \geq b$$

where m is the binary decision variable for PMU placement, whose entries are defined as

$$A_i = \begin{cases} 1, & \text{if PMU is installed at } i\text{th bus} \\ 0, & \text{otherwise} \end{cases}$$
$$\text{For } i = 1, 2, \ldots, M$$

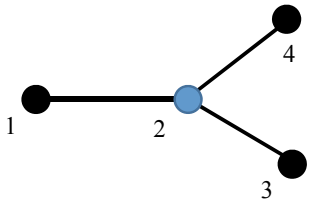

Fig. 1 Simple system for PMU measurements representation

3 Proposed Method

In this research, a graph theory-based intellectual search technique has been proposed. The complete proposed method has been discussed below.

3.1 Graph Theory Essentials

Graph theory is an essential element to analyze the power system networks. To identify the co-optimal PMU placement locations, primarily the system network is converted into a graph. All nodes are considered as vertices, and connected lines are edges. Degree of a vertex is considered as the number of connected edges. Pendant vertices are those types of vertices whose degrees are one. For instance, in Fig. 1a, simple 4 bus system has been considered. Here, four vertices and three edges form this graph. The degree of vertex 2 is 4. In this figure, vertices 1, 3 and 4 are pendant vertices as the degrees of these vertices are one.

3.2 Intellectual Search Technique

PMUs can observe the nodes, where these devices are installed, and all the connected lines of these nodes. PMU provides time synchronized node voltage, line currents, frequency and the changing rates of frequency.

For test case-1, bus number 14 is selected as the location of DG. Now the PMU placement for complete observability is conducted as follows.

Steps to be followed for observing the remaining unobserved buses:

Step-1: Initially, install PMUs at all the DG installed nodes.
Identify the initial observed and unobserved areas.
Step-2: Identify the pendant edges of the unobserved area (Table 1).
Step-3: Install PMUs at the nodes connected to the pendant edges.
Step-4: Check the remaining unobserved area.
Step-5: Install PMU at the highest degree vertex of the remaining unobserved area.

Table 1 Number of DGs and their respective locations

Test systems	No. of DGs	DG locations
Test case-1	1	14
Test case-2	5	15, 19, 21, 24, 30

Step-6: Repeat from step-3 until the system completely is observable.

3.3 Redundant Measurement

Redundant measurement is calculated as the percentage of ratio of the total number of extra measurements of every buses by all installed PMUs to the number of buses.

$$\text{Redundant Measurement} = \frac{\text{Total number of extra measurement of all the buses}}{\text{Total number of buses of the } system} \times 100\%$$

4 Result Analysis

Several researches have been conducted for optimal placement and sizing of DG. For IEEE 14 bus system, the optimal locations of DG have been indicated as bus number 14 in [10]. In [11], researchers have found buses of 15, 19, 21, 24 and 30 are the best solution for multiple DG locations in IEEE 30 bus system.

4.1 Proposed Method on Test Case-1

IEEE 14 bus system which is shown in Fig. 2a consists of 14 nodes and 20 connected lines. To initiate the proposed minimum PMU allocation method, a PMU is placed at bus number 14 where DG is installed. Consequently, voltage phasors of buses 9, 13 and 14 are assessable using direct voltage measurement of bus 14 and lines current measurements of lines 9–14 and 13–14. Now, the observed and unobserved areas can be separated, which creates some pseudo-pendant vertices and pendant edges. Figure 2b is showing the initially observed and remaining unobserved areas which are connected through line marked as red. Indicated steps are followed to observe the remaining unobserved areas, and it is found that the co-optimal locations of the PMUs are 2, 6, 7, 9 and 14. The tabularized form of the result of IEEE 14 bus system is given in Table 2.

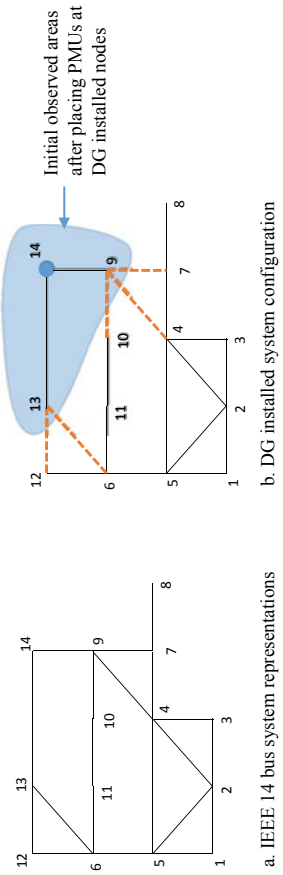

Fig. 2 **a** IEEE 14 bus system representations, **b** DG installed system configuration

Table 2 Result of the proposed method on selected test cases

Bus system	No. of PMUs	PMU locations	Redundant measurement (%)
Test case-1	5	2, 6, 7, 9, 14	57.14
Test case-2	12	2, 4, 6, 9, 10, 12, 15, 19, 21, 24, 25, 30	90.0

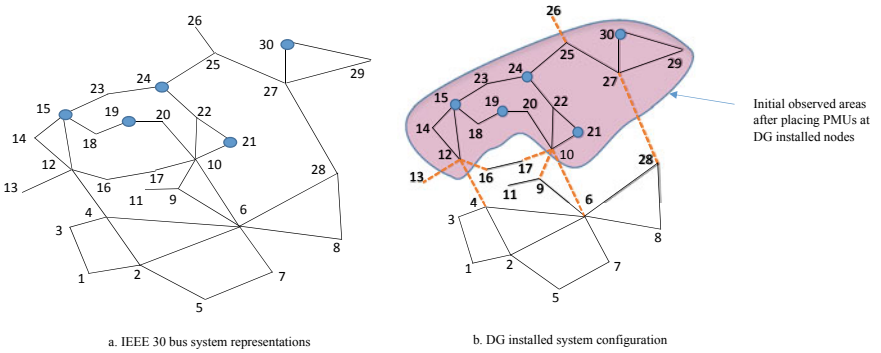

Fig. 3 **a** IEEE 30 bus system representations, **b** DG installed system configuration

4.2 Proposed Method on 30 Bus System

Figure 3a is showing the test system which consists of 30 nodes and 41 connected lines. Initially installed PMU locations due to having installed DGs are 15, 19, 21, 24 and 30. The starting observed area and remaining unobserved areas connected with red-colored lines are shown in Fig. 3b. Table 2 shows the final results of PMU requirements throughout the system, and the respective locations are given in Table 2.

5 Conclusion

The proposed technique in this paper addresses co-optimal synchrophasor placement considering the new strategy of having preinstalled DGs in the given power system. Preinstalled DGs have been considered as the initial PMU locations by default which leads to the separations of the initial observed islands and remaining unobserved islands. Application of this efficient method on IEEE standard test system shows significant improvement of the redundant measurements which is more important for continuous state estimation.

References

1. Chatterjee, S., Roy, B.K.S.: An analytic method for allocation of Distributed Generation in radial distribution system. Ann. IEEE India Conf. (INDICON) New Delhi **2015**, 1–5 (2015)
2. Rahmani-andebili, M.: Distributed generation placement planning modeling feeder's failure rate and customer's load type. IEEE Trans. Industr. Electron. **63**(3), 1598–1606 (2016)
3. Ettehadi, M., Ghasemi, H., Vaez-Zadeh, S.: Voltage stability-based DG placement in distribution networks. IEEE Trans. Power Delivery **28**(1), 171–178 (2013)
4. Dalali, M., Kazemi Karegar H.: Optimal PMU placement for full observability of the power network with maximum redundancy using modified binary cuckoo optimisation algorithm. In: IET Generation, Transmission & Distribution, vol. 10, no. 11, pp. 2817–2824 (2014). https://ieeexplore.ieee.org/document/7542747
5. Rahman, N.H.A., Zobaa A.F.: Integrated mutation strategy with modified binary PSO algorithm for optimal PMUs placement. In: IEEE Transactions on Industrial Informatics, vol. 13, no. 6, pp. 3124–3133 (2017). https://ieeexplore.ieee.org/abstract/document/7950984
6. Aghaei, J., Baharvandi, A., Rabiee, A., Akbari M.: Probabilistic PMU placement in electric power networks: an MILP-based multiobjective model.In: IEEE Transactions on Industrial Informatics, vol. 11, no. 2 pp. 332–341 (2014). https://ieeexplore.ieee.org/document/7004810
7. Gou, B.: Generalized integer linear programming formulation for optimal PMU placement. IEEE Trans. Power Syst. **23**(3), 1099–1104 (2008). https://doi.org/10.1109/TPWRS.2008.926475
8. Ghosh, P.K., Chatterjee, S., Roy, B.K.S.: Optimal PMU placement solution: Graph theory and MCDM-based approach. IET Gen. Trans. Distrib. 11, 3371–3380 (2017). https://digital-library.theiet.org/content/journals/10.1049/iet-gtd.2017.0155
9. Chatterjee, S., Ghosh, P.K., Roy, B.K.S.: PMU-based power system component monitoring scheme satisfying complete observability with multicriteria decision support. Int. Trans. Electric. Energy Syst. **30**(2), e12223 (2020). https://doi.org/10.1002/2050-7038.12223
10. Dulău, L.I., Abrudean, M., Bică, D.: Optimal location of a distributed generator for power losses improvement. Procedia Technol. **22**, 734–739 (2016). https://doi.org/10.1016/j.protcy.2016.01.032
11. Ramamoorthy, A., Ramachandran, R.: Optimal siting and sizing of multiple DG units for the enhancement of voltage profile and loss minimization in transmission systems using nature inspired algorithms. Sci. World J. **2016**, 1086579 (2016). https://doi.org/10.1155/2016/1086579

A Comprehensive Review of Remote and Passive IDMs of Utility Grid Integrated MG System—Part I

Ravikant Shastri, Akshit Samadhiya, and Kumari Namrata

1 Introduction

With the rising global power uses and risk of exhausting of traditional combustible, addition of DG set becomes important [1], and for that, advancement in the technology is needed. Advances in technologies as fuel chargeable cells, diesel engines, small wind, hydropower and solar power as well as new developments in the power electronics, deregulation of the energy market, consumer demand for improved power quality (PQ) and reliability; most important environmental issues are pushing the power industry towards the distributed generation. DGs can be described as generation units, other than utility units, which are generally located near to consumers end. By rising the DGs in the electrical system, it can reduce the distribution and transmission losses and improves the voltage (V) profile and power quality [2]. Before the DGs are added to the grid, various obstacles should be resolved. Such concerns include frequency stabilization, voltage stability, renewable resource intermittency, and problems with power quality. Major problem of the distribution system caused during the disconnecting of the central grid, the disconnection of the central grid is called islanding, i.e. shown in Fig. 1, where load is able to get the power from DG only, which might be intentional or unintentional. Intentional islanding is that although they are isolated from the main grid, DGs still supply electricity efficiently to local load. This is a controllable mode of operation, and mostly, this is done for the

R. Shastri (✉) · A. Samadhiya · K. Namrata
Department of Electrical Engineering, National Institute of Technology, Jamshedpur, Jamshedpur, India
e-mail: rkshastri123@gmail.com

A. Samadhiya
e-mail: akspinnacle1@gmail.com

K. Namrata
e-mail: namrata.ee@nitjsr.ac.in

O. H. Gupta and V. K. Sood (eds.), *Recent Advances in Power Systems*, Lecture Notes in Electrical Engineering 699, https://doi.org/10.1007/978-981-15-7994-3_45

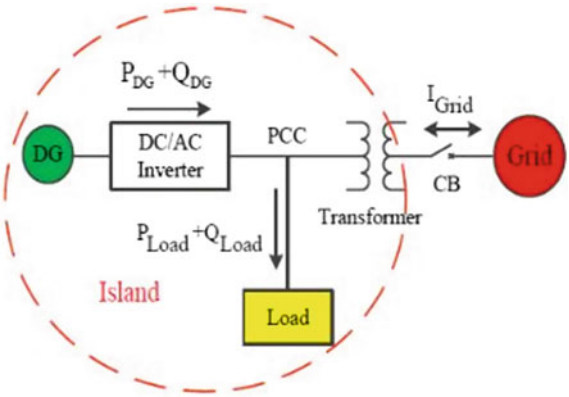

Fig. 1 Power islanding condition

Table 1 Islanding detection time (D.t), quality factor (Q.f), frequency (f) and voltage (V) range of different standards [4, 5]

Standard	Q.f.	D. t. (ms)	Frequency range (Hz)	'*V*' range
IEEE: 1547	1	Less than 2000	59.3–60.5	88–110%
IEC: 62116	1	Less than 2000	f0-1.5 $\leq$ f $\leq$ f0 + 1.5	88–110%
IEEE: 929–2000	2.5	Less than 2000	59.3–60.5	88–110%

maintenance purpose, but unintentional islanding is an unacceptable phenomenon due to line tripping, malfunction of metres, etc. [3], and this is an uncontrollable mode of operation.

The unintentional islanding of DG leads to several problems like safety issue, fluctuation of the voltage and frequency, stability issue and many more. Hence, it has to be detected as soon as possible within a specified NDZ and DG standards given in Table 1, so that the distributed generators must detect islanding and immediately disconnect, called anti-islanding (AI) detection.

As due to many problems like safety concern, instruments/equipments concern, etc, this paper looks in depth of islanding detection (ID) of remote and passive methods with their pros and cons and also very helpful to researchers when choosing an appropriate ID technique for future islanding detection.

2 Indices/Parameters of Islanding Detection Methods

NDZ became the primary cause for failing of IDMs. NDZ is mainly due to slight power difference between DG and load utilization that leads to variation in V, I and f but not significantly [6]. Detection time also plays an important role, expound as time interval between (b/w) the disconnecting of the central grid and detecting islanding

by IDMs, and during islanding events power quality should be maintained as per standard.

3 Islanding Detection Methods (IDMs)

Different IDMs given till now, but these are mainly classified as remote islanding detection (RID) and local islanding detection (LID) methods. RID techniques are concerned with realization on central side, while LID methods are concerned with realization on DG side [7]. LID methods are further categorized as passive islanding detection (PID), active islanding detection (AID) and hybrid islanding detection (HID) methods.

3.1 Remote Islanding Detection Methods

RID approaches are planted as interaction with the power grid and DGs. RID methods work adequately having better reliability than LID methods and also have very negligible NDZ. The main drawbacks of communication-based IDMs are high computational burden, higher cost and complexity in their operations [8]. A transmitter and receiver are used for the communication, i.e. shown in Fig. 2.

PLC method. In power line communication (PLC) method, continuous signal is broadcasted from the main grid to DGs using power line as the path of the signal. Here, there would be need of the signal transmitter and receiver unit. Signal transmitter is equipped with the grid and signal receiver at the DGs. Generally, the transmitting signal is optimized for the 4 successive cycles and if signal vanishes for 2 or more cycles, islanding events get realized [9]. Due to the rising costs and other complexities, system is ideal for large-scale distributed power networks.

Transfer trip (TT) method. TT method is tangled islanding realization method having additional control of DG via the main grid is attained [10]. Generally, TT method is incorporated into the SCADA program for controlling the running switches

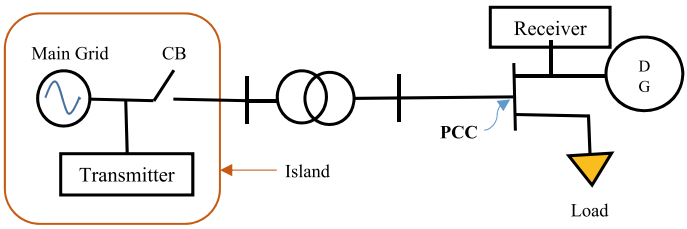

Fig. 2 Power line of remote islanding consisting of transmitter and receiver

while maintaining good synchronization between MG and utility. These processes have almost zero NDZs and giving fast realization of islanding, but limitations are high cost, hardware implementation, etc [11].

Supervisory control and data acquisition (SCADA) method. It is planted as the regular tracking of breaker, recloser, switching device and their control circuit. In a SCADA system, sensitive sensors monitor electrical data such as V, I and f to detect any alteration or failure in the network. When islanding event happens, the grid data are changed immediately, so relay operates and disconnects the DG sources [11].

3.2 Passive Islanding Detection Methods

These methods operate on the principle of measuring of local data such as V, f and power variation as well as harmonic distortion at PCC. These data vary significantly when utility grid is isolated from the integrated power distribution networks or DGs or microgrid. A threshold value has to be set so that islanding and non-islanding (disturbance, slight load variation, etc.) conditions are recognized clearly. PID methods are fast and do not have any issue on power quality but having the large NDZ [12, 13], i.e. the main drawback of passive IDMs. The basic flowchart of PID methods is shown in Fig. 3, and after that various passive IDMs are discussed briefly.

Over/Under voltage and Over/Under frequency (OUV/OUF). Methods of OUV and OUF allow the realization of islanding phenomena by measuring the V and f

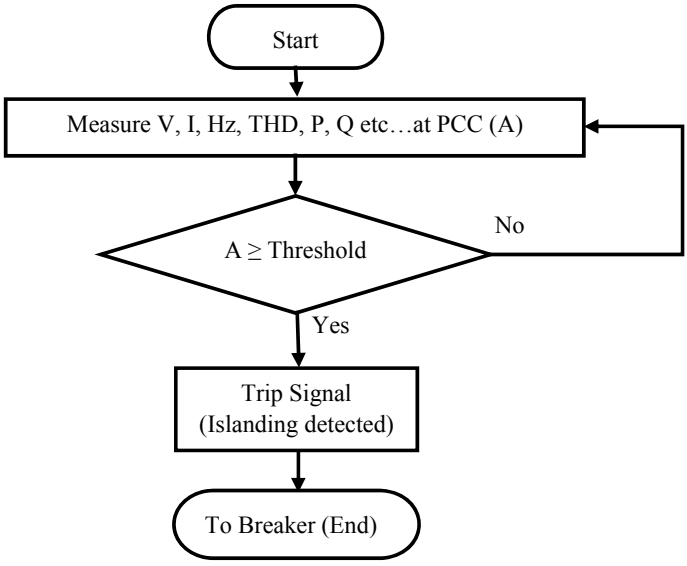

Fig. 3 Flowchart of passive IDMs

at PCC or DG terminals and subsequently compared with the threshold values for the proper operation [14]. Active power difference leads to V variation, while large fluctuation in the f is due to reactive power difference ($\Delta Q \neq 0$) b/w supply (DG) and demand (load). Approach has reasonable cost, no influence on PQ, and limitations of this approach are having large NDZ. Prediction of detection time is difficult as Δt varies from 4 to 2000 ms, sometime may be more [15].

Rate of change of frequency (ROCOF). Efficiency of passive ROCOF method is centred on frequency measurement at PCC. During sudden power imbalance, the ROCOF (df/dt) is analysed continuous for the five cycles to abolish the false detection due to the present of transients and compared with the threshold value for generating the trip signal [16]. Generally, it is said that a large system has small ROCOF while a small system has large ROCOF as df/dt has inverse relation to the moment of inertia and generation capacity. Detection time is up to 24 ms [17], and it is highly efficient.

Rate of change of power output (ROCOP). Principle of ROCOP (dP/dt) depicts as detection of the changes in the output power of DG network. Owing to loss of main grid, changes in the output power are much greater than the non-islanding case. Realization time of this practice is nearly 24–26 ms [18]. This practice is very responsive when the microgrid has unbalanced burden in lieu of balance load.

Rate of change of frequency over active power (ROCOFOAP). In small generation network, it is shown that df/dP value is bigger compared to the larger capacity network. ROCOFOAP uses the same concept to determine the islanding condition. A slight change in the power mismatch leads to higher df/dP value, and thus, it is more sensitive, having smaller NDZ and has lower error detection ratio as well as higher reliability. Expected detection is about 100 ms [19]. Difficulty with this method is in selecting the threshold limit as both things (ROCOF and ROCOP) are required.

Rate of change of frequency over reactive power (ROCOFORP). Among entire PID methods, it is said to be the best one [20]. Approach discriminates the islanding and non-islanding conditions perfectly, but in case of OUV/OUF, ROCOF, ROCOP perfectly discrimination is not possible [21]. Whenever ROCOFORP crosses the preset threshold value, islanding gets detected. It has very narrow NDZ and can say almost zero NDZ.

Phase jump detection (PJD). PJD involves checking for a sudden "jump" of the phase difference between the inverter V & I [22]. In usual mode, the current waveform of inverter is proportioned to the V of the power grid with the help of phase-locked loop (PLL). Whenever phase difference becomes more than threshold value, then islanding detects [23].

The phase difference phenomena occur because only the inverter current is controlled, that is why PCC voltage may deviate their path while current not.

Figure 4 shows the variation of voltage when DG operates just after disconnection of the main grid. Key benefits are easy in implementation and fast detection within

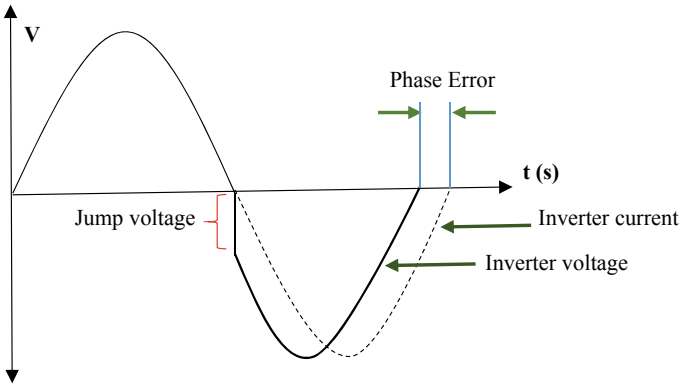

Fig. 4 Principle used in PJD operation

10–20 ms [24]. Yet problem will come during selection of preset value, as phase may be changed during load switching generally motor load.

Voltage unbalance (VU). Whenever islanding occurs, DG has the burden of their local load. If the changes in the V, f and phase displacement are large at the PCC, then islanding is detected easily but not effective during small changes. So during small change, VU topology used, as it varies despite of the small changes [7, 25, 26]. VU is planted as the deviation of V at time t during unbalance and steady state. If VU of 3-phase voltage output of microgrid exceeds the threshold value, then islanding detected. The VU at the time t is described as the proportion of negative and positive sequence voltage.

$$\mathrm{VU}_t = \frac{\mathrm{NSV}_t}{\mathrm{PSV}_t} \tag{1}$$

where NSV_t and PSV_t are degree of negative (-ve) and positive (+ve) sequence voltages at time t. The realization time is around 53 ms [27]. Problem will come during selection of preset value as −ve sequence V is changed by sudden spike too.

Total harmonic distortion (THD) of voltage and current. Method implements the measure of harmonics in AC signal. During integrated mode, there is almost perfect sinusoidal wave generated, and thus, their THD is near to zero. Due to change in impedance of the load, whenever main grid gets disconnected, large changes occur in their waveform, and hence, THD value rises, after comparing to the threshold value, a trip signal is generated and islanding gets detected [28]. Method is effective for multi-DGs. Drawback is that sometimes nuisance tripping occurs due to nonlinear load switching as THD is sensitive to perturbation.

Voltage unbalance (VU) and THD. Whenever two or more passive parameters are used their accuracy get improved, sometimes NDZ also reduced [29]; thus, effectiveness of the THD method gets increased when THD of current combined with VU method. Additionally, it utilized the voltage magnitude as well. Whenever average

voltage get lowered/above more than preset value (around 5%), then it makes immediate trip signal for islanding. Otherwise, it measures ΔTHD and ΔVU in a specified sampling time, and if both exceed their preset value simultaneously, then islanding get detected [30]. This method is capable of detection of islanding correctly.

Rate of change of reactive power (ROCORP) and THD. Practice is based on ROCORP and THD of current. Parameters are measured at DG's output, orderly to decide islanding and non-islanding events. ROCORP is measured at the first stage, and their threshold value is taken small. Whenever ROCORP exceeds their threshold value, then the analysis would be done on current harmonic, if current THD also crosses their preset value then islanding gets detected [31].

Change in impedance. By computing of V and I at the PCC, impedance can be obtained. Usually, impedance at the utility grid is lesser compared to the microgrid. Whenever the main grid is getting disconnected, the impedance rise suddenly and thus by continuously monitoring of the source impedance, islanding or non-islanding events get detected [7, 32].

Rate of change of voltage and change in power factor (ROCOV and CPF). It is based on the parameters (dv/dt) and (Δpf). Method is particularly helpful in case of the DG having capacity close to the main generator, it is also helpful in detection of the loss of the parallel feeders. Whenever utility grid disconnected from the integrated distribution network, variation in the voltage degree and power factor occurred at PCC, and thus islanding realized. Its realization time is around 35 ms [33].

Rate of change of negative sequence voltage/current (ROCONSV/C). By the help of sequence analyser, components +ve, -ve and zero sequence of V and I might be separated. The +ve sequence component remains in both (islanding and grid-connected) modes, and −ve sequence component remains during the islanding operation. After comparing the ROCONSV/ROCONSC with their respective set value, an islanding event is being realized easily [34].

Rate of change of positive sequence voltage/current (ROCOPSV/C). As +ve sequence components of V and I are present in all the modes, hence its magnitude will play the role of islanding detection. Positive sequence components are being computed by sequence analyser and compared to the preset defined value; if ROCOPSV/ROCOPSC value crosses that defined value, then balanced islanding condition is realized with zero NDZ [35]. This method will eradicate the switching events and islanding condition perfectly.

ROCO(PSV and PSC). This PID technique is the union of rate of change of +ve sequence V and I. Island gets realized if both ROCOPSV and ROCOPSC exceed the set threshold value. Some of the passive approaches are not capable of detecting islanding condition at low power mismatch, but this method is capable of islanding even at very low power mismatch. Method eliminates islanding condition and non-islanding condition easily. Realization time is also low, i.e. around 10 ms [36].

Rate of change of exciter voltage, over reactive power (ROCOEVORP). Within this method, exciter voltage and power (reactive) are chosen for islanding realization as exciter voltage and reactive power are proportionally vary with the variation of excitation and not depend upon inertia constant, while frequency and active power depend upon inertia constant but not with excitation variation [37]. The affectivity of reactive power and excitation for a variety of excitement is very quick. After measuring of voltage excitation and reactive power, ROCOEVORP (dE/dQ) is obtained and compared with the preset value for islanding detection [38]. On the basis of exciter voltage, one more technique is used, and name is given as rate of change of exciter voltage with circuit breaker switching strategy (ROCOEV with CBSS). For detection, this technique takes more time compared to ROCOF, OUV/OUF. Advantage is having the small NDZ [39].

Phase angle between negative sequence voltage and current (PANSVNSC). This practice is established upon the principal of phasor estimation of negative sequence V and I by least squares method. The NSV and NSC are obtained by sequence analyser. Absolute phase angle is symbolized as

$$|\emptyset| = |\angle V_{\mathrm{NS}} \text{ and } \angle C_{\mathrm{NS}}|$$

If the absolute value of phase angle crosses the set point, hence islanding is realized. Advantage of this technique is fast detection, and it works also on zero power imbalance, and hence, NDZ is reduced [40].

Forced Helmholtz oscillator (FHO). This islanding detection method uses the modified frequency at the PCC. In the proposed literature [41], inverter and synchronous-based DGs are used. Method uses chaos concept principle, and forced Helmholtz oscillator, oscillator input is modified frequency. Change between chaotic motion and normal motion has their own advantage of this oscillator. This method detects the $\pm$ 0.4% active power mismatch, and hence, their NDZ is negligible.

4 Comparison of IDMs

After reviewed of many islanding detection methods, a healthy comparison is made among the RID and PID methods on the basis on (NDZ), detection time and PQ, i.e. shown in Table 2. Every technique has its own merits and demerits. There is no any IDM which will work accurately in all conditions, but according to need, IDM can be chosen. On the basis of cost, IDMs can also be classified as, generally PID has lowest cost, RID has highest cost, AID and HID cost are in between the two. Comparisons are made according to the prescribed references.

Table 2 Comparison of IDMs on the basis of NDZ, detection time (Δt) and power quality (PQ)

Method's name (RID)	NDZ	Δt (ms)	PQ
PLC	Zero	200	N.A.
TT	Zero	N.R.	N.A.
SCADA	Zero	Slow speed in busy grid	N.A.
OUV/OUF	Large	4–2000	N.A.
ROCOF	Large	24	N.A.
ROCOP	<than OUV/OUF	>One cycle	N.A.
ROCOFOP	<ROCOF	100	N.A.
ROCOFORP	Very small	N.R.	N.A.
PJD	Large	10 to 20	N.A.
VU	Large	53	N.A.
THD (V/I)	Large, (Q high)	45	N.A.
VU AND THD	Small	25–2000	N.A.
ROCOV and CPF	Small	35	N.A.
ROCONSV (ac)	Zero	80	N.A.
ROCOPSV (ac)	Zero	10	N.A.
ROCO(PSV & PSC)	Zero	10	N.A.
ROCOEVORP	Zero	N.R.	N.A.
ROCOEV with CBSS	Zero	100 to 300	N.A.
PANSVNSC	Zero	Within 4.16	N.A.
FHO	Very small	Up to 440	N.A.

#*N.R.* Not Reported, *N.A.* Not Affected

5 Conclusion

In this paper, different kinds of IDMs (remote, passive) have been described for the utility connected microgrid system. The IDMs comparison is made on the basis of standards of Table 1. Remote methods are based on the communication scheme, that is why cost is high and most reliable, as NDZ is zero and no power quality issue. But in case of local methods, these indices vary as per the different kinds of local methods named as passive, active and hybrid. Passive technique does not cause any problem on power quality and has high NDZ, but the modified or integrated passive has somehow less NDZ; i.e. why integrated passive IDMs are more beneficial. Generally, passive detection time is low compared to other methods. Due to the high cost and complexity during installation, RID methods are not chosen. After being the above-mentioned limitation of PID methods, still it is chosen over RID due to their lesser cost and easy

implementation, but PID and modified PID are more suitable for the small microgrid system. For large system, RID is best. Hence, this literature is providing a good concept over islanding detection, and it will be helpful for the future research.

References

1. Dutta, S., Sadhu, P.K., Reddy, M.J.B., Mohanta, D.K.: Shifting of research trends in islanding detection method-a comprehensive survey. Protect. Control Modern Power Syst. **3**(1), 1 (2018)
2. Acharya, N., Mahat, P., Mithulananthan, N.: An analytical approach for DG allocation in primary distribution network. Int. J. Electric. Power Energy Syst **28**(10), 669–678 (2006)
3. Chiang, W.J., Jou, H.L., Wu, J.C.: Active islanding detection method for inverter-based distribution generation power system. Int. J. Electr. Power Energy Syst. **42**(1), 158–166 (2012)
4. Basso, T.S.: IEEE 1547 and 2030 Standards for Distributed Energy Resources Interconnection and Interoperability with the Electricity Grid; National Renewable Energy Laboratory: Golden, vol. 15013. CO, USA (2014)
5. CH, R.R., Reddy, K.H.: Islanding detection techniques for grid integrated DG–A review. Int. J. Renew. Energy Res. **9**(2), 960–977 (2019)
6. Ye. Z., Kolwalkar, A., Zhang, Y., Du. P., Walling, R.: Evaluation of anti-islanding schemes based on nondetection zone concept. IEEE Trans. Power Electron. **19**(5), 1171–6 (2004)
7. Mahat, P., Chen, Z. and Bak-Jensen, B.: Review of islanding detection methods for distributed generation. In: Third International Conference on Electric Utility Deregulation and Restructuring and Power Technologies, pp. 2743–2748. IEEE (2008)
8. Rumbayan, M.: Development of power system infrastructure model for the island communities: a case study in a remote island of Indonesia. In: International Conference on Advanced Mechatronic Systems, pp. 515–518 (2017)
9. Wang, W., Kliber, J., Zhang, G., Xu, W., Howell, B., Palladino, T.: A power line signaling based scheme for anti-islanding protection of distributed generators: Part II: Field test results. IEEE Trans. Power Deliv **22**, 1767–1772 (2007)
10. Raza, S., Mokhlis, H., Arof, H., Laghari, J.A., Wang, L.: Application of signal processing techniques for islanding detection of distributed generation in distribution network: A review. Energy Conversion Manag. **96**, 613–624 (2015)
11. Kim, M.S., Haider, R., Cho, G.J., Kim, C.H., Won, C.Y., Chai, J.S.: Comprehensive review of islanding detection methods for distributed generation systems. Energies **12**(5), 837 (2019)
12. Bikiran, G., Rami, J.H., Youakim, K.: A novel passive islanding detection technique for converter based distributed generation systems. In: IEEE Power & Energy Society Innovative Smart Grid Technologies Conference, pp: 1–5 (2015)
13. Zhao, J., Zhang, D., He, J.: A passive islanding detection method based on inter harmonic impedance. In: IEEE Conference on Energy Internet and Energy System Integration pp. 1–6 (2017)
14. IEEE 929. IEEE recommended practice for grid interface of photovoltaic (PV) systems. New York, NY: Institute of Electrical and Electronics Engineers; April, (2000)
15. Jones, R.A., Sims, T.R., Imece, A.F.: Investigation of potential islanding of a self-commutated static power converter in photovoltaic systems. IEEE Trans. Energy Convers. **5**(4), 624–631 (1990)
16. Gupta, P., Bhatia, R.S., Jain, D.K.: Active ROCOF relay for islanding detection. IEEE Trans. Power Deliv. **32**(1), 420–429 (2016)
17. Guha, B., Haddad, R.J., Kalaani, Y.: A passive islanding detection approach for inverter-based distributed generation using rate of change of frequency analysis. In South east Conference, pp 1–6. IEEE (2015)

18. Nasir aghdam, H., Ghadimi, N., Farhadi, P., Hashemi, F., Ghadimi, R.: Detecting the anti-islanding protection based on combined changes of active and reactive output powers of distributed generations. In: 2011 3rd International Conference on Computer Research and Development, pp. 285–289. Shanghai (2011)
19. Nikolovski, S., Baghaee, H.R.: Islanding detection of synchronous generator-based DGs using rate of change of reactive power. IEEE Syst J **13**(4), 4344–4354 (2019)
20. Raza, S., Mokhlis, H., Arof, H., Mohamad, H., Laghari, J.A.: Prioritization of different passive parameters for islanding detection on the basis of response analysis. IEEE International Conference on Power and Energy (PECon), pp. 615–619. Melaka (2016)
21. Raza, S., Mokhlis, H., Arof, H., Laghari, J.A., Mohamad, A.: A sensitivity analysis of different power system parameters on islanding detection. IEEE Trans. Sustain. Energy **7**(2), 461–470 (2016)
22. Hu, W., Sun, Y.: A compound scheme of islanding detection according to inverter. Asia-Pacific Power and Energy Engineering Conference, pp. 1–4. Wuhan (2009)
23. Khichar, S., Lalwani, M.: An analytical survey of the islanding detection techniques of distributed generation systems. Technol Econ Smart Grids Sustain Energy **3**, 10 (2018)
24. Singam. B., Hui, L.Y.: Assessing SMS and PJD schemes of anti-islanding with varying quality factor. IEEE International Power and Energy Conference, pp. 196–201. Putra Jaya (2006)
25. Mahat, P., Chen, Z., Bak-Jensen, B.: Review on islanding operation of distribution system with distributed generation. IEEE Power and Energy Society General Meeting, pp. 1–8. Detroit, MI, USA (2011)
26. Sung-Il, J., Kwang-Ho, K.: An islanding detection method for distributed generations using voltage unbalance and total harmonic distortion of current. IEEE Trans. Power Deliv. **19**(2) 745–752 (2004)
27. Tzelepis, D., Dyśko, A., Booth, C.: Performance of loss-of-mains detection in multi-generator power islands. 13th International Conference on Development in Power System Protection (DPSP), pp. 1–6 Edinburgh (2016)
28. Jose, B.K., Vincent, G.: Harmonic current based islanding detection for grid connected PV systems. 2017 IEEE International Conference on Circuits and Systems (ICCS), pp. 191–195. Thiruvananthapuram (2017)
29. Zeineldin, H.H., Kirtley, L.A.: A simple technique for islanding detection with negligible nondetection zone. IEEE Trans. Power Deliv. **24**(2), 779–786 (2009)
30. Laaksonen, H.: New multi-criteria-based algorithm for islanding detection in smart grids. 3rd IEEE PES, (ISGT Europe), pp. 1–8. Berlin (2012)
31. Danandeh, A., Seyedi, H., Babaei, E.: Islanding Detection Using Combined Algorithm Based on Rate of Change of Reactive Power and Current THD Techniques. 2012 Asia-Pacific Power and Energy Engineering Conference, pp. 1–4. Shanghai (2012)
32. Jun, L., Xue-liang, H., Xiao-hu, C., Miao, X., Wen, X.: Two islanding detection circuits based on the impedance variation for the micro-grid. The 2nd International Symposium on Power Electronics for Distributed Generation Systems, pp. 859–863. Hefei (2010)
33. Salman, S.K., King, D.J., Weller, G.: New loss of mains detection algorithm for embedded generation using rate of change of voltage and changes in power factors (2001)
34. Kumar, K.M., Naresh, M., Singh, N.K. and Singh, A.K.: A passive islanding detection approach for distributed generation using rate of change of negative sequence voltage and current. IEEE Uttar Pradesh Section International Conference on Electrical, Computer and Electronics Engineering pp. 356–360. IEEE, (2016)
35. Rostami, A., Jalilian, A., Naderi, S.B., Negnevitsky, M., Davari, P., Blaabjerg, F.: A novel passive islanding detection scheme for distributed generations based on rate of change of positive sequence component of voltage and current. Australasian Universities Power Engineering Conference, Melbourne, VIC, pp. 1–5 (2017)
36. Reddy, C.R., Reddy, K.H.: An efficient passive islanding detection method for integrated DG system with zero NDZ. (IJRER), 8, pp. 1994–2002 (2018)
37. Rostami, A., Bagheri, M., Naderi, S.B., Negnevitsky, M., Jalilian, A., Blaabjerg, F.: A novel islanding detection scheme for synchronous distributed generation using rate of change of

exciter voltage over reactive power at DG-Side. Australasian Universities Power Engineering Conference, Melbourne, VIC, 2017, pp. 1–5 (2017)
38. Naveen, G., Reddy, K.H., Reddy, C.R., Ramakrishna, B., Bramaramba, P., Reddy, L.B.: Passive islanding detection method for integrated DG system with balanced islanding. Int.J. Pure Appl. Maths **120**(06), 4041–4058 (2018)
39. Rostami, A., Jalilian, A., Hagh, M.T., Muttaqi, K.M., Olamaei, J.: Islanding detection of distributed generation based on rate of change of exciter voltage with circuit breaker switching strategy. IEEE Trans. Ind. Appl. **55**(1), 954–963 (2018)
40. Bashir, J., Jena, P., Pradhan, A.K.: Islanding detection of a distributed generation system using angle between negative sequence voltage and current. In Eighteenth National Power Systems Conference (NPSC), pp. 1–5. IEEE (2014)
41. Bakhshi, M., Noroozian, R., Gharehpetian, G.B.: Novel islanding detection method for multiple DGs based on forced helmholtz oscillator. IEEE Trans. Smart Grid **9**(6), 6448–6460 (2017)

Optimal Share of DG and DSTATCOM in Distribution Network Using Firefly Algorithm

Jitendra Singh Bhadoriya and Atma Ram Gupta

1 Introduction

Distribution system (DS) plays very important role in value chain as it is the last end of electricity supply. Mainly DS are of radial nature which makes it flexible to supply power at different areas. DS suffers problem with higher active and reactive loss, over and under voltage when it is subjected to different kind of load types and demand. Several attempts have been made to minimize the problem occurring in DS. Capacitors are used for compensating voltage and balancing reactive power management. Voltage regulators are also introduced to eliminate the effect of voltage overloading. Distributed generation is capable to reduce active power (AP) as well as reactive power loss (RPL) with improved voltage profile (VP). Since voltage regulators are slow in nature and can regulate only 10% voltage deviation, DSTATCOM is new emerging technology to improve VP and RPL. Integration of DG and DSTATCOM makes DS active network from passive network, it also become more resilient toward any unhealthy conditions such as fault, blackout etc. integration of these devices make DS more reliable and secure.

Several studies have been made to allocate DGDST simultaneously as well as individually by different optimization algorithms. Integration of these devices has negative impact also, like reverse power flow, undesirable voltage level, increased fault current, and power loss. To rectify this problem optimal location and sizing is determined satisfying various constraints [1, 2]. Multi-objective optimization (MOO) for optimal allocation of DG (OAD) for various load models and impact is also shown

J. S. Bhadoriya (✉) · A. R. Gupta
Department of Electrical Engineering, NIT Kurukshetra, Haryana, India
e-mail: jitendra_61900077@nitkkr.ac.in

A. R. Gupta
e-mail: argupta@nitkkr.ac.in

O. H. Gupta and V. K. Sood (eds.), *Recent Advances in Power Systems*, Lecture Notes in Electrical Engineering 699, https://doi.org/10.1007/978-981-15-7994-3_46

with several indices like power loss indices, capacity indices etc. by genetic algorithm (GA) [3]. GA and Particle Swarm Optimization (PSO) is applied to obtain the optimal location of DGs with different type depending upon the providing and absorbing active and reactive power, in practical bus system with several other parameter like ATC, reliability index ENS to show the impact in DS after installation of these device [4]. PSO is implemented to allocate multiple distributed generation to reduce losses [5]. PSO is implemented with PSAT software for finding optimal location of DG is DS [6]. DSTATCOM is optimally allocated through method based on sensitivity with load growth considering the load is modeled according to time variation, with impact in terms of reduction in energy loss, energy cost saving and voltage stability margin (VSM) enhancement [7]. Simultaneous allocation of DG and capacitor is introduced using strength pareto evolutionary algorithm 2 (SPEA2) with uncertainty in load modeling, the impact of reverse power flow is also shown in DS with techno economic analysis [8].the impacts of DG is briefly explained, that technical issues can be mitigated by use of different indices, so the complexity of integration these DGs can be made simpler [9]. The Whale optimization algorithm is applied successfully for managing reactive power by optimal allocation of TCSC and SVC to reduce active power loss (APL) and reactive power loss (RPL) [10]. The dispatch and management of DGs is taken into account with economic benefit from the distribution company's point of view, that will encourage electrical utility to make DG is best choice among all remedy methods for DS [11]. A biogeography based optimization (BBO) is presented intended for OAD based on solar photovoltaic generation to decrease AP loss and harmonics with maintaining appropriate voltage profile [12]. An optimization technique Sine Cosine Algorithm (SCA) and chaos map theory is used for finding multiple OADs [13]. The OAD by implementing hybrid GA-APSO algorithm based on harmony search (HS) is revealed in published work [14]. Many researchers focused on mainly two objectives by optimally placing DG to minimize AP and RP power loss and increasing VP enhancement in DS, it is better way to strengthen the DS rather than placement of capacitor and network reconfiguration [15]. Differential evolution algorithm is implemented for optimal allocation of DSTATCOM to reduce losses as well as maximizing the profit to lessening the total planning cost of DSTATCOM [16]. The impact of DG and DSTATCOM allocation using stability index is presented in radial DS by minimizing the losses and Harmonics [17]. The impact of integrating for single and multiple DSTATCOM is presented in DS under load growth on voltage stability, losses and energy saving by GAMS software and PSO [18]. Optimal placement of DSTATCOM is evaluated by new sensitivity index with probabilistic load model [19]. For diminish losses and improve VP, DSTATCOM is allocated using Jaya algorithm [20]. The performance of DSTATCOM is analyzed in radial DS with UPQC using power loss index [21]. DG is optimally allocated with simultaneous reconfiguration of network to coordinating optimizing the distribution network with adequacy and security [22]. Deployment of DG and DSTATCOM simultaneously can make DS more flexible by providing adequate active and reactive power support, which will make DS more reluctant toward various challenges that have been faced by DS.

In proposed work, FA optimization is used to allocate DGDST for reducing the losses and VP improvement. The proposed algorithm is implemented in IEEE-33 RDS. Section 2 describes the DGDST. Section 3 formulated the objective function with necessary constraints. Section 4 describes the FA optimization. Section 5 describes results followed by conclusion.

2 DG and DSTATCOM

2.1 DG

Renewable based DG like solar, wind, biomass etc., getting very popular because of its neat, clean and green energy property throughout globe. In India the rate of growth of SOLAR based DG is 30% while wind based is 10%. The profits of DG are given [23] as follows:

- Suitable place DG can reduce losses and enhanced voltage stability.
- Additional amount of power generated by DG reduces the burden on generator as well as transmission lines, so it provides security and reliability to whole value chain.
- Renewable based DG also participates in making environment neat clean and green because of not producing carbon emission.
- DG installation is simple and does not require complex infrastructures.
- The use of DG is increasing day by day, so participation of new players will introduce the competition in the market that will reduce the cost of DG.

In this presented work, we have taken DG which will inject active power with unity power factor in the DS.

2.2 DSTATCOM

DSTATCOM is a static synchronous compensator (STATCOM) shunt connected reactive compensation device that will closely regulate voltage in case of rise and decline in system voltage, since the reactive power is mutually related to voltage so by providing adequate voltage supply reactive power remain within limit and does not cause any harmful situation for DS. DSTATCOM insert current into the system by raising the value of voltage with compared to DS voltage, which in turn support in correction of power factor, reactive power management, and filtering of unwanted high frequency power overlapping as harmonic, etc. The following objectives can be achieved by allocation of DSTATCOM [24, 25]:

(a) APL and RPL reduction	(b) VP improvement
(c) Reliability improvement	(d) Load balance improvement
(e) Making DS more efficient and smooth functioning	

DSTATCOM is suitable choice among all power electronics-based devices because it has wide range of variety to regulate system voltage. In this paper the DSTATCOM is modeled as constant source of reactive power injecting in the DS.

3 Solution Strategy for Optimization Problem

3.1 Objective Function

The objective function (OF) is obtained by way of a minimization function subjected under numerous constraints which are classified as equality and inequality to fulfill the prerequisite of the DS to allocate DGDST.

I. Active Power Loss (APL)	II. Reactive Power Loss (RPL)
$\text{APL} = \sum_{b=1}^{Nbr} \lvert i_b \rvert^2 * R_b$	$\text{RPL} = \sum_{b=1}^{Nbr} \lvert i_b \rvert^2 * X_b$

Minimum value of voltage (MVV): It is the minimum value of voltage among all buses in the DS.

$$MVV = \min\|V_1, V_2 \ldots V_{n-1}, V_n\| \tag{1}$$

The overall multi-objective weighted (W) function is given by following below mentioned Eq. (4).

$$\text{OF} = \min\{W_1 * APL + W_2 * RPL + W_3 * (1/MVV)\} \tag{2}$$

$$\sum_{I=1}^{3} W_i = 1 \tag{3}$$

3.2 Constraints

The OF is exposed to under given constraints. Equality Constraints:

I. *Power Mismatching Constraints*:

$$P_{\text{loss}} + \sum P_{D(t)} = \sum P_{\text{DG}} \tag{4}$$

$P_{D(t)}$ The demand of active power at bus t P_{DG}. DG penetration power
Inequality Constraints:

II. *Voltage Extent Constraints:* The value of voltage should be within its predefined limits. It is given as

$$V_a^{\min} \leq |V_a| \leq V_a^{\max} \tag{5}$$

III. *Power Compensation*: The injecting AP and RP provided by DG for every candidate at each solution bus must obey tolerance limit.

$$P_{\text{DG}(t)}^{\min} \leq P_{\text{DG}(t)} \leq P_{\text{DG}(t)}^{\max}, \quad Q_{\text{DSTATCOM}(t)}^{\min} \leq Q_{\text{DSTATCOM}(t)} \leq Q_{\text{DSTATCOM}(t)}^{\max} \tag{6}$$

Power flow limits on feeder line:

$$S_{ac} \leq S_{ac}^{\max} \tag{7}$$

Where, S_{ac} is the thermal limit through the distributed line tied between bus ***a*** and ***c***. It is the maximum power transference capability of that line.

4 Firefly Optimization

Optimization methods can be categorizing as exact algorithms and heuristic algorithms. For exact algorithm there is no boundless of time, but for a global optimization problem their time may be increase exponentially according to dimension of time. Heuristic algorithms finds a reasonable solution in finite amount of time, however it may be slightly worse than optimal solution. A meta-heuristic is a high-level algorithm framework that is problem-independent and provides some certain rules to develop heuristic optimization algorithm [26]. FA is one of a meta-heuristic optimization solution method that is based on the fireflies flashing behavior and the phenomenon of bioluminescent communication. This algorithm uses real random numbers and communication within swarm particles since many algorithm particles communicate with neighbor particles only.

There are some fundamental rules of FA growth:

Attractiveness: The function of attractiveness in firefly is given by equation since sex is eliminated for fireflies because they are unisex when programmed virtual fireflies.

$$\beta_r = \beta_o * \exp(-\gamma r_{ij}^m) \tag{8}$$

where r = (mutual distance of fireflies) $\beta 0$ = (attractiveness at initial stage) γ = (coefficient of absorption)

Distance: Distance is updated using given formula for firefly because brightness is function of attractiveness, and it decreases according to distance from the other firefly rises because the air grips light.

$$r_{ij} = \left\| x_i - x_j \right\| = \sqrt{\sum_{k=1}^{\dim} (x_{i,k} - x_{j,k})^2} \tag{9}$$

where, xi, k = (k*t*h spatial coordinate component) xi =(*i*th firefly) dim= (dimensions number).

Movement: *The* firefly with largest brightness is found most eligible attractive, all neighbors move toward it. If there is no brightest firefly, then it moves in any possible direction

$$\begin{aligned} x_i = {} & x_i\{\text{current\_position}\} + \beta_o * \exp(-\gamma r_{ij}^2) * (x_j - x_i)\{\text{attractiveness}\} \\ & + a^*(\text{rand} - 0.5)\{\text{movement}\} \end{aligned} \tag{10}$$

As FA does not consider velocity so it eliminates problem associated with dynamically changing variable. The convergence speed is quite high compared to other optimization algorithms. It is very flexible and easily merges with other techniques to form hybrid optimization algorithm. Other details regarding firefly algorithm is given in [27]. FA implemented flow chart is shown in Fig. 1.

4.1 Implementation Step

1. The swarm of firefly is initialized with initial value of objective function by calculating the flashing light intensity.
2. Load all data needed for load flow analysis.
3. Start iteration after limiting the size and location of DGDST.
4. Load data is modified according to the decision variables of DGDST.
5. Obtained and store them OF value until maximum iteration is reached according to updation given in Eqs. (8), (9) and (10).
6. Print final optimizes solution.

5 Results and Discussion

All the data taken for analysis of test IEEE-33 BRDS is given in [28]. The load flow of BRDS is done by direct load flow method [29].The results of the proposed methodology are determined with MATLAB (2014a) with the system configuration

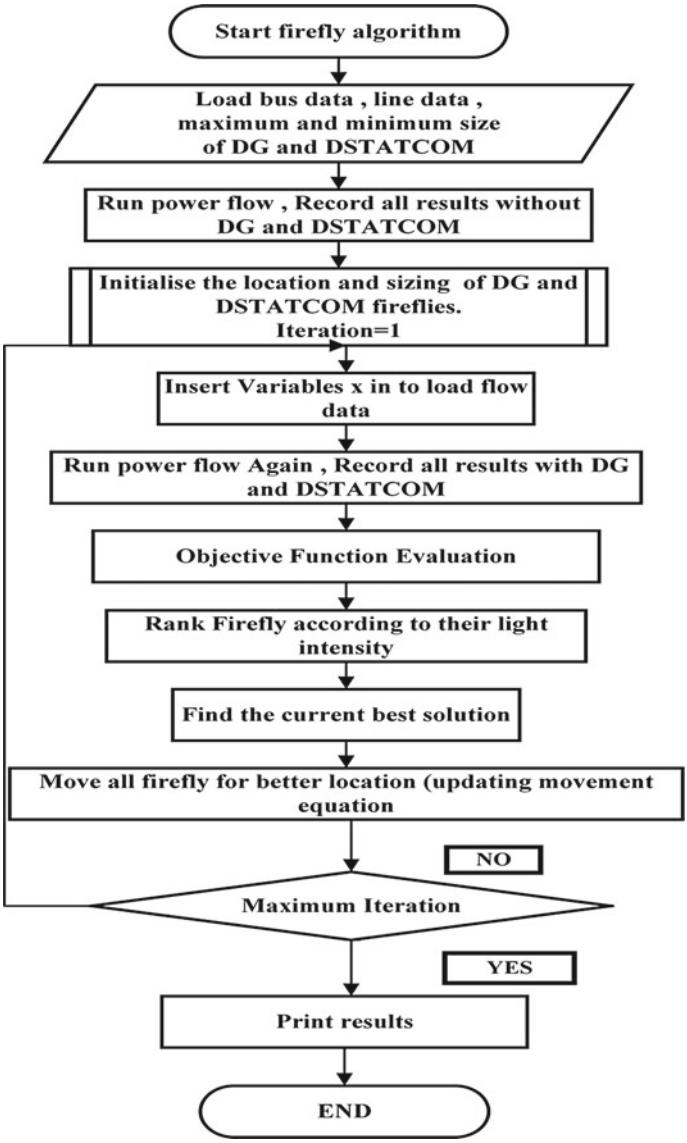

Fig. 1 Flowchart of flow chart

windows-7, Intel® core ™ i7-3770 CPU, 3.4 GHz, 4.0 GB RAM. The values of different coefficients are given in Table 1 is taken for optimization based on solution accuracy, computational time and robustness after running algorithm several number of times.

The Implementation is done based on following cases formulation.

Table 1 The parameter value for FA optimization techniques

Parameter	Maximum No. of Iteration	Number of fireflies	Alpha	Beta	Gamma
Value	30	10	0.25	0.2	1

Base Case : Without DGDST. Case1 : Single DGDST.
Case2 : Two DGDST. Case3 : Three DGDST.

Figure 2 shows convergence characteristics for all different cases for given number of iteration obtained during optimization of objective function. Figure 3 shows the VP of the 33 buses of the test DS in all cases. It is cleared that voltage profile goes on improving, as we tend to move from base case to case 3. Optimal multiple placements of DGDST provide almost flat voltage profile by injecting adequate supply of reactive power in the system. Table 3 represents the different solution parameters obtained with all the cases with reference to base case. The MVV is 0.9131pu at bus 18 and

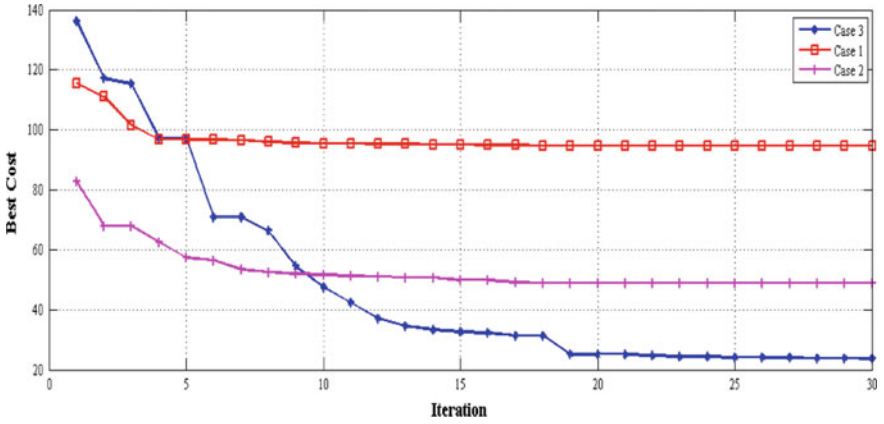

Fig. 2 Convergence characteristics for all cases

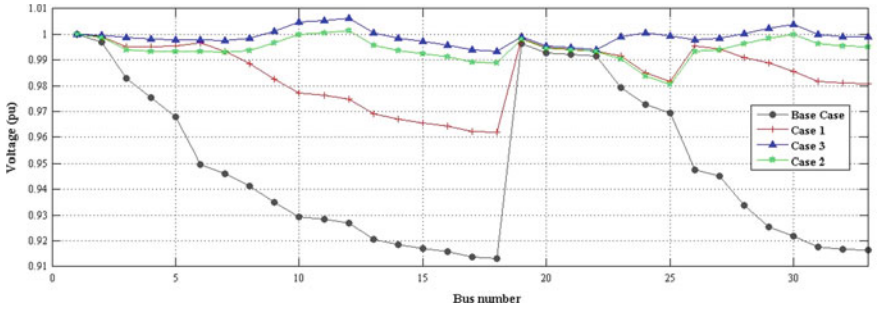

Fig. 3 Voltage profile for all cases

there are many other under voltage buses. The APL and RPL before the installation of DGDST are 202.70 kW and 135.16 kVAr, respectively. In Case1 when the single DGDST is installed on the bus no. 6 and 29 the APL and RPL is reduced to 53.34 kW, 41.26 kVar with MVV is 0.9618 pu. In case 2 when two DG and DSTATCOM are placed, then APL and RPL are reduced to 28.6874 kW and 20.3142 kVAr with MVV 0.9806 pu at bus 25. In case 3 when three DG and DSTATCOM are placed, then APL and RPL are reduced to 13.4707 kW and 10.6239 kVAr with MVV 0.9935 pu at bus 18. It is incidental that power flows in certain lines are controlled; no reverse power flow takes place due to placement of DGDST that is shown in Figs. 4 and 5 considering all cases (Table 2).

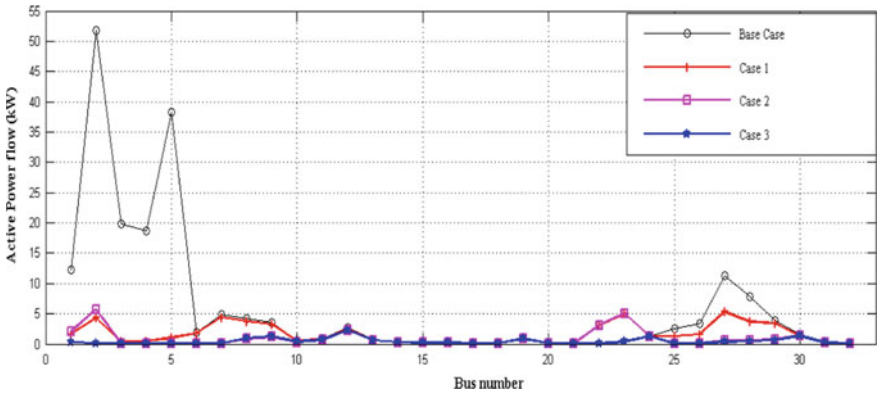

Fig. 4 Active power flow for all cases

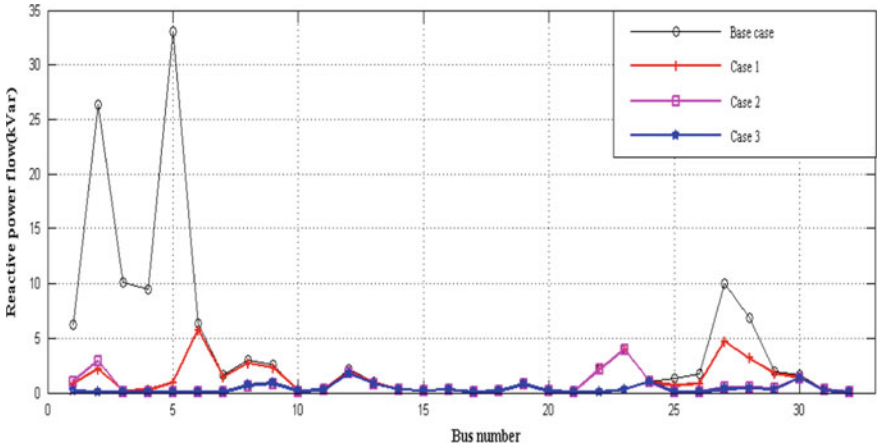

Fig. 5 Reactive power flow for all cases

Table 2 All comparative results

	APL	RPL	MVV	Location		Size		OF value
Cases	kW	kVar	p.u.	DG Bus	DST Bus	DG (kW)	DST (kVar)	–
Base case	202.7	135.1	0.9131	–	–	–	–	337.8
Case 1	53.3	41.2	0.9618	6	29	2476.7	1327.8	94.6
Case 2	28.6	20.3	0.9806	12,30	30,11	1000,1049.3	619.9,500	49
Case 3	13.4	10.6	0.9935	24,12, 30	30,25, 10	1086.3,1014.4, 1014.6	611.2, 650.2, 529.7	24

6 Conclusions

In this paper, FA with weighted objective function is presented for finding the DGDST optimal location and capacity for IEEE-33 radial DS. The FA optimization successfully applied including different cases, starting from base case without DGDST and with one, two and multiple DGDST as case 1, case 2 and case 3 for designing the problem. The APL and RPL are minimized along with installation of integrating devices. The DS becomes more efficient and reliable due to improvement in VP with controlled power flow due to DGDST. The total AP and RP loss of the system in case 3 are better among all cases.

References

1. Selim, A., Kamel, S., Alghamdi, A.S., Jurado, F.: Optimal placement of DGs in distribution system using an improved Harris Hawks optimizer based on single- and multi-objective approaches. IEEE Access **8**, 52815–52829 (2020). https://doi.org/10.1109/ACCESS.2020.2980245
2. MEl-Zonkoly, A.: Optimal placement of multi-distributed generation units including different load models using particle swarm optimization. Swarm Evol Comput.1, 50–59. (2011). https://doi.org/10.1016/j.swevo.2011.02.003
3. Singh, D., Singh, D., Verma, K.S.: Multiobjective optimization for DG planning with load models **24**(1), 427–436 (2009)
4. Bohre, A.K., Agnihotri, G., Dubey, M.: Optimal sizing and sitting of DG with load models using soft computing techniques in practical distribution system. IET Gener. Trans. Distrib. **10**(11), 2606–2621 (2016). https://doi.org/10.1049/iet-gtd.2015.1034
5. Fanish, R., Bhadoriya, J.S.: Optimal placement of multi DG in 33 bus. IJAREEIE **4**(4), 3758–3764 (2015)
6. Pandey, D., Bhadoriya, J.S.: Optimal placement & sizing of distributed generation (DG) to minimize active power loss using particle swarm optimization (PSO). Int. J. Sci. Technol. Res. **3**(7), 246–254 (2014)
7. Gupta, A.R., Kumar, A.: Optimal placement of D-STATCOM using sensitivity approaches in mesh distribution system with time variant load models under load growth. Ain. Shams. Eng. J. **9**(4), 783–799 (2018). https://doi.org/10.1016/j.asej.2016.05.009

8. Biswal, S.R., Shankar, G.: Simultaneous optimal allocation and sizing of DGs and capacitors in radial distribution systems using SPEA2 considering load uncertainty. IET Gener. Trans. Distrib. **14**(3), 494–505 (2020). https://doi.org/10.1049/iet-gtd.2018.5896
9. Ochoa, L.F., Member, S., Padilha-feltrin, A., Harrison, G.P.: Impacts with a multiobjective index. **21**(3), 1452–1458 (2006)
10. Raj, S., Bhattacharyya, B.S.C.: Swarm Evol Comput BASE DATA (2018). https://doi.org/10.1016/j.swevo.2017.12.008
11. Ameli, A., Bahrami, S., Khazaeli, F., Haghifam, M.R.: A multiobjective particle swarm optimization for sizing and placement of DGs from DG owner's and distribution company's viewpoints. IEEE Trans. Power Deliv. **29**(4), 1831–1840 (2014). https://doi.org/10.1109/TPWRD.2014.2300845
12. Duong, M.Q., Pham, T.D., Nguyen, T.T., Doan, A.T., Van Tran, H.: Determination of optimal location and sizing of solar photovoltaic distribution generation units in radial distribution systems. Energies **12**(1) (2019). https://doi.org/10.3390/en12010174
13. Selim, A., Kamel, S., Jurado, F.: Efficient optimization technique for multiple DG allocation in distribution networks. Appl. Soft. Comput. J. **86**, 1–20 (2020). https://doi.org/10.1016/j.asoc.2019.105938
14. Pandey, R.S., Awasthi, S.R.: A multi-objective hybrid algorithm for optimal planning of distributed generation. Arab. J. Sci. Eng. (0123456789) (2020). https://doi.org/10.1007/s13369-019-04271-1
15. Sultana, U., Khairuddin, A.B., Aman, M.M., Mokhtar, A.S., Zareen, N.: A review of optimum DG placement based on minimization of power losses and voltage stability enhancement of distribution system. Renew. Sustain. Energy Rev. **63**, 363–378 (2016). https://doi.org/10.1016/j.rser.2016.05.056
16. Sanam, J.: Optimization of planning cost of radial distribution networks at different loads with the optimal placement of distribution STATCOM using differential evolution algorithm. Soft Comput. (2020). https://doi.org/10.1007/s00500-020-04739-5
17. Tagore, A.K., Gupta, A.R.: Impact of DG and D-STATCOM allocation in radial distribution system for reducing harmonics. In: 8th International Conference on Computer *Engineering and* Networks Technology ICCCNT 2017 (2017). https://doi.org/10.1109/icccnt.2017.8204087
18. Murty, V.V.S.N., Kumar, A.: Impact of D-STATCOM in distribution systems with load growth on stability margin enhancement and energy savings using PSO and GAMS. Int. Trans. Electr. Energy Syst. **28**(11), 1–24 (2018). https://doi.org/10.1002/etep.2624
19. Gupta, A.R., Kumar, A.: Optimal placement of D-STATCOM in distribution network using new sensitivity index with probabilistic load models. In: 2nd International Conference *on* Recent *Advances in* Engineering Computer Science RAECS 2015. (2016). https://doi.org/10.1109/raecs.2015.7453316
20. Ei-Ela, A.A.A., Mouwafi, M.T., Shammah, A.E.S., Abdel-Ghany, D.Y.: Optimal placement of D-STATCOM in distribution systems using JAYA algorithm. In: 2018 20th International Middle East Power System Conference on MEPCON 2018—Proceedings (2019). https://doi.org/10.1109/mepcon.2018.8635133
21. Gupta, A.R., Kumar, A.: Performance analysis of radial distribution systems with UPQC and D-STATCOM. J. Inst. Eng. Ser. B. **98**(4), 415–422 (2017). https://doi.org/10.1007/s40031-016-0254-4
22. Ahmadi, S.A., Vahidinasab, V., Ghazizadeh, M.S., Mehran, K., Giaouris, D., Taylor, P.: Co-optimising distribution network adequacy and security by simultaneous utilisation of network reconfiguration and distributed energy resources. IET Gener. Transm. Distrib. **13**(20), 4747–4755 (2019). https://doi.org/10.1049/iet-gtd.2019.0824
23. Rezaee, Jordehi A.: Allocation of distributed generation units in electric power systems: a review. Renew. Sustain. Energy Rev. **56**(March), 893–905 (2016). https://doi.org/10.1016/j.rser.2015.11.086
24. Gupta, A.R., Kumar, A., Deployment of Distributed Generation with D-FACTS in distribution system: A Comprehensive Analytical Review. IETE J. Re. Taylor & Francis Group (2019). https://doi.org/10.1080/03772063.2019.1644206

25. Sirjani, R., Rezaee, J.A.: Optimal placement and sizing of distribution static compensator (D-STATCOM) in electric distribution networks: A review. Renew. Sustain. Energy Rev. **77**, 688–694 (2017). https://doi.org/10.1016/j.rser.2017.04.035
26. Johari, N.F., Zain, A.M., Mustaffa, N.H., Udin, A.: Firefly algorithm for optimization problem. Appl. Mech. Mater. **421**, 512–517. https://doi.org/10.4028/www.scientific.net/AMM.421.512
27. Yang, X.-S.: Firefly algorithms. In: Nature-Inspired Optimization Algorithms (2014). https://doi.org/10.1016/b978-0-12-416743-8.00008-7
28. Taher, S.A., Afsari, S.A.: Electrical power and energy systems optimal location and sizing of DSTATCOM in distribution systems by immune algorithm. Int. J. Electr. Power Energy Syst. **60**, 34–44 (2014). https://doi.org/10.1016/j.ijepes.2014.02.020
29. Teng, J.H.: A direct approach for distribution system load flow solutions. IEEE Trans Power Deliv. **18**(3), 882–887 (2003). https://doi.org/10.1109/TPWRD.2003.813818

A Comprehensive Review of Conventional and Computational Islanding Diagnosis of Distributed Generator in Distribution Network

Akshat Kumar, Shaik Riyaz, and R. N. Mahanty

1 Introduction

Over last several years, renewable energy power generation mode has been a major global priority. These energy generation techniques emit low pollution than their conventional counterparts. From this standpoint the Distributed Generation (DG) approach takes significance and it serves as phenomenal shift from centralized stations [1, 2]. DG refers to micro scale generation situated close to load which has grid integration potential. It is one of the ways to utilize renewable energy in effective and efficient manner. The number of DG is growing as it can avoid transmission and distribution capital investments as well as maintenance, curtail losses in transmission and distribution line, revamp voltage profile, enhance power quality and many other benefits [3]. Most of the utilities across the globe are having significant intrusion of DG. Apart from these benefits, there are some issues involved with DG and one such concern is occurrence of islanding.

The term "islanding" is a condition in DGs which refers to electric phenomena that occurs when injected energy to the network is interrupted because of many factors meanwhile DGs continue stimulating some part of the load or entire distribution network as depicted by Figs. 1 and 2. Consequently power grid loses control over this secluded part of distribution network that consists of generators as well as loads. Under this circumstance may trade-off reliability and system security of power system network [4, 5]. Imbalance in power system as a result of line and

A. Kumar (✉) · S. Riyaz · R. N. Mahanty
Department of Electrical Engineering, NIT Jamshedpur, Jamshedpur, India
e-mail: akshat.eee@gmail.com

S. Riyaz
e-mail: nitjsrriyaz@gmail.com

R. N. Mahanty
e-mail: rnmahanty.ee@nitjsr.ac.in

O. H. Gupta and V. K. Sood (eds.), *Recent Advances in Power Systems*, Lecture Notes in Electrical Engineering 699, https://doi.org/10.1007/978-981-15-7994-3_47

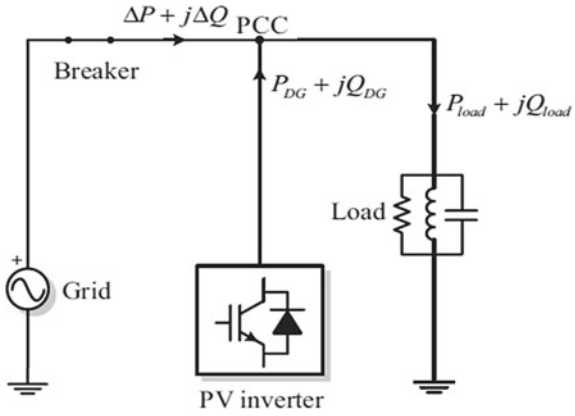

Fig. 1 Just before islanding

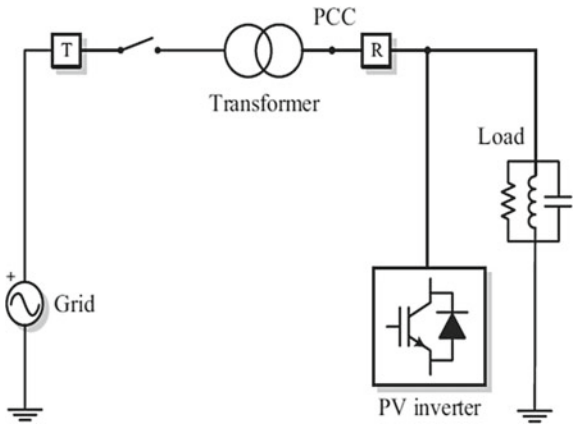

Fig. 2 Just after islanding

generator outages, faults or disturbances that would give rise to snapping of distribution network leading to islanding [6]. On the other hand, because of large number of DGs, this technique is not an economical option, and might lead to wastage of power from DG units. There may be intentional or unintentional islanding. Intentional islanding can decrease congestion of distribution and transmission networks enhance overall performance of the system by reduction of power losses as well as revamping of voltage profiles [7]. Hence, islanding action is a feasible option as long as all the issues concerned to it are adequately addressed. Many diversified researches are going on in order to make islanding a prolific reality [8, 9].

Islanding diagnosis methods are segmented as remote, local, and hybrid ones which are shown in Fig. 3. The local islanding technique can be again split into passive and active ones. These methodologies have their own merits as well as demerits. Therefore, research interest aligns toward computational intelligent methodologies for islanding diagnosis. These methodologies are robust and have ability to deal with complex system as well as situations. Whenever the distribution network gets

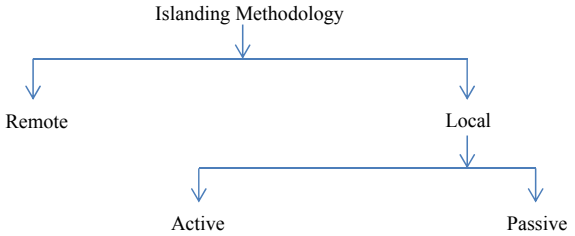

Fig. 3 Islanding diagnosis methodologies

detached, the very first step should be to diagnose islanding which requires efficient islanding diagnosis schemes.

Time and accuracy play major role in tracing islanding. This is utmost important, as failing to precisely identify islanding may lead to the failure of whole distribution system like cascading failures and ultimately results into blackout [10, 11]. Before proceeding toward different methodologies for islanding diagnosis, it is imperative to have a look on two key features for better understanding of islanding phenomena. One of them is "Non-Detection Zone" (NDZ) which means the limit up to which islanding remains untraced and other one is the type of load. These loads can be modeled as parallel RLC circuit in accordance with IEEE test frame because of its difficulty to diagnose islanding. Those loads which produce harmonics and constant power loads are non-linear in nature and they do not show great trouble in islanding [12]. The values of resistance, inductance and capacitance can be related using quality factor equation which is given by

$$Q = R\sqrt{\frac{C}{L}} \tag{1}$$

where Q is called the Q factor or quality factor which relates the maximum energy stored in the circuit, i.e., reactance to the energy dissipated, i.e., resistance during each cycle. RLC load with high quality factor value possess difficulty for islanding detection. In the next sections appropriate islanding techniques including computational methods are addressed.

2 Remote Islanding Detection Techniques

These methodologies principally rely upon communication channel between DGs and utilities. After diagnosis of islanding, the DGs are communicated to trip with the help of transmitters and receivers. A transmitter and receiver combination is properly placed at the grid and receiver sides respectively at every DG units in order to carry out communication regarding information through power line carrier communication (PLCC) channel. When distributed network is disconnected or islanded, the

receiver does not get corresponding command due to communication lapse. Ultimately islanding is diagnosed. Transfer trip scheme, power line signaling scheme and Supervisory Control and Data Acquisition (SCADA) are the prominent remote islanding diagnosis methodology [15]. In spite of the fact that remote methodologies have appreciable reliability than local techniques still they are uneconomical. Therefore, local techniques are vastly employed for islanding diagnosis.

3 Local Islanding Detection Schemes

Those methodologies employ measurement or calculation of parameters like current, voltage, frequency, phase etc. on the DG (inverter) side. Local schemes are categorized as passive mainly on the presumption of these parameters and active wherein small perturbations are introduced at inverter side and monitor whether the aforesaid parameter are influenced [13].

3.1 Passive Methodology of Island Detection

These methodologies are based upon system parameter measurements such as current, frequency, voltage etc. at PCC [16]. These parameter values are checked with pre-set threshold value for motive of islanding detection. These methodologies are economical and fast with no interjection of disturbance but at the same time NDZ is large where they could not diagnose islanding [17]. Rate of change of Output Power (ROCOP) is one of the techniques in which idea for diagnosing changes in the distributed generators' output power (dP/dt) as loss of grid usually causes load changes. On islanding dP/dt measured would be much greater than grid-connected case. When the change crosses the limit, the DG gets disconnected and stops supplying power to load. This method is much effective when power imbalance would be increasing. Other one is Rate of Change of Output Frequency (ROCOF) in which the DG gets disconnected from main grid whenever power mismatch occurs resulting into change in frequency [20]. The limitation of ROCOF is that it is sensitive to power fluctuations and load switching which may cause erroneous detection and threshold selection is also difficult. Thus, ROCOF is good for loads with fewer fluctuations.

Current and voltage harmonic detection method works on the basis of measurement of total harmonic distortion (THD) at PCC to diagnose islanding whenever THD exceeds pre-set values. Threshold selection is not easy for this as grid disturbance easily cause error detection. Under or over voltage and under or over frequency (OUV/OUF) methodologies rely on establishing limit for voltage as well as frequency. If voltage/frequency exceeds thresholds at PCC, DGs will be detached and stopped supplying power to load. It is low cost, has hardly influences power quality. NDZ is bigger in OUF/OUP and diagnosis time is hardly anticipated. Another passive

technique, i.e., intrinsic time decomposition methodology is widely used nowadays which utilizes voltage signal and dissects it into residual and baseline signals [18].

Another methodology is Phase Jump Detector which involves tracking of abrupt jumps in inverter's voltage as a result of deviation in inverter voltage as well as output currents. Ease of implementation is the biggest reason why PJD is used. Another method of islanding diagnosis is voltage unbalance (VU) which primarily occurs due to disconnection of DG with grid. If this unbalance is more than threshold value islanding occurs.

$$\mathrm{VU} = \frac{\mathrm{NS}}{\mathrm{PS}} \tag{2}$$

The voltage imbalance is given by Eq. (2) where NS is negative sequence current and PS is positive sequence. Because of variation, it is difficult to trace error. Influence of harmonics in negative sequence causes further difficulty in anticipating threshold values. This technique can be applied where capacitor bank switching is used.

3.2 Active Methodology of Islanding Detection

The main ideology of active methodology based upon usage of high frequency signals and perturbation in voltage and current. Whenever distribution network is connected to the grid; the augmentation of small perturbation would be negligible variation in system parameter. On other hand when islanding occurs, the system observes large variation in parameter due to same perturbations which lead to detection of islanding. Even under perfect match of load and generator, islanding can be diagnosed which is impossible in passive techniques. Active methodologies have unique advantage of reducing or even no NDZ meanwhile power quality of grid voltage is affected which may cause instability. Some of the active islanding diagnosis techniques are discussed in this section. The first one is Impedance Measurement [21] which is based upon measurement of impedance to diagnose changes at inverter side when distribution grid which has low impedance gets disconnected from the system. It has advantage of having small NDZ but disadvantage while working with multiple inverters. Other one is harmonic Injection/Impedance Detection [22]: Involves adding a specific current harmonic at point of common coupling. If impedance of grid is smaller than load impedance on grid connection, then the injected harmonics will pass onto the grid.

Another widely used methodology is Slide Mode Frequency Shift (SMS) or Active Phase Shift (APS) [22] which employs positive feedback that varies phase angle of current at inverter w.r.t. deviation of frequency at PCC. This method can be easily implemented and has small NDZ. SMS also has unique advantage of utilizing multiple inverters. One of the most prominent ways is Active Frequency Drift [22] whose main philosophy relies upon variation of frequency of current by using positive feedback. Whenever system gets disconnected, a phase mismatch between current and voltage waveform appears at PCC. This technique can be applied to multiple

inverters but at the same time power quality is degraded and inverter exhibits NDZ which is dependent on chopping factor.

Another technique is Sandia Frequency Shift [22] which is an expedited edition of AFD technique. With positive feedback, it is used to prevent false islanding. This methodology has smallest NDZ in comparison to other active methods. Sandia Voltage Shift [22] is also one of the techniques whose basic concept is similar to Sandia Frequency Shift. It is easily implementable. Slight deterioration of power quality is one of its demerits. Also affects maximum power point tracking (MPPT) computation of inverter and finally reduces inverter's operational efficacy.

4 Hybrid Islanding Detection Schemes

These methodologies employ composite attributes of both active as well as passive diagnosis schemes. In these methodologies, active schemes are employed solely when passive methods are unable to decide islanding phenomenon. Some of the hybrid islanding methodology is based on proportional power spectral density as well as real power drift, rate of change of voltage and active power shift [6], monitoring current real power of circuit breaker etc. These diagnosis methods have very small NDZ. Hence, power quality is largely improved but at the same time the diagnosis speed reduces. The two significant issues precision and swift diagnosis are still unresolved. Some of the techniques based upon modified Slantlet transform along with machine learning are widely employed [19]. Therefore, intelligence methodologies for islanding diagnosis may be an appropriate explication for the two issued dealt earlier.

5 Computational Islanding Detection Schemes

A group of techniques which are employed to mimic human intelligence is called computational intelligence. Artificial Immune System (AIS), Artificial Neural Network (ANN), Fuzzy Logic Control (FLC), Support Vector Machine (SVM), Adaptive Neuro-Fuzzy Inference System (ANFIS) and Decision Tree (DT) classifier are some of intelligence techniques used [14]. These techniques have dexterity to resolve non-linear multi objective issues which could not be resolved by conventional methodologies with coveted precision as well as speed. The applications of some of the computational techniques for islanding diagnosis are dealt in upcoming section.

5.1 *Artificial Neural Network (ANN) Based Islanding Diagnosis*

ANN has been extensively employed as one stop solution for wide range of science and engineering issues [23]. Neurons are analogous to biological synapse is considered as an ANN. Multi-layered feed forward networks are widespread employed for power system analysis. ANN based islanding diagnosis methodology is intended for multiple and hybrid based DG [24]. The transients in voltage signal as well as in three phase currents [25] are some of the parameters used for islanding purpose. Both are classified as passive islanding diagnosis technique because they have nothing to do with power quality. Wavelet transform is utilized to take out information, then it is passed to train ANN so as to differentiate between islanding and non-islanding process. Load raise and load lower, association and disassociation of capacitive load, SLG fault, L-L fault, DLG fault at required position of DG and its operating states come under non-islanding phenomena. ANN based upon hybrid islanding diagnosis methodology is appropriate for synchronous DG. This methodology utilizes both active and passive technique for better precision as well as reliability. The change or adjustment of frequency is employed as input variable to the islanding diagnosis compensators and regulate real power reference value to DG while the adjustment of magnitude of voltage signal is employed as input variable to islanding compensator which regulates reactive power reference values to DG in active and reactive power approaches respectively. Some other ANN based passive islanding diagnosis methodology is apt for Doubly Fed Induction Generator (DFIG) wind turbines are based upon symmetrical component of second harmonic voltage and current signal. Fourier transform is utilized to process these harmonics. The symmetrical components are measured at wind farm side and fed to ANN for the purpose of islanding diagnosis. The findings reflect proposed ANN method has capability to decide between islanding or other incidents which can diagnose islanding phenomena in swift manner. Some types of ANN like self-organizing maps (SOM), probabilistic neural networks (PNN), extension neural networks (ENN) etc. are also widely employed.

5.2 *Fuzzy Logic Control (FLC) Based Islanding Diagnosis Technique*

It is an emerging technique for modeling of system which is not systematically or well-illustrated by mathematical formulae. Fuzzy logic control depicts the proficient human knowledge with respect to language variables called fuzzy rules. This technique is employed for islanding diagnosis problems. FLC technique is used for rotating type of DG which is in [26]. This literature utilizes passive parameters, i.e., voltage to diagnose islanding phenomena quite precisely. The relevant computation looks after change in parameters as well as fuzzy laws used to diagnose islanding

phenomena. This methodology is corroborated on radial distribution networking with diverse kind of loads and found capable of distinguishing between islanding phenomena and other events [26]. Δf, ΔV, $\Delta f/\Delta t$, $\Delta V/\Delta t$, $\Delta P/\Delta t$, $\Delta f/\Delta P$, current THD, voltage THD, $\Delta P, f$, absolute (v/p.f), gradient (v/p.f) for islanding diagnosis are intended in [27, 28]. This paper executes initial categorization by decision tree (DT) methodology, membership functions of fuzzy is established and corresponding rule is developed based on islanding diagnosis. The simulation results provide 100% precision by FLC based islanding detection scheme. In addition, inline implementation of FLC is simpler that renders it concrete for real time application [27, 28].

5.3 Decision Tree (DT) Classifier Based Islanding Diagnosis Technique

DT is a kind of pattern classifier and recognition tool that purports to provide a considerable resolution for different inputs by accounting statistical variations using different analytical methods. Main merit of this technique is quick training in comparison to other pattern recognition facilities. DT algorithm crumbles much complex decision making process into unions of various elementary decisions which ultimately makes it convenient to interpret Partition may be done from child nodes. A leaf or terminal node is where there is not any more partition [29]. Forecasts are done on the make-up of leaf nodes. To utilize DT for forecasting, the split/broken decisions are succeeded till leaf node is attained in the concerned system. DT classifier has been extensively used for islanded diagnosis purposes. A DT classifier based islanding diagnosis scheme is proposed in [29]. The concerned attributes are analyzed and processed by DT for islanding diagnosis. The simulation result depicts among three signals, particularly voltage signal is quick in islanding diagnosis with simpler structure and economical in comparison to other ways. This method is precise with accuracy till 98% and could diagnose islanding in one cycle [29].

6 Discussion

This work has addressed the capability of computational intelligence techniques in obtaining precise islanding diagnosis within limited time frame. It is observed in review that computational based intelligent methodologies are given more preference over conventional techniques like active, passive, remote and hybrid islanding diagnosis schemes as observed in Table 1.

During grid disconnections, computational techniques have ability to perform swift and higher precision islanding diagnosis as depicted in Table 2. In this the accuracies of different islanding methodologies have been compared. Moreover, it can be pointed out that computational islanding diagnosis techniques are largely

Table 1 Comparisons

Characteristic	Active techniques	Passive techniques	Remote techniques	Hybrid techniques
Principle	Introduce frequency signal/introduce perturbation	Inspect variation in system parameter	Communication system between utility and DG	Combined passive and active
Diagnosis Time	Long	Short	Short	Long
NDZ	Small	Large	None	Very small
Reliability	High	Low	High	High
Power quality	Worst	No effect	No effect	Very small effect
Price	Low	Low	High	Low
Examples	Impedance measurement, HD. SMS, AFD. AFDPF. FJ, SFS, SVS	ROCOP, ROCOF, THD, OUV/OUF, ROCOFOP, PJD, VU	PLCC, SCADA	Based on positive feedback, VU and voltage and reactive power shift

Table 2 Percentage Precision

Islanding diagnosis techniques	Precision (%)	Islanding diagnosis techniques	Precision (%)
Under/over frequency [33]	90.24	SOM neural networks [37]	98.19
Under/over voltage [33]	78.81	SOM neural networks [36]	97.92
VVS [33]	74.05	MPNN [32]	97.4
DT classifier [34]	96.43	PNN [31]	90
ROCOF [33]	93.81	ANFIS [30, 38]	100
Voltage based DT [29]	98	Fuzzy and DT [27, 28]	100
Intelligent based [35]	83.33	SVM [31]	78
ANN [24]	97.77	DT [31]	99.61

precise with accuracy more than 95%. Some of them have precision up to 99% while fuzzy with DT based methodologies assert to have 100% precision. Because of unique attributes like robustness and ability to deal non-linear complex system make computational based intelligence methodologies attain higher precision despite

of the fact that these techniques also utilize same parameters as that of active, passive, hybrid and remote.

7 Conclusions

An extensive review of both conventional and computational intelligence based islanding diagnosis techniques in distributed generation system has been presented in this work. This paper also dealt with limitations of all possible conventional methods with their merits and demerits which ultimately require computational intelligence based methodologies for greater precision and swift diagnosis of islanding. The intelligent techniques have highest precision of 100% and shortest islanding diagnosis duration. It can also be inferred that computational methodologies play significant role in successful operation of islanding in DG which enhance power system reliability along with power quality. Therefore, computational intelligence based methodologies are preferred over conventional or existing techniques.

References

1. Dincer, I.: Renewable energy and sustainable development: a crucial review. Renew. Sustain. Energy Rev. **4**(2), 157–175 (2000)
2. de Alegría Mancisidor, I.M., de Basurto Uraga, P.D., de Alegría Mancisidor, I.M., de Arbulo López, P.R.: European Union's renewable energy sources and energy efficiency policy review: the Spanish perspective. Renew. Sustain. Energy Rev. **13**(1), 100–114 (2009)
3. Acharya, N., Mahat, P., Mithulananthan, N.: An analytical approach for DG allocation in primary distribution network. Int. J. Electr. Power Energy Syst. **28**(10), 669–678 (2006)
4. Pietzsch, M.: Convertidores CC/CA para la conexio´n directa a red de sistemas fotovoltaicos: comparacio´n entre topologı´as de 2 y 3 niveles. Bachelor thesis. U.P.C. (2004, December)
5. PVPS, I.: Evaluation of islanding detection methods for photovoltaic utility-interactive power systems. Report IEA PVPS T5-09 (2002)
6. Laghari, J.A., Mokhlis, H., Karimi, M., Bakar, A.H.A., Mohamad, H.: Computational Intelligence based techniques for islanding detection of distributed generation in distribution network: a review. Energy Convers. Manag. **88**, 139–152 (2014)
7. Velasco, D., Trujillo, C.L., Garcerá, G., Figueres, E.: Review of anti-islanding techniques in distributed generators. Renew. Sustain. Energy Rev. **14**(6), 1608–1614 (2010)
8. Mohamad, H., Mokhlis, H., Ping, H.W.: A review on islanding operation and control for distribution network connected with small hydro power plant. Renew. Sustain. Energy Rev. **15**(8), 3952–3962 (2011)
9. Mahat, P., Chen, Z., Bak-Jensen, B.: Review on islanding operation of distribution system with distributed generation. In 2011 IEEE Power and Energy Society General Meeting, pp. 1–8. IEEE
10. Hines, P., Apt, J., Talukdar, S.: Large blackouts in North America: historical trends and policy implications. Energy Policy **37**(12), 5249–5259 (2009)
11. Wang, J.W., Rong, L.L.: Robustness of the western United States power grid under edge attack strategies due to cascading failures. Saf. Sci. **49**(6), 807–812 (2011)
12. Aghamohammadi, M.R., Shahmohammadi, A.: Intentional islanding using a new algorithm based on ant search mechanism. Int. J. Electr. Power Energy Syst. **35**(1), 138–147 (2012)

13. Pahwa, S., Youssef, M., Schumm, P., Scoglio, C., Schulz, N.: Optimal intentional islanding to enhance the robustness of power grid networks. Physica A **392**(17), 3741–3754 (2013)
14. El-Zonkoly, A., Saad, M., Khalil, R.: New algorithm based on CLPSO for controlled islanding of distribution systems. Int. J. Electr. Power Energy Syst. **45**(1), 391–403 (2013)
15. Chen, Y., Xu, Z., Østergaard, J.: Security assessment for intentional island operation in modern power system. Electr. Power Syst. Res. **81**(9), 1849–1857 (2011)
16. Nale, R., Biswal, M., Kishor, N.: A transient component based approach for islanding detection in distributed generation. IEEE Trans. Sustain. Energy **10**(3), 1129–1138 (2018)
17. Nale, R., Biswal, M.: Comparative assessment of passive islanding detection techniques for microgrid. In: 2017 International Conference on Innovations in Information, Embedded and Communication Systems (ICIIECS), pp. 1–5. IEEE
18. Nale, R., Venkatanagaraju, K., Biswal, S., Biswal, M., Kishor, N.: Islanding detection in distributed generation system using intrinsic time decomposition. IET Gener. Trans. Distrib. **13**(5), 626–633 (2018)
19. Ahmadipour, M., Hizam, H., Othman, M.L., Radzi, M.A.M., Chireh, N.: A novel islanding detection technique using modified Slantlet transform in multi-distributed generation. Int. J. Electr. Power Energy Syst. **112**, 460–475 (2019)
20. Funabashi, T., Koyanagi, K., Yokoyama, R.: A review of islanding detection methods for distributed resources. In: 2003 IEEE Bologna Power Tech Conference Proceedings, vol. 2, p. 6. IEEE
21. Dyśko, A., Booth, C., Anaya-Lara, O., Burt, G.M.: Reducing unnecessary disconnection of renewable generation from the power system. IET Renew. Power Gener. **1**(1), 41–48 (2007)
22. Bower, W., Ropp, M.: Evaluation of islanding detection methods for photovoltaic utility-interactive power systems. International Energy Agency. Report IEA PVPS, 5 (2002)
23. Dias, F.M., Antunes, A., Mota, A.M.: Artificial neural networks: a review of commercial hardware. Eng. Appl. Artif. Intell. **17**(8), 945–952 (2004)
24. Fayyad, Y., Osman, A.: Neuro-wavelet based islanding detection technique. In: 2010 IEEE Electrical Power & Energy Conference, pp. 1–6. IEEE
25. ElNozahy, M.S., El-Saadany, E.F., Salama, M.M.: A robust wavelet-ANN based technique for islanding detection. In: 2011 IEEE Power and Energy Society General Meeting, pp. 1–8. IEEE
26. Eugeniusz, R., Burek, A., Jedut, L.: A New Method for Islanding Detection in Distributed Generation. Wroclaw University of Technology, Department of Electrical Power Engineering, Poland (2007)
27. Samantaray, S.R., El-Arroudi, K., Joos, G., Kamwa, I.: A fuzzy rule-based approach for islanding detection in distributed generation. IEEE Trans. Power Deliv. **25**(3), 1427–1433 (2010)
28. Kumarswamy, I., Sandipamu, T.K., Prasanth, V.: Analysis of islanding detection in distributed generation using fuzzy logic technique. In: 2013 7th Asia Modelling Symposium, pp. 3–7. IEEE
29. Heidari, M., Seifossadat, G., Razaz, M.: Application of decision tree and discrete wavelet transform for an optimized intelligent-based islanding detection method in distributed systems with distributed generations. Renew. Sustain. Energy Rev. **27**, 525–532 (2013)
30. Yin, G.: A distributed generation islanding detection method based on artificial immune system. In 2005 IEEE/PES Transmission & Distribution Conference & Exposition: Asia and Pacific, pp. 1–4. IEEE
31. Lidula, N.W.A., Rajapakse, A.D.: Fast and reliable detection of power islands using transient signals. In: 2009 International Conference on Industrial and Information Systems (ICIIS), pp. 493–498. IEEE
32. Mohanty, S.R., Ray, P.K., Kishor, N., Panigrahi, B.K.: Classification of disturbances in hybrid DG system using modular PNN and SVM. Int. J. Electr. Power Energy Syst. **44**(1), 764–777 (2013)
33. Lidula, N.W.A., Rajapakse, A.D.: A pattern-recognition approach for detecting power islands using transient signals—Part II: Performance evaluation. IEEE Trans. Power Deliv. **27**(3), 1071–1080 (2012)

34. Lidula, N.W.A., Rajapakse, A.D.: A pattern recognition approach for detecting power islands using transient signals—Part I: Design and implementation. IEEE Trans. Power Deliv. **25**(4), 3070–3077 (2010)
35. El-Arroudi, K., Joos, G., Kamwa, I., McGillis, D.T.: Intelligent-based approach to islanding detection in distributed generation. IEEE Trans. Power Deliv. **22**(2), 828–835 (2007)
36. Moeini, A., Darabi, A., Karimi, M.: Clustering governor signal of distributed generation for islanding detection. In: 2010 IEEE Region 8 International Conference on Computational Technologies in Electrical and Electronics Engineering (SIBIRCON), pp. 493–498. IEEE
37. Moeini, A., Darabi, A., Rafiei, S.M.R., Karimi, M.: Intelligent islanding detection of a synchronous distributed generation using governor signal clustering. Electr. Power Syst. Res. **81**(2), 608–616 (2011)
38. Bitaraf, H., Sheikholeslamzadeh, M., Ranjbar, A.M., Mozafari, B.: Neuro-fuzzy islanding detection in distributed generation. In IEEE PES Innovative Smart Grid Technologies, pp. 1–5. IEEE

Economic Power Wheeling Using MW-MILE Method Through Gravitational Search Algorithm

Anumeha, Kaushik Paul, Pratul Arvind, K. B. Yadav, and Jayendra Kumar

1 Introduction

The electrical energy is a vital need for our daily life. The electrical power sector is considered as one of the largest industry. It is composed of mainly three-component power generation, the transmission of power to load centers, and distribution of power at load centers to the consumers. Since many years the power industry is operating in regulating the manner or monopolistic way. Traditionally, this industry is run by a single company that is serving all three activities generation, transmission, and distribution. This system of operation has some drawbacks such as low efficiency, less cost-effective, and limited financial support. The appreciable results of deregulation in the sector of communication, natural gas, and airline industry, it is felt by the researchers the necessity to deregulate the electric power industry [1]. It results in higher operational efficiency and lower energy cost to the consumers.

The power system deregulation has opened the door for the private sector to invest and expand the power market. Several reforms have been made in the sector of generation, transmission, and distribution of power industries. Deregulation has benefited the consumers with a variety of options in energy purchases [2–4]. The

Anumeha (✉)
Government Women's Polytechnic Jamshedpur, Jamshedpur, Jharkhand, India
e-mail: amehanitjsr@gmail.com

K. Paul · J. Kumar
Department of Electrical Engineering, BIT Sindri, Sindri, Jharkhand, India
e-mail: kaushiksunnypaul@gmail.com

P. Arvind
Department of Electrical Engineering, ADGITM, New Delhi, India

K. B. Yadav
National Institute of Technology Jamshedpur, Jamshedpur, Jharkhand, India

O. H. Gupta and V. K. Sood (eds.), *Recent Advances in Power Systems*, Lecture Notes in Electrical Engineering 699, https://doi.org/10.1007/978-981-15-7994-3_48

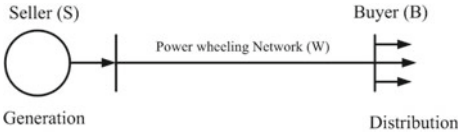

Fig. 1 Power wheeling structure for power system

transmission open access facilitates the utilization of transmission structure by more than two market players maintaining some regulatory norms [5].

The power wheeling in the transmission system refers to the usage of a third party transmission system to enable the power transaction between a buyer and seller [6]. An example of power wheeling is presented in Fig. 1.

In this example, S represents power seller and *B* represents power buyer. They do not have the transmission link between them of their own. So path *W* is used for power exchange. There may be more than one wheeling transmission going on simultaneously. The interconnected transmission system provides multiple routes to deliver/wheeling power to the utilization point or load centers. Since interconnecting transmission lines create large networks, they do more than transmit power from generating plant to load centers. They provide an alternative path for power flow serves as a source of reactive power flow (Vars) and provide stability and other ancillary supports.

The wheeling power cost is computed by several methods such as MW-Mile method, postage, contract path method, stamp method, boundary flow method, and MW-Mile method [7, 8]. In MW-Mile method, the wheeling power cost is computed based on wheeling transaction, i.e., wheeling power multiplied by the actual distance in miles of power flow. The MW-Mile strategy endeavors to dispense the wheeling cost dependent on real framework utilization as close as could reasonably be expected [9, 10].

A number of population-based metaheuristic optimization methods are developed and implemented for solving power system problems [11]. Recently, a new meta-heuristic method known as Gravitational Search Algorithm (GSA) [12] has been applied to optimum power flow problem of power system [13] and other fields of electrical engineering [14]. In this paper, it is proposed to use MW-Mile method for solving the economic operation of the power wheeling problem of power system through GSA. This problem is also solved by Particle Swarm Optimization (PSO) [15] and the results obtained by the two methods are compared. It has been shown that the GSA method is more efficient than PSO. In the next section, the optimization problem of power wheeling is formulated. A 4-grid power system is used for GSA implementation and the results are compared with PSO. It has been shown that GSA outperforms PSO method. Lastly, the conclusion and comment are presented.

2 Problem Formulation

An interconnected power system is shown in Fig. 2. It is assumed that there are N areas/grids interconnected by transmission lines. It is further assumed that first r grids have additional power available then the base load requirement says $Sg_1, Sg_2, \ldots, Sg_t$ which can be sold to a buyer and there is a buyer who purchases power which is to be transferred to $N - r$ grids say $Pd_{r+1}, Pd_{r+2}, \ldots, Pd_N$. The total power available for selling (wheeling) at the seller level to the buyers at r grids is represented by Eq. (1).

$$S_G = S_{g1} + S_{g2} + \cdots + S_{gr} \tag{1}$$

The total power purchased and distributed at $r + 1$ to N grids is given by Eq. (2).

$$P_D = Pd_{r+1} + Pd_{r+2} + \cdots + Pd_N \tag{2}$$

It is assumed that neither the buyer nor the seller has a network to transfer power from the seller point to buyer point. It has to be transferred by a third party who owns the transmission network connecting seller point to buyer point. The party charges for the transmitted power on the basis of absolute value of MW-Mile of the power transferred (wheeling power) and it is assumed that it is constant per MW-Mile (λ) for each line. Let there are m numbers of transmission lines connecting "N" grids. The length of the lines is $d_1, d_2 \ldots d_m$ miles and the power transferred by lines is P_1, $P_2 \ldots P_m$. If the power flow is in the opposite direction, then it should be considered as negative. Total cost (J) of power wheeled is computed as the product of λ and total MW-Mile of all the lines represented by Eq. (3).

$$J = \lambda \sum_{i=1}^{m} abs(p_i d_i) \tag{3}$$

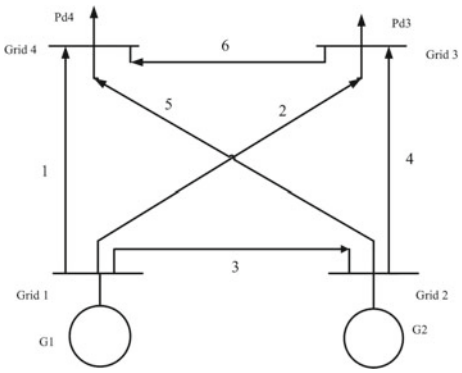

Fig. 2 Grid representation of interconnected power system

Since λ is constant, minimization of (3a) represents minimization of (3).

$$JJ = \sum_{i=1}^{m} abs(p_i d_i) \tag{3a}$$

Hence, the problem is designed as "To find out the wheeling power Pi in each line for a given total power demand P_D (buyer) and available total power generation *Sg* (seller) such that the total power wheeling cost involved represented by Eq. (3) is minimum subject to constrains." The economic operation of the power system is given in [2]. The solution to the problem by GSA method is proposed.

2.1 Gravitational Search Algorithm

The GSA method of solution is based on Newton's laws of gravity and motion. It was formulated by Rashedi et al., in 2009. The force between two masses is used as a primary concept for this algorithm. The GSA is discussed as follows.

A "*n*" number of agents have considered each of them having a mass M_i. Each mass position is represented as:

$$X_i = (x_{i1}, x_{i2}, \ldots, x_{im}) \quad for\ i = 1, 2, \ldots, n \tag{4}$$

$$Q_i^k = \frac{\text{fit}_i^k - \text{worst}_i^k}{\text{best}^k - \text{worst}^k} \tag{5}$$

$$M_i^k = \frac{Q_i^k}{\sum_{i=1}^{n} Q_i} \tag{6}$$

Here k denotes the iteration number, M_i^k and fit_i^k are considered as the mass and fitness component for the ith agent corresponding to the kth iteration number, respectively. The worst^k and best^k are shown as:

$$\text{best}^k = \min_{i \in 1 \text{ to } n} \left\{\text{fit}_i^k\right\} \tag{7}$$

$$\text{worst}^k = \max_{i \in 1 \text{ to } n} \left\{\text{fit}_i^k\right\} \tag{8}$$

The agent's acceleration is determined based on the sun of the forces experienced from the group of heavier masses. Representation of total forces is shown in Eq. (9).

$$F_{ij}^{k} = \sum_{l \in k \text{ best}, l \neq i} \text{rand}_i G^K \frac{M_l^k M_i^k}{(R_{il} + \delta)} \left(x_{lj}^k - x_{ij}^k\right) \tag{9}$$

where *rand* varies from [0, 1] and is randomly distributed. δ represents a constant value. R_{il} in Eq. (10) denotes the Euclidean distance between ith and lth agent. Equation (11) gives the expression for the gravitational.

$$R_{il}^k = \left\| X_i^k, X_i^k \right\|_2 \tag{10}$$

$$G^k = G_0 e^{-(\beta \frac{k}{m})} \tag{11}$$

where G_0 represents the gravitational constant with initial value and k_m represents maximum iterations and β is taken as a constant.

$$\alpha_{ij}^k = \frac{F_{ij}^k}{M_i^k} = \sum_{l \in k \text{best}, l \neq i} \text{rand}_i G^k \frac{M_l^k}{R_{il}^k + \delta} \left(x_{lj}^k - x_{ij}^k\right) \tag{12}$$

The velocity of the agent is determined based on the acceleration by Eq. (13).

$$V_{ij}^{k+1} = \text{rand}\, V_{ij}^k + \alpha_{ij}^k \tag{13}$$

The position update for the agent is expressed in Eq. (14).

$$X_{ij}^{k+1} = x_{ij}^k + V_{ij}^{k+1} \tag{14}$$

The complete solution step for the optimization problem by GSA is shown in Fig. 3.

The solution to the problem is considered under following simplifying assumptions.

1. The power wheeling company is not responsible for line loss incurred during power wheeling. It has to be taken care either by the seller or by the buyer of power, i.e., first party or second party.
2. The total power demand P_D (as per Eq. (2)) is less than the total power available for wheeling S_G (as per Eq. (1)).

Under the above assumed operating conditions, the total power demand P_D is equal to total the total power supplied S_s for wheeling for power wheeling company as the company is not responsible for loss during power wheeling.

$$P_D = S_s \tag{15}$$

The constraining equations are the sum of all the power input is equal to the sum of all the power out at each grid (equality constraints). Mathematically, it can be

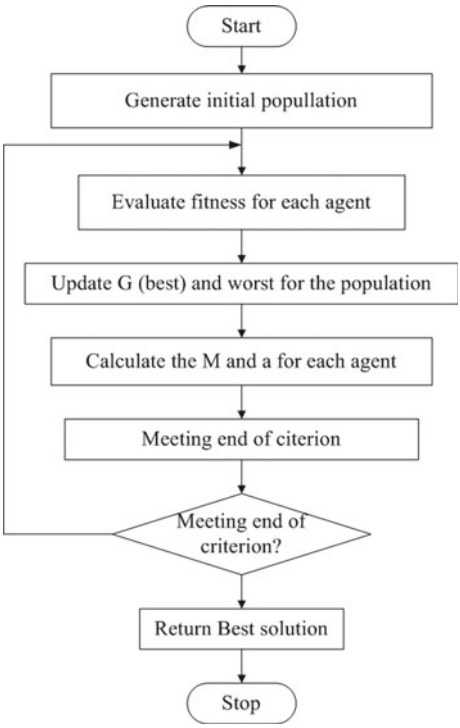

Fig. 3 Flow chart for GSA

represented as

$$\sum P \text{ into } \text{grid} = \sum P \text{ out of grid (at each grid)} \tag{16}$$

Now, the solution to the problem is discussed. The GSA method is a population-based optimization method. Hence the size of the population (the number of the objects/agents) is selected to be "n". The dimension of each agent is the number of variables of the problem. The variables are the power flow in each transmission line. In this case, the dimension of each agent is m.

The initial position of each agent is initialized keeping in view of per the equality and inequality constraints. The initial velocity is initialized in a random way in low-velocity limit may be between 10 and -10.

The value of other constants G_0,δ, and β are selected. The maximum number of iterations k_m for the process is also selected. The stopping criterion of the iterative process is selected based on the result of (worst $-$ best) when relatively smaller as compared to tolerance value or maximum iteration number. MATLAB 7 platform is used to develop coding for the problem. The complete solution has been demonstrated with a framework of four-grid interconnected power system.

3 Results and Discussion

A four-grid interconnected power system example is considered in Fig. 2 to illustrate the optimal power wheeling problem as proposed above. The buyer "*B*" buy power from seller "*A*" at grid 1- 282 MW and at grid 2–418 MW and ask the power wheeling company "W" to transfer 400 MW to grid 3 (distribution load) and 300 MW (distribution load) to grid 4. The distances of the transmission lines are indicated in Table 1.

The equality constraining equations are presented below as per Eq. (16).

At grid 1:

$$P_1 + P_2 + P_3 = 282 \tag{16a}$$

At grid 2:

$$P_4 + P_5 - P_3 = 418 \tag{16b}$$

At grid 3:

$$P_4 + P_2 - P_6 = 400 \tag{16c}$$

At grid 4:

$$P_1 + P_5 + P_6 = 300 \tag{16d}$$

For the proposed problem G_0 is taken as 10.0 and other constants assumed are $\beta = 10$ and $\varepsilon = 0.9$. Here (m) is variable taken as 6 due to the number of transmission lines are 6. Since the GSA is population-based optimization method, the population (number of agents/objects $= n$) assumed is 7 which is considered a little higher than the count of variables. The solution of this problem is computed under two conditions first without a power limit of transmission lines and secondly with transmission lines limits.

- **The solution by not considering transmission lines power limit**:

Table 1 Distance of transmission lines and power flow in lines

SN.	From grid	To grid	Nomenclature of distance	Distance in miles	Power flow
1	1	4	d_1	200	p_1
2	1	3	d_2	300	p_2
3	1	2	d_3	150	p_3
4	2	3	d_4	220	p_4
5	2	4	d_5	250	p_5
6	3	4	d_6	100	p_6

Table 2 Initial position of agents

Agents	p_1	p_2	p_3	p_4	p_5	p_6
1	100	100	82	200	300	−100
2	120	100	62	250	230	−50
3	200	150	−68	100	250	−150
4	100	200	−18	200	200	0.0
5	160	22	100	318	200	−60
6	130	80	72	300	50	20
7	150	250	−118	200	100	50

Table 3 Initial velocity of agents

Agents	V_1	V_2	V_3	V_4	V_5	V_6
1	8	7	6	5	4	2
2	1	2	3	4	5	6
3	7	8	−2	2	6	2
4	3	1	4	7	8	−5
5	3	4	−4	3	2	1
6	−4	3	2	8	−7	0
7	1	4	6	5	3	1

The position of each agent is initialized as per Eqs. (16a), (16b), (16c), and (16d), and presented in Table 2.

The velocity of each agent is initialized in a random way between 10 and −10 and presented in Table 3.

The values of other constants required for solution are assumed as follows:

Initial value of gravitational constant $G_0 = 10$. Maximum number of iterations Km = 1000, $\delta = 0.9$, and $\beta = 10$. The program is developed using the MATLAB 7 software. The stopping criterion for the iterative method is assumed as the absolute value of (worst-best) is less than 1. The computed results are indicated below.

$$P_1 = 282,\ P_2 = 0,\ P_3 = 0,\ P_4 = 400,\ P_5 = 18 \text{ and } P_6 = 0$$

Number of iterations for convergence = 243. Computation time taken = 0.181366 s. The minimum cost computed (J) = 148,900 MW-Mile. This problem has also been solved by Particle Swarm Optimization (PSO) for comparison. The line flows and minimum cost are the same as in GSA shown above. Number of iterations for convergence = 1330. Computation time taken = 0.248479 s.

- **Solution with power limit of transmission lines**:

In addition to the problem considered above it is considered here that the power limit of each transmission line is 350 MW and stopping criterion abs (worst-best) < 0.1.

The computed results by GSA method are as follows.

$$P_1 = 247.2,\ P_2 = 34.8,\ P_3 = 0,\ P_4 = 350,\ P_5 = 68 \text{ and } P_6 = -15.2$$

Number of iterations for convergence = 295. Computation time taken = 0.217166 s. The minimum cost computed (JJ) = 155,400 MW-Mile. This problem has also been solved by Particle Swarm Optimization (PSO) for comparison. The results are indicated below:

$$P_1 = 247.6,\ P_2 = 7.4,\ P_3 = 0,\ P_4 = 350,\ P_5 = 68 \text{ and } P_6 = -42.6$$

Number of iterations for convergence = 6586. Computation time taken = 1.156848 s. The minimum cost computed (JJ) = 155,400 MW-Mile. The optimum value is achieved at around 300 runs.

At optimum, all the agents have the same value of the optimum cost. At optimum, all the agents have the same value of wheeling power in each line. At optimum, both the velocity and acceleration will be zero for GSA method. It has been observed that for different run the power flow in the linear is different but the cost is the same when the power limit for different lines is considered. It shows that in this condition the solution has multiple optima having the same cost. But for unconstrained line flow only one value of the power flow is observed and the optimal cost is due for different runs.

PSO has greater computation time and the iteration numbers are also high than GSA method in both the cases with and without limitation on transmission line. In case of without limiting transmission line power flow, the computed minimum cost and power flow in each line is the same by both the methods of solution GSA and PSO. In the case of limiting power flow in transmission line the optimum power flow computed is different by the methods PSO and GSA. However, for both the techniques, the optimum cost determined is approximately the same. This shows that the problem has multiple optima with the same optimum value of cost. In the case of transmission line limit, the optimum cost computed is more than the optimum cost computed without limiting the transmission line.

4 Conclusion

Under deregulated environment, the economic operation and control power wheeling of interconnected power system by GSA method is presented. With an example of four-grid interconnected power system, the complete procedure is explained. The result computed by GSA has been contrasted with the output with PSO. The performance of GSA has been much more enhanced than PSO due to its low computational time as compared to PSO. Without power limit of transmission line, the result (wheeling power in each transmission line and the total cost of transmission) is the

same in both the methods GSA and PSO. In the case of power limit of transmission lines, the wheeling power in transmission lines computed by GSA and PSO are different but the cost computed by both the methods is the same. It indicates that the problem space has multiple optima having the same cost.

References

1. Talati, P.S.: Transmission System Management & Pricing. William Barclay Parsons Fellowship, Parsons Brinckerboff, Monograph-12, (1998)
2. Paul, K., Kumar, N., Agrawal, S., Paul, K.: Optimal rescheduling of real power to mitigate congestion using gravitational search algorithm. Turkish J. Electric. Eng. Comput. Sci. **27**(3), 2213–2225 (2019)
3. Paul, K., Kumar, N.: Cuckoo search algorithm for congestion alleviation with incorporation of wind farm. Int. J. Electric. Comput. Eng. **8**(6), 4871–4879 (2018)
4. Raj, S.Y., Padhy, N.P., Gupta, H.O.: Wheeling of power under deregulated environment of power system-a bibliographical survey. IEEE Trans. Power Syst. **17**(3), 870–878 (2002)
5. Jiuping, P., Yonael, T., Saifur, R., Koda, J.: Review of usage-based transmission cost allocation methods under open access. IEEE Trans. Power Syst. **15**(4), 1218–1224 (2000)
6. Paul, K., Kumar, N., Agrawal, S.: Optimal rescheduling of real power to mitigate congestion with incorporation of wind farm using gravitational search algorithm in deregulated environment. Int. J. Renew. Energy Res. **7**(4), 1731–1740 (2017)
7. Murali, M., Kumari, M.S., Sydulu, M.: An overview of transmission pricing methods in a pool based power market. Electric. Electron. Eng. **1**(1), 33–41 (2011)
8. Lee, W.J., Lin, C.H., Swift, L.D.: Wheeling charge under a deregulated environment. IEEE Trans. Ind. Appl. **37**(1), 178–183 (2001)
9. Shrmohammadi, D., Filho, X.V., Gorenstin, B., Pereira, M.V.P.: Some fundamental technical concepts about cost based transmission pricing. IEEE Trans. Power Syst. **11**(2), 1002–1008 (1996)
10. Paul, K., Kumar, N.: A review on some aspects of transmission pricing in power system network. In: 6th International conference on Computer Application in Electrical Engineering-Recent Advaces (CERA), pp. 175–180, IEEE, IIT Roorkee (2017)
11. Behesti, Z., Shamsuddin, S.M.: A review of population-based Meta heuristic algorithms. Int. J. Adv. Soft Comput. Appl. **5**(1), 1–35 (2013)
12. Rashedi, E Nezamabadi-Pour, H., Saryazd S.: GSA: a gravitational search algorithm. Inf. Sci. **179**(13), 2232–2248 (2009)
13. Duman, S., Guvenc, U., Sonmez, Y., Yorukeren, N.: optimal power flow using gravitational search algorithm. Energy Convers. Manag. **59**, 86–95 (2012)
14. Swain, R.K., Sahu, N.C., Hota, P.K.: Gravitational search algorithm for optimal economic dispatch. Procedia Technology **6**, 411–419 (2012)
15. Del Valle, Y., et al.: Particle swarm optimization: basic concepts, variants and applications in power systems. IEEE Trans. Evol. Comput. **12**(2), 171–195 (2008)

Materials and Methods for Performance Enhancement of Perovskite Photovoltaic Solar Cells: A Review

Divya Sharma, Rajesh Mehra, and Balwinder Raj

1 Introduction

In 1839, LA Perovski a Russian scientist had discovered a cubic crystal structure with chemical composition $CaTiO_3$. This structure was named calcium titanium oxide ($CaTiO_3$) which had calcium ion (Ca^{2+}) at the corners, titanium ion (Ti^{2+}) BCC (body cubic-centred) and oxygen (O_2^-) at the FCC (face cubic-centred) in a cubic crystal. Between both the cation, i.e. calcium and titanium, calcium ion was bigger in size. And the compounds having similar structure to $CaTiO_3$ were named as perovskites in the honour of Russian scientist LA Perovski. Perovskites exibit general configuration ABX_3 which represents A as cation of bigger size, *B* as cation of smaller size, whereas *X* represents negative ion mostly of oxygen or halogens. In perovskites crystals, cation *A* is located between BX_6 octahedron connected through apex angle while cation *B*, possessing sixfold coordination, is surrounded by an octahedral of anions is shown in Fig. 1 [1]. To form a perovskite structure, radius of ions *A*, *B* and *X* must obey the following rules [2].

Rule of Tolerance Factor (TF):

$$0.81 < \mathrm{TF} = \frac{R_A + R_X}{\sqrt{2}(R_B + R_X)} < 1.11$$

D. Sharma · R. Mehra · B. Raj (✉)
Department of Electronics and Communications Engineering, NITTTR, Chandigarh, Chandigarh 160019, India
e-mail: balwinderraj@gmail.com

D. Sharma
e-mail: divya13jan@gmail.com

R. Mehra
e-mail: rajeshmehra@nitttrchd.ac.in

O. H. Gupta and V. K. Sood (eds.), *Recent Advances in Power Systems*, Lecture Notes in Electrical Engineering 699, https://doi.org/10.1007/978-981-15-7994-3_49

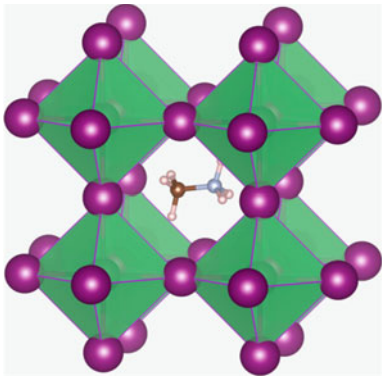

Fig. 1 Unit cell structure of OIH perovskite surrounded by BX_6 octahedra [1]

Rule of octahedral factor (OF):

$$0.44 < \mu = \frac{R_B}{R_X} < 0.9$$

Perovskites materials possess various astonishing properties, e.g. ferroelectricity, spintronics and superconductivity.

In 2009, Miyasaka et al. from Tsutomu, Tokyo, used perovskites for the first time as a photosensitizer in lieu of organic dye in a DSSC. They utilized $CH_3NH_3PbI_3$ ($MAPbI_3$) and $CH_3NH_3PbBr_3$ ($MAPbBr_3$) as photosensitizer. Mesoporous TiO_2 was used as an electron transport medium (ETM). In addition LiI/I_2 in methoxyacetonitrile (CH_3OCH_2CN) and $LiBr/Br_2$ in acetonitrile were utilized as electrolytes for $MAPbI_3$ and $MAPbBr_3$, respectively, for two different DSSCs. However, these cells had low efficiencies of 3.81% and 3.13%, respectively, as well as these cells were not stable.

Further, this cell was improved by Gratzel et al. where Spiro-OMeTAD was utilized in the form of solid-state hole transport medium (HTM), which possessed the efficiency of 9.7%. This aroused the interest among scientists towards the unexceptional properties of perovskites and resulted in formation of perovskites solar cells (PSCs). These cells are further classified into organic–inorganic halide perovskites (OIH-PSCs) [2] and all inorganic halide perovskites (IH-PSCs).

2 Organic–Inorganic Halide Perovskite Solar Cells (OIH-PSCs)

The first OIH-PSC made was consisted of glass as a substrate which is further coated by a FTO film. This resultant substrate is further annealed at 500 °C for 20 min after deposition with compact layer TiO_2 by spin coating process. This TiO_2 layer acts as ETM which constricts the motion of holes. Also, it acts as a shield between

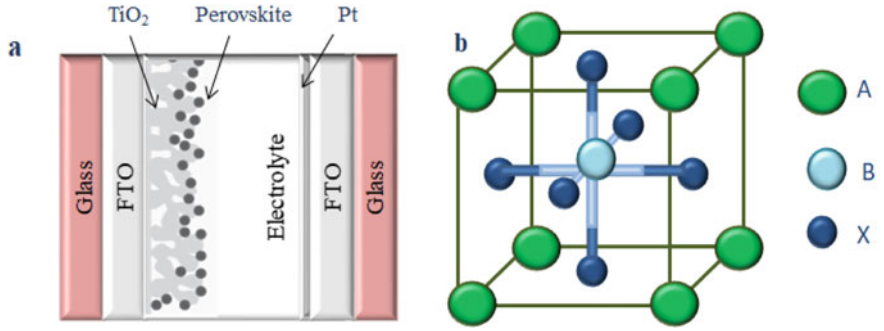

Fig. 2 **a** Schematic structure and **b** crystalline configuration of perovskite photovoltaic cell

FTO and perovskite layer. Thereafter, the resultant stack was coated with mesoporous TiO_2 (m-TiO_2) layer by doctor blading technique followed by sintering at 550 °C for 45 min. Further, resultant substrate was coated with $MAPbI_3$. This final stack is heated at 100 °C for 10 min which resulted in the formation of $MAPbI_3$ nanocrystal layer. Further, a thin coating of Spiro-OMeTAD was deposited using spin coating method. This Spiro-OMeTAD layer acted as HTM. Ultimately, the cell was completed with deposition of gold (Au) of 60-nm-thin layer by thermal evaporation as counterelectrode. Schematic structure and crystalline configuration of first perovskite photovoltaic cell are shown in Fig. 2a [2] and Fig. 2b, respectively.

In 2013, Gratzel et al. preferred in situ deposition of perovskite layer over mesoporous TiO_2 (m-TiO_2) film which resulted in controlled formation of perovskite film and this layer could be absorbed deeply in m-TiO_2 layer. Consequently, efficiencies of this cell are stepped up to 15%.

In 2013, H Snaith et al. from Oxford University prepared a perovskite cell with methyl ammonium lead iodide chloride ($CH_3NH_3PbI_2Cl$) as a light absorber and the mesoporous layer of TiO_2 was replaced by mesoporous layer of Al_2O_3. Astonishingly, solar cell with mesoporous Al_2O_3 (an insulator) stored 10.9% efficiency which was greater than the efficiency (7.9%) of solar cell consisting of m-TiO_2 as ETM.

Since Al_2O_3 was an insulator, still electron transport mechanism was as good as with the use of TiO_2. Consequently, it was confirmed that electron transport occurred within perovskite itself. Therefore, Snaith et al. substituted the mesoporous CiO_2 (m-CiO_2) with compact CiO_2 (c-CiO_2) and synthesize a solar cell consisting ascending layer of FTO/c-CiO_2/OIH perovskite/Spiro-OMeTAD/Gold; however, its efficiency was only 2%. Although the efficiency received was quite low, they found that for electron transportation, mesoporous structure is not essential as it could be done by perovskite itself. Subsequently, Snaith et al. enhanced the quality of perovskite film in planar hetrojunction (PHJ) structure. Thus, the optimized PHJ perovskite showed an efficiency of 11.4%. The morphology and compactness play a vital role in determination of cell efficiency of perovskite cell as it affects several parameters like electron–hole separation, diffusion length (L_D) and electron–hole recombination in perovskite films [2].

Interestingly, they prepared a perovskite film in PHJ by thermal evaporation method which resulted in increased of PCE to 15%. PHJ structure is categorized into two types: (i) normal planar hetrojunction (n-i-p PHJ), (ii) inverted planar hetrojunction (p-i-n PHJ). The n-i-p PHJ contains glass/TCO/ETM/OIH perovskite/HTM/Au electrode which is illustrated through Fig. 3 while p-i-n contains glass/TCO/HTM/OIH perovskite/ETM/metal. In recent years, Yang et al. have upgraded the capability of ETM by doping the compact TiO_2 (c-TiO_2) layer with yttrium (Y) which resulted in the increased cell efficiency of 19.3% [3]. The power conversion rate in OIH-PSC has taken a major leap from 3.8% [4] to 25.2% between 2009 and 2020 [10] which is illustrated in Table 1 [4–10] and graphically shown in Fig. 4.

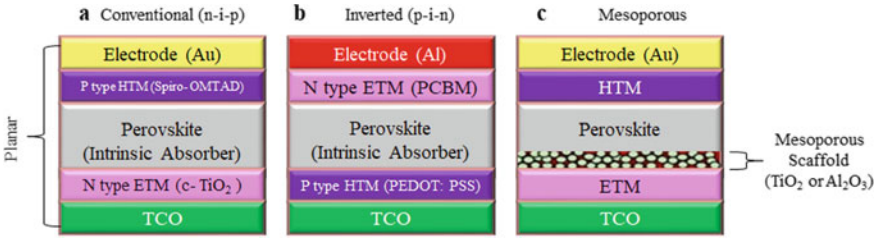

Fig. 3 Device structure **a** conventional n-i-p PHJ; **b** inverted p-i-n PHJ; and **c** mesoporous n-i-p of an OIH-PSCs

Table 1 Development of perovskite solar cells w.r.t. efficiencies from 2009 to 2020

Sr. No.	Perovskite Structure	Voc (V)	Jsc (m A per cm^2)	FF (%)	1_L(%)	Year	Ref. No.
1	CII,NI I J'bI-; perovskite sensitizer on $Ti0_2$	0.61	11	57	3.81	2009	4
2	Glass/ FTO/c-TiOj/Mesoporous Oxide Perovskite/Spiro-OMeTAD/Ag	-	-	-	10.9	2012	5
3	Glass/TC0/$Ti0_2$/MASnI$_3$(CHjNH3Snl3)/Spii0-OMeTAD/ metal	0.92	31.59	79.99	23.36	2016	6
4	Glass/TC0($Sn0_2$:F)/Cri, Zu_sS/ defect layer 1/ MAPblj.ˆCy defect layer 2/CuI/ Back Contact Metal	1.21	25.33	84.11	25.68	2018	7
5	Glass/TCO ($Sn0_2$: F)/$Ti0_2$/MASnI$_3$/CuSbS$_2$/Ag	0.936	31.7	81.1	24.1	2019	8
6	n-i-p planar-Au/CZT S-Cu_2ZiiSiiS+/MAPbI$_3$/$Ti0_2$/FT0				17.5	2020	9
7		-			25.2	2020	10

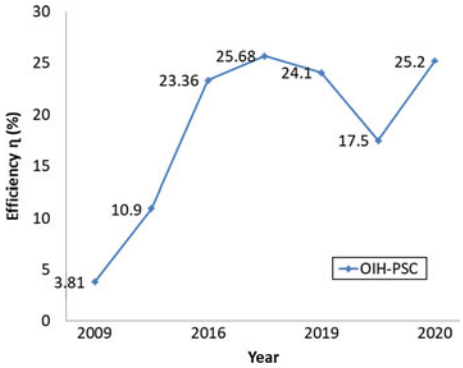

Fig. 4 A graph of the improvements in efficiency of OIH-PSC

2.1 Material Used as Perovskite

The most common materials used as perovskites for PV application are $CH_3NH_3PbI_3$ ($MAPbI_3$), $CH_3NH_3PbBr_3$ ($MAPbBr_3$), mixed $CH(NH_2)_2Pb(I_{1-x}Br_x)_3$ $\{FAPb(I_{1-x}Br_x)_3\}$, mixed $CH_3NH_3Pb(I_{1-x}Br_x)_3$ $\{MAPb(I_{1-x}Br_x)_3\}$, mixed $CH_3NH_3PbI_{3-x}Cl_x$ ($MAPbI_{3-x}Cl_x$), $CH(NH_2)_2PbI_3$ ($FAPbI_3$) and $CH_3NH_3SnI_3$ ($MASnI_3$) [3].

'A' Site. MA cation, formamidinium (FA) and ethylammonium (EA) are the common cations used at 'A' site in OIH perovskite material. Methylammonium (MA) cation possesses tetrahedron crystal structure instead of cubic crystal structure due to its smaller size along with a band gap between the range of 1.51–1.55 eV is found that exceeds Shockley–Queisser limit. The cation with larger ionic radii, e.g. ethylammonium (EA), possesses orthorhombic crystal structure. Though the EA structure possess band gap of 2.2 eV, they show efficiency of only 2% [11, 12].

'B' Site. Location B of OIH perovskite material is captured by elements of group IVA, e.g. lead (Pb), germanium (Ge) and tin (Sn). Among these, lead is used meticulously. It has been observed that $MASnX_3$ has lower band gap than $MAPbX_3$. Also, $MASnX_3$ is unstable as it swiftly oxidizes in air.

'X' Site. Location X of OIH perovskite structure is occupied by halogens (group VII A). It is well known that atomic size of an element increases as moving down the group. Therefore, as the size of halogens at *X* site increases, it results in the absorption of longer wavelength along with decrease in energy. Among these, iodine has been widely used; however, bromine (Br) has the property to regulate the band gap (E_g) of perovskites.

Mixture of cations and anions. Different kinds of mixed anions and cations have also been utilized the band gap of perovskite materials. Some common examples are methyl ammonium formamidinium lead iodide ($MA_xFA_{1-x}PbI_3$), 5-aminovaleric acid $(5\text{-AVAI})_xMA_{1-x}PbI_3$ [8], $CH_3NH_3Sn_{1-x}Pb_xI_3$ ($MASn_{1-x}Pb_xI_3$),

Table 2 Band gap of various perovskite materials

A Site		B site		X site	
Perovskite material	Band gap E_e in eV	Perovskite material	Band gap E? in eV	Perovskite material	Band gap E_g in eV
$FAPbI_3$	1.4	MASnL	1.1	MAPblj	1.5
$MAPbI_3$	1.5	MAS1io.9Pbo.jI_3	1.18	MAPbClj	3.11
EAPblj	2.2	MAPblj	1.5	$MAPbBr_3$	2.2
		MAS1io.3Pbo.7I3	1.31	MAPbljBr	1.8
		MASno.5Pbo.5I3	1.28		

$CH_3NH_3PbI_{3-x}Br_x$ ($MAPbI_{3-x}Br_x$) and $CH(NH_2)_2PbI_{3-x}Br_x$ ($FAPbI_{3-x}Br_x$). The band gap (E_g) of various perovskite materials is given in Table 2 [11].

2.2 *Methods Involved in Fabrication of OIH Perovskite Films*

Mainly there are three methods for manufacturing of OIH perovskite films [12, 14] as shown in Fig. 5.

(i) Solution processing technique
(ii) Vapour deposition method

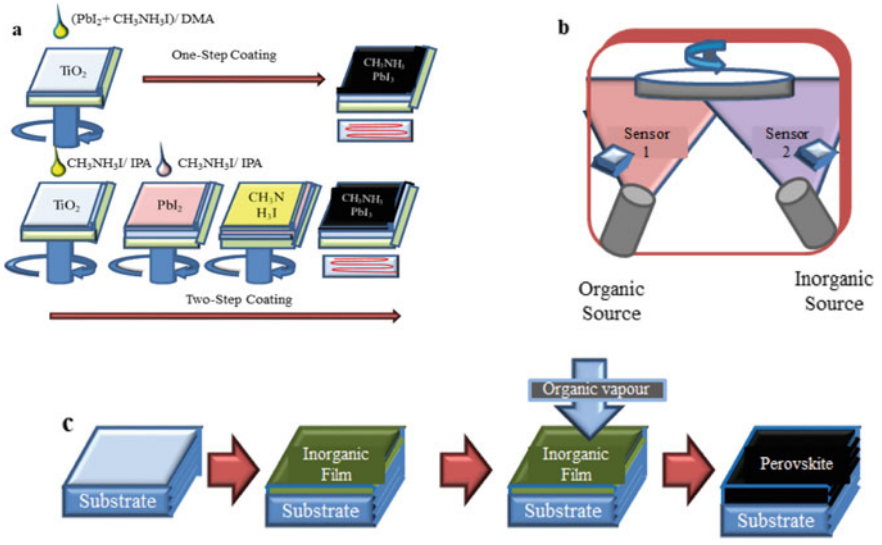

Fig. 5 **a** one-step and two-step methods; **b** vapour deposition method; and **c** evaporation-aided solution processing technique

(iii) Evaporation-aided solution processing technique.

Solution processing technique. This method adopts a simpler and low-cost technique, in which the perovskites can be coated over the substrate by two processes, i.e. one-step spin coating technique and two-step spin sequential deposition method.

One-step spin coating technique. In this process, a solution prepared by mixing MAX (methylammonium halide) powder and PbX_2 in 1:1 ratio or by mixing MAX powder and polar solvents like gamma-Butyrolactone (GBL), N,N-dimethylformamide (DMF) and dimethyl sulfoxide (DMSO) in 3:1 ratio is spin coated over the substrate. Further, the resultant substrate is heat treated (annealed) at various temperature as per solvent used. The film obtained by this process shows amorphous structure.

Two-step spin sequential deposition method. Firstly, PbI_3 layer is spin deposited over m-TiO_2 film with specific speed for a definite time. The resultant substrate is then introduced to 2-propanol (IPA) solution having optimum amount of MAI (methylammonium iodide). This process resulted in 15% efficiency of perovskite solar cells. The film obtained by this techniques shows cubic crystal structure.

Vapour deposition method. This process is discovered by Snaith et al. from Oxford University to produce perovskite film. In this process, MAI and $PbCl_2$ are simultaneously deposited by the process of evaporation on fluorine-doped Tin oxide (FTO) substrate from two different containers which is kept at 120 °C and 350 °C, respectively, in a nitrogen-filled glove box under vacuum. Thus, a layer of $MAPbI_{3-x}Cl_x$ is obtained post-heat treatment (annealing). This is an expensive process.

Evaporation-aided solution processing technique. It is a low-temperature deposition technique. The layer of perovskites produced by the process exhibits full surface coverage and uniform micro-sized crystal grains. This process is cheaper than vapour deposition technique.

In Table 3, the physical and electronic properties of various OIH perovskite materials, i.e. $CH_3NH_3PbI_3$ ($MAPbI_3$), mixed $CH_3NH_3PbI_{3-x}Cl_x$ ($MAPbI_{3-x}Cl_x$), $CH_3NH_3PbBr_3$ ($MAPbBr_3$), are summarized [15].

2.3 Advantages of OIH-PSCs

(i) Tunable band gap by changing organic, metal cations or halide anions.
(ii) Lower recombination.
(iii) High optical absorption.
(iv) Comparatively rapid efficiency increase within ten years.
(v) High open-circuit voltage (V_{oc}).

Table 3 Properties of various OIH perovskites

Properties	MAPblj	MAPI.Br_3	MAPb, Clx
Weight percentage of lead (Wl%)	33.4	43.3	39.2
Band gap Energy E_g (eV)	1.5	2.02	1.55
Mobility (cm sq V"^{1}/s"^{1})	66	-	-
Density (gram/mol)	4.1	-	-
Dielectric constant (g)	6.5	4.8	-
Absorption length (1/a)(11111)	100	-	100–200
Electron diffusion length L_D (11111)	129 ± 11	-	$1069 + 204$
Hole diffusion length L_D (11111)	105 ± 32	-	$1213 = 243$
Exciton binding energy (meVKT)	37 (1.5)–50 (2.0)	2.9	-
LUMO energy level $E_{Lt}tm_0$ (e\)	−3.9	−3.36	−3.75
HOMO energy level Ehomo (eV)	−5.4	−5.38	−5.3

2.4 Disadvantages of OIH-PSCs

(i) Since OIH perovskites are highly sensitive to humidity, oxygen, UV rays and temperature, they easily get degraded. Therefore, stability of perovskites is major concern.
(ii) Toxicity of lead.
(iii) Diminishing of current flow due to the formation of current–voltage (J–V) hysteresis, as a result of ferroelectric behaviour of perovskites.

3 All Inorganic Halide Perovskite Solar Cells (IH-PSCs)

In IH-PSCs {$CsPbI_{3-x}Br_x(x = 0, 1$ and $2)$}, organic group is substituted with inorganic cesium cation (Cs^+) at 'A' site of ABX_3 perovskite structure. This resulted in improved stability of perovskites solar cells under harsh environmental condition. The first, IH-PSCs was assembled by Snaith et al. in 2015. These cells had an efficiency of 2.9%. Till date, IH-PSCs have touched 18.4% efficiency which indicates huge potential in nearby future. Recent researches w.r.t IH-PSCs are described in succeeding paragraphs.

3.1 Crystalline Structure of IH-Perovskites

Similar to OIH perovskites, all inorganic possess ABX_3 perovskite structure, where Cs^+ bigger cation (A site) is located between BX_6 octahedron connected through apex angle while smaller cation B (Pb^{2+}or Sn^{2+}), possessing six coordination is enclosed

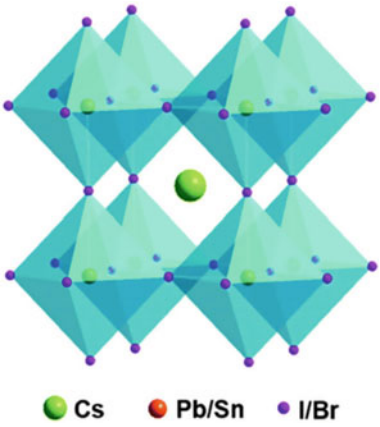

Fig. 6 Unit cell structure of an inorganic $CsMX_3$ perovskite [13]

by an octahedron of halogen anions ($X = Cl^-, Br^-, I^-$). Further, Cs^+ occupies corner Pb^{2+} or Sn^{2+} is body-centred and halogen anions occupied face-centred of unit cell which is shown in Fig. 6 [16].

3.2 Durability of IH Perovskites

The unstability of OIH perovskite is known worldwide due to the presence of volatile, highly reactive organic cation. However, $CsPbBr_3$ perovskites have emerged as the best among all perovskites in terms of stability [17]. Another advantage of all inorganic perovskites is that there are free from moisture-absorbing organic cation as these are hygroscopic in nature. Therefore, it can be concluded that the stability of inorganic perovskites is unaffected by external factors to some extent in comparison with OIH perovskites. Decomposition, oxidation and polymorphic transition can be the intrinsic factor for instability.

3.3 Architecture of IH-PSCs

Construction of IH-PSCs is similar to organic perovskite solar cell. These are also fabricated in a regular n-i-p and inverted p-i-n formation [18]. This cell can also be designed using a mesoporous scaffold either semiconducting (TiO_2) or insulating (Al_2O_3). All the three formations are illustrated in Fig. 7. In all the above formation, the perovskites layer is packed between n-type ETM and p-type HTM [19]. In this section, IH-PSCs engineered from compositional, interfacial, doping and spectral criteria are systematically demonstrated, and the photovoltaic parameters of various IH-PSCs are given in Table 4 [13, 20].

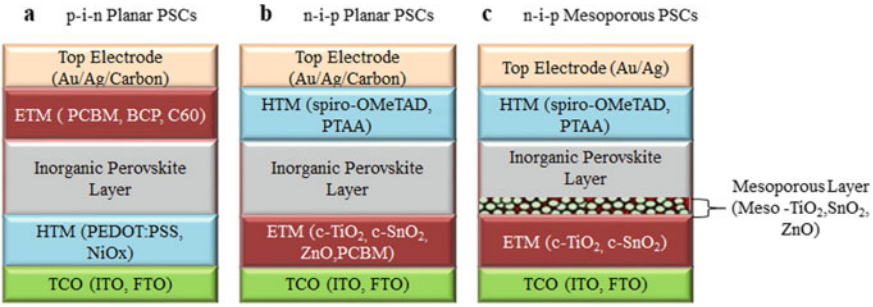

Fig. 7 Device structure **a** planar p-i-n; **b** planar n-i-p; and **c** mesoporous n-i-p of IH-PSCs

3.4 Methods Involved in Fabrication of IH Perovskite Films

All inorganic halide perovskite ($CsPbI_{3-x}Br_3$) film is to combine $PbI_2/PbBr_2$ and CsI/CsBr [21]. This can be done using solution processing technique, i.e. one-step or two-step spin coating process, vapour deposition technique and evaporation-aided solution processing technique as adopted in fabrication of organic perovskite film [21].

3.5 Advantages of IH-PSCs

(i) Higher thermal stability than organic–inorganic halide perovskites.
(ii) Higher open-circuit voltage.
(iii) Fabrication cost is comparatively lower than OIH-PSCs.

3.6 Disadvantages of IH-PSCs

(i) Comparatively lower efficiency than OIH perovskites.
(ii) Lower light absorption.
(iii) Toxicity of lead.

4 Conclusion

The power conversion rate of 25.2% has been attained by OIH-PSCs, which is equivalent to commercially available silicon solar cells whose efficiency is more than 23%. However, OIH-PSCs are confronting the problem of thermal stability and short life operation lifetime. The problem of thermal stability has been eradicated to some

Table 4 Device performances for various IH-PSCs

Peiovskite materials	Structure of Peiovskite cell	PCE (%)	Operation conditions	Year
CsPbBi;	FTO/m-TiO_2/$CsPbBr_3$ (Peiovskite Absorber (PA))/PTAA/Au	5.72	Ambient	2015
	FT0/c-$Ti0_2$/m-$Ti0_2$/$CsPbBr_3$(PA)/C	6.7		2016
	rT0/c-TiO/ni-$Ti0_7$/$CsPbBr_1$(PA)/ZiiS: SnS/C	10.26		2018
	FT0/c-$Ti0_2$/CsPbBrj(PA)/spn0-0MeTAD/Ag	10.91		2019
$CsPbIBr_2$	FT0/m-TiO_2/$CsPbIBr_2$(PA)/Au	4.7	Glovebox	2016
	ITO/SnO_2/C60/$CsPb_{1.:1}SiiIIBi'_2$(PA)/spiio-OMeTAD/Au	11.53		2018
	IT0/c-TiO_2/$CsPbI_2Br$(PA)/Spir0-0MeTAD/Au	16.07		2019
	FT0/bl-$Fi0_2$/mp-$Ti0_2$/CsPbIBi:(PA)/Spir0-0MeTAD./Au	6.3	Ambient	2016
	FTO/c-TiO_2/m-TiO_2/$CsPb_{0\,9}Sn_0$ JBrˆPAVC	11.33		2017
	FTO/ $Ti0_2$/$CsPbI_2Br$/$CsPbI_3$ QDs/PTAA/Au	14.45		2018
	FT0/c-$Ti0_2$/m-$Ti0_2$/BaI_2:CsPbLBr(PA)/P3HT/Au	14.85		2019
	FTO/c-TiO_2/m-TiO_2/$CsPb_{0\,98}Sr_{0\,02}I_2Br$(PA)/P3HT/Au	11.3	n_2	2017
	ITO/$Sii0_2$/ZnO/$CsPbI_2Br$(PA)/Spiro-OMeTAD/$Mo0_3$/Ag	14.6		2018
	ITO/$Sn0_2$/$CsPbI_2Br$(PA)/PTAA/$Mo0_3$/A]	13.8		2019
	FTO/bl-TiO_2/$Cs0_{\,925}$ko $_{075}PbI_2Br$(PA)/Spiro:Li-TFSi-tBP/Au	10	20 °C. Hi I 20%	2017
	ITO/Ca/C60/$CsPbI_2Br$(PA);TAPC/TAPC: $Mo0_3$/Ag	11.8	Vacuum	2017
	IT0/$Sn0_2$/$CsPbI_2Br$(PA)/CsBr/Spir0-0MeTAD/Au	16.37	N_2 glovebox	2019
CsPllI,	FT0/c-TiO_2/$CsPbI_3$ QDs/Spiro-OMeTAD/MoO_s/A]	10.77	Dry ambient	2016
	FTO/bl-TiO_2/mp-TiO_2/CsPbl3(PA)/P3HT/M0O3/Au	4,68	n_2	2016
	FT0/c-TiO_2/$CsPbI_3$ (PA)/CuI/Au	13.21		2017
	FTO/ TiOj/a-$CsPbI_3$ (PA)/Spii o-OMeT AD/Ag	4.13	Ambient	2016
	FT0/c-TiO_2/$BA_2CsPb_2I_7$(PA)/Spir0-0MeTAD/Au	4.84		2017
	rTO/c-$Ti0_2$/$CsPbI_3$(PA)/Spiro-OMeTAD/Ag	13.5		2018
	FTO/c-TiCyCsPbI_3(PA)/Spiro-OMeTAD/Au	2.9	Vacuum	2015
	ITO/PT AA/C sPbI_3 (PA)/PCBM/C 60/BCP/A1	11.4	glovebox	2017
	FT0/c-TiO_2/PTABr-$CsPbI_3$(PA)/Spiia-0MeTAD/Ag	17.01		2018
	Glass/FT0/$Ti0_2$/$CsPbI_3$ QDs/PTAA/MoOˆ/Ag	14.10	N_2 glovebox	2019

extent by inorganic halide is maximum of 18.4% which is still on some side. Therefore, a lot of researches are in progress to improve the stability of OIH-PSCs and to enhance the power conversion rate of IH-PSCs. From previous results, the target seems to be achievable, however, lots of efforts are required. In future, the days are not far away when the perovskites will power the household appliances.

References

1. Eames, C., Frost, J.M., Barnes, P.R.F., O' Regan, B.C., Walsh, A., Islam, M.S.: Ionic transport in hybrid lead iodide perovskite solar cells. Nature Comm. **6**, 1–8 (2015)
2. Kumar, P.: Organic Solar cells-Device Physics, Processing, Degradation, and Prevention, 1st edn. CRC Press Taylor & Francis Group, New York (2017)
3. Zhou, H., Chen, Q., Li, G., Luo, S., Song, T., Duan, H.S., Hong, Z., You, J., Liu, Y., Yang, Y.: Interface engineering of highly efficient perovskite solar cells. Science **345**, 542–546 (2014)
4. Kojima, A., Teshima, K., Shirai, Y., Miyasaka, T.: Organometal halide perovskites as visible-light sensitizers for photovoltaic cells. J. Am. Chem. Soc. **131**, 6050–6051 (2009)
5. Lee, M.M., Teuscher, J., Miyasaka, T., Murakami, T.N., Snaith, H.J.: Efficient hybrid solar cells based on meso-superstructured organometal halide perovskites. Science **338**, 643–647 (2012)
6. Du, H.J., Wang, W.C., Zhu, J.Z.: Device simulation of lead-free $CH_3NH_3SnI_3$ perovskite solar cells with high efficiency. Chin. Phys. B **25**(10), 1–8 (2016)
7. Thakur, N., Mehra, R., Devi, C.: Efficient design of perovskite solar cell using parametric grading of mixed halide perovskite and copper Iodide. J. Electron. Mater. **47**, 6935–6942 (2018)
8. Devi, C., Mehra, R.: Device simulation of lead-free $MASnI_3$ solar cell with $CuSbS_2$ (copper antimony sulfide) J. Mater. Sci. **54**(7), 5615–5624 (2019)
9. Syafiq, U., Ataollahi, N., Scardia, P.: Progress in CZTS as hole transport layer in perovskite solar cell Sol. Energy **196**, 399–408 (2020)
10. National Renewable Energy Laboratory, Best research-cell efficiencies (2020). https://www.nrel.gov/pv/assets/images/best-research-cell-efficiencies.20200406
11. Mutalikdesai, A., Ramasesha, S.K.: Emerging solar technologies: perovskite solar cell. J. Sci. Edu. **22**, 1061–1083 (2017)
12. Sharma, S.K., Ali, K.: Solar Cells-From Materials to Device Technology. Springer Nature Switzerland AG (2020)
13. Mei, A., Li, X., Liu, L., Ku, Z., Liu, T., Rong, Y., Xu, M., Hu, M., Chen, J., Yang, Y.: A hole-conductor-free, fully printable mesoscopic perovskite solar cell with high stability. Science **345**, 295–298 (2014)
14. Liu, M., Johnston, M.B., Snaith, H.J.: Efficient planar hetrojunction perovskite solar cells by vapour deposition. Nature **501**, 395–398 (2013)
15. Stranks, S.D., Eperon, G.E., Grancini, G., Menelaou, C., Alcocer, M.J., Leijtens, T., Herz, L.M., Petrozza, A., Snaith, H.J.: Electron-hole diffusion lengths exceeding 1 micrometer in an organometal trihalide persovskite absorber. Science **342**, 341–344 (2013)
16. Duan, J., Xu, H., Sha, W.E.I., Zhao, Y., Wang, Y., Yang, X., Tang, Q.: Inorganic perovskite solar cells: An emerging member in photovoltaic community. J. Mater. Chem. A **7**, 21036–21068 (2019)
17. Wang, H., Wu, Y., Ma, M., Dong, S., Li, Q., Du, J., Zhang, H., Xu, Q.: Pulsed laser deposition of CsPbBr films for application in perovskite solar cells. ACS App. Energy Mater. **2**, 2305–2312 (2019)
18. Wang, L., Fan, B., Zheng, B., Yang, Z., Yin, P. G., Huo, L.: Organic interlayer materials: recent advances in all inorganic perovskite solar cells. Sus. Energy Fuels, 2134–2148 (2020)
19. Mora, J.U., Benito, I.G., Ontoria, A.M., Martin, N.: Hole transporting materials for perovskite solar cells: a chemical approach. Chem. Soc. Reviews **47**, 8541–8571 (2018)
20. Zhu, Y., Poddar, S., Shu, L., Fu, Y., Fan, Z.: Recent progress on interface engineering for high-performance, stable perovskites solar cells. Adv. Mater. Interfaces (2020)
21. Ouedraogo, N.A.D., Chen, Y., Xiao, Y.Y, Meng, Q., Han, C.B., Yan, H., Zhang, Y.: Stability of all-inorganic perovskite solar cells. Nano Energy **67** (2020)